Functional gold and silver complexes and supramolecules based on 9,10-diphenylanthracenes : photoactivity, catalysis and chiroptical properties

Zhen Cao

N° d'ordre :

THÈSE

Présentée à

L'UNIVERSITÉ DE BORDEAUX

École Doctorale des Sciences Chimiques

Pour obtenir le grade de

DOCTEUR

Spécialité: Chimie Organique

Par Zhen CAO

Functional gold and silver complexes and supramolecules based on 9,10-diphenylanthracenes: Photoactivity, catalysis and chiroptical properties

Complexes fonctionnels d'or et d'argent et supramolécules à base de 9,10-diphenylanthracènes: photoactivité, catalyse et propriétés chiroptiques

---

Directrice de thèse: Mme. Brigitte BIBAL
Co-directeur de thèse: M. Dario BASSANI

Soutenue publiquement le: 15 Octobre 2020

Devant la commission d'examen composée de:

M. Louis FENSTERBANK, *Professeur, Sorbonne Université*	Rapporteur
M. Abderrahmane AMGOUNE, *Professeur, Université de Lyon I*	Rapporteur
M. Didier ASTRUC, *Professeur Emérite, Université de Bordeaux*	Président, Examinateur
Mme. Isabelle LERAY, *Directrice de Recherche CNRS, ENS Paris-Saclay*	Examinatrice
Mme. Brigitte BIBAL, , *Maître de Conférences, Université de Bordeaux*	Directrice
M. Dario BASSANI, *Directeur de Recherche CNRS,Université de Bordeaux*	Co-directeur

Preface

L'écriture de ce manuscrit de thèse a représenté un défi de taille, mais ce fût aussi un grand voyage qui a approfondi ma réflexion sur mes accomplissements et leur sens. Il ne fait aucun doute que, ces années de thèse ont constitué un moment de vie scientifique important qui ouvre la voie à de futurs apprentissages et réflexions.

Cette thèse, débutant en novembre 2016, est le fruit de quatre années (2016.11-2020.10) de travail réalisées sous la supervision des docteurs Brigitte Bibal et Dario Bassani à l'Institut des Sciences Moléculaires de l'Université de Bordeaux au sein du groupe de recherche « Nano-structures Organiques » (NEO).

Dedicated to those who inspired me

Acknowledgements

Almost four years has elapsed since I came to Bordeaux I felt in love with which is a colorful journey in my life as I encountered a number of lovely people here. At the end of the journey, I would like to thank people who inspired or helped me.

I would like to express deep thanks to my supervisors Dr. Brigitte Bibal and Dr. Dario Bassani who were always available to discuss my recent results and gave me timely feedback to establish a clear goal. They also showed me a lot of respect to what I was doing which makes me feel full of satisfactory and confidence. Meanwhile, they gave me much patience when I happened to obstacles. Not only confined to academic problems they helped me, but also the difficulties I met in my everyday life such as writing French letters and special thanks to Dr. Dario Bassani for helping me get reunited with my wife and little son in France.

In this special time, I would express my great thanks the jury members who accepted my thesis defense. Please take good care of yourself and I wish you have a safe and good voyage to Bordeaux city.

I would like to thank the members of the CESAMO group for their wonderful work in characterizations including NMR, X-ray diffraction and mass spectroscopy. They are very kind people and special thanks to Aline Lacoudre, Cybille Rossy, Claire Mouche and Christelle Absalon who gave me a lot of patience and helped me on many occasions.

I would thank to Mr. Damien Jardel who is a genius in repairing machines and teaches me a lot, and I appreciated our discussions about life. I would also thank to Mrs. Pascale Godard and Mrs. Clothilde Davies for their available and kind help whatever I demanded. Special thanks to my previous colleague Dorian Sonet who is a peaceful and responsible man that shared the same office for three years, but a great pity for not finalizing his Ph.D and he finally decided to embark on a teaching career. I would thank to Dr. André Del Guerzo and Dr. Guillaume Raffy who shared their office to me for writing the thesis manuscript. Great thanks to the excellent master students Simon Plaize, Guillaume Chamelot, Morgan Wolch, Mathilde Berthe who also shared a great time with me. I would also thank other NEO members: Dr. Jean-Marc Vincent, Dr. Nathan D. McClenaghan, Dr. Jean-luc Pozzo, Dr. Vicente Marti Centelles, Dr. Leire G. Rivero, Dr. Shilin Yu, Dr. Das Avijit, Dr. Luca Pisciottani, Axel Almansa, Baptiste Abadie, Yu-Yu Hsieh, Amaury Furet, Maxime Douarre. They are all lovely, kind, smart and enthusiastic NEO-ers that I will put in a significant position in my heart. And no matter where I go, I am proud to be one of the NEO members.

I would thank my collaborators Dr. Emillie Pouget and Dr. Reiko Oda that allowed me to work in IECB and tested something new, and many thanks to Dr. Antoine Scalabre for providing me the silica helices and Peizhao Liu for helping me to measure the CD and CPL of chiral sulfoxides which is now in progress.

Many thanks to Mrs. Iman Traboulsi and Jonathan Lusseau for lending me chemicals and instruments.

Special thanks to Veng-Chan Choi and Luming Zhao who taught me to be a humble person. I would also thank to Rosa Ren and Jianhong Ren who gave me the opportunity to do a part-time job in Asia-shop Bordeaux for one and half year and thank Zhengyan Sheng, Wenjuan Wang and Yuechao Dong for their kind help during the lockdown.

I would thank my good friend Changcong Neng and Dr. Jian Zhao who shared a great experience of basketball playing and interesting discussions. I would also remember my friends Dr. Qian Li, Dr. Jie Gao, Dr. Jinhua Wang, Dr. Shiliu Lv, Dr. Fangyu Fu, Mrs. Xinghui Qi, Mr. Wenbin Guo, Mrs. Naixin Kang, Mr. Junjie Hao, Dr. Zhenhui Chen, Mr. Zaicheng Zhang and Mr. Wei Chen in Bordeaux and cherish our friendship.

I would also thank China Scholarship Council (CSC) for the financial funding.

I would like to express my deep thanks to my parents from who I saw the character of fortitude and a mentally strong heart. Special thanks to my beloved family, they are always my motivations to go forward.

Abbreviations

Solvents and compound motifs and reagents:

CH_2Cl_2: Dichloromethane

CD_2Cl_2: Dichloromethane-d2

DMSO: Dimethylsulfoxide

DMSO-d_6: Deuterated dimethylsulfoxide-d6

CH_3CN: Acetonitrile

CD_3CN: Deuterated acetonitrile

THF: Tetrahydrofuran

DCE: Dichloroethane

DMF: Dimethylformamide

Et_2O: Diethyl ether

TREN: Tris(2-aminoethyl)amine

NaBArF: Sodium tetrakis[3,5-bis(trifluoromethyl)phenyl]borate

CsBArF: Cesium tetrakis[3,5-bis(trifluoromethyl)phenyl]borate

DPA: Diphenylanthracene

DIPEA: N,N-diisopropylethylamine

Et_3N: Triethylamine

Ad: Adamantyl

NHC: *N*-heterocyclic carbene

bpy: 2,2'-bipyridine

tmbn: 2,4,6-trimethoxybenzonitrile

DBV: Divinylbenzene

Techniques and characterizations:

TLC: Thin-layer chromatography

XRD: X-ray diffraction

MS: Mass spectroscopy

CPL: Circularly polarized luminescence

UV-vis: Ultraviolet-visible

EDS: Energy dispersive spectroscopy

TEM: Transmission electron microscopy

STEM: Scan transmission electron microscopy

NMR: Nuclear magnetic resonance

CD: Circular dichroism

HPLC: High-performance liquid chromatography

Unities

mL: Milliliter

mM: Millimole

µL: Microliter

µM: Micromole

min: Minutes

nm: Nanometer

mg: Milligram

Hz : Hertx

Kcal: Kilocalorie

KJ: Kilojoule

Å: Angström

°C: Celsius degree

h: Hour

Others

rt: room temperature

Contents

Résumé

1 Introduction

The development of novel molecular systems affords the world with plenty of diversification. Functional systems are nowadays pursued by organic chemists.

"*The primary motivations that once induced chemists to undertake natural product syntheses no longer exist. Instead of target structures themselves, molecular function and activity now occupy center stage.*"

—— Dieter Seebach, 1990[1]

As chemists in organic chemistry, we do know that a lot of challenging issues are to be overcome. For example, developing efficient and environmentally friendly catalysis is still a big challenge with practical applications.

In our group, we are interested in developing (supra)molecular systems and templated metal complexes which are capable of displaying catalytic activity or photoactivity, including hydrogen bonding organocatalysis for ring-opening polymerization,[2-6] photoreduction of gold complexes,[7, 8] and switchable organic molecular cage system based on diphenylanthracene (DPA) upon cycloaddition of singlet oxygen.[9]

This thesis is mainly related to ligand design to achieve functional gold complexes for catalysis. In chapter 1, a short history about the development of homogeneous gold catalysis is provided as a background including representative gold(I) and gold(III) complexes and their differences in gold catalysis. Gold as a carbophilic π acid for activation of unsaturated carbon-carbon bonds toward necleophilic addition is also discussed. More importantly, this introduction highlights the newly-emerging catalytic gold redox chemistry through several strategies which is aimed to inspire new idea for gold catalyzed transformations. The sections entitled 'Dual photoredox and gold catalysis' and 'light-triggered redox gold catalysis' are partially based on the chapter in in Specialists Periodical Reports in Photochemistry (Z. Cao, D. M. Bassani and B. Bibal. 'Light activation of gold complexes.' *Photochemistry*, **2020**, 47, 421-456.).

Chapter 2, Photoreduction of gold(III) complexes and homogeneous catalysis, presents results showing that the oxidation state of gold could be steered by photoreduction and enable the utility of both gold species in a one-pot fashion. The mechanistic study of photoreduction is investigated and preliminary results concerning the photoreduction of dichloro(2-pyridinecarboxylato)gold(III) complex ($PicAuCl_2$) are aimed towards the transformation from gold precatalyst to cationic gold.

Chapter 3 concerns heterogeneous gold catalysis using supported metal complex on silica nano-objects. Functionalized phosphine ligands were elaborated and the corresponding gold complexes covalently bound to chiral silica helices for heterogeneous catalysis. The use of chiral silica nanohelix allowed to form a

chiroptical 3D ensembles observed by circular dichroism. Even though chiral induction was not observed for a spirocyclization reaction, this approach opens a route to achieve chiral catalysis from an inorganic template. Chapter 4 describes the development of hindered bis-thioether ligands that take advantage of DPA atropisomerism (*syn vs. anti*), an under-exploited property of polyaromatic compounds. We chose to investigate the corresponding thioether silver complexes for homogeneous catalysis and to prepare their chiral sulfoxides to elucidate their chiroptical properties. The thioether silver complexes self-assembled differently depending on the nature of the anion and thioether substituents and were efficient as homogeneous catalysts for tandem addition/cycloisomerizations of alkynes. The chiral sulfoxides based on DPA can react with singlet oxygen to switch off their chiroptical properties. Meanwhile, preliminary results towards developing DPA-based hemilabile P,P(O) or P,P(S) ligands were shown for further formation of coinage complexes and their applications in homogeneous catalysis.

Finally, chapter 5 introduces a self-assembled switchable imine cage by using $^1O_2$ stimulus. The rigid [2+3] imine cage with three chromophoric pillars exhibits good reversibility and high affinity toward metal ions. Meanwhile, a [2+2] imine macrocycle is also described. The overall frame work of this thesis is presented in Figure I.

Thesis framwork

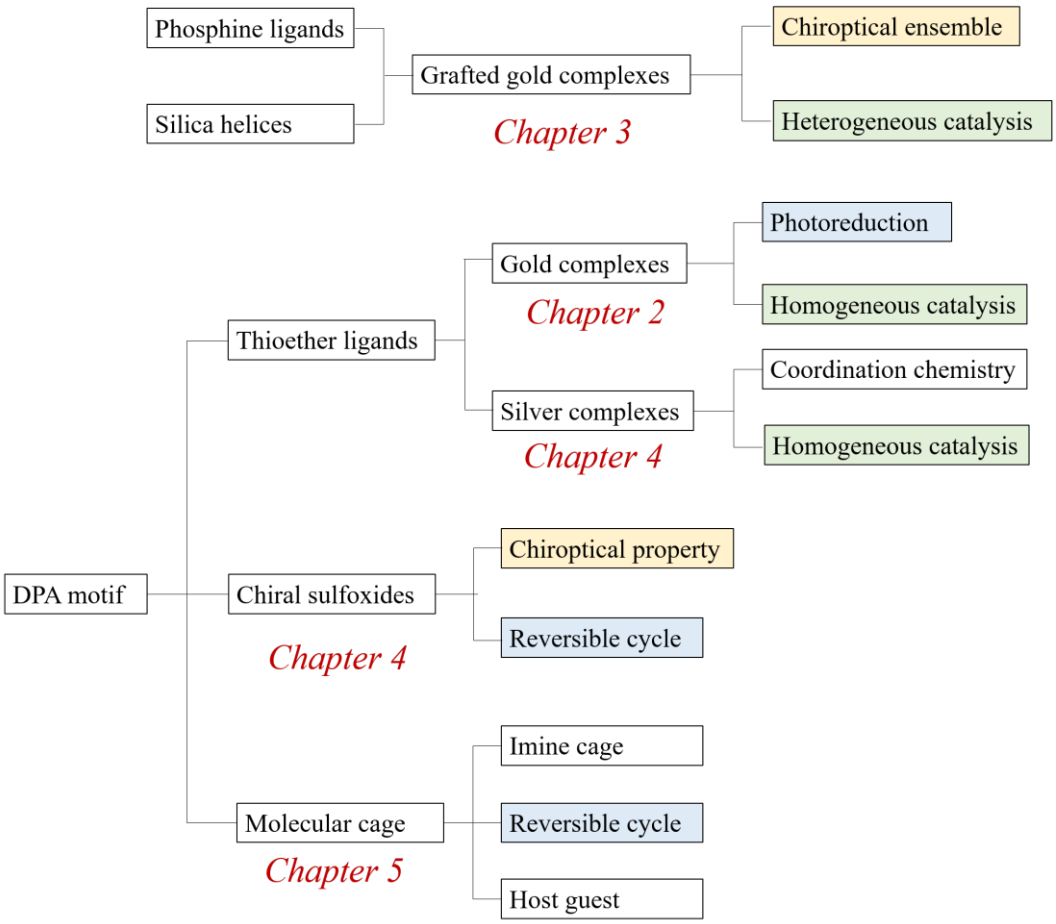

Figure I. Thesis framework of my Ph.D research. The columns in light yellow represent chiroptical property; the columns in light green represent catalysis; the columns in light blue represent switches.

2 Photoreduction of gold(III) complexes and homogeneous catalysis

The two most common oxidation states of gold are (+I) and (+III). Generally, gold(I) exhibits linear coordination and gold(III) planar coordination geometries. In most cases, the gold(III) complexes undergo thermal reductive elimination into gold(I) at elevated temperatures[10, 11] or, rarely at exceptionally low temperature[12] which leads to C-C bond C-X bond formation and generation of the corresponding gold species (**Scheme I**). Early studies reported by Kochi and co-workers[13-15] demonstrated seminal mechanistic studies of a series of four-coordinated alkyl gold(III) complexes, such as PPh_3AuMe_3, which readily undergo fast reductive elimination. Dissociation of phosphine ligand from gold leading to a tri-coordinate complex is proposed to be the rate-limiting step as the reductive elimination process was severely suppressed by addition of extra phosphine.

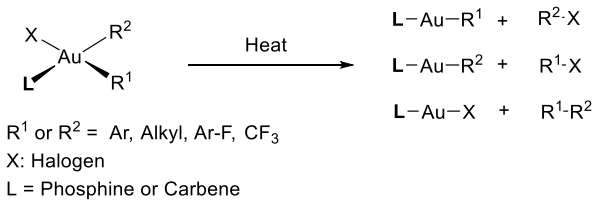

Scheme I. Representative thermal reduction of organogold(III) complexes.

In contrast, the photoreduction of gold(III) chloride complexes was considered as a robust approach to produce gold nanoparticles in the presence of water under UV light irradiation [16-20] Nocera and co-workers[21] reported a pioneering contribution of halogen reductive elimination in mono- and dinuclear phosphine gold(III) complexes under 320 nm irradiation for 60 h. The Au-X bond was proposed to be activated through significant ligand-to-metal charge transfer (LMCT) which allows two-electron photoelimination of X_2 from each monomeric gold center (**Scheme II**). The photoreduction process was also achieved in *N*-heterocyclic carbene gold(III) complexes under 280 nm irradiation in Monkowius's group[22] and Rosenthal's group[23].

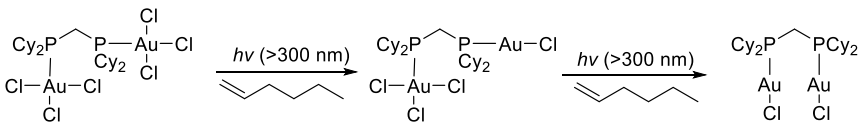

Scheme II. Photoinduced halogen reductive elimination of phosphine gold(III) complex.[21]

In 2015, we developed a thioether gold(III) chloride complex appended with a 9,10-diphenylanthracene (DPA) chromophore which undergoes rapid photoreduction (around 30 min) to gold(I) species under 365 nm irradiation.[7] The mechanism involves intramolecular energy transfer from the DPA chromophore to the bounded gold. To gain a better understanding of the mechanism, three new dialkyl-thioether ligands with or without the DPA chromophore were synthesized and the corresponding gold(III) trichloride complexes were

straightforwardly prepared through a liquid-liquid extraction. The thioether gold(III) complexes underwent a rapid reductive elimination under a 365 nm irradiation or ambient light in dichloromethane and toluene solutions to afford the corresponding gold(I) complexes (**Figure II**). The mechanism of photoreduction through Cl_2 elimination is discussed based on a kinetic study and the chemical trapping chlorine species: Cl_2, radical Cl· and possibly Cl^+ by stepwise radical pathway or an ionic pathway with a tri-coordinated intermediate. The kinetic study showed that the presence of DPA has no impact on the reductive rate which is consistent with efficient energy transfer from DPA to the gold atom.

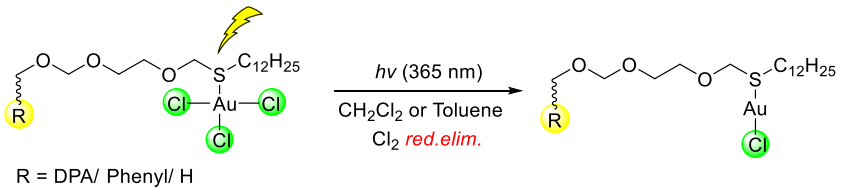

Figure II. Schematic representation for photoreduction of thioether gold(III) complexes.

The catalytic activity of gold(III) chloride complexes and the corresponding gold(I) ones obtained by *in situ* reduction were evaluated in the cyclization of *N*-propargylic amides to oxazoles. Finally, a cascade reaction catalyzed by the thioether gold complexes allowed the synthesis of a 4*H*-quinolizin-4-one in high yields and illustrates the convenience of such photoreducible complexes in homogeneous gold catalysis (**Figure III**).

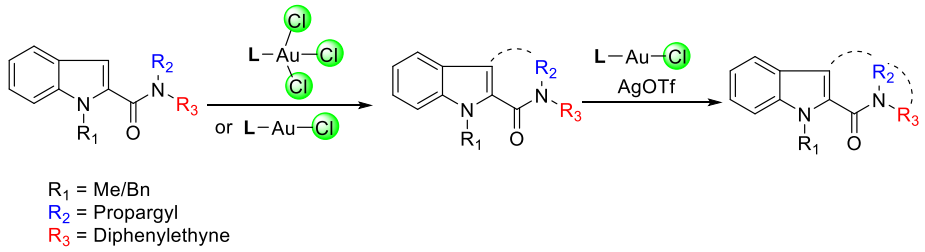

Figure III. Gold catalyzed cascade catalytic process of substituted *N*-propargylic amide.

Dichloro(2-pyridinecarboxylato)gold(III) complexes ($PicAuCl_2$) is a highly stable gold(III) precatalyst[24] which has been widely employed in many cyclization reactions for alkynyl activation.[25-31] Based on the proposed mechanism, the photoreduction of $PicAuCl_2$ was examined in various solvents and followed by UV-vis spectroscopy (**Figure IV**). The shift and subsequent loss of gold absorbance indicates that a new gold species was formed. A strong solvent effect was observed in DMSO and dichloromethane, consistent with a mechanism involving ionic or radical pathways. The determination of the photoreduced species, only soluble in DMSO, is still in progress.

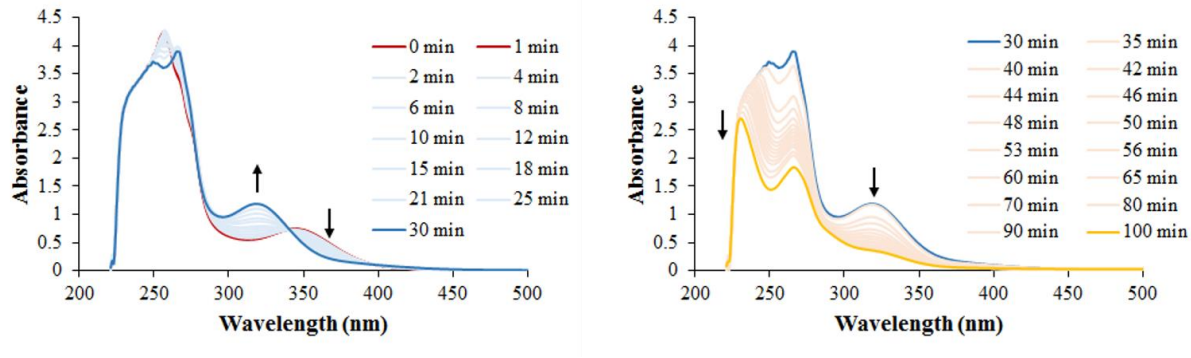

Figure IV. Photoreduction of $PicAuCl_2$ followed by UV-vis spectroscopy (0-100 min) (490 µM, CH_2Cl_2).

3 Silica helices supported heterogeneous gold catalysis

Immobilization of metal nanoparticles or metal complexes onto a solid support for heterogeneous catalysis has attracted considerable attention in synthetic chemistry as it offers removable catalysts with facile product purification. The recyclability and reusability of the supported catalysts provide waste-reduction and greener processes. In the field of heterogeneous gold catalysis, the vast research efforts has focused on metal oxides (TiO_2, Al_2O_3, CeO_2 etc.) or polymer supported gold nanoparticles (AuNPs) for greener catalysis.[32-35] The grafting of gold complexes onto a solid support made an increasing progress in gold catalysis. The early examples of polystyrene supported cationic gold(I) catalysts were reported in 2011 by Akai's[36] and Yu's groups[37]. Subsequently, phosphine, carbene, and pyridine gold complexes have been bound onto various solid supports such as organic polymers,[38-41] mesoporous silica[42-46] and magnetic nanoparticle,[47, 48] which exhibited comparable efficiency and enantioselectivity as the corresponding homogeneous systems. Depending on the systems, high performance can be maintained through 4 to 8 catalytic cycles.

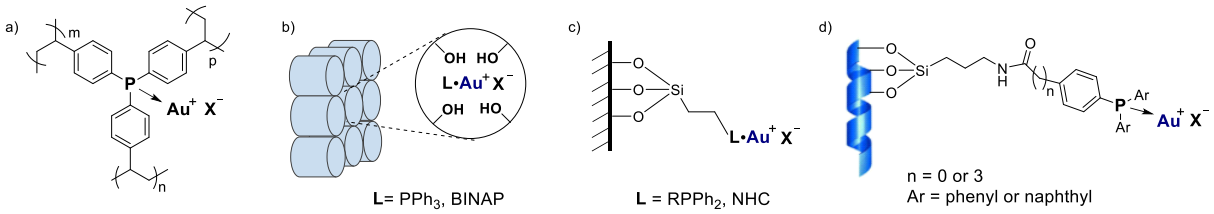

Figure V. Main strategies for supporting gold complexes in heterogeneous catalysis: a) insertion in an organic (porous) polymer; b) adsorption on silica mesopores to benefit from an acidic assistance, c) covalent grafting on silica particles or mesoporous silica and d) our work: grafting on a chiral silica nanohelix to form a chiroptical assembly for a long-term monitoring.

In our case, the phosphine gold complexes were covalently bound onto chiral silica helices by peptide condensation (**Figure V**) and the gold content was determined by energy dispersive spectroscopy (1 mol% compared to silicon). In the presence of a silver salt, the reactivity of the immobilized gold catalyst was

examined in the cyclization of propargylic amide and 1,6-enyne and water addition to terminal alkyne and was found to be similar to homogeneous conditions. In addition, the bound gold catalyst exhibit high efficiency in the dearomative spirocyclization of aryl alkynoate esters (**Figure VI**) which can be carried out with a catalytic loading of 0.05 mol%. The heterogeneous catalysts were easily recovered and can be recycled up to 7-8 times without loss of efficiency. However, the reaction was found to be much slower after 7 cycles while adding extra silver salt can accelerate the reaction. The observation probably accounts for the participation of silver species (Ag^+/SiO_2 or silver NPs)[49] to the long-lasting catalytic process as the silver nanoparticles were observed in the TEM image of the heterogeneous mixture after four catalytic cycles.

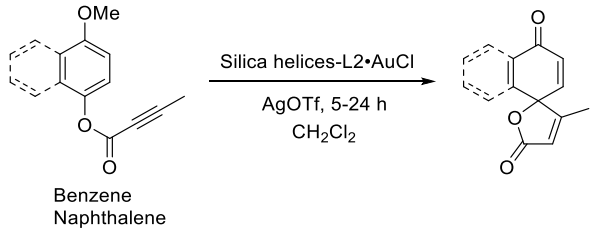

Figure VI. Dearomative ipso-cyclization of aryl alkynoate esters by silica helices bound gold complexes.

4 DPA-based thioethers or sulfoxides: Coordination complexes and chiroptical property

Diphenylanthracene (DPA) has been applied in the field of organic light-emitting diodes[50] and fluorescence probes[51] with blue emission.[52, 53] We were interested in two under-exploited properties of DPA: a) their reversible reactivity with singlet oxygen that potentially offers a switchable functionality, and b) their hindered ortho-substituted derivatives that provide *syn* and *anti* atropisomers for different types of metal coordination. At first, the reversible [4+2] Diels-Alder cycloaddition reaction of substituted anthracene and singlet oxygen[54] leading to 9,10-endoperoxides and subsequent thermal cycloreversion are well-known since 1980s.[55-57] This chemical transformation can be used to modify *in situ* the optical properties of DPA. Secondly, the ortho-substituted DPAs can offer *syn* and *anti* atropisomers. When the ortho substituent on the aryl ring is not hydrogen, the rotation around the C-C single bond is sterically hindered (**Figure VII**) as the experimental value for rotational barrier increase from 75 kJ/mol for *ortho*-H and 123 kJ/mol for *ortho*-CH_3[58-60] which are thermally stable even above 300 °C.[61] We were interested in the use of syn and anti atropisomers as platforms for metal (gold and silver) coordination.

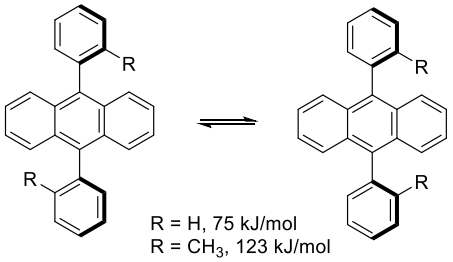

Figure VII. Rotational barrier for ortho-substituted DPA.

4.1 Coordination complexes between DPA-based thioether ligands and silver salts

Thioether silver complexes have been widely developed since 1990s, including macrocyclic thioether ligands.[62-66] Unlike the coordination mode of gold, the chelating mode of silver complexes is much more versatile as linear,[67, 68] planar[69] and octahedral,[70] even coordination polymer[71-73] and cyclic oligomer[74] structures can be isolated. The coordination topology can be controlled by ligand design. Besides, only a few elaborated silver complexes were reported for homogeneous catalysis since simple inorganic silver salts can be highly efficient. In our case, DPA was employed as a directional platform that offers two identical thioether ligands in *syn* and *anti* configurations to better control the formation and the self-assembly of silver complexes.

Four thioether ligands were prepared to form silver(I) complexes whose geometry can be tuned by the nature of anion or by extending the length of coordination chain (part of silver complexes were listed in **Figure VIII**). Their activity in homogeneous catalysis was proven in two tandem addition/cycloisomerization of alkynes using 0.5-1 mol% of catalytic loading.

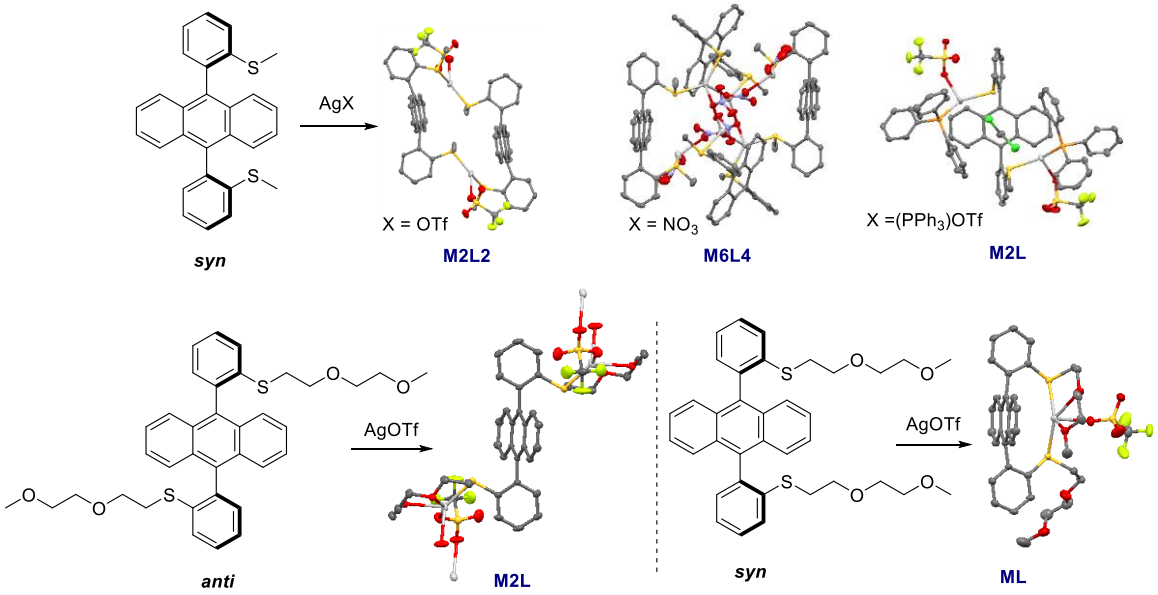

Figure VIII. X-ray structures for part of DPA-based thioether silver complexes

Preliminary results concerning DPA-based bidentate P,P ligand and hemilabile P,P(O) or P,P(S) ligands were also obtained, aiming to access to the corresponding gold complexes. (**Figure IX**) such as bidentate P,P gold π complexes or hemilabile gold complexes for the oxidative addition of aryl iodide.[75, 76]

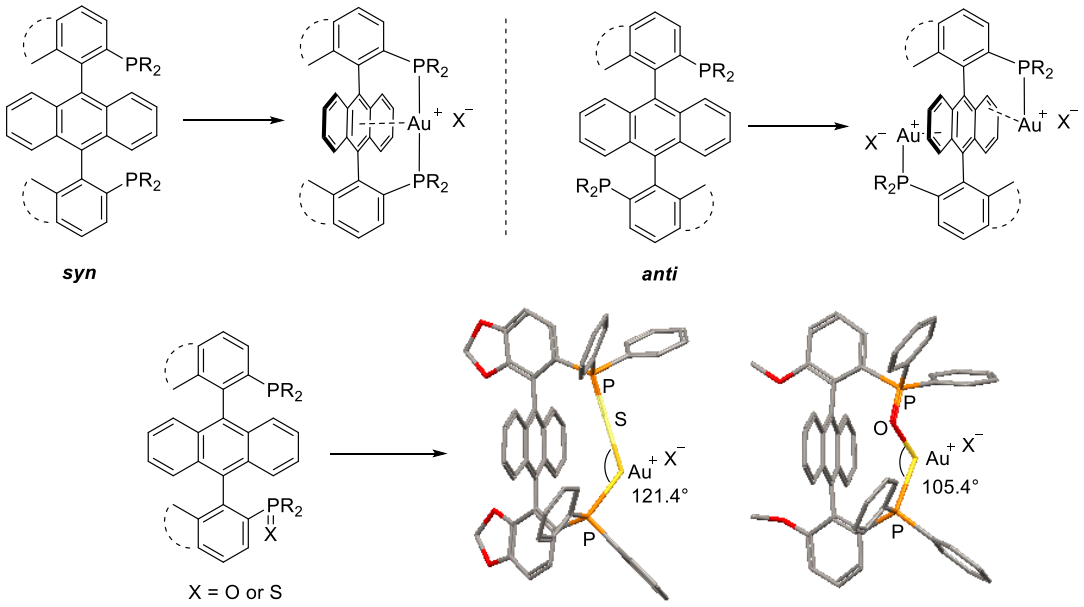

Figure IX. Bidentate P,P or hemilabile P,P(O) or P,P(S) for gold complexes.

4.2 Switchable chiroptical property of DPA-based chiral sulfoxides

Chiroptical properties have been achieved in chiral supramolecular systems,[77, 78] lanthanide complexes[79, 80] and polymer systems[81, 82] Small organic molecules displaying CPL present advantages such as facile synthesis and easy modification. So far, small organic molecules for CPL have been documented in many systems, such as chiral binaphthyl skeletons,[83-85] chiral spiro scaffold,[86, 87] and chiral helicene systems.[88-90] We were interested in the exploration of a chiroptical switch based on DPA that could be stimulated by either singlet oxygen or by ionic recognition through fluorescence quenching occurring due to a heavy-metal atom effect. By taking advantage of the prochirality of the sulfoxide and the reversibility of the DPA chromophore, sulfoxides based on DPA platform were obtained by oxidation of thioethers (**Figure X**). The chiral sulfoxides were separated via chiral HPLC and the absolute configuration was determined by comparison with calculated and experimental electronic circular dichroism (ECD) spectra. The photo-oxidation of DPA monosulfoxides to its corresponding 9,10-endoperoxides afforded a major **DPAO4** product under conventional conditions (in the presence of methylene blue and oxygen) which might due to the electronic effect or steric effect at the *ortho*-position. As a result, the thermal cycloreversion was only partially recovered. The CPL measurement of chiral sulfoxides is ongoing and an alternative photocycloreversion will be evaluated in the near future.

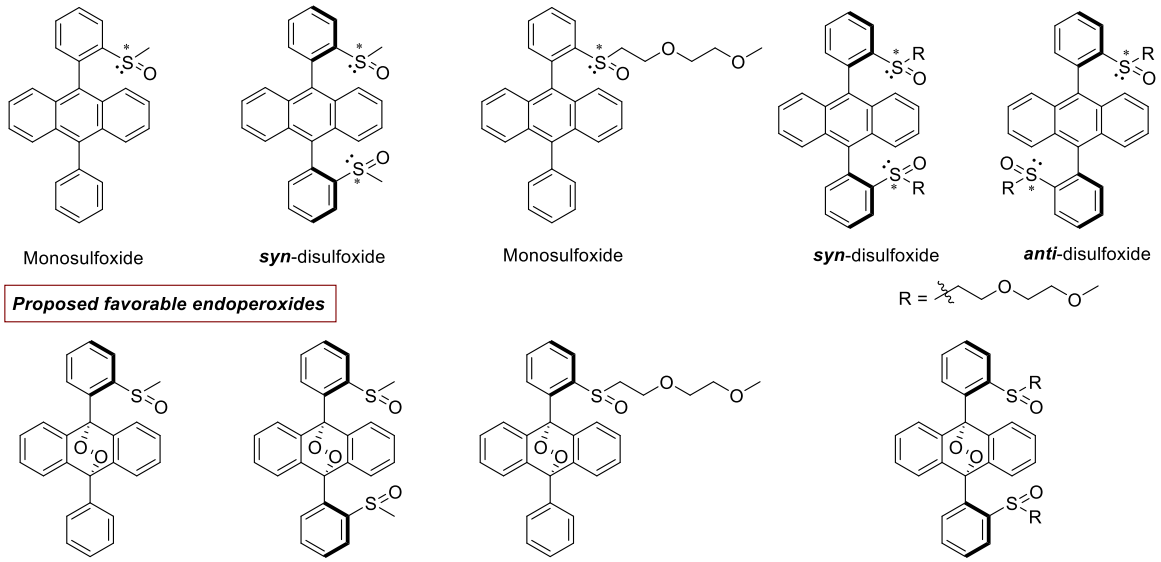

Figure X. DPA-based sulfoxides and their corresponding endoperoxides.

5 Self-assembled switchable imine cage by using singlet oxygen stimulus

Organic molecular cages are well known as a class of molecular containers that possess an inner cavity defined by several macrocycles. Among them, stimuli-responsive molecular cages play an important role due to the capability of modifying their structure or properties in response to light, heat, pH or solvent.[91] In contrast to self-assembled metallocages prepared by metal coordination, multi-step synthesis is needed for the preparation of a reversible organic cage unless employing the dynamic covalent chemistry as illustrated by a recent example of the self-sorted cryptands[92] We were interested in the investigation of self-assembled organic molecular cages that combine ionic binding and reactivity with $^1O_2$ which could lead to switchable functional cages. Herein, a facile preparation of a self-assembled fluorescent [2+3] imine cage with reversible DPA pillars is presented. Singlet oxygen is employed as the stimulus to switch between structures.[9] The reversible photo-oxidation/thermal reduction processes (**Figure XI**) can be followed by UV-vis and emission spectra and the endoperoxide cage was further characterized by ^{1}H NMR and mass spectra. The kinetic study in 3-chorotoluene showed a different rate (0.2522 h^{-1} for oxidation *vs* 0.1683 h^{-1} for reduction). In addition, the fatigue cycles for imine cage were evaluated and DOSY study provides approximate diffusion coefficients for the imine cage and the oxidized cage. The (host: guest) titration experiments showed a high affinity towards metal ions which is also evidenced by ^{1}H NMR.

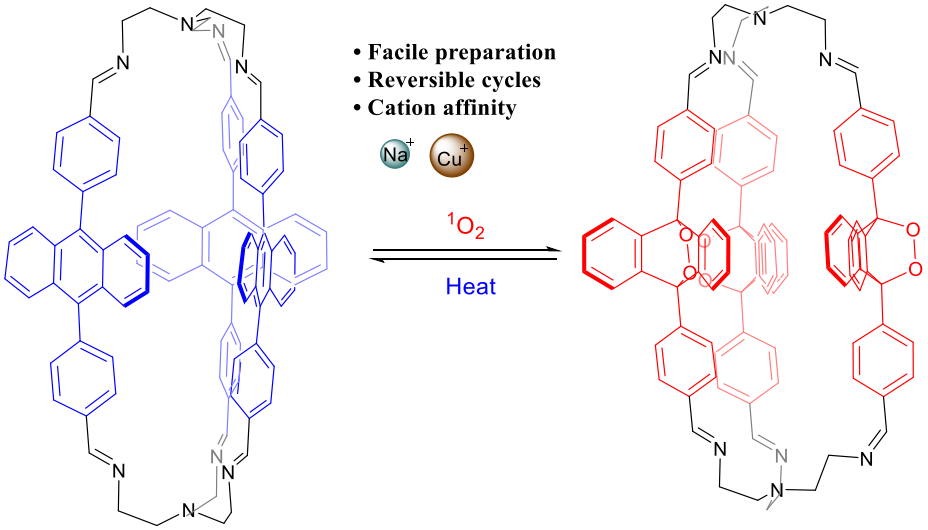

Figure XI. Reversible transformation of imine cage.

Nobody can casually succeed, it comes from thorough self-control & the will.

From library of Harvard university

Chapter 1

1 Introduction

1.1 Introduction to gold catalysis

1.1.1 The early examples of homogeneous gold catalysis

First discovered as shining yellow nuggets, gold element is closely correlated with the evolution of human culture due to its natural beauty and nobleness. However, gold was considered to be catalytically inactive due to its inertness. As a result, the use of gold as a homogeneous catalyst has long been neglected until the first application reported by Ito and Hayashi in 1986, who described a catalytic asymmetric aldol reaction with isocyanoacetate employing a chiral ferrocenylphosphine gold(I) complex (Scheme 1-1a).[93] The first report of the transformation of alkyne compounds into ketones or acetals was realized in 1991 by using $NaAuCl_4$ in protic solvents (methanol and water).[94] The field of homogeneous gold catalysis really began to blossom in 1998 when Teles unveiled its potential in the activation of alkynes in 1998 (Scheme 1-1b).[95]

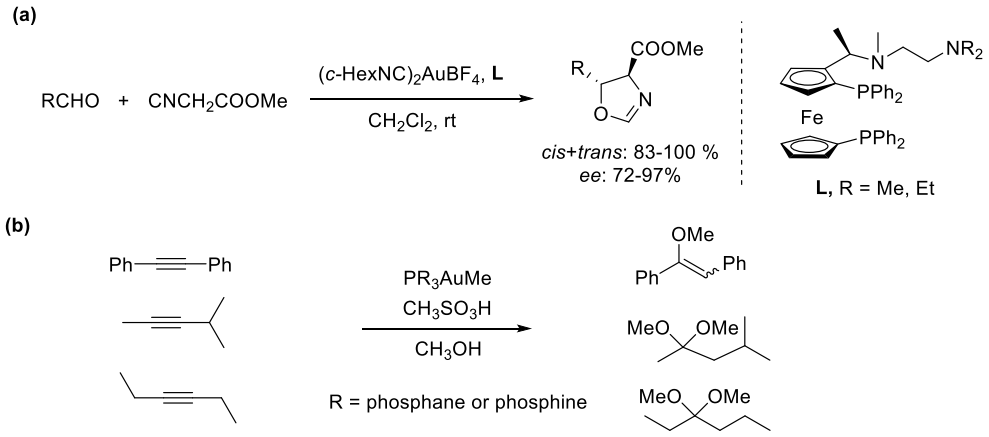

Scheme 1-1. Early reports for homogeneous gold catalysis. (a) Gold catalyzed asymmetric aldol reaction with isocyanoacetate; (b) Gold catalyzed alcohol addition to alkynes.[93, 95]

Another classic example was presented by Hashmi's group[96] where a gold(III) catalyzed transformation of propargyl ketones to furan compounds which can be further transformed to a phenol product by using $AuCl_3$ in acetonitrile.

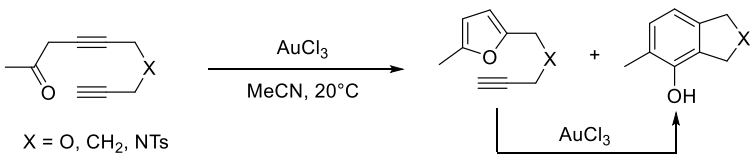

Scheme 1-2. Gold catalyzed arene synthesis from propargyl ketone.[96]

In the early stages of gold catalysis, gold(I) and gold(III) were mainly used as their chloride salts until the ligand effect was recognized. Since then, homogeneous gold catalysis has experienced an explosive

development. The catalysis of organic reactions by gold compounds has been recently shown to be a powerful tool in synthesis which is now well-recognized as a soft carbophilic lewis acid which efficiently activate the C-C π bonds toward nucleophilic attack under mild conditions.

1.1.2 Relativistic effects in gold

Relativistic effects in chemistry are due to the high speeds of electrons when they move near a heavy nucleus. Atoms with a high nuclear charge (Z) often result in relativistic effects. Gold (Z = 79) exhibits a large relativistic effect, as the orbital energies of non-relativistic (NR) 5d and relativistic (R) 6s on gold are quite similar (Figure 1-1).[97] Thus, the electron configuration of gold is $[Xe]4f^{14}5d^{10}6s^{1}$ but it could also be written as $[Xe]4f^{14}(5d6s)^{11}$. The relativistic effect of gold has also been discussed mathematically based on the relativistic quantum theory.[98, 99] From another point of view, the chemical properties of gold are strongly influenced by relativistic effects as illustrated by the electronegativity of Au (2.54 versus Pt (2.28) and Hg (2.0)) which is resulting from the relativistic contraction of the valence orbitals 6s and 6p. Furthermore, gold shows a maximum of relativistic effects by measuring the ratio of relativistic (R) and non-relativistic (NR) 6*s* shell radii in the atomic ground states (Figure 1-2).[100, 101]

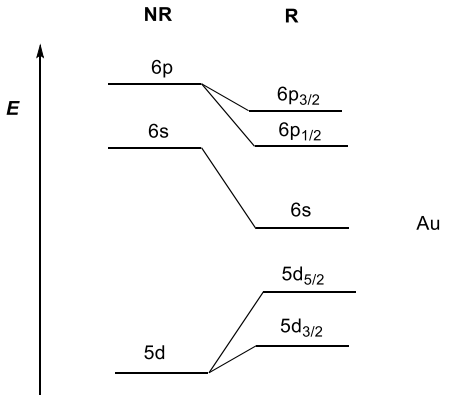

Figure 1-1. Schematic view of the molecular orbital energies for hypothetic gold compounds in non-relativistic (NR) orbitals and relativistic (R) orbitals.[97]

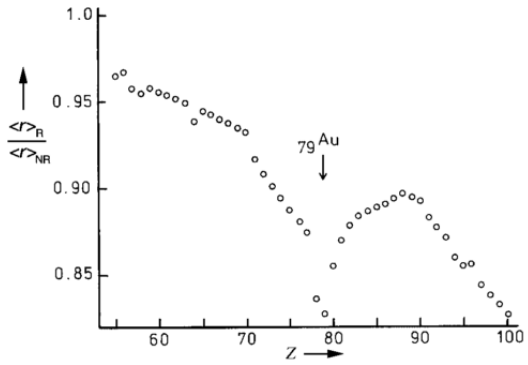

Figure 1-2. The ratio of relativistic (R) and non-relativistic (NR) 6s-shell radii in the atomic ground states of the elements 55–100.[100] Notably, Au, Pt, Hg are the metals markedly affected by relativistic effect.

Gold complexes exhibits a strong lewis acidity for the activation of alkynes, coupled with the potential to stabilize the cationic gold intermediates. In order to rationalize the observed reactivity of gold, Toste and Gorin evaluated the relativistic effects in homogeneous gold catalysis experimentally and theoretically.[102] The contracted 6s orbital and expanded 5d orbitals account for the strong lewis acidity of cationic gold catalyst based on the calculations. Of note, the 5d electrons of gold atom remain too low in energy, suggesting their delocalization into lower-energy, vacant non-bonding orbitals in the π-bonding gold complexes.

1.2 Gold complexes

The commonly observed oxidation states of gold are (+I) and (+III). With the remarkable development of novel ligands, the numerous gold complexes containing gold(I) and gold(III) that are accessible and show exciting outcomes as homogeneous gold catalysts was involved. Generally, gold(I) predominantly adopts a linear, bicoordinate geometry and gold(III) enables a prevalent square planar geometry. In this part, the selected representative examples of gold(I) complexes are outlined with phosphine and carbene ligands. Concerning enantioselective gold catalysis, the chiral ligands featured on various skeletons for asymmetric catalysis are reviewed including phosphines, carbenes and phosphoramidites. Moreover, several exceptionally stable cationic gold(I) complexes, novel Z-type gold(I) complexes and tricoordinated gold(I) complexes are also displayed. As is often the case, gold(III) complexes are considered as less stable than gold(I) due to their higher electrophility and they are sensitive to light and moisture. However, stable gold(III) complexes are also accessible via ligand design or by oxidation of gold(I), as a result, selected gold(III) complexes are listed. Notably, the representative examples of ligand enabled gold(III) complexes via oxidative addition were also displayed. Finally, the difference between gold(I) and gold(III) catalysis was illustrated with a few examples to demonstrate the catalytic selectivity or reactivity.

1.2.1 Gold(I) complexes

In 1995, Green described a method for classifying covalent bonds in transition metals.[103] According to the definition, the three types of ligands (L, X, and Z type) are defined based on the bonding mode of the ligating atom belonging to the ligand (Figure 1-3). The L ligands, for instance phosphine, carbon monoxide, and olefins, provide two-electrons for occupying an empty orbital on the metal center. The X ligands (hydride, alkyl and halogen) provide one electron to the metal to form covalent bonds. Lewis-acidic ligands such as borane, aluminum, and silicon, are classified as Z-type ligands. Gold(I) is the common and stable oxidation state of gold which possesses an electron configuration of $[Xe]4f^{14}5d^{10}$ with an empty 6s orbital. Normally, gold(I) readily coordinates with mainfold donating ligands to form gold(I) complexes such as thioethers,[104] *N*-heterocyclic carbenes,[105, 106] and phosphines[107] which could be commercially available.

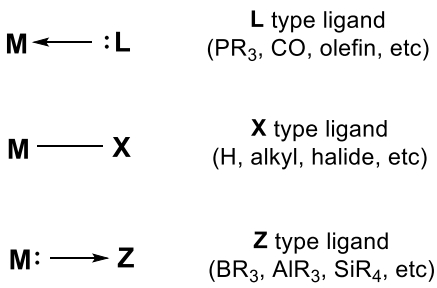

Figure 1-3. Classification of the three bonding modes in metal complexes.[103]

During the past decade, the development of homogeneous gold chemistry significantly benefited from the extensive discovery of novel ligands. The conventional representative ligands for gold(I) complexes were showed in figure 1-4.[105, 106, 108] In some cases, the reactivity and selectivity can be tuned through modification of electronic effect and steric effects on the ligands.

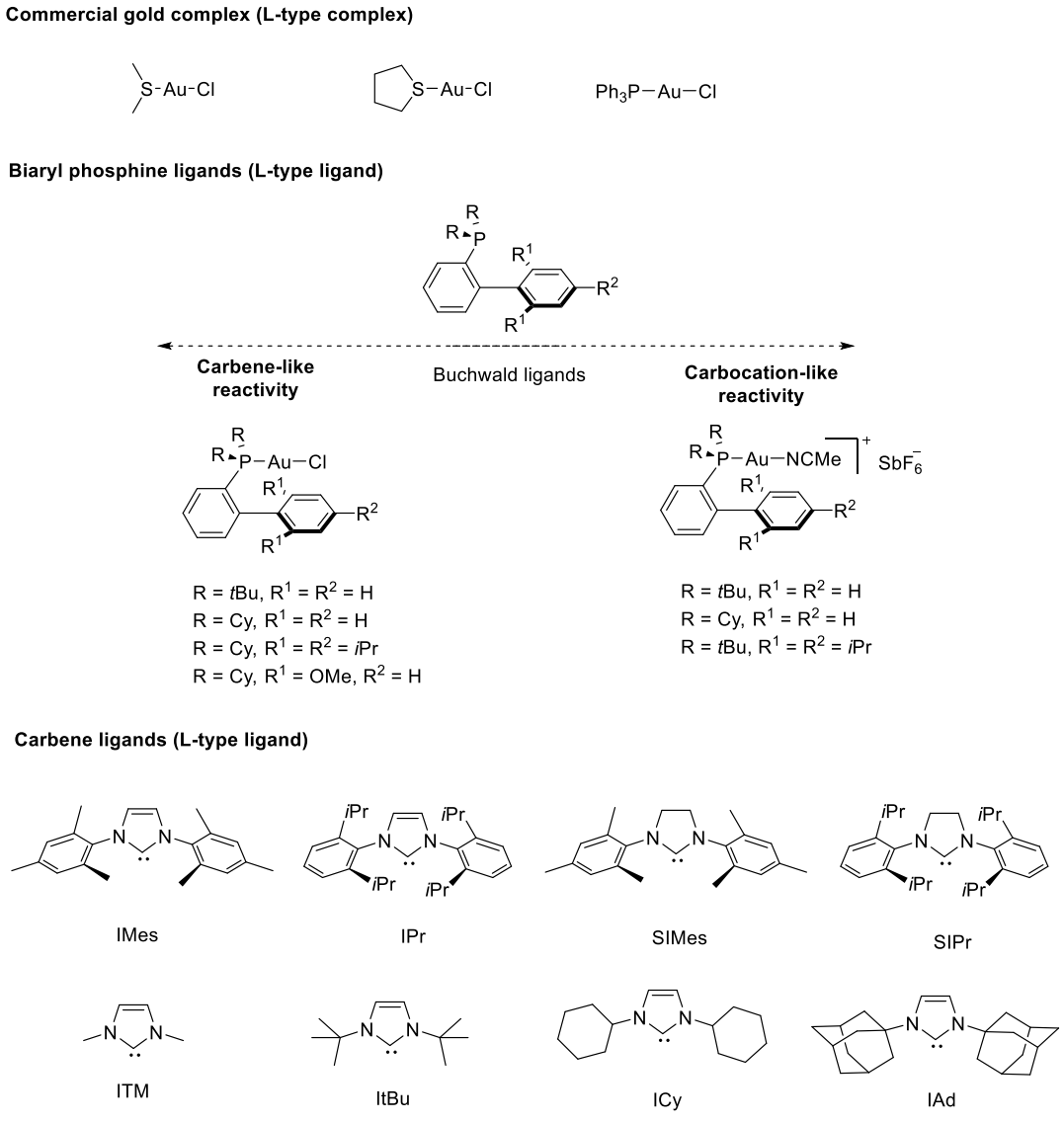

Figure 1-4. Representative widely-exploited gold(I) complexes and ligands.[105, 106, 108]

Enantioselective gold catalysis has also been broadly documented by using various chiral ligands, such as chiral phosphines, carbenes and phosphoramidities. Selected chiral ligands are listed in figure 1-5.[107, 109-114] All the other chiral ligands were elaborated to achieve a rigid system where the linear gold(I) is forced to adopt a one-direction coordination except for the axially chiral phosphines. Impressively, the enantioselectivity can be controlled by a distal chiral auxiliary or a chiral anion.[109, 110]

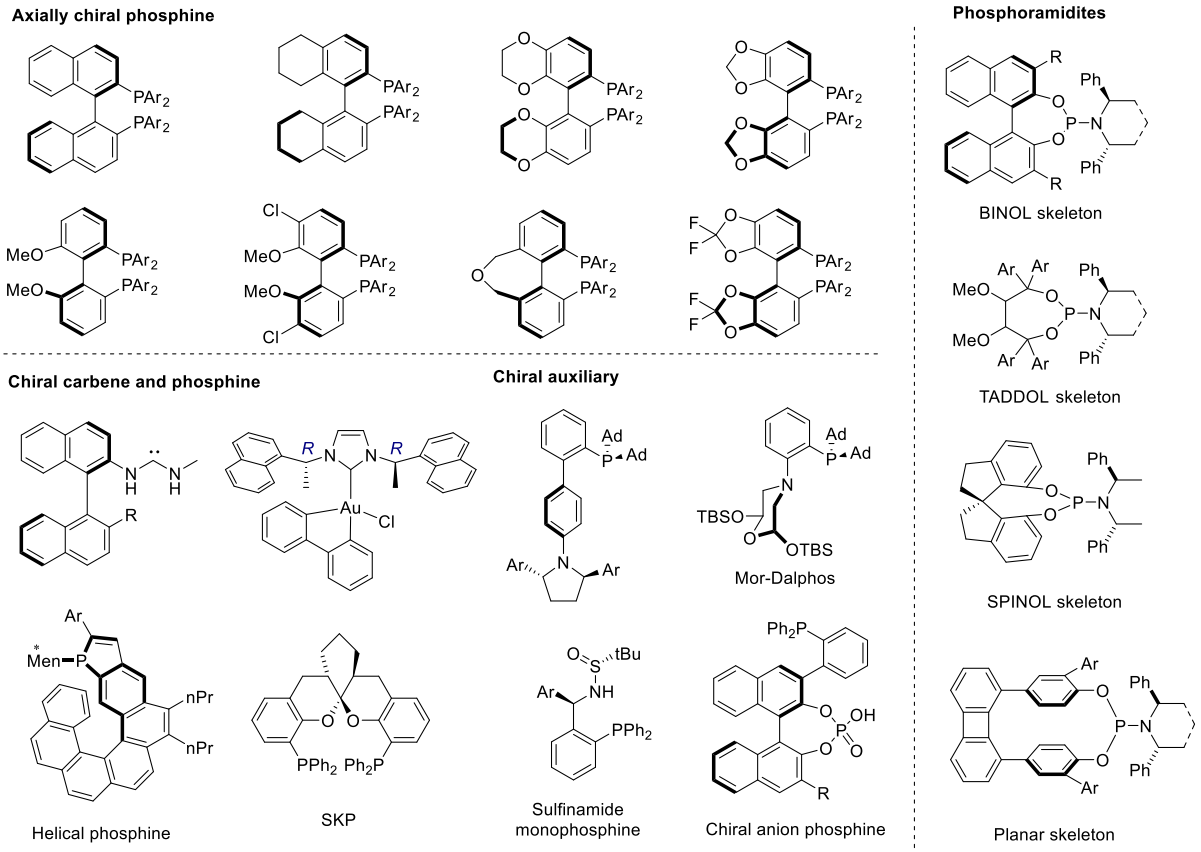

Figure 1-5. Selected chiral ligands that form gold(I) complexes involved in asymmetric catalysis.[107, 110-116]

Apart from the various phosphines and carbenes, two types of gold(I) complexes are worth to note as they exhibit special reactivity: firstly the stable cationic gold complexes and secondly the Z-type gold complexes and tricoordinated gold complexes (Figure 1-6).

Cationic gold complexes are effective in the electrophilic activation. However, their thermal stability is usually very low and they undergo significant degradation during reactions. Shi *et al*. developed a class of triazole-based stable cationic gold complexes which are active in intermolecular internal alkyne hydroamination and reactions with unprotected aliphatic amines.[117] After a while, Echavarren's group described a super stable cationic gold(I) precursor[38] which is readily transformed to a series of cationic gold complexes by adding a phosphine ligand. By employing this method, the gold catalyst precludes the silver effect and its application in heterogeneous gold catalysis showed good recyclability due to the stability of the catalyst. Another important class of Z-type gold complexes[118-124] were initially reported by Bourissou, later

investigations revealed exceptional reactivity in enyne cyclization while cationic $Au(PPh_3)_2$ was discovered to be non-reactive (Figure 1-6). In 2014, Bourissou and Amgoune developed a carborane-based tricoordinated gold(I) complex which first achieved the oxidative addition to form stable organogold(III) (Figure 1-6).[76] The success of this ligand preorganization might spur new discoveries in gold catalysis and future applications.

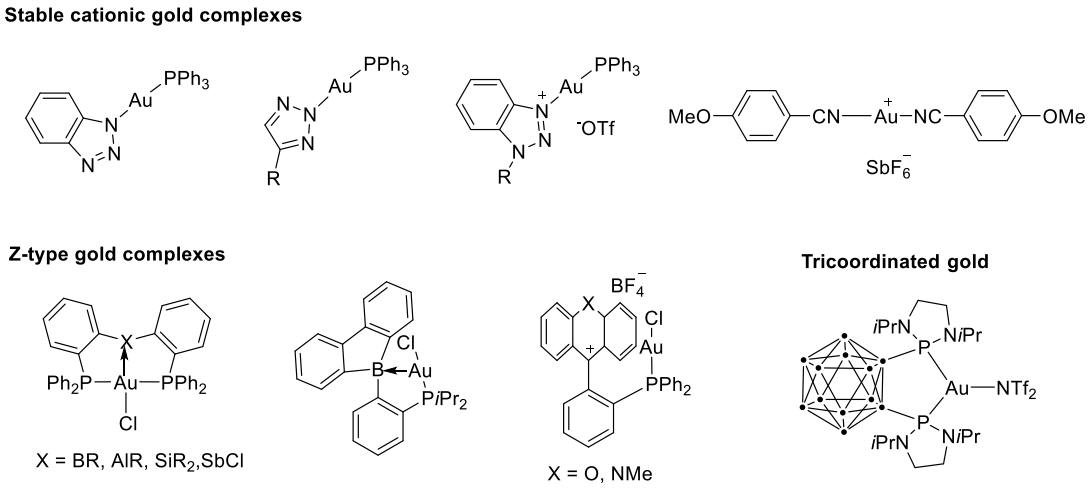

Figure 1-6. Novel gold(I) complexes with an exceptional stability (Top) or special coordination mode (Bottom).[38, 76, 117-124]

1.2.2 Gold(III) complexes

Previously, gold(III) halides (AuX_3) were mostly used to catalyze organic transformations with excellent to modest results. But a significant loss of reactivity was observed with more complicated substrates. The fragile stability under light or moisture makes AuX_3 catalyzed reactions extremely difficult to handle. A class of stable gold(III) complexes with pyridine were first described by Hashmi[24] which were found to be thermally stable[1] and effective catalysts in many alkyne-related transformations.[125-128] In contrast, other readily accessed gold(III) complexes, such as biphenyl gold(III), porphyrine gold(III), were rarely reported be useful catalysts (Figure 1-7).[129]

Recently, numerous organogold(III) complexes have been obtained based on new strategies, such as the oxidative addition of gold(I) complexes using a photoredox method in the presence of aryldiazonium.[130, 131] Here, we highlighted the ligands that enabled a facile oxidative addition of gold(I) complexes to form gold(III) complexes without external oxidants[75, 76, 132, 133] as shown in figure 1-8.

[1] The thermal stability was evaluated in toluene up to 100°C and no decomposition was observed. Details are given in Chapter 2.

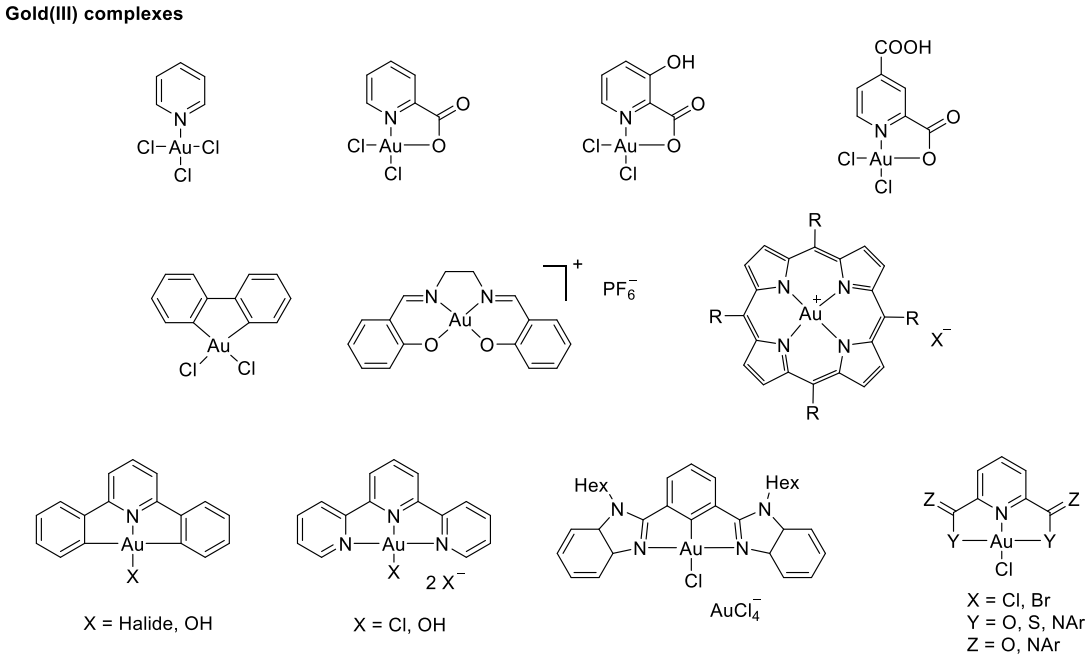

Figure 1-7. Stable gold(III) complexes.[24, 129, 134]

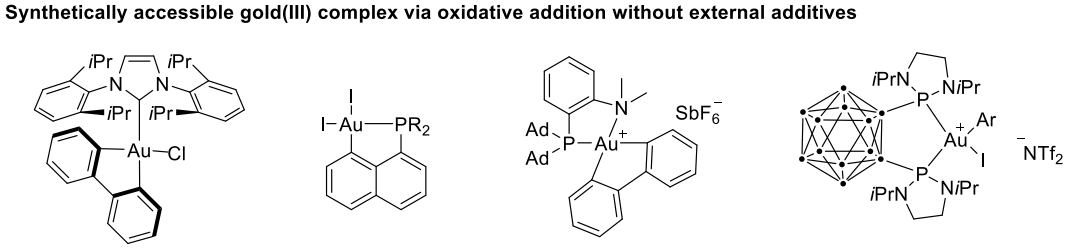

Figure 1-8. Easily accessible gold(III) complexes via oxidative addition.[75, 76, 132, 133, 135]

1.2.3 Gold(I) *vs* Gold(III) catalysis

In general, gold precatalysts are gold complexes coordinated with simple halides such as stable linear dicoordinated gold(I) chloride complexes [LAuCl], where L is phosphine, thioether, phosphite or other donating ligand. In most cases, gold precatalysts require to be activated by chloride abstraction using a scavenger agent such as a silver salt, leading to monocoordinated cationic gold(I) complexes. Usually, cationic gold catalysts exhibit a higher reactivity in activating unsaturated π bonds due to their higher electrophilicity.

Most gold-catalyzed reactions rely on the use of stable gold(I) complexes whereas the catalytic reactivity of gold(III) complexes has been less explored. Gold(III) complexes exhibit a higher electrophilicity than gold(I) complexes. So, switching from gold(I) to a gold(III) catalyst can have a profound effect on the reaction outcome which often leads to divergent reaction pathways. In 2005, Zhang reported that gold(I) and gold(III) catalyzed reactions of indole-based propargylic ester yielding to disparate cyclization products.[136] In the

presence of PPh_3AuCl and $AgSbF_6$, an indolenine-fused cyclobutane was obtained by a formal [2+2] cycloaddition between the indole and an allene formed *in situ*. In contrast, the use of $PicAuCl_2$ delivered a fused product by a [3+2] cycloaddition (Scheme 1-3).

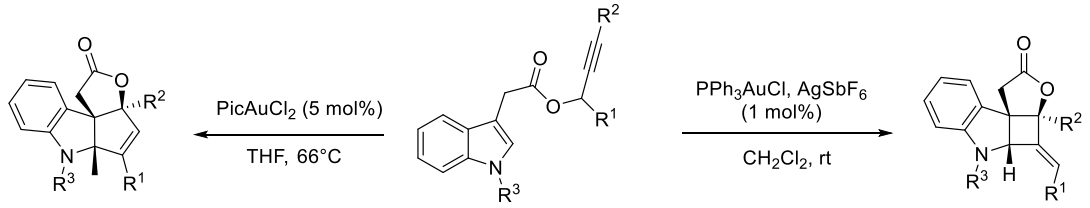

Scheme 1-3. Reactivity of gold(I) versus gold(III) complexes in the cyclisation of indole-based propargylic esters.[136]

A dramatic effect was also found in the cyclization reaction of alkynyl-substituted indole using gold(I) and gold(III) catalysts (Scheme 1-4).[137] A 7-exo-dig cyclization was found for gold(I) catalyst whereas $AuCl_3$ led to a rare 8-endo-dig cyclization product. It was suggested that chloride atom ligation is responsible for this change in the cyclization mode.

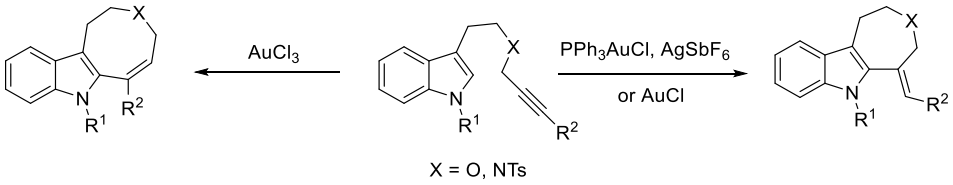

Scheme 1-4. Formation of seven- and eight-membered indole-fused rings using gold(I) *vs*. gold(III) catalysis.[137]

Recently, a selective synthesis of *N*-sulfonyl enaminone isomers from sulfonamides and ynones was achieved by employing an electron-rich gold(I) phosphine complex or a biphenylcarbene gold(III) catalyst in a chemo-controlled manner (Scheme 1-5).[138] A hydroamidation versus a proton-assisted carbonyl activation followed

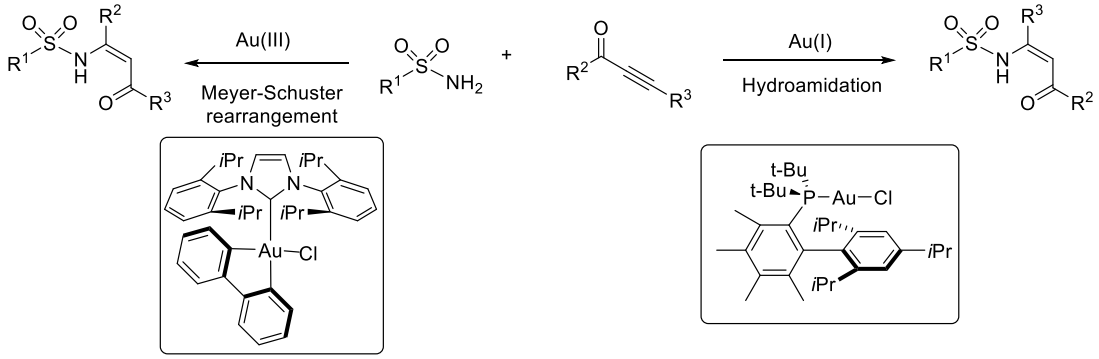

Scheme 1-5. Formation of *N*-sulfonyl enaminones from two pathways using gold(I) and gold(III) catalysis.[138]

by a Meyer−Schuster rearrangement were proposed as mechanisms for the reactions. A wide range of substrates afforded moderate to excellent yields and selectivities.

1.3 Homogeneous gold catalysis

In this decade, gold catalyzed organic transformations have been extensively reviewed from broad perspectives.[107, 108, 139-150] In this section, the various gold intermediates obtained though electrophilic activation of alkynes are discussed and selected classic cyclization reactions of C-C π bonds are listed with a few examples including cycloisomerization of 1,*n*-enynes, oxidative cyclization reactions, domino reactions for construction of molecular complexity. The aim of this part is to roughly show the robust efficacy of gold catalysis in the activation of unsaturated carbon-carbon bonds. Here, the conventional activation of alkynes for diverse nucleophilic additions is not covered for the sake of briefness.

1.3.1 Gold intermediates through electrophilic activation

Over the last decade, the use of gold complexes as carbophilic π-acids has become a powerful tool for building molecular complexity in an atom-economical fashion. The gold readily activates unsaturated C-C bond for nucleophilic additions while generating a vinylgold intermediate (Figure 1-9) which was first experimentally isolated in the Hammond's group in 2008[151, 152] by using an electron deficient allene. Notably, a gold carbene was also proposed as the key intermediates in many gold catalyzed transformations. The common methods for the generation of gold carbene intermediates[153, 154] are summarized in figure 1-10 including the 1,2-acyloxy migration of propargylic carboxylates, cycloisomerization of 1,6-enyne, decomposition of diazo compounds, oxidation of alkyne with pyridine *N*-oxides and acetylenic Schmidt reaction.

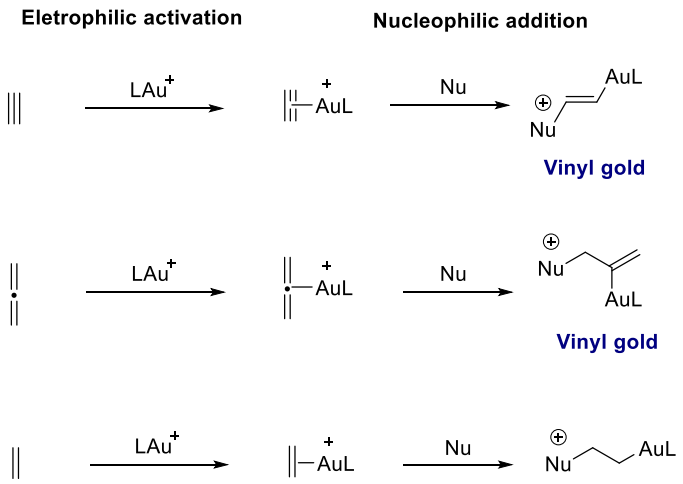

Figure 1-9. Unsaturated C-C bonds transformations in homogeneous gold catalysis: Electrophilic activation and followed by a nucleophilic addition.

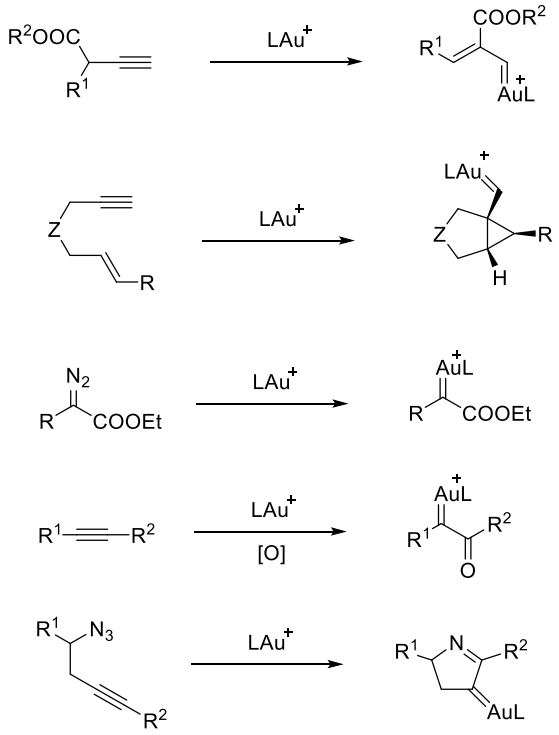

Figure 1-10. General methods for the generation of gold carbenes.[153]

1.3.2 Selected gold catalyzed organic transformations

1.3.2.1 Cycloisomerization of 1,*n*-enynes

The cycloisomerization of 1,*n*-enynes is undoubtedly an important case of gold catalyzed transformations as it reveals a diverse chemistry with two general pathways: a 5-exo-dig cyclization or 6-endo-dig cyclization leading to a vinyl gold intermediate or a 6-endo-dig cyclization that forms gold carbenes (Figure 1-11).[155] The skeletal rearrangement takes place on gold carbene **I** and forms dienes while the deauration of gold carbene **II** leads to a cyclopropane product.

Generally, coordination of transition metals such as Pt or Pd to the alkyne and alkene leads to metal π complexes, which usually evolve by β-hydrogen elimination to give Alder-ene type products. In contrast, gold complexes are unique in their high reactivity as carbophilic π acids. They exclusively bind to the alkyne function and therefore the oxidative cyclometalation to form cyclobutene is not favored. However, the cyclobutene could also be obtained by conrotatory ring-opening of gold carbene **I**. Further DFT calculations also suggested that the *anti* attack of the alkene is more favorable than the *syn* attack. However, the skeleton rearrangement is disfavored when the alkyne or alkene is substituted.

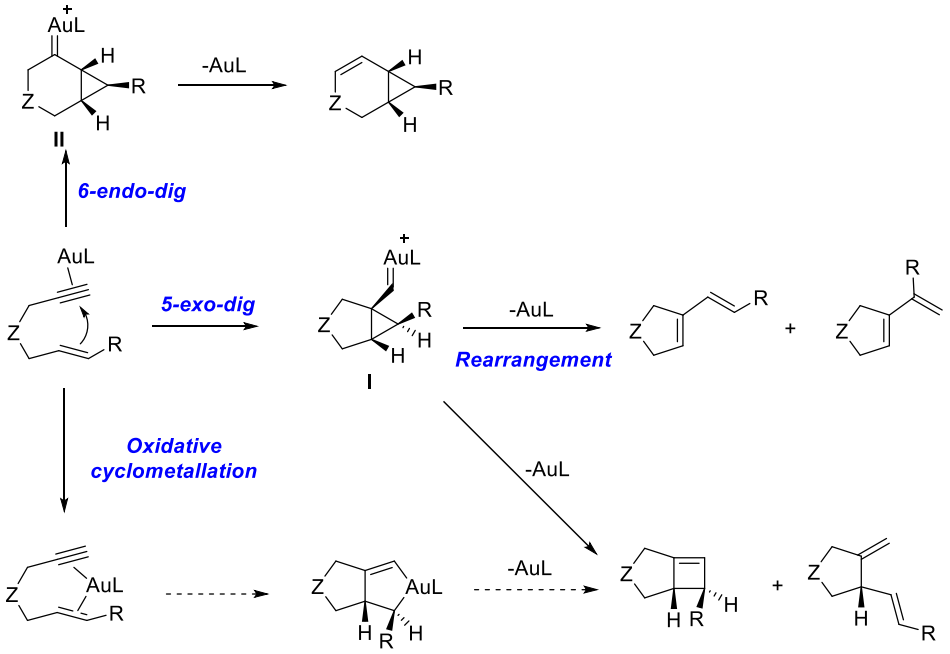

Figure 1-11. Activation mode of enynes by gold.

In 2005, Echavarren's group demonstrated that the cyclization of a cyclohexene- or a cyclooctene- tethered alkyne (1,7-enyne) led to a ring-fused tricyclic scaffold under two different gold(I) catalysts at room temperature (Scheme 1-6).[156] Both reactants proceed via a similar [2+2] cycloaddition to form a cyclobutene. The outcome of the reaction is in accordance to the calculation of the skeleton rearrangement.

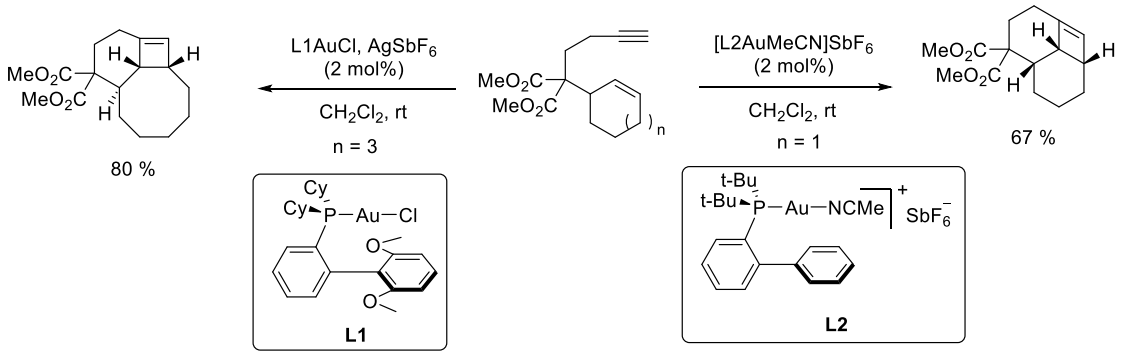

Scheme 1-6. Gold catalyzed cyclization of 1,7-enynes with gold(I) complexes.[156]

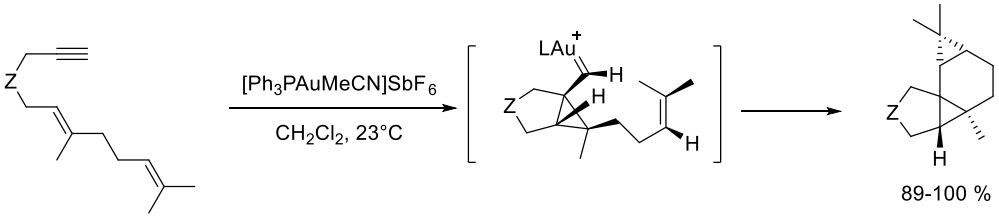

Scheme 1-7. Gold catalyzed intramolecular cyclopropanation of dienynes with a gold(I) complex.[157]

Notably, intramolecular cyclopropanation of dienynes was achieved by a gold(I) catalyst (Scheme 1-7).[157] The reaction was proposed to undergo via a 5-exo-dig cyclization gold carbene intermediate followed by a second activation to exclusively deliver a ring-fused product. The stereoselectivity of the cyclopropanation appears to be the result of the kinetically controlled intermediate, which presents an antiperiplanar arrangement of the cyclopropane and the metal carbene.

Recently, Echavarren's group described an intermolecular enyne cyclization of alkenes with acetylene gas generated *in situ* from calcium carbide and water, which leads to (*Z*,*Z*)-1,4-disubstituted 1,3-butadienes and biscyclopropanes (Scheme 1-8).[158] Of note, the reaction of acetylene with 1,5-dienes stereoselectively gives rise to tricycle[5.1.0.0]octanes. This method was further applied in the total synthesis of waitziacuminone in one step.

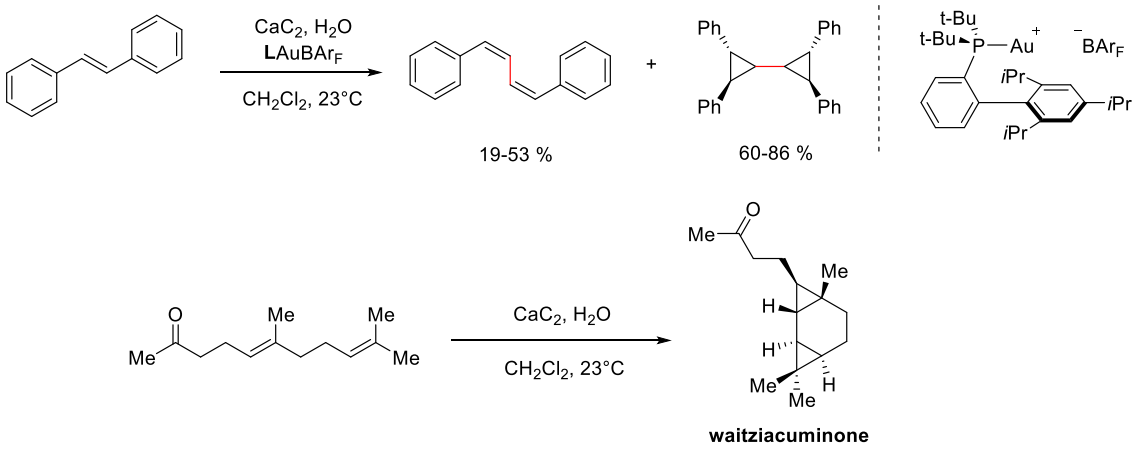

Scheme 1-8. Gold catalyzed intermolecular alkene and alkyne cyclization and the one-step synthesis of waitziacuminone.[158]

1.3.2.2 Oxidative cyclization

The gold catalyzed oxidative cyclization reaction affords a cyclization product in the presence of an intra/intermolecular oxidant. In 2007, Toste and Zhang independently reported the oxidative cyclization of alkynyl sulfoxides to benzothiepinones where the tethered sulfinyl group could serve as an intramolecular nucleophilic oxidant (Scheme 1-9).[159, 160] It is important to note that both gold(I) and gold(III) complexes exhibited an excellent reactivity and lead to the formation of the 7-membered thiepinone ring. However, the mechanistic pathway might involve different intermediates. When employing a gold(I) catalyst, a gold-carbenoid intermediate formed through oxygen atom transfer from the sulfoxide was postulated. For the gold(III) catalyzed process, an α-oxo gold carbene intermediate generated upon an initial gold-catalyzed nucleophilic attack at the alkyne was proposed instead. The latter forms a 5-exo-dig intermediate, and followed by a gold-promoted heterolytic fragmentation of the S–O bond. Finally a Friedel–Crafts type cyclization with the electron-deficient carbene moiety to deliver the product.

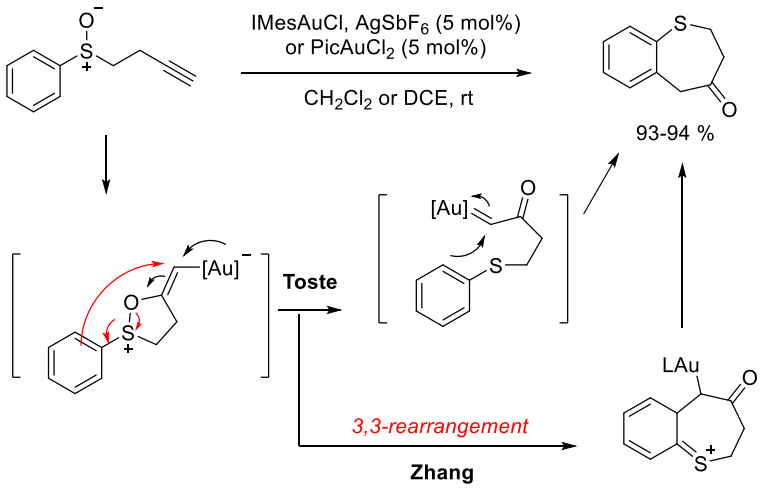

Scheme 1-9. Gold catalyzed intramolecular oxidative cyclization.[159, 160]

Intermolecular oxidative cyclization can also be performed with an external oxidant.[161] In 2013, Liu's group developed a gold(I) catalyzed reaction of 3,5- and 3,6-dien-1-ynes with 8-alkylquinoline *N*-oxides which results in an oxidative cycloaddition product through the activated quinoline framework (Scheme 1-10).[162] The mechanism of this transformation probably involves an α-oxo pyridinium ylide intermediate, which undergoes a concerted [3+2] cycloaddition with the tethered alkene to form the ring-fused product.

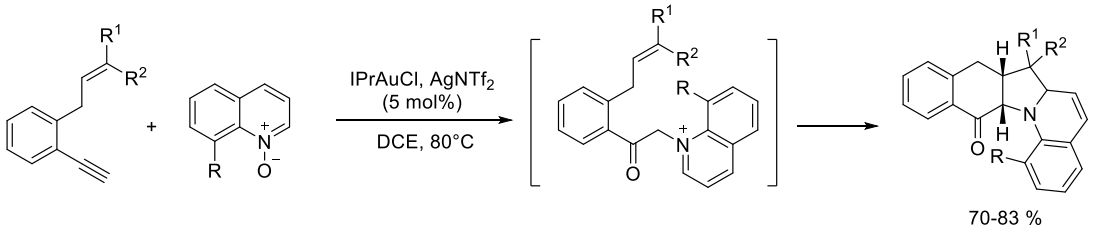

Scheme 1-10. Gold catalyzed intermolecular oxidative cyclization.[162]

In 2015, Zhang's group described an asymmetric intramolecular cyclopropanation of dienynes in the presence of 8-methylquinoline *N*-oxide (Scheme 1-11).[111] This enantioselective oxidative gold catalysis relied on a chiral P,N bidentate ligand (Mor-Dalphos) which enables the *in situ* formation of α-oxo gold carbene intermediates. This class of P,N ligands were further proven to be effective for the facile oxidative addition of aryl iodide on gold(I) atoms.[75]

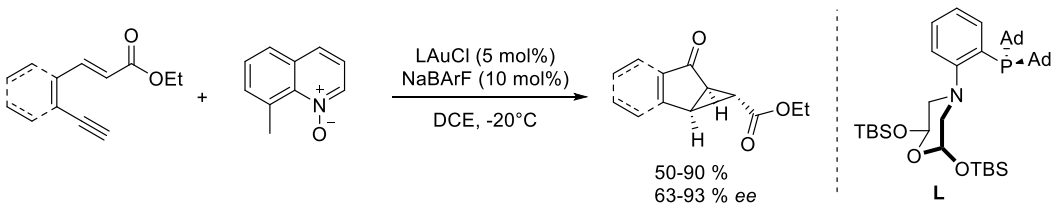

Scheme 1-11. Enantioelective gold catalyzed intermolecular oxidative cyclization.[111]

1.3.2.3 Cascade reactions for molecular complexity

The gold catalyzed cascade reaction is an efficient approach to construct molecular complexity in one step.[163] In 2012, an Ugi four-component reaction of propargylamines with 3-formylindoles, acids, and isonitriles was coupled with a gold(I) catalyst to prepare substituted tetracyclic spiroindolines in moderate to excellent yields (Scheme 1-12).[164] The remarkable efficiency showed the huge potential of one-pot gold catalysis in natural products synthesis.

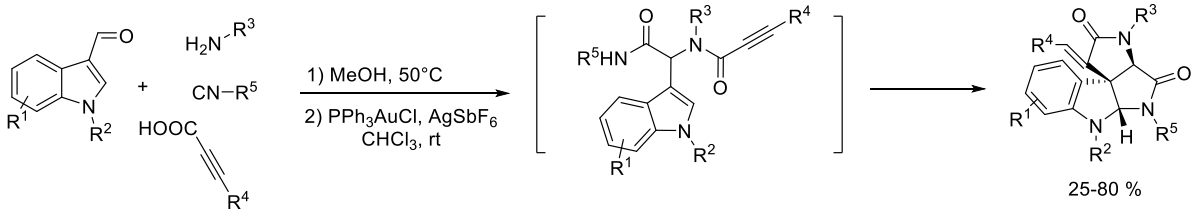

Scheme 1-12. Synthesis of substituted spiroindolines from gold catalysis and Ugi four-component adducts.[164]

In 2014, Wang's group highlighted the use of gold catalysis to access to polycyclic indole alkaloids.[165] In the case of indoles bearing a nucleophilic functional group and an alkynyl chain, the reaction gives tetracyclic indolines in one single step with high yields (Scheme 1-13).

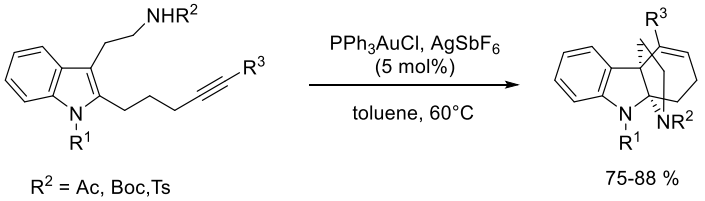

Scheme 1-13. Synthesis of tetracyclic indolines by gold catalyzed hydroarylation and intramolecular nucleophilic addition.[165]

This strategy is also applicable to furan-yne precursors, Hashmi reported the cyclization of furan-ynes via a dearomative pathway, resulting in tetracycles containing two heteroatoms and two new stereocenters under mild conditions (Scheme 1-14).[166] The first step of the reaction is initiated by a 6-endo-dig cyclization to form a gold carbene, which subsequently undergo a Friedel-Crafts annulation leading to the tetracycles.

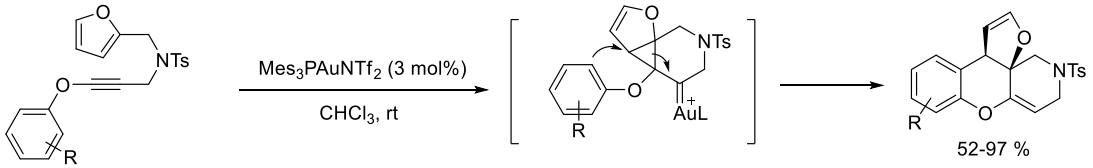

Scheme 1-14. Furan-yne cyclization and Friedel-Crafts annulation.[166]

1.4 Silver in gold catalysis

Gold(I) chloride has been extensively used as homogeneous catalyst in the presence of silver salts (chloride scavenger) to form a cationic gold complex which is generally believed as the active catalytic species. However, a rising problem is that silver has also been effective in many organic transformations due to its excellent alkynophilicity.[167] In 2009, Gagné reported that vinylgold species can be trapped by another equivalent of gold or silver as exemplified with phenyl tethered allenes (Scheme 1-15).[168] A few years later, Shi's group revealed that the gold complex PPh_3AuOTf prepared from PPh_3AuCl/AgOTf, with or without AgCl (withdrawn by filtration) led to different chemical shifts on ^{31}P NMR,[169] in accordance with the results of Gagné. In 2015, Zhdanko and Maier conducted an extensive *in situ* NMR investigation and further confirmed the formation of a dinuclear metal complex.[170]

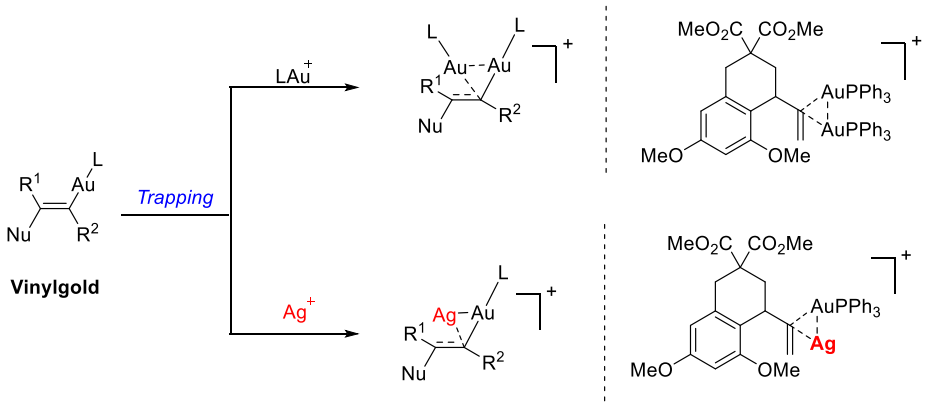

Scheme 1-15. Trap vinylgold intermediate with gold or silver and form dinuclear metal complexes.[168, 171]

Subsequently, Echavarren demonstrated the formation of a chloride-bridged dinuclear gold complex in the presence of one equivalent or of an excess silver salt (Scheme 1-16).[172] This finding further proved that silver is not totally innocent in gold catalysis even if silver itself might not catalyze all gold-catalyzed transformation.

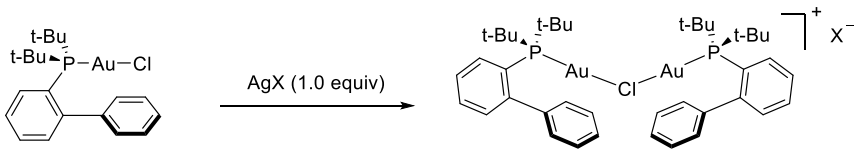

Scheme 1-16. Access to chloride-bridged dinuclear gold complex in the presence of silver salts.[172]

A profound silver effect was observed in the gold catalyzed enantioselective cyclization of allenes (Scheme 1-17). The *in situ* generated cationic gold(I) complex lead to the best outcome of 72 % *ee*, while a significant decrease (21% *ee*) was observed when using an isolated pure gold complex by removing the AgCl generated *in situ*. The addition of additional AgOTf did not improve the stereoselectivity. Of note, an excess of AgCl

afforded a better outcome of 34 % ee.[173] This result in line with the discovery that the innocent AgCl might coordinate with the gold intermediate or lead to a new gold species.[168, 172]

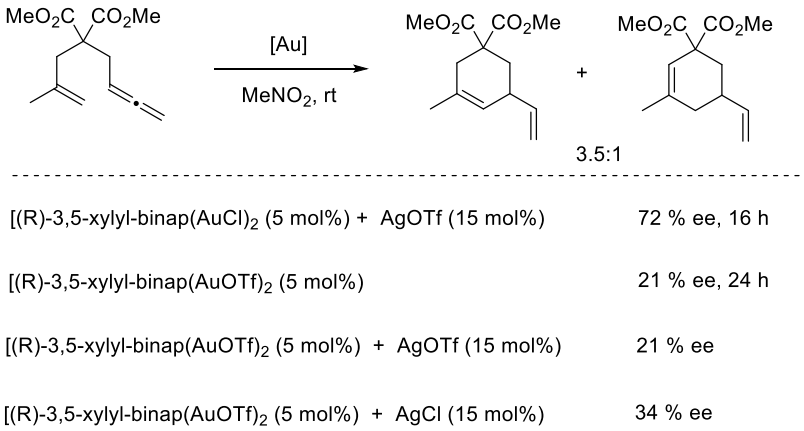

Scheme 1-17. Silver effect on gold catalyzed enantioselective cyclization of allene.[173]

Recently, Bebbington and Lee discussed the regioselectivity controlled by silver in the gold catalyzed region-divergent hydroamination of terminal alkynyl sulfamides (Scheme 1-18).[174] In the presence of silver(I), a 6-endo-dig cyclization was observed while in its absence, the major 5-exo-dig cyclization product was obtained. The different possible π-silver acetylides and σ-π-digold intermediate might account for this dramatic change in regioselectivity.

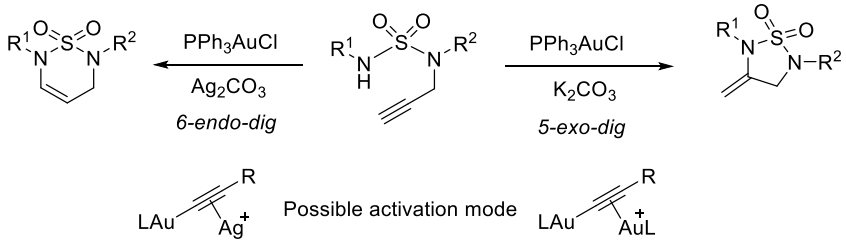

Scheme 1-18. Regioselective cyclization of alkynyl sulfamides with or without silver salts.[174]

Most investigations in gold catalysis focus on the catalysts and neglect the crucial control experiments. Based on the aforementioned results, silver can either form a dinuclear complex with gold, or lead to the less active chloride-bridged dinuclear gold. A higher standard is thereby required on future condition optimizations of gold catalyzed reactions. For example, three basic control experiments by utilizing *in situ* generated cationic gold complex, the pre-isolated gold complex, and the silver itself as catalyst are at least needed.

1.5 Catalytic redox gold catalysis

Gold has been considered to be an inert metal in catalysis until the seminal work of Teles and Hashmi unveiled the potential of homogeneous gold catalysis which has experienced strong development over the

last few decades. Acting as a Lewis acid, numerous gold complexes are now considered to be robust and versatile catalysts that efficiently activate carbon-carbon π bonds toward nucleophilic attack. However, the exceptionally high redox potential is considered to be an intrinsic limitation for gold as a transition metal to undergo Au(I)/Au(III) cycles. To address this problem, the field of catalytic redox gold catalysis is pursuing several strategies in the last decade. Herein, redox gold catalysis was reviewed along four major strategies: Au(I)/Au(III) catalysis with an oxidant, dual photoredox and gold catalysis including photosensitizer-free redox gold catalyst, light-triggered gold catalysis with dinuclear complexes and ligand enabled Au(I)/Au(III) catalysis. Each approach is presented with a general mechanism and followed with organic transformation scope.

1.5.1 Au(I)/Au(III) catalysis with oxidant

The application of Au(I)/Au(III) catalysis was extremely limited due to the high redox potential which can be achieved by using an external stoichiometric oxidant. For a long period, the development of gold catalyzed coupling reaction was limited to use stoichiometric amount of gold catalyst.[175] The first catalytic Au(I)/Au(III) catalysis was illustrated by Tse and coworkers,[176] with the direct oxidative homocoupling of non-activated arene in the presence of $HAuCl_4$ and $PhI(OAc)_2$ as an oxidant. However, low selectivity was observed as the homocoupling step was a competitive process with ligand exchange. As a result, the cross coupling reaction often led to a mixture of the cross-coupled biaryl product and homodimers. Notably, the oxidative coupling reaction can also be achieved in moderate yield by using gold(I) complexes and Selectfluor™.[177, 178] In this part, selected examples of cross coupling reactions using the Au(I)/Au(III) redox catalysis in the presence of $PhI(OAc)_2$ are depicted.

1.5.1.1 General mechanism for gold catalyzed cross coupling reactions

From the recent development of gold catalyzed cross coupling reactions, two major pathways were involved. The first one refers to the cross coupling of functionalized aryls and non-activated arenes: the first step involves the transmetalation of functionalized aryl compound resulting in a gold(I) species **A** which can be further oxidized to a gold(III) intermediate **B** in the presence of hypervalent iodine. This electrophilic gold(III) undergoes a selective C-H activation of an arene leading to a diarylgold(III) **C** which proceeds via a reductive elimination to generate the coupling product (Figure 1-12a). The second coupling type involves two arenes via a double selective C-H activation: the arene substituted by an electron withdrawing group can be activated by the gold(I) complex to form a gold-arene species **D** which is oxidized to gold(III) intermediate **E**. The highly electrophilic gold(III) species was expected to undergo a selective C-H activation of an electron-rich arene and lead to diarylgold(III) **F** which generates the coupling product after a reductive elimination (Figure 1-12b).

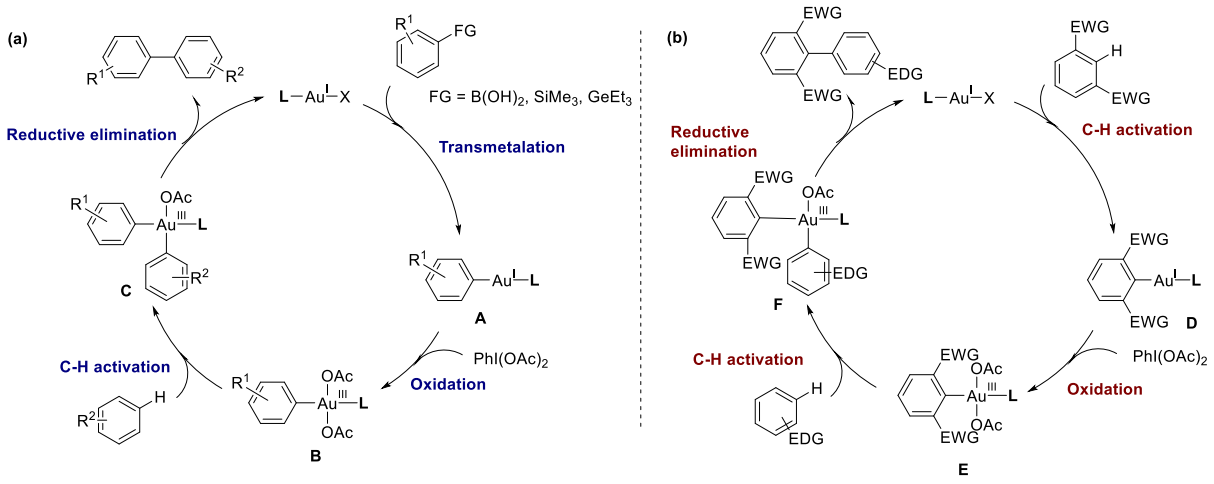

Figure 1-12. General mechanism for gold-catalyzed cross coupling reactions in the presence of $PhI(OAc)_2$.

1.5.1.2 Gold catalyzed oxidative cross coupling

In 2010, Nevado's group reported the successful synthesis of arylacetylenes from electron-rich arenes and electron-deficient alkynes by using a catalytic amount of gold(I) catalyst and $PhI(OAc)_2$ as an oxidant (Scheme 1-19).[179] The possible intermediate might be a arylynegold(III) which then undergoes reductive elimination.

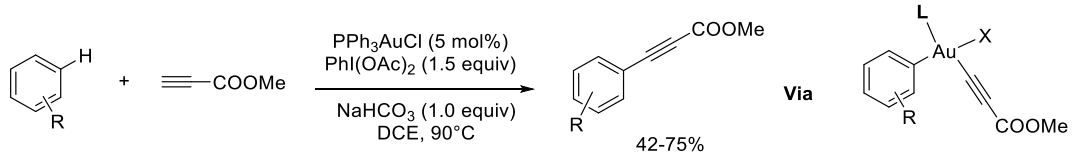

Scheme 1-19. Gold-catalyzed ethynylation of arenes.[179]

Two years later, the cross coupling of arylsilanes and aryl halides was achieved by using a low catalytic loading of gold(I) complex (1 mol%) in the presence of hypervalent iodine and camphorsulfonic acid at room temperature. This process was superior to the conventional palladium catalysis with mild conditions and a tolerance to halide groups (Scheme 1-20a).[180] Notably, the coupling product can be further transformed to the nonsteroidal anti-inflammatory diflunisal. The mechanism was discussed by the same group based on the kinetic isotope effects and the stoichiometric experiments. Noteworthy, the use of camphorsulfonic acid was proved to enhance the electrophilic character of gold(III) and facilitate the C-H auration to form a diarylgold(III) and its subsequent reductive elimination.[181] Recently, electron-deficient arylboronates were also employed for the arenes coupling in good yields (Scheme 1-20b). The gold(III) intermediate was isolated and characterized after the oxidation by $PhI(OAc)_2$. The acetate anion as an internal base has been revealed as a crucial parameter for expanding the reaction scope.[182] More recently, the chemoselective coupling reaction of polyfluoroarenes with aryl germanes was achieved by a cationic gold(I) catalyst associated with

a mesylate anion (PPh_3AuOMs)[183] that promotes the transmetalation of aryl germanes (Scheme 1-20c). Further studies revealed that the aryl germanes exhibit a higher reactivity than arylsilanes and arylborates. Later, a similar coupling reaction with a greatly larger scope was realized by using an *in situ* umpolung strategy with the assistance of silver.[184] This approach showed compatibility with electro-poor or -rich aryl germanes and gave rise to a series of electron-poor biaryls (Scheme 1-20d).

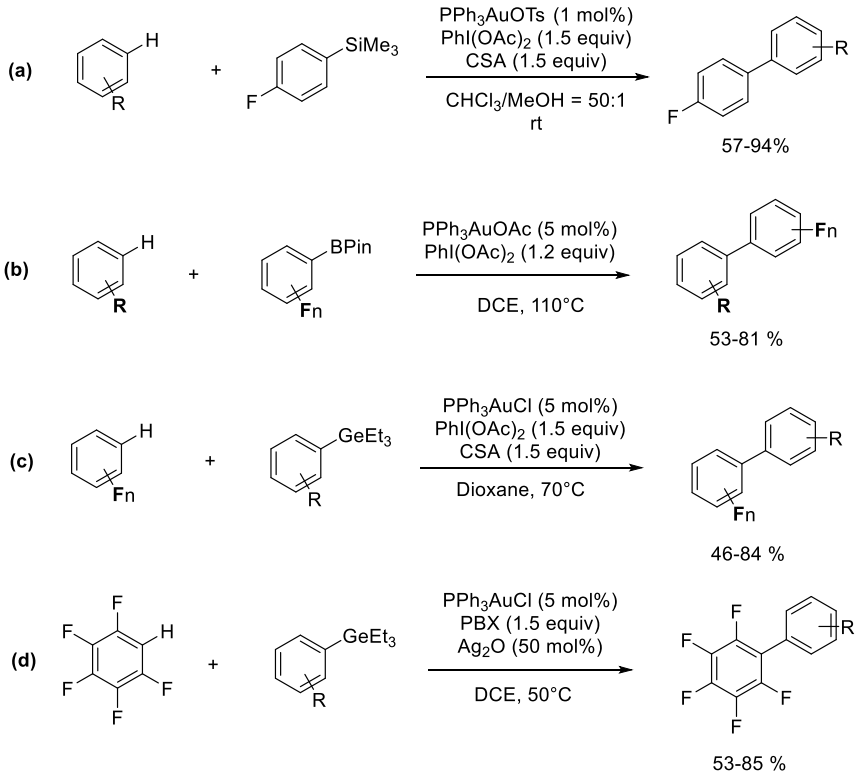

Scheme 1-20. Gold catalyzed cross coupling of functionalized arenes and electron-poor or -rich arenes.[180, 181, 183, 184]

The direct oxidative cross coupling of two arenes is an efficient method to construct biaryls, while the reactivity or selectivity is often difficult to control. The selective C-H activation of arenes can be achieved by tuning the electronic density of the arenes. An electron-poor arene favors the C-H activation by a gold(I) complex whereas an electron-rich arene is readily activated by an electrophilic gold(III) catalyst. Thus, the double C-H activation can be selectively controlled to result in the biaryl coupling product. This approach was illustrated in the cross-couplings of electron-poor fluorinated arene and electron-rich arenes or indoles with good yields and excellent selectivities (Scheme 1-21).[185, 186]

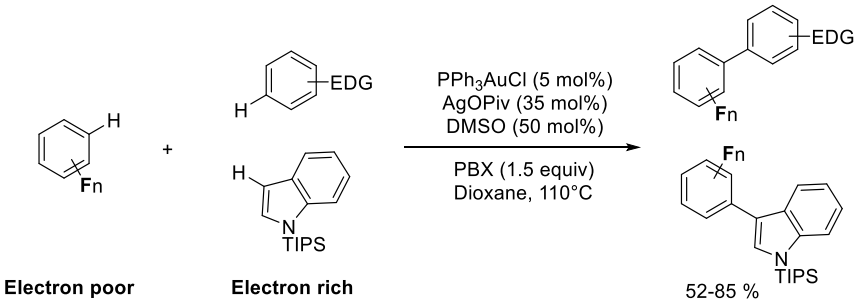

Scheme 1-21. Gold catalyzed cross coupling via double C-H activation.[185, 186]

1.5.2 Dual photoredox and gold catalysis

Before being applied to gold, the concept of cooperative photoredox catalysis was already investigated with various organocatalysts, Lewis acids and other transition metal catalysts such as nickel and palladium.[187] Light-induced gold catalysis provides an alternative, elegant route to the Au(I)/Au(III) redox cycle without the use of excess oxidants. In the presence of a photocatalyst and a aryldiazonium reagent (in most cases), gold(I) complexes can be converted into gold(III) species through a two-electron oxidation process. A broad investigation of the reactions scope led to the discovery of novel transformations. In this section, the concepts of dual gold/photoredox catalysis are presented with the proposed mechanisms supported by DFT calculations. The concept of photosensitizer-free light-mediated reactions is also discussed.

1.5.2.1 Concept

Owing the development of classic transition metal catalysis (such as palladium), gold complexes were shown to achieve Au(I)/Au(III) redox cycles in the presence of an oxidant. Indeed, the high potential of the Au(I)/Au(III) redox couple limits its ability to undergo an oxidative addition step crucial for cross coupling reactions. Several oxidants, such as hypervalent iodine or selectfluor were employed to generate the gold(III) oxidation state and enable oxidative cross coupling.[180, 188-193] Some obvious disadvantages of using superstoichiometric amounts of oxidant are poor atom economy and restricted functional group tolerance. In order to achieve the elementary oxidation step, gold(III) species were designed to be obtained through a stepwise two-electron oxidation processes from gold(I) by using photoredox catalysis: (a) a photocatalyst triggers the formation of a carboradical R• which reacts with the Au(I) complex to form a Au(II) intermediate and (b) a single electron transfer (SET) from the photocatalyst to the gold atom to form the cationic Au(III) species (Scheme 1-22). Then, a reductive elimination step provides the product and the initial gold(I) catalyst required to complete the catalytic cycle. The active catalytic species can be either the Au(I) or Au(III) species. This concept is based on the studies of Puddephatt[194] in the 1970's and Corma in 2006,[195] who reported that organic radicals can react with gold(I) to afford organogold(III) intermediates. In 2013, Glorius introduced an elegant strategy to carry out the oxidant-free Au(I)/Au(III) redox catalysis by merging visible light photoredox and gold catalysis under mild conditions.[196] The first two model reactions are presented in

the next paragraph: (a) the intramolecular oxyarylation of alkenes (Glorius), and (b) an arylative ring expansion reaction of vinylcyclopropanol (Toste and Frei).[197]

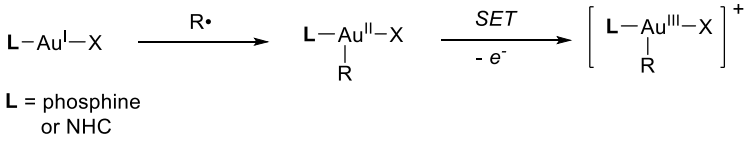

Scheme 1-22. The concept of photo-induced two electron oxidation to generate gold(III) species.

Hashmi and coworkers reported pioneering work in light-mediated Au(I)/Au(III) redox catalysis by using blue or visible light LED in the absence of any photosensitizer. This approach was illustrated in the gold-catalyzed 1,2-difunctionalization of alkynes and cross coupling reactions.[198] Light was proposed to favor the oxidative addition step and the elimination of nitrogen. Under these conditions, the oxidation of gold seems to occur through a SET followed by radical addition, which is the reverse order compared to the general mechanism of dual gold/photoredox catalysis. Importantly, gold(I) has no absorption in the region of blue LED to visible light and can hardly act as photocatalyst, whereas the unsubstituted benzenediazonium reactant shows a strong absorption maximum at $\lambda_{max} \approx 300$ nm and 261 nm in solution. Methanol (solvent) as an electron donor can contribute to the generation of aryl radical. The role of gold complexes, light and solvent during the oxidative addition step is therefore still under investigation.

1.5.2.2 General mechanism

From the initial studies by Glorius and Toste,[196, 197] both dual catalytic processes with similar reactants and identical $Ru(bipy)_3$/Ph_3PAuCl catalysts involve a radical addition and a single electron transfer to generate a gold(III) species (Scheme 1-23**)**. One classic example is the oxyarylation of alkenes (Scheme 1-5, Path I).[196] The cationic gold(I) activates the alkene and initiates nucleophilic cyclization resulting in the alkylgold(I) intermediate **A** which undergoes addition of the photo-generated aryl radical to afford a gold(II) species **B**. This unstable intermediate is expected to be further oxidized by Ru^{III} through a SET process to generate a highly electrophilic gold(III) species **C**. The smooth reductive elimination of **C** gives rise to the coupling product and regenerates the gold(I) catalyst (Scheme 1-23, Path I). In this mechanism based on experimental evidence, gold(I) catalysis is followed by the action of photocatalyst to form the final intermediate **C** before the reductive elimination. A theoretical study by Yu suggested that the favorable pathway for this reaction is first the action of the photocatalyst on gold(I) followed by gold(III) catalysis on the substrate.[199]

A slightly different mechanism was proposed for the arylative ring expansion reaction (Scheme 1-23, Path II).[197] Based on the observation of the reductive elimination product PPh_3AuPh **D**, the authors proposed that the two electron oxidation process of gold(I) complex into gold(III) **E** triggered by the photocatalyst occurs first, followed by classical gold(III) catalysis, *i.e.* the activation of the alkene towards the ring-expansion step, followed by reductive elimination.

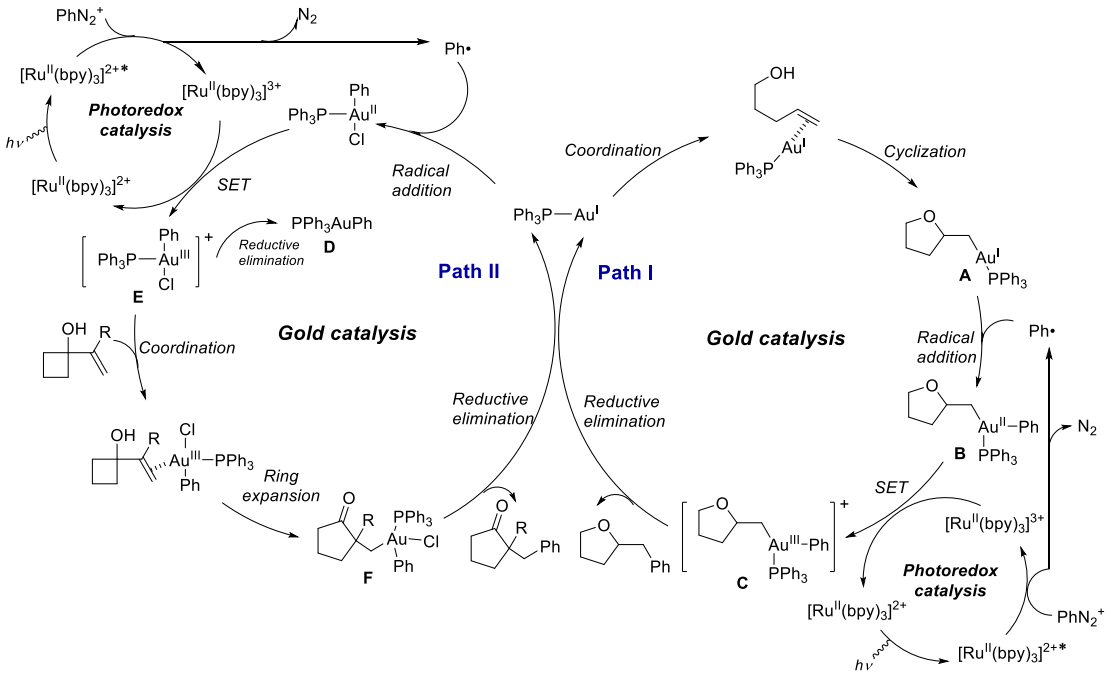

Scheme 1-23. The general mechanism of dual photoredox and gold catalytic system (Path I: For oxy- and aminoarylation of alkene; Path II: For arylative ring expansion reaction).[196, 197]

Recent reports of photosensitizer-free light-mediated gold catalyzed organic transformations[198, 200-202] developed by Hashmi raised a series of questions with respect to the mechanism: (i) the role of PPh_3AuCl, as a catalyst and/or a photocatalyst, (ii) the action of visible or blue LED light on gold(I)/(III) species, (iii) in the absence of a photosensitizer, the aryldiazonium salt reactivity under irradiation, and (iv) the key actors of the oxidation addition step.

To explain the new results, a distinct mechanism than the previous ones (Scheme 1-23) was proposed by Hashmi for two model reactions (Scheme 1-24): a cross coupling reaction and a 1,2-difunctionalization of an alkyne. Initially, a single electron transfer process occurs from neutral gold(I) complex to the aryldiazonium salt generates a gold(II) aryldiazo radical exciplex **A**, which undergoes an intramolecular aryl radical addition on the gold(II) center to afford cationic gold(III) species **B**. Assisted by light irradiation, the elimination of N_2 affords arylgold(III) species **C**.

Depending on the experimental conditions, this common intermediate can react with two different reactants. In the cross-coupling reaction, an *in situ* transmetallation of arylboronic acid to **C** gives diarylgold(III) species **D**, which upon fast reductive elimination delivers the cross coupling product. Notably, the scope of the coupling partner ranges from arylboronic acids,[200] arylboronates, potassium trifluoroboronates, to trimethoxysilanes and bis(catecholato)silicates.[201] In the case of TMS reagents as coupling partners, cationic gold(I) (PPh_3AuNTf_2) performs better than a neutral gold(I) catalyst (PPh_3AuCl) and the chlorine anion plays a crucial role in the 1,2-difunctionalization reaction of alkynes.[198]

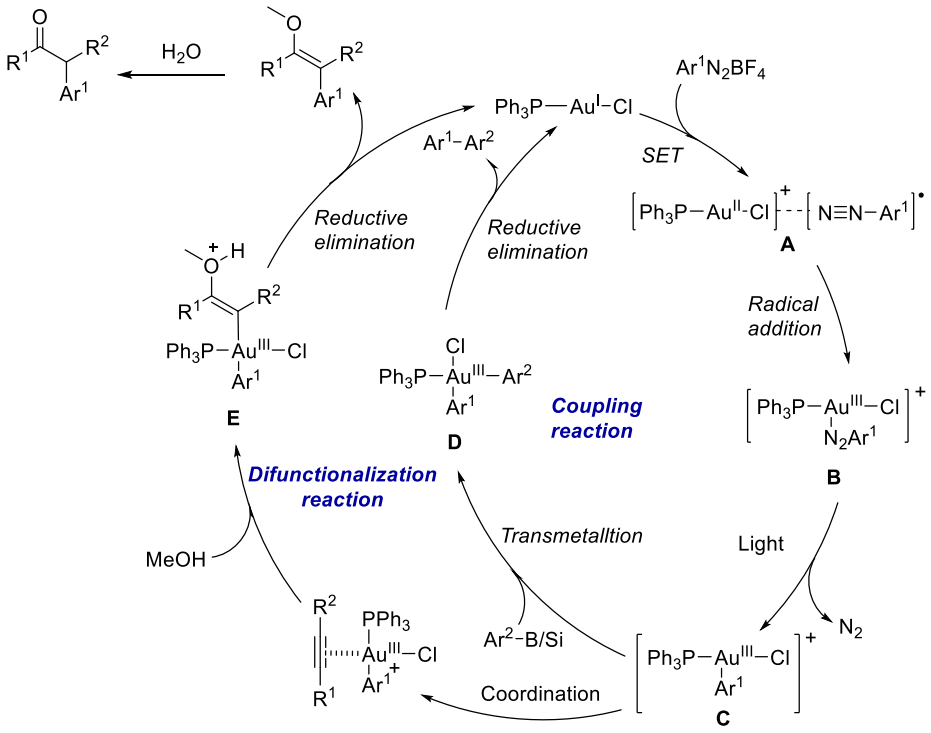

Scheme 1-24. The plausible mechanism of photosensitizer-free light-mediated gold catalyzed cross coupling reaction and 1,2-difunctionalization of alkyne.[198]

Concerning the 1,2-difunctionalization reaction of alkynes (Scheme 1-24), the gold(III) intermediate **C** can catalyse the activation of the alkyne followed by the nucleophilic addition of methanol to deliver the substituted ketone. Recently, Zhu and Zhang published a theoretical study of the mechanism of the 1,2-difunctionalization of alkynes.[203] The DFT calculations suggest that the first steps involve the formation of a charge-transfer complex between gold(I) complex and the phenyldiazonium salt, which can be excited by visible light and further undergoes a SET process to afford gold(II) and the carbon-centered radical. The radical addition can then occur on gold(II) or gold(I) centers, followed by the classical elementary steps. Here, the DFT calculations are important in highlighting the possible dual role of the gold(I) complex in gold catalysis under light, both as a catalyst and as a precursor of a photocatalyst.

1.5.2.3 Oxidative addition on gold(I) complex: experimental evidence

As stated above, the oxidative addition step is the main stumbling block for the Au(I)/Au(III) redox catalysis. Thorough understanding of this two-electron oxidation step is also difficult to achieve solely from experimental evidence. A theoretical study by Bickelhaupt and co-workers indicated that the oxidative addition of arylhalides or aryl triflates is feasible on some gold(I) complexes.[204] The authors suggest that the oxidative addition process is steered by the strain energy associated with the deformation of the reactants from their equilibrium geometries to the geometries they adopt in the corresponding concerted transition state. Experimentally, the oxidative addition onto gold(I) complexes was reported in absence of any light source or

external oxidant, for specific reactants or ligands: Toste described a *NHC* gold(III) complex obtained by the insertion of gold(I) into a strained biphenylene.[205] Meanwhile, Bourissou *et al.* developed a hemilabile *P,N*-ligand that stabilized gold(III) species after the oxidative addition of an aryliodide on the corresponding gold(I) complex.[206]

Under dual gold/photoredox catalysis conditions, Glorius reported the formation of (*C,N*)-cyclometalated arylgold(III) complexes directly from the stoichiometric reaction between a 2-pyridyl-substituted aryldiazonium salt and the gold(I) complex, which indirectly evidences the aryl radical addition to a gold(I) complex (Scheme 1-25A).[207] The square planar gold(III) product is stable and prone to undergo reductive elimination. Hashmi's group obtained a similar (*P,N*)-cyclometallated arylgold(III) from the reaction of a phosphine gold(I) complex and benzendiazonium salt in methanol under blue LED irradiation and in absence of any photocatalyst (Scheme 1-25B).[198] In 2019, Toste and co-workers[208] prepared a cationic *NHC* gold(III) complex from the corresponding gold(I) complex under visible-light photoredox conditions (Scheme 1-25C). Clearly, the search for new strategies to access diverse gold(III) complexes from gold(I) would provide more possibilities for their application in homogeneous gold catalysis.

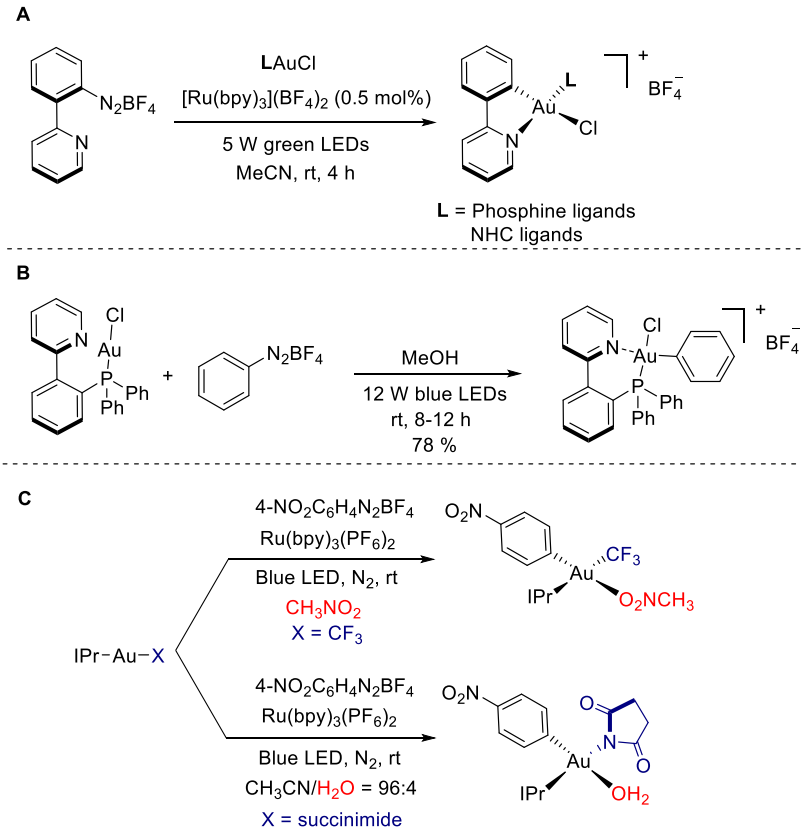

Scheme 1-25. Experimental evidence for oxidative addition of various gold(I) complexes to gold(III) with aryldiazonium salts through photoredox catalysis.[198, 208]

1.5.2.4 Selected organic transformations based on dual catalytic system

Following the initial report of the dual gold/photoredox catalysis for the 1,2-functionalization of alcohol-alkenes using a $Ru(bipy)_3/Ph_3PAuCl$ catalytic system (Scheme 1-23), Glorius's group presented an intermolecular three-component oxyarylation reaction of non-activated alkenes (Scheme 1-26).[209] The reaction proceeds under benign conditions and delivers α-arylated ether products in good yield. Interestingly, the reaction can be achieved by using different photocatalysts such as inexpensive organic dyes and a diaryliodonium salt as an alternative radical source.

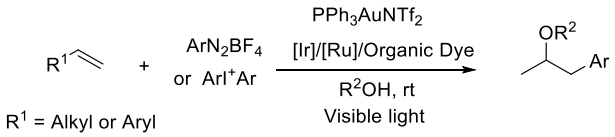

Scheme 1-26. Other photocatalyst and radical precursor for dual photoredox and gold catalysis.[209]

In the last few years, a series arylative cyclization reactions were developed based on the dual photoredox and gold catalytic system. The major principle of arylative cyclization reaction design is that the generated arylgold(III) is an efficient Lewis acid catalyst to activate C-C π bonds and further be attacked by a nucleophile. It is also reasonable that, in some cases, the initial gold(I) catalyst leads to the nucleophilic attack, and followed by a two-electron oxidation process to generate the arylgold(III) intermediate which readily proceeds through reductive elimination to afford the final product. Based on this principle, in 2016, Fensterbank, Ollivier, and co-workers described the arylative cyclization of *o*-alkynylphenols as a pratical method to afford benzofurans.[210] In the same year, Zhu's group presented aminoarylation of alkynes, affording a series of multisubstituted indoles in excellent yields (Scheme 1-27).[211]. In 2017, Patil revealed an intramolecular *ipso*-arylative cyclization of aryl-alkyniates and *N*-arylpropiolamides through merged gold/visible light photoredox catalysis.[212]

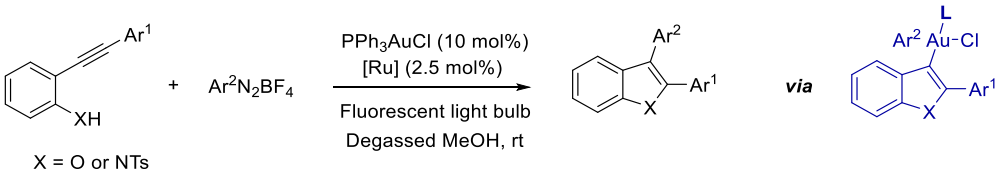

Scheme 1-27. Arylative cyclization of *o*-aminoalkyne or *o*-alkynylphenols.[211]

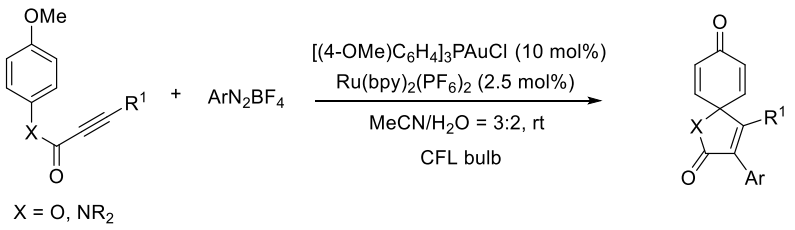

Scheme 1-28. Intramolecular ipso-arylative cyclization reaction of alkynes.[212]

The arylgold(III) was generated by radical addition and SET process and further promotes the dearomative cyclization, providing an access to arylated spirocarbocycles in moderate to good yield (Scheme 1-28).

The arylative cyclization of chiral homopropargyl sulfonamides using a diazonium salt was reported by Ye to occur under dual gold/photoredox catalysis conditions (Scheme 1-29).[213] The catalytic process afforded chiral 2,3-dihydropyrroles possessing two aryl substituents without any racemization. Alcaide *et al.* described a similar two-fold arylation reaction of TMS-protected alkynes.[214, 215] The reaction offers a versatile methodology to access a wide range of disubstituted heterocyclic compounds. The proposed mechanism involves two successive arylgold(III) intermediates (Scheme 1-30). The same group also developed a tandem oxycyclization/coupling sequence to transform allenols in 2,5-dihydrofurans under visible light irradiation using a $Ru(bipy)_3^{2+}$/PPh_3AuCl catalytic system.[216]

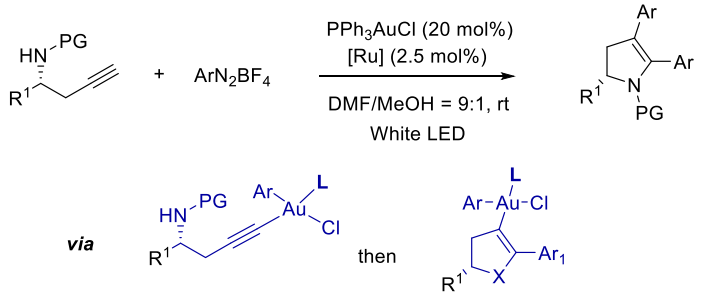

Scheme 1-29. Arylative cyclization of homopropargyl sulfonamides under dual photoredox/gold catalysis.[213]

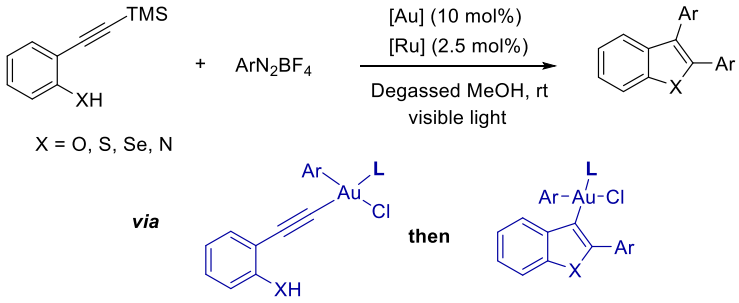

Scheme 1-30. Photoinduced gold-catalyzed domino *C(sp)*- arylation/benzoheterocyclization of TMS-protected alkynes.

A recent review by Patil describes the progress in oxidant-free cross-coupling reactions catalyzed by gold, in the presence and absence of light.[217] In 2015, Toste reported a *C-P* bond coupling between *H*-phosphonates and aryldiazonium salts with a large functional group tolerance, using the $Ph_3PAuCl/Ru(bipy)_3(PF_6)_2$ catalytic system under visible light (Scheme 1-31).[218] Importantly, other metal sources such as Pd, Ag, Cu exhibit lower or no reactivity for this cross coupling reaction. The mechanism involves an electrophilic arylgold(III) intermediate, which can be coupled to the *H*-phosphonate nucleophile.

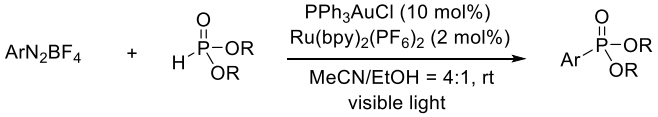

Scheme 1-31. Dual gold/photoredox catalyzed arylation of phosphonates.[218]

In 2016, Glorius described the arylation of alkyl and aromatic terminal alkynes using dual gold/photoredox catalysis (Scheme 1-32).[219] This method allows the preparation of diversely-functionalized arylalkynes from aryldiazonium salts, under mild and base-free conditions. In the same year, Toste's group described a similar cross-coupling reaction from alkynyltrimethylsilanes and aryldiazonium tetrafluoroborates (Scheme 1-33A).[220] Under these conditions, no reactivity was observed by employing a terminal alkyne. In 2017, Patil published the cross coupling reaction of aryldiazonium salts with allylsilanes under quite similar conditions (Scheme 1-33B).[221] Later, the same group described the cross coupling between arylsilanes and aryldiazonium salts.[222] The presence of a copper(II) catalyst (20 mol%) is essential and might involve the transmetallation of arylsilanes (Scheme 1-33C).

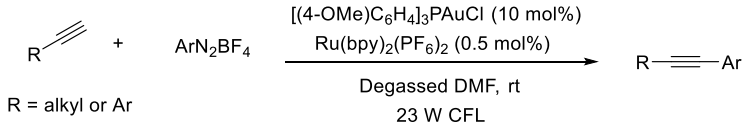

Scheme 1-32. *C(sp)-H* arylation of terminated alkynes.[219]

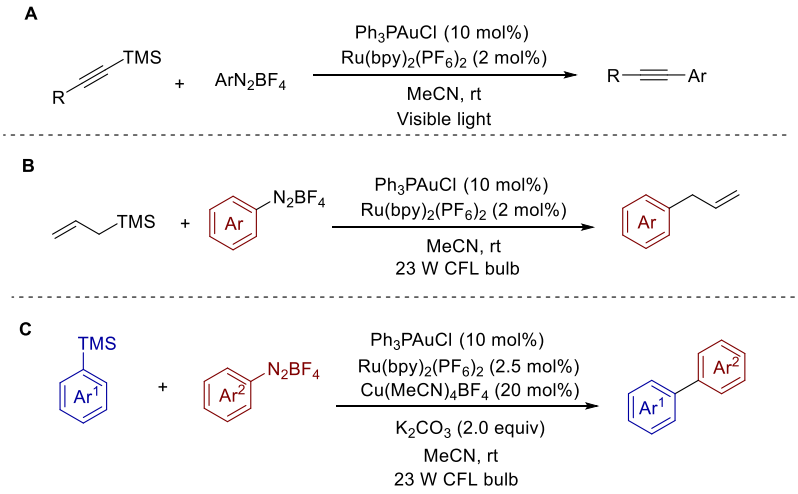

Scheme 1-33. Various trimethylsilyl-substituted reagents as partner in cross coupling reaction.[220-222]

In 2016, two research groups described the synthesis of biaryl compounds from arylboronic acids and aryldiazonium salts under similar conditions. Fouquet and Hermange employed 9-mesityl-10-acridinium tetrafluoroborate or $Ru(bpy)_3(PF_6)_2$ as a photocatalyst in the presence of blue LED light (Scheme 1-34).[223] Meanwhile, Lee revealed that the $Ph_3PAuNTf_2/Ru(bipy)_3(PF_6)_2$ catalytic system was most efficient in the presence of water.[224] A mechanistic study suggests two possible pathways depending on the gold source: a transmetallation of the arylboronic acid by gold(I) may occur prior to the oxidation of gold(I) to gold(III) if using cationic gold(I) catalysts, whereas the oxidation of gold(I) to gold(III) precedes transmetallation when using neutral gold(I) catalysts. One year later, the same group achieved the aryl–aryl cross coupling with a large scope of reactants via gold-catalyzed *C–H* activation using the $Ph_3PAuNTf_2/Ru(bipy)_3(PF_6)_2$ catalytic system under blue LED irradiation (Scheme 1-35).[225] The reaction proceeds through the oxidative addition of aryldiazoniums followed by the *C-H* auration and the aryl-aryl reductive elimination.

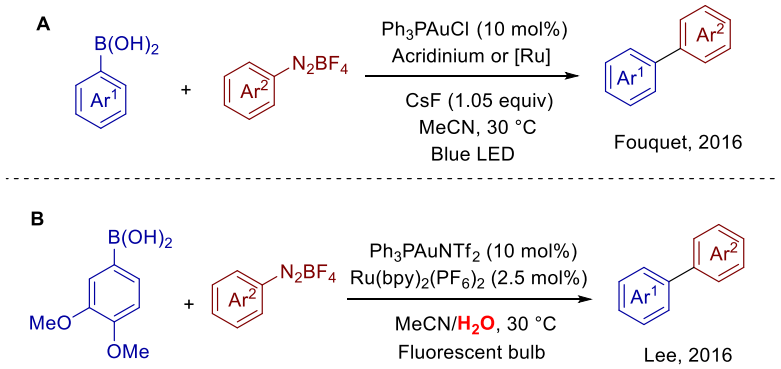

Scheme 1-34. Cross coupling reaction by using arylboronic acid as coupling partner.[223]

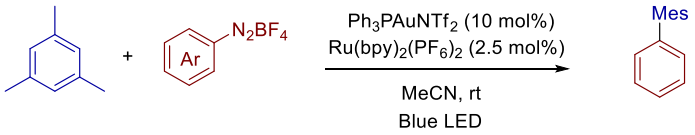

Scheme 1-35. Aryl-aryl cross coupling via light-mediated gold-catalyzed *C-H* activation.[225]

1.5.2.5 Photosensitizer free light-mediated organic transformations

As discussed in the general mechanism part with the initial example of 1,2-difunctionalization of alkyne (Scheme 1-24), arylgold(III) species can be generated *in situ* in the absence of a photosensitizer.[198] Nonetheless, even with support from DFT calculations,[203] the formation of the arylgold(III) intermediates is not fully understood. In 2017, Hashmi reported a cross coupling reaction between arylboronic acids and aryldiazonium salts in methanol under blue LED light in the presence of $(4\text{-}CF_3\text{-}C_6H_4)_3PAuCl$ catalyst at 10 mol% loading (Scheme 1-36A).[200] The proposed mechanism involves an oxidative addition to species **B**. After the loss of dinitrogen, the gold(III) intermediate **C** is transmellated to form the diarylgold(III) **D** which

undergoes reductive elimination to afford the coupling product. The same year, Bandini, Protti and co-workers achieved a cross coupling reaction in acetonitrile/methanol between an arylboronic acid and a photolabile arylazosulfone as the radical source, using PPh_3AuCl (5 mol%) as a catalyst and bipyridine (20 mol%) under blue LED irradiation (Scheme 1-36B).[226] The proposed mechanism relies on the photo-generation of aryl and methanesulfonyl radicals from arylazosulfone which leads to the same arylgold(III) intermediate.

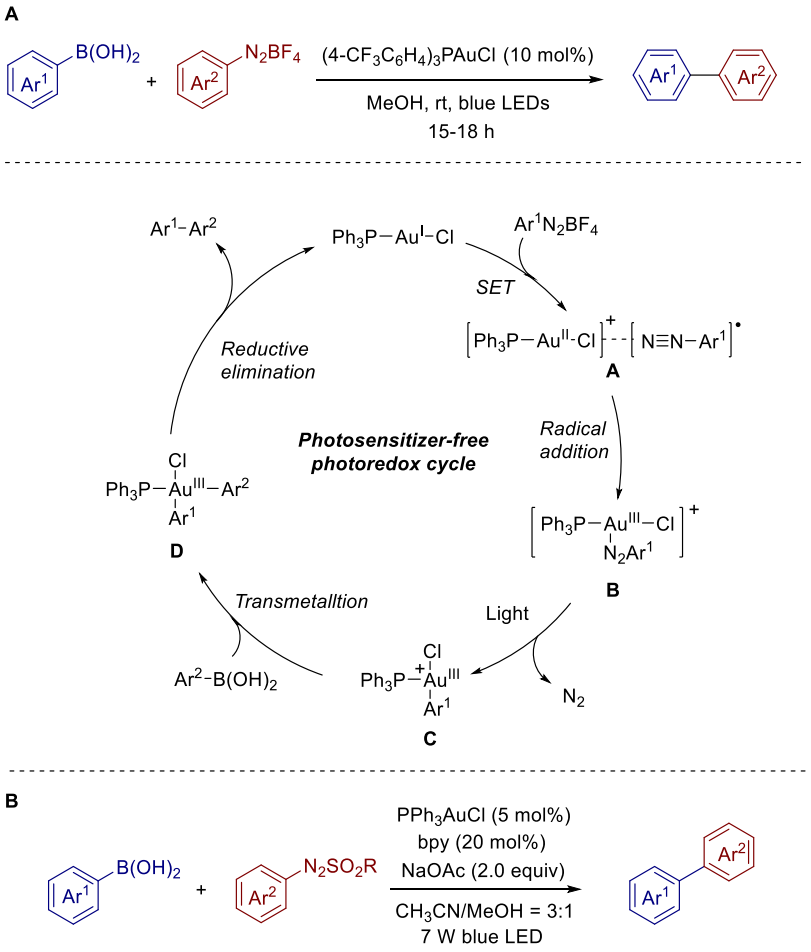

Scheme 1-36. Cross coupling reactions of arylboronic acid and aryldiazonium salts/arylazosulfones catalyzed by gold and irradiation with UV light.[200, 226]

With the hypothesis that the electrophilic arylgold(III) generated by a photoredox process in the presence of aryldiazoniums could still serve as an efficient Lewis acid activate C-C π bonds, the very initial example of 1,2-difunctinalization of alkynes was achieved by generating the arylgold(III) catalyst in the absence of photosensitizer.[198] However, the detailed process for the formation of arylgold(III) intermediate remains obscure. In 2017, Hashmi reported the cross coupling reaction between an arylboronic acid and an aryldiazonium salt under LEDs light in the presence of a neutral phosphine gold(I) complex.[200] The proposed mechanism involves the formation of a diarylgold(III) intermediate through radical addition, oxidation and transmellation, followed by reductive elimination to afford the coupling product (Scheme 1-

37).

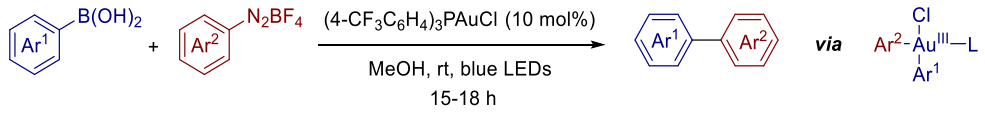

Scheme 1-37. Cross coupling reaction of arylboronic acid and aryldiazonium salts in the presence of neutral gold(I) and light.[200]

Shortly after this, cross coupling reactions in the presence of aryldiazoniums with various boron or silicon reagents as coupling partners to afford diaryl products were reported.[201] Interestingly, an obvious electronic effect was observed when the yield is low while introducing electron rich methoxyl groups. It is also important to mention that the neutral gold catalyst is essential to afford high yields (Scheme 1-38), this observation is in line with previous studies of 1,2-difunctionalization of alkynes.[198] More recently, a photochemical gold-catalyzed chemo-selective Hiyama arylation[202] was achieved to access diarylboronates which could further be transformed to form new C-C bond or C-X bonds (Scheme 1-39). Interestingly, Wong described a visible light-mediated gold-catalyzed difunctionalization of silyl-substituted alkyne to afford fluorescent silyl-substituted quinolizinium derivatives with excellent regioselectivity and good function group compatibility.[227] Furthermore, the fluorophores possess tunable emission properties and were used in photo-oxidative amidations as efficient photocatalyst (Scheme 1-40). In addition, apart from switching the reagent for the transmetallation step, Bandini, Protti and co-workers[226] achieved a cross coupling reaction with arylboronic acids by employing a photolabile arylazosulfone as a radical source. However, bipyridine was proved to be essential for the coupling reaction (Scheme 1-41).

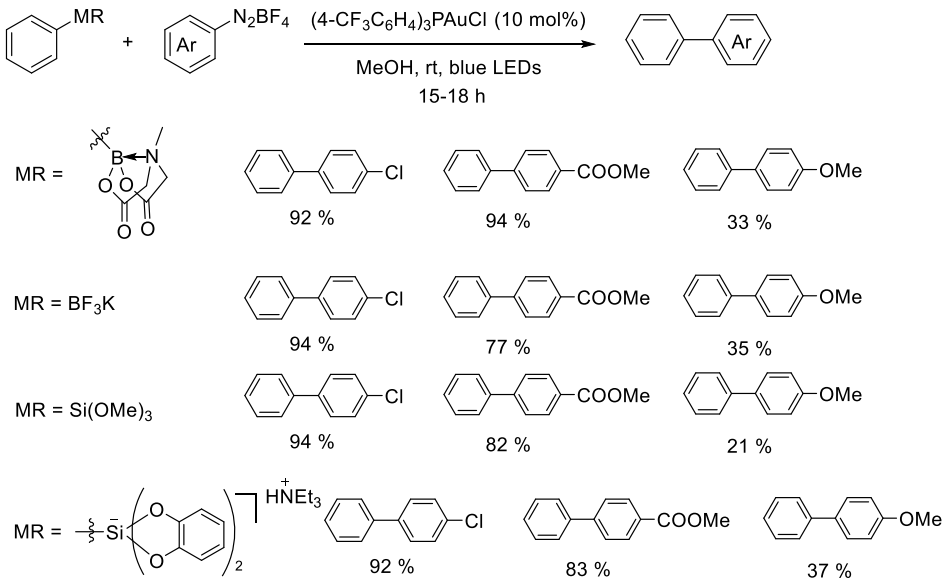

Scheme 1-38. Photosensitizer-free light-induced gold-catalyzed cross coupling reaction of aryldiazonium salts and various boron or silicon reagents.[201]

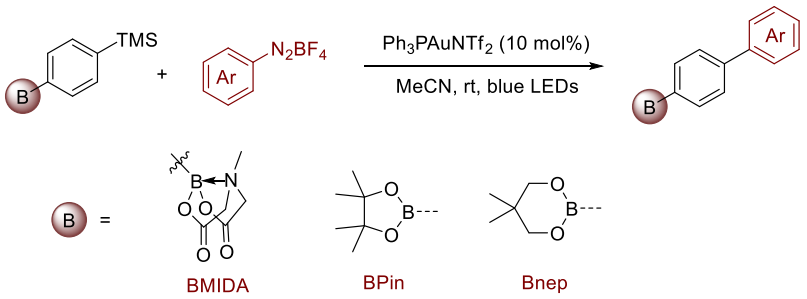

Scheme 1-39. Photochemical gold-catalyzed chemo-selective Hiyama arylation.[202]

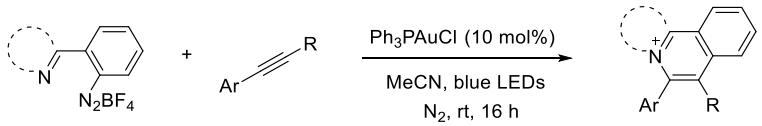

Scheme 1-40. Photosensitizer-free light mediated gold catalyzed cross coupling reaction of aryldiazonium and arylalkyne.[227]

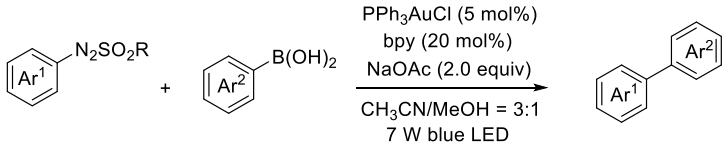

Scheme 1-41. Bench-stable arylazosulfones as radical source in cross coupling reaction with arylboronic acid.[226]

1.5.3 Light-triggered redox gold catalysis

Several reviews about dimeric gold photoredox catalysis are available.[228-230] This section is centered on the mechanistic aspects and the key advances in organic transformations. During the last decade, several metal complexes, such as $[Ru(bpy)_3Cl_2]$ and *fac*-$[Ir(ppy)_3]$, have uncovered their potential in harvesting light and converting it into electronic energy that can be engaged in a single-electron-transfer process within organic transformations, such as for the generation of carbon-centered radical intermediates. In 1989, Che and co-workers[231] reported that the dinuclear gold complex $[Au_2(\mu\text{-dppm})_2]^{2+}$ (λ_{max} = 292 nm and 267 nm) exhibits a room temperature photoluminescence and possess a powerful one-electron reducing ability when in the excited state, as the electron could be trapped by a pyridinium ion to deliver a pyridinyl radical species under irradiation conditions. Moreover, the excited state of $[Au_2(\mu\text{-dppm})_2]^{2+}$ can undergo either an oxidative or a reductive quenching pathway in the presence of methylviologen (MV) or *N,N,N',N'*-tetramethyl-*p*-phenyl-enediamine (TMPD), respectively (Scheme 1-43). Interestingly, common halides can serve as a quenchers, which then generate carbon-centered radicals. This therefore represent a novel and mild way to access transformations from commercially available halides. In 2013, Barriault and Gagosz developed a radical intramolecular cyclization reaction of bromo-alkenes and bromo-arenes catalyzed by $[Au_2(\mu\text{-dppm})_2]X_2$ salts

(X: OTf, Cl) at 1 mol% in the presence of *i*Pr$_2$NEt (2 equiv.) under sunlight (Scheme 1-42).[232] This transformation was inefficient (0-5 % yield) in the presence of classical Ru- or Ir-based polypyridyl complexes due to a less energetic outer-sphere metal-to-ligand charge transfer (MLCT) state. The main advantage of the process over traditional redox reactions is that the dimeric gold complex acts as photoredox catalyst which *in situ* generates the active catalyst by light excitation.

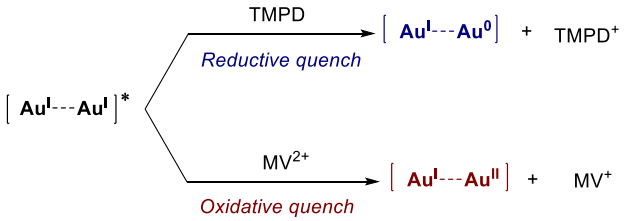

Scheme 1-42. Excited state of dimeric gold complex was quenched by various quencher.[231]

1.5.3.1 General mechanism

Recently, Che and co-workers elucidated the photochemical excitation pathways for a binuclear gold(I) complex.[233] According to the ultrafast time-resolved spectroscopy and computational studies, this complex shows minimal aurophilic interactions in the ground state (2.962 Å) which is strongly enhanced upon excitation with UVA light when an electron from the anti-bonding $5d_z^2$ orbital is populated into the $6s/6p_z$ bonding orbital (^{1}5ds*6ps) inducing robust Au-Au interactions (2.677 Å). Dinuclear complexes exhibit a lifetime of ~510 ps in dichloromethane which enable light induced C-X bond cleavage transformations. Generally, dimeric gold photoredox catalysis can proceed through either an oxidative or reductive quenching pathway. In the reductive quenching pathway, the initial photo-excited complex is reduced through single electron transfer (SET) in the presence of an electron donor reagent such as triethylamine. The resulting species can act as a reductant with respect to an acceptor such as bromoalkenes and regenerate the ground state complex (Scheme 1-43A). In the oxidative quenching pathway, the inner-sphere exciplex is oxidized by an acceptor leading to a $[Au^I\text{-}Au^{II}]^{3+}$ intermediate along with a carbon-centered radical for further transformation. The resulting radical can reduce the intermediate into dimeric gold(I) complex(Scheme 1-43B). In 2016, laser flash photolysis experiments were carried out by Barriault and Scaiano, concluding that trialkylamine and bromoalkanes were both capable of quenching excited dimeric gold complex $[Au_2]^*$. Time-resolved absorption and emission measurements indicate that the inner-sphere interaction which might derive from an exciplex.[234]

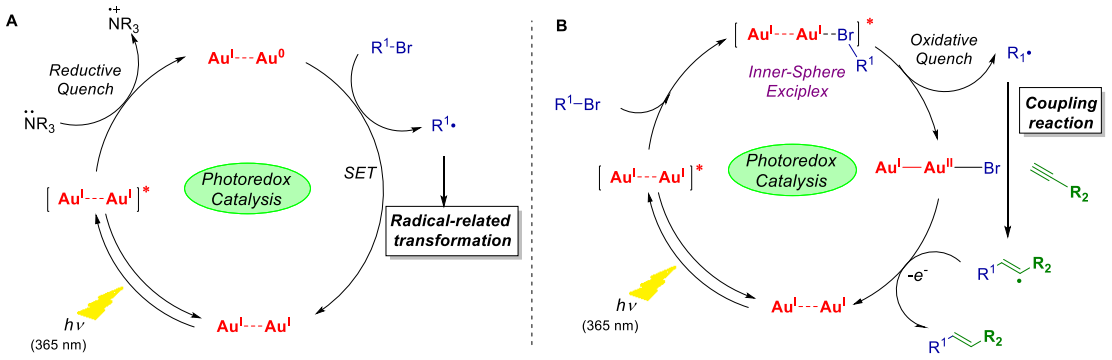

Scheme 1-43. The oxidative quenching/reductive quenching pathway for dimeric gold photoredox catalyst.[234]

1.5.3.2 Organic transformations expansion based on gold photoredox catalytic system

The very first example of radical cyclization in the presence of dimeric gold photoredox catalyst was developed by Barriault in 2013.[232] This methodology provides an access to various heterocyclic and polycyclic products in intra/intermolecular manner under mild conditions (Scheme 1-44). Since then, a series of radical cyclization to unsaturated systems, such as indoles[235] and arenes. Such radical cyclization was also applied to construct fused cyclic skeleton in the total synthesis of Triptolide.[236] In 2018, a [5+2] cyclization catalyzed by dimeric gold(I) photoredox catalyst featured in the total synthesis of pyrroloazocine indole alkaloid[237] and was used to build bridge-ring scaffold in 91 % yield with excellent *endo*-diastereoselectivity (*dr* > 50:1) (Scheme 1-45).

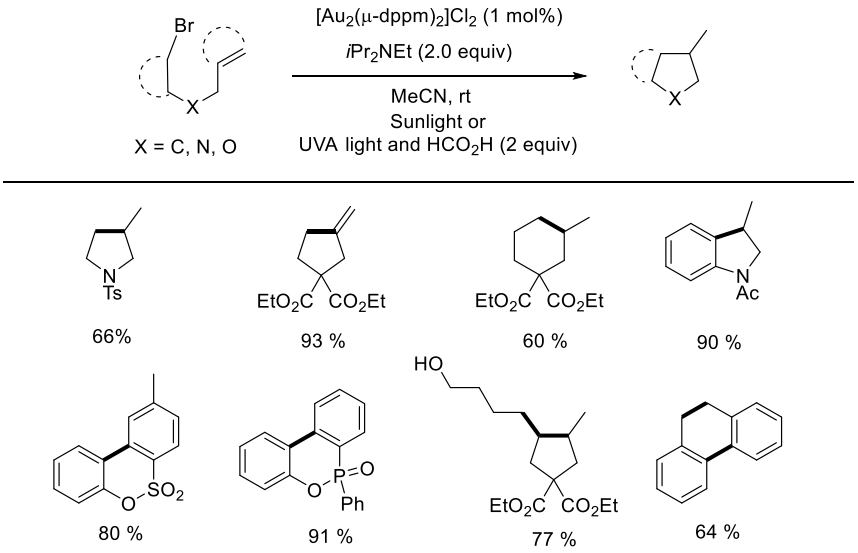

Scheme 1-44. Visible light-mediated radical cyclization to unsaturated π system under dimeric gold photoredox catalyst.[232]

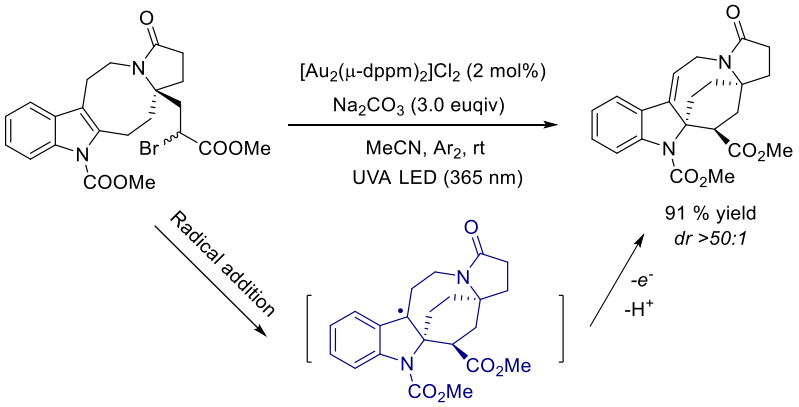

Scheme 1-45. Light-mediated [5+2] cyclization to indole using dimeric gold photoredox catalyst.[237]

Recently, based on the photoredox system, Barriault reported mild intermolecular cyclization to afford a large scope of phenanthridine products in good yield by using readily available bromides (Scheme 1-46A)[238]. Moreover, the corresponding amides were obtained in the presence of water (Scheme 1-46B).

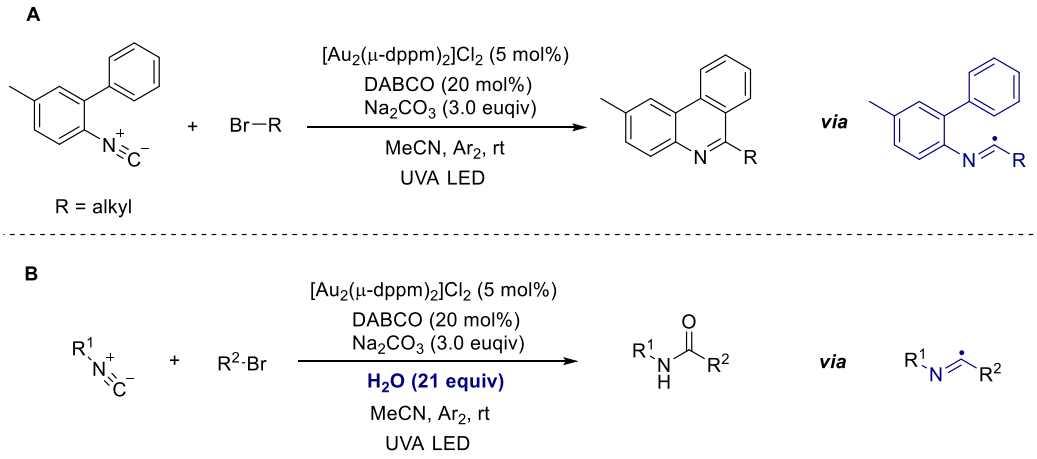

Scheme 1-46. Light-mediated transformations of isonitrile compound using dimeric gold photoredox catalysts.[238]

In 2016, Barriault group presented Minisci-type alkylation of heteroarenes using dimeric gold photocatalysts in mild condition.[239] The *C-H* fuctionalization of heteroarenes was previously accessible under harsh condition by employing stoichiometric oxidant and under elevated temperature. This methodology provides a pratical *C(sp³)-C(sp²)* cross coupling involving nonactivated bromoalkanes (Scheme 1-47A). Furthermore, a polarity reversal radical addition strategy was implemented in a three-component reaction by introducing an alkene as radical acceptor. Upon alkyl radical addition to alkene, the electrophilic radical turns to nucleophilic, gaining access to *C-H* fuctionalization of heteroarenes (Scheme 1-47B).

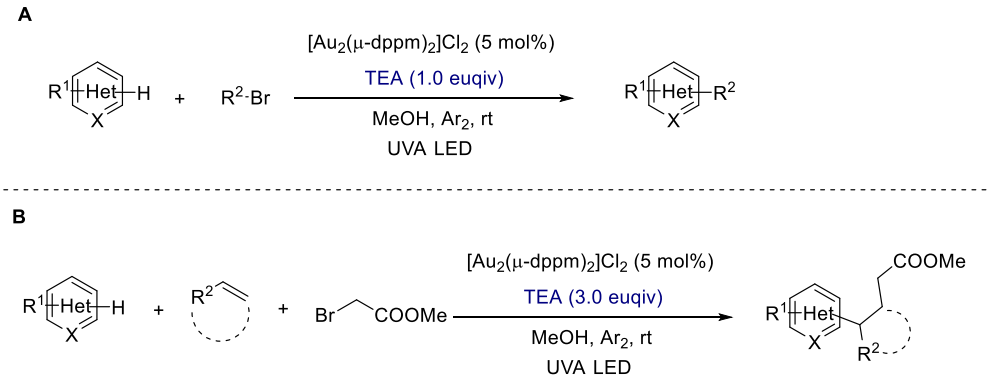

Scheme 1-47. Alkylation of heteroarenes under dimeric gold photoredox catalyst.[239]

In 2015, Barriault published a pratical one-pot protocol for the reductive deoxygenation of primary alcohols.[240] The primary alcohol is first brominated in the presence of CBr_4, and the resulting bromide can further be reduced by $[Au_2(dppm)_2]Cl_2$ photoredox catalyst with UVA light illumination (Scheme 1-48). Later, the homocoupling of bromoalkanes via dimeric gold(I) photoredox catalyst was reported.[241] Interestingly, the use of deuterated solvents dramatically promoted the ratio of homocoupling product compared with radical cyclization product from 3:1 to 10:1 while bromoalkene as substrate. The process involves the reductive quenching mechanism and probably undergoes two steps of single electron transfer to form gold(III), then reductive elimination from gold(III) center to afford homocoupling product (Scheme 1-49).

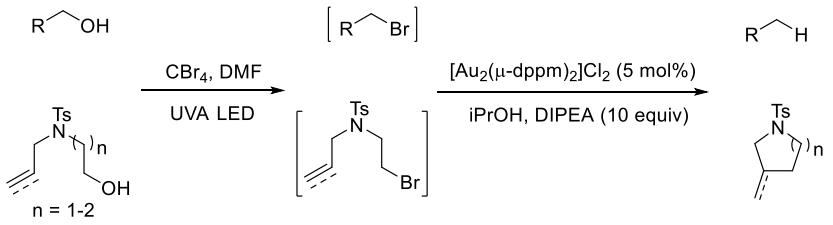

Scheme 1-48. Deoxygenation of primary alcohol under dimeric gold photoredox catalyst.[240]

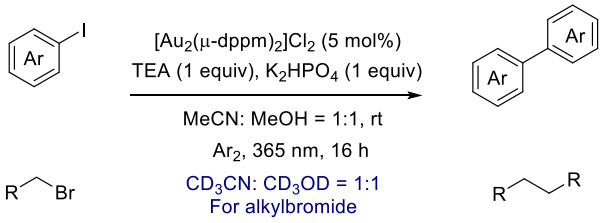

Scheme 1-49. Homocoupling of aryliodide or alkylbromdie under dimeric gold photoredox catalyst.[241]

Finding new applications in material science, in 2015, Ollivier, Goddard, Fensterbank and co-workers reported a controlled radical polymerization (CRP) of methactylates and ethyl α-bromophenylacetate (EBPA) in the presence of dimeric gold photocatalyst upon 350 nm irradiation in dichloromethane.[242] Compared to

EBPA/Ir(ppy)$_3$ system, it exhibits faster rate of polymerization with better solubility and low cost. Notably, the chain length can be further extended by adding more methyl methacrylate or benzyl methacrylate under the same condition (Scheme 1-50).

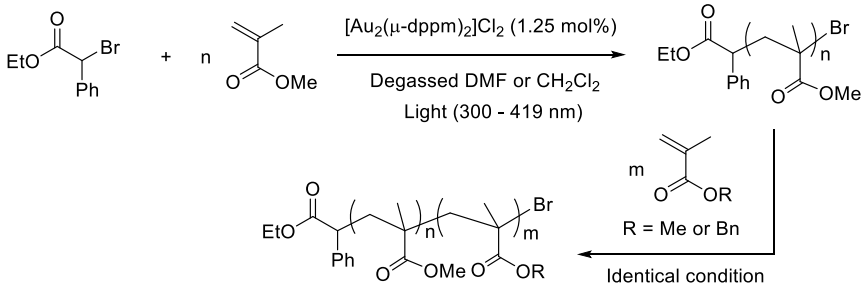

Scheme 1-50. Radical polymerization under dimeric gold photoredox catalyst.[242]

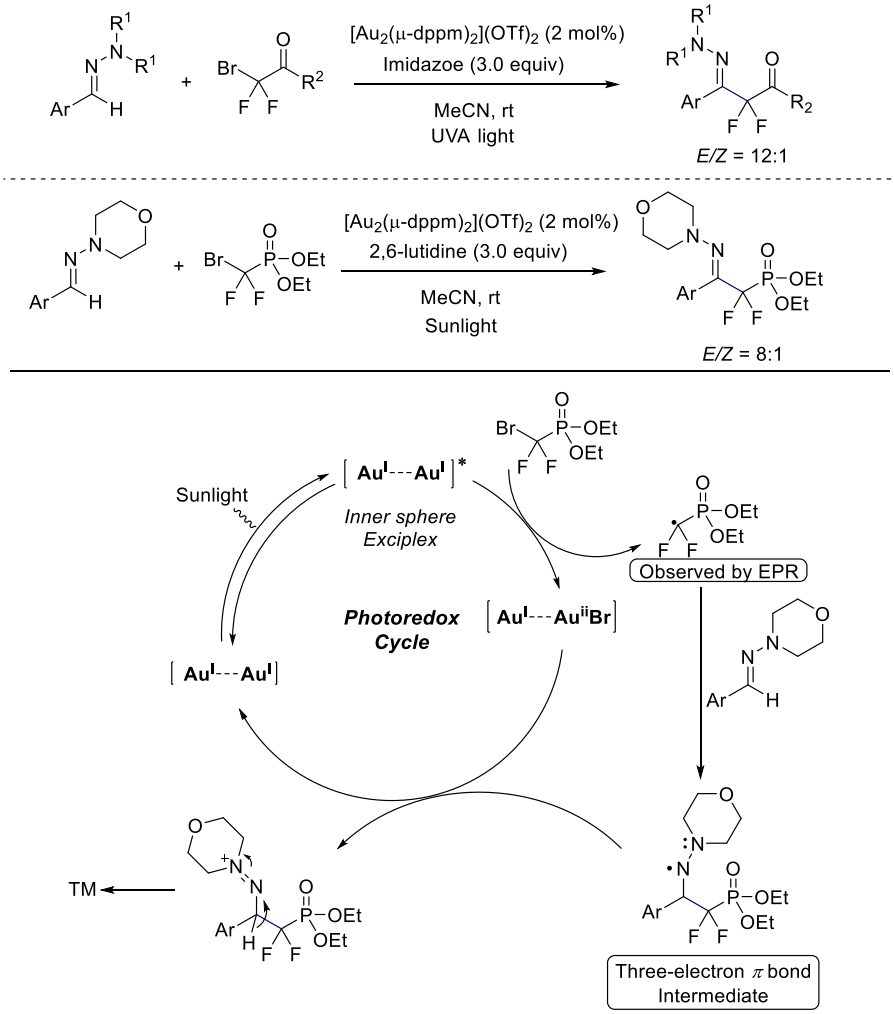

Scheme 1-51. Intermolecular difluoroalkylation and perfluoroalkylation of hydrazones under dimeric gold photoredox catalyst.[243]

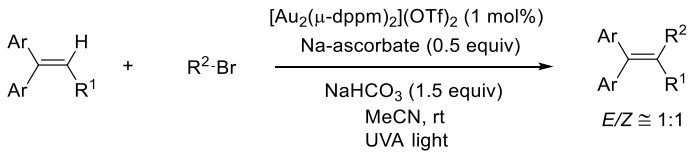

Scheme 1-52. Heck-type reaction of unactivated alkyl bromides under dimeric gold photoredox catalyst.[244]

In 2016, Hashmi's group described an interesting gold-catalyzed photoredox *C(sp²)-H* intermolecular difluoroalkylation and perfluoroalkylation of hydrazones with a readily available α-bromodifluoroalkyl ester.[243] After optimization, hydrozones proved to be the optimal acceptor with respect to the radical addition of a difluoroalkyl radical. The mechanism involves the three-electron π-bonding aminyl radical intermediate which can be oxidized and lead to the difluoromethylated product (Scheme 1-51). Following this work, Hashmi published a Heck-type reaction of unactivated alkyl bromides and poly-substituted alkenes in the presence of a gold photocatalyst.[244] The alkyl radical was generated by oxidative quenching pathway and nonactivated bromoalkanes were formed. Notably, this catalytic system is superior to traditional Heck condition where the β-H elimination product is difficult to surpass (Scheme 1-52).

In 2015, Hashmi's group investigated a novel synthetic application in *C(sp³)-H* alkynylation of unactivated aliphatic amines under sunlight by using the dimeric gold complex $[Au_2(dppm)_2]^{2+}$ as a photocatalyst.[245] The proposed mechanism involves an oxidative quenching pathway to generate an alkynyl radical followed by tertiary amine oxidation, finally leading to radical-radical coupling (Scheme 1-53). More recently, Chan's group further described a C1-alkynylation of *N*-alkyl-1,2,3,4-tetrahydroisoquinolines (THIQs) reaction in the presence of $[Au_2(dppm)_2]Cl_2$ under UVA light with the moderate yield.[246] The difference of selectivity by using alkynylbromide and alkynyliodide is discussed, with the formation of dimerization product favored when employing alkynyliodide as the coupling partner. The proposed mechanism refers to a reductive quenching pathway which initially generates a carbon-centered THIQ radical and is followed by reductive cleavage of the *C(sp)*-I bond (Scheme 1-54)

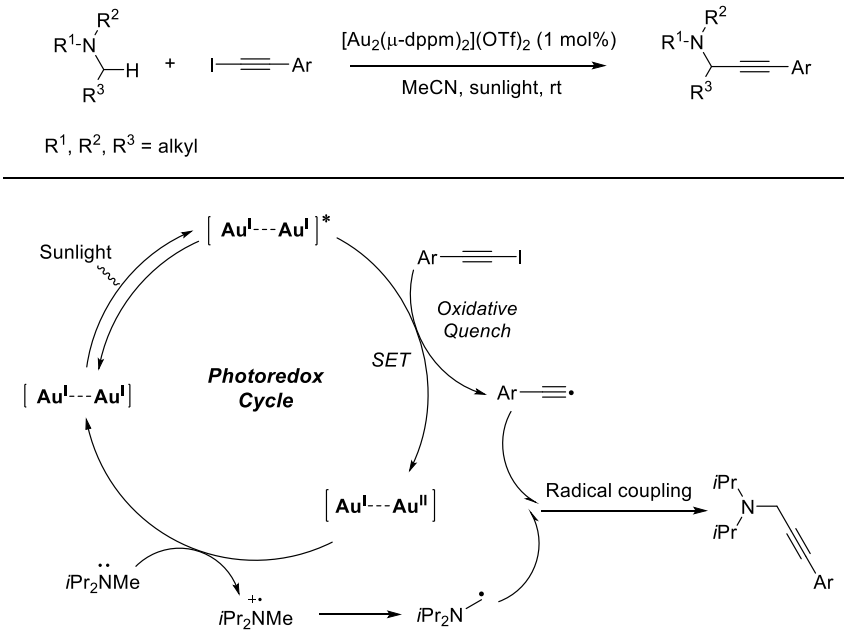

Scheme 1-53. *C(sp³)-H* alkynylation of unactivated aliphatic amines under dimeric gold photoredox catalyst.[245]

.

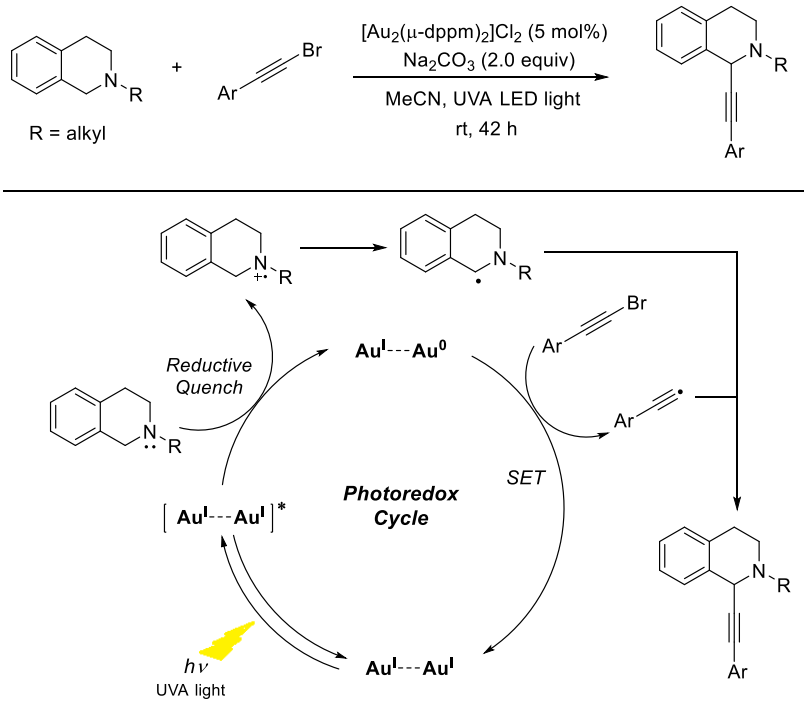

Scheme 1-54. C1-alkynylation of THIQs reaction under dimeric gold photoredox catalyst.[246]

1.5.4 Ligand enabled Au(I)/Au(III) catalysis without external oxidants

The reluctance of gold to undergo oxidative addition is the major bottleneck for the development of cross coupling reactions. The problem can be somewhat solved by using stoichiometric oxidant. However, this approach would be extremely limited as the substrate might also be oxidized in the presence of strong oxidants. In order to perform oxidative addition process in the absence of stoichiometric oxidant, several approaches were achieved by tailoring suitable substrates or by ligand-enabled Au(I)/Au(III) catalysis.

In 2014, Toste's group outlined gold catalyzed inter- or intramolecular cross coupling of allylbromides and aryl boronic acids in the absence of a sacrificial oxidant (Scheme 1-55). The use of a bimetallic catalyst bearing a bis(phosphino)amine ligand is the key to achieve the cross coupling reaction which has been described to accelerate the oxidative addition process. The plausible mechanism of this reaction involves the transmetalation of the aryl boronic acid then followed by oxidative addition to the C-Br bond, and finally undergoes reductive elimination to furnish the Csp^3-Csp^2 product.[247]

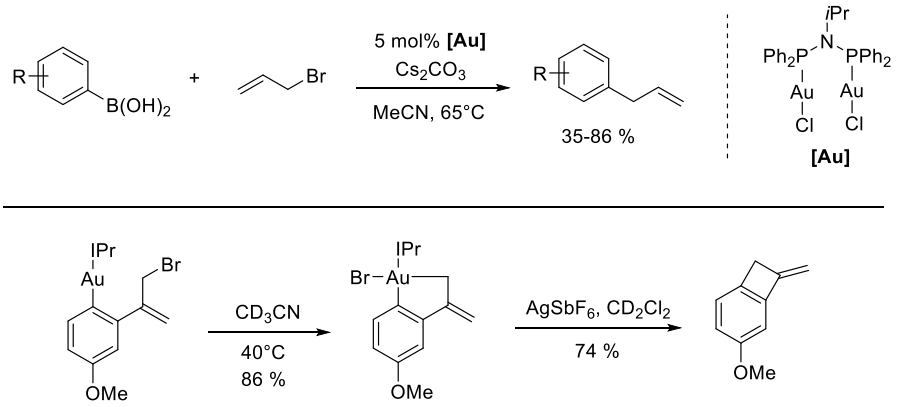

Scheme 1-55. Gold catalyzed inter- and intramolecular cross coupling of allylbromide and aryl boronic acids.[247]

Oxidant-free C-N and C-O bond cross-coupling was also achieved by using pyridine-directed oxidation of the aryl bromide to form a gold(III) complex with cationic carbene gold(I) without an external oxidant (Scheme 1-56). This gold(III) is well-characterized and meanwhile active toward O- or N-nucleophiles leading to C-O or C-N coupling products. Notably, the reaction showed great tolerance including to aromatic and aliphatic alcohols and amines, as well as water and amides.[248] In addition, the employment of strong electrophilic aryldiazoniums can oxidize the gold(I) species into gold(III) with the assistance of bipyridine ligands in the absence of oxidants (Scheme 1-57). The bipyridine ligand revealed to be essential for the coupling reaction as it facilitates nitrogen extrusion, and the *in situ* formed gold(III) readily undergoes reductive elimination under room temperature.[249] Porcel's group further evidenced that the diazonium compound can oxidize the triphenylphosphinegold(I) and dimethylsulfidegold(I) complex in DMSO at <50°C where the DMSO also serve as a coordination ligand to stabilize gold(III).[250]

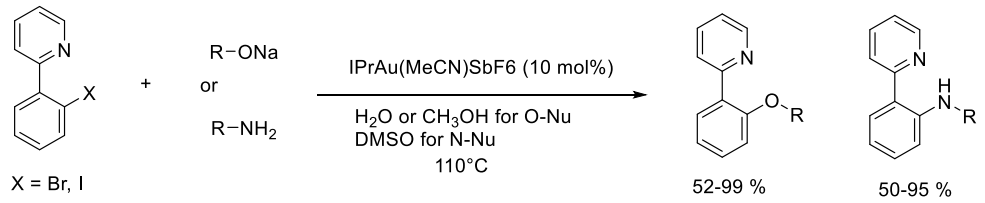

Scheme 1-56. Gold catalyzed oxidant-free C-O and C-N bond formation.[248]

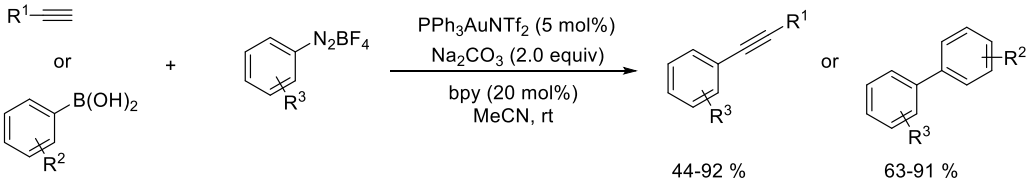

Scheme 1-57. Bipyridine assisted gold catalyzed Csp^2-Csp and Csp^2-Csp^2 cross coupling.[249]

In 2017, Bourissou and Amgoune's group employed rational ligand design to achieve Au(I)/Au(III) catalysis under mild condition (Scheme 1-58). The use of the bulky hemilabile MeDalphos (P,N) ligand is essential to achieve the facile oxidative addition to arylhalide which is explicitly evidenced. The following arene C-H activation affords to diarylgold(III) which readily undergo reductive elimination and achieve cross coupling.[75]

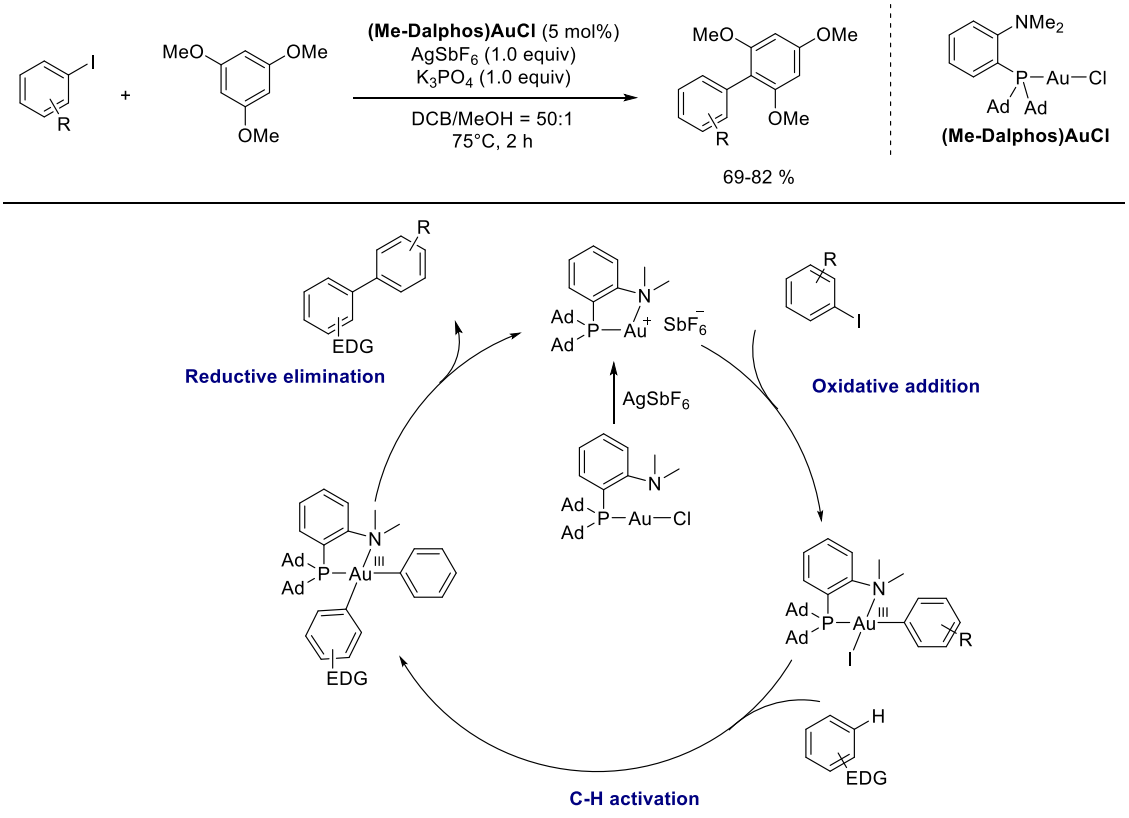

Scheme 1-58. (Me-Dalphos)AuCl catalyzed cross coupling of aryliodide and 1,3,5-trimethoxybenzene and proposed mechanism.[75]

Later, the same catalyst was used in several new bond-forming reactions by combination of the π-bond activation and redox character of gold catalysis. Bourissou's group published a robust heteroarylation of alkenes with aryl iodides which showed a broad substrate scope (Scheme 1-59). The variation on the alkene substrate was revealed to significantly affect in regioselectivity, as the *E*-alkene favors 6-endo cyclization and the *Z*-alkene favors 5-exo cyclization. The reaction begins by oxidative addition of the aryl iodide to form a gold(III), then activation of the alkene double bond to facilitate the cyclization, and finally proceeds reductive elimination to afford the coupling product (Scheme 1-60).[251] Almost at the same time, Patil's group reported a similar 1,2-heteroarylation of alkenes by using methanol as the nucleophile. The examination of other hemilabile (P,N) ligands further elucidated the uniqueness of MeDalPhos in achieving oxidative addition of arylhalides.[252] Furthermore, the (MeDalphos)AuCl complex was also employed for the efficient C-N bond formation by taking the advantage of the facile oxidative addition to aryl iodide under mild condition. Mechanistic studies using ^{15}N NMR suggest that the oxidative addition step precedes transmetalation.

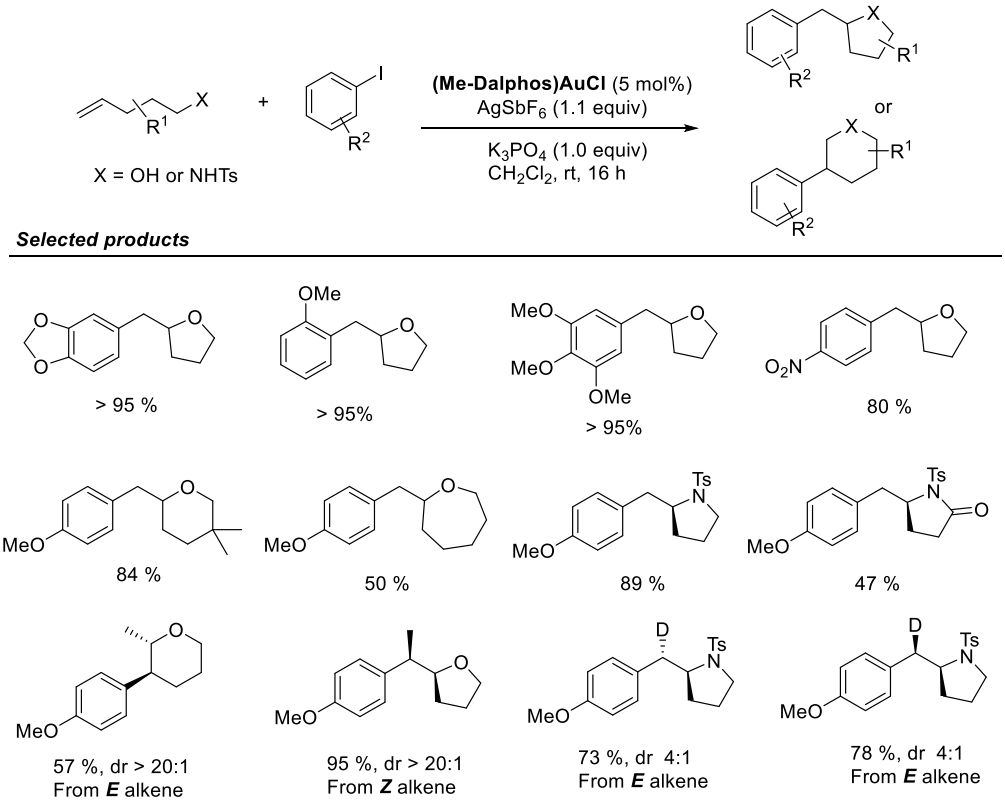

Scheme 1-59. Gold catalyzed heteroarylation of alkenes with aryl iodides.[251]

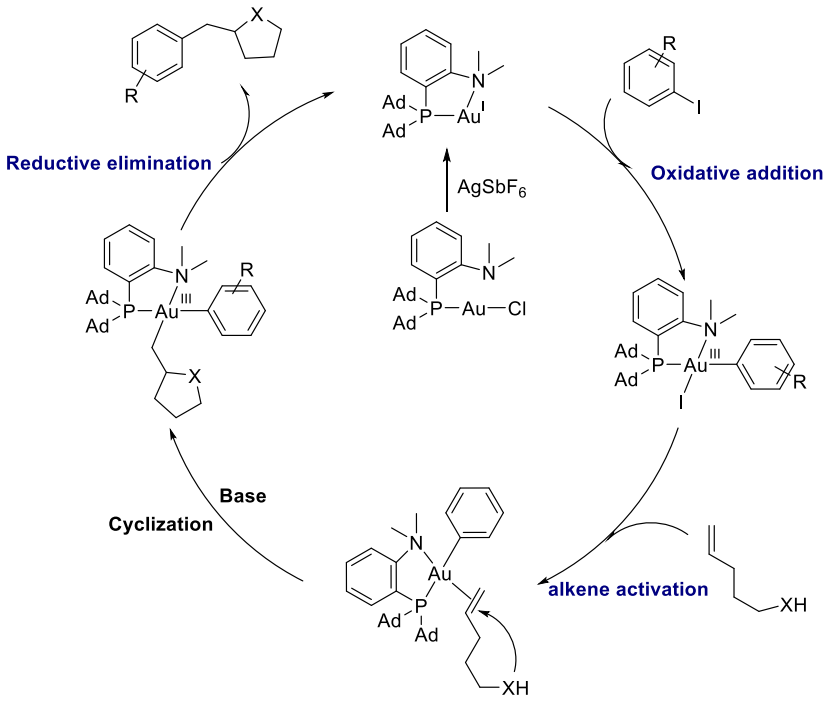

Scheme 1-60.Proposed mechanism for gold catalyzed heteroarylation of alkenes with aryl iodides.[251]

1.6 Conclusion

Although gold has a very short history in homogeneous catalysis, it has experienced the sharpest burst of interest witnessed in the last two decades. Particularly, the Lewis acidity of gold for selective activation of carbon-carbon π-bonds toward nucleophilic attack which leads to the construction of diverse molecular complexity and often performs under mild condition. Of note, both gold(I) and gold(III) electrophiles are able to activate the C-C multiple bonds for further nucleophilic addition and a little difference was observed by these two catalytic systems. However, the more electrophilic gold(III) complexes were also reported to favor aryl C-H or Csp-H activation to form organogold(III) species, thus allowing the formation of new C-C bonds. Meanwhile, significant ligand and anion effects on the activity of gold complexes was observed as little variations in ligands or anions might lead to disparate selective products, while the selectivity preference is still elusive. Some studies pointed out that the anion might coordinate with the substrate, thus facilitating the reaction. Additionally, the use of silver salts as chloride scavengers for numerous gold catalyzed alkyne-related transformations made it much more difficult to distinguish the real active species. Thus, in order to develop new gold catalyzed organic transformations, the use of well-defined gold catalysts is strongly necessary either to avoid the use of a silver source or simultaneously examine the ractivity of silver.

So far, gold complexes have also been proven to be efficient catalytic redox catalysis. Several strategies were employed to circumvent the high redox potential of gold which all showed both advantages and limitations. The cross coupling reactions were achieved under benign conditions by the addition of a stoichiometric

oxidant such as hypervalent iodine. However, this approach is confined to certain substrate that are stable toward oxidation and it exhibits a low atom efficiency. The dual photoredox and gold catalysis is an elegant approach to afford diverse arylation products although the transformation is limited to strong electrophilic aryldiazonium substrates. Light triggered gold redox catalysis can lead to a series of radical-related transformations even polymerization. However, gold photoredox catalysis is limited to certain dimeric gold complexes. Finally, ligand enabled catalytic redox gold catalysis pointed out a promising route, where to date Au(I)/Au(III) catalysis can be achieved by rational ligand design, albeit for certain ligands. In the field of catalytic redox gold catalysis, huge effort is still needed as significant perspectives in new organic transformations exist.

La chance ne sourit qu'aux esprits bien préparés.
Cultivez l'esprit critique

French microbiologist and chemist
Louis Pasteur (1822-1895)

Chapter 2

2 Photoreduction of gold(III) complexes and homogeneous catalysis

2.1 Reductive elimination in gold(III) complexes

Reductive elimination is an elementary step in metal catalytic cycles and this process is well documented for a variety of transition metal complexes. Reductive elimination in organogold(III) complexes which can lead to the formation of new carbon-carbon or carbon-heteroatom bonds and generates the corresponding gold(I) species. During the last decade, novel gold(III) complexes were developed which readily undergo reductive elimination under thermal conditions. In order to gain an in-depth understanding of this redox mechanism and explore further applications, the reductive elimination of various gold(III) complexes is reviewed in the following section.

2.1.1 C-C bond formation

Pioneering work was contributed by Kochi and coworkers in 1970s. A trialkyl(triphenylphosphine)gold(III) complex proceeds reductive elimination to generate a C(sp^3)-C(sp^3) bond via a high energy T-shaped trialkylgold intermediate formed by the dissociation of the PPh_3 ligand. Under thermal conditions, reductive elimination of *cis*- and *trans*- gold(III) complexes generates a C-C bond by the loss of two *cis*-alkyl groups (Scheme 2-1).[13, 15] Similarly, reductive elimination was also achieved in cationic dialkylgold complexes[253] and a *cis*-dimethyl(alkoxycarbonyl)gold(III) complex.[254]

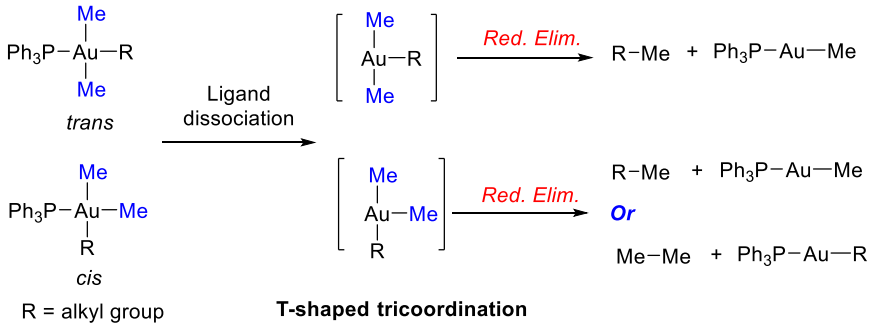

Scheme 2-1. Reductive elimination of trialkylgold(III) complexes.[13, 15]

Recently, two triphenylphosphine organometallic halide complexes (Ph_3P)Au(4-Me-C_6H_4)(CF_3)(X) and (Cy_3P)Au(4-F-C_6H_4)(CF_3)(X) (X = I, Br, Cl, F), were reported to undergo both C(sp^2)-X and C(sp^2)-CF_3 reductive elimination (Scheme 2-2) under thermal conditions (at 122 °C). Mechanistic studies reveal a dramatic reactivity and kinetics selectivity dependence on the halide ligand.[10] A similar difluoromethylated organogold(III) complex *cis*-[Au(PCy_3)(4-F-C_6H_4)(CF_2H)(Cl)] was synthesized by oxidative addition of 4-fluorobenzenediazonium chloride to [(Cy_3P)Au(Cl)] in CH_3CN under irradiation of blue LED light. The reductive elimination proceeds smoothly at 115°C to generate the corresponding C(sp^2)-CF_2H product (Scheme 2-3).[255]

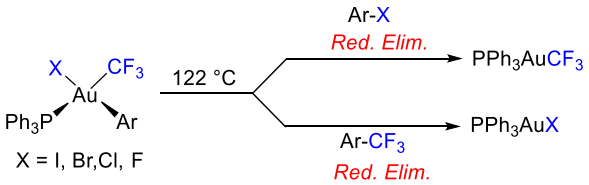

Scheme 2-2. Halide dependent reductive elimination.[10]

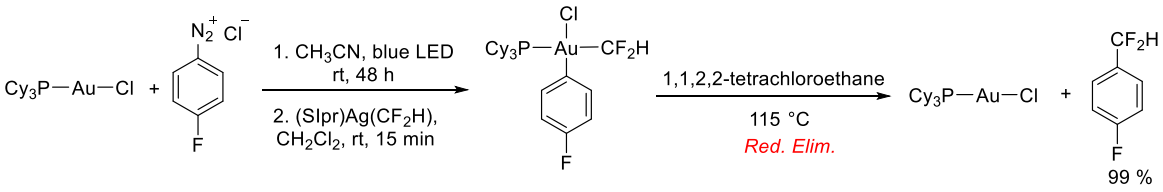

Scheme 2-3. Reductive elimination of difluoromethylated organogold(III) complex.[255]

An elegant example of controlling alkyl-alkyl reductive elimination from dialkylgold(III) was achieved by Raymond and Toste employing a self-assembled supramolecular complex which facilitates halide dissociation followed by the transient and reversible encapsulation of the nascent cationic species and, finally, an irreversible reductive elimination event within the cluster cavity (Scheme 2-4).[256]

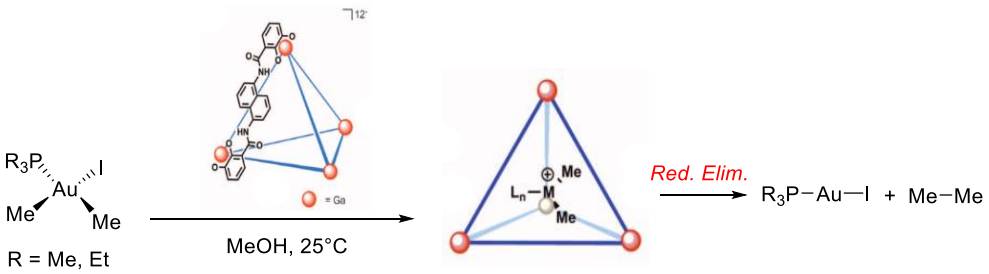

Scheme 2-4. Reductive elimination of dialkylgold(III) with a supramolecular encapsulate.[256]

In 1990s, Vicent and coworkers reported several 2-phenylazophenylgold(III) complexes which further transform to the diaryl(triphosphine)gold(III) by a ligand exchange triggered by the addition of a phosphine ligand (Scheme 2-5).[257] A C(sp^2)-C(sp^2) coupling product was generated during the reductive elimination process. A similar methodology was described by Bochmann and coworkers where protodeauration followed by addition of one equivalent of dimethylsulfide leads to the quantitative generation of the thioether complexes [(C,N-CH)Au(aryl)(SMe_2). The pyridine ligand is displaced upon the addition of a second dimethylsulfide, which triggers the reductive aryl-aryl reductive elimination (Scheme 2-6).[258]

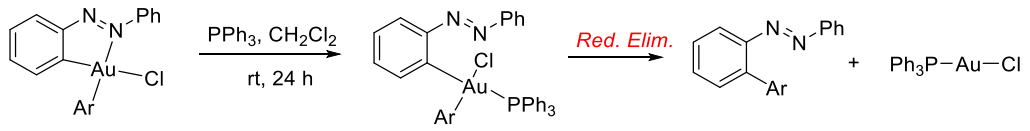

Scheme 2-5. Reductive elimination of diarylgold(III) complex.[257]

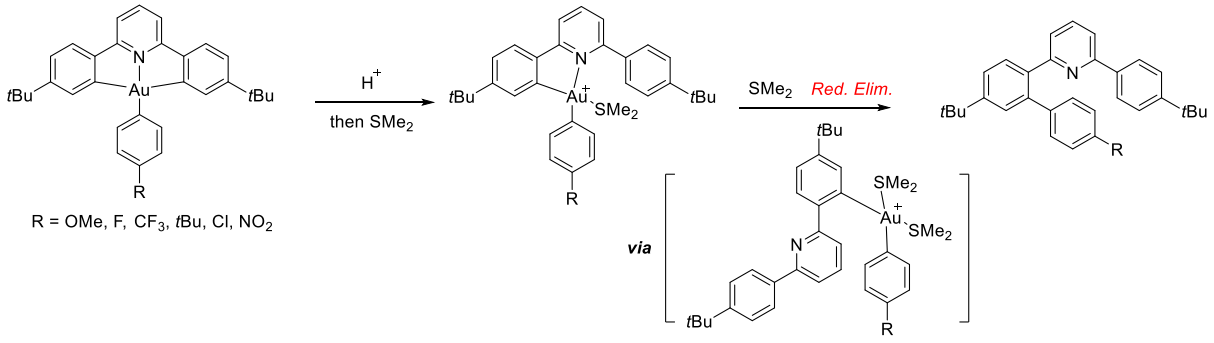

Scheme 2-6. SMe_2-induced $C(sp^2)$-$C(sp^2)$ reductive elimination within a bis(aryl)gold(III) complex.[258]

In 2017, Shen described a series of phosphine-ligated diarylgold(III) complexes that undergo reductive elimination under elevated temperature while generating $C(sp^2)$–$C(sp^2)$ coupling products (Scheme 2-7).[11] The mechanistic study disclosed that steric hindrance plays a major role in promoting the biaryl-forming reductive elimination through a concerted pathway from a four-coordinated gold(III) center. Futhermore, the weak electronic effect of ligands was observed (i.e. the complexes bearing weaker electron-withdrawing aryl ligands undergo reductive elimination more quickly) and the elimination rate is not sensitive to the polarity of the solvent.

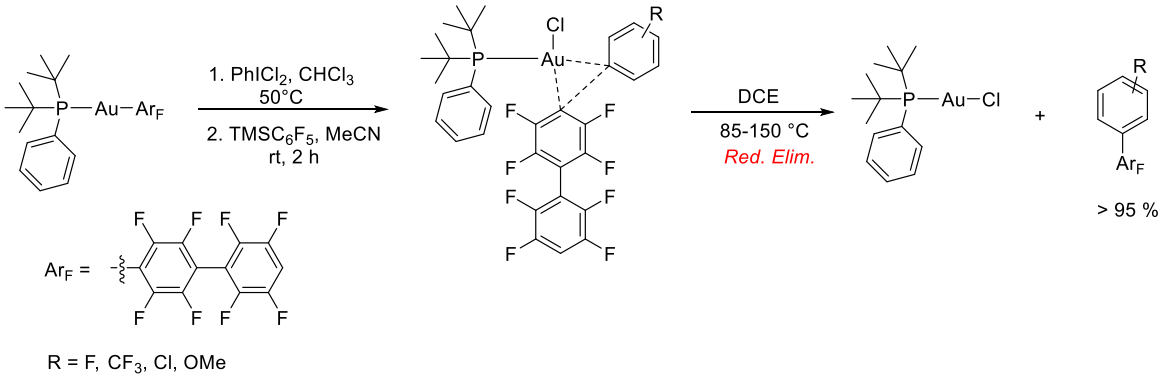

Scheme 2-7. $C(sp^2)$-$C(sp^2)$ reductive elimination from diarylgold(III) complexes.[11]

An exceptionally fast reductive elimination that allows the formation of $C(sp^2)$–$C(sp^2)$ from a monometallic *cis*-diarylgold(III) complex at low temperature was reported by Toste.[12] Contrary to the established dissociative mechanism, this biaryl reductive elimination exhibits fast rates even at -52°C through a concerted

mechanism from a four coordinated gold(III) center (Scheme 2-8).

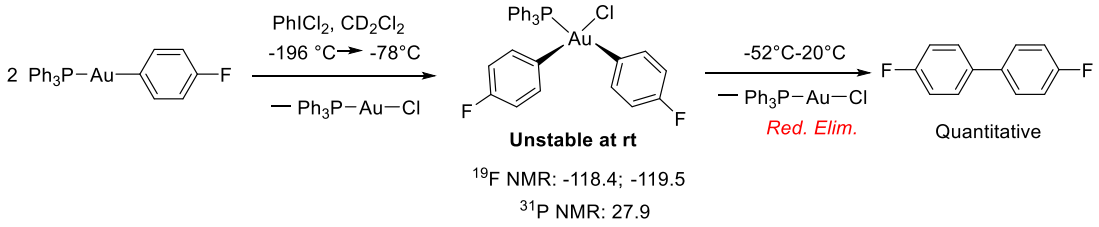

Scheme 2-8. Oxidation of a monometallic gold(I) complex and the subsequent biaryl reductive elimination.[12]

More recently, Nevado and coworkers[259] uncovered a family of phosphine-ligated dicyanoarylgold(III) complexes and their reactivity towards reductive elimination where a C(sp^2)-C(sp) bond was formed (Scheme 2-9). An asynchronous concerted reductive elimination was elucidated. Importantly, the reductive elimination of *cis* and *trans* gold(III) led to same product due to the favorable rearrangement of the *cis* gold(III) complex to *trans* conformation.

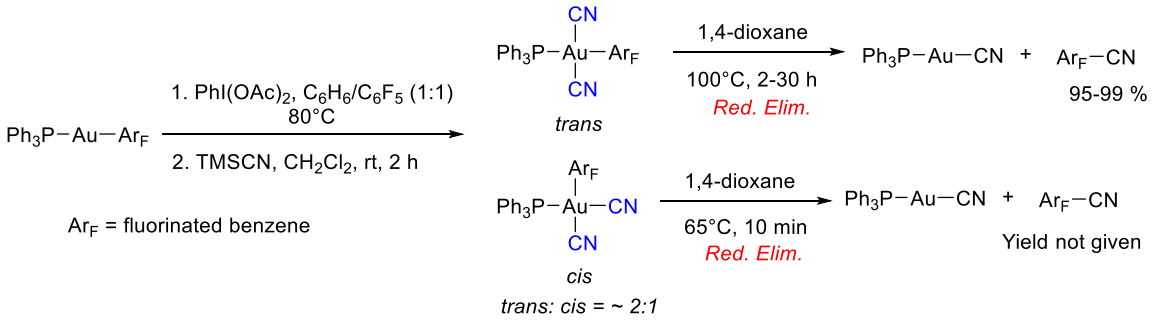

Scheme 2-9. Thermally-induced reductive elimination from phosphine-ligated dicyanoarylgold(III) complexes.[259]

2.1.2 C-N/S bond formation

The reductive elimination of Au(III) complexes can also allow the formation of carbon-heteroatom bonds. A pioneering example was depicted by Wong and coworkers[260] where associative ligand exchange occurs in the presence of cysteine as an ancillary ligand, and followed by the reductive elimination of the cyclometalated gold(III) complex to achieve a C-S bond and then a chemoselective modification of cysteine (Scheme 2-10).

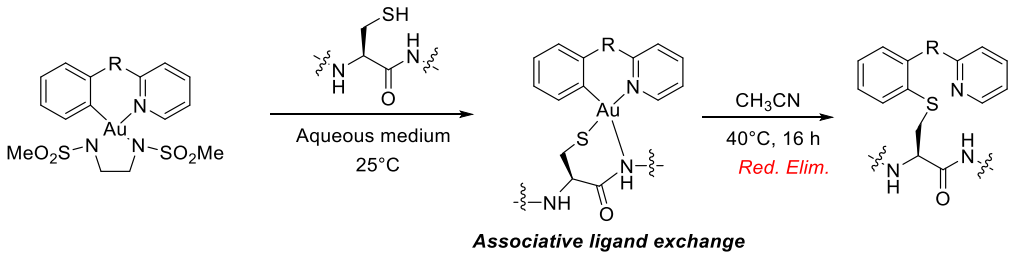

Scheme 2-10. C–S bond formation on cysteine using a cyclometalated gold(III) complex.[260]

Years later, Bochmann disclosed carbon–sulfur bond formation through the reductive elimination of gold(III) thiolates accompanied by S-H bond cleavage. [261] From a (N^C^C^) gold(III) complex, one molecule of adamantylthiol was added on the metallic center, accompanied by S-H bond cleavage. One more equivalent of thiol enabled the displacement of the N-donor to form a conformationally flexible gold(III) thiolate which undergoes facile reductive elimination (Scheme 2-11).

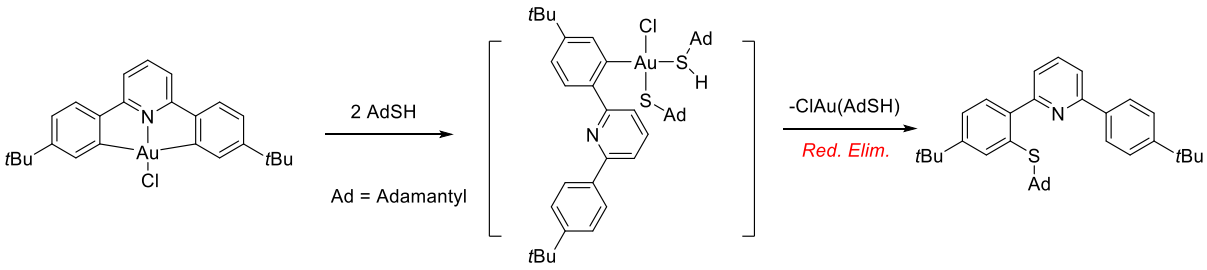

Scheme 2-11. Reductive C–S elimination pathway induced by thiols.[261]

Recently, an intramolecular C(sp^2)-N(sp^2) reductive elimination was achieved from a cationic (C,N) cyclometalated *N*-heterocarbene (NHC) gold(III) complex. The direct reductive elimination at 110°C results in the formation of a benzoylpyridinium and a stable NHC gold(I) complex (Scheme 2-12).[262]

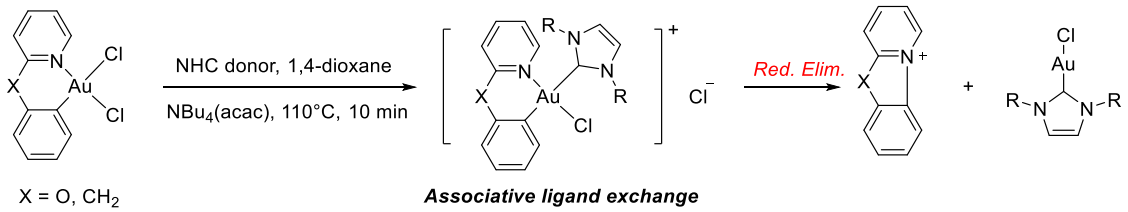

Scheme 2-12. Direct reductive elimination of cationic (C,N) cyclometalated NHC gold(III) complex.[262]

In 2017, Ribas and coworkers described the first example for an oxidant-free C–N and C–O cross coupling catalysis via a two-electron redox process.[248] The cationic (C,N,N) bis-pyridine gold(III) species was stabilized by adding pyridine as an external donor which is prone to favor a ligand exchange with *O*- or *N*-tethered nucleophiles and then forming a new gold(III) intermediate that readily undergoes a reductive

elimination (Scheme 2-13). The catalytic reactivity of aryl cycloaurated species with arylboronic acids was investigated by You and coworkers.[263] In this case, the reactive cyclometalated gold(III) species was accessible in the presence of selectfluor and underwent transmetalation and reductive elimination.

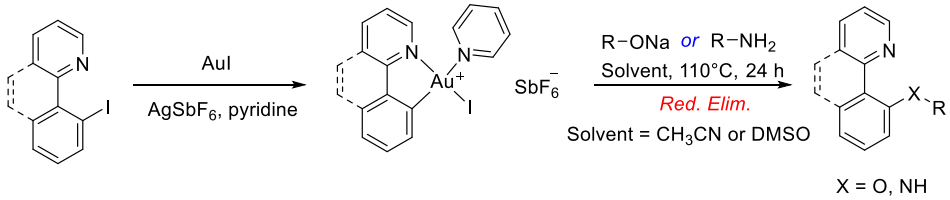

Scheme 2-13. C-N and C-O cross coupling in the presence of a cationic bis-pyridine gold(III) complex.[248]

2.1.3 Halide and halogen reductive elimination

In 2009, Nocera and co-workers reported a pioneering contribution in the dihalogen reductive elimination process leading to gold(I) complexes without any further reduction products (Scheme 2-14).[21] This controlled photoreduction was conducted on mono- and di- nuclear phosphine gold(III) complexes under 320 nm irradiation and in the presence of 2-hexene as a chemical trap. The Au–X bond cleavage was proposed to be activated through a ligand-to-metal charge transfer (LMCT) state which allowed a slow two-electron photoelimination of X_2 from each monomeric gold center.

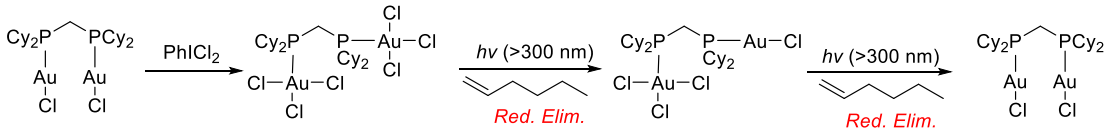

Scheme 2-14. Dihalogen photoelimination from dimeric phosphine gold(III).[21]

Two years later, Monkowius and co-workers[22] treated (NHC)AuBr with iodine or bromine to afford (IPr)$AuBrI_2$ and (IPr)$AuBr_3$ respectively. The irradiation of the obtained gold(III) complexes with UV light cleanly yielded gold(I) species (Scheme 2-15). Recently, Rosenthal and co-workers[23] described a thermally stable (IPr)$AuCl_2(C_6F_5)$ complex which undergoes photo-reductive elimination to deliver (IPr)AuCl and C_6F_5Cl upon excitation (>275 nm) in $CHCl_3$. DFT calculations support that the photoexcitation of (IPr)$AuCl_2(C_6F_5)$ produces an excited state which significantly weakens the Au-Cl bond and thus leads to the dissociation of the halide, facilitating reductive elimination (Scheme 2-15). In the same year, Bercaw and Vicente[264, 265] synthezied a series of stable gold(III) complexes[Au(CF_3)(X)(Y)(IPr)] by oxidation of the corresponding trifluoromethyl gold(I) which undergo smooth reductive elimination upon photoirradiation to generate halotrifluoromethane (Scheme 2-16).

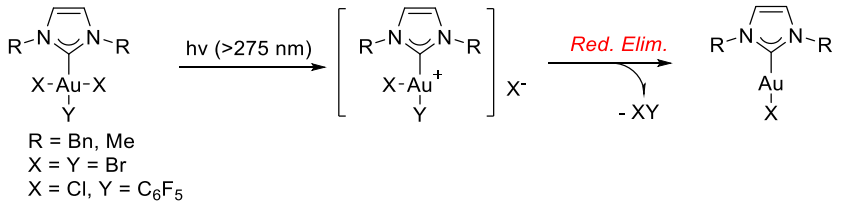

Scheme 2-15. Photoelimination of NHC gold(III) complexes.[22, 23]

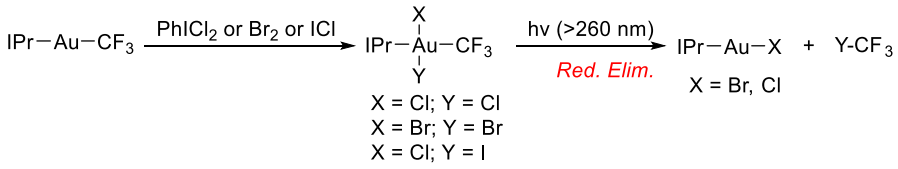

Scheme 2-16. Photoelimination of trifluoromethyl(NHC)(X_2) gold(III).[264, 265]

In conclusion, the reductive elimination of gold(III) complexes enables the formation of various carbon-carbon and carbon-hetero bonds under either thermal conditions or irradiation. However, the preparation of gold(III) complexes greatly relies on the use of strong oxidants and stoichiometric amount of gold complexes were needed. As a result, the developments of a facile oxidative addition to form gold(III) complexes and coupling reactions in the presence of catalytic gold catalyst remaining a challenge to be solved. In addition, the reductive elimination from gold(III) complexes affords the corresponding gold(I) species whose catalytic activity has not yet been evaluated. In a promising approach, the gold(III) complexes and *in situ* generated gold(I) complex are both active and expected to be used as a switch to control the selectivity of a reaction.

2.2 Photoreduction of thioether gold(III) complexes and catalysis

2.2.1 Objectives

In contrast to thermal reduction, photoinduced reductive elimination proceeds smoothly under mild condition. Generally, a ligand to metal charge transfer mechanism is involved.

In 2015, we reported a thioether gold(III) trichloride complex appended with a 9,10-diphenylanthracene (DPA) unit which undergoes a fast dihalogen reductive elimination to yield a gold(I) species under 365 nm irradiation in toluene or dichloromethane (Scheme 2-17).[7] Based on ultrafast transient absorption spectrocopy, the initial step was shown to involve intramolecular energy transfer from the anthracene chromophore to the coordinated gold species (antenna effect).

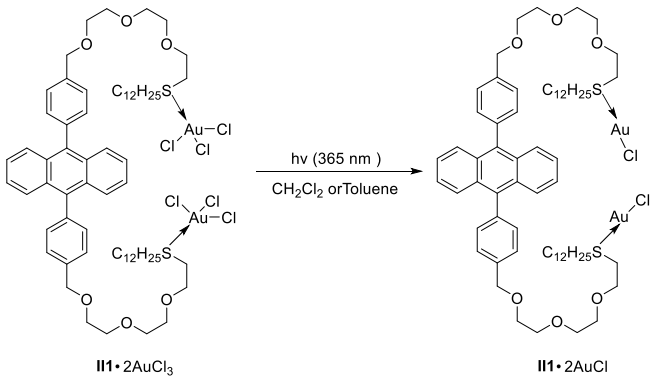

Scheme 2-17. Dihalogen photoelimination of thioether gold(III) complex.[7]

To gain an in-depth understanding of the mechanism, a series of dialkyl-thioether gold(III) trichloride complexes with or without a DPA chromophore were straightforwardly prepared through liquid-liquid extraction without any oxidation step. Our aim is to elucidate the mechanism of this Au(III) chloride photoreduction by comparing the photoreductive behavior of different dialkyl-thiether gold(III) complexes and, importantly, to evaluate the activity of gold(III) and photoreduced gold(I) species in homogeneous catalysis.

2.2.2 Materials and instruments

MilliQ purified water was used for the synthesis of the gold(III) complexes on an orbital shaker. The photoreduction was carried out in the quartz cuvette (length: 1 cm) with a stirring bar, under the irradiation of a medium pressure Xenon-Mercury lamp equipped with a monochromator at a concentration of 60 µM. The thermal reduction was carried out in a sealed glassware possessing a round flask (25 mL) and a cuvette (1 cm). $Pd(PPh_3)_4$ was prepared with a modified procedure[2] and stored in the freezer under argon atmosphere.

2.2.3 Results and discussion

2.2.3.1 Synthesis of thioether ligands

Based on our previous report,[7] the existence of lipophilic polyether group facilitates the solubility of the thioether gold(III) complex in low-polar organic solvents such as dichloromethane and toluene. The stability of the thioether gold(III) complexes may also benefit from the assistance of the polyether chain. Thus, three thioether ligands **II2-4** were designed to probe the role of the DPA chromophore and the effect of the thioether chains (Figure 2-1). Thioether ligand **II2** contains only one thioether coordination site and it was designed to

[2] An 100 mL flask equipped with stirring bar was charged with palladium chloride (355 mg, 2.0 mmol) and triphenylphosphine (2.63 g, 10.0 mmol) followed by adding dry dimethylsulfoxide (40 mL). The suspension was stirred and heated at 350 °C under air until the solution turned to transparent orange solution. Hydrazine hydrate (0.5 mL, 10 mmol) was added leading to instant yellow precipitation. The solid was filtered and washed with absolute ethanol and diethyl ether and finally dried to afford a bright yellow solid (2.2 g, 95 % yield).

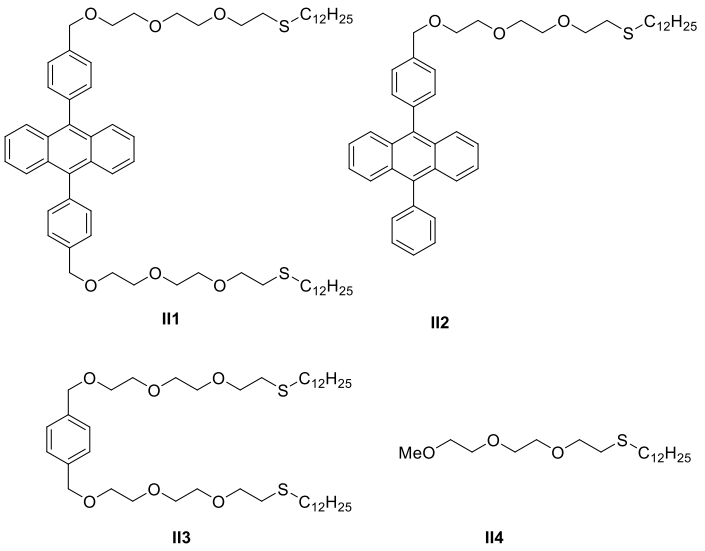

Figure 2-1. Thioether ligands designed for gold(III) complexes.

reveal the effect of gold atom number within complexes during photoreduction. Ligand **II3** (benzene connected thioether chain) and **II4** (single thioether chain) were designed to evaluate the function of chromophore upon photoirradiation. The approach for the synthesis of **II1-3** involves formation of the corresponding mesylate then followed by a SN_2 nucleophilic attack with sodium hydride as a base (Scheme 2-18). Ligand **II4** was achieved through a thiol radical addition to diethylene alcohol in the presence of 2,2-dimethoxy-2-phenylacetophenone (DMPA) as a photoinitiator (92% yield) and followed by a methylation reaction in 75 % yield (Scheme 2-19). Meanwhile, the thioether ligands with a *t*Bu substituent were also synthesized using a similar method.[3]

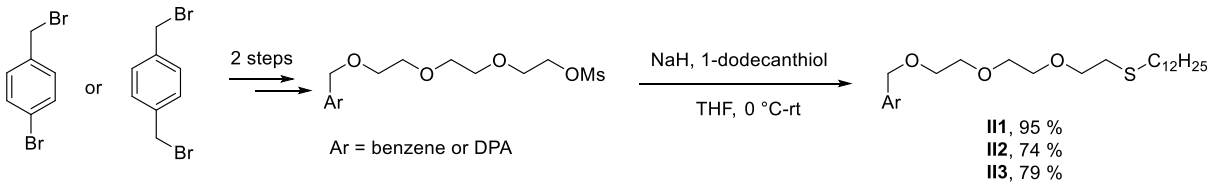

Scheme 2-18. The final step to introduce thioether moiety.

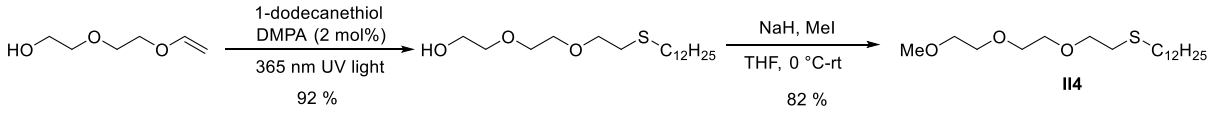

Scheme 2-19. Synthesis of ligand **II4**.

[3] The thioether ligands **II23-26** were synthesized (see Experimental Section) aiming to disclose the steric effect sulfur atom by either influent the complexation with gold or the photoreductive process. The gold complexes with ligands **II23-26** were obtained. However, UV-vis spectroscopy of the gold complexes showed an unclear gold stoichiometry (for example, less than two equivalent of gold was observed with ligand **II23**). Meanwhile, the ^{1}H NMR showed ambiguous formation of pure gold complex. Thus, we did not continue the investigation of photreductive elimination on these gold complexes.

2.2.3.2 Preparation of gold chloride complexes

The thioether gold(III) chloride complexes were synthesized via liquid-liquid extraction in the absence of light by mixing a solution of the thioether ligand in toluene and an aqueous solution of $NaAuCl_4 \cdot 2H_2O$ (5.0 equiv for ligands **II1** and **II3**; 3.0 equiv for ligands **II2** and **II4**) (Figure 2-2). The mixture was shaken for 1 to 2 hours and, after centrifugation, the gold complexes were obtained as a yellow organic solution while the free inorganic gold(III) was confined to the aqueous phase. Finally, the organic phase was collected and dried to afford the pure gold complexes. All the gold(III) complexes were characterized by ^{1}H NMR and mass spectroscopy.[4] Interestingly, the mass spectra also revealed the occurrence of reduced species and unusual ionic complexes that reflects the lability of these gold complexes under the conditions of analysis.

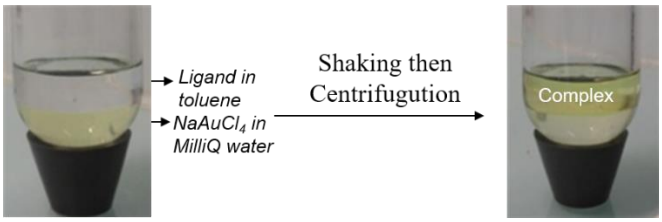

Figure 2-2. Schematic illustration of preparation of thioether gold(III) complexes.

The gold stoichiometry in the complexes was determined by comparing the absorption of the gold(III) complexes with the absorption at around 330 nm, which mainly corresponds to the main contribution of gold(III) and not the ligands.[266] Based on the absorption at 330 nm (Figure 2-3, Table 2-1), the observed gold stoichiometry in the complexes corresponds to the number of thioether ligands.

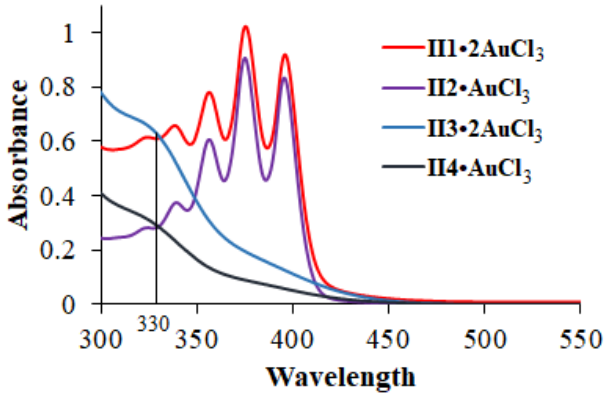

Figure 2-3. UV-Visible spectra of thioether gold(III) complexes (c = 60µM, toluene) with the main gold(III) absorption at 330 nm.

[4] For gold(III) complexes **II1**·2AuCl$_3$ and **II2**·AuCl$_3$, mass spectroscopy ananlysis performed by Field Desorption (FD) technique showed a mixture of gold(I) and gold(III) complexes under mass-detecting condition. For the complexes **II3**·2AuCl$_3$ and **II4**·AuCl$_3$, mass spectroscopy using Electrospray Ionization (ESI) showed the peaks assigned to the mass of gold complexes, [**II3**·AuCl$_2$]$^+$ and [2**II4**·Au]$^+$ respectively.

Table 2-1. Absorption of gold(III) at 330 nm in toluene with a concentration of 60 µM

Gold(III) complexes	Absorption at 330 nm
II1•2$AuCl_3$	0.609
II2•$AuCl_3$	0.285
II3•2$AuCl_3$	0.617
II4•$AuCl_3$	0.284

The stability of the gold(III) complexes under dark conditions was also examined by measuring the UV-vis spectroscopy of gold(III) complexes solution after two month.[5] Interestingly, the thioether gold(III) complexes turn out to be stable after months in the dark (Figure 2-4), except gold complex **II3**·2$AuCl_3$ whose mass analysis revealed [**II3**·$AuCl_2$]$^+$ and [**II3**·Au]$^+$ species with only one equivalent of gold remained. Since the intra/intermolecular aurophilic interaction has been known in many polynuclear gold complexes.[267, 268], This observation suggests a possible rearrangement of the gold complex **II3**·2$AuCl_3$ in the solution that the two thioether chains can be stabilized by gold-gold interaction or as an ionic form (Figure 2-5) due to the short distance, then promoting the release of one equivalent of gold.

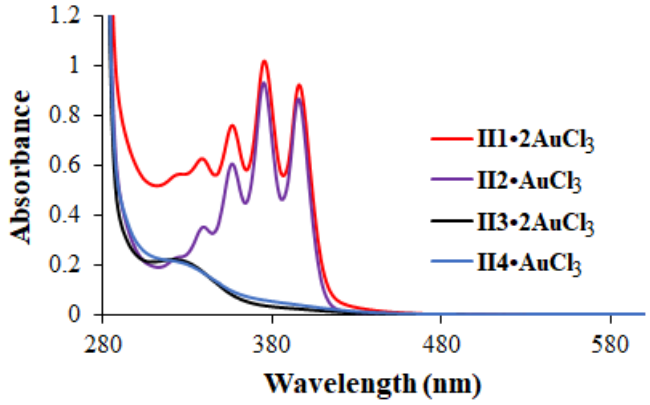

Figure 2-4. UV-vis spectra of thioether gold (III) complexes in toluene solution under dark condition at ambient temperature after two months (60 µM).

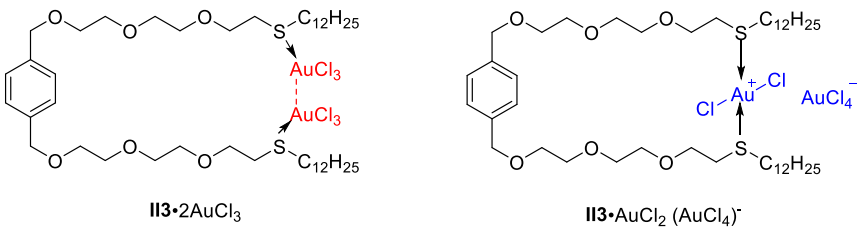

Figure 2-5. Two possible forms of gold complex **II3**·2$AuCl_3$ in the solution.

[5] The gold(III) complexes were prepared as toluene solutions with a concentration of 60 µM in 20 mL. The solutions were kept at room temperature in the dark. The same batch of the solutions was analyzed by UV-vis spectra after two months.

2.2.3.3 Photoreduction *vs* thermal reduction

The photoreduction was carried out under 365 nm irradiation using a medium pressure Xenon-Mercury lamp equipped with a monochromator and followed by UV-vis spectroscopy. A significant loss of absorption at 330 nm was observed during a period of 30 min (Figure 2-6) which indicates the reduction of gold(III) complexes into gold(I) species since gold(I) species exhibit no appreciable absorption in the region of 250-650 nm.[266]

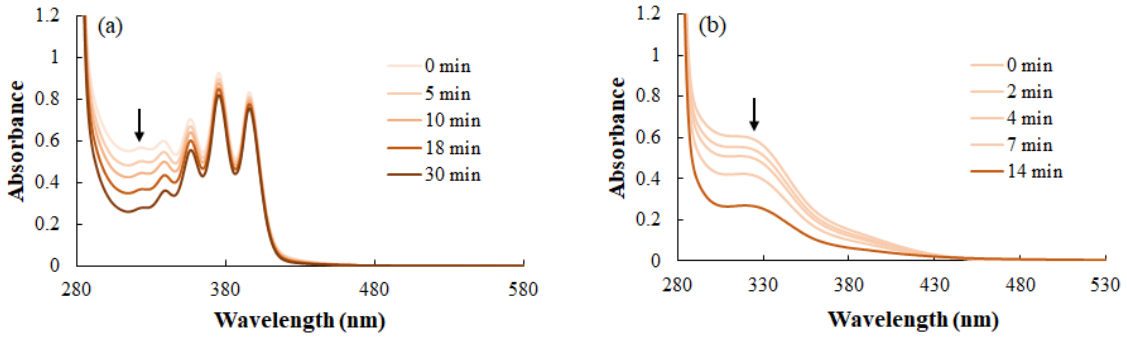

Figure 2-6. Representative photoreduction process under 365 nm with a medium pressure Xenon-Mercury lamp (60 µM, in toluene) followed by UV-vis spectroscopy (a) photoreduction of **II1**•2AuCl$_3$; (b) photoreduction of **II3**•2AuCl$_3$.

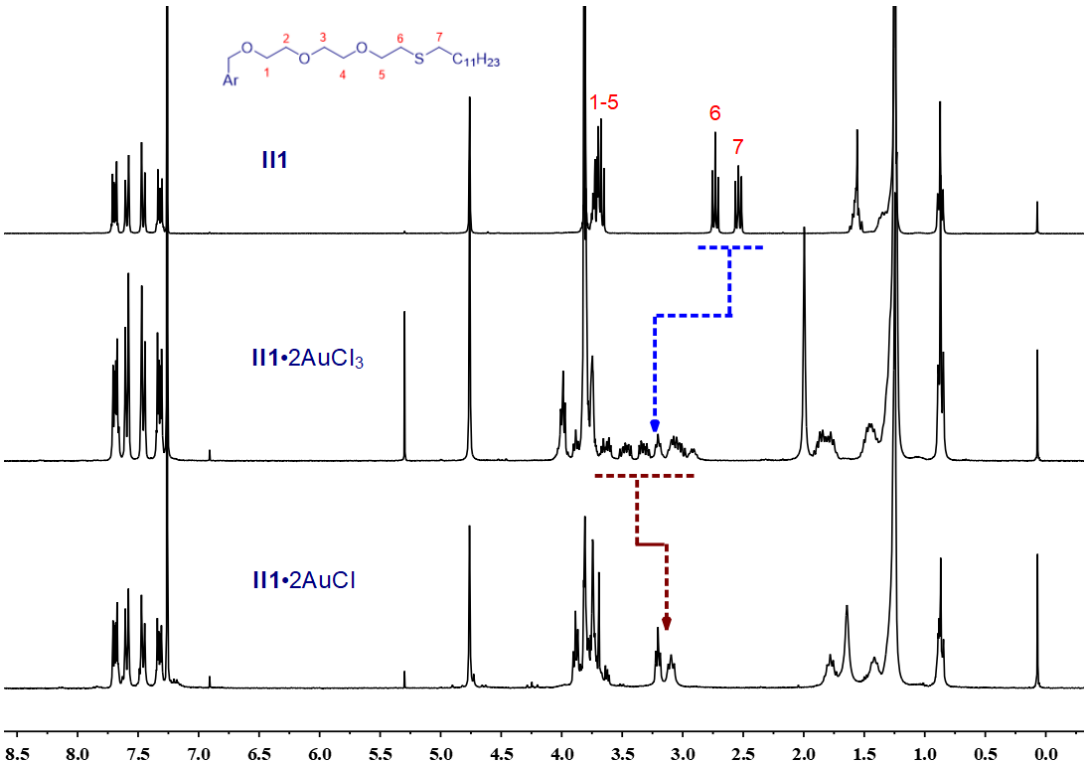

Figure 2-7. Comparison of ^{1}H NMR of ligand **II1**, gold(III) complex **II1**·2AuCl$_3$ and photoreduced **II1**·2AuCl (after purification).

The photoreduced species was further characterized by ^{1}H NMR and mass spectrometry. A representative NMR comparison between the ligand, the corresponding gold(III) complexes, and the photoreduced gold(I) species is displayed in Figure 2-7. Compared to the ligand, the protons near the sulfur atom were observed to be shifted to low-field and split into separate signals in the corresponding gold(III) complexes, suggesting a dissymetric environment. Surprisingly, these protons converged into two major peaks upon photo-irradiation which is possibly due to a more symmetric environment around the coordination site.

The analysis by mass spectroscopy of a freshly prepared gold(III) complex before and and after irradiation are shown in Figure 2-8. Taking into account the fragility of gold complexes upon this analysis (decomposition, reduction), gold(III) and gold(I) chloride complexes are identified in each independent sample. In particular, the intensity of the peaks corresponding to the gold(III) complexes is weak in the spectrum of the photoreduced sample, which further confirms the transformation of gold(III) into gold(I) species.

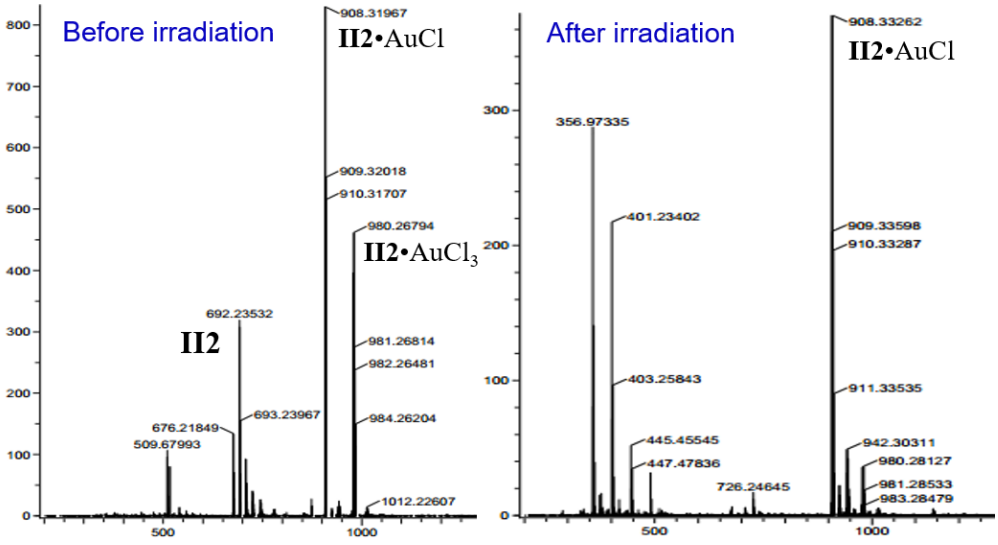

Figure 2-8. The mass spectroscopy of complex **II2**•$AuCl_3$ (before irradiation) and **II2**•AuCl (after irradiation) by FD (Field Desorption)[6]

Aside from photoreduction, the gold(III) complexes can also be reduced under thermal conditions. **II1**•2$AuCl_3$ was chosen as a model gold complex to study the thermal reduction process at a concentration of 70 µM in toluene under elevated conditions. The thermal reduction performed from 25°C to 75°C, using a gradient of 10°C with each period of 20 min and followed by UV-vis spectroscopy (Figure 2-9a). The complexes are thermally stable under 65°C as no loss of gold absorption is observed below this temperature. An absorption decrease was only observed at 75°C. To further investigate the impact of the temperature, a solution of **II1**•2$AuCl_3$ in toluene was monitored by UV/Vis spectroscopy at 80°C over a period of 12 hours

[6] The exact mass for **II2**•$AuCl_3$: HRMS (FD): m/z calculated for $C_{45}H_{56}O_3SAuCl_3$ $[M]^{+\bullet}$: 978.2681; found: 978.2698. The exact mass for **II2**•AuCl: HRMS (FD): m/z calculated for $C_{45}H_{56}O_3SAuCl$ $[M]^{+\bullet}$: 908.3304; found: 908.3326.

needed to complete the thermal reduction process. The decrease in gold(III) absorption at 330 nm is similar to that observed during photoreduction, but much slower (12 h *vs.* 30 min). The thermal reduction product was also confirmed by ^{1}H NMR and mass spectra to be similar to those of the photoreduced species obtained under 365 nm light.

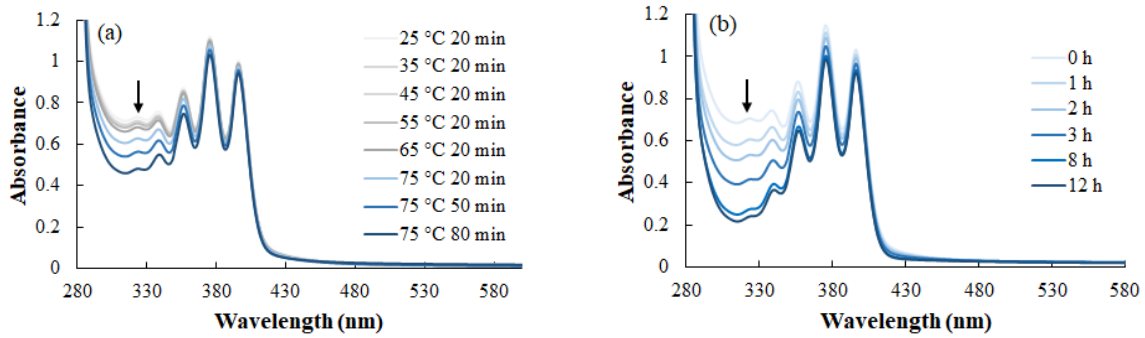

Figure 2-9. UV-vis spectroscopy monitored thermal reduction of gold complex **II1**•2$AuCl_3$ (70 µM in toluene) (a) heating by a gradient of 10°C for 20 min/period from 25°C to 75°C; (b) heating at 80 °C

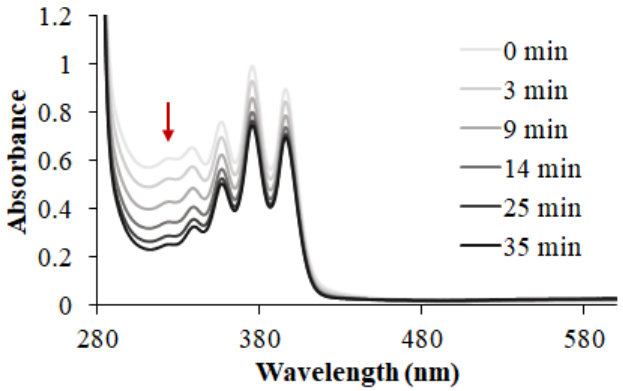

Figure 2-10. Photoreduction of **II1**•2$AuCl_3$ under indoor visible light (60 µM, in toluene).

Remarkably, solutions of the **IIn**•x$AuCl_3$ (n = 1 or 2, x = 1 or 2) complexes are stable in the dark but sensitive to ambient visible light. We found that solutions of the gold(III) complexes inside the laboratory were prone to photoreduction to gold(I) complexes exposed to daylight at rates similar to samples exposed to 365 nm irradiation as the photoreduction process can be completed in around 35 min (Figure 2-10).

Finally, the strong fluorescence emission of 9,10-diphenylanthracene is quenched in the complexes **II1**•2$AuCl_3$ and **II2**•$AuCl_3$ due to intramolecular energy transfer from the polyaromatic ligand to the gold(III) atom, as previously evidenced. The characteristic emission of anthracene is recovered after the photoreduction to the corresponding **II1**•2AuCl and **II2**•AuCl complexes, as gold(I) species do not absorb in the range of 260–600 nm (Figure 2-11 and Figure 2-12). To possibly conclude about the impact of the intramolecular energy transfer in the photoreduction process, we will investigate the kinetic aspects (see

below).

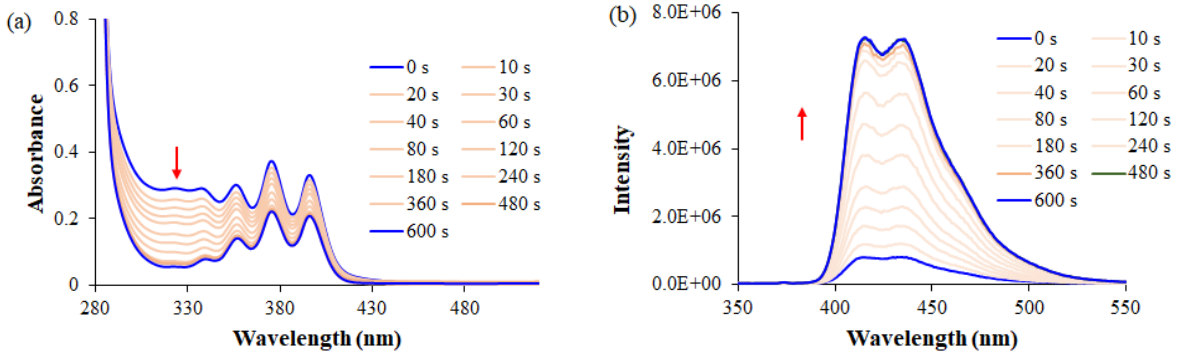

Figure 2-11. Photoreduction of **II1**•2$AuCl_3$ (30 µM, in toluene) upon irradiation under 365 nm. (a) UV-vis spectra monitoring (b) Emission spectra (λ_{ex} = 340 nm).

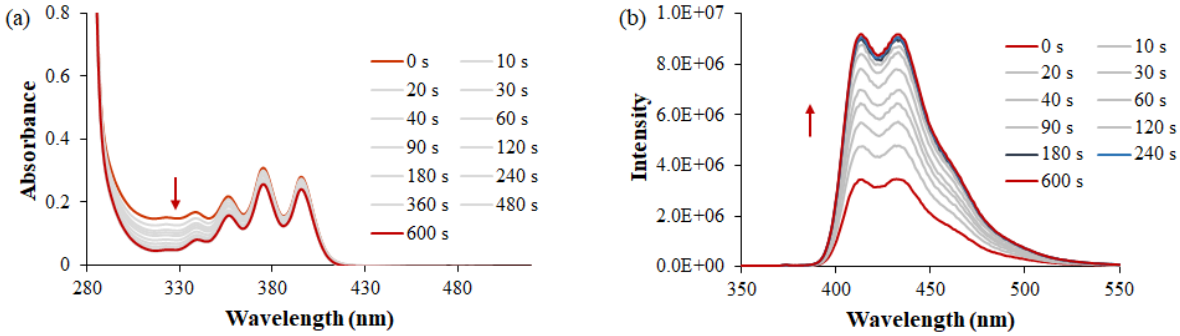

Figure 2-12. Photoreduction of **II2**•$AuCl_3$ (30 µM, in toluene) upon irradiation under 365 nm. (a) UV-vis spectra monitoring (b) Emission spectra (λ_{ex} = 340 nm).

2.2.3.4 Mechanism investigation

2.2.3.4.1 Kinetic study

Despite the intramolecular energy transfer occurs in the DPA complexes, a raised question concerns its participation to the reduction process. In order to discuss the function of chromophore during the photoreduction, the kinetics of reduction were investigated under irradiation at 365 nm or ambient daylight by monitoring the absorption of the gold(III) species with or without a DPA chromophore. For each **IIn**•x$AuCl_3$ (n = 1-4, x = 1 or 2) complex, the decrease in absorbance was fitted to a pseudo first-order relation.

$$\ln \frac{C_0}{C_t} = k_1 t \qquad \text{(equation II-1)}$$

Table 2-2. Pseudo-first-order rate constants for the photoreduction of gold(III) complexes under 365 nm irradiation and daylight [a,b]

Gold complexes	Under 365 nm	Under daylight[c]
	k^{365} (min^{-1})	$k^{daylight}$ (min^{-1})
II1•2$AuCl_3$	0.0802 (0-9 min) R^2 = 0.9987	0.0733 (0-7 min) R^2 = 0.999
II2•$AuCl_3$	0.0571 (0-9 min) R^2 = 0.9976	0.0539 (0-6 min) R^2 = 0.9955
II3•2$AuCl_3$	0.0836 (0-9 min) R^2 = 0.9982	0.079 (0-7 min) R^2 = 0.9995
II4•$AuCl_3$	0.0644 (0-6 min) R^2 = 0.999	0.0673 (0-6 min) R^2 = 0.9979

[a] All solutions of gold(III) complexes were at a 60 µM concentration in toluene and were fully photoreduced within 0-30 min. [b] The calculation of k_1 constants was fitted with the pseudo-first-order reaction equation (R^2: correlation coefficient), using absorption monitoring at 323 nm; [c] Daylight is indoor light on a sunny day without any direct sunlight irradiation.

The photoreductive kinetics of all the four gold(III) complexes over the first 10 min of irradiation were evaluated (Table 2-2), with similar rates observed upon irradiation at 365 nm (k^{365}) and under ambient daylight ($k^{daylight}$). Moreover, the reductive rate for gold complexes bearing two equivalent of gold is twice the speed of gold complexes with one equivalent gold which suggest that two gold might influent each other as the distance is sufficiently close to form binuclear gold complexes alongside the formation of short lived halide-bridged intermediates. More importantly, the complexes without chromophore exhibit a similar reductive rate that indicates the intramolecular energy transfer is not the main factor leading to photoreduction. Thus, we can conclude that the photoreduction process might directly occur on gold center, as the incident light can be absorbed by gold(III) whose absorption ranges from 280 to 430 nm.

2.2.3.4.2 Chemical trapping experiment

To explore the elimination of dichlorine, the photoreduction of **IIn**·x$AuCl_3$ (n = 1-4, x = 1 or 2) complexes (*ca.*20-30 mM in CH_2Cl_2) was conducted in the presence of cyclohexene (380 mM) as a chemical trap. The crude mixture was analyzed by GC-MS, which revealed the presence of chlorocyclohexane and 1,2-dichlorocyclohexane, as well as 2-chlorocyclohexanol (Scheme 2-20). This result suggests that Cl_2 and $Cl^{\bullet}$ are released following photo-excitation of the gold(III) complex. In presence of alkenes, the excitation of the LMCT band was shown to induce the ejection of $Cl^{\bullet}$ to give a gold(II) intermediate that was further reduced. On the contrary, the *in situ* dichlorine formation is characteristic of a non-radical reductive elimination mechanism in agreement with Kochi's proposed mechanism or a direct *cis*-elimination process.[15, 21] Therefore, both radical and non-radical photoreduction pathways appear to be operating during the reduction of the gold(III) chloride thioether complexes. Surprisingly, the GC-MS analysis of the crude photoreduced gold(III) complexes indicates that 2-chlorocyclohexanol is also formed. This compound may be generated from cyclohexene and electrophilic Cl^+ in the presence of residual water. To the best of our knowledge, this

is the first time that the cleavage of Au-Cl bond to generate $[Au^{III}]^-$ and Cl^+ was indirectly observed through a chemical trap.

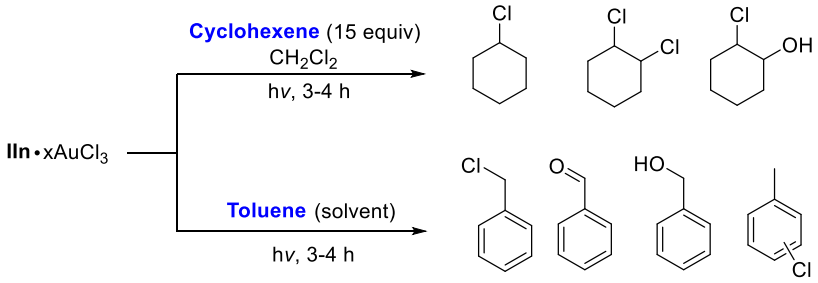

Scheme 2-20. Photoreduction (365 nm irradiation) of gold(III) chloride complexes in the presence of cyclohexene as chemical trap in CH_2Cl_2 or directly in toluene.

A second experiment of photoreduction was conducted in toluene in the absence of cyclohexene. The analysis of the crude irradiated gold(III) chloride complexes revealed the presence of benzaldehyde and chlorinated toluene, *i.e*. benzyl chloride and *ortho*- and *para*- chlorotoluene (Scheme 2-20). These products may be obtained from toluene through oxidation by Cl_2 (PhCHO), radical substitution by radical $Cl^{\bullet}$ ($PhCH_2Cl$) and electrophilic substitution by Cl^+ ($Cl\text{-}C_6H_4\text{-}CH_3$). The formation of the chloronium ion is unexpected, although supported by the formation of both 2-chlorocyclohexanol and *o*,*p*-chlorotoluene. The chloronium ion may arise from an ionic pathway that is a complementary to the mechanism initially proposed by Kochi. This ionic pathway would imply the formation of a chloronium cation and a tricoordinated gold(III) $[\mathbf{IIn}\cdot xAuCl_2]^-$ species. The reactive Cl^+ would then react with toluene to form *o*- and *p*- chlorotoluene. If the chloronium is not captured by toluene, then $[\mathbf{IIn}\bullet xAuCl_2]^-$ can undergo a reductive elimination of Cl_2 followed by a recombination with Cl^+ to lead to the expected **IIn**•xAuCl complex.

Based on the kinetic study and the outcome of chemical trapping experiments, we conclude that the Au-Cl bond is photo-excited and two possible mechanism pathways might co-exist (Figure 2-13). One is a stepwise radical pathway, where a chlorine radical is released from the gold(III) to generate a gold(II) intermediate, and then further reduced to gold(I) by releasing one more chlorine radical. Another is related to an ionic

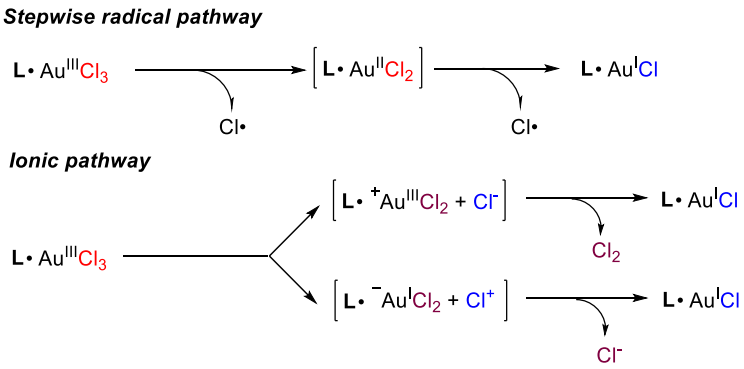

Figure 2-13. Plausible radical and ionic pathways for the photoreduction of thioether gold(III) complexes.

pathway: after the Au-Cl bond cleavage leading to the release of a chloride or a chloronium, the possible tri-coordinate cationic gold(III) with positive or negative charge readily undergo *cis*-elimination to generate gold(I) by releasing chlorine and followed by recombination of the chloride or the chloronium.

2.2.3.5 Homogeneous gold catalysis

The catalytic properties of the thioether-based complexes of $AuCl_3$ and AuCl (obtained by *in situ* photoreduction) were investigated as homogeneous catalysts in two model reactions.

2.2.3.5.1 Gold precatalyst *vs* cationic gold catalyst

In a first example, the cyclization of *N*-propargylic amides developed by Hashmi was chosen as a model reaction[269] as it gives two different isomers depending on the nature of the catalyst. Aromatic oxazoles (compounds **II8-10**) were isolated in the presence of gold precatalyst, due to a 5-exo-dig cyclization followed by a step of isomerization. Meanwhile, in the presence of a cationic gold(I) catalyst, the product of a 5-exo-dig cyclization leading to dihydrooxazole (compounds **II11-13**) was instead observed. Our study was focused on three different propargylic amides appended with aliphatic (**II5**), electron rich thiophene (**II6**) and phenyl (**II7**) substituents (Table 2-3). The catalytic activities of gold(III) chloride **II*n*·*x***$AuCl_3$ (*n* = 1-4, *x* = 1 or 2), the corresponding gold(I) chloride **II*n*·*x***AuCl obtained by *in situ* photoreduction at 365 nm and the cationic **II*n***·x$AuNTf_2$ complexes (obtained from the latter **II*n*·*x***AuCl in the presence of $AgNTf_2$) were compared to PPh_3AuNTf_2, an efficient gold(I) phosphine complex for homogeneous catalysis.

Amides **II5–7** were converted to the aromatic 2,5-disubstituted oxazoles **II8-10** using either the gold(III) chloride catalysts (85–99% conv.) or the gold(I) chloride catalysts (80–99% conv.) in a similar fashion as $AuCl_3$. To the best of our knowledge, this is the first report showing that complexes of AuCl can also catalyze this transformation. As expected, dihydrooxazoles **II11-13** were obtained by employing cationic **II*n*·*x***$AuNTf_2$ complexes (79–96% conv.) or commercially available PPh_3AuNTf_2 (94–96% conv.) through a 5-exo-dig cyclization without further isomerization. The model cyclization of *N*-propargylic amides can thus be readily controlled by employing **II*n*·*x***$AuCl_3$ and **II*n*·*x***AuCl gold chloride catalysts or cationic gold(I) catalyst, **II*n*•*x***$AuNTf_2$. It is interesting to note that the gold(I) chloride obtained under daylight and thermal reduction less efficient catalysts that the species obtained by irradiation at 365 nm (Table 2-3, entry 2 *vs*. 3 and 4, 80-92 % *vs*. 40-67 % and 77-80 %). A representative example for the different catalytic process using gold precatalyst and cationic gold catalyst toward the cyclization of thiolphenyl substituted is illustrated using ^{1}H NMR (Figure 2-14 and figure 2-15).

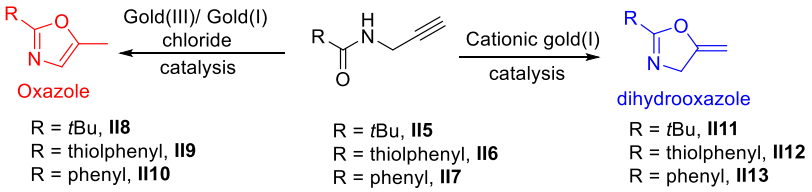

Table 2-3. Catalytic activity of gold(III) chlorides and gold(I) catalysts obtained by photoreduction.

Substrate	Entry[a]	Catalyst	Product (Conv. %)[b]
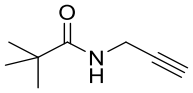 **II5**	1	gold(III) chloride	85-90, **II8**
	2	gold(I) chloride[c]	80-92, **II8**
	3	gold(I) chloride (daylight)[d]	77-80, **II8**
	4	gold(I) chloride (thermal reduction)[e]	40-67, **II8**
	5	gold(I) chloride/$AgNTf_2$[f]	85-93, **II11**
	6	PPh_3AuNTf_2[g]	95, **II11**
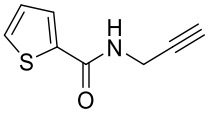 **II6**	7	gold(III) chloride	86-99, **II9**
	8	gold(I) chloride[c]	96-99, **II9**
	9	gold(I) chloride/$AgNTf_2$[f]	91-96, **II12**
	10	PPh_3AuNTf_2[g]	94, **II12**
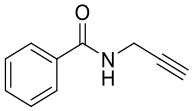 **II7**	11	gold(III) chloride	95-99, **II10**
	12	gold(I) chloride[c]	90-99, **II10**
	13	gold(I) chloride/$AgNTf_2$[f]	79-95, **II13**
	14	PPh_3AuNTf_2[g]	96, **II13**

[a] Unless specified, all the reactions were carried out in an NMR tube ($CDCl_3$) without stirring, using an amide substrate (0.11 mmol), **IIn**·x$AuCl_3$ or **IIn**·xAuCl (obtained through a TLC lamp irradiation at 365 nm) as a catalyst (n = 1–4, x = 1–2; 2 mol% loading), at room temperature in the dark. Reactions were monitored by ^{1}H NMR for 24-30 h until full conversion was reached; [b] Determined by ^{1}H NMR; [c] Obtained through photo-irradiation at 365 nm; [d] Obtained by photoreduction under ambient daylight. [e] Obtained by thermal reduction. [f] Prepared by mixing gold(I) chloride complex and $AgNTf_2$ for 1h. [g] Reaction performed in a 10 mL vial with stirring.

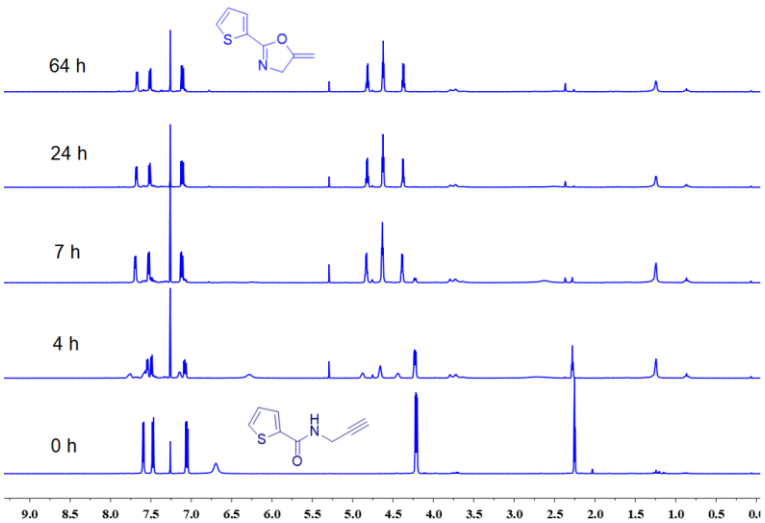

Figure 2-14. Catalyzed by **II1**•2AuCl (2.4 µmol, 2 mol%) and $AgNTf_2$ with substrate (0.12 mol).

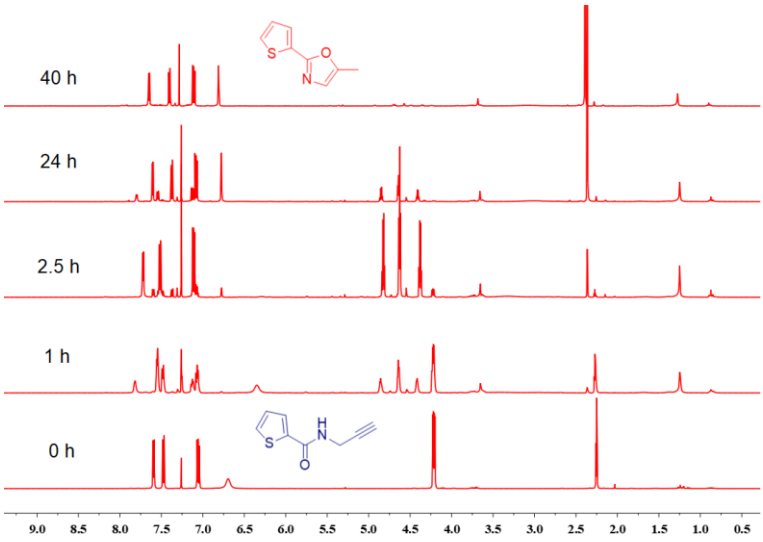

Figure 2-15. Catalyzed by **II3**•2$AuCl_3$ (2.4 µmol, 2 mol%) with substrate (0.12 mol)

Concerning the mechanism of the cyclization of propargylic amides in the presence of gold precatalyst or the cationic gold catalyst, it is proposed that the Lewis acid activity of the catalytic species is involved. The alkyne or the corresponding allene can be activated by gold to form a vinyl gold species. In the presence of a cationic gold catalyst, the vinyl gold intermediate undergoes a proto-metallation to deliver the 5-exo-dig cyclization product without isomerization. Using a gold(I) chloride precatalyst, the 5-exo-dig cyclization intermediate further proceeds through isomerization to form the aromatic oxazole (Figure 2-16).

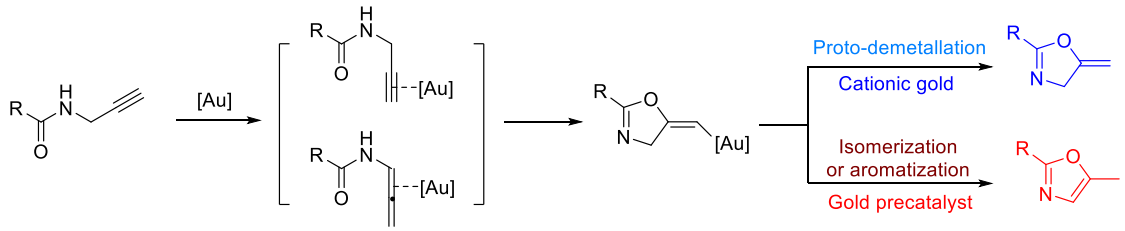

Figure 2-16. Proposed mechanism for gold precatalyst and cationic gold catalyzed cyclization of *N*-propargylic amides.

2.2.3.5.2 One pot cascade reaction

In order to demonstrate that thioether gold(III) complex and the corresponding photoreduced gold(I) chloride obtained by irradiation at 365 nm are efficient gold chloride and cationic gold catalysts, their Lewis acid activity is evaluated in a one-pot two steps reaction that plays on the sequential reactivity of mono- and di-substituted alkynes to access complex heteropolyaromtaic compounds.The one pot reaction constitutes two sequential chemoselective cyclizations that are catalyzed by different gold species: the monosubstituted alkyne is first activated by the gold(III) chloride catalyst, whereas the disubstituted alkyne reacts in the presence of cationic gold(I). Step 1 is a 6-*exo*-dig cyclization followed by an isomerization leading to the

new β-carbolinone **II19**. A similar electrophilic activation of monoalkynes by gold(III) was described by A. Padwa using $AuCl_3$.[270] Step 2 is a novel 6-*endo*-dig cyclization towards indolino-4*H*-benzoquinolizin-4-one **II20**, inspired by the synthesis of a related regioisomer.[271] Straightforward routes to *4H*-quinolizin-4-ones are rare and mainly based on Pd or Rh catalysis.[272, 273] Herein, we propose a cascade strategy towards model compound **II20** that can be attained using gold catalysts at different oxidation states: either gold(III) or gold(I) that is obtained from photoreduction of the corresponding gold(III) complex. Based on our experience in the cyclization of *N*-proparylamide, a more sophisticated amide **II18** possessing both an *N*-propargyl amide and an *N*-diphenylacetylene group was designed and synthesized in four steps with an overall yield of 37 % (Scheme 2-21).

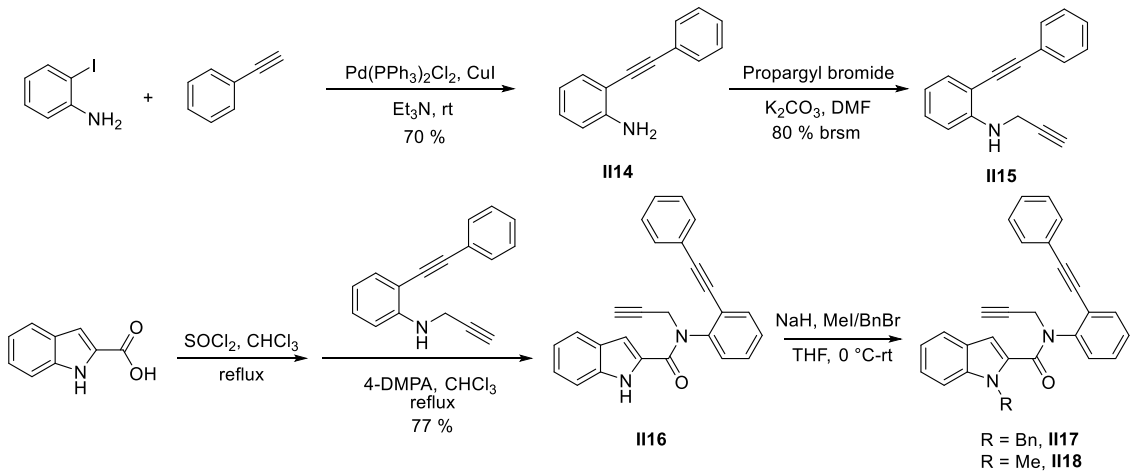

Scheme 2-21. Synthesis of indole-based *N*-propargyl amide.

Initially, the reaction was tested using $AuCl_3$ as a catalyst (Table 2-4, entry 1). Several products were observed by TLC but the expected cyclization product was not detected. The smooth transformation of amide **II18** to **II19** (step 1) was seen when thioether gold(III) chlorides **II*n***·*x*$AuCl_3$ (*n* = 1–4, Table 2-4, entries 2–5, 90–95% yield) were used. Notably, indole **II19** can be obtained with 99% conversion within 5 h in the presence of **II1**·2$AuCl_3$ and this product was isolated in 93 % yield (Table 2-4, entry 2). As noticed for the catalyzed cyclization of propargylic amides, the synthesis of indole-pyridone **II19** is catalyzed by thioether complexes with gold(III) chloride or gold(I) chloride.

To catalyze the second cyclization and obtain the desired quinolizin-4-one 10 (step 2), the higher activity of a cationic gold species is required. The classical cationic gold(I) species obtained from **IIn**·xAuCl complexes in the presence of silver salts were firstly evaluated with success (Table 2-4, entries 6-7). The sequential cyclization product **II20** can be obtained in excellent yield (71–80 %, entries 7–8) by tuning the Au(I) catalyst over the two sequential steps: gold(I) chloride complex was used in the first step (99% conv.) whereas, in the second step, the corresponding cationic gold(I) complex was *in situ* generated by the addition of AgOTf in

the reaction medium. Along step 2, the role of silver triflate was shown to be restricted to chloride exchange, as no catalytic activity was detected in step 2 (Table 2-4, entry 8) for AgOTf alone. Commercial dimethylsulfide gold(I) and silver salt also showed good yield to deliver the cascade cyclization product (79 %, Table 2-4, entry 9). We then decided to try an alternative catalytic system composed of **II*n***·*x*$AuCl_3$ complexes in the presence of silver salts in the absence or presence of irradiation along step 2. This system should be composed of cationic gold(III) species and possibly traces of cationic gold(I). The catalytic effect of gold(III) chloride complexes (**II1**·2$AuCl_3$ and **II2**·$AuCl_3$) alone for the first step and in the presence of a silver triflate for the second step, allowed the synthesis of compound **II20** in excellent yield (72–76 %, entries 10–11). It should be noted that several gold(III) active species can exist and no data was available concerning their nature under these homogeneous reaction conditions. We also cannot exclude the occurrence of gold(I) traces (through undesired photoreduction) that might participate in the final cyclization.

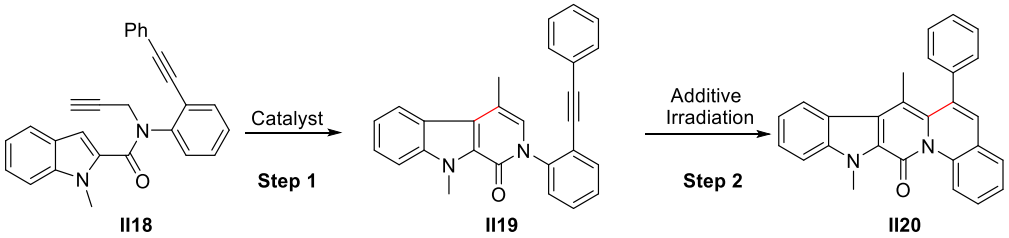

II18 II19 II20

Table 2-4. Condition study for one pot reaction

Entry[a]	Catalyst	Time 1	Conv. 6[b]	Irradiation[c]	Additive	Product[d]
1	$AuCl_3$	16 h	-[e]	-	-	-
2	**II1**•2$AuCl_3$	5 h (48 h)	Full	-	-	93 %, **II19**
3	**II2**•$AuCl_3$	12 h	Full	-	-	90 %, **II19**
4	**II3**•2$AuCl_3$	12 h	Full	-	-	95 %, **II19**
5	**II4**•$AuCl_3$	12 h	Full	-	-	92 %, **II19**
6	**II1**•2AuCl[f]	16 h	Full	-	AgOTf	80 %, **II20**
7	**II2**•AuCl[f]	16 h	Full	-	AgOTf	71 %, **II20**
8	AgOTf	16 h	-	-	-	n. d.[g]
9	$AuCl(SMe)_2$	16 h	Full	-	AgOTf	79 %, **II20**
10	**II1**•2$AuCl_3$	16 h	-	-	AgOTf	76 %, **II20**
11	**II2**•$AuCl_3$	16 h	-	-	AgOTf	72 %, **II20**
12	**II1**•2$AuCl_3$	12 h	Full	Yes	AgOTf	83 %, **II20**
13	**II2**•$AuCl_3$	12 h	Full	Yes	AgOTf	72 %, **II20**
14	**II3**•2$AuCl_3$	12 h	Full	Yes	AgOTf	80 %, **II20**
15	**II4**•$AuCl_3$	12 h	Full	Yes	AgOTf	73 %, **II20**

[a] Unless specified, all the reactions were performed in dry dichloromethane at ambient temperature and in the dark in the presence of a catalyst (2 mol%), amide **II18** (0.1 mmol), and, when necessary, AgOTf (6 mol%) was added after the completion of step 1; [b] Monitored by TLC; [c] TLC lamp (6 W), irradiation for 2 h; [d] Isolated yield; [e] Compound **II19** was not detected by TLC; [f] Freshly prepared through irradiation of the corresponding gold(III) complex at 365 nm. [g] n.d.=not detetected.

To better investigate the possible effect of *in situ* reduction of gold(III) into gold(I), we proceed to the final cyclization product using gold(III) chloride complexes, in the presence of AgOTf and under 365-nm irradiation (entries 12–15). Compound **II20** was isolated in excellent yields (72–82 %) that are similar to those determined in the dark. The catalytic system composed of AgOTf and complexes based on thioether ligands **II3-4** and gold(III) chloride are efficient gold species for the cyclization of disubstituted alkynes, with a performance similar to that of cationic gold(I) catalysts.

2.2.4 Conclusion

Homogeneous gold(III) complexes with well-defined stoichiometry are readily obtained by liquid-liquid extraction using dialkylthioether ligands. The complexes are stable in the dark for months. Independently of the ligand nature (anthracene, phenyl, alkyl), all the gold(III) chloride complexes are rapidly photoreduced to the corresponding gold(I) chloride complexes using 365-nm irradiation. The course of this photoreduction was more rapid (30 min) than the thermal reduction at 80°C (12h). The photoreduction under a conventional TLC lamp (365 nm) also induced the formation of gold(I) showing a higher catalytic activity than those obtained by daylight exposure or heating.

Under the conditions explored, we found no acceleration or reduction of photoreduction ascribable to the presence of the diphenylanthracene chromophore. The photoreductive elimination of X_2 seems to occur under 365 nm or daylight irradiation as evidenced by the formation of chlorinated organic by-products observed in toluene. In the case of the dialkyl thioether gold complexes, the reductive elimination might be triggered through a direct excitation on the gold center, possibly accompanied with the formation of a chloronium ion. The catalytic properties of the gold complexes at different oxidation states were evaluated in the cyclization reactions of alkynes under homogeneous reaction conditions for single and sequential double cyclization. All gold(III) chloride and *in situ* generated gold(I) chloride complexes showed excellent efficiency (high yield, reasonable reaction times). The corresponding cationic gold(I) complexes obtained in the presence of AgOTf were also active. Interestingly, the catalytic system composed of the gold(III) chloride catalyst and AgOTf (in the dark) showed a similar activity to classical cationic gold(I) catalysts. The complexes of thioethers and $AuCl_3$ are therefore highly versatile complexes with the possibility to prepare and tailor their catalytic activity by using light to control the oxidation state and silver salts to modify the coordination sphere of the gold center.

2.3 Solvent and light induced reduction of picolinic gold(III) complex[7]

2.3.1 Objectives

The dichloro(2-pyridinecarboxylato)gold(III) complex ($PicAuCl_2$) is a highly stable gold(III) precatalyst[24] and readily dissolved in organic solvents. It has been widely employed in numerous reactions in terms of alkyne or allene activation for nucleophilic attack.[29, 274-276] We anticipated to be able to obtain a cationic gold(I) directly from this gold(III) precatalyst through photoreduction and further explore the reactivity of both species as catalysis.

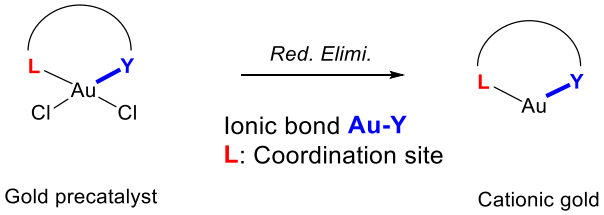

Figure 2-17.Transformation of gold(III) catalyst to cationic gold(I) through reductive elimination.

Based on the results obtained for the thioether gold(III) complexes, the Au-Cl bond can be photoactivated to generate a radical or by forming a tri-coordinated ionic gold center. Apart from photoreduction, the formation of the cationic gold(III) intermediate by introducing a stronger coordinated ligand[248, 262] through associative ligand exchange is also an efficient approach to realize reductive elimination. To the best of our knowledge, it has not yet been documented that the associative ligand exchange induced by polar solvent. Hence, the reduction of $PicAuCl_2$ under light irradiation was examined in various solvents (for example, CH_2Cl_2, acetone, DMSO, MeOH, toluene) and monitored by UV-vis spectroscopy. The absorption shift or the loss of gold absorbance indicates the formation of new gold species. Based on the radical and ionic mechanism, the photoreduced product might be a pyridinium or an ionic gold(I) species. The exploration of photoreduction and determination of the photoreduced species is still in progress.

2.3.2 Results and discussion

2.3.2.1 Solvent effect on dichloro(2-pyridinecarboxylato) gold(III) complex

Toluene and dichloromethane were generally employed as solvents for gold catalytic process. However, few reports discussed the solvent effect on gold catalysis. In 1990, Vicente described a C,N gold(III) complex[257]

[7] To prove that the reduction of $PicAuCl_2$ complex can be induced by light irradiation or coordination property of polar solvent, the photoreduction or solvent induced reduction of pyridine $AuCl_3$ complex should also be examined for two factors: 1) a coordinating solvent such as DMSO can modify the structure of the gold complex by either with chloride or pyridine; 2) the pyridine $AuCl_3$ complex is reported as a highly stable gold(III) complex which is stable under visible light or thermal conditions. So, the reduction would only be triggered by the external factors such as 365 nm light or polar solvents.

was able to activate acetone and form a new gold(III) species. The strong solvent effect on the gold complex $PicAuCl_2$ was observed through the chemical shift of the aromatic protons in deuterated solvents (Figure 2-18) which indicates a solvent interaction with gold complex. The exact chemical shift comparison is given in the table 2-5. Excluding the solvent coordination effect in less polar solvents (CD_2Cl_2), the coordination sphere of the complex might be affected in a polar solvent such as DMSO-d_6.

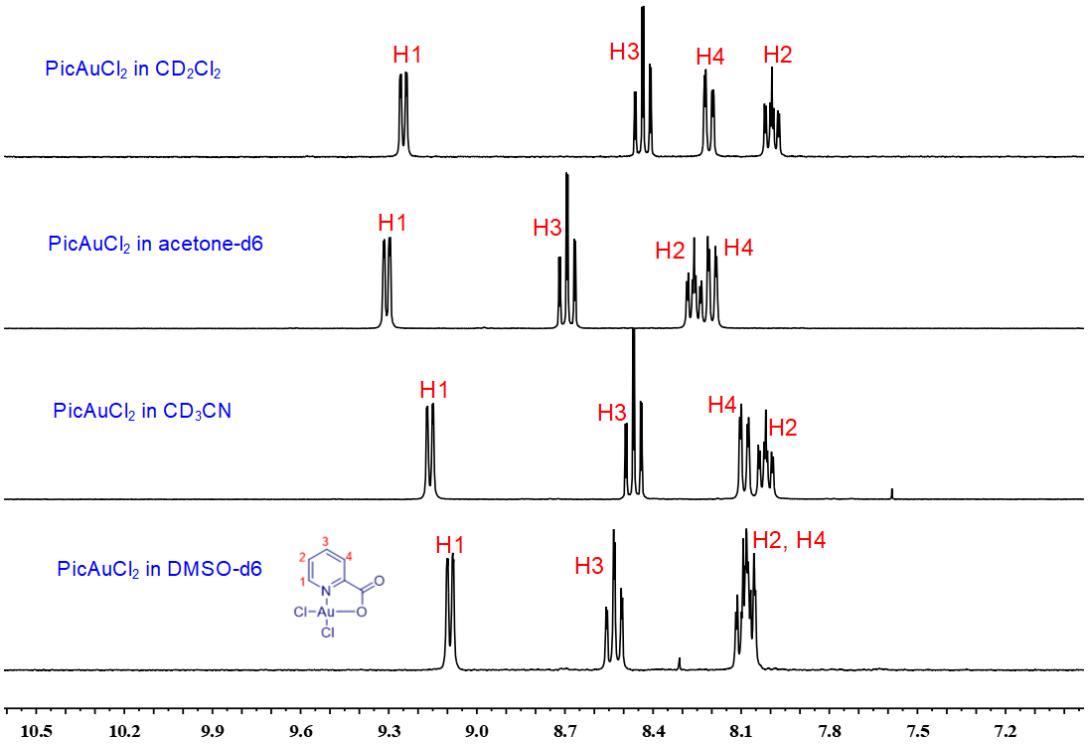

Figure 2-18. ^1H NMR (300 MHz) of $PicAuCl_2$ in various deuterated solvents.

Table 2-5. Chemical shift comparison.

Proton atoms	Gold complex ($PicAuCl_2$) in various deuterated solvents			
	In CD_2Cl_2	In DMSO-d_6	In acetone-d_6	In CD_3CN
H1	9.25; dq	9.09; dq	9.31; dq	9.16; dq
H3	8.43; td	8.53; td	8.69; td	8.46; td
H2	7.99; sept	8.05-8.11; m	8.26; sept	8.02; sept
H4	8.21; dd		8.20; dd	8.09; dd

2.3.2.2 Thermal stability of $PicAuCl_2$

Generally, gold(III) complexes are able to be reduced to gold(I) at elevated temperatures. Thus, thermal reduction was examined in toluene under a temperature gradient and followed by UV-vis spectroscopy (Figure 2-19). The outcome suggests that the $PicAuCl_2$ gold complex is stable at least until 100°C[8] as no

[8] To test the thermal stability, temperature can be elevated up to 150°C by using 1,1,2,2-tetrachloroethane as solvent.

gold absorption loss or shift was observed.

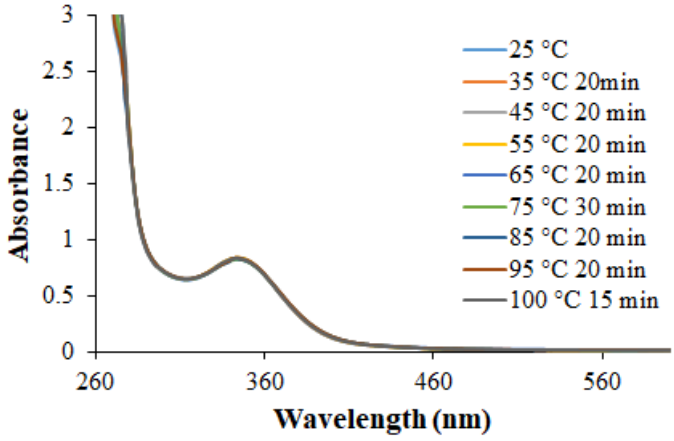

Figure 2-19. Stability of $PicAuCl_2$ under thermal conditions (490 µM, in toluene) as followed by UV-Vis spectroscopy.

2.3.2.3 Light induced reduction of $PicAuCl_2$

In view of the strong solvent effect observed in the $PicAuCl_2$ complex (Figure 2-18), the photoreduction process was investigated in polar solvents (DMSO and MeOH) and less polar solvents (CH_2Cl_2 and THF). With DMSO as the solvent, the reduction of $PicAuCl_2$ under 365 nm light irradiation leads to a significant loss of gold absorption over a period of 1 hour (Figure 2-20a). The reduction process was also monitored in methanol under the same conditions (Figure 2-20b). In contrast to toluene, a partially decrease of the gold absorption was observed accompanied by a small blue shifted, which implies a new gold species is formed. This phenomenon was then followed by a rapid absorption decrease which could be related to the gold reduction. Similarly to the experience in methanol, the photoreduction proceeds smoothly in THF with a decline of the gold absorption (Figure 2-21b). In these three cases, the successive decreases of the gold absorption during irradiation can be characteristic of the formation of gold(I) species.

To gain an in-depth understanding of the photoreduction, the reduction process in dichloromethane was carried out. An obvious absorption shift from 350 nm to 320 nm occurs over 30 min and then a subsequent decrease of the gold absorption was observed (Figure 2-21a), which indicates two different steps. Over the first 30 min, a new gold species were formed that still absorb, i.e. possibly a different gold(III) species or eventually gold(II) ones obtained through the loss of a radical chlorine. After 30 min of irradiation, the absoprtion decrease could reveal a reduction into gold(I) that does not absorb.

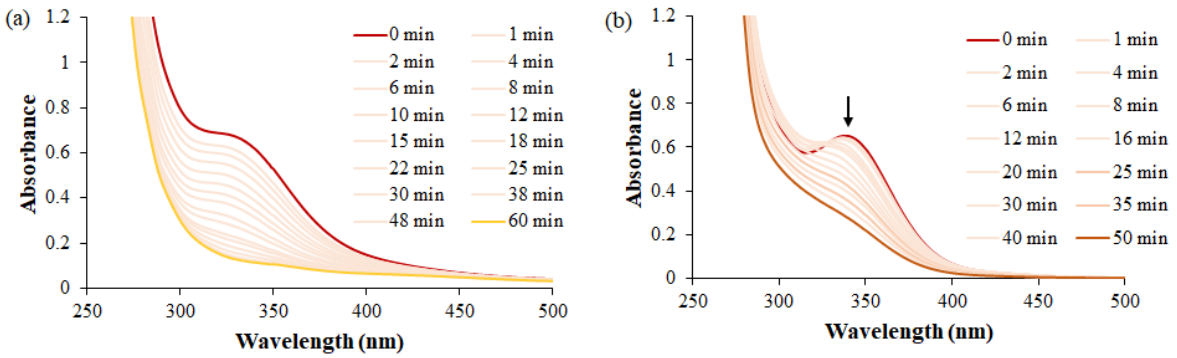

Figure 2-20. UV-vis spectra monitored photoreduction of $PicAuCl_2$ (490 µM) in polar solvents under 365 nm UV lamp. (a) in dry DMSO (b) in dry MeOH.

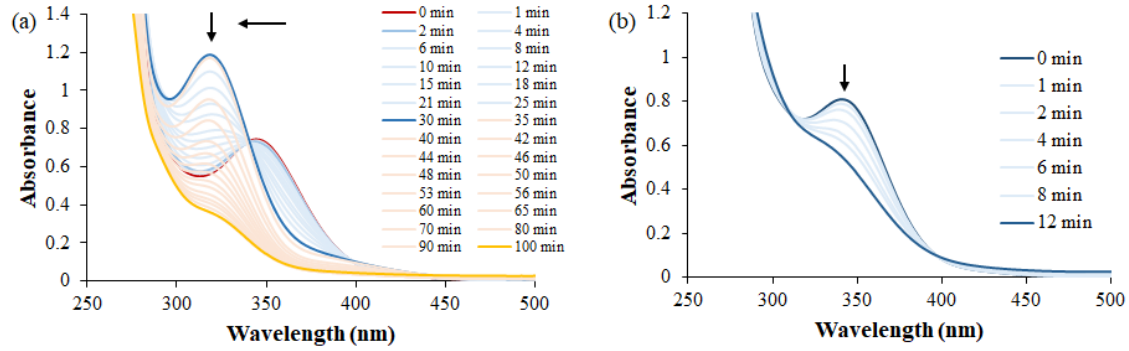

Figure 2-21. UV-vis spectra monitored photoreduction of $PicAuCl_2$ (490 µM) in less polar solvents under 365 nm UV lamp. (a) in dry dichloromethane; (b) in dry THF

In order to identify the photoreduction products, the reduction process was initially monitored by ^1H NMR spectroscopy using a 365 nm irradiation[9] at a complex concentration of 28 mM in DMSO-d_6 (Figure 2-23). After irradiation over 2h, the spectrum of $PicAuCl_2$ was converted to a new gold species and the three sets of protons were all shifted. Notably, the presence of water showed no impact on the photoreduction process as the same experiment conducted in the presence of 3 equivalents of water leads to the identical species. The irradiation at 365 nm of a solution of $PicAuCl_2$ complex in dichloromethane led to the same species observed after irradiation in DMSO.

In contrast, the $PicAuCl_2$ complex is stable in CD_2Cl_2 under visible light. This result is also different from the observation for the thioether gold(III) complexes, leading to the formation of new gold(I) species under a 365 nm photoirradiation (Figure 2-24).

[9] TLC lamp (6 W) was used for 365 nm light source.

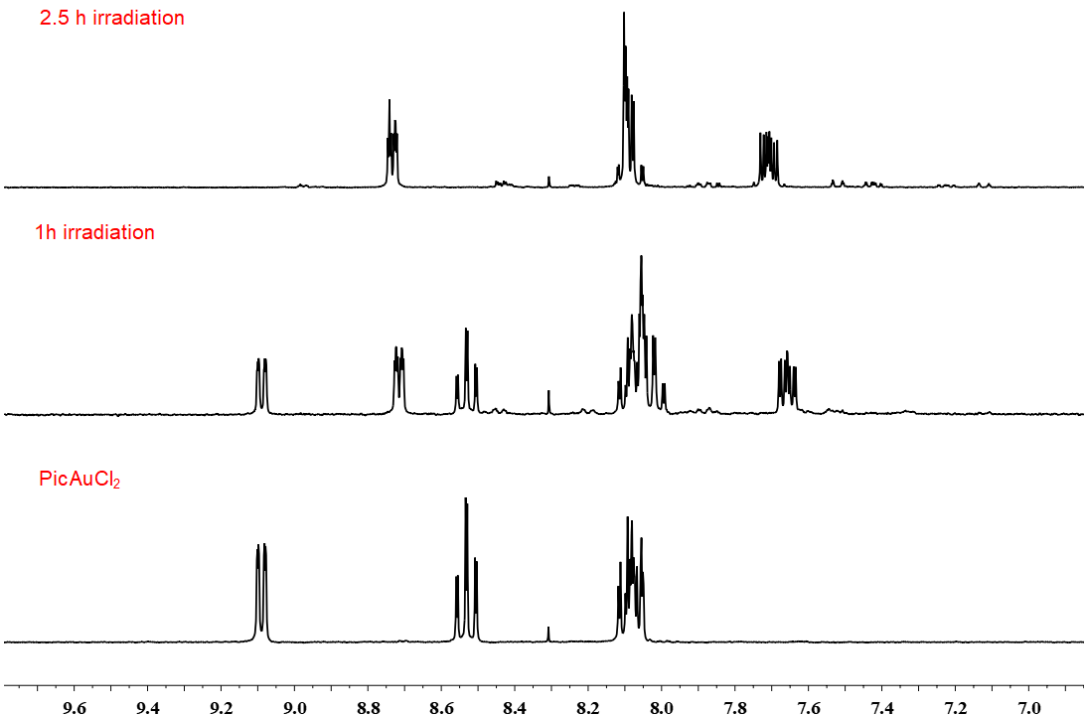

Figure 2-22. Monitoring the photoreduction of $PicAuCl_2$ (6.6 mg, 1.7 mmol, 28.2 mM) by ^1H NMR in DMSO-d_6 (0.6 mL) under 365 nm.

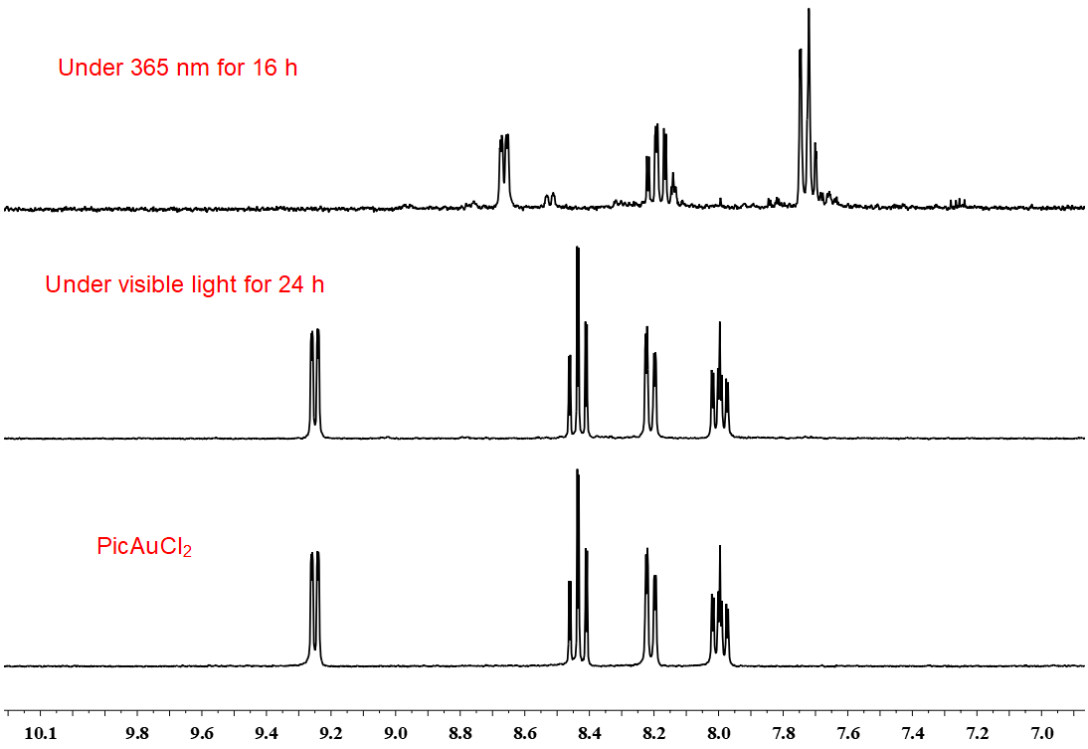

Figure 2-23. Monitoring photoreduction of $PicAuCl_2$ (3.0 mg, 7.7 µmol, 12.8 mM) by ^1H NMR in CD_2Cl_2 (0.6 mL) under indoor daylight and 365 nm irradiation (TLC lamp).

2.3.2.4 Solvent induced reduction of $PicAuCl_2$

Generally, the reduction of gold(III) complexes to gold(I) complexes can be achieved under either photochemical or thermal conditions. To the best of my knowledge, no report was documented that this reduc-

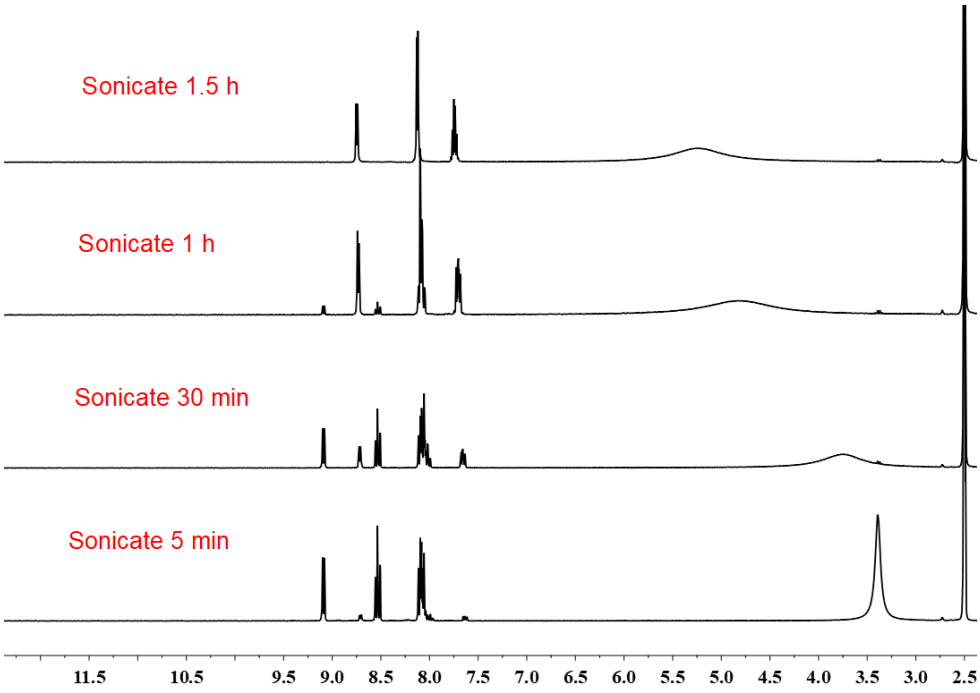

Figure 2-24. Monitoring photoreduction of $PicAuCl_2$ (3 mg, 7.7 µmol, 12.8 mM) by ^1H NMR in DMSO-d_6 (0.6 mL) under sonication condition.

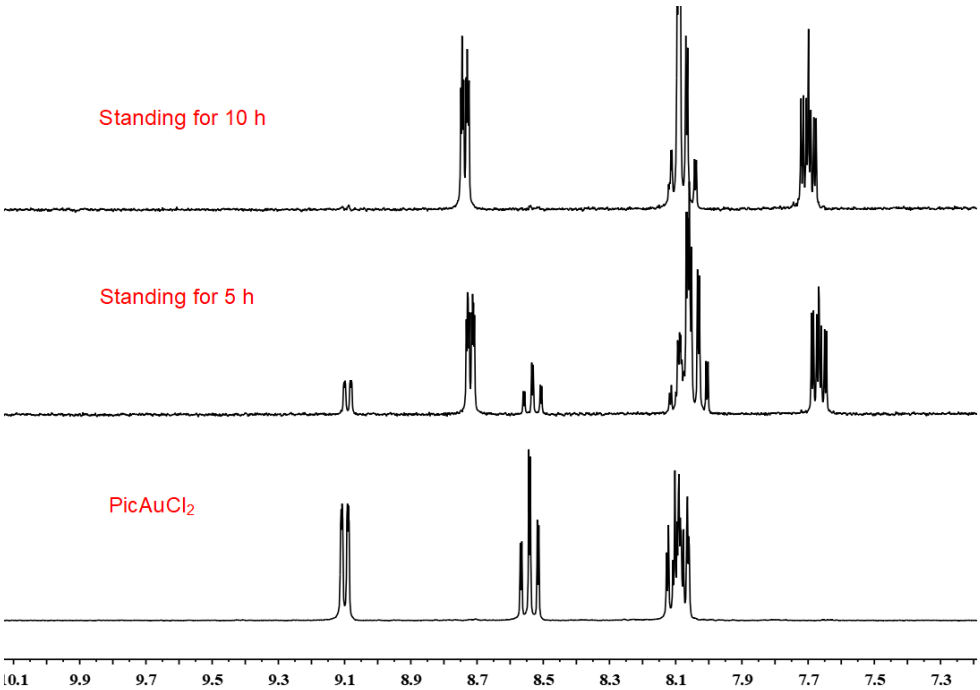

Figure 2-25. Monitoring photoreduction of $PicAuCl_2$ (3 mg, 7.7 µmol, 12.8 mM) by ^1H NMR in DMSO-d_6 (0.6 mL) standing in the dark.

tive elimination process can be realized in the absence of light or heat. A strong solvent effect was observed in dimethylsulfoxide for complex $PicAuCl_2$ which undergoes a rapid reduction (1.5 h). Without light and heating, the strong donor property of dimethylsulfoxide was attributed to be the main factor for the reduction. Under sonication condition, the ligand exchange with chloride was accelerated and led to the formation of a cationic gold(III) which is readily to undergo elimination and generate a new gold species, the process was evidenced by ^{1}H NMR (Figure 2-25). Surprisingly, the reduction process occurs even in a standing solution of $PicAuCl_2$ under dark condition without any treatment. In contrast to sonication condition, a longer period (10 h) was taken to achieve the full conversion (Figure 2-26). Moreover, a new gold species also appeared in methanol solution in the dark condition over 48 h with 40 % conversion. Based on the above results, an associative ligand exchange could be involved during the course of reduction.

A full comparison of the reduced species in DMSO-d_6 was provided for a better vision (Figure 2-27). Based on the NMR spectra, the $PicAuCl_2$ complex can be reduced to gold(I) species either by light irradiation or solvent coordination effect. However, difference between the reduced species still exist as the proton NMR are not entirely superposed. For the reduction speed in dimethylsulfoxide, a shortest time (1.5 h) was found under sonication condition, while the photoreduction under 365 nm takes 2.5 h to reach the full conversion and standing in dimethylsulfoxide solution without any treatment, a longer period (10 h) is required. The ^{1}H NMR and ^{13}C NMR of the picolinic ligand, $PicAuCl_2$ complex, and reduced species were detailed respectively (Table 2-6 and Table 2-7).

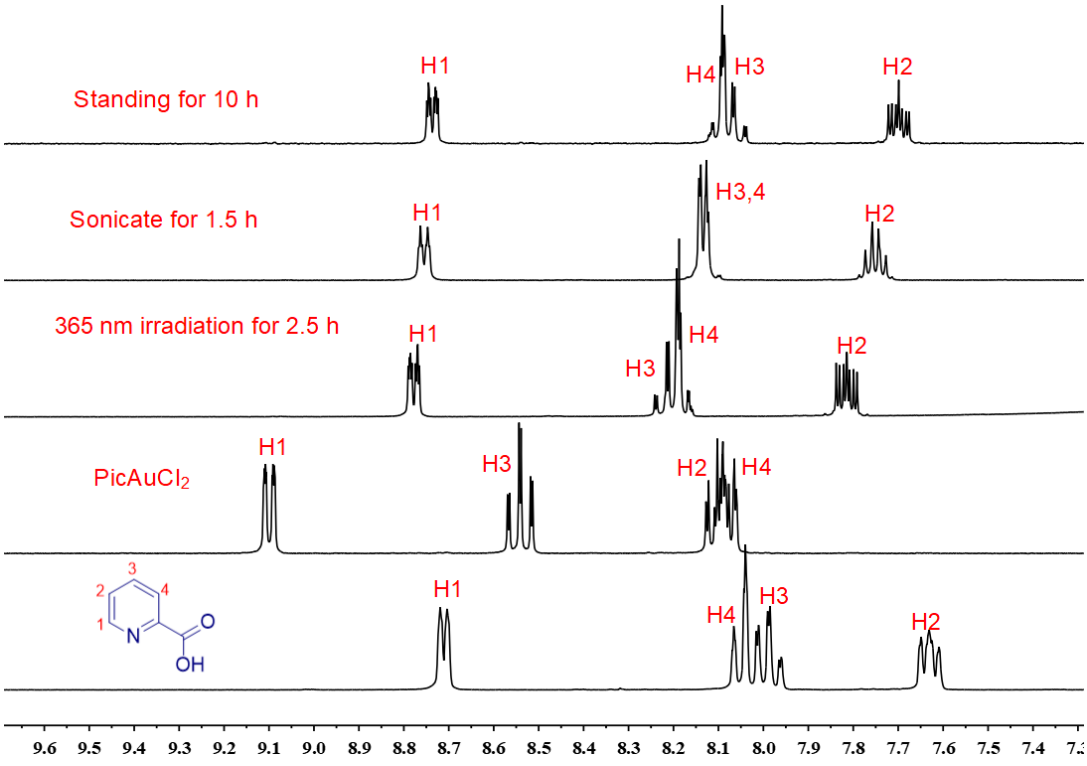

Figure 2-26. Overview of ^{1}H NMR for reduced species in DMSO-d_6 through various methods.

Table 2-6. Chemical shift comparison for $PicAuCl_2$ complex in ^1H NMR spectra.

Atoms	Ligand	Complex	After irradiation	After sonication	Standing
H1	8.70; dq	9.09; dq	8.76; dq	8.74; dq	8.72; dq
H2	7.60-7.64; dq	8.06-8.11; dq	7.77-7.82; dq	7.70-7.77; sept	7.64-7.69; dq
H3	7.95-8.00; td	8.50-8.56; td	8.174-8.178; d	8.08-8.16; m	8.00-8.11; m
H4	8.02-8.06; td	8.05-8.08; dq	8.15-8.22; dq		

The attribution of the proton based on 2D *g* cosy and HMQC spectra.

Table 2-7. Chemical shift comparison for $PicAuCl_2$ complex in ^{13}C NMR spectra.

Atoms	Ligand	Complex	After irradiation	After sonication	Standing
C1	149.4	144.6	147.7	148.2	149.0
C2	127.0	131.2	127.9	127.6	128.0
C3	137.5	145.1	140.2	139.3	139.3
C4	124.6	129.8	125.3	125.1	125.5
C5	148.3	147.2	146.3	146.9	147.7
C6	166.1	171.1	164.6	165.1	165.9

The attribution of the carbon based on the 2D NMR HMQC and gcosy spectra.

2.3.2.5 Plausible mechanism

Based on the observed results and the well-established mechanism of reductive elimination, two possible pathways exist: a concerted pathway through associative ligand exchange and a stepwise radical pathway by generating a gold(II) intermediate. For the reduction process in DMSO, the pyridine ligand is replaced by dimethylsufoxide to form a four coordination gold(III) intermediate with *cis* and *trans* conformations and, subsequently, proceeds by *cis*- reductive elimination by releasing chlorine and delivering an ionic gold(I) species (Figure 2-27). The generation of ionic gold(I) might explain the poor solubility of this photoreduced species in less polar solvents.

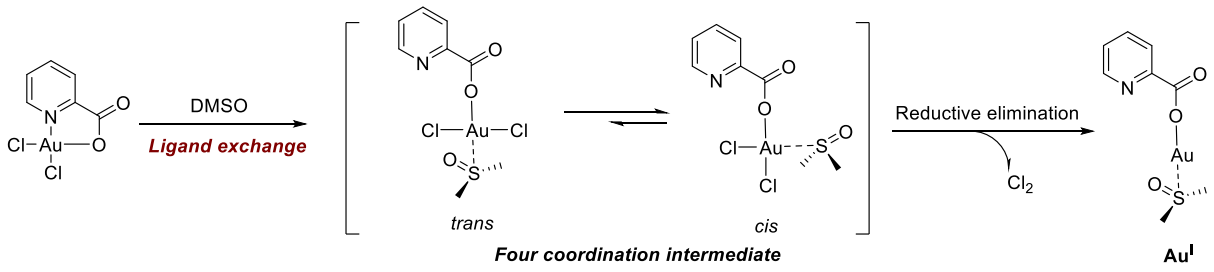

Figure 2-27. Plausible pathway for DMSO induced reduction of $PicAuCl_2$.

Both Au-Cl bond and Au-O bond in $PicAuCl_2$ complex can be photo-activated upon light irradiation. Two possible pathway might be implicated in the photoreduction of $PicAuCl_2$ in dichloromethane. In one, the Au-Cl bond is activated, releasing a chlorine radical to form a gold(II) species which is further reduced into gold(I) (Figure 2-28a). A different possibility is activation of the Au-O bond leading to a unstable tri-coordinated gold(III) that undergo a rapid reductive elimination to generate gold(I) (Figure 2-28b). This is

consistent to the photoreduced species detected which might be gold(II) species or a new gold(III) species based on the UV-vis spectra (Figure 2-21a).

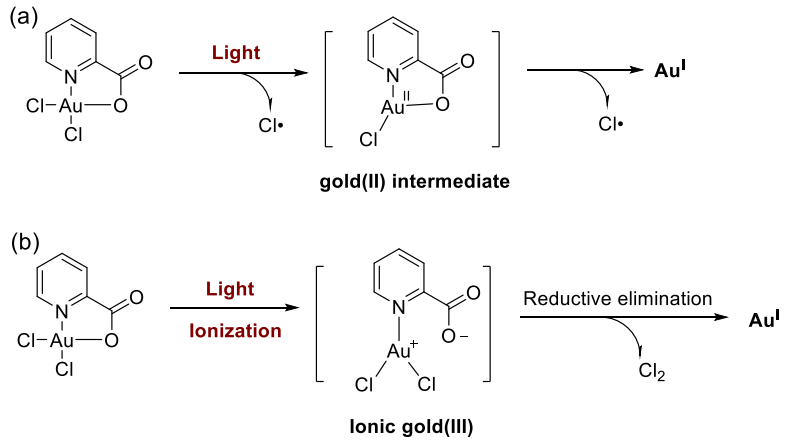

Figure 2-28. Plausible radical pathway and ionic pathway for the photoreduction of $PicAuCl_2$ in CH_2Cl_2.

2.3.4 Conclusion and perspectives

The dichloro(2-pyridinecarboxylato)gold(III) complex ($PicAuCl_2$) is a thermally stable gold(III) precatalyst that exhibit excellent efficiency in terms of alkyne or allene activation towards nucleophilic attack. A strong solvent effect was observed in the $PicAuCl_2$ complex as the proton NMR showed large differences in polar and less polar solvents. The $PicAuCl_2$ complex is stable under visible light but sensitive to 365 nm UV irradiation. The photoreduction behavior of $PicAuCl_2$ was examined in various solvents (including polar and less polar solvent), and a relative loss of gold absorption was observed which indicates gold(I) species was generated. Interestingly, the reduction processes of the $PicAuCl_2$ complex are able to proceed in the absence of light and heating which, to our best knowledge, is the first example of a solvent-induced reductive elimination in a gold(III) complex. The mechanisms for solvent-induced reduction and photoreduction were proposed. Concerning solvents with electron donor properties such as DMSO, the ligand exchange was involved to form a four-coordinate gold(III) intermediate, while a radical pathway or ionic pathway might occur during photoreduction.

In order gain an in-depth understanding of the reduction process induced by light irradiation or by electron donor polar solvents, the photoreduction or solvent induced reduction of pyridine $AuCl_3$ complex should also be examined for two factors: 1) a coordinating solvent such as DMSO can modify the structure of the gold complex by either with chloride or pyridine; 2) the pyridine $AuCl_3$ complex is reported as a highly stable gold(III) complex which is stable under visible light or thermal conditions. So, the reduction would only be triggered by the external factors such as 365 nm light or polar solvents.

2.4 Chapter summary

During the last decade, novel gold(III) complexes were developed which readily undergo reductive elimination processes under thermal conditions. Reductive elimination in gold(III) complexes which leads to new carbon-carbon or carbon-heteroatom bonds formation. However, many people neglect the fact that reductive elimination of gold(III) halides is also an approach to adjust the oxidation state of gold and both of them can be applied as homogeneous catalysts in a controlled way.

We have developed thioether ligands with polyether group which can stabilize the formation of thioether gold(III) complexes. The photoreduction of these gold(III) complexes into gold(I) complexes was achieved under visible light or 365 nm UV light even though they are thermally stable to 65°C.

For the photoreduction of thioether gold(III) complexes, three points are needed to be pointed out:

First, this work is complementary to the halogen photo-elimination in gold(III) halide complexes, as the photoreductions in phosphine gold(III) chloride complexes in the presence of chlorine chemical trap (slow process) and *N*-heterocyclic carbene gold(III) bromide complex in methanol have been reported.[21, 22]

Second, a richer mechanism of photoreductive elimination was proposed to account for kinetics in the presence or absence of the chromophore. In addition to classic routes, an ionic pathway involving one-negative-charge gold(III) anion is proposed as a chloronium was trapped by toluene or cyclohexene.

Third, this is the first time that the *in situ* photoreduced gold(I) complex was evaluated as homogeneous catalysis and illustrated in a one pot cascade cyclization reaction.

No catalytic difference was found between the thioether gold(III) complexes and the photoreduced gold(I) complexes. In order to *in situ* prepare cationic gold(I) complexes by photoreduction, a $PicAuCl_2$ precatalyst was submitted to photoreduction. Interestingly, we observed that the reduction processes are able to proceed in DMSO in the absence of light and heating, which is the first example that solvent-induced reductive elimination in gold(III) complex. A mechanism were proposed based on these results. Chemical trapping experimentS and the determination of final reduced gold species are necessary to further elucidate the detailed mechanism.

Si nous attribuons les phénomènes inexpliqués au hasard,
ce n'est que par des lacunes de notre connaissance.

French astronomer and mathematician
Pierre Simon de Laplace (1749-1827)

Chapter 3

3 Heterogeneous gold catalysis with supported silica nano-objects

3.1 Heterogeneous gold catalyst

Immobilization of metal nanoparticles and metallic complexes onto a solid support has attracted considerable attention in synthetic chemistry in the last four decades, 1965 masked the discovery of the very first heterogeneous catalyst containing gold, which was developed by the German company Knapsack as a catalyst for the oxidative acetoxylation of ethylene to vinyl acetate.[277] Compared to homogeneous conditions, the recyclability and reusability of the supported catalysts potentially provide waste-reducing, cost-saving and greener processes. In the field of heterogeneous gold chemistry, the vast research efforts towards greener catalysts have focused on gold nanoparticles (NPs) supported on metal oxides (TiO_2, Al_2O_3, CeO_2 etc.),[278, 279] or polymer resins.[32-35] These supported AuNPs have been implemented in various types of reactions: low-temperature oxidation of carbon monoxide,[280] selective oxidation of alcohols[281, 282] or nitro compounds,[283] or the hydration of alkynes,[284] the isomerization of ω-alkynylfuran to phenols,[285] cross-coupling reactions,[286] and even in industrial applications such as the oxidative esterification of methacrolein to methyl methacrylate and the hydrochlorination of acetylene.[287]

In the recent decade, supported gold(I) complexes were also employed as heterogenized catalysts to diversify the nature of transformations. To date, numerous solid supports have been used for gold complexes, such as organic polymers, silica nanoparticles and magnetic nanoparticles. We became interested in silica nano-helices as chiral silica supports for gold(I) complexes for two reasons: (i) to benefit from the the grafting of metallic complexes chromophores on chiral silica to form a chiroptical 3D ensemble. This new property for an immobilized gold catalysis can allow its monitoring along successive catalytic processes; (ii) to evaluate the asymmetric induction for such a chiral system.

Here, a background of various supported heterogeneous gold(I) catalysts in organic transformations is presented.

3.1.1 Polymer supported heterogeneous gold(I) catalysis

In 2011, Akai and coworkers[36] reported a polystyrene(**PS**)-bound cationic triphenylphosphinegold(I) which is reusable and active in the cyclization of propargyl amide, as well as the spiro-cyclization of methyl 2-acetylhept-6-ynoate, and the intramolecular cyclization reaction to furans via alkyne activation (Figure 3-1). The particle size of 100-200 mesh for the polymer resin was found to be the most effective when it comes to coordination or catalytic activity. The cylization of alkynol compound into furan product was evaluated by using such immobilized catalyst (0.5 mol%) for 8 cycles without losing yield (2-7 h, 94-99 %).

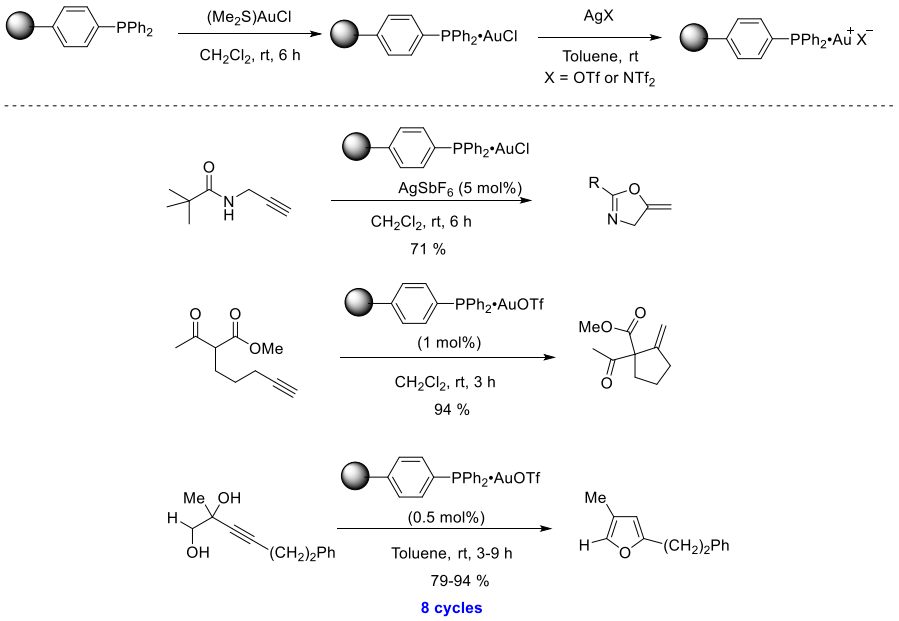

Figure 3-1. Intramolecular cyclization reactions using the ***PS***-immobilized cationic gold(I) catalysts.[36]

Almost simultaneously, a divinylbenzene (DBV) cross-linked polystyrene-supported stable cationic (benzotriazole)(triphenylphosphine)gold(I) was described as a robust catalyst in three model reactions,[37] including the tandem 3,3-rearrangement and Nazarov reaction of an enynyl acetate, the cyclization of a 1,6-enyne, and the rearrangement of an alkyne-furan (Figure 3-2). However, a considerable prolongation of reaction time was found after each cycle which might be attributed to the aggregation of the polymer and the degradation of the cationic gold catalyst. Four years later, the same group described an immobilized cationic phosphine gold complex for the cyclization of 1,6-enyne to the endocyclic product.[39]

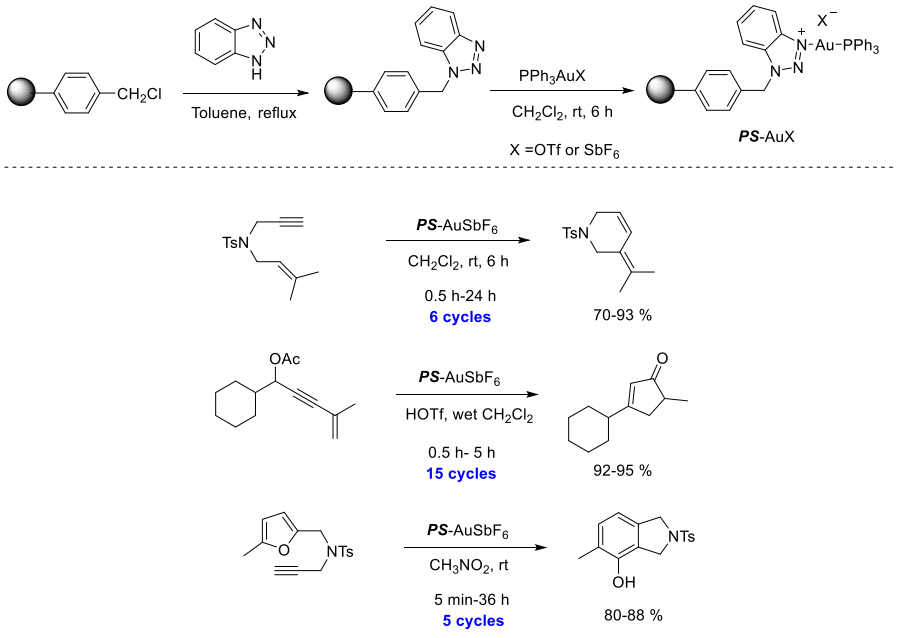

Figure 3-2. Cyclization reactions using the ***PS***-immobilized cationic gold(I) catalysts.[37]

In the same year, Echavarren's group developed an air stable electron-rich cationic gold(I) complex $[Au(tmbn)_2]SbF_6$ with 2,4,6-trimethoxybenzonitrile (tmbn). The corresponding supported phosphine gold complexes **PS**n-P (Figure 3-3, n = 1-3) were readily prepared by coordination of the cationic gold(I) complex to the phosphine functionalized polystyrenes (Figure 3-3). The triphenylphosphine complex **PS3**-PAu exhibited excellent reactivity and recyclability in the cyclization of 1,6-enyne.[38]

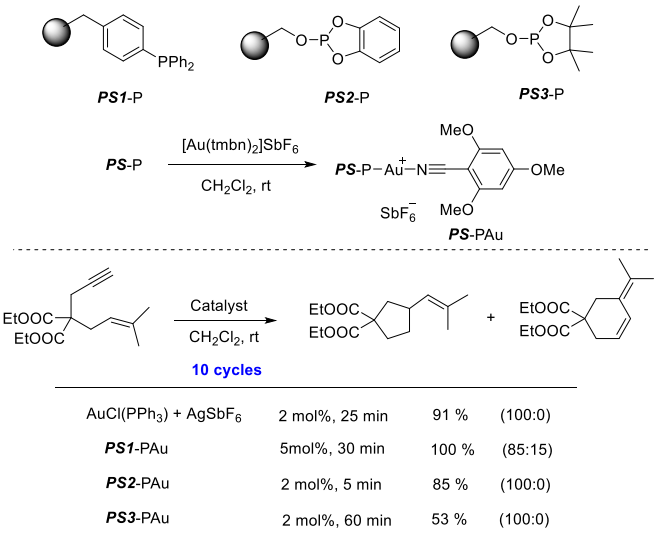

Figure 3-3. Cyclization of 1,6-enyne by ***PS***-bound cationic gold(I).[38]

In 2009, a class of stable cationic triazole phosphine gold(I) complexes was developed by Shi and coworkers.[117] From an immobilized triphenylphosphine gold chloride complex, a stable cationic triazole-gold(I) supported on polystyrene POP-TA-Au was synthesized avoiding the formation of silver chloride, a undesirable side-catalyst . Such heterogeneous gold(I) catalysts exhibit remarkable Lewis acid reactivity in a wide range of reactions with alkynes and allenes (Figure 3-4).[40] In addition, an oxidative alkyne coupling

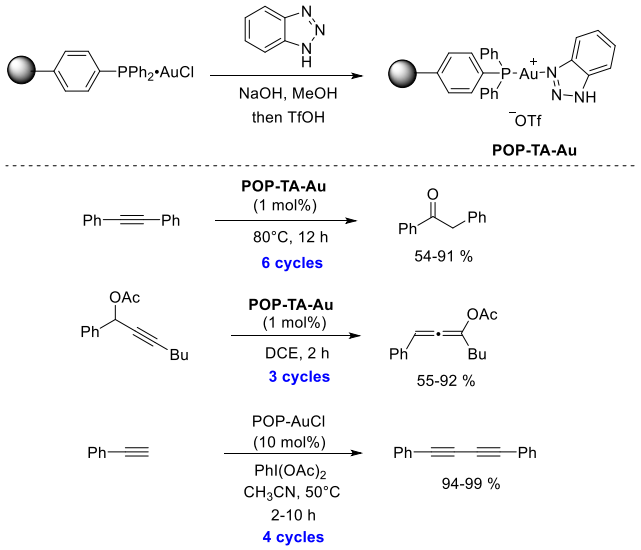

Figure 3-4. Various reaction catalyzed by stable cationic gold(I) POP-TA-Au.[40]

was also described.

In 2018, a mesoporous polymer FDU-15 bound phosphine-gold(I) complex catalyst was evaluated for the amination of allylic alcohols and intramolecular cyclization reaction of ynol to substituted furan under a super low catalytic loading (0.1-0.5 mol%) (Figure 3-5) was reported by Wu et al.[288]

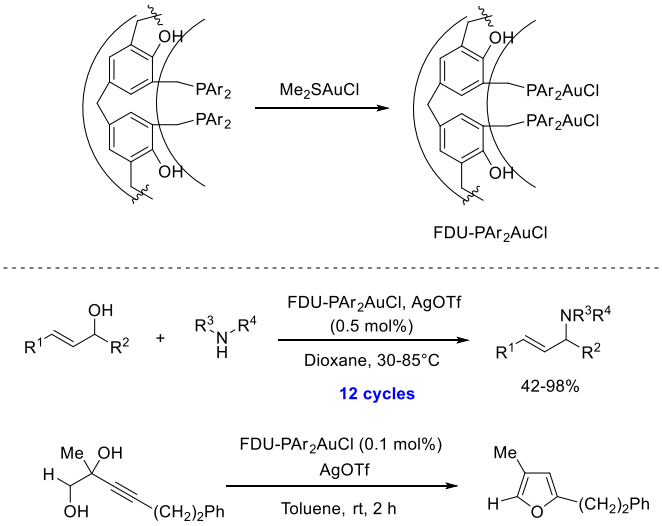

Figure 3-5. Amination of allylic alcohol by FDU supported gold complex.[288]

3.1.2 Mesoporous silica supported gold(I) complexes

In 2012, a series of NHC gold(I) complexes supported on mesoporous hexagonal silica MCM-41 were employed as catalysts in a three component coupling reaction of amines, aldehydes, and alkynes (Figure 3-6).[42] The heterogenized complexes were stable and recoverable for at least six cycles. Higher reaction conversions were observed under homogeneous conditions compared to heterogeneous conditions. Heterogenized cationic carbene gold(I) complexes were assembled on a polystyrene backbone and used for the continuous flow for the cyclization of propargylic amide and phenol synthesis.[289, 290]

In 2017, two immobilized bulky NHC-Au(I) complexes, silica-[(IPrR)Au]Cl and silica-[(IPrAdR)Au]Cl were implemented in the hydration, hydroamination, hydroarylation, or cycloisomerization of various alkynes (Figure 3-7).[291] The results are comparable to those obtained under homogeneous conditions. However, a significant loss of catalytic activity was observed after the 5th cycle. In addition, the reaction solvents are restricted since the silica support (Merk 230-400 mesh) is sensitive to methanol and water.

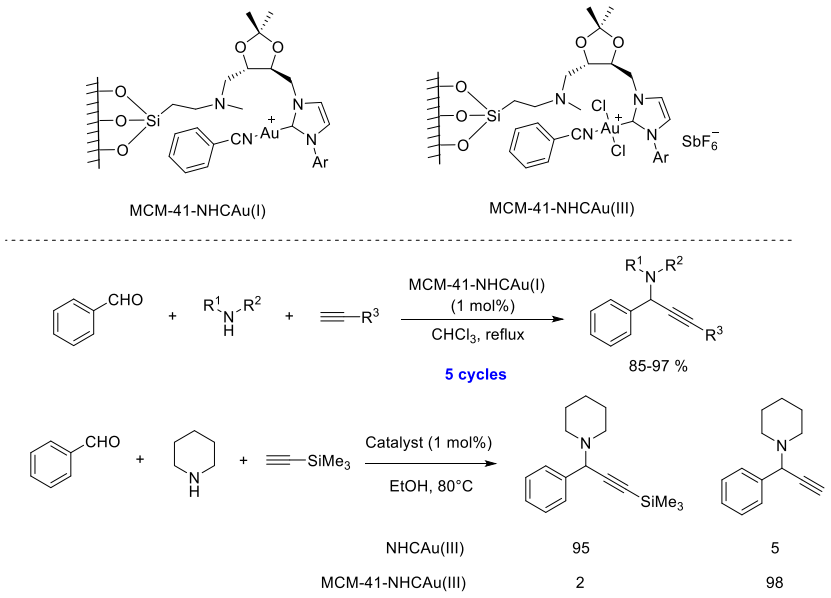

Figure 3-6. Heterogenized gold complexes for multicomponent reactions of aldehydes, terminal alkynes, and amines.[42]

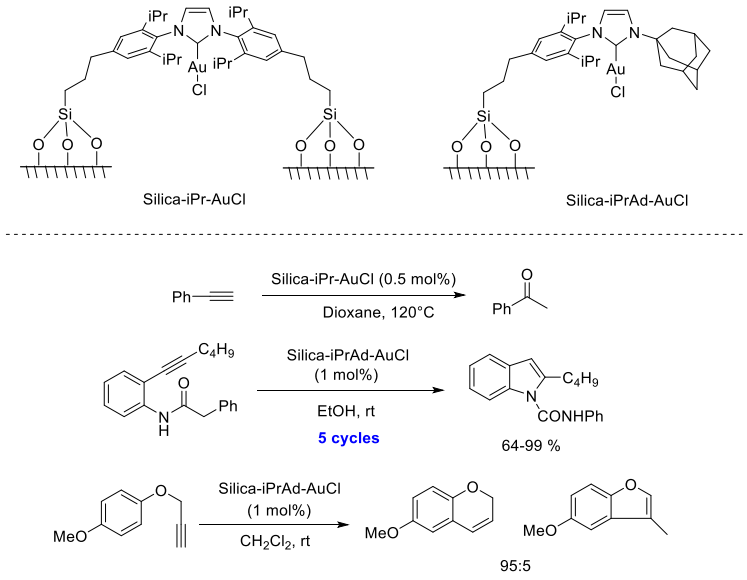

Figure 3-7. Silica-immobilized NHC-gold(I) complexes for functionalization of alkynes.[291]

Also in 2017, a similar functionalization of a hexagonal mesoporous silica (MCM-41) was employed to prepare immobilized cationic gold(I) catalysts for the [2 + 2 + 1] annulation of terminal alkynes and nitriles in the presence of 8-methylquinoline *N*-oxide leading to 2,5-disubstituted oxazoles (Figure 3-8).[43] This supported phosphine gold catalyst can also be combined with silver carbonate for the functionalization of arylalkynes to amides in moderate yield through a nitrogenation process.[44] The silver salt was proved to be necessary to achieve the transformation. In the absence of silver salts, the MCM-41 supported gold chloride catalyzed the cyclization of ynals and amidines to 2,4-disubstituted pyrimidines under mild conditions

(Figure 3-8).[292]

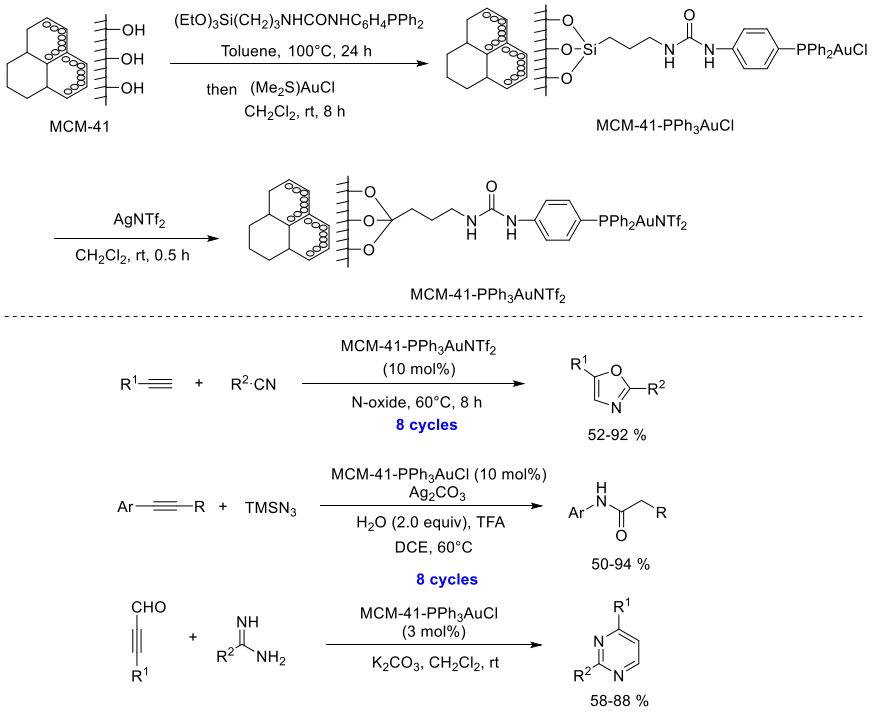

Figure 3-8. MCM-41 supported gold complexes catalyzed various reaction of alkynes.[43, 292]

3.1.3 Magnetic nanoparticle supported heterogeneous gold(I) catalysis

In 2016, a phosphine gold(I) complex supported on magnetic nanoparticles was reported (Figure 3-9). The heterogeneous gold catalyst was prepared from commercially readily available reagents and can easily be separated from the reaction mixture using an external magnet > 10 times without loss in yield. This catalyst was recyclable and highly efficient for the direct reductive amination of aldehydes and ketones at room temperature in the presence of an ethyl Hantzsch ester (Figure 3-9).[48] Such magnetic NPs supported gold catalysis provide an easier way for a long-lasting catalysis as the reaction yield dramatically decreased under homogeneous conditions. The same gold catalyst can also be employed in the ring expansion of unactivated alkynylcyclopropanes with sulfonamides leading to (*E*)-2-alkylidenecyclobutanamines.[293] One year later, a highly efficient heterogeneous oxidative cross coupling of tertiary amines with nitroalkanes and ketones was achieved by using a magnetic nanoparticle-immobilized bipyridine gold(III) complex as catalyst and air as the sole oxidant to afford the corresponding C-C coupling products in good to excellent yields under mild reaction conditions upon the activation of the α-Csp^3–H bond of tertiary amines (Figure 3-9).[47]

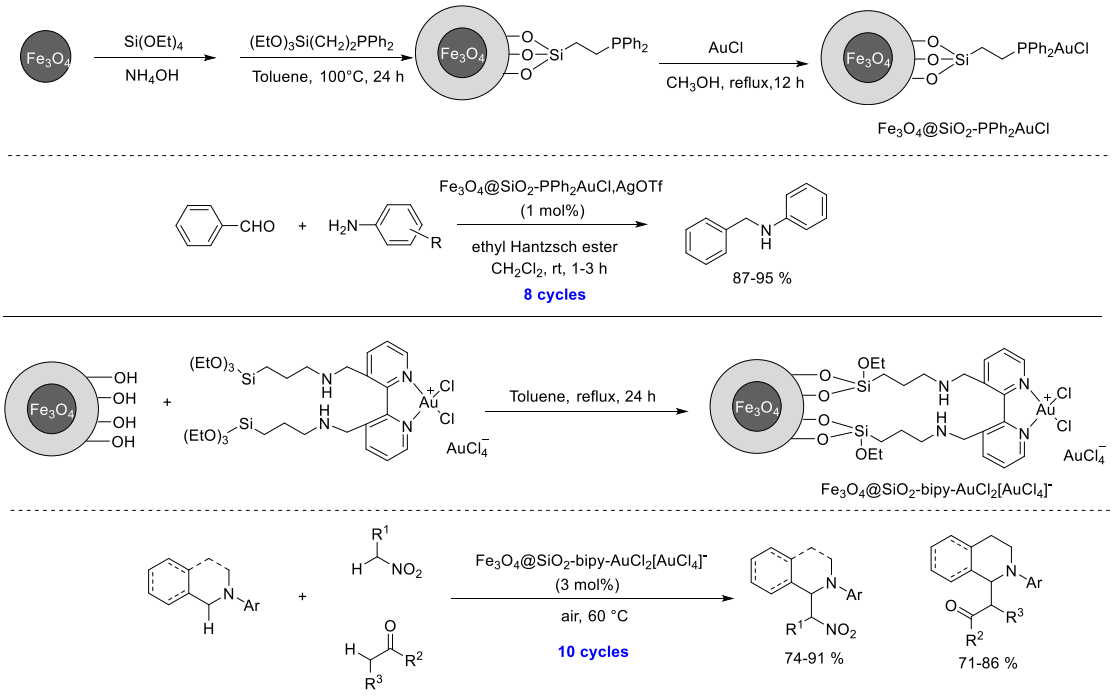

Figure 3-9. Magnetic nanoparticle supported gold catalysis.[47, 293]

3.1.4 Carbon material supported heterogeneous gold(I) catalysis

Gold complexes can also be covalently anchored onto carbon nanotubes[294] as reusable catalysts for the cyclization of enynes(Figure 3-10). However, low yields were obtained after 4 cycles which might be ascribed to significant gold leaching or the degradation of the cationic gold complex. Moreover, an inferior selectivity of the cyclization product was found compared to homogeneous conditions.

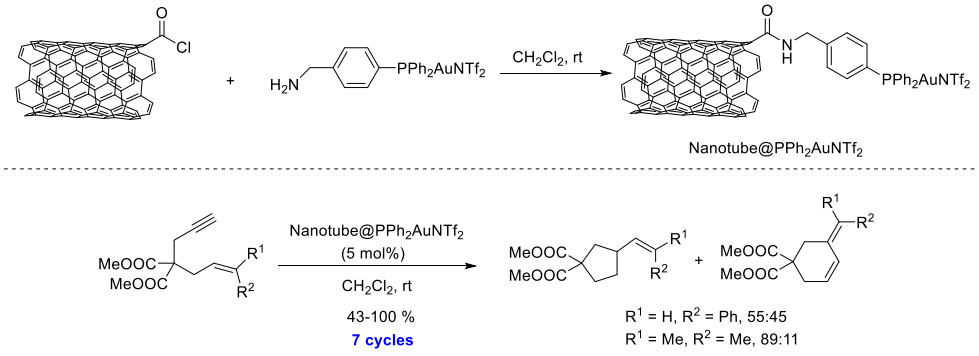

Figure 3-10. Nanotube grafted cationic gold complex catalyzed cyclization of enynes.[294]

A heterogeneous gold catalyst was obtained by the adsorption of a pyrene-tagged gold(I) complex on multi-walled carbon nanotubes through π-π stacking interactions. The non-covalent immobilization of the pyrene-tagged gold was evaluated in cyclization of 1,6-enynes with excellent reactivity (Figure 3-11).[295] Nevertheless, the reactivity is specifically dependent on the solvent polarity as the strength of the π-π interactions is strongly dependent this parameter. Later on, the same group reported the use of a pyrene-

tethered cationic NHC gold(I) complex on carbon nanotubes for the intermolecular hydroamination of alkynes possessing a high reactivity. A better stability of the immobilized gold catalyst was observed compared to homogeneous conditions.[296]

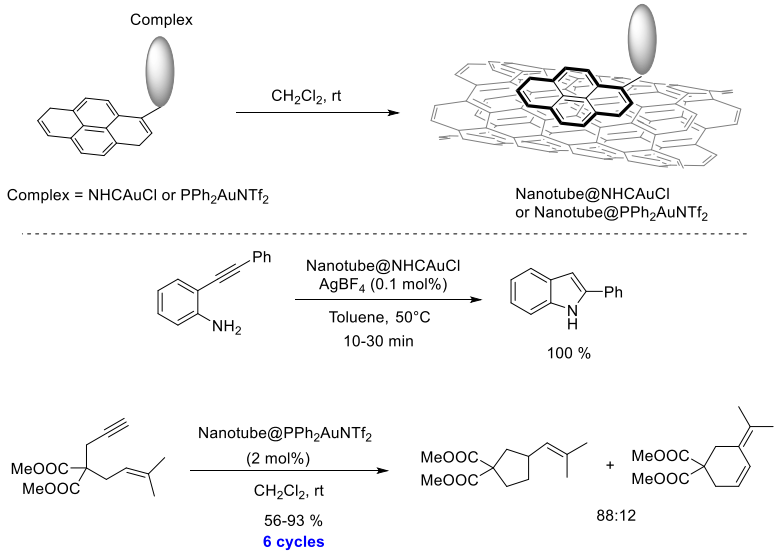

Figure 3-11. Immobilized gold complex by π-π stacking as heterogeneous catalyst for hydroamination and cyclization of enyne.[295]

3.1.5 Supported chiral heterogeneous gold(I) catalysis

In the field of homogeneous gold complexes, ligands play a significant role in achieving high reactivity and selectivity. As the ligand for immobilized gold catalysis is tunable, the immobilization of chiral catalyst onto solid supports for asymmetric catalysis provides a novel approach for sustainable asymmetric catalysis.

A few years ago, Toste's group described chiral cationic biaryl phosphine gold(I) complexes encapsulated in acidic silica pores of SBA-15.[46] This system was effective in various reactions of alkyne activations and it

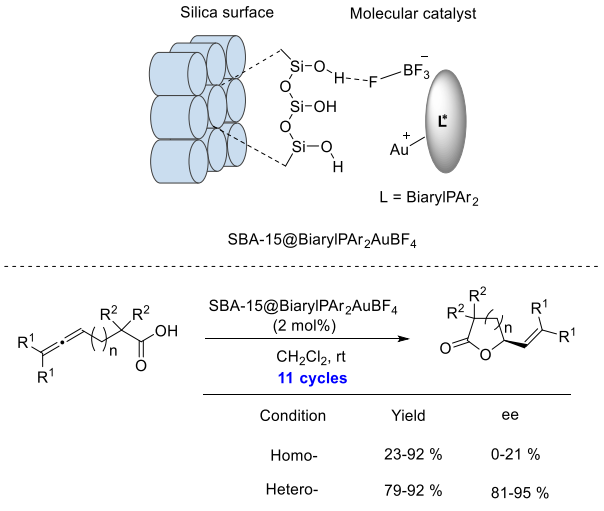

Figure 3-12. SBA-15 localized chiral biaryl phosphine gold complex for as chiral catalyst.[46]

was proposed to be a bifunctional gold/Brønsted acid catalyst that take advantages of the hydroxyl groups available on surface (Figure 3-12). More importantly, the heterogeneous gold catalysts exhibited a superior catalytic activity toward various reactions with protodeauration as the rate limiting step, and showed significant enhancement in regio- and enantioselectivity compared with homogeneous catalysts.

In the same year, Zhang's group developed a polymer-bound chiral phosphine gold(I) complex which is efficient toward the cycloaddition of 2-(1-alkynyl)-2-alken-1-ones and nitrones to bicyclic products with excellent diastereo- and enantioselectivity (Figure 3-13).[41] It was also noted that 5 % of divinylbenzene for copolymerization with chiral ligands leads to less cross-linking than reactions without DVB. However, the partial oxidation of the phosphine ligand can not be excluded during the course of preparation of such supported gold complex.

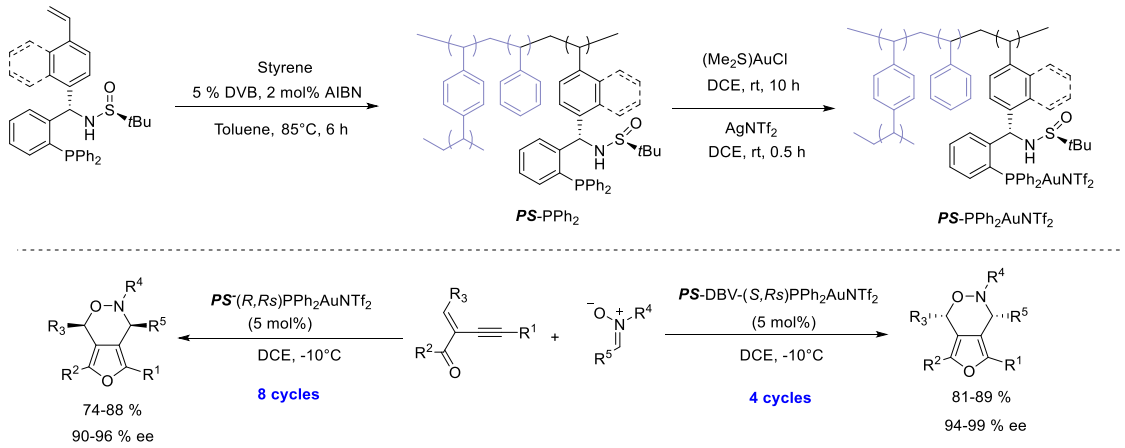

Figure 3-13. Polymer supported chiral gold complex for asymmetric cyclization.[41]

In conclusion, whereas huge progress has been made in the field of homogeneous gold catalysis, the immobilization of gold complexes onto solid supports is an emerging strategy for developing an efficient and sustainable catalysis. Generally, such heterogeneous gold catalysts are employed as Lewis acids and lead to similar performance as observed in homogeneous condition, and are reusable and applicable in continuous flow synthesis. In some of the cases, an enhancement of reactivity or selectivity was achieved thanks to the inorganic support contribution to stabilize the cationic gold complexes or to participate in the catalytic process.

3.2 Objectives

Up to now, the supported gold complexes on various solid supports can be used as heterogeneous gold(I) catalyst and showed a moderate reactivity and recyclability. A large difference for the surface area of the solid supports was observed, the surface area of commonly used solid supports for heterogeneous gold(I) catalyst are compared in the table 3-1.

Table 3-1. Surface area of solid support materials.

Materials	Surface area (m^2/g)
MCM-41	1030
SBA-15	401-439
Activated carbon	257-974
Polystyrene	615-758
Magnetic NPs	28
Silica NPs	50
Silica helices	170

As reported in the literature, the value of the surface area were measured by the Brunauer–Emmett–Teller (BET) method using nitrogen adsorption isotherms.

Silica nanohelices, as a chiral support, was obtained through a sol-gel transcription of molecular self-assembly whose handedness (Plus or Minus for the right handed (L-) and left handed (D-) helices respectively), morphology and size can be controlled.[297, 298] Recently, chirality induction from such chiral silica template to large polyoxometalate (POM) clusters,[299] gold nanoparticles[300] and organic fluorophores were observed. As far as this work is concerned, using silica nanohelices as a chiral solid support, combining with gold complexes as heterogeneous catalyst, have not been evaluated. Despite the surface area of silica helix is not larger than many other supporting materials, we anticipated to covalently graft gold complexes onto chiral silica nanohelices, leading to a 3D ensemble as a heterogeneous chiroptical catalyst in which life cycle could be monitored by circular dichroism spectroscopy.

3.3 Experimental

In this approach, silica nanohelices were prepared from 16-2-16 gemini amphiphiles with tartrate counterions and the silica nano-objects were functionalized via a surface chemical modification with (3-aminopropyl) triethoxysilane (APTES).[10] Three phosphine ligands were synthesized and covalently grafted onto the functionalized silica nano-objects (silica helices and silica NPs). In addition, the silica helices grafted gold complexes were characterized with transmission electron microscopy (TEM), energy dispersive spectroscopy, and circular dichroism (CD). The silica supported gold complexes were evaluated as heterogeneous catalyst in the cyclization of propargylic amide, 1,6-enyne, and hydration of terminal alkyne. In addition, spirocyclization of aryl alkynoate esters was examined as a benchmark substrate under various catalytic conditions for the evaluation of efficiency and recyclability of the heterogeneous catalyst.

[10] **This is a collaboration project with Dr. Reiko Oda and Dr. Emilie Pouget and the silica helices was fabricated in Institut Européen de Chimie et Biologie (IECB) by Dr. Antoine Scalabre. The fuctionalization of silica NPs and silica nanohelix were supervised by Dr. Emilie Pouget.** The detailed procedure for the synthesis of silica helices and functionalization are illustrated in the literature.[297, 298]

3.4 Results and discussion

3.4.1 Synthesis of ligand and gold complexes

Phosphine ligands are strong donors and readily coordinate with gold chloride to form gold(I) chloride complexes. In order to covalently bond gold complexes to silica materials (helices and nanoparticles), three triarylphosphine ligands bearing a carboxylic acid group were designed for further reacting on silica surface functionalized by amines (Figure 3-14) through a stable amide group. The triphenylphosphine ligand **III1** with a carboxyl group in the *para* position was chosen as the model ligand. The phosphine **III2** with two naphthyl substituents was designed to examine the aryl effect on the chiroptical properties, and the ligand **III3** with an additional pentyl spacer compared to **III1** was envisioned to evaluate the impact of the distance between the coordination site and the surface of silica helices on the chiroptical and the catalytic properties.

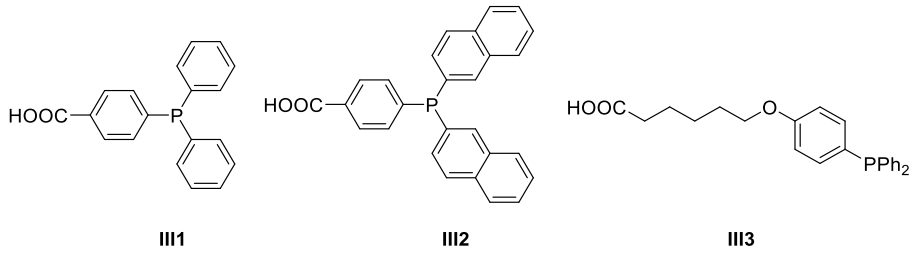

Figure 3-14. Phosphine ligands bearing a carboxylic acid group for grafting on silica nanohelices.

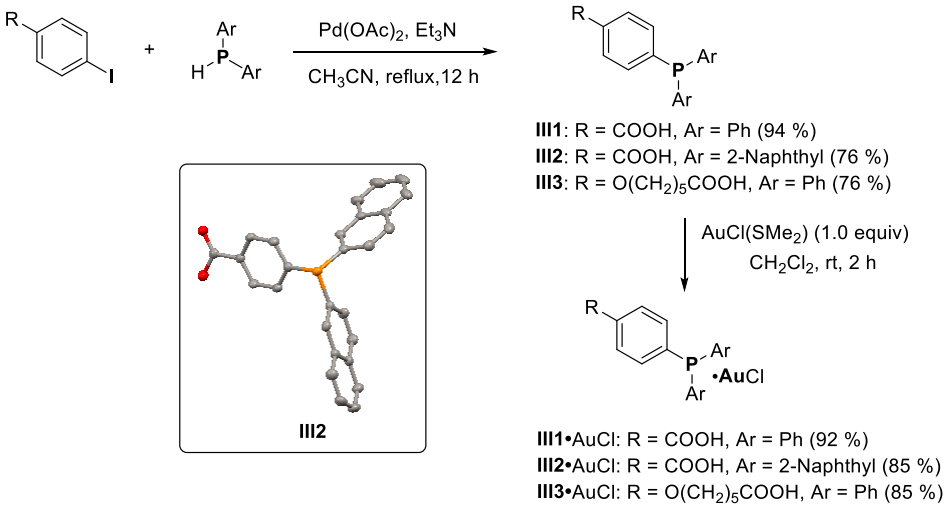

Scheme 3-1. Synthesis of phosphine-gold chloride complexes **IIIn**·AuCl (n = 1–3) for grafting on silica nanoparticles and helices functionalized with amines. Inset: crystallographic structure of ligand **III2** (CCDC number 2006391).

Palladium catalyzed coupling of aryliodide with the three different diarylphosphines was achieved in good

to excellent yield (76-94 %). The corresponding phosphine gold complexes were prepared in excellent yield (85-92 %) by treatment of chloro(dimethylsulfide) gold(I) (1.0 equiv) with the phosphine ligand (1.0 equiv) in CH_2Cl_2 at room temperature for 2 h. Meanwhile, the crystal structure of ligand **III2** was obtained and showed that the phosphine is available for metal coordination (Scheme 3-1).

3.4.2 Grafting of gold complexes

Initially, we expected to achieve the grafting of gold complexes to silica surface based on the widely-documented approach, that is to bind the ligand as the first step followed by forming the metal complex.[36, 44, 47] According to a recent method developped by Antoine Scalabre under the direction of D. Bassani and R. Oda, an amide condensation proceeds smoothly between ligands **III1** and **III3** and functionalized chiral silica helices (P- or M- Helix-NH_2) when the carboxylic acids were transformed in activated esters (ethyl chloroformate, Et_3N, dry acetone, 0–20°C). To our delight, the CD spectra of phosphine grafted P- and M-

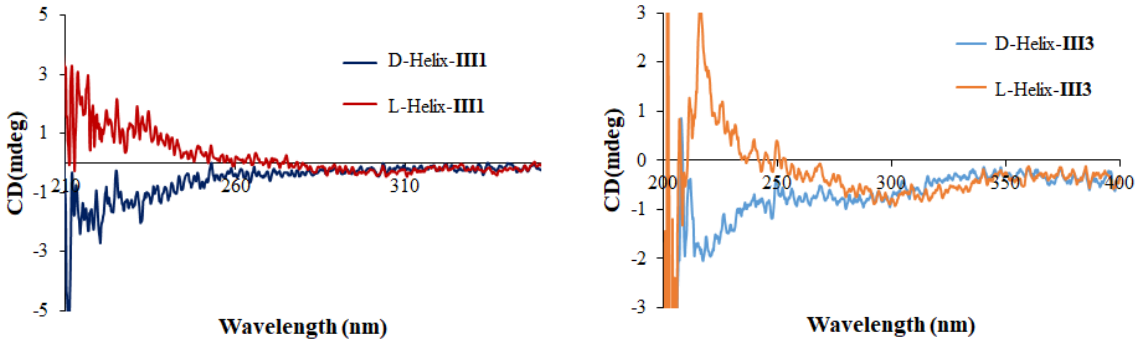

Figure 3-15. Circular dichroism spectra of L/D-silica helices grafted phosphine ligands **III1** and **III3**.

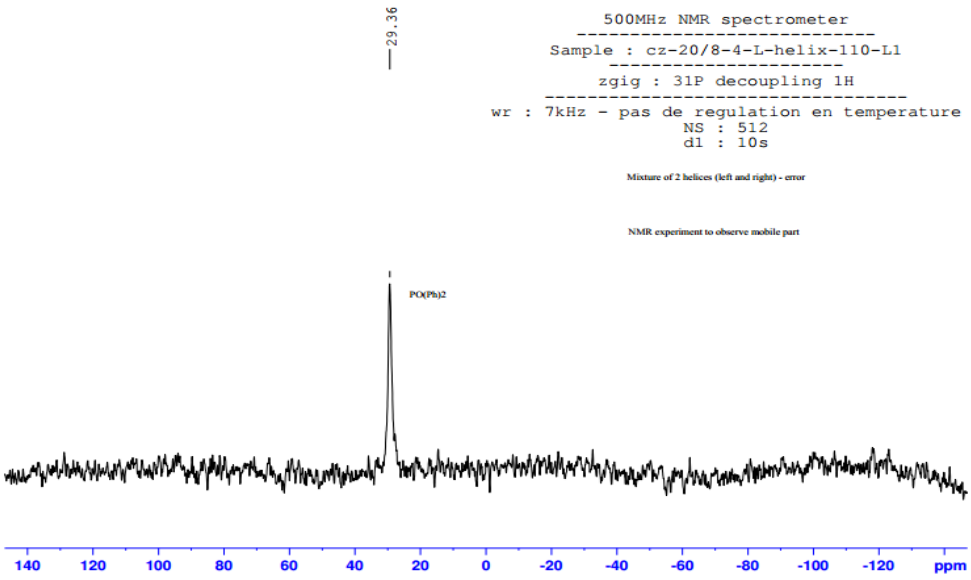

Figure 3-16. Solid state ^{31}P NMR (202 MHz, 298 K) of L-**Helix-III1** in absence of gold.

helices were mirror images (Figure 3-15) which confirms the successful grafting of the ligand, and the chirality transfer from the inorganic silica helix to phosphine ligands chromophores. However, the solid state ^{31}P NMR of the supported phosphines showed a peak at 29.4 ppm (Figure 3-16) which indicates the oxidation of the phosphine ligand into phosphine oxide, which is not suitable for gold coordination. This oxidation could be attributed to the long exposure to air during the post-treatment of the silica material.

To avoid this undesirable oxidation, we attempted to directly graft the gold complexes to the silica nano-objects (silica helices and NPs) under the same conditions (Scheme 3-2). Again, the CD spectra of gold phosphine complexes grafted P- and M- helices were mirror images (Figure 3-17) which suggests the successful grafting of the complexes. The absorption of the gold complexes is observed at 200-350 nm. The chiroptical properties of the 3D ensembles are similar, with a strong effect for the naphthyl derivative **III3** possibly due to a closer packing.

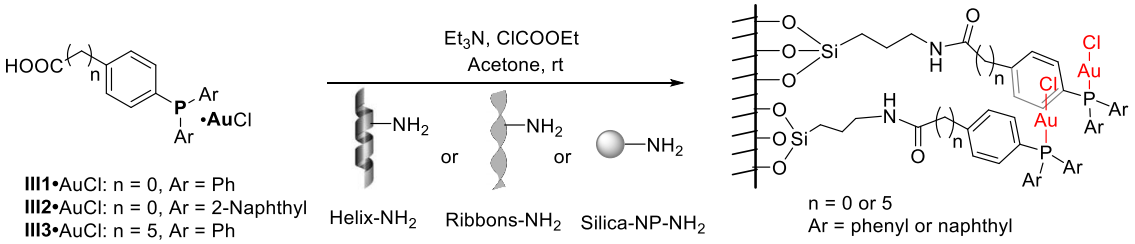

Scheme 3-2. A peptide coupling allows the covalent grafting of gold complexes on silica nanoparticles and helices to get heterogeneous catalysts Si-NP and helix-**IIIn**·AuCl (n = 1-3).

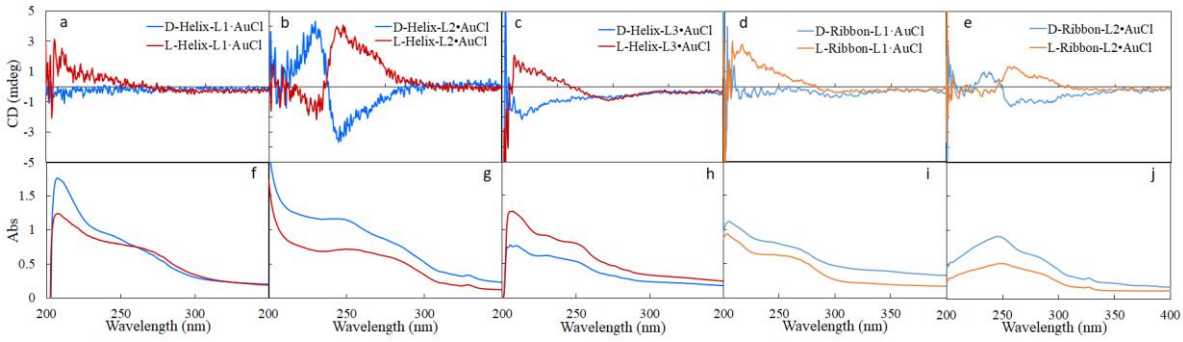

Figure 3-17. Circular dichroism (CD) spectroscopy and UV-vis absorbance spectra of chiral silica helices or silica ribbons grafted phosphine gold complexes measured in absolute ethanol (Concentration: 500 µg/mL which are based on the amount of silica helices or ribbons) (a and f) Silica helices grafted with **III1**•AuCl, (b and g) Silica helices grafted with **III2**•AuCl, (c and h) Silica helices grafted with **III3**•AuCl, (d and i) Silica Ribbons grafted with **III1**•AuCl, (e and f) Silica ribbons grafted with **III2**•AuCl.

Interestingly, by comparing the CD signal of the silica-helix grafted **III1**•AuCl and **III3**•AuCl, the behavior of chirality transfer is not affected by the longer distance from the silica surface which possibly suggests an interaction between the adjacent phosphine gold complex (Figure 3-17a *vs* Figure 3-17c). Moreover, when the aryl group turned to a larger naphthyl π ring (Figure 3-17b *vs* Figure 3-17a and Figure 3-17c), a slightly

higher CD signal is observed (Figure 3-4b) which further indicates the likely stacking of the aryl ring, inducing a Cotton effect. Based on the analysis of the X-ray structure of ligand **III2**, a pileup mode of nathphyl stacking (distance between the aromatic planes is 3.57 angstroms in solid state) was found as the distance between the phenyl rings and naphthyl rings, with the assistance of hydrogen bond formed by carboxyl group, are 3.57 Å and 3.79 Å respectively (Figure 3-18). However the organization of the grafted gold complex on the silica surface is undetermined so far, such as the distance between two adjacent chains or the distribution of the grafted chains containing the gold complexes (Outer surface or inner surface). However, the chirality transfer should originate from the directionality of helical geometry as the silica helices is the only chiral source. Ideally, the two neighboring chains are close enough and interact each other with both hydrogen bond from amide and π stacking duo to the aryl rings. Thus, an possible model to explain the observed chiroptical properties of the immobilized gold complexes was proposed (Figure 3-19)

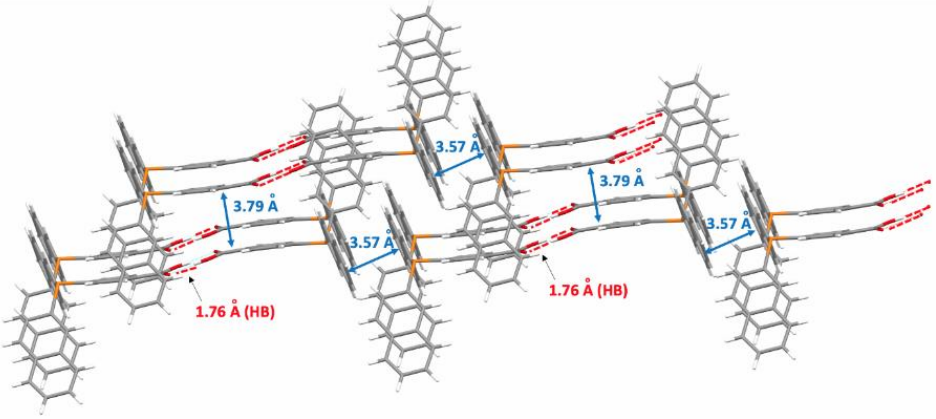

Figure 3-18. Pileup mode of ligand **III2** in solid state.

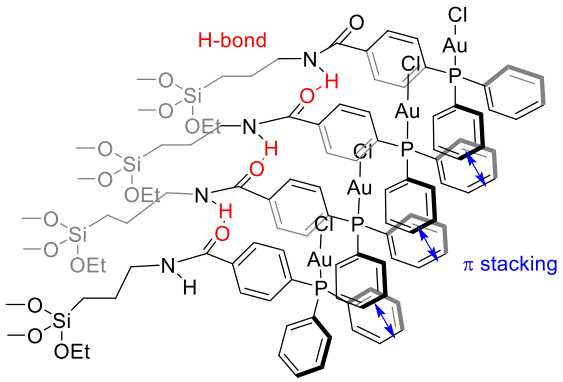

Figure 3-19. Possible model for chirality induction from silica helices to phosphine gold complex.

To further characterize the immobilized gold complexes, TEM spectroscopy of the silica helices[11] is displayed in figure 3-20. An obvious darkening surface was observed in both right/left handed silica helices after treatment with complex **III1•**AuCl which also ambiguously certificated the successful grafting of gold complex. On the nanoparticles, no difference can be visualized because of the higher silica thickness induces a denser material than the helices. In order to quantify the gold content on the surface of silica nano-objects, EDS (this method should be explained before) spectroscopy of grafted gold complex was also measured, the STEM image and elemental mapping of gold and silicon were all provided in the figure 3-21. Based on the EDS result, the atomic percentage of gold (versus silicon) for these new organic-inorganic materials is: 0.3 ± 0.1 % for Silica-NP **IIIn•**AuCl (n = 1-3) and 0.9 ± 0.2 % for Helix-**IIIn•**AuCl (n = 1-3) with very good reproducibility for several (3 to 8) samples. The measured gold density on the silica surface was 0.5 Au/nm² for the helices and 0.6 Au/nm² for the NPs based on their specific surfaces.

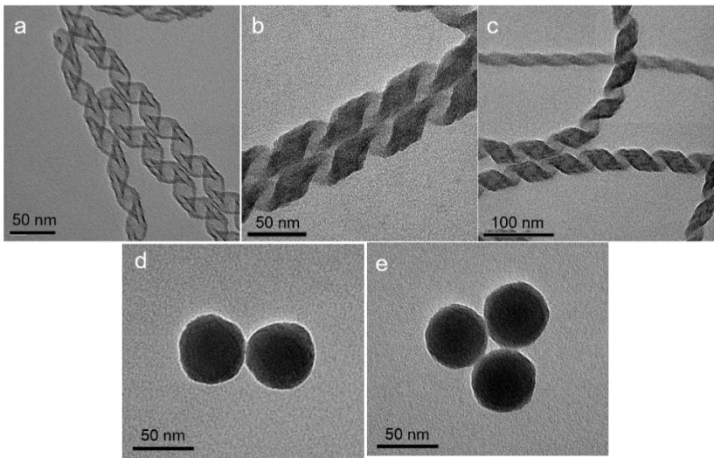

Figure 3-20. TEM spectroscopy of chiral silica helices (a) Before grafting gold complex, (b) D-silica helix grafted **III1•**AuCl and (c) L-silica helix grafted **III1•**AuCl, (d) Silica NP before grafting, (e) Silica NP grafted **III2•**AuCl

[11] For helical ribbons (silica helix), when ee equal to 1, the pitch length is 79.39 ±7.63 nm, and the width is 27.92 ±5.50 nm based on the result of Dr. Jie Gao in her thesis manuscript. [Oda's group (IECB)].

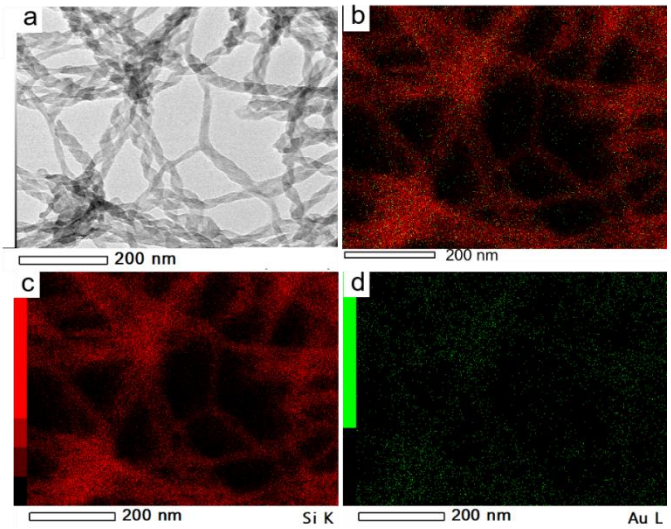

Figure 3-21. (a) STEM images of silica helices (L)-**III1**·AuCl; (b) elemental mappings of gold (Au) and silicon (Si); (c) elemental mapping of Si; d) elemental mapping of Au.

Knowing that the amine density on silica is generally comprised between 0.7 and 1 amine per nm^2,[300] it can be considered that the maximum loading of gold complexes is reached. The gold complex grafting on both silica NP and helices is therefore high, homogeneous and reproducible.

3.4.3 Heterogeneous catalysis

The Lewis acid activity of the supported cationic gold complexes was evaluated in three classical alkyne activation reactions using Helix **III2**·AuCl as a model catalyst (2 mol%) in the presence of silver triflate as a chloride scavenger (6 mol%) in dichloromethane at room temperature over 24h (Scheme 3-3). Under heterogeneous conditions, the cyclization of the propargylic amide afforded a mixture of the 5-*exo*-dig product and its oxazole isomer in a (2:1) ratio (70% conv., Scheme 3-3a). This activity is similar to other gold complexes under homogeneous conditions (79% conv., 36h).[269] The supported complex was also effective for the cyclization of 1,6-enyne into the 5-*exo*-dig product,[37] i.e. a vinyl cyclopentene (100% conv., Scheme 3-3b) and the hydration of 1-phenylprop-2-ynylacetate (99% yield, Scheme 3-3c),[284, 301] with reaction times of 24h. The three model reactions were similarly catalyzed by gold complexes under homogeneous and helix-supported conditions.

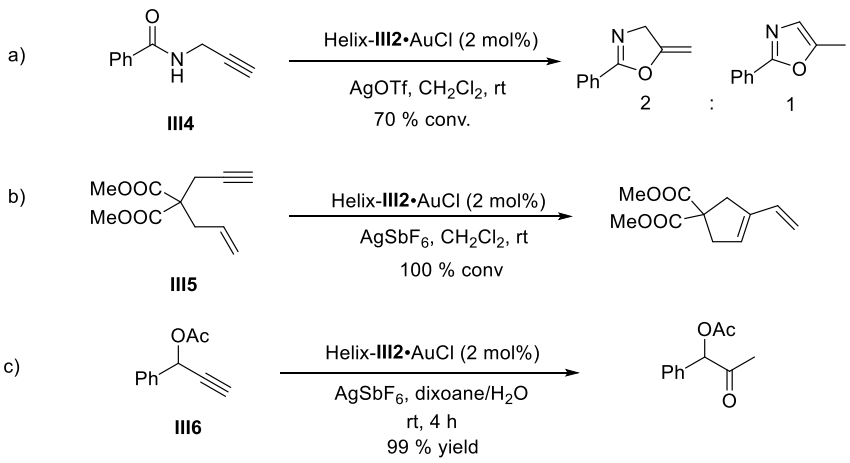

Scheme 3-3. Alkyne activation under heterogeneous conditions over 24h using Helix-**III2**·AuCl (2 mol%) as a catalyst for the transformation of : a) a propargylic amide (**III4**) into the 5-*exo*-dig product and its oxazole isomer in a (2:1) ratio; b) a 1,6-enyne (**III5**) into the 5-*exo*-dig product; c) an terminal alkyne (**III6**) into a ketone by water addition

To further investigate the catalytic activity of the supported gold complexes, the dearomative spirocyclization of aryl alkynoate esters **III7** and **III8** was selected as a benchmark reaction (Table 3-1). Under homogeneous conditions, Vadola et al. showed that Ph_3PAuCl (5 mol%) and AgOTf (5 mol%) catalyzed the reaction in dichloromethane, in the presence of water (1 equiv.) that assists the demethylation step.[302] The transformation of **III7** is described as rapid (90% yield, 30 min) and it was reproduced under slightly different conditions (90% yield, 12h, Table 3-2, entry 1). In our hands, the process was found to be concentration dependent, requiring at least a concentration of 50 mM in substrate to observe any conversion of **III7**. By employing gold chloride complexes supported on silica NP and helices (3-10 mol%) and silver triflate (30 mol%) as the catalytic system, the reaction proceeds smoothly with alkynes **III7** and **III8** (Table 3-2, entries 2-7) in 99% conversion into the corresponding spirocycles. Both silica NP and helices supports have no impact on the catalytic activity over 12-16 h. To better compare the supports, a kinetic study should be conducted. To assess the catalytic role of gold, control experiments were carried out. A silica nanoparticle NP-NH_2 without any gold complex,[12] no catalytic difference was observed in these two systems. As expected, the silica itself can not catalyze the reaction (Table 3-2, entry 8). Besides, the silver triflate alone does not catalyse this reaction, even after 48 h (Table 3-2, entry 9). Interestingly, the reaction is slowly achieved by the combination of Si-NH_2 nanoparticle and silver triflate, in the presence of water and can reach 16% conversion after 24 h (66 % yield after 6 days) which suggests the generation of silver nanoparticles. As reported by Taylor and Unsworth,[49] silver nitrate salts in the presence of silica can catalyze similar spirocyclisations.

[12] Non-chiral spherical nanoparticles (Si-NP, diameter: 52 nm) and chiral nano-helices (diameter: 37 nm) that have larger specific surfaces: 50 m^2/g for Si-NP and 170 m^2/g for helices.

Table 3-2. Dearomative spirocyclization of aryl alkynoate esters **III7-8** catalyzed by gold complexes grafted on silica nano-objects

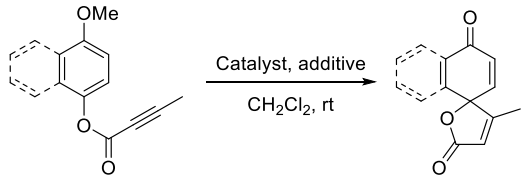

Entry[a]	Substrate	Catalyst	Catalytic loading	Additive	Reaction time	Yield[c]
1[b]	**III7**	PPh_3AuCl	10 mol%	AgOTf	12 h	99 % (90 %[d])
2	**III7**	NP-**III1**·AuCl	3 mol%	AgOTf	5 h	99 %
3	**III8**	NP-**III2**·AuCl	3 mol%	AgOTf	5 h	99 %
4	**III8**	NP-**III3**·AuCl	1.5 mol%	AgOTf	24 h	99 %
5	**III7**	Helix-**III1**·AuCl	5 mol%	AgOTf	16 h	99 %
6	**III8**	Helix-**III2**·AuCl	10 mol%	AgOTf	5 h	99 %
7	**III7**	Helix-**III3**·AuCl	5 mol%	AgOTf	16 h	99 %
8	**III7**	NP-NH_2	10 mol%[e]	-	3 days	Trace
9	**III7**	AgOTf	30 mol%	-	2 days	Trace
10	**III7**	NP-NH_2	10 mol%[e]	AgOTf	24 h	16%[f]
11	**III8**	Helix-**III2**·AuCl	1 mol%	AgOTf	24 h	99 %
12	**III8**	Helix-**III2**·AuCl	0.1 mol%	AgOTf	24 h	99 %
13	**III8**	Helix-**III2**·AuCl	0.05 mol%	AgOTf	16 h	99 % (97 %[d])

[a] Standard procedure: the reaction was performed by stirring substrate **III7** or **III8** (0.04 mmol), H_2O (10 uL), the gold chloride catalyst (10 mol%) and AgOTf (30 mol%) in CH_2Cl_2 (3 mL) at room temperature in aluminium foil. [b] Under homogeneous conditions, the reaction appeared to be dependent on substrate concentration, requiring at least 50 mM. [c] Conversion was determined by ^1H NMR. [d] Isolated yield. [e] Calculated for available amine groups. [f] Conversion reached 66% after 6 days.

Nonetheless, the secondary catalytic activity of AgOTf with silica is marginal compared to the one observed with supported cationic gold complexes, with short reaction times (5-24 h) such as used in this study. Finally, the catalyst loading was optimized for Helix **III2•**AuCl towards the dearomative *ipso*-cyclization reaction of **III8** (Table 3-2, entries 11-13). The reaction was achieved with a catalytic loading as low as 0.05 mol% in 16 h with an excellent yield of 97% (Table 3-2, entry 13). Compared to the documented supported gold complexes which are typically efficient in a range of 1-10 mol% for different reactions over a maximum of 24 h, this result for Helix **III2**·AuCl at 0.05 mol% is remarkable and could be attributed to the strategy of catalyst preparation in which pure gold-phosphine complexes were grafted on the acidic supports which is an opposite strategy compared to the literature.

As the silica helix support is chiral, the enantiomeric ratio of spirocycles obtained in the presence of gold catalyst supported on P- and M- helices was analyzed by chiral HPLC. No chiral induction from enantiopure Helix **III2•**AuCl to the molecular scale (spirocycles) chirality was observed (no detectable enantiomeric

excess). This result is expected for such a "large scale" chiral ensemble (over 100 nm), as asymmetric catalysis is reported for homogeneous gold complexes provided by bulky chiral ligands that impact on the coordinated substrate.[107]

It is also worth to note that other homogeneous conditions avoid the participation of silver salt failed to get the *ispo*-cyclization product and exhibit no reactivity (Table 3-3). For instance, without silver salt, no reaction was observed using triphenylphosphine gold(I) chloride alone (Table 3-3, entry 1). Moreover, other anion alternatives (NaOTf, KOTf and $NaBAr_F$) with PPh_3AuCl are not able to catalyse the reaction (Table 3-3, entry 2-4). As expected, silica-NPs bearing lewis acid sites showed no catalytic activity. Thus, the presence of the gold and silver as cocatalyst is necessary to this dearomative cyclization of **III7-8**.

Table 3-3. Complementary conditions for dearomative cyclization of **III7-8**.

Entry[a]	Substrate	Condition	Results
1	**III7**	PPh_3AuCl (10 mol%), H_2O (10 µL), CH_2Cl_2 (3 mL), 72 h	N.R
2	**III8**	PPh_3AuCl (10 mol%), NaOTf (30 mol%), H_2O (10 µL), CH_2Cl_2 (3 mL), 72 h	N.R.
3	**III8**	PPh_3AuCl (10 mol%), KOTf (30 mol%), H_2O (10 µL), CH_2Cl_2 (3 mL), 72 h	N.R
4	**III7**	PPh_3AuCl (10 mol%), $NaBAr_F$ (20 mol%), H_2O (10 µL), CH_2Cl_2 (3 mL), 72 h	N.R
5	**III7**	Silica-NP (10 mg), H_2O (10 µL), CH_2Cl_2 (3 mL), 72 h	N.R

[a] Standard procedure: the reaction was performed by stirring substrate **III7** or **III8** (0.04 mmol), H_2O (10 uL), the gold chloride catalyst (10 mol%) with or without sodium/potassium salt in CH_2Cl_2 (3 mL) at room temperature in aluminium foil.

3.4.4 Recycling experiments

In order to take advantage of its heterogeneous nature, the silica nano-particle and silica helix were all evaluated for the dearomative cyclization. Initially, the recyclability of silica-supported Helix **III2**·AuCl with an initial loading of 10 mol% and silver triflate (30 mol%) was evaluated in the reaction the dearomative spirocyclization of substrates **III8**. During the recyclability process, each Helix **III2**·AuCl catalyst was readily recovered simply by centrifugation after the reaction completion (monitored by TLC and ^1H NMR) and it was used for next catalytic cycle without any further treatment. The reaction showed a durable catalytic performance for 8 cycles without loss of yield (Figure 3-22). However, the reaction time increased from 5 h to 24 h during the cycles.

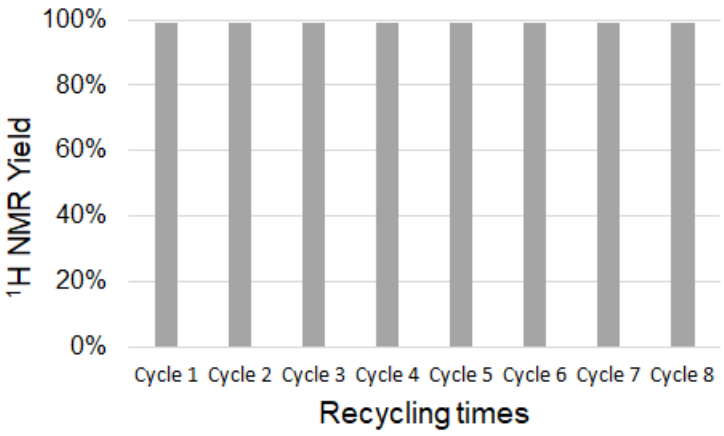

Figure 3-22. Consecutive catalytic cycles of helix-**III2**·AuCl (9 mg, 5 mol%) and AgOTf (30 mol%) in the presence of substrate **III8** (0.03 mmol for each cycle). Full conversion was reached over 8 cycles meanwhile the reaction time gradually increased from 5 to 24h

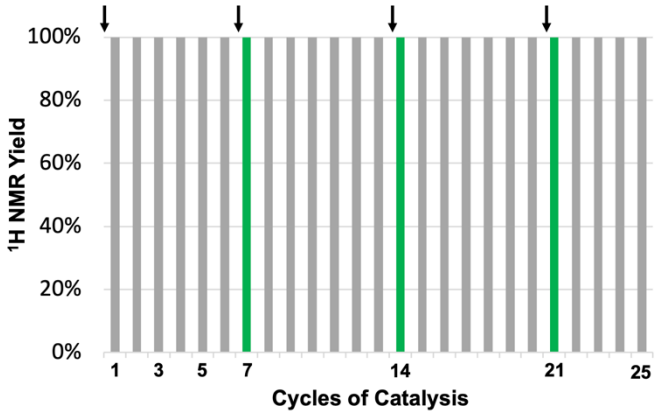

Figure 3-23. Recyclability of Silica NP-**III1**•AuCl catalyst (10 mol%) for the spirocyclization of substrate **III7** over 25 cycles. In this case, reasonable reaction times (ca. 24h max) are maintained by adding AgOTf (30 mol%) every 7th cycle (black arrow).

In addition, silica NP-**III1**·AuCl was also examined in the *ipso*-cyclization of **III7** (Figure 3-23). Full conversion was reached at each cycle, with reaction times gradually increasing from 5 h (initial cycle) to 24 h at the seventh cycle which is similar as silica helix supported gold catalyst. However, a higher loss of silica NP was observed during the recycling process when washed with dichloromethane. Concomitant to the prolongation of the reaction time, an additional portion of AgOTf (30 mol%) was added every 7 cycles. This experiment was followed over 25 cycles with full conversion. Compared to homogeneous cationic gold complexes that rapidly deactivate over 24 h-48 h and were not refreshed by silver salts, the durability of these supported gold complexes with an additional silver assistance deserves further investigation. For this reason, the nature of the silica supported catalysts was examined after four cycles by TEM, EDS and CD spectroscopy (Figure 3-24). Circular dichroism showed that the phosphine ligand is still covalently linked to

silica, with a similar signature to the freshly prepared gold complex material. Notably, the UV-Visible spectra presented a broad absorbance in the 400-500 nm region, which is characteristic of the presence of AgNPs in contrast with AuNPs that absorb in the 500-600 nm region.[303, 304] TEM images indicated the presence of small nanoparticles (~3 nm) on the surface of the helices and larger aggregates (~100-500 nm) in the medium. Those nanoparticles can be compared of Au(0) and Ag(0). Finally, the EDS analysis of this recycled catalytic material revealed the main presence of silver (1.7 ± 0.6 %), forming large aggregates (100-500 nm, Figure 3-24, b-c) and a large decreased in gold surface concentration (0.9% after preparation versus 0.1% after 4th cycle).

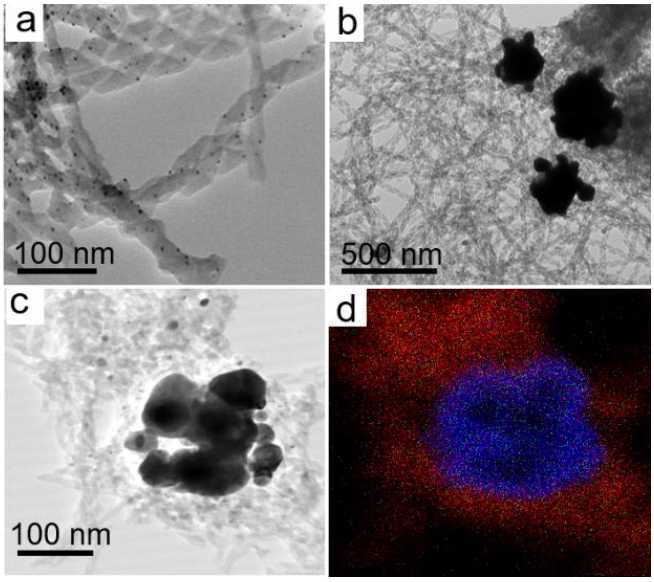

Figure 3-24. TEM images of Helix-**III2**·AuCl after four catalytic cycles showing the still presence of helices and the apparition of small (a) and larger (b and STEM image c) particles. The EDS mapping (d) shows that the particles are silver (red is silicon and blue is silver)

This observation also confirmed that gold leaching from the silica support, which is a classical phenomenon for most immobilized metallic complexes. Based on these analyses, the recycled material appeared to gradually transform over time and cycles, with a decrease in cationic gold(I) catalyst and the possible presence of Ag(I)-SiO_2 catalytic species,[49] as the catalytic activity is boosted by the addition of AgOTf after seven cycles. The *in situ* reduction of gold(I) and Ag(I) into of nanoparticles accounts for uncontrolled pathways of catalyst deactivation. The exact nature of catalytic species is still under investigation in our laboratory. In a more general view, our report is questioning previous examples of supported gold complexes even embedding ones, that are recycled over 5-8 runs. A plausible catalytic activity emerging from supported Ag(I) or AgNP should be carefully taken into account.

3.5 Conclusion and perspectives

Two new phosphine ligands **III2-3** were designed for conjugation to silica nano-helices through peptide coupling. Metal ion based catalysts i.e. gold chloride phosphines were successfully grafted to silica by directly linking to the support and avoiding any phosphine oxidation. The chiroptical properties of these supported gold complexes were exploited for monitoring the ligand linkage to the support. Furthermore, we highlighted that the combination of the inorganic silica nano-objects and gold complexes provides an efficient approach for several types of alkyne-related cyclizations. More importantly, the heterogeneous catalysts could be recycled up to an average 7 cycles without any loss of efficiency in the dearomative spirocyclization reaction of aryl alkynoate esters.

Interestingly, the recycled silica material appeared to be gradually transformed over time and reaction cycles, from pure supported cationic gold(I) catalysts into a complex catalytic system based on silica and different metallic species. Whereas the catalytic system can be boosted by adding silver triflate, a plausible catalytic activity emerging from supported Ag(I) or AgNP may account for gold chloride complexes associated to silica in the presence of silver salt additives.

From a practical view, Vries and Farina pointed out that the heterogenization adds complexity to the system, increasing risk and prolonging process development while suffering from metal leaching and catalyst deactivation.[305] The immobilized transition catalyst showed limited efficiency over cycles which also questions their economic benefits *versus* their cost of preparation which might not be suitable as catalyst for industry process. Moreover, in our case, the preparation of the silica helix is quite sophisticated. However, for a positive perspective, developing materials that form 3D helical superstructures with chiroptical properties is a promising field. In our case, as the chirality induction is enhanced by employing a larger π ring on phosphine ligand, we believe that other phosphine ligands with much larger π moiety would lead to a higher CD signal and, hopefully, a further chiral induction. In addition, this supported gold complexes might exhibit a better chirality control in organic transformations.

Cogito ergo sum

French mathematician, physicist and philosopher
René Descartes (1596-1650)

Chapter 4

4 DPA-based thioethers and sulfoxides: Coordination complexes and chiroptical properties

4.1 Introduction

9,10-Diphenylanthracene (DPA) is a chromophore with blue emission that has been modified and applied in preparation of organic light-emitting diodes,[50] fluorescence probe for singlet oxygen,[51] and intense luminophores.[52, 53] *Ortho*-substituted DPA possesses *syn*- and *anti*- atropisomers due to the high rotational barrier. The theoretical rotational barrier for non-substituted 9-phenylanthracene was calculated to be 87 kJ/mol[60] which is close to the experimental rotational energy 75 kJ/mol for 9,10-diphenylanthracene.[58] The rotational barrier increase when the substituted group is larger, reaches 123 kJ/mol for *ortho*-CH_3 DPA[59] (Figure 4-1). Moreover, they are highly thermally stable atropisomers, for instance, the *ortho*-OCH_3 DPA undergoes the *syn*- to *anti*- transformation at around 320 °C.

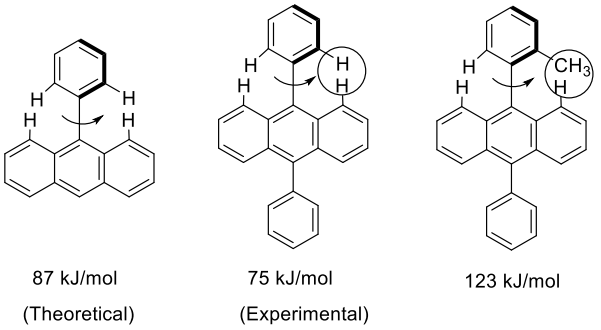

Figure 4-1. Rotational barrier for DPA and *ortho*-CH_3 substituted DPA.[58-60]

DPA has also been reported to be a good candidate for reversible [4+2] Diels-Alder cycloaddition reaction in the presence of singlet oxygen leading to 9,10-endoperoxides and subsequent thermal cycloreversion to recover the anthracene moiety.[54] Linker and coworkers described photo-oxidation of the *anti*-DPA compounds led to the formation of sole *syn*- endoperoxide and the cycloreversion under 110 °C gave back to *syn*- DPA compound while the *syn*- to *anti*- transformation was achieved above 320 °C (Figure 4-2).[61, 306]

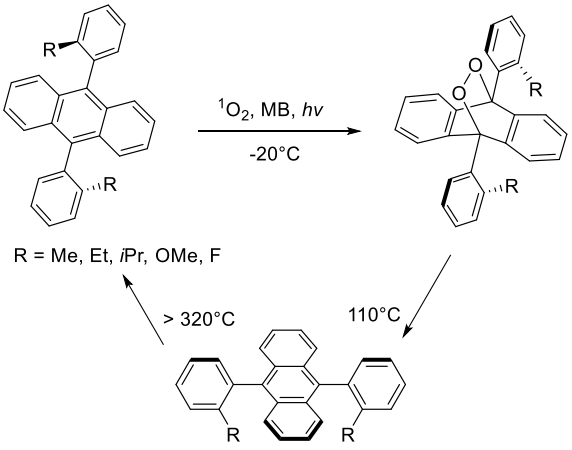

Figure 4-2. DPA-based molecular rotary switches.[61, 306]

4.2 Coordination complexes between DPA-based thioether ligands and silver salts

4.2.1 Introduction

Silver has been known to adopt various chelating modes with thioether ligands, the early examples of silver complexes with various macrocyclic thioether ligands were described in the 1990s,[62, 64, 65, 70] as tetrahedral, sandwich, and octahedral silver complexes were obtained and characterized based on X-ray analysis (Figure 4-3).

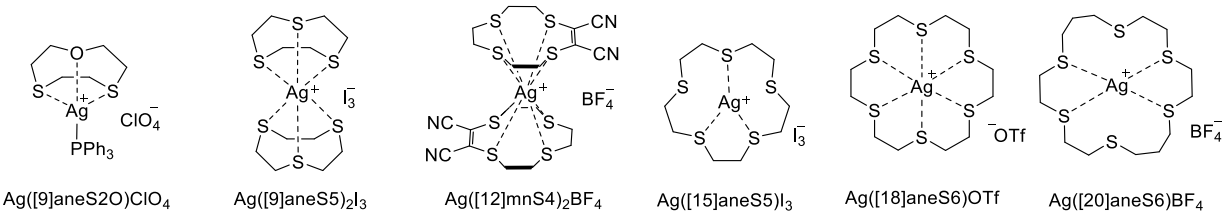

Figure 4-3. Silver complexes with macrocyclic thioethers.[62, 64, 65, 70]

By altering the anion to 1,1,1,5,5,5-hexafluoro-2,4-pentanedione (hfpd) or 2,2-dimethyl-6,6,7,7,8,8,8-heptafluoro-3,5-octanedionat (fod), silver coordination polymers[71, 73] were obtained using thioether macrocycle building blocks. Notably, the rare five-coordinate silver complexes was observed when using [14]aneS4 and [9]aneS3 ligands (Figure 4-4). The self-assembly of silver salts with bidentate thioether α,α'-bis(8-thioquinoline)-*m*-xylene (*m*-XYTQ) afford a helical silver complex. In this case, the xylylene moiety was proven to be the crucial spacer for the formation of the helical morphology.[307]

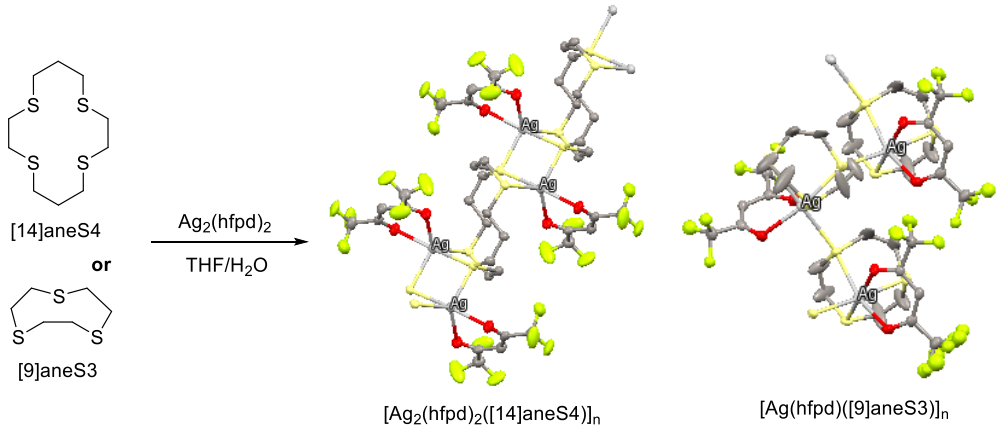

Figure 4-4. Synthesis of silver coordination polymer with thioether macrocycles.[71, 73]

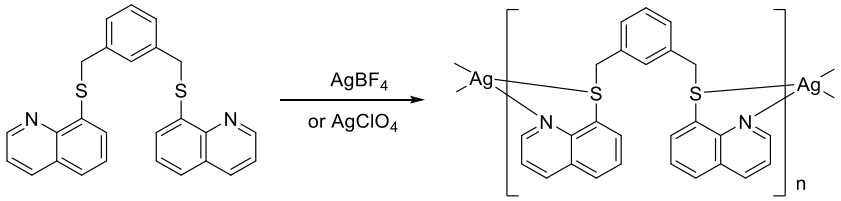

Figure 4-5. Self-assembled helical silver complex with N,S bidentate ligand.

Another representative example for the diverse coordination of silver complexes was described by Lee and Lindoy's groups. By using three isomeric NS2-macrocycles, a series of self-assembled silver complexes was obtained: cyclic tetramer or hexamers with the amine ligand, *vs*. linear or helicoidal polymers with the deprotonated amine ligands (Figure 4-6).[74] The access to these diverse topologies is proposed to arise from the flexibility of the macrocyclic rings.

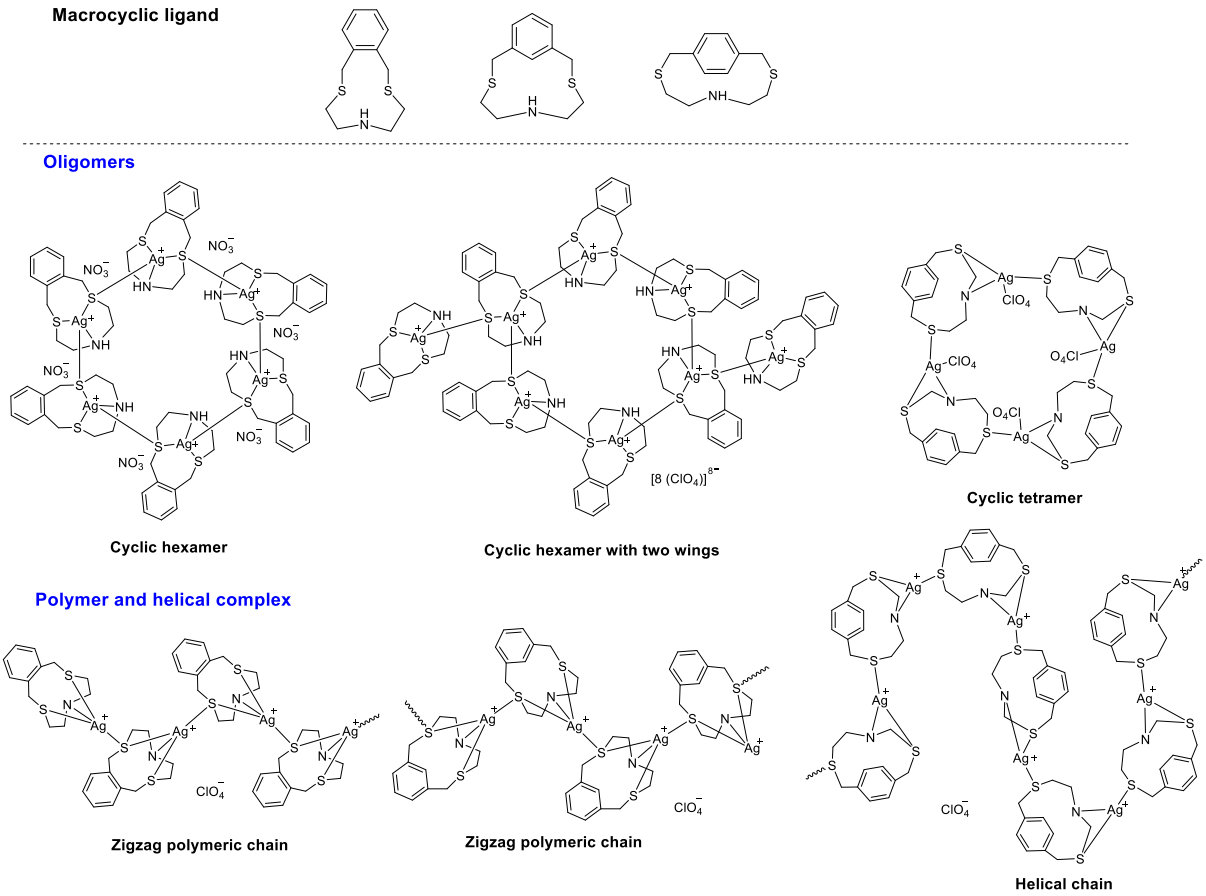

Figure 4-6. The diverse topologies of silver complexes obtained from the NS_2-macrocyclic ligands.[74]

In conclusion, diverse chelating modes for silver complexes are known and the rational ligand design led to the diversity of silver coordination chemistry. We were interested in using of *syn* and *anti* DPA atropisomers as platforms appended with thioether ligands for metal coordination, whose coordination topologies might

be controllable. Besides, we were also interested in using the well-defined silver complexes for homogeneous catalysis as few cases are documented.

4.2.2 Objectives

Hindered *ortho*-substituted diphenylanthrancene derivatives with *syn*- and *anti*- configurations are stable atropisomers due to the significantly high rotation barrier which was theoretically and experimentally calculated.[58-60] Often, these two isomers can be readily separated by column chromatography. Thus, rational molecular design based on the DPA skeleton was expected to control the coordination mode of the metal complexes. We are interested in developing DPA-based thioether ligands that enable to access to diversely coordinated silver complexes as silver have been known to adopt a versatile chelation topology with thioethers. Whereas few cases of homogeneous silver catalysis were documented, the thioether silver complexes as homogeneous catalysis are to be evaluated which can be a promising approach to lower the catalytic loading as usually a high amount of silver is needed in the silver catalyzed transformations. Additionally, DPA-based diphosphine ligands and hemilabile ligands for functional gold complexes are also discussed.

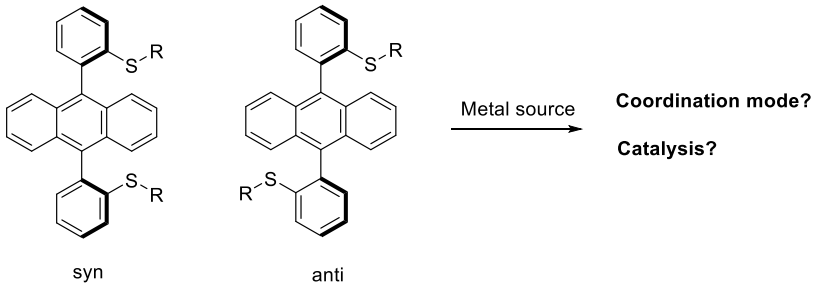

Scheme 4-1. *Syn*- or *anti*- DPA atropisomers with thioether substituents for metal coordination and catalysis.

4.2.3 Experimental abstract

In this research, we developed four DPA-based thioether ligands (**IV2**, **IV4-6**) which readily form self-assembled silver complexes with various geometries. A bis-*ortho*-thioether-9,10-diphenylanthracene was synthesized as a *syn*- atropisomer as revealed by X-ray diffraction. This alkylaryl-thioether ligand **IV2** can form silver complexes with different coordination modes depending on the nature of the anion such as M2**L**2 for AgOTf and AgOTFA, M6**L**4 for $AgNO_3$, M2**L** for bulky PPh_3AgOTf which were further characterized by XRD analysis. Their activity in homogeneous catalysis was observed in two tandem addition/cycloisomerization of alkynes using 0.5-1 mol% of catalytic loading. By extending the length of coordination chain, the *anti* and *syn* atropisomers were isolated and their complexes with AgOTf were found to be M2**L** for *anti*- thioether ligand **IV4** and M**L** for *syn*- thioether ligand **IV5**. In addition, other silver

complexes with $AgPF_6$ were also obtained even though the exact geometries were unidentified.

4.2.4 Results and discussion

4.2.4.1 Synthesis of thioether ligands

The DPA-based bisthioether compound with an undetermined configuration was obtained[13] by a one-step coupling reaction from commercially available 9,10-dibromoanthracene and 2-(methylthio)phenylboronic acid in dry toluene.[50] In contrast, using the same Suzuki-Miyaura cross-coupling reaction in a mixed solvent (toluene/EtOH/H_2O = 4:1:1), we only isolated a mere principal thioether ligand **IV2** in low yield (26%). The X-ray analysis of monocrystals revealed it possesses the *syn*- conformation of **IV2** (Scheme 4-2). Thus, the previous thioether compound was probably obtained in an *anti*- configuration as its ^{1}H NMR spectrum was very different from that of *syn*-thioether **IV2**. Such difference in the product configurations possibly results from the different favored configurations of four-coordinated palladium species after the transmetalation process in the presence of a protic solvent.

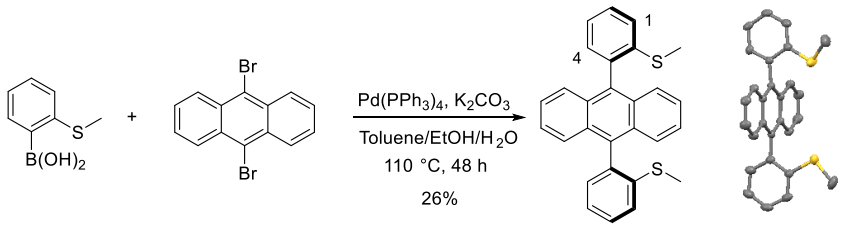

Scheme 4-2. Synthesis of bisthioether ligand **IV2**. The *syn*- structure was confirmed XRD analysis.

Variable temperature ^{1}H NMR (VT-NMR) experiment of **IV2** in $C_2D_2Cl_4$ in the range of –30 to 110 °C showed the fluctuation of protons on benzene rings (Variations of chemical shift: 0.17 ppm for H1, 0.24 ppm for H4, 0.25 ppm for methyl group) (Figure 4-7) mainly due to the restricted rotation of the 9,10-aryl substituents respect to the anthracene core, which somewhat indicates a certain flexibility of the benzene rings with *ortho*-substituents, and importantly, without any indication of a *syn* to *anti* isomerization. Meanwhile, the broadening of proton signals under high temperature was also observed.

[13] In this literature, the thioether compound was synthesized in the similar approach with 58 % yield which is probably *anti*-configuration as the ^{1}H NMR description was severely disparate from the well-characterized *syn*-thioether **IV2** we obtained. The only difference of the preparation is the dry toluene was used in the literature, and in our case, a mixed solvent (toluene/EtOH/H_2O = 4:1:1) was employed which suggests the different configurations of four-coordinated palladium species after transmetalation process in the presence of protic solvent. This might also provide a way to access to *syn*-atropisomer, as always the case, *anti*- product was favored in this system due to less steric hindrance.

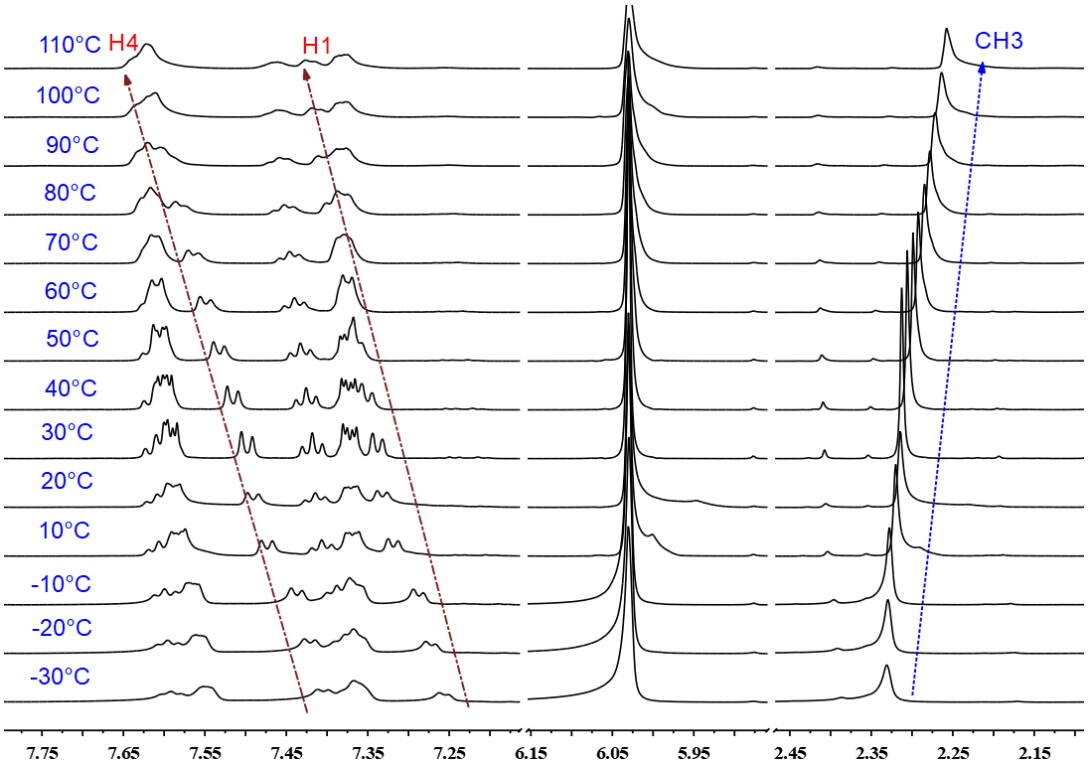

Figure 4-7. Variable temperature ^{1}H NMR of **IV2** in $C_2D_2Cl_4$ from -30°C to 110°C.

4.2.4.2 Synthesis of silver complexes and VT NMR

Initially, attempts to access to gold complexes with various gold sources led to no reaction or unknown products[14] which suggests that the arylalkyl thioether is not a good candidate for gold(I) or gold(III) coordination. However, the formation of descrete complexes can be readily achieved with several silver salts in good yield (77-92 %) according to the general procedure.[15] Interestingly, the coordination modes were strongly depended on the nature of anions as macrocyclic M2**L**2-type silver complexes were found for AgOTf and AgOTFA, a M6**L**4-type metallocage was observed for $AgNO_3$ and a discrete M2**L**-type silver complex was obtained in the presence of bulky PPh_3AgOTf. All complexes were characterized by X-ray diffraction analysis (Scheme 4-3). However, their analysis by mass spectroscopy was unsuccessful, leading to only the mass of the ligand. Although the silver complexes are stable in solution, we presume that they are not stable under the experimental conditions used for mass spectrometry analysis since the signals for the corresponding molecular ions were not observed. For macrocyclic silver complex **IV21**, two different morphologies were isolated and characterized by X-ray diffraction analysis.

[14] Gold sources such as $NaAuCl_4{\cdot}2H_2O$, $HAuCl_4{\cdot}3H_2O$, PPh_3AuCl, $AuCl(SMe_2)$, AuCl(tht), PPh_3AuOTf, $Au(tht)_2OTf$ were examined in mixed solvents (CH_3CN/H_2O, CH_2Cl_2/CH_3CN, $CH_2Cl_2/MeNO_2$, $EtOH/Et_2O$) or single solvent (CH_2Cl_2, THF) with a ratio of ligand/gold (1:2).

[15] General procedure for the synthesis of silver complexes: To a solution of **IV2** (1.0 equiv) in dichloromethane (1 mL) was added silver salts (1.0 equiv) under argon atmosphere at room temperature. The mixture was stirred at room temperature for 4-6 h. Then the solution was concentrated to *ca.* 0.3 mL and diethyl ether (2 mL) was added to afford a white precipitate. The solid was filtered, washed by diethyl ether and dried under reduced pressure to afford corresponding silver complexes.

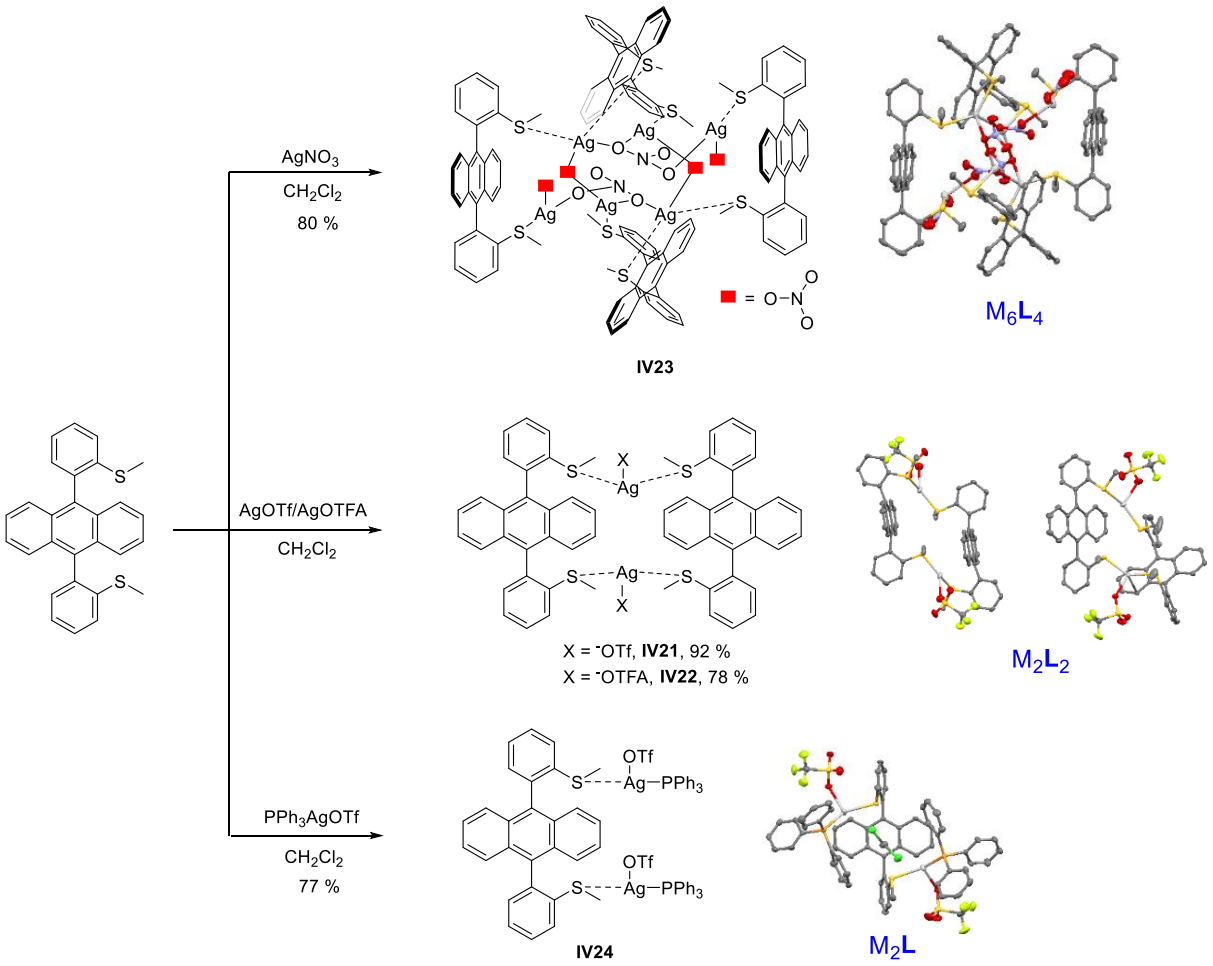

Scheme 4-3. Synthesis of silver complexes with *syn*-thioether ligand **IV2**. The structure of silver complexes were characterized by X-ray diffraction analysis.

As the sulfur atom is prochiral, the coordination of a metal atom by the lone pair of sulfur generates an (*R*) or (*S*) configuration. Because ligand **IV21** possess two sulfur atoms, its coordination to silver creates two new asymmetric centers: one (*R*) and one (*S*). Finally, two possible self-assemblies by coordination are observed: the head-to-head mode (**IV21a**) when the same configuration are connected to the silver atoms or the head-to-tail mode (**IV21b**) when (*R*) and (*S*) sulfur atoms are connected to the silver atoms (Figure 4-8). Based on the ^{1}H NMR spectra, slight differences were also observed for the methyl group connected to the sulfur atom and certain protons on the benzene ring , which were ascribed to the different twist degree of the benzene ring as the VT-NMR of ligand **IV2** also showed certain flexibility that lead to the variation of the protons on benzene ring.

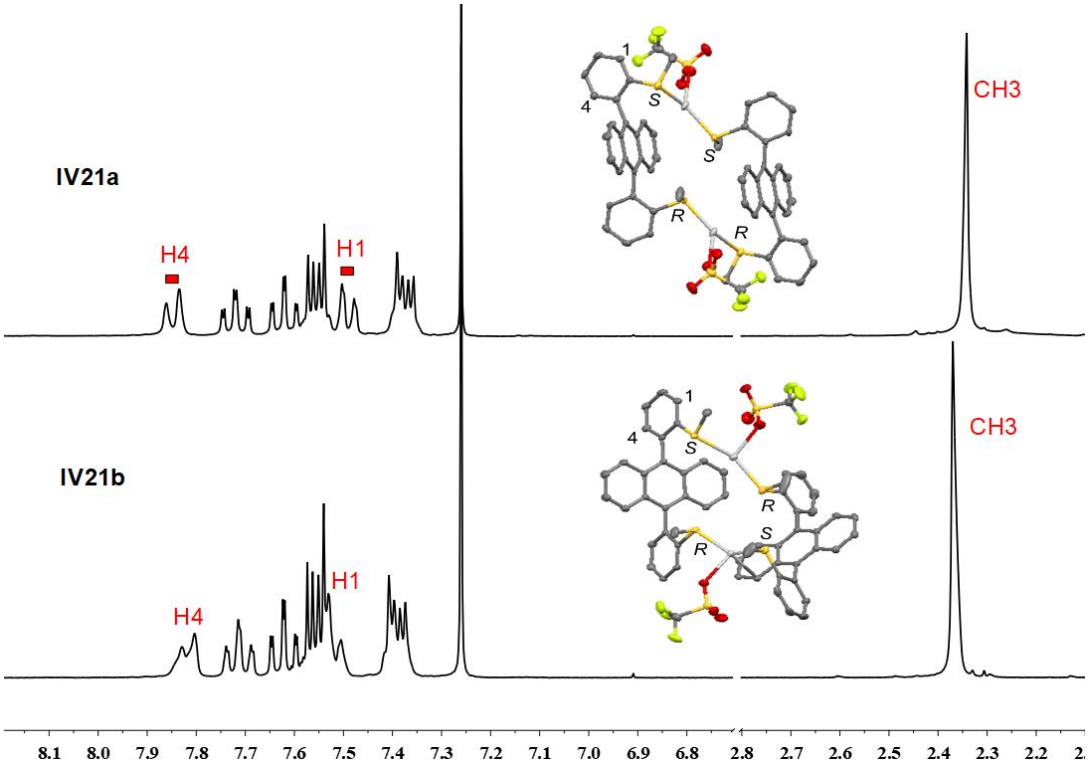

Figure 4-8. ^{1}H NMR comparison and X-ray structures of macrocyclic silver complex **IV21.** Head-to-head coordination (**IV21a**) and head-to-tail coordination (**IV21b**).

We envisioned that the flexibility also exists in the silver complexes. Thus, VT-NMR analysis for the silver complex **IV21** was carried out from -30°C to 60°C in $CDCl_3$ (Figure 4-9), as expected, the variation of the proton peaks on benzene rings was observed as H1 and H4 shifted to low field and high field respectively upon elevated temperatures with a 0.2 ppm fluctuation. In addition, a 0.1 ppm shift of methyl peaks was also observed. The variation of the proton signals accounts for the different environment of protons under different temperatures where mainly the protons on the benzene ring are affected due to restricted rotation, which also implied that more than two morphologies of macrocyclic silver complex exist at different temperatures. A rational speculation would be that the several morphologies of silver complex are not rigid conformations and readily convert near room temperature.

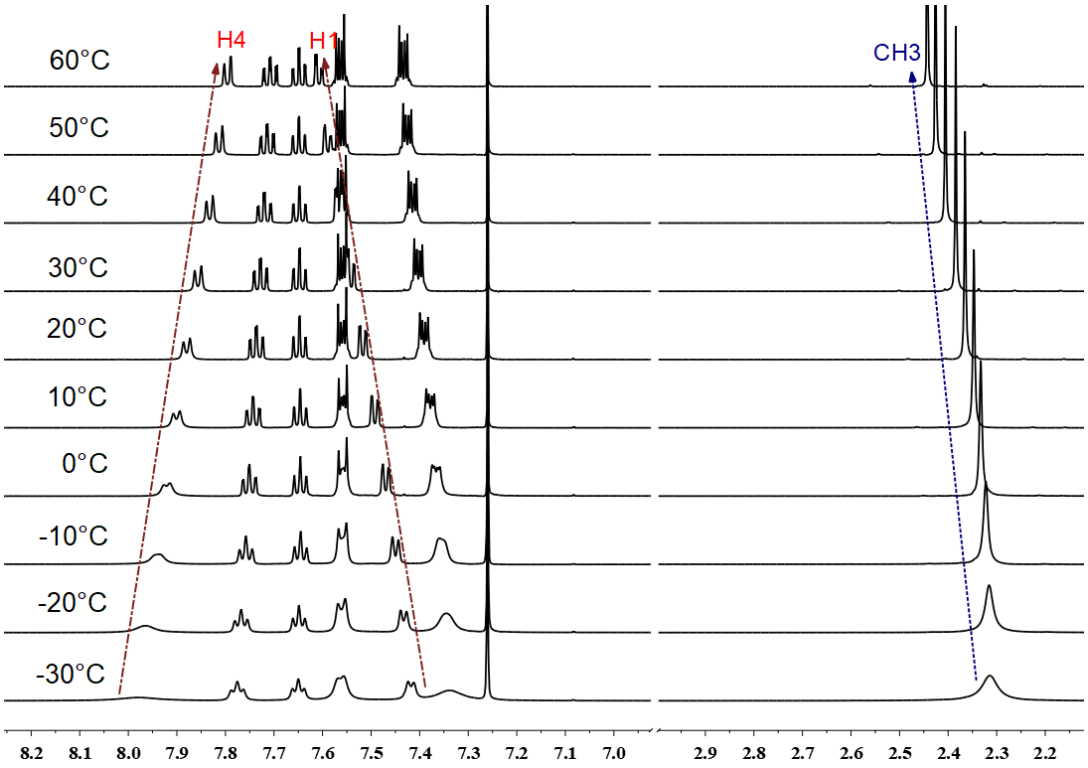

Figure 4-9. Variable temperature ^{1}H NMR of silver complex **IV21** from -30°C to 60°C in $CDCl_3$. The assignment for H1 and H4 protons was based on their multiplicity, a simulation and partially on the 2D NMR.

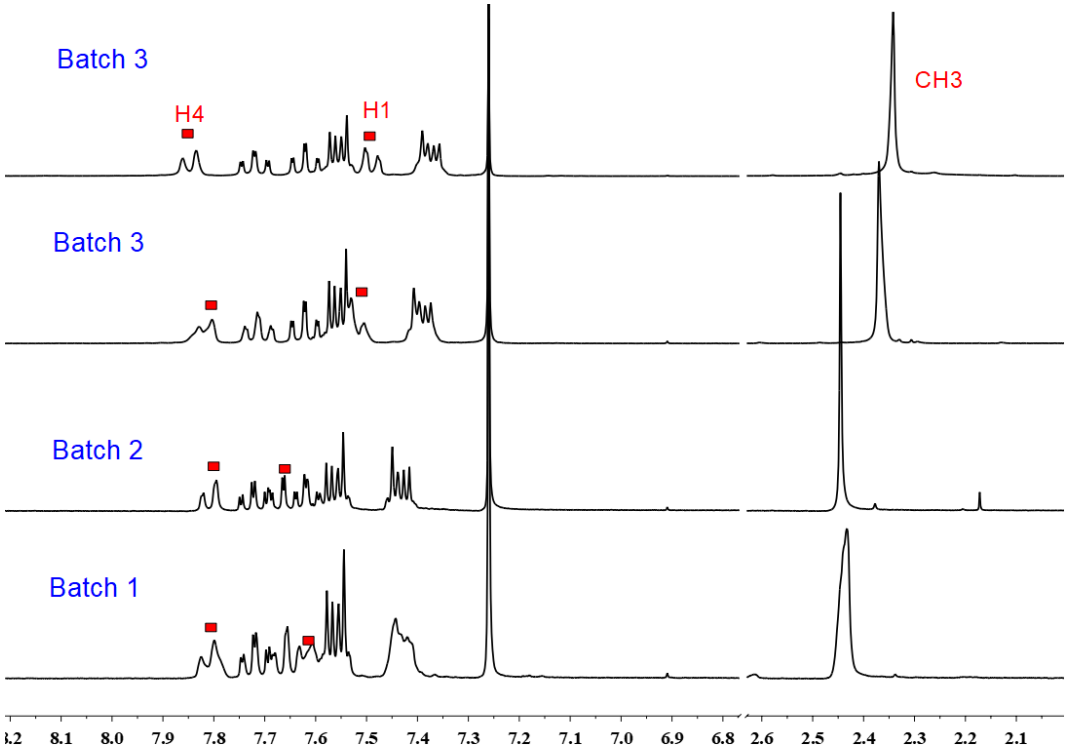

Figure 4-10. ^{1}H NMR of silver complexes **IV21** synthesized with different batches of ligand **IV2** based on the general procedure without any modification.

Surprisingly, the silver complexes prepared from different batches, or even the same batch of ligand **IV2** led to different ^{1}H NMR spectra which showed small shifts (0.05 ppm for H4 and 0.10 ppm for H1) of proton signal[16] (Figure 4-10), while no other difference was found for the several batches of ligand **IV2**. The silver coordination topologies could proceed randomly and are not limited to the two morphologies. The VT-NMR of silver complexes **IV22** also showed a similar trend for the proton variations on the benzene ring.[17] More complicated variations of both protons of on the benzene ring and the anthracene core in silver complex **IV23** were observed based on VT-NMR which can be ascribed to the complex environment inside the metallocage at elevated temperatures.

In order to examine the photophysical properties of ligand and silver complexes, their absorption and emission spectra were collected at concentrations of 20 or 40 µM depending on their chemical structures (Figure 4-11)., Compared to ligand **IV2** (dark blue), the fluorescence emission of silver complexes **IV21-IV23** was slightly quenched probably due to internal conversion whereas the silver complex **IV24** was a little enhanced due to the presence of triphenylphosphine group (Figure 4-11).

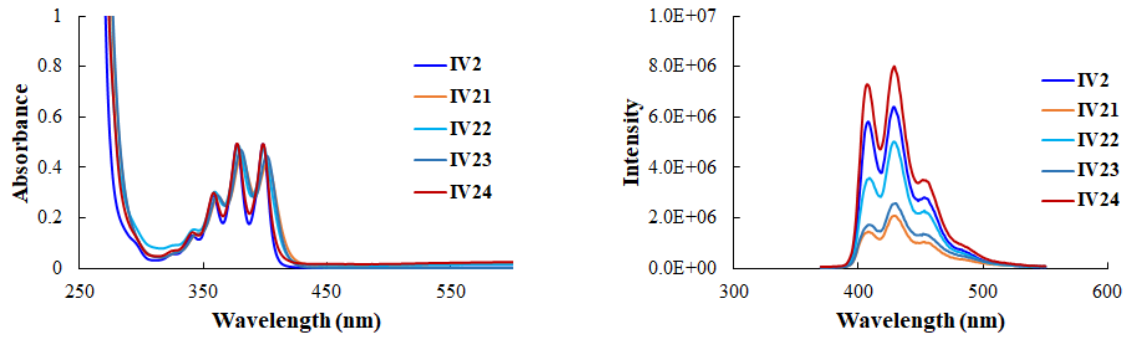

Figure 4-11. UV-vis (left) and fluorescence (right, λ_{ex} = 340 nm) spectroscopy of ligand **IV2** (40 µM, in CH_2Cl_2) and its silver complexes **IV21-22** (20 µM), **IV23** (20 µM) and **IV24** (40 µM).

4.2.4.3 DOSY study

DOSY experiments were conducted to identify the species of silver complexes in solution. Thus, the diffusion coefficients were calculated according to the DOSY study performed in $CDCl_3$ under similar concentrations for comparison (Table 4-1). However, the value of diffusion coefficient showed an average error of ± 15–20% even for the repeat measurement of the identical solution or two separated samples from the same batch with same concentration (Table 4-1, batch 2-3). Furthermore, a large difference was observed between different batches of silver complexes under the same concentration (Table 4-1, batch 2 *vs* batch 3) as two times of the diffusion coefficient were observed for batch 3 compared to batch 2. This observation again implied that

[16] The silver complexes **IV22** and **IV23** also showed similar behavior whose ^{1}H NMR always differs between several complex batches.

[17] Details of the other variable temperature ^{1}H NMR can be found in the Electronic Support Information (ESI) of the publication: Z. Cao, A. Lacoudre, C. Rossy and B. Bibal. *Beilstein J. Org. Chem.*, **2019**. *15*, 2465-2472.

various morphologies of the silver complexes coexist in solution.

Table 4-1. Measurements of diffusion coefficients for silver complexes.

Diffusion coefficient[a]	First series Batch 1 (conc.) ($\times 10^{-9}$ m^2/s)	Second series Batch 2 (conc.) ($\times 10^{-9}$ m^2/s)	Third series Batch 3 (conc.) ($\times 10^{-9}$ m^2/s)
IV21	1.85 (6.1 mM)	0.73 (5 mM)[b]; 0.58 (5 mM)[b]	1.69 (5 mM)[c]; 2.00 (5 mM)[c]
IV22	1.76 (6.5 mM)	0.80 (5 mM)[b]; 0.89 (5 mM)[b]	1.69 (5 mM)[c]; 1.35 (5 mM)[c]
IV23	0.93 (7 mM)	0.76 (5 mM)[b]; 0.81 (5 mM)[b]	-[d]
IV24	0.91 (5.7 mM)	0.85 (5 mM)[b]; 0.80 (5 mM)[b]	-[d]

[a] Average diffusion coefficient values calculated for aromatic and aliphatic protons, with estimated errors of ± 15–20%. [b] Measurements were done twice on the same NMR tube. [c] Measurements were carried out on the same batch of complex but done in different NMR tube. [d] Not tested yet

4.2.4.4 Homogeneous silver catalysis

Because silver(I) salts exhibit a high alkynophilicity,[167] silver complexes **IV21-24** were evaluated as homogeneous catalysts in two tandem addition/cycloisomerization of model alkynes **IV34** and **IV36**.

2-Alkynylbenzaldehyde **IV34** was chosen as the first model substrate for a cyclization reaction in the presence of methanol as a second nucleophile.[308] This tandem acetalization/cycloisomerization was previously described in high yields (>95%) using 5 mol% catalyst loadings on quinoline derivatives with AgOTf and on 2-alkynylbenzaldehyde in the presence of an aza-macrocyclic complex of Ag(I) as a catalyst.[309] In our hands, alkyne **IV34** was converted into product **IV35** in good yield (88 %) using AgOTf

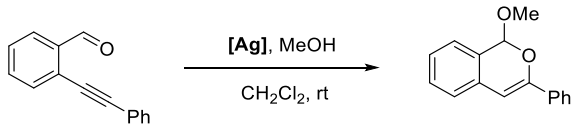

IV34 **IV35**

Table 4-2. Addition/cycloisomerization of alkyne **IV34**.

Entry[a]	[Ag] catalyst	Catalytic loading (mol%)	Yield[b]
1	AgOTf	5	88
2	AgOTf	1	89
3	**IV21**	1	92
4	**IV21**	0.5	92
5	**IV22**	1	73
6	**IV23**	1	85
7	**IV24**	1	65

[a] Unless specified, all the reactions were carried out in dry CH_2Cl_2 at room temperature for 12-16 h with alkyne **IV34** (0.15 mmol), MeOH (0.45 mmol) and a silver(I) catalyst (0.5-5 mol%). [b] Isolated yield.

at 5 mol% (Table 4-2, entry 1). Interestingly, we were also able to isolate 1-methoxy-isochromene **IV35** in 89 % yield, using 1 mol% AgOTf (Table 4-2, entry 2). All silver complexes **IV21-24** (1 mol%) efficiently catalyzed the intramolecular cyclization with 73-92% yields (Table 4-2, entries 3-7). The transformation reached 92 % yield by employing **IV21** at 0.5 mol% (Table 4-2, entry 4). Compared to literature, catalyst **IV21** is efficient for the tandem cyclization of 2-alkynylbenzaldehyde **IV34** at lower loadings and under smooth conditions (20°C, full conversion after 12h). As previously observed for inorganic Ag salts, the catalytic efficiency for this cyclization slightly depends on the nature of the anion.

To further demonstrate the catalytic property of silver(I) complexes **IV21-24**, we investigated their performance in the cyclization of alkynone **IV36** in the presence of benzylamine, as a nucleophile that lead to substituted pyrrole **IV37**. This tandem condensation/cycloisomerization was previously reported in 78% yield using AgOTf at 5% mol (reaction time 3.5 h, 50°C).[310] It is noteworthy that at 50°C, the transformation occurs in 35 % yield without any catalyst (Table 4-3, entry 1). In our hands, using AgOTf (2.5 mol%), gave the product in 73 % yield, whereas 67–76 % yield was reached when silver complexes **IV21-24** at 1 mol% were employed (Table 4-3, entries 2-6). Interestingly, a lower catalytic loading of 0.5 mol % allowed the isolation of 73 % of pyrrole **IV37** in the presence of catalysts **IV21** and **IV22** (Table 4-3, entries 7-8). Under the same conditions, the catalytic efficiency of **IV23** and **IV24** was slightly lower (64–67 % yield) but similar to AgOTf at 2.5 mol% (Table 4-3, entries 9-10). For this second tandem model cyclization, the effect of the anion on the catalyst's efficiency was small.

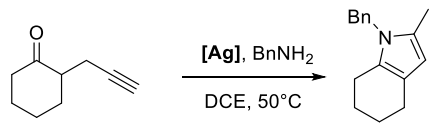

IV36 **IV37**

Table 4-3. Condensation/cycloisomerization of alkyne **IV36**.

Entry[a]	[Ag] catalyst	Catalytic loading (mol%)	Yield[b]
1	-	-	35
2	AgOTf	2.5	73
3	**IV21**	1	76
4	**IV22**	1	67
5	**IV23**	1	72
6	**IV24**	1	76
7	**IV21**	0.5	73
8	**IV22**	0.5	73
9	**IV23**	0.5	67
10	**IV24**	0.5	64

[a] Unless specified, all the reactions were performed at 50 °C under argon atmosphere in dry 1,2-dichloroethane for 12-16 h, in the presence of alkyne **IV36** (0.2 mmol), benzylamine (0.3 mmol) and a silver(I) catalyst (0.5 mol%-2.5 mol%). [b] Isolated yield.

In conclusion, the well-defined thioether silver complexes as homogeneous catalysis exhibit similar or slightly higher efficiency compared to simple AgOTf. In the future, a better opportunity for the application of these silver complexes might be searching bifunctional catalysis based on their macrocyclic structures.

4.2.4.5 New thioether ligands and silver complexes

To illustrate the differences of the *anti*- and *syn*- thioethers in controlling the metal coordination, we turned to design novel DPA-thioether ligands by extending the coordination chain. To our delight, two thioether ligands were obtained as *anti*- (**IV4**) and *syn*- (**IV5**) configurations with a ratio of 3:1 using a cross-coupling reaction between (2-bromophenyl)(2-(2-methoxyethoxy)ethyl)sulfane (**IV3-1**) and 9,10-anthracene diboronic acid bis(pinacol) esters. *Anti*- ligand **IV4** was characterized by XRD analysis. In addition, the *para*-substituted ligand **IV6** was also synthesized[18] to examine the coordination for silver when the two chains are far separated and possibly favoring the intermolecular coordination to form a coordination polymer.[73]

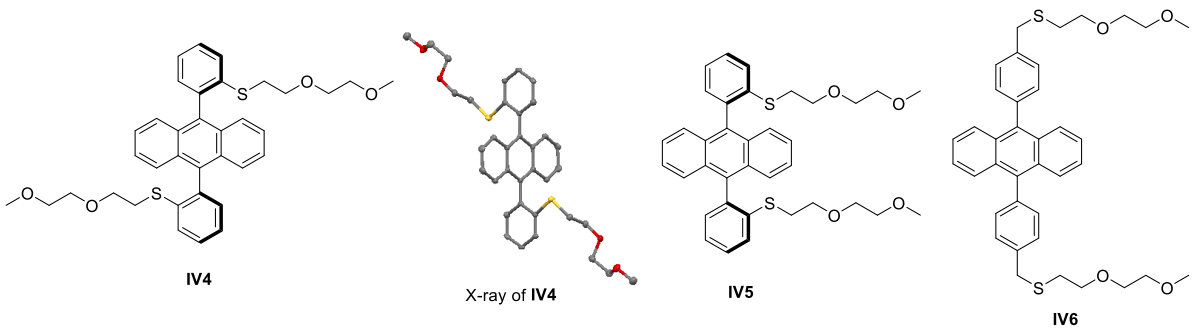

Figure 4-12. New S,O ligands **IV4-6** synthesized for silver coordination by extending the length of coordination chain. The structure of **IV4** was identified by X-ray diffraction analysis.

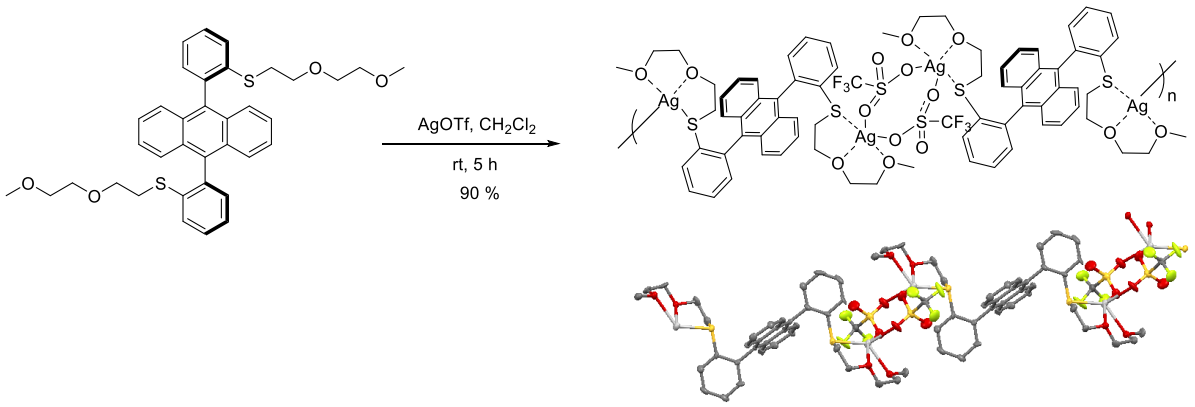

Scheme 4-4. Synthesis of silver complex **IV25** and its structure was determined by XRD analysis.

With the thioether ligands in hand, the silver complexes were readily synthesized by mixing silver triflate

[18] This ligand was also used for synthesis of gold(III) complex by using liquid-liquid extraction to discuss the impact of the chromophore on the reductive speed, the ^{1}H NMR showed a partially coordinated gold(III) complex was obtained as the signal for the ligand remained.

and the ligand. Using the general procedure with anti-ligand **IV4** in CH_2Cl_2 a silver complex **IV25** was isolated in 90 % yield (Scheme 4-4). The slow diffusion of hexane into a solution of complex **IV25** in $CDCl_3$ with a drop of acetonitrile led to white needle crystals. Their X-ray analysis revealed a M2**L**-type coordination polymer through anion contact. The complex **IV27** with silver hexafluorophosphate was synthesized using same approach (the full characterization see Experiment Section). Based on the well-characterized structure of silver complex **IV25**, plausible structures of the silver complex **IV27** could be a discrete or polymeric M2**L**-type complex. Furthermore, the emission spectra was also examined both silver complexes and a fluorescence suppression was observed especially in the case of silver complex **IV27** (Figure 4-13).

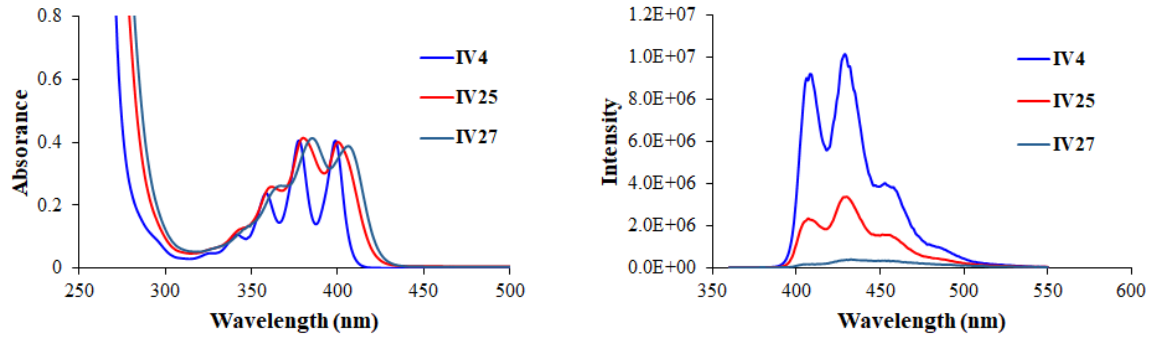

Figure 4-13. UV-vis (left) and emission (right, λ_{ex} = 340 nm) spectra of *anti*-thioether ligand **IV4** and silver complexes **IV25**, **IV27** (30 µM, in CH_2Cl_2)

Similarly, silver complexes **IV26, IV28** involving *syn*- ligand IV5 were synthesized and the structure of the silver complex **IV26** was further characterized by X-ray diffraction analysis with a M**L**-type coordination while the complex **IV28** with $AgPF_6$ probably exhibit similar structures (Scheme 4-5). The emission spectra also showed a fluorescence suppression for both complexes due to an intramolecular energy transfer (Figure 4-14). Finally, the complex between *para*-substituted ligand **IV6** with AgOTf and $AgPF_6$ were also achieved and led to identified structures which could be similar to those of anti-ligand IV4: discrete or polymeric M2L type complexes.

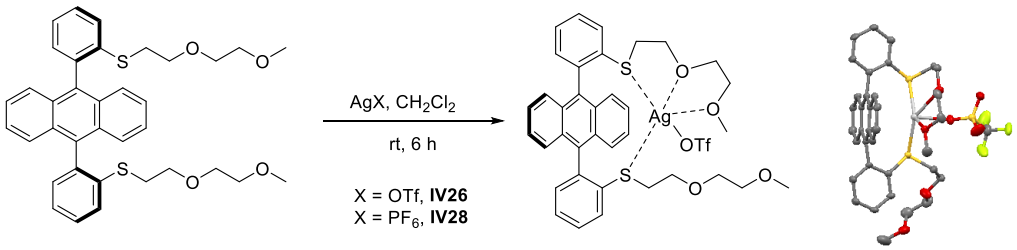

Scheme 4-5. Synthesis of the silver complex **IV26** from *syn*-thioether ligand **IV5**. The structure of the silver complex was identified by XRD analysis.

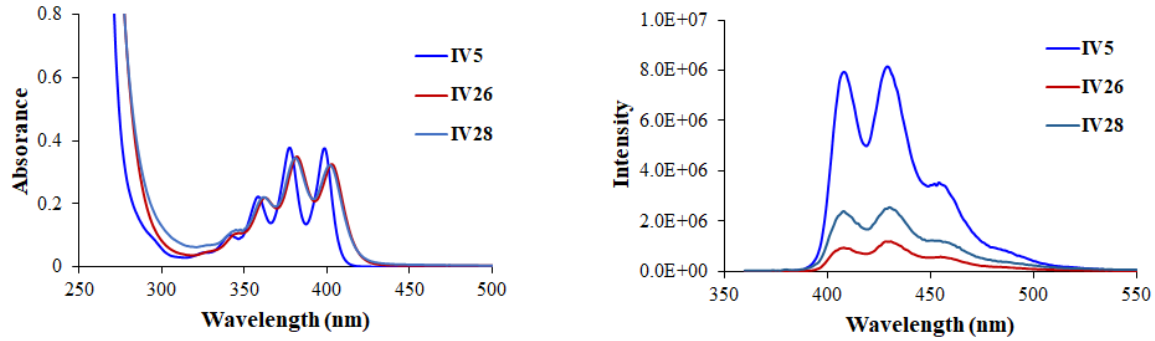

Figure 4-14. UV-vis (left) and emission (right, λ_{ex} = 340 nm) spectra of *syn*-thioether ligand **IV5** and silver complexes **IV26**, **IV28** (30 µM, in CH_2Cl_2)

4.2.5 Conclusion

9,10-diphenylanthracene with two *ortho*-substituted thioether functional groups is an interesting scaffold which allowed us to design and prepare stable *syn*- and *anti*- atropisomers to control metal coordination. Thus, four DPA-based thioether ligands were designed and synthesized. They were readily formed complexes with various silver salts whose geometry can be tuned by the nature of anion or by extending the length of coordination chain.

The thioether ligand **IV2** was first obtained in the *syn*- configuration by a cross coupling reaction in the presence of a protic solvent. Three macrocyclic silver complexes with ligand **IV2** were then synthesized and their coordination modes as revealed by X-ray diffraction were depended on the nature of the anion, for instance, M2**L**2 for $^-$OTf/$^-$OTFA, M6**L**4 for NO_3^- and M2**L** for bulky PPh_3AgOTf. Notably, the ^{1}H NMR and DOSY experiment of silver complex **IV21** prepared from different batches showed a large difference which indicates the morphologies of silver complex might not confined to two isolated diastereoisomers (head-to-head or head-to-tail). These silver complexes were evaluated as homogeneous catalysts in two tandem addition/ cycloisomerization of model alkynes in excellent yields using 0.5 mol% catalytic loading, with efficiencies similar to those obtained with inorganic silver catalysts employed at higher loadings (2.5-5 mol%).

By extending the coordination chain, three DPA-based S,O ligands **IV4-6** were synthesized and six silver complexes were obtained: Two of them showed a M2**L** and M**L** coordination as revealed by XRD analysis.

In conclusion, various silver complexes with DPA-based thioether ligands can be accessed such as macrocyclic M2**L**2, metallocage M6**L**4, discrete M2**L**, polymeric M2**L** and cyclic M**L**. The morphologies of self-assembled silver complexes **IV21-23** are obtained randomly and are probably interconvertible[19] with

[19] To prove the interconversion of the morphologies, the ^{1}H NMR of silver complex under specific temperature need to be evaluated. For instance, measuring the ^{1}H NMR of silver complex in the same NMR tube at 0°C and then 50°C, the system was cooled back to 0°C to check the ^{1}H NMR to see if they are interconvertible. (Notes: the VT-NMR should be evaluated, as no variation was observed when heated and cooled measuring on the normal NMR spectrometer)

a low barrier as the ^{1}H NMR of silver complex showed difference even for different batches.

4.2.6 Perspectives: DPA-based bisphosphine ligand and hemilabile ligands

4.2.6.1 DPA-based bidentate phosphine ligand for gold-π complex

Gold π complexes are gold complexes containing a π-coordination. The first example of a gold(I) π complex(1,5-cyclooctadiene)$(AuCl)_2$ was reported by Chalk and coworkers in 1964 (Figure 4-15).[311] Among the early examples of cationic gold(I) π complexes, Zhang reported that phosphine ligands with a *N*-tethered anthracene unit were able to form cationic gold(I) η^2-arene complexes with strong interaction as Au-C distances are 2.958 and 3.020 Å.[312, 313] Subsequently, Echavarren described cationic η^1 and η^2 gold(I) complexes containing simple arene such as benzene and 1,4-dimethylbenzene that showed the shortest gold to arene distance of 2.20 Å.[314] Since then, examples of gold atom bound to alkene, alkyne, diene, allene have been well documented.[315]

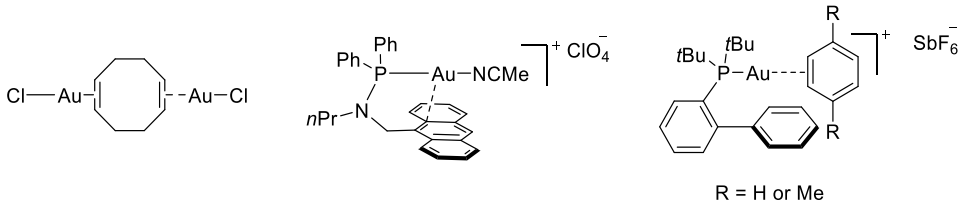

Figure 4-15. Early examples of neutral and cationic gold(I) π complexes.

Based on these results, we thought that the *ortho*-substituted DPA-based bidentate diphosphine ligand could be a good model to form cationic gold(I) arene (probably η^6) complex[312] with the directionality of *syn*-atropisomer. Similarly, the *anti*- atropisomer might lead to dimeric gold(I) arene (probably η^2) complex[313] (Figure 4-16).

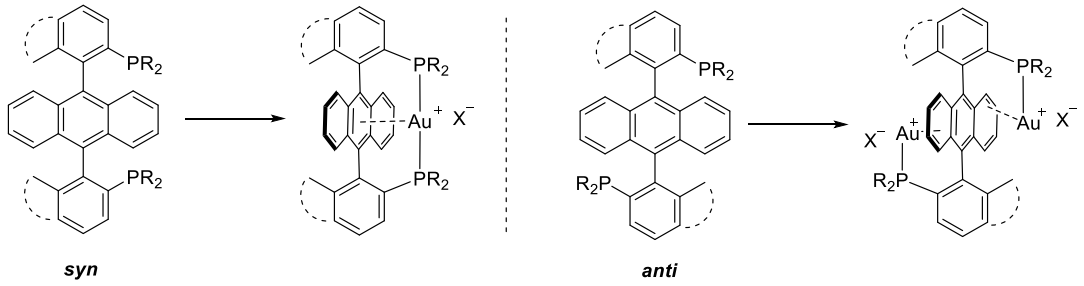

Figure 4-16. DPA-based bidentate diphosphine ligand as model to form gold(I) arene complex.

4.2.6.2 DPA-based hemilabile P,P(X) ligands for gold complex and catalysis

The facile oxidative addition of aryl halides to preorganized carborane-based bidentate phosphine gold complex was reported by Bourissou and Amgoune[76] where the chelating angle is around 90° while no

reaction was observed with a linear coordinated bidentate phosphine gold complex even heated at 120 °C (Figure 4-17). Recently, these authors reported a gold complex based on an hemilabile P,N ligand (Me-Dalphos) that readily proceeded an oxidative addition of aryl halides under mild conditions which circumvented the high redox potential necessary to form gold(III).[75]

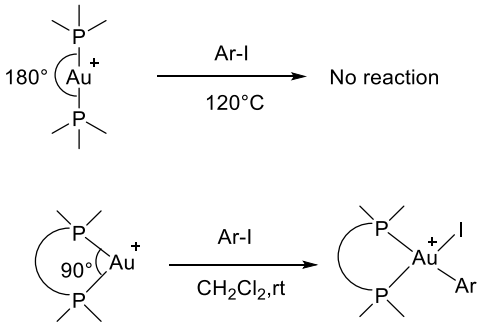

Figure 4-17. Ligand preorganization for gold complex to turn on the oxidative addition of aryl iodides.

Based on the simulated models of gold complex with hemilabile bisphosphane oxide or sulfide gold complexes, the chleating angles are 105.4°and 121.4° respectively (Figure 4-18) might be a candidate to access to the ensuing oxidative addition product.

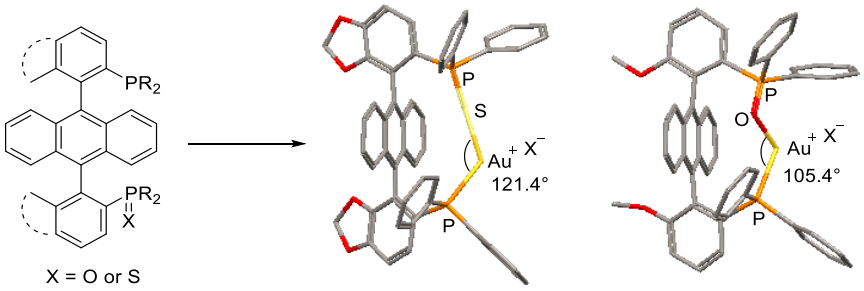

Figure 4-18. Simulated models of gold chelated hemilabile P,P(X) ligands.

4.2.6.3 Preliminary synthesis

The attempts to access to diphosphine ligands via cross coupling reaction showed frustrated results when using 9,10-anthracene diboronic acid bis(pinacol) ester and (2-bromophenyl)diphenylphosphine oxide. While the synthesis of diphosphine oxide can be achieved in 25 % yield by treatment of dibromo-substituted DPA with *tert*-butyllithium and chlorodiphenylphosphine, followed by oxidation by hydrogen peroxide after quenching the reaction

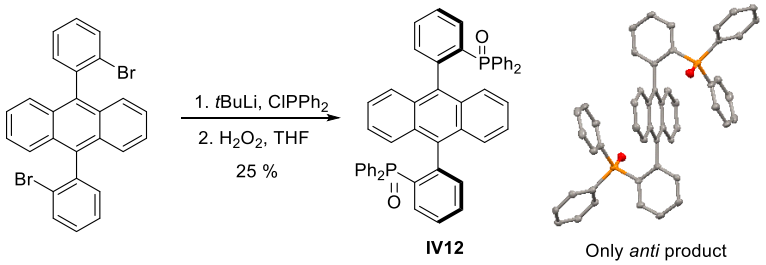

Scheme 4-6. Synthesis of DPA-based bisphosphine oxide **IV12**.

Notably, only *anti*- product was obtained as revealed by X-ray diffraction analysis (Scheme 4-6). Alternatively, an iodide compound was synthesized from 1-bromo-3-methoxybenzene in 2 steps which was expected to possess high reactivity for the Suzuki-Miyaura reaction, that failed to get the desired product (Scheme 4-7). However, the similar approach to access to the bisphosphine sulfide from 5-bromo-1,3-benzodioxole gave 11 % overall yield (Scheme 4-8). The configuration of the phosphine sulfide has not been determined yet.

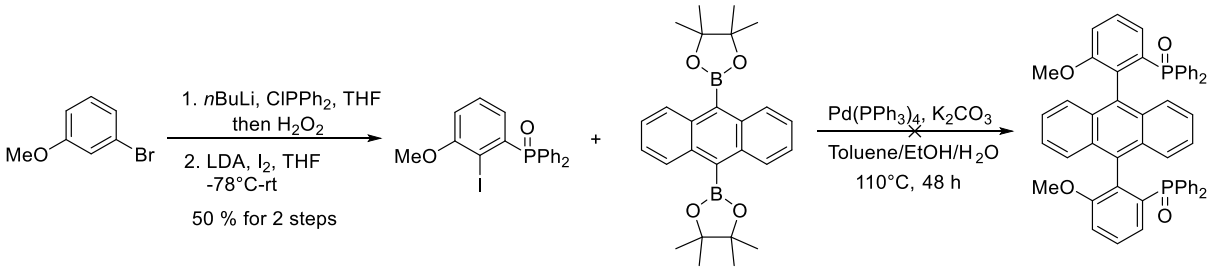

Scheme 4-7. Synthesis of DPA-based bisphosphine oxide via cross coupling reaction.

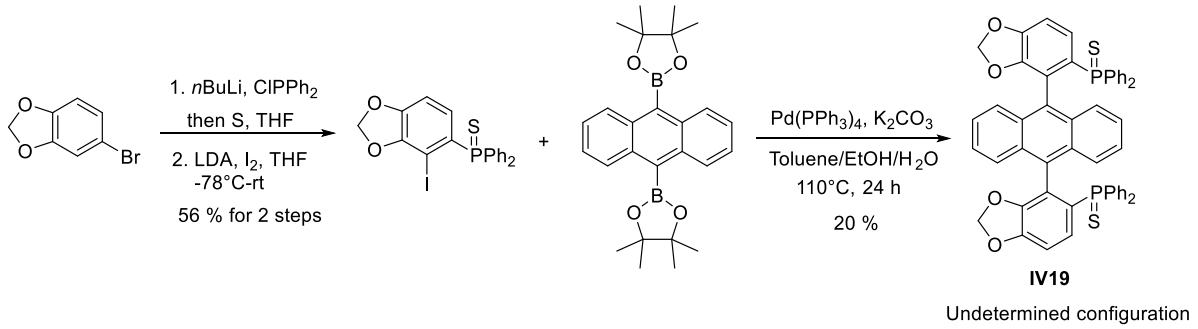

Scheme 4-8. Synthesis of bisphosphine sulfide **IV19**.

Based on these results, future work will be focused on three directions. First, it is important to isolate both *anti*- and *syn*- phosphine atropisomers and further characterize them by XRD if possible. Subsequently, effort can be put to reduce the phosphine oxide to phosphine and examine the formation of gold π complexes, Meanwhile, their photophysical properties are also interesting in view of the relativistic effect of gold. Secondly, the phosphine oxide or sulfide can be partially reduced to a hemilabile P,P(X) ligand, allowing

evaluation of their coordination complexes for catalysis, especially of coinage metal complexes. For the gold complex, the oxidative addition of aryl halides could be evaluated. Finally, the variation of the *ortho*-substituted group might also offer potential for conceiving a bifunctional catalysis merging metal catalysis and organocatalysis.

4.3 Switchable chiroptical property of DPA-based chiral sulfoxides

4.3.1 Introduction

Circular dichroism (CD) originates from the difference between the absorption for left and right circularly polarized light in chiral environment. Circularly polarized luminescence (CPL) spectroscopy refers to the chiroptical property of the fluorescence emission difference between right and left handed circularly polarized light from intrinsically chiral fluorophores or fluorophores in chiral environments, which can be considered as an emission analog of CD. A substantial difference between them is that CD involves the chirality in electronic ground state while CPL pertains to chirality in the emissive excited state. Despite the luminescence dissymmetry factor $|g_{lum}|$ is usually low ranging from 10^{-5} to 10^{-3}, small chiral organic molecules for CPL still are of interest in view of understanding factors influencing CPL. More importantly, on/off switching of CPL might be tuned by external stimuli.

4.3.1.1 Circularly polarized luminescence of small organic molecules

The circularly polarized luminescence of small organic molecules was reviewed by Mori's group in 2018.[316] In this context, a selection of examples of some representative chiral organic molecules that show reliable CPL are presented in Figure 4-19: including chiral cyclic ketones, planar chiral cyclophanes, axially chiral biaryls, helicenes and chiral BODIPY compounds.

4.3.1.2 Circularly polarized luminescence switching

Developing molecules with switchable chiroptical property might lead to novel multifunctional molecular materials for information processing and storage. So far, the control of CPL switching was achieved by changing the conformation changes in the presence of external stimuli.

In 2011, Maeda's group developed controllable CPL by using anion-responsive π-conjugated molecules with a BINOL-boron moiety.[317] Conformation changes by inversion (flipping) of two pyrrole rings due to the anion binding control the chiroptical properties of the anion receptors (Figure 4-20). An OFF/ON switching of CPL was achieved by an oxophilic interaction of homochiral sulfoxide-containing *ortho*-phenylene ethynylene foldamers with a silver cation.[318] The folding induced by silver cation led to stable complexes that present both high g_{lum} values and high quantum yield (Figure 4-21). Recently, Crassous and Autschbach presented an organic helicene equipped with a chiral bipyridine moiety for CPL switching which can be achieved by adjusting the pH (Figure 4-22).[319] More recently, a solvent-induced CPL inversion was realized by using hydrogen bonding to control excimer chirality (Figure 4-23).[320]

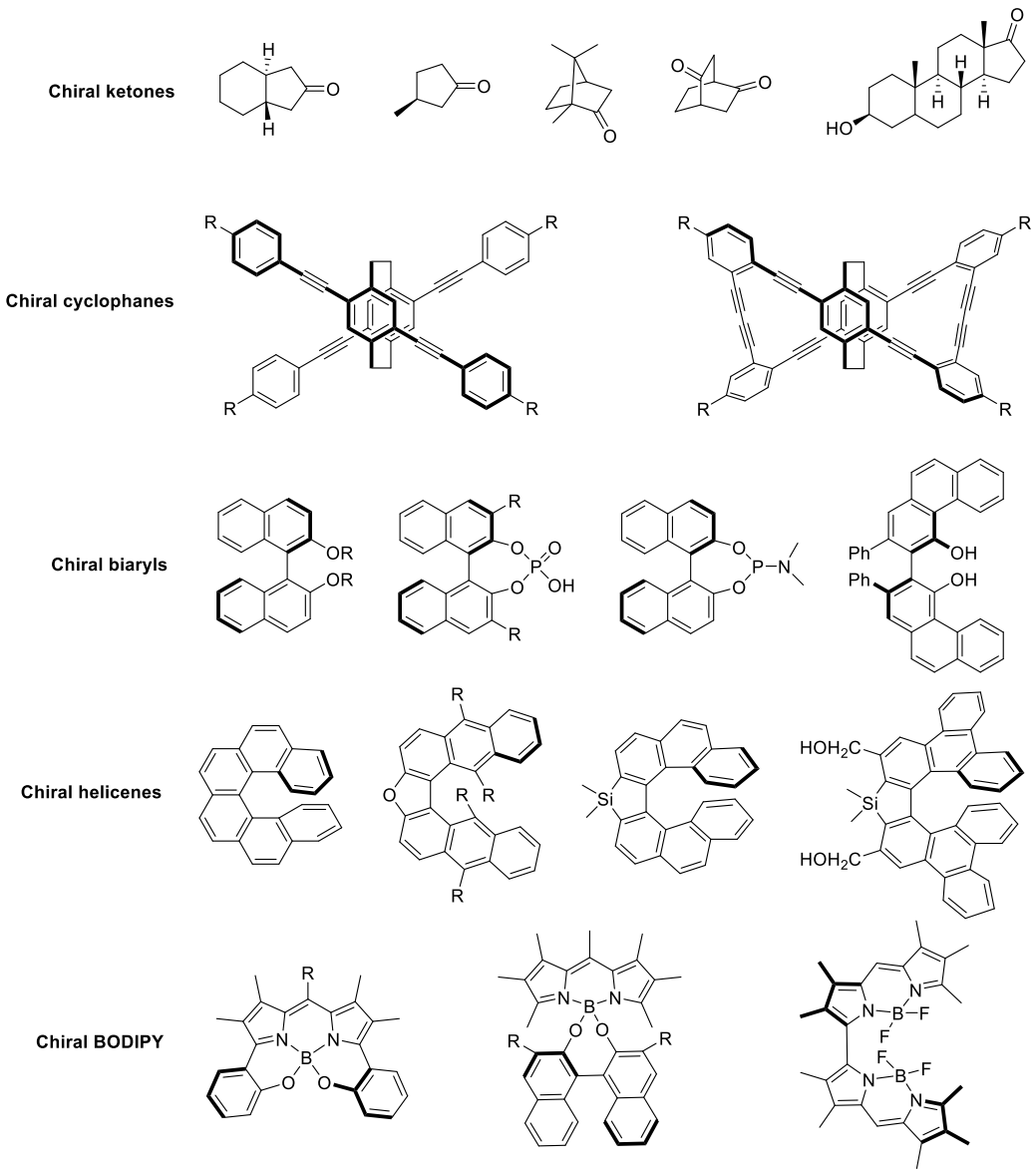

Figure 4-19. Representative chiral organic molecules with CPL properties.[316]

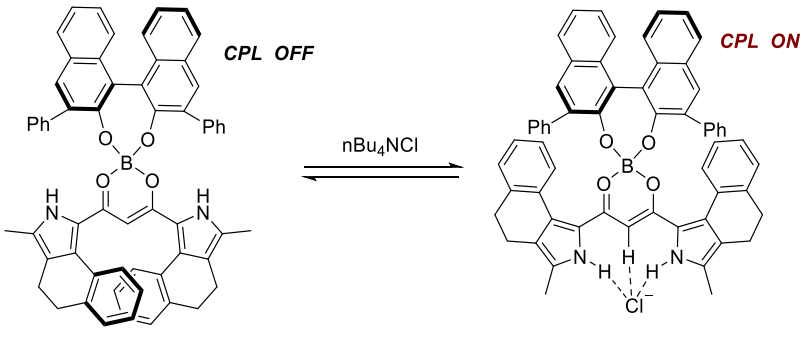

Figure 4-20. Chemical structure of BINOL-based anion receptor and its anion-binding mode.[317]

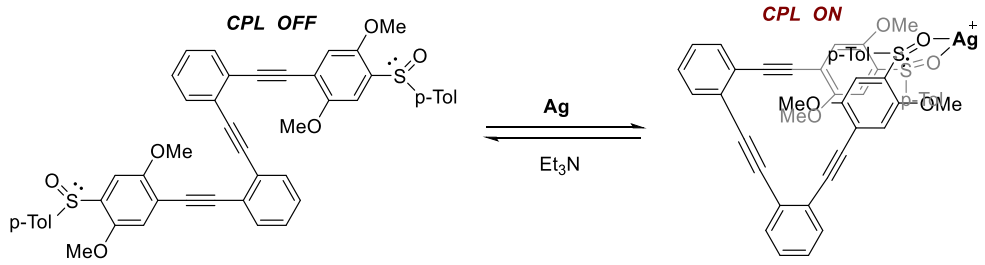

Figure 4-21. OFF/ON switching of CPL by oxophilic interaction of homochiral sulfoxide-containing *ortho*-phenylene ethynylene foldamers with silver cation.[318]

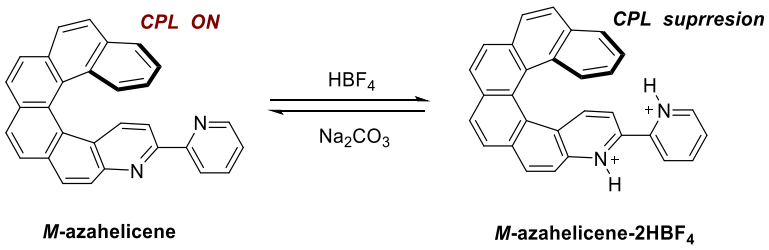

Figure 4-22. pH-triggered CPL switching of azahelicene.[319]

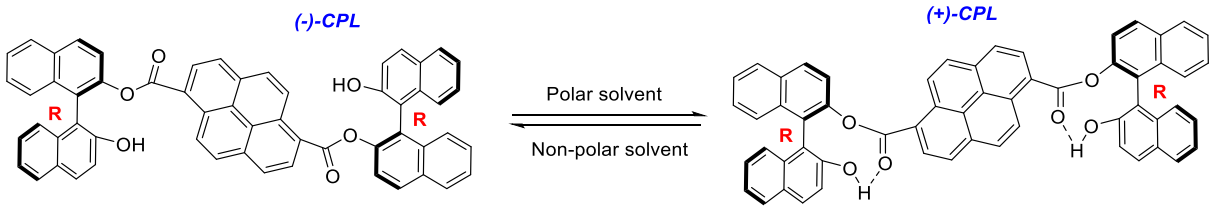

Figure 4-23. Solvent induced inverse CPL switching by hydrogen bonding.[320]

In conclusion, numerous chiral organic molecules exhibit chiroptical properties. The development of switchable CPL systems is interesting for further multi-functional materials sensitive to external stimuli: ion, pH, solvent or temperature.[321] However, the current access to chiral molecular systems is still a bit more complicated due to multi-step synthesis. The development of simpler molecular systems for further practical uses is rare.

4.3.2 Objectives

Simple organic molecules capable of chiroptical properties are attractive due to their facile synthesis, easy modifications and importantly, tunable properties via external stimuli. Circularly polarized luminescence (CPL) has already been obtained in many chiral systems such as chiral binaphthyl skeleton,[83-85] chiral spiro scaffold,[86, 87] and chiral helicene systems.[88-90] So far, progress has been made in controlling on/off CPL

switching by external stimuli. [322, 323] We seek to develop simpler fluorescent molecules incorporating with a chiral group that are sensitive to an external stimulus controlling the CPL signal in an on/off manner. Thus, a DPA provided with a chiral sulfoxide groups is anticipated to perform a modification of the CPL signal in the presence of singlet oxygen through the fluorescence emission quench (Scheme 4-9). In addition, the coordination of metal ions to the sulfoxide group may also be another stimulus for the chiroptical properties variation.

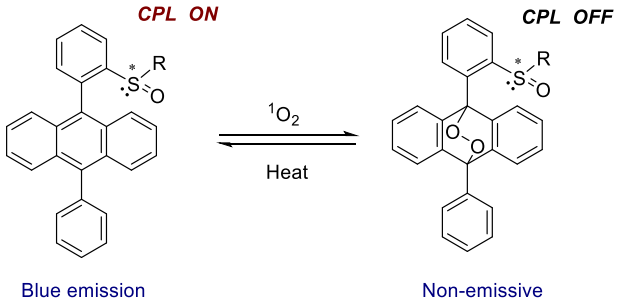

Scheme 4-9. Concept of switchable CPL by using singlet oxygen stimulus.

4.3.3 Experimental

Five sulfoxides **IV7-11** placed at the *ortho*- position of DPA were synthesized by oxidation of the corresponding thioethers. The chiral sulfoxides were separated via chiral HPLC and the absolute configuration was determined by comparison of the calculated and experimental Electronic Circular Dichroism (ECD) spectra. The sulfoxides readily formed complexes mainly with silver, sodium and cesium. The preliminary results of cyclooxidation of DPA sulfoxide **IV7** in the presence of methylene blue and oxygen showed a minor product of 9,10-endoperxoide and a major diendoperoxide **DPAO4** as characterized by mass and ^{1}H NMR. The cycloreversion under thermal conditions (110°C in toluene for 5 h) can partially give back the **DPA**. The chiroptical study of sulfoxides using circular dichroism (CD) and circularly polarized luminescence (CPL) spectroscopy is in progress.

4.3.4 Results and discussion

4.3.4.1 Synthesis of sulfoxides

Five DPA-based thioether ligands were designed (Figure 4-24) as precursors for the corresponding sulfoxides. Mono-thioether **IV1** and **IV3** were synthesized for a comparison with bisthioether ligands (**IV2**, **IV4-5**) toward metal coordination and photo-oxidation in the presence of singlet oxygen. The thioether ligands **IV1** and **IV3** were all synthesized via Suzuki-Miyaura cross-coupling reaction in excellent yield (91 %) and three bisthioether ligands (**IV2**, **IV4-5**) were afore-described to access to various silver complexes.

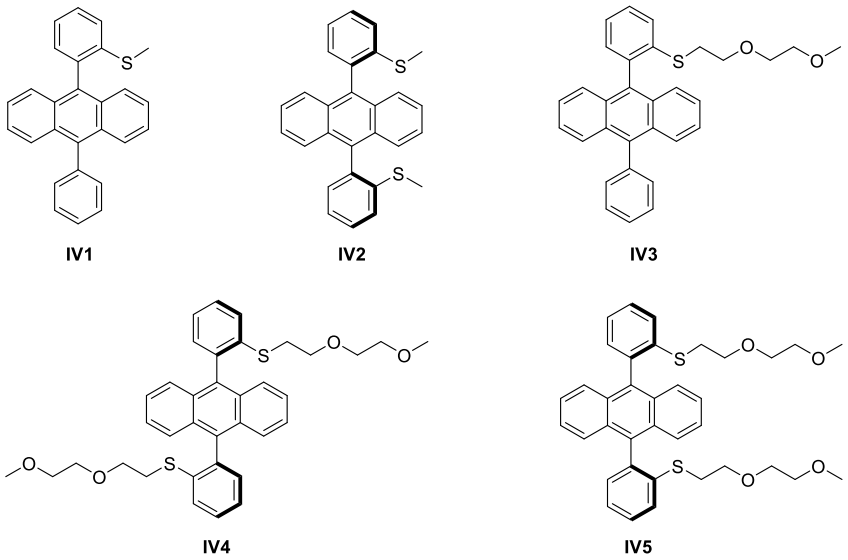

Figure 4-24. DPA-based thioethers as precursors for sulfoxides.

As expected, the DPA-based sulfur monoxides (**IV7-11**) were smoothly obtained via oxidation from corresponding thioethers by treatment with hydrogen peroxide (1.5 equiv for **IV1** and **IV3**, 2.5 equiv for **IV2**, **IV4-5**) in good yield (72-97 %) (Figure 4-25). Noteworthy, the addition of excess hydrogen peroxide (around 30 equivalent) led to sulfone compounds.

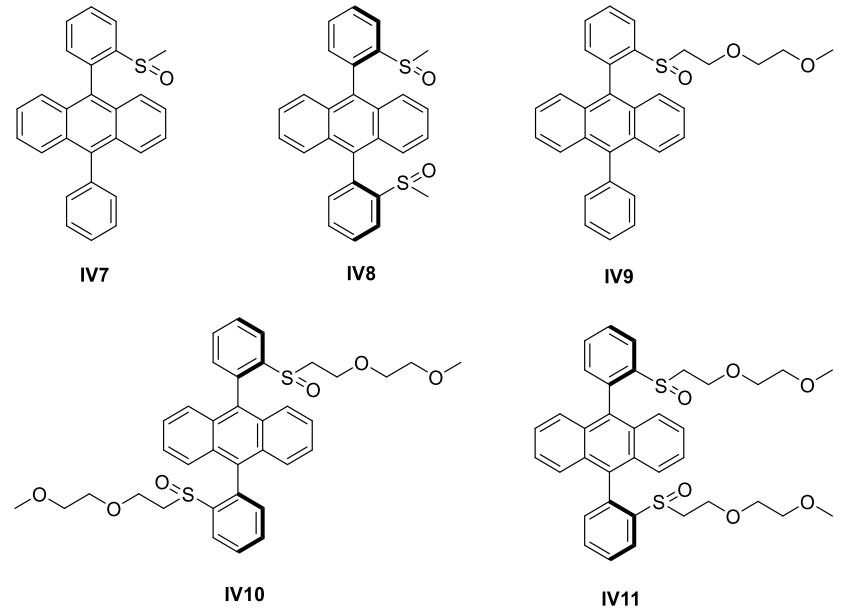

Figure 4-25. DPA-based sulfoxides synthesized from corresponding thioethers via oxidation.

4.3.4.2 Chiral separation and absolute configuration determination[20]

The chiral sulfoxides can be separated by chiral preparative HPLC[21] by using a chiral column of (*S*,*S*)-Whelk-O1 or Chiralpak ID with a solvent mixture of hexane/ethanol/dichloromethane. The purified chiral sulfoxide enantiomers showed reversed optical rotation values.[22] Furthermore, the absolute configurations of the sulfoxides were determined by comparison of the experimental and calculated ECD spectra where the DFT and TD-DFT calculations were performed using Gaussian 16 package, with the default parameters for the solvent used in SMD. Similar electronic circular dichroism (ECD) and UV spectra were obtained for all the sulfoxide enantiomers as strong CD peaks appeared in the region of 185-300 nm while feeble CD signals were observed in the region of 330-410 nm which are in line with the corresponding absorption for the arylsulfoxide and anthracene moieties respectively. Representative ECD and UV spectra of (*S*)-**IV7** and (*R*)-**IV7** are shown in Figure 4-26.

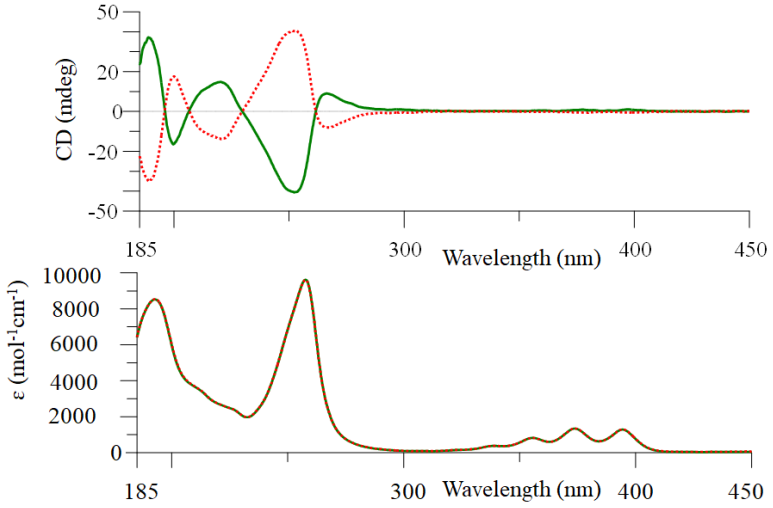

Figure 4-26. ECD and UV spectra[23] of (*S*)-**L1** (Green solid line) and (*R*)-**L1** (Red dotted line) in acetonitrile (180 µM).

[20] The chiral separation and the determination of absolute configuration of the sulfoixdes have been done by Dr. Nicolas Vanthuyne in Institut des Sciences Moléculaires de Marseille, UMR CNRS 7313, Aix-Marseille Université, Campus de Saint Jérôme, Avenue Escadrille Normandie Niemen, 13013 Marseille, France

[21] Exact conditions for chiral separation: For **IV7**, (*S*,*S*)-Whelk-O1 (250 x 10 mm), hexane / ethanol / dichloromethane (20/40/40) as mobile phase, flow-rate: 5 mL/min, UV detection at 280 nm, t1 = 3.80 min (*S*), t2 = 5.53 min (*R*). For **IV8**, Chiralpak ID (250 x 10 mm), hexane / ethanol / dichloromethane (30/40/30) as mobile phase, flow-rate: 5 mL/min, UV detection at 280 nm, t1 = 5.04 min (*S*,*S*), t2 = 6.04 min (*R*,*R*). For **IV9**, (*S*,*S*)-Whelk-O1 (250 x 10 mm), hexane / ethanol / dichloromethane (20/40/40) as mobile phase, flow-rate: 5 mL/min, UV detection at 280 nm, t1 = 3.73 min (*S*), t2 = 4.46 min (*R*). For **IV10**, (*S*,*S*)-Whelk-O1 (250 x 10 mm), hexane / ethanol / dichloromethane (20/40/40) as mobile phase, flow-rate: 5 mL/min, UV detection at 290 nm, t1 = 4.50 min (*S*,*S*), t2 = 8.31 min (*R*,*R*). For **IV11**, (*S*,*S*)-Whelk-O1 (250 x 10 mm), hexane / ethanol / dichloromethane (30/40/30) as mobile phase, flow-rate: 5 mL/min, UV detection at 280 nm, t1 = 4.56 min (*S*,*S*), t2 = 5.50 min (*R*,*R*).

[22] Optical rotations were measured on a Jasco P-2000 polarimeter with a halogen lamp (589, 578, 546 and 436 nm), in a 10 cm cell, thermostated at 25°C with a Peltier controlled cell holder. See detailed optical rotaion under different wavelengths in the Experimental Section

[23] Acquisition parameters: 0.1 nm as intervals, scanning speed 50 nm/min, band width 2 nm, and 3 accumulations for each sample.

4.3.4.3 Metal complex with DPA-based sulfoxide

In order to evaluate metal coordination with sulfoxides, a screening of metal ions were examined. Initially, sulfoxide **IV9** with three potential coordination sites was employed as a model of ligand for coinage metals which enabled fluorescence quenching upon formation of complexes perhaps due to the heavy-metal atom effect of the metal ion. However, complexes with cooper and gold showed no reaction (Table 4-4, entries 1 and 3) while the silver complex was obtained with $AgPF_6$ (Table 4-4, entry 2). To our surprise, the reaction with KPF_6 showed no reaction (Table 4-4, entry 5), while a complex seems to appear in the presence of $NaBAr_F$. Concerning the disulfoxide ligand **IV10**, a complex with $AgPF_6$ also obtained (Table 4-4, entry 7). The ^1H NMR proton shift of complexes with $NaBAr_F$ and $CsBAr_F$ were observed (Table 4-4, entries 4 and 6). Subsequently, the disulfoxides (**IV8**, **IV10-11**) were examined to coordinate with $CsBAr_F$ and all led to formation of new species as the protons were shifted compare to the ligand. However, the identification of the metal complexes structures is in progress.

Table 4-4. Coordination with metal ions.

Entry[a]	Sulfoxides	Metal source	Results
1	**IV9**	$Cu(MeCN)_4PF_6$	No reaction
2	**IV9**	$AgPF_6$	NMR matched silver complex
3[c]	**IV9**	$AuCl(SMe)_2 + AgPF_6$	No reaction
4	**IV9**	$NaBAr_F$	Protons shifted,[b] N. D.[d]
5	**IV9**	KPF_6	No reaction
6	**IV9**	$CsBAr_F$	Protons shifted,[b] N. D.[d]
7	**IV10**	$AgPF_6$	NMR matched silver complex
8	**IV8**	$CsBAr_F$	Protons shifted,[b] N. D.[d]
9	**IV10**	$CsBAr_F$	NMR matched cesium complex
10	**IV11**	$CsBAr_F$	NMR matched cesium complex

[a] All the reactions were performed with sulfoxide (0.01 mmol) and metal source (0.01 mmol); [b] Both aromatic and aliphatic protons were shifted; [c] $AuCl(SMe_2)$ and $AgPF_6$ mixed for 5 min before adding the sulfoxide; [d] N. D. = not determined.

4.3.4.4 Photo-oxidation of anthracene

Initially, the sulfoxide **IV7** was used as a model for the photo-oxidation reaction due to its simplicity. It was fully converted under the conventional cycloaddition conditions (in the presence of 2 mol% methylene blue as photosensitizer and an oxygen atmosphere) (Scheme 4-10). Preliminary results showed that a minor expected 9,10-endoperoxide (**DPAO2**) was formed which was only detected by mass spectroscopy and could not be isolated by column chromatography. A major product **DPAO4** (the sulfoxide compound **IV7** attached with four oxygens) was separated as a pure compound and its chemical formula was confirmed by mass spectra. The speculated structure of the diendoperoxide **DPAO4** might be the double cycloaddition of singlet oxygen to 1,4- and 9,10- positions according to the splitting peaks. However, the configuration of the

diendoperoxide has not been fully confirmed.

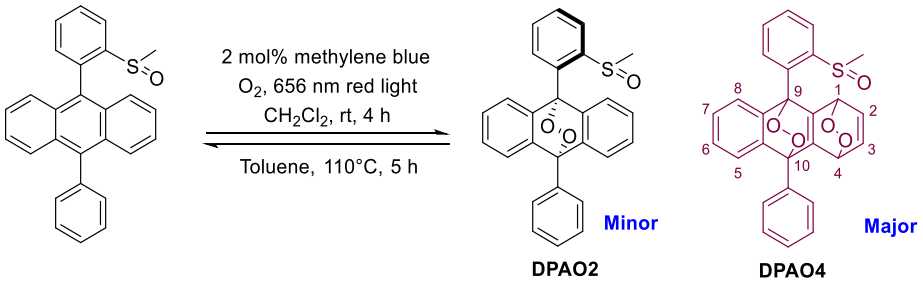

Scheme 4-10. Cyclooxidation of sulfoxide **IV7** by singlet oxygen in the presence of methylene blue under 656-nm red light.

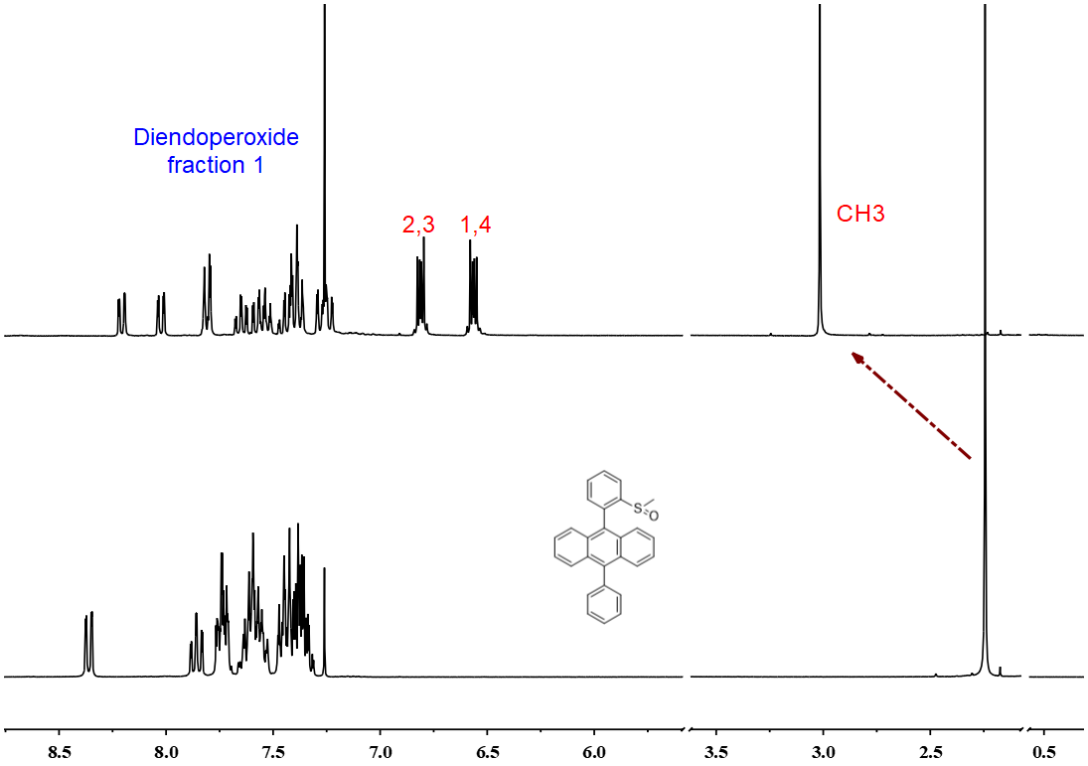

Figure 4-27. ^{1}H NMR comparison of sulfoxide **IV7** and the unidentified endoperoxide **DPAO4** obtained by photo-oxidation.

Based on the ^{1}H NMR obtained, a significant difference of the chemical shift of protons on the methyl group was observed which suggest that the methyl group might exist in a steric hindered environment or be involved in H-O interactions. So far, no reports involving the photo-oxidation of DPA compound containing a sulfur monoxide group was described. Therefore, questions including the unknown stability of sulfoxide in the presence of singlet oxygen, the steric and electronic effects of sulfoxide group for directing a selective formation of unusual DPA endoperoxides remain unanswered. The cycloreversion of the system was also examined by heating at 110°C in toluene for 5 h: partial cycloreversion was observed based on the TLC

analysis. This result could be correlated to the small portion of 9,10-endoperoxide **DPAO2** which was detected by mass spectrometry. Furthermore, the pure endoperoxide **DPAO4** was found to be a thermally stable compound even when heated at 110°C for 30 h.

4.3.5 Conclusion and perspectives

Five DPA-based sulfoxides **IV7-11** were synthesized by the oxidation of their corresponding thioethers. The enantiopure sulfoxides were separated by chiral HPLC separation and the absolute configuration was determined by comparison of calculated and experimental Electronic Circular Dichroism (ECD) spectra. The preliminary chiroptical characterization of (*S*)-**IV7** and (*R*)-**IV7** showed reverse CD and CPL signals..

To achieve the switchable chiroptical property, the reversibility of DPA-based sulfoxide would be the essential problem to be solved. The preliminary result showed that the reaction of DPA sulfoxide and singlet oxygen led to an unusual diendoperoxide product[24] **DPAO4** possibly due to the electronic or steric effects at of sulfoxide. Generally, the 9,10-endoperoxides can be reduced under thermal condition, but this diendoperoxide showed a relatively high thermal stability even heating at 110°C in the toluene for 30 h. Thus, the photocycloreversion of the new diendoperoxide might be an alternative strategy as anthracene endoperoxides were also reported to undergo a photodissociation process towards the anthracene fragment.[324, 325] The *in situ* switchable CPL will be examined once the reversible transformation of DPA-based sulfoxide will be achieved.

From another perspective, the photo-oxidation of other ortho-substituted DPA should be examined to understand this new reactivity on the anthracene core. Carbonyl and phosphoryl substituents could be attractive groups for this study.

[24] A similar ^{1}H NMR was also observed for oxidation of **IV9** under photo-oxidation condition (in the presence of methylene blue and oxygen in CD_2Cl_2 under 656 nm red light for 1 h) and the mass spectra of the crude system is to be tested.

4.4 Chapter summary

Metal complexes with tunable structures maybe of potential use in homogeneous catalysis. We are interested in developing tunable complexes with gold or silver by using thioether ligands. Unlike gold, silver adopts versatile chelating modes with thioether ligands such as linear, planar, and octahedral coordination, even coordination polymer, and cyclic oligomer morphologies where the design is also important.

Several well-defined *syn* and *anti* DPA atropisomers with thioether groups were synthesized and their silver complexes showed diverse coordination modes depending on the nature of the anion and the directionality of the atropisomers as M2**L**2-type macrocyclic, M6**L**4-type metallocage, M2**L**-type dinuclear, M2**L**-type polymeric, M**L**-type arm-closing morphologies were well-identified by XRD analysis and meanwhile, the structures of other six silver complexes are yet to be determined. In conclusion, the DPA-based thioethers are effective to form silver complexes with various morphologies.

DPA provided with chiral sulfoxides were anticipated to perform switchable circularly polarized luminescent (CPL) property in the presence of the singlet oxygen stimulus. Despite the photo-oxidation of DPA-based sulfoxide by singlet oxygen led to a diendoperoxide **DPAO4** product, no thermal cycloreversion was observed. Therefore, the photocycloreversion of the diendoperoxide could be used as an alternative strategy. Once this is solved, the switchable CPL might be realized *in situ*.

Le bonheur est parfois caché dans l'inconnu.

Artiste, écrivain, Poète, Romancier
Victor Hugo (1802 - 1885)

Chapter 5

5 Self-assembled switchable imine cage by using singlet oxygen stimulus

5.1 Introduction

Self-assembled organic molecular cages based on the formation of dynamic reversible bonds went through a large development over the last few decades. In principle, two primary synthetic approaches towards organic cage molecules can be differentiated. One route is a stepwise pathway via irreversible bond formation such as cross-coupling or amidation reactions. The advantages for this approach is the relative chemical robustness thanks to the irreversibility and stability of the cage, which is often obtained in a low overall yield. The second synthetic approach concerns the one-step formation of a thermodynamically preferred products by a reversible bond formation with high yields, leading to cages with a relatively lower chemical stability towards pH for instance.

In 1988, Nelson first described the facile high-yield synthesis of cage molecules by using a one pot route to [2 + 3] imine cages based on the Schiff-base condensation between two TREN molecules and three aromatic dialdehydes.[326] This procedure was later used by others to make even larger hemicarcerands related to known resorcinarenes reported by Cram and Quan.[327] Years later, similar cages were obtained by adding $MgSO_4$[328] or catalytic TFA (5 mol%) [329] under mild conditions. The concept of dynamic combinatorial chemistry (DCC) was first introduced by Jean-Marie Lehn in 1999[330] which features to synthesis of molecular cages in fewer steps from simple precursors. To date, numerous novel functional imine cages were obtained by applying the dynamic covalent chemistry concept. We are interested in investigating switchable molecular cages[9] by introducing an anthracene building-block in the structure. This moiety can be involved in a (4+2) reaction with singlet oxygen to form the corresponding 9,10 endoperoxides and thermal cycloreversion can lead back to the parent anthracene. So far, the anthracene embedded molecular cages are scarce except for some macrocycles derived from anthracene.[331-334] In this regard, a new self-assembled switchable imine cage with three diphenylanthracene pillars are presented, such a rigid cage might exhibit a high modularity as the so-called ‘shape persistent’ cages do. As a result, the background of this work is provided with the following recent examples of imine cages obtained from simple precursors by dynamic covalent chemistry and a few imine cages with tunable properties. The selected examples were presented with classified triamines.

5.1.1 Imine cages

All chosen examples are shape persistent cages with rigid scaffolds. Shape persistent imine cages synthesized through the formation of dynamic covalent bonds represent cage molecules that are not very flexible and contain a cavity that is able to bind small molecules or ions.

In 2007, Warmuth’s group[335] developed an efficient [6+8] reaction towards an exceptionally large covalent rhombicuboctahedral nanocapsule which possesses 14 square- and triangular-shaped molecular components

by using formyl cavitands and 1,3,5-tris(*p*-aminophenyl)benzene (Scheme 5-1). The binding studies showed good encapsulating ability of tetraalkylammonium salts in toluene with binding constants: $K_1 = 10^{(3.6\pm0.1)}$ M^{-1} and $K_2 = 10^{(3.0\pm0.1)}$ M^{-1}.

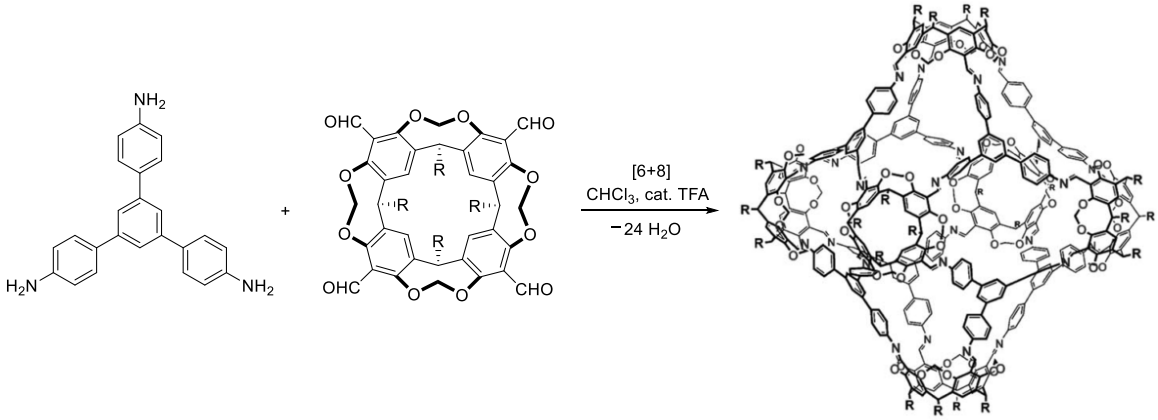

Scheme 5-1. Covalent assembly of giant rhombicuboctahedron imine cage by a [6+8] imine condensation.[335] Reproduced with permission from literature.

In 2008, a shape-persistent *endo*-functionalized [4+6] adamantoid cage[336] was synthesized from a triptycene triamines and a *tert*-butyl-substituted 2,6-diformylphenol via imine condensation (Scheme 5-2). The introduction of the rigid *tert*-butyl group is beneficial to form a hydro-inner cavity due to the steric hindrance.

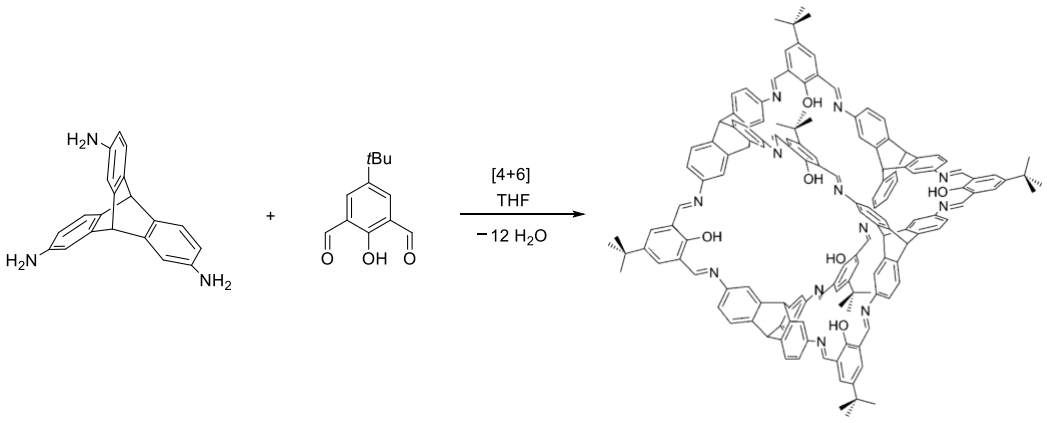

Scheme 5-2. Synthesis of functionalized adamantoid cage based on a triptycene triamine.[336] Reproduced with permission from literature.

In 2006, Roelens reported that the treatment of 1,3,5-tris(aminomethyl)-2,4,6-triethylbenzene with pyrrole-2,5-dicarboxaldehyde in methanol affords a [2+3] imine cage as the single product in quantitative yield (Scheme 5-3). The reaction is driven by the poor solubility of the cage in methanol and, more importantly, this C_{3h} symmetric imine cage is the thermodynamically favored product that arises from condensation of five reacting molecules. Based on the X-ray structure, all the ethyl groups were pointing outward, and the pyrrole rings were facing the cavity. Further binding studies evidenced specific recognition of β-

glucopyranosides.[337] In 2014, a fluorescent [2+3] self-assembled nanoscopic organic cage was obtained in chloroform at reflux via similar approach using a tribenzylamine derivative (Scheme 5-3). The corresponding amine cage obtained by reduction with $NaBH_4$ was further exploited for the highly selective detection of the explosive picric acid monitored by fluorescence emission titration.[338] Recently, Schmidt and coworkers described a porous [4+4] imine cage containing perfluorinated aromatic panels (Scheme 5-3) where the introduction of fluorine on the cage significantly facilitates the CO_2 and H_2 absorption (19 wt% for CO_2 at 273 K, 1 bar and 1.5 wt% for H_2 at 77 K, 1 bar).[339]

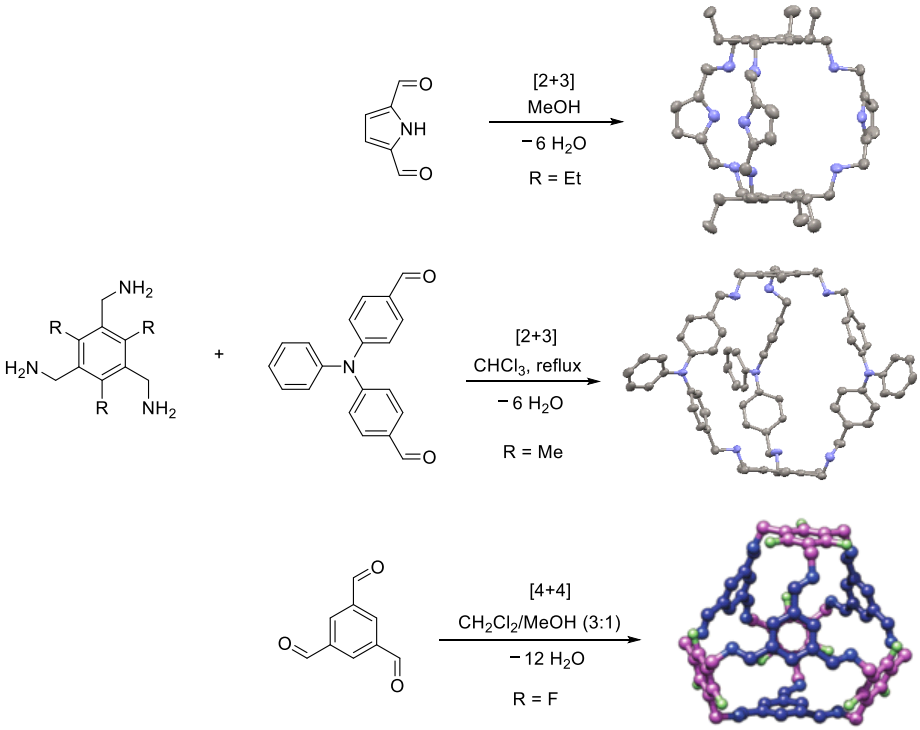

Scheme 5-3. Imine cages formed based on similar tribenzylamines with various aldehydes with the corresponding crystallographic structures (the third X-ray structure is reproduced with permission form the literature[339]).[337-339]

In 2018, a more sophisticated [4+4] imine cage with a truncated tetrahedral geometry was delineated by using conformationally rigid precursors with steric functional groups which is proven to be crucial to form the cage with the assistance of geometrical pre-orientation of reacting groups (Scheme 5-4), otherwise leading to thermodynamic polymerization product.[340] The porous cages were finally evaluated in gas absorption toward CO_2 and CH_4 (13.8 wt% for CO_2, 2.17 wt% for CH_4 at 273 K, 1 bar).

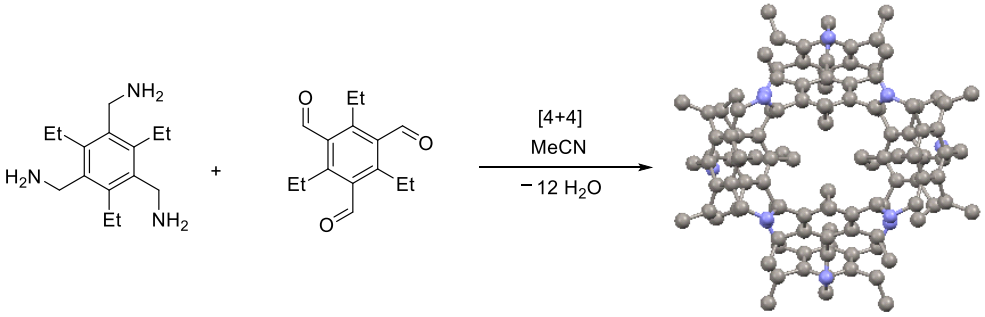

Scheme 5-4. Synthesis of a [4+4] truncated tetrahedral imine cage with corresponding crystallographic structure.[340]

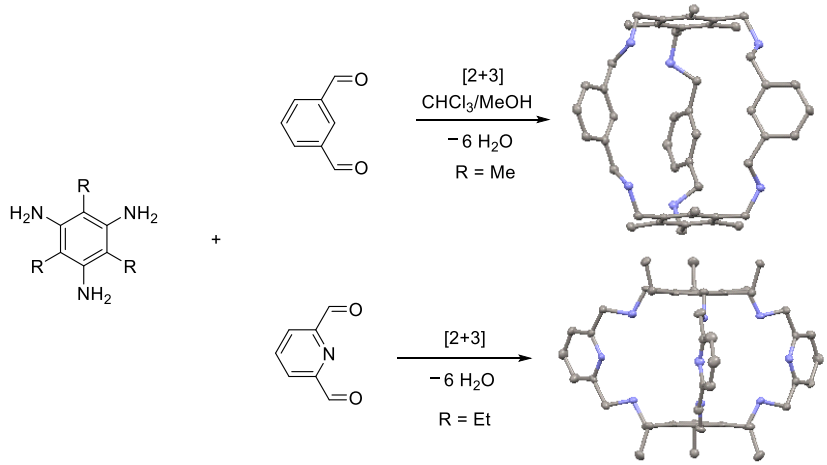

Scheme 5-5. Synthesis of [2+3] imine cage based on similar triaminobenzene and dialdehydes with the corresponding crystallographic structures.[341, 342]

Recently, two smaller [2+3] imine cages with C_3-symmetric macrobicycles were also obtained by dynamic covalent bond formation (Scheme 5-5). The first hexaprotonated cage can encapsulate halides such as chloride and iodide,[341] while the polyazacryptand with three pyridine moieties is a selective receptor for dihydrogen phosphate with protonation constants from 8.72 to 40.39.[342] The same year, using a trisaminobenzene building block, Cooper and coworkers made a computational screening followed by the automatized synthesis of selected organic cages and catenanes (Scheme 5-6). By using this method, 78 precursor combinations were investigated by computation and experiments and finally 33 cages that were successfully formed in one-pot syntheses.[343]

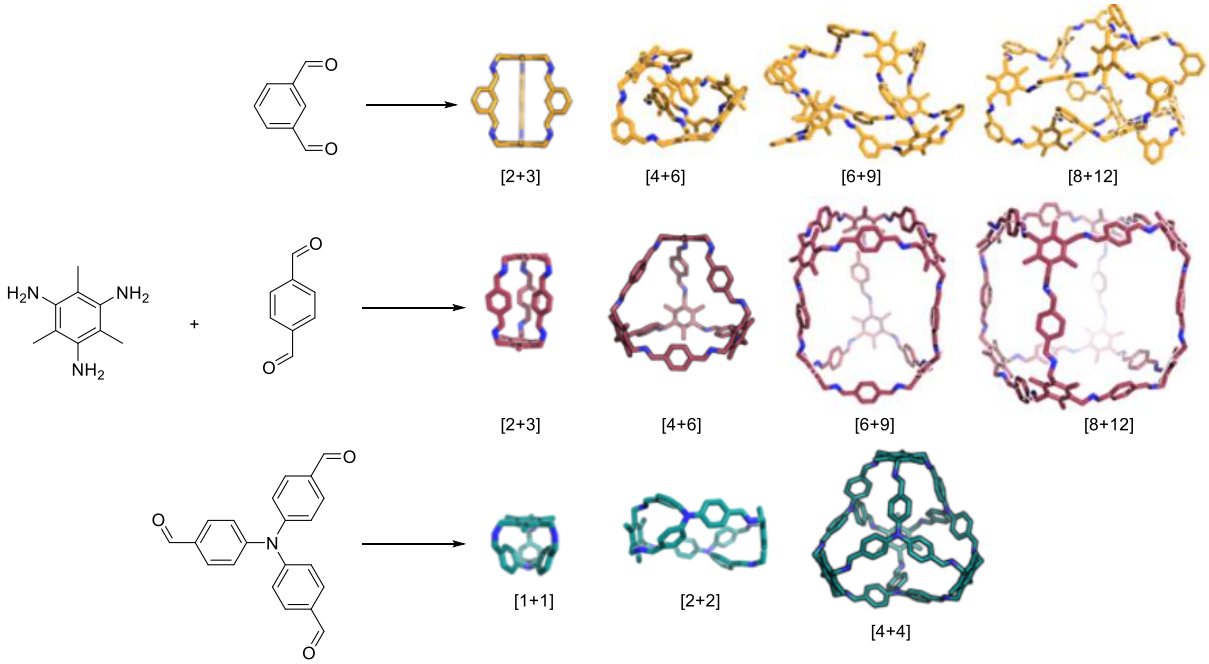

Scheme 5-6. Computationally favorable combinations from trisaminobenzene to form imine cages.[343] The structures are the optimized topologies obtained y modeling.

Enantiopure cyclohexane-1,2-diamine is an important linker for the synthesis of imine cages. In 2011, Cooper's group reported a large self-assembled [8+12] chiral imine cage with inner diameters of 1.2 nm and the cavity of 7500 $Å^3$ obtained from trisaminobenzene and (*R*,*R*)-2-cyclohexanediamine (Scheme 5-7).[344] In 2012, using the smaller 1,3,5-triformylbenzene, the same group developed a shape-persistent porous [4+6] imine cage which is stable in the boiling water and can reversibly absorb 20.1 wt% water.[345] In 2019, an identical cage combined with ultra-small palladium nanoparticle was employed as heterogeneous catalysis in oxidation of carbon monoxide (Scheme 5-7),[346] the cage serves as a stabilizer or support to trap the palladium nanoparticles. In 2015, a well-characterized large chiral triazine-based [4+6] organic molecular cage was obtained by reaction with a large tris-aldehyde in $CHCl_3$.[347] The tetrahedral cage features a large cavity of 2070 $Å^3$ and a surface area of 1181 m^2/g which exhibited selective absorption of CO_2 over N_2 (16.4 cm^3/g for CO_2 and 3.8 cm^3/g for N_2 at 273 K, 1.08 bar).

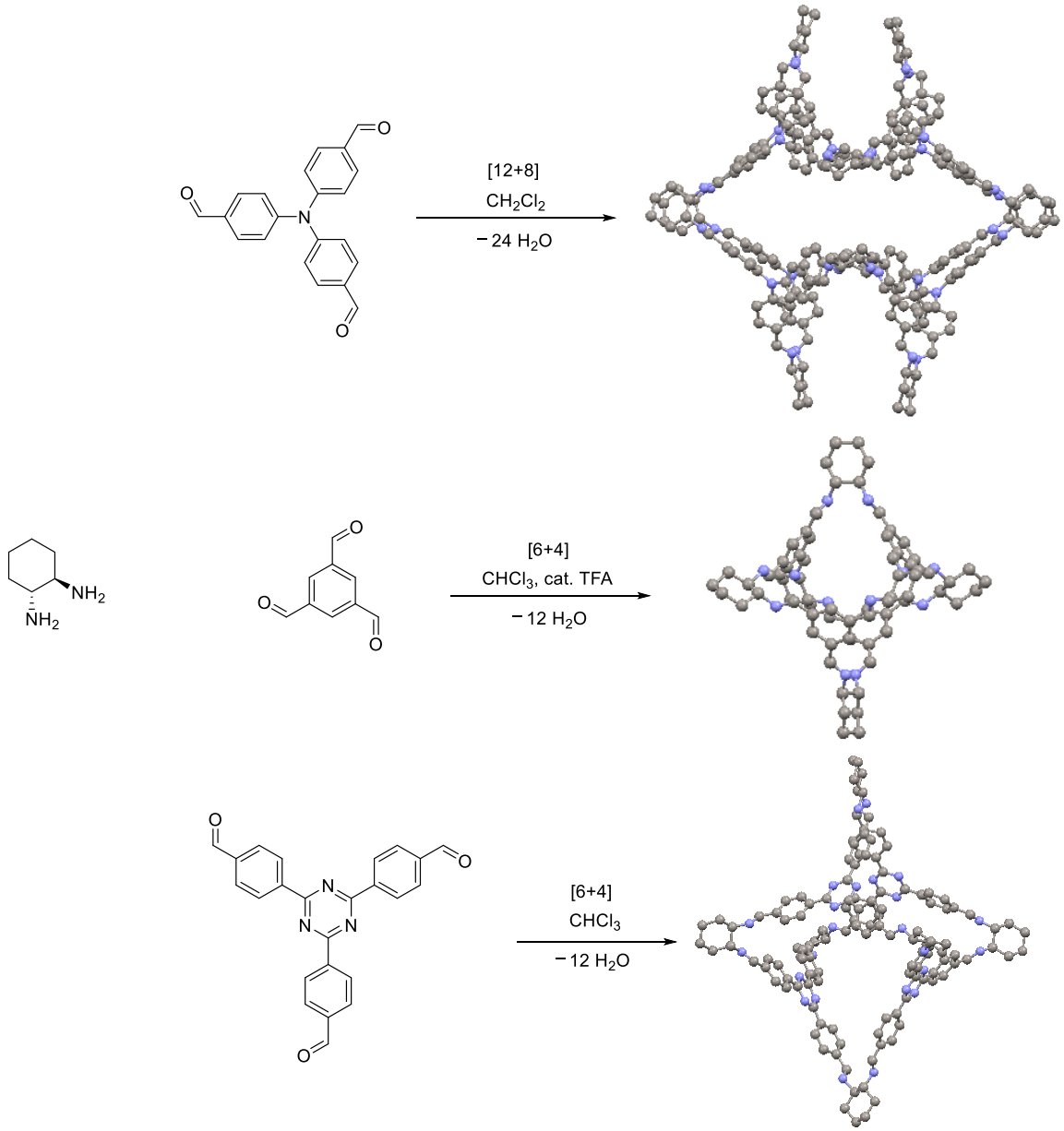

Scheme 5-7. Chiral imine cages based on 1,2-cyclohexanediamines with the corresponding X-rays structures.[344-347]

Interestingly, Cooper and coworkers reported a subtle directionality change on the linker, leading to large differences in cage size: A [4+6] imine cage was formed by using 1,2-cyclohexanediamine with a trialdehyde in one-pot synthesis while the use of 1,3-cyclohexanediamine led to a larger [8+12] imine cage (Scheme 5-8) with a much larger cavity and a surface area of 1750 m^2/g.[348]

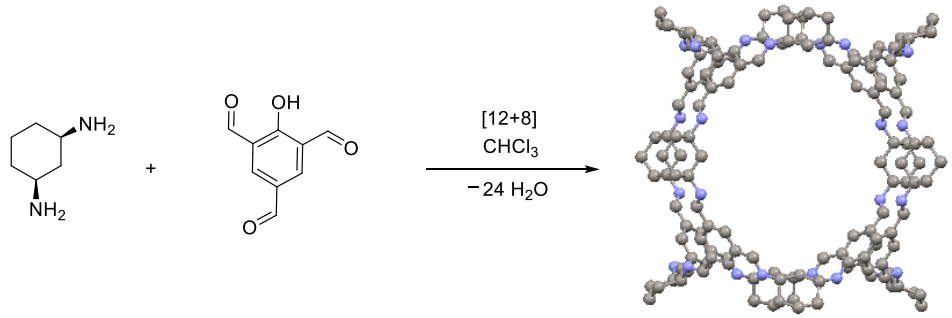

Scheme 5-8. Synthesis of [8+12] imine cage with 1,3-cyclohexanediamine.[348] The cage structure is from X-ray structure analysis.

The self-sorting of reactants involves a spontaneous association through mutual recognition of complementary building units into a well-defined ordered architecture, within a random reaction mixture.[349] This concept was first described by Lehn[350] with the exclusive formation of a helical metal complex from a mixture of several ligands and metal ions. In 2014, Mukherjee's group reported a hydrogen-bond-driven controlled [2+3] covalent cage by employing 2-hydroxybenzaldehyde derivative and a flexible tris(2-amino-ethyl)amine (TREN) (Scheme 5-9). The intramolecular hydrogen bonding involving the phenol and amine groups played a decisive role in selective formation of an imine based organic cage in a mixture of similar dialdehydes.[351] In 2019, Lehn prepared a series of dynamic polyimine macrobicyclic cryptands by using TREN in presence of two bis-formyl aromatics. The self-sorting process was favor of the pyridine containing [2+3] imine cage which was exclusively obtained in 92 % yield. This selection was attributed to intramolecular interactions of imine C-H bonds and pyridine N lone pair.[352]

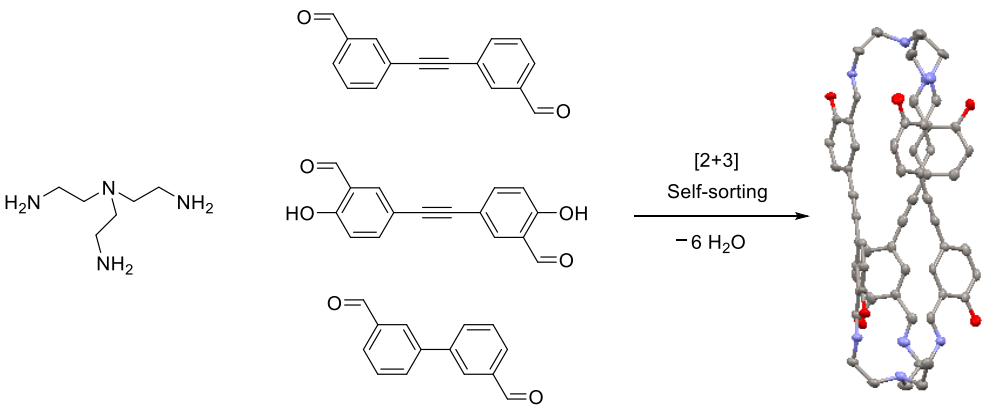

Scheme 5-9. Exclusive formation of cage in Self-sorting approach.[351] The cage structure is from X-ray analysis.

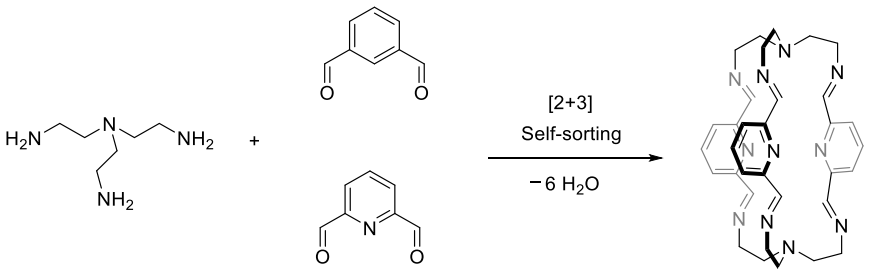

Scheme 5-10. Selective formation [2+3] imine cage with pyridine based dialdehyde in self-sorting approach.[352]

5.1.2 Responsive imine cages

Despite the extensive progress of molecular switches, only a few cases were documented in controlling the properties of molecular cages. A recent case is reported by Mukherjee's group that a spiropyran-functionalized [2+3] imine cage was synthesized via dynamic covalent synthesis which showed reversible thermochromism and photochromism in both solid and solution states (Scheme 5-11).[92]

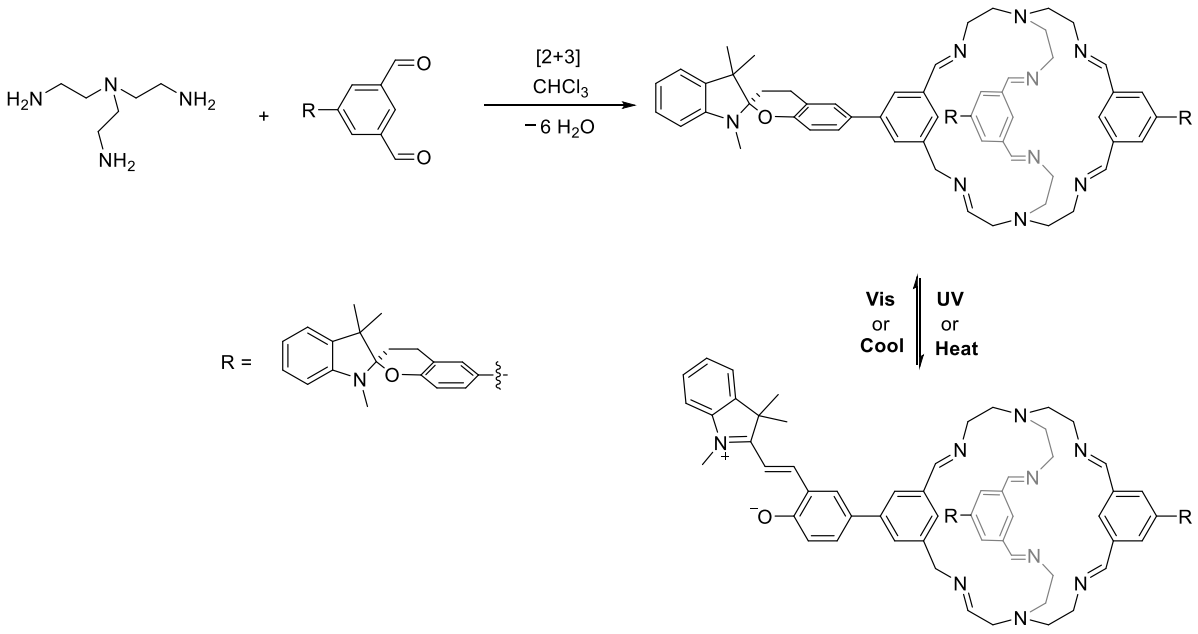

Scheme 5-11. Synthesis of a spiropyran-functionalized imine cage and its reversibility chroism under photo- or thermal conditions.[92]

In 2018, using cyclohexane-1,2-diamine and trisformylbenzene as building-blocks, a porous switchable [4+6] imine cage was developed which is exceptionally stable even in concentrated acid or basic conditions (Scheme 5-12). Interestingly, two different morphologies were obtained simply by changing the solvent. The difference between these two morphologies is the orientation of methoxyl group (cage α with one methoxyl group outside the cavity, cage β three methoxyl groups inside the cavity) which led to selective porosity

towards nitrogen (Conformation I was porous to nitrogen while conformation II not).[353]

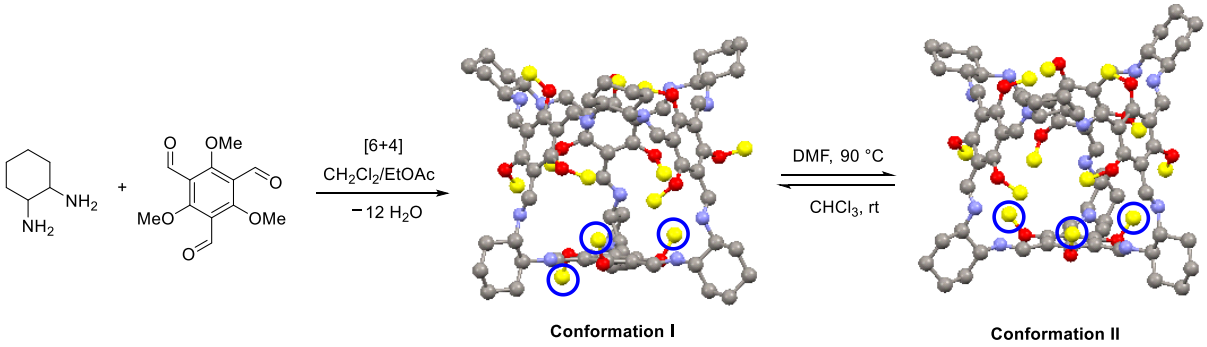

Scheme 5-12. Synthesis of [4+6] imine cage and the reversibility of the morphologies in different solvents with X-ray structures.[353] The methyl connected to oxygen were all marked with yellow color and circles for a better vision of the difference.

In conclusion, dynamic covalent chemistry is a highly efficient approach to obtain self-assembled imine cages with a defined size which can be further transformed into functional amine cages. A subtle change in the chemical structure in building-blocks can lead to dramatic differences in the cage formation or cage size. Recently, a few responsive molecular cages with a switchable morphology has been few documented. Despite the huge progress made in molecular switches, the development of the cages with switchability is still a big challenge. Thus, the development of functional molecular cages obtained by a facile preparation is of great importance, especially when a switchable property is also simultaneously exhibited.

5.2 Objectives

Numerous examples of dynamic covalent molecular cages with different morphologies are known, and some of the them exhibit tunable properties by introducing an external reversible molecular switch[92, 354] or with the assistance of metal coordination.[355] In 2020, Bassani and Bibal published a switchable organic cage by using the reversible addition of singlet oxygen to DPA as a molecular switch. They showed that a classical multi-step synthesis based on covalent chemistry and a final templated metathesis ring-closure successfully gave access to two model cages.[9] The binding property of the cages and their corresponding endoperoxides toward cations were different in strength and, for the first time, the endoperoxide group was demonstrated to be involved in cation coordination (Scheme 5-13).

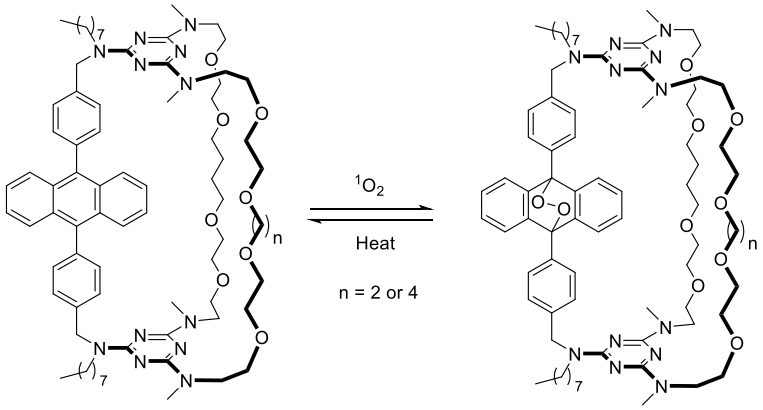

Scheme 5-13. Reversible transformation of DPA-based cage in the presence of singlet oxygen.[9]

We intended to alternatively synthesize switchable molecular cages via the dynamic covalent chemistry approach in one step as the triamines as caps and DPA aldehyde as pillars (Scheme 5-14). The reversible transformation of the cage using singlet oxygen as a stimulus is envisioned. Finally, the binding property of imine cage toward cations are also to be evaluated.

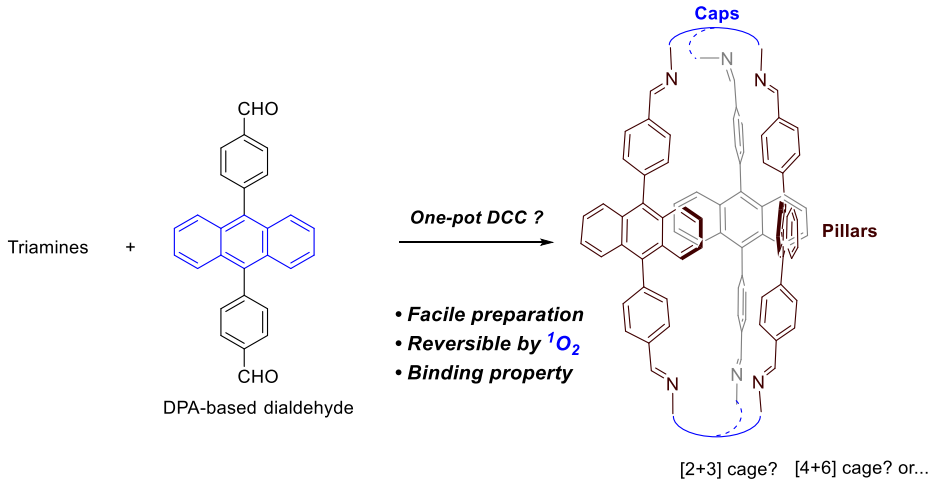

Scheme 5-14. Objectives for accessing a reversible cage by one pot dynamic covalent chemistry.

5.3 Experimental

In this section, the dynamic covalent imine bond formation is exploited to prepare a self-assembled [2+2] imine macrocycle (**V1**) and a [2 + 3] imine cage (**V3**) with chromophoric pillars synthesized by using amine caps (diethylenetriamine and tris(2-aminoethyl)amine (TREN)) and a DPA-based dialdehyde (**V3-1**) pillars in one step. Interestingly, variations of amine caps (**V5-2** and **V6-3**) and methoxyl-substituted DPA based aldehyde (**V7-2**) were all failed to access the corresponding imine cages. The reversible photo-oxidation/thermal reduction processes of the cage (**V3**) in the presence of singlet oxygen was followed by UV-vis and emission spectroscopy. The endoperoxide cage was further characterized by ^{1}H NMR and mass

spectrometry. In addition, the kinetics study and the fatigue cycles in 3-chlorotoluene were also examined. Finally, the qualitative affinity for cations was followed by ^{1}H NMR and the titration experiments were monitored by fluorescence emission.

5.4 Results and discussion

5.4.1 Synthesis of imine macrocycle and cages

The imine macrocycle **V1** was smoothly synthesized in excellent yield by adding a solution of diethylenetriamine in CH_3CN into a solution of DPA-based aldehyde in CH_2Cl_2 with a ratio of 1:1 at room temperature. Notably, the solubility of the DPA-bis-aldehyde is limited to CH_2Cl_2. Furthermore, under the classic reduction condition the corresponding macrocyclic amine **V2** can be obtained in 79 % yield by the treatment of imine marcrocycle **V1** with $NaBH_4$ in a mixed solvent (methanol and CH_2Cl_2) at ambient temperature (Scheme 5-15).

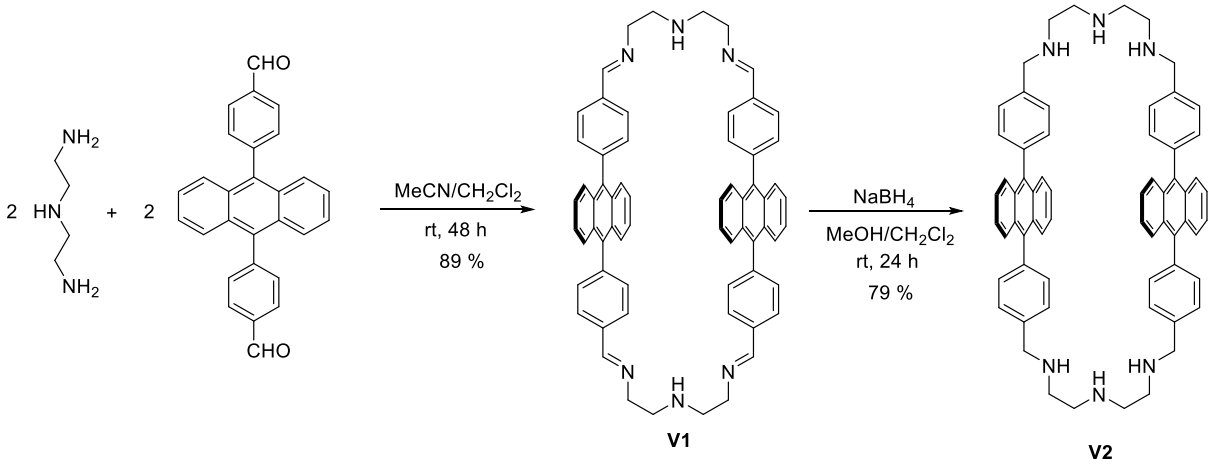

Scheme 5-15. Synthesis of imine macrocyle **V1** and reduction to amine macrocycle **V2**.

Based on the successful synthesis of the macrocycles **V1** and **V2**, a self-assembled [2 + 3] imine cage **V3** was achieved in chloroform with high yield when switching the amine cap to 'TREN'. Generally, polar solvents, such as DMSO, CH_3CN or MeOH were employed for the synthesis of imine cages that precipitate *in situ* and are collected by filtration. In our case, the use of polar solvents led to no reaction while the cage appears as a light yellow precipitate in chloroform at room temperature (Scheme 5-16). Cage **V3** was isolated with a good yield of 74% after a reaction time of 72 h. Notably, the cage can be dissolved in refluxing chloroform but this simultaneously lead to a small decomposition based on ^{1}H NMR. Moreover, several attempts to reduce **V3** into the corresponding amine cage failed using $NaBH_4$, probably due to the poor contact between the reactants of different solubilities.

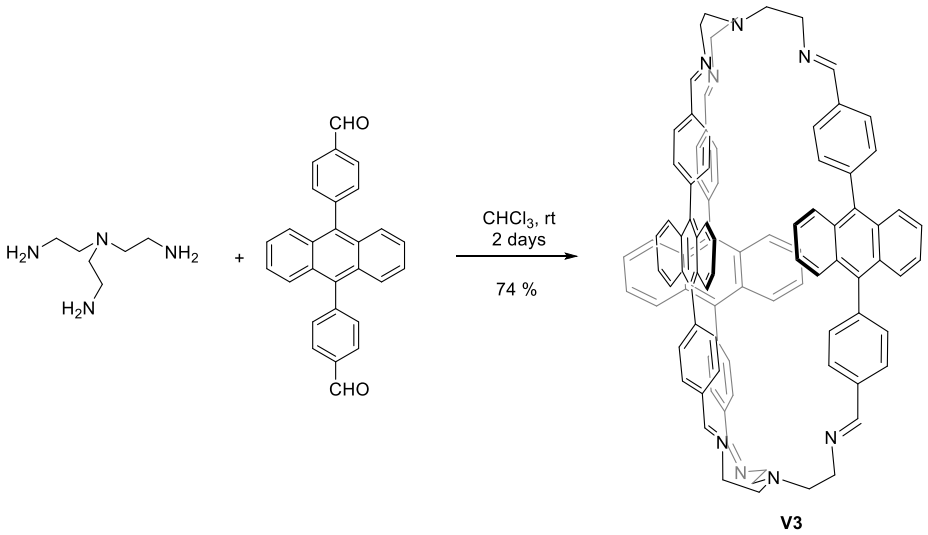

Scheme 5-16. Synthesis of [2 + 3] imine cage **V3** with DPA pillars.

5.4.2 Failed building-block variations towards a series of cages

In order to investigate the scope of the new DPA-imine cages, several combinations of triamines and aldehydes were also examined. Concerning triamines with a C3 symmetry, we synthesized tribenzylamine **V5-2** with a similar length as TREN and a more flexible triamine **V6-3**[25] (Figure 5-1) that could impact the size and flexibility of cages. Meanwhile, a 2,3,6,7-tetra-methoxyl-DPA bis-aldehyde **V7-2** was fabricated to modify the solubility of cages and also to evaluate the steric hindrance impact on the formation of cages.

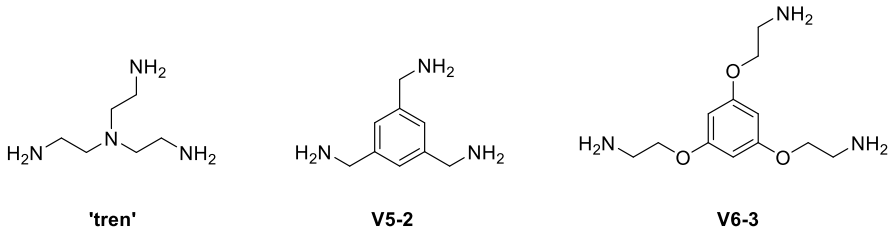

Figure 5-1. Triamines as caps for the synthesis of imine cage.

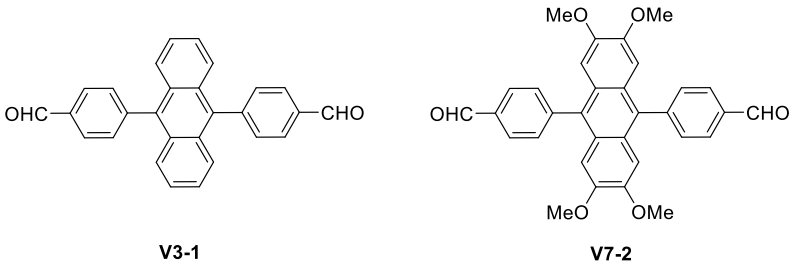

Figure 5-2. Aldehydes as pillars for synthesis of imine cage.

[25] An alternative mild route for the synthesis of triamine **V6-3** was employed and obtained as a hydrochloric salt, details can be seen in the Experimental Section.

To our disappointment, the formation of all desired cages failed using the same conditions as the ones for the obtention of imine cage **V3** (Figure 5-3). Other conditions[26] by varying solvent or adding additives or under heating condition led to no reaction or polymerization, a membrane-like material which is insoluble in any solvent was obtained. Compared to cage **V3**, the failure to access to cages **V5** and **V6** might be due to undetermined directionality of the triamines used. Substituents on anthracene influence the formation of a cage which also imply that imine cage **V3** is a high-rigidity cage.

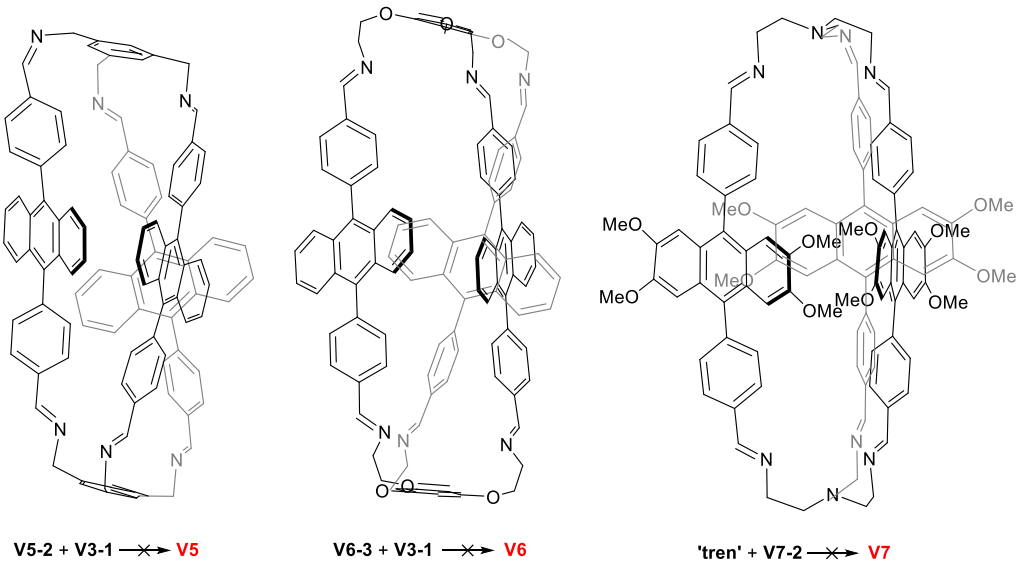

Figure 5-3. Failed combinations for [2 + 3] imine cages.

5.4.3 Reversibility of imine cage V3

5.4.3.1 Reversible transformation of imine cage V3

Diphenylanthracene is well known for its ability to smoothly react with singlet oxygen ($^1O_2$) and form stable 9,10-endoperoxides whose thermal cycloreversion is also highly efficient and affords the parent anthracene chromophore. These reactions are conducted under the conditions developped by our group and were monitored by TLC. Initially, the cyclooxidation process was conducted using the widely-employed photocatalytic approach by using methylene blue as photosensitizer in dichloromethane under near red light irradiation (656 nm) which can be completed in 30 min. The cycloreversion process was carried out in refluxing toluene solution for 12 h (Scheme 5-17).

[26] A clean and dried 10 mL vial equipped with stirring bar was charged with DPA aldehyde (1.5 equiv) and triamine (1.0 equiv). Solvent (MeCN, MeOH, $CHCl_3$ or mixed solvent) (6 mL) was added, and followed with or without base (TEA or DIPEA) (8.0 equiv), with or without $MgSO_4$ (3.0 equiv). The resulting mixture was stirred at room temperature or under heating condition for around 2 or 3 days.

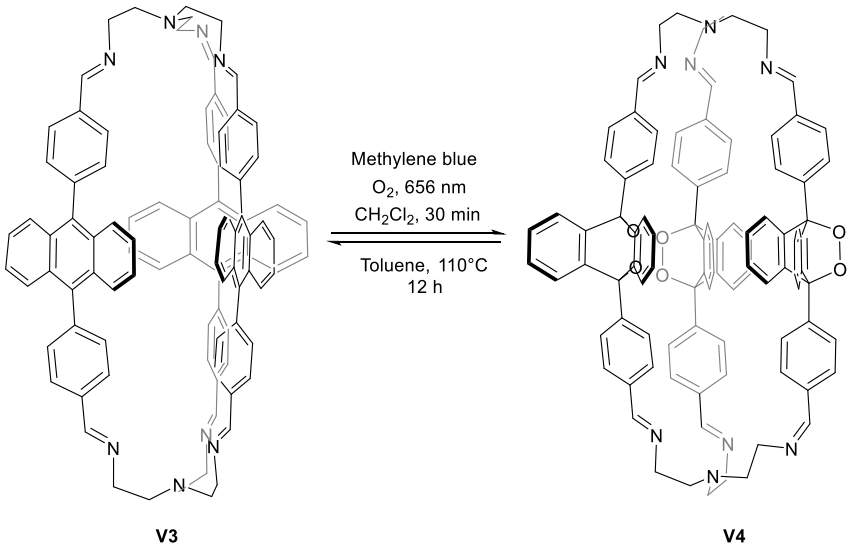

Scheme 5-17. Reversible transformation of imine cage **V3**/ endoperoxide cage **V4**.

The reversible processes were also monitored by UV-vis and fluorescence emission spectroscopy (Figure 5-4) as a drastic decrease of absorbance and emission intensity was observed when DPA is oxidized by singlet oxygen which indicates the complete formation of endoperoxide **V4**. The absorbance and emission of DPA can be recovered during the thermal cycloreversion process. This was further proved by ^{1}H NMR and mass spectrometry (Figure 5-5). However, after the full cycle of $^{1}O_2$ addition and the thermal cycloreversion, partial decomposition (14%) of imine cage **V3** was observed based on the ^{1}H NMR spectra.

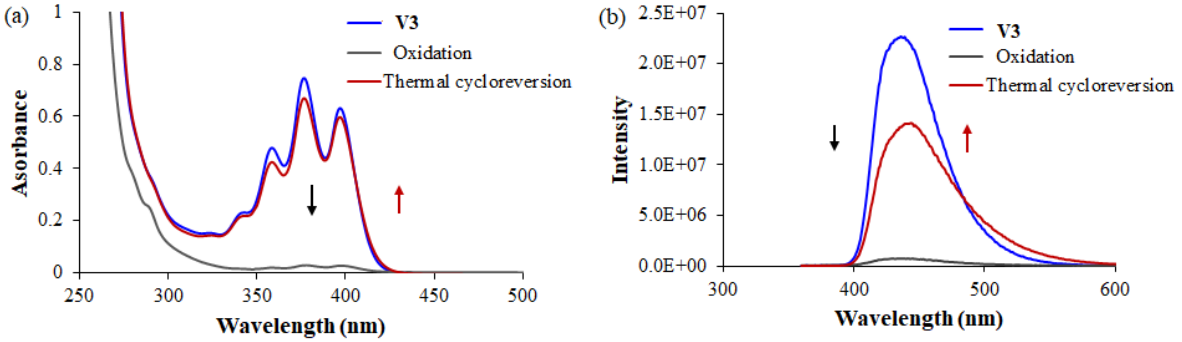

Figure 5-4. Reversible oxidation/reduction of imine cage **V3** (9 µM in CH_2Cl_2, calculated according to the extracted volume) monitored by (a) UV-vis spectra and (b) Fluorescence spectroscopy (λ_{ex} = 340 nm). Imine cage **V3** before irradiation (blue line); Oxidation in the presence of methylene blue and oxygen for 30 min (grey line), thermal cycloreversion at 110°C for 12 h (red line).

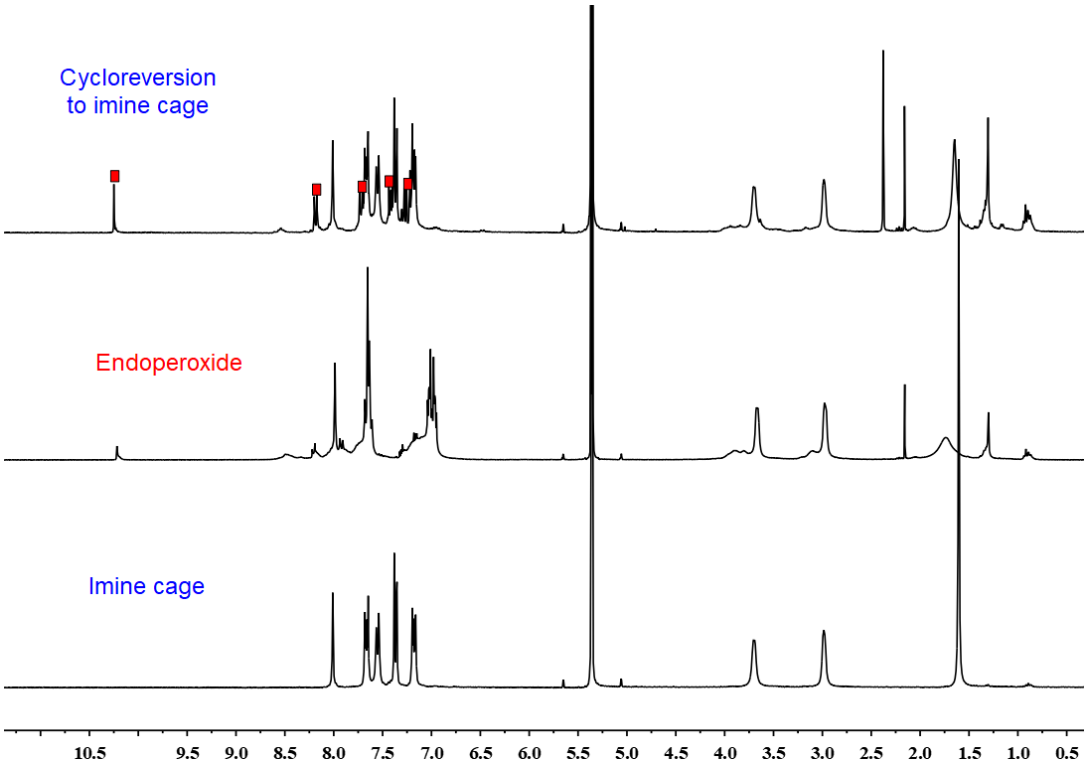

Figure 5-5. ^{1}H NMR monitored reversible transformation of cage **V3**/ endoperoxide **V4.** (Oxidation in the presence of methylene blue (40 mol%) in CH_2Cl_2 and cycloreversion in toluene)

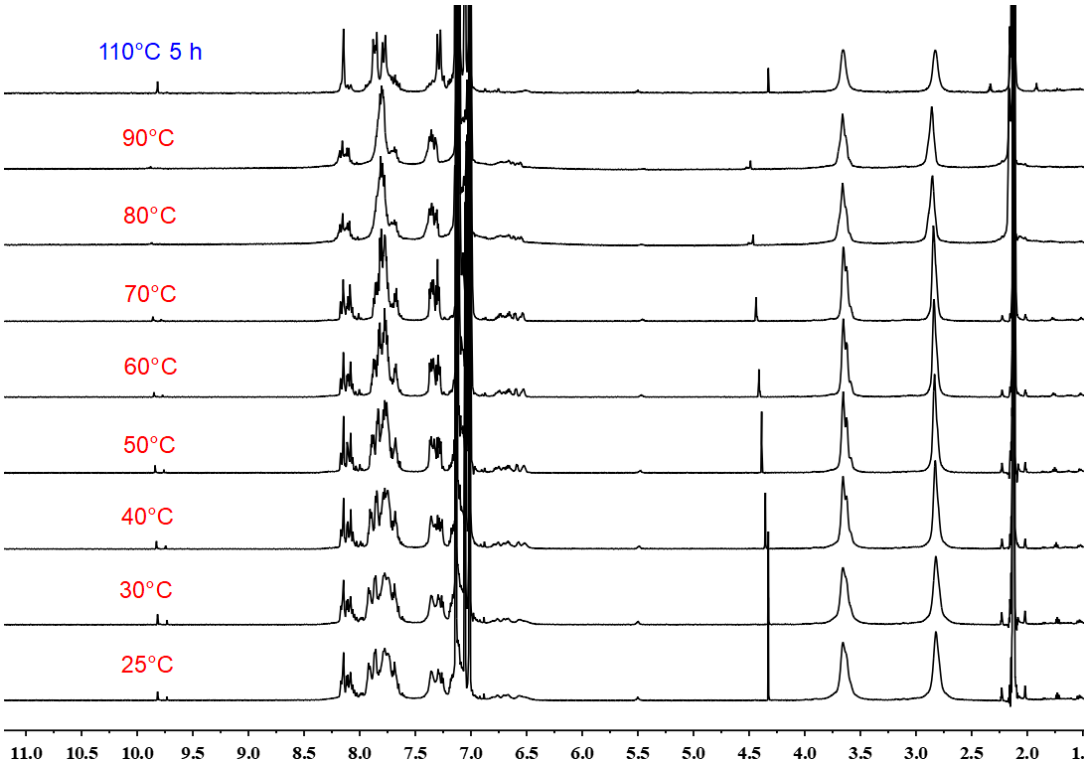

Figure 5-6. Variable temperature ^{1}H NMR of endoperoxide **V4** from 25°C to 90°C and thermal cycloreversion under 110°C for 5 h.

In principle, the [4 + 2] cycloaddition of singlet oxygen to DPA may occur both interior and exterior of the cage which might lead to several rotamers for the hindered endoperoxide and results in a mixture of isomers, Unfortunately, no single crystal of pure the endoperoxide was obtained to clarify the arrangement of the pillars in **V4**. The variable temperature NMR was also evaluated for the purpose of thermal cycloreversion in situ (Figure 5-6). However, the ^{1}H NMR showed no variation of splitting peaks which indicates the configuration stability of the endoperoxide at 90 °C. Even so, the endoperoxide mixture can be reversed back to the exclusive imine cage upon heating (110 °C for 5 h).

5.4.3.2 Conditions optimization for reversible transformation

In order to control the cage stability, various solvents and the effect of catalytic loading of methylene blue were examined. As expected, by employing less loading of methylene blue (2 mol% vs 40 mol%), the decomposition of the cage during the oxidation and cycloreversion process can be decreased with shorter time to reach the full cycloreversion (Table 5-1, entry 1 vs entry 2 and 3). To achieve both oxidation and cycloreversion in the same solvent, the reversible cycle was tested in 1,1,2,2-tetrachloroethane: a higher decomposition was found by using 30 % methylene blue which is in line with the aforementioned observation (Table 5-1, entry 5 vs entry 6). However, the degradation was found to be 14 % in the presence of 2 % methylene blue and a lower decomposition was obtained with dried solvent (Table 5-1, entry 3 vs entry 6 and 7). It is also worth to note that the thermal cycloreversion in $C_2D_2Cl_4$ ends up with an entirely decomposed cage. Similar results were obtained in 1,2-dibromoethane (Table 5-1, entry 8) which suggests that toluene is the most suitable solvent for the thermal cycloreversion process. However, the oxidation of cage **V3** cannot be conducted in toluene as no conversion was observed due to the insolubility of methylene blue (Table 5-1,

Table 5-1. Condition optimization for reversible cycles of oxidation-cycloreversion of cage **V3**.

Entry	Loading of MB[a]	Solvent for oxidation	Percentage[b] of decomposition	Solvent for thermal reduction	Percentage[b] of decomposition
1	40 %	CH_2Cl_2	10 %	Toluene[d]	14 %
2	6 %	CH_2Cl_2	1 %	Toluene[e]	3 %
3	2 %	CH_2Cl_2	< 1 %	Toluene[e]	3 %
4	2 %	CD_2Cl_2	2 %	Toluene[e]	5 %
5	30 %	$C_2D_2Cl_4$	28 %	$C_2D_2Cl_4$	All decompose
6	2 %	$C_2D_2Cl_4$	14 %	$C_2D_2Cl_4$	All decompose
7	2 %	$C_2D_2Cl_4$ (dried)[c]	10 %	$C_2D_2Cl_4$	All decompose
8	5 %	1,2-dibromoethane	8 %	1,2-dibromoethane	All decompose
9	2 %	Toluene	N. R.[f]	-	-
10	2 %	CH_2Cl_2	1 %	CH_2Cl_2	N. R.[f]
11	2 %	CH_2Cl_2 and toluene	2 %	CH_2Cl_2 and toluene	5 %
12	2 %	3-chlorotoluene	3 %	3-chlorotoluene	8 %

[a] MB = methylene blue (Photosensitizer) under an excitation wavelength of 656 nm; [b] percentage calculated based on ^{1}H NMR; [c] The solvent was dried by 4Å molecular sieves overnight; [d] Heating for 12 h; [e] Heating for 3 h; [f] N. R. = no reaction.

entry 9). In addition, the thermal cycloreversion in CH_2Cl_2 under reflux condition was unsuccessful (no conversion of endoperoxide) (Table 5-1, entry 10) showing that dichloromethane is a solvent suitable for oxidation but not for cycloreversion. To our delight, the oxidation-cycloreversion cycle can be achieved in a mixed solvent (CH_2Cl_2 and toluene, 1:1) (Table 5-1, entry 11). However, a second cycle can not be properly achieved because of the uncontrolled evaporation of dichloromethane during cycloreversion. 3-Chlorotoluene as an alternative solvent for cages **V3** and **V4** in the presence of methylene blue. The [4+2] reaction between cage **V3** and singlet oxygen was achieved with only small decomposition even over a long period (around 11 h) while the thermal cycloreversion was completed in 5 h with an acceptable degradation (Table 5-1, entry 12). Thus, 3-chlorotoluene appeared as the optimized solvent for reversibility even if the decomposition is higher than those obtained under the best conditions (Table 5-1, entry 3). For the moment, the observed solvent effects on the cycles are not fully understood.

5.4.3.3 Kinetic study

Under the optimized conditions and the subsequent general procedure using 3-chlorotoluene as a solvent, both the oxidation and cycloreversion processes were monitored by UV-vis spectroscopy according to the general procedure[27] using 3-chlorotoluene as the solvent and a dioxygen atmosphere during cycloreversion. During the oxidation process, a decreased of absorption was observed at 350-420 nm in the region attributed to anthracene meanwhile this signal was recovered upon heating (Figure 5-7). The oxidation process was found to be completed after 11 h, a long period compared to the 30 min necessary to reach completion when dichloromethane was employed as a solvent. This phenomenon was attributed to the difference of solubility of MB in those solvents. For both oxidation and reduction processes, the decrease in absorbance can be fitted

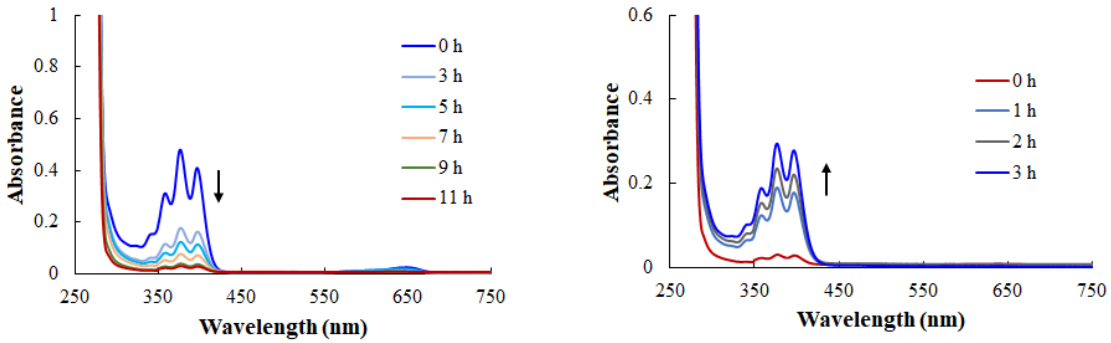

Figure 5-7. UV-vis spectroscopy monitored oxidation process (left) and cycloreversion process (right, λ_{ex} = 340 nm) in 3-chlorotoluene on a concentration of 5.6 µM in CH_2Cl_2.

[27] *General procedure for oxidation and reduction processes*: An oven-dried Schlenk tube equipped with stirring bar was charged with imine cage **3** (7 mg, 5.2 µmol), the system was evacuated and flushed with oxygen for five times. Then a solution of methylene blue (0.03 mg, 0.1 µmol, 2 mol%) in dry dichloromethane (2 mL) was injected via a syringe. The mixture was stirred at room temperature under the 656 nm-irradiation for 30 min. The solvent was removed and dry toluene (2 mL) was added, the resulting solution was heated for 3 h. Each measurement was carried out by extracting 7.5 µL solution and diluted with dichloromethane (3 mL) (5.6 µM) in 10 mm cuvette. The kinetics were calculated based on the loss of absorption at 377 nm.

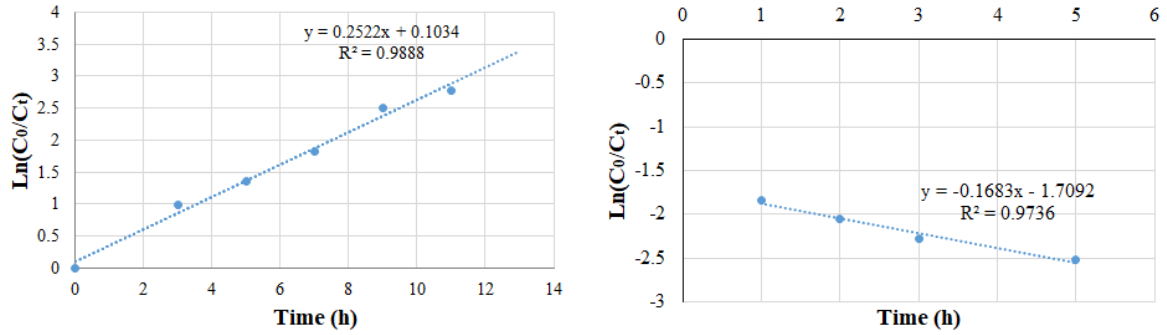

Figure 5-8. Plot of first order relation of oxidation process (left) and cycloreversion process (right) in 3-chlorotoluene.

to first-order relationship. The linear plots of $\ln([A]/[A]_0)$ *vs* time were obtained according to the absorption value at 377 nm (Figure 5-8). The extracted values for rate constants are listed in table 5-2. The oxidative and reductive rates were found to be 0.25 h^{-1} and 0.17 h^{-1} respectively. Such a low rate for the thermal cycloreversion could be due to the steric hindrance for the endoperoxide that may prevent a fast and controlled release of a dioxygen.

Table 5-2. Kinetics of oxidation and cycloreversion process in 3-chlorotoluene for cage **V3** at 377 nm on a concentration of 20 µM.

Processes	**First order kinetics k_1 (h^{-1})**
Oxidation process	0.25 (0-11 h) R^2 = 0.9888
Cycloreversion process	-0.17 (1-5 h) R^2 = 0.9736

5.3.3.4 Fatigue cycles

The oxidation-cycloreversion cycles in 3-chlorotoluene were monitored along 5 cycles using the general procedure: the oxidation process was completed in 15-17 h and the cycloreversion was proceeded for 5 h. The detailed absorptions were displayed in table 5-3. According to the monitoring by UV-Vis spectroscopy, the first cycle seems perfectly reversed as the approximate absorption was recovered after the thermal reduction. A weaker absorption than the initial one was found from the second cycle and the following ones with a decreasing trend. The fatigue cycles are shown in figure 5-9. The absorption of the medium after 5 cycles is consistent with the aforementioned degradation percentage (Table 5-1).

Table 5-3. Fatigue cycles monitored by absorption at 377 nm.

Processes	Time/h	Cycles	Abs	Degradation rate (%)
Initial	0	0	0.378	0
Oxi-1	17	0.5	0.016	-
REV-1	3	1	0.373	1.5
Oxi-2	16	1.5	0.071	-
REV-2	4	2	0.297	21
Oxi-3	17	2.5	0.094	-
REV-3	4	3	0.283	26
Oxi-4	15	3.5	0.087	-
REV-4	4.5	4	0.231	39
Oxi-5	15	4.5	0.069	-
REV-5	5	5	0.217	43

Oxi-n represents the n^{th} oxidation process; REV-n represents the n^{th} cycloreversion. The measurement procedure is the same as procedure for the kinetics measurement.

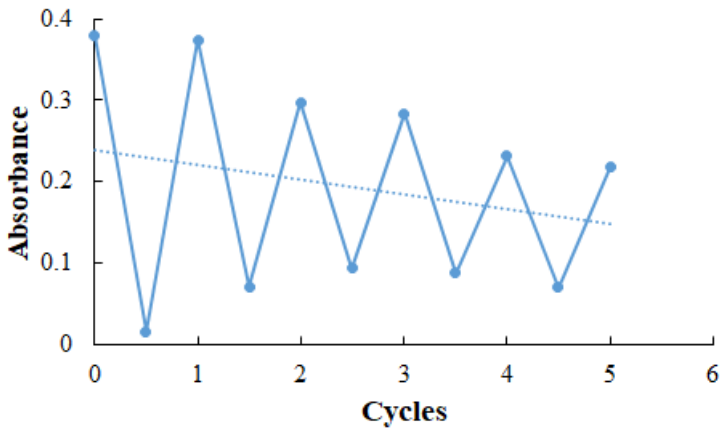

Figure 5-9. Fatigue cycles for the imine cage **V3/V4** conversion in 3-chlorotoluene in the presence of methylene blue as a photo-sensitizer. The photo-oxidation process lasts for 15-17 h and the cycloreversion process lasts for 3-5 h.

5.4.4 DOSY studies

To evaluate the difference between imine cage **V3** and endoperoxide **V4**, the DOSY experiments were carried out at room temperature under several concentrations in the presence of an internal standard (hexamethylbenzene). The diffusion coefficient values of cage **V4** (obtained after a (4+2) reaction with singlet oxygen) and cage **V3** (obtained from the cycloreversion of previous cage **V3**) were listed in table 5-4. Subtle differences (D = 2.3-2.8×10^{-10} m^2/s) were observed under various concentrations. By taking into account the undefined compact shape of both cages, these similar values account for similar morphologies for cages **V3** and **V4** and more importantly, the DOSY experiments confirmed that the cage structure is intact

after an oxidation-cycloreversion cycle

Table 5-4. Diffusion coefficient comparison of imine cage **V3** and its endoperoxide cage **V4** under different concentrations in toluene-d_8.

Concentration	Diffusion Coefficient of endoperoxide cage V4 (m^2/s)	Diffusion Coefficient of thermally reduced cage V3 (m^2/s)
1.76 mM	2.28×10^{-10}	2.60×10^{-10}
2.8 mM	3.09×10^{-10}	2.86×10^{-10}
2.75 mM	2.49×10^{-10}	2.68×10^{-10}
4.8 mM	2.82×10^{-10}	2.82×10^{-10}

All solutions of cages were prepared according to the general procedure[28] showing identical ^{1}H NMR spectra to figure 5-5.

5.4.5 Cation binding properties

Subsequently, we examined the binding properties of the imine cage **V3** toward various cations (2.0 equivalents) in CH_2Cl_2 to synthesize metal complexes.[29] Initially, the use of high-valence rare earth metals such as neodynium, europium and terbium salts led to the full decomposition of the imine cage which might be ascribed to their known lewis acidity (Table 5-5, entry 1-3). Even when employing less acidic $Zn(OTf)_2$ and $Cu(OTf)_2$, similar results were observed (Table 5-5, entry 4-5). A treatment of **V3** with $Mg(OTf)_2$ led to the formation of magnesium cage complex which appears in the ^{1}H NMR spectrum with shifted signals compared to the parent cage (Figure 5-10). However, the metallated cage is accompanied with a significant amount of DPA-bisaldehyde, resulting from a partial decomposition (37 %) of the cage based on the ^{1}H NMR (Table 5-5, entry 6). No coordination was seen for smaller cations such as potassium and sodium as no change in chemical shift occurred. This assertion was further confirmed by mass spectrometry (Table 5-5, entry 7-8). Interestingly, copper(I) was shown to be effective to coordinate the cage using $Cu(MeCN)_4BF_4$. The metallic complex was identified by mass spectrometry.[30] Even slightly broad, the ^{1}H NMR spectrum of the complex (Figure 5-11), presented in the disappearance of cage **V3** signals and the appearance of new complex signals, which could account for the different architectures (Table 5-5, entry 9). An identical NMR signature was obtained when using two equivalent $Cu(MeCN)_4PF_6$ (Table 5-5, entry 10).

[28] In a dried Schlenk tube was charged with Imine cage (7.6 mg, 5.6 μmol) was added a solution of methylene blue (0.09 mg, 0.28 μmol, 5 mol%) in dry dichloromethane (2 mL) under oxygen atmosphere at room temperature. The mixture was irradiated under red light (656 nm) for 30 min. The resulting solution was transferred to a 5 mL vial and dried to afford a yellow solid. Then the solid was dissolved in toluene-d_8, the suspension was pass through a pipette equipped with cotton and control the volume of toluene-d_8 to be 0.6 mL. Hexamethylbenzene (0.617 mg/0.778 mg, 4.8 μmol) was added as an internal standard reagent to calculate the mass of oxidized imine cage **V4**. According to this procedure, several concentrations (2.8 mM/4.8 mM/2.75 mM/ 1.76 mM) of oxidized imine cage **V4** were prepared. After monitoring the DOSY, the cage **V4** was thermally reduced in NMR tube under 105°C in oil bath for 2.5 h. The ^{1}H NMR was tested again in order to confirm the thermal reduction has been finished and to see if there is any variation of the concentration before measure the DOSY of thermal reduced imine cage **V3**.

[29] The mixture of imine cage **V3** and two equivalent of metal source was stirred at room temperature for 8 h. The solution was concentrated to *ca.* 0.5 mL, diethylether (2.0 mL) was added to afford a precipitation.

[30] The mass of $[M+2Cu]^{2+}$ was found 734.2483, theoretical mass for $[M+2Cu]^{2+}$: 734.2465.

Table 5-5. Cation binding experiments.

Entry	Cation source	^{19}F NMR (ppm)	^{1}H NMR	Mass[a]	Remarks
1	$Nd(OTf)_3$	-	No aliphatic protons	-	Decomposition
2	$Eu(OTf)_3$	-	No aliphatic protons	-	Decomposition
3	$Tb(OTf)_3$	-	No aliphatic protons	-	Decomposition
4	$Zn(OTf)_2$	-78.2	No aliphatic protons	-	Decomposition
5	$Cu(OTf)_2$	-	-	-	Decomposition
6	$Mg(OTf)_2$	-78.9	Shifted	D.	A mixture[b]
7	KOTf	-78.7	No shift	N. D.	No reaction
8	NaOTf	-78.7	No shift	N. D.	No reaction
9[c]	$Cu(MeCN)_4BF_4$	-152.2 -71.5	Shifted	D.	61 % yield
10[d]	$Cu(MeCN)_4(PF)_6$	-74.0 -78.8	Shifted	D.	81 % yield

[a] N. D. = Not detected; D. = Detected. [b] The NMR showed it contains decomposed aldehyde and magnesium cage complex. [c] **HRMS (ESI$^+$):** calculated m/z $[M\text{-}B_2F_8]^{2+}$ for $[C_{96}H_{78}N_8Cu_2]^{2+}$: m/z 734.2465, found 734.2468. [d] **HRMS (ESI$^+$):** calculated m/z $[M\text{-}P_2F_{12}]^{2+}$ for $[C_{96}H_{78}N_8Cu_2]^{2+}$: m/z 734.2465, found 734.2483. [e] Based on ^{1}H NMR

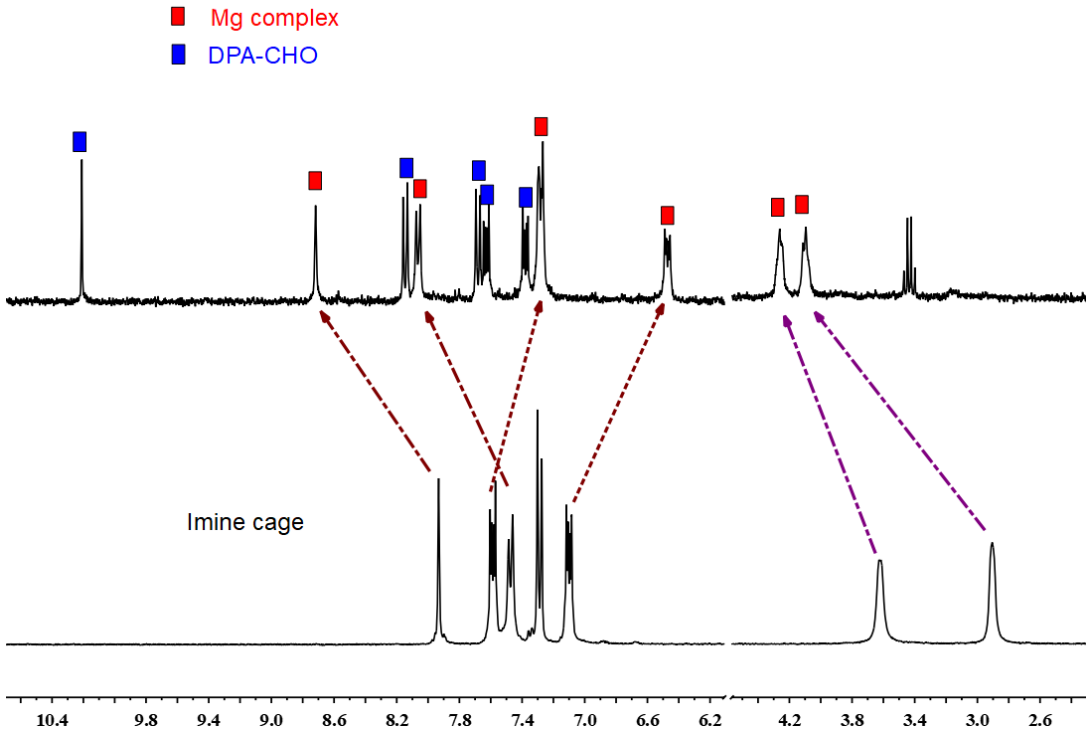

Figure 5-10. ^{1}H NMR of magnesium cage complex accompanied with decomposition.

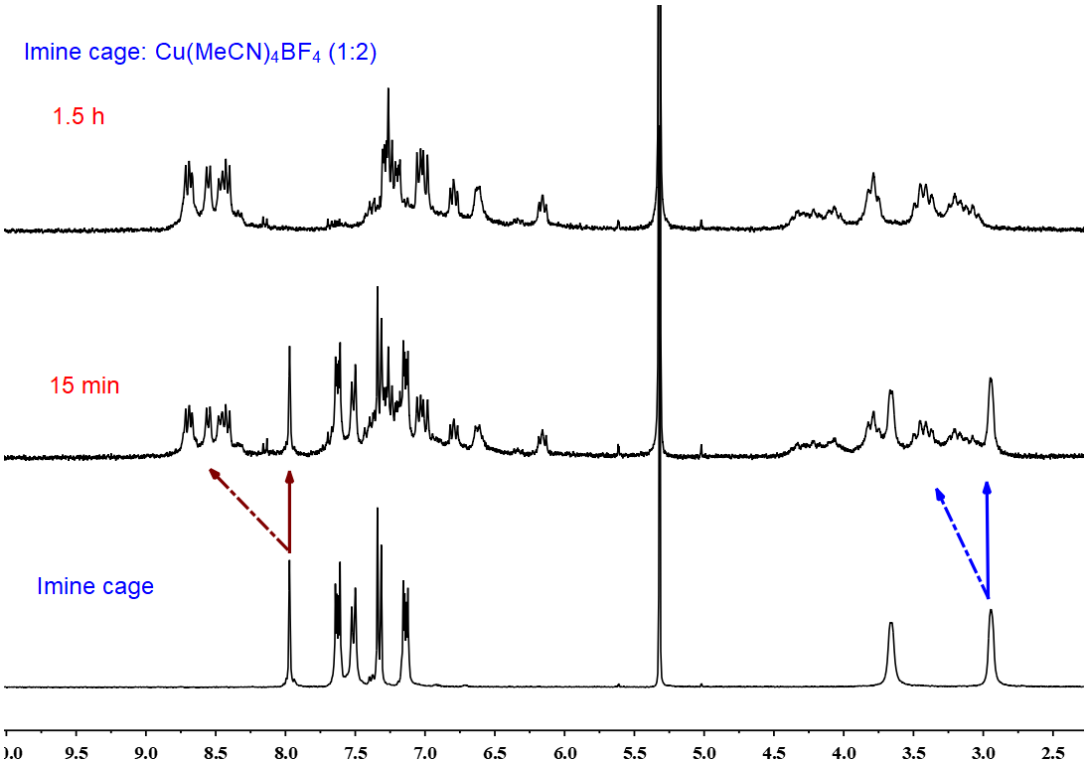

Figure 5-11. Formation of complexes between cage **V3** and cooper(I) salts monitored by ^{1}H NMR.

Notably, the full emission quench was observed for both cooper complexes which could reveal the intramolecular energy transfer from cage to cooper (Figure 5-12).

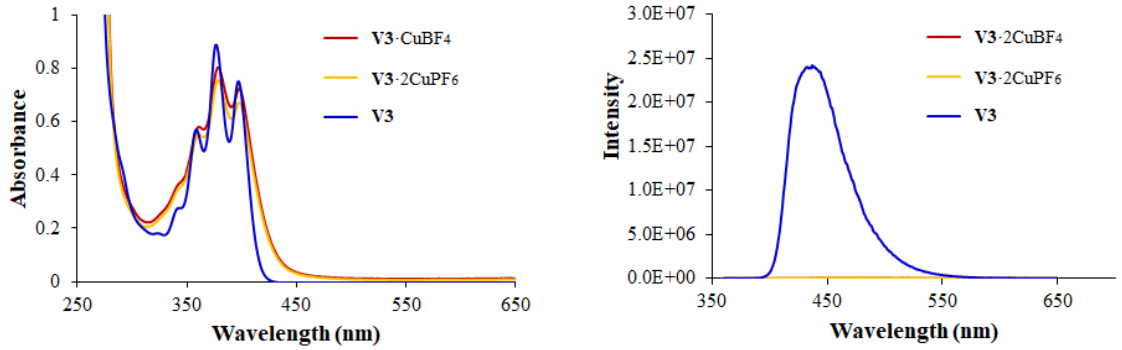

Figure 5-12. Absorption and fluorescence emission spectroscopy of cooper complexes and the parent imine cage (20 uM, in CH_2Cl_2) under a 340 nm excitation.

The anion effect was also investigated by using a lipophilic anion tetrakis[3,5-bis(trifluoromethyl)phenyl]borate (BAr_F) which promotes the solubility of an inorganic salt in organic solvents. Thus, $NaBAr_F$ and $CsBAr_F$ were examined as guests for the imine cage. The imine cage can bind two equivalents of sodium in few minutes which is accompanied by an explicit proton shift on the ^{1}H NMR spectrum. The protons on the imine and benzene groups were shifted low-field and the protons on the

anthracene ring moved to high field. The aliphatic protons showed a little difference (Figure 5-13). Besides, by adding only one equivalent of $NaBAr_F$ to the cage solution, the equilibrium was reached in 2 h (Figure 5-14). Two sets of signals appear in a (50:50) ratio of integration: one set is identical to the cage signals meanwhile the second set is shifted in a similar manner as previous observed in figure 5-13, when using a (1:2) ratio of (cage:cation). To this point, the identification of the species is not obvious as two situations are possible: (i) the unique formation of a (1:1) (cage:cation) complex or the formation of a more favored (1:2) (cage:cation) complex in the presence of the same amount of cage (50%) . Indeed, as the cage is a ditopic receptor, a (1:1) (cage:cation) complex would lead to two different environments for similar protons then resulting in two sets of signals. The mixture of cage and its (1:2) complex also would present two groups of signals. However, the chemical structure of **V3** is highly constrained. If a metal is coordinated in one site, its close proximity to the second site should also impact on all proton signals. Further analysis (mass spectrometry, elemental analysis) should be conducted to understand the behaviour of cage **V3** during coordination. However, we were interested in the formation of (1:2) complex. As expected, no variation of ^{19}F NMR was observed as the large BAr_F anions are outside the cage.

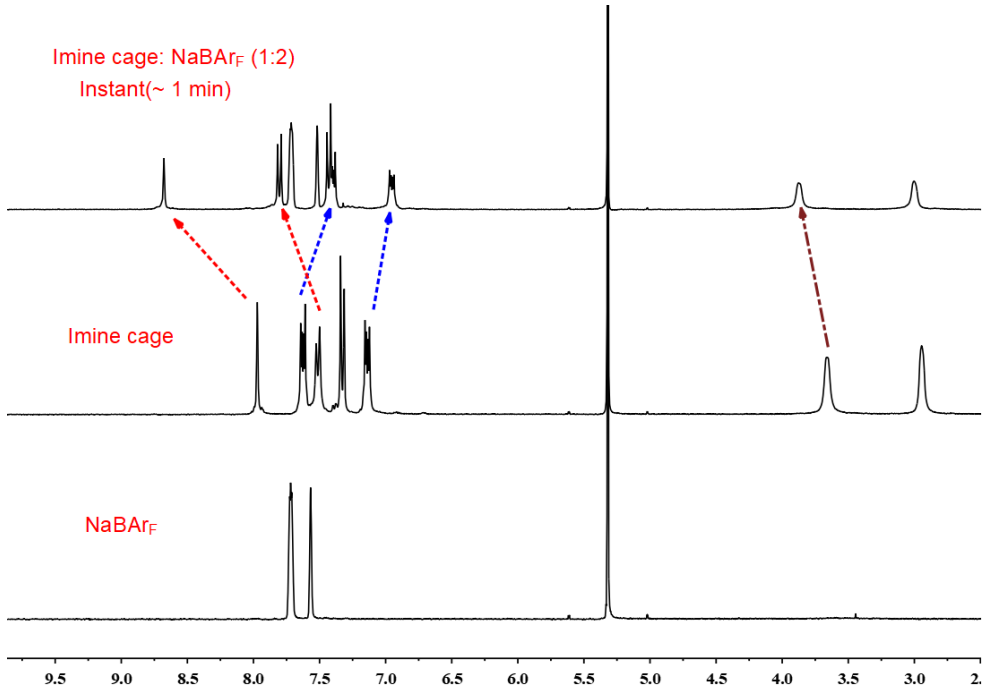

Figure 5-13. ^1H NMR (300 MHz, CD_2Cl_2) monitored imine cage **V3** binding sodium in the presence of two equivalent $NaBAr_F$.

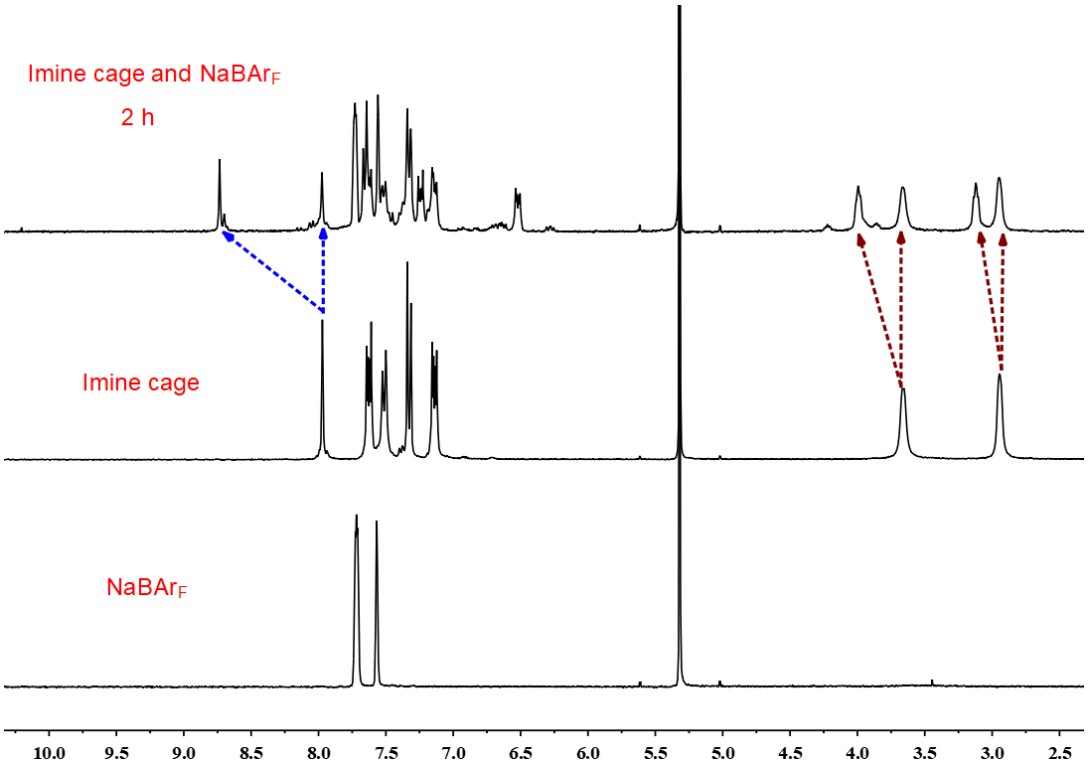

Figure 5-14. ^{1}H NMR(300 MHz, CD_2Cl_2) monitoring of the $NaBAr_F$ (1 equivalent) coordination by imine cage **V3**.

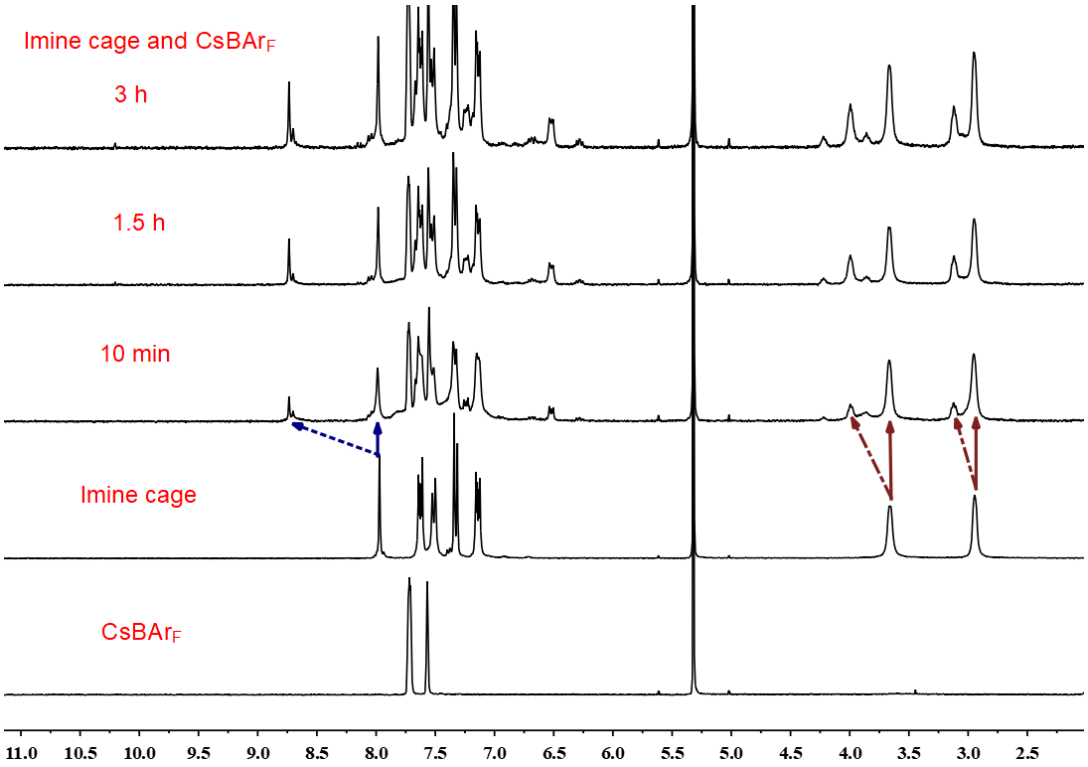

Figure 5-15. ^{1}H NMR (300 MHz, CD_2Cl_2) monitoring of the $CsBAr_F$ (2 equivalents) coordination by imine cage **V3**.

Subsequently, a much larger cation, CsBArF (2 equivalents), was tested for the coordination to **V3**. The ^{1}H NMR spectrum of the mixture showed again two sets of signals: one similar to the parent cage and a shifted one which could be attributed to coordinated complex. Further investigation is planned to identify the species in solution

5.4.6 Titration monitored using fluorescence emission

As the imine cage exhibited binding properties toward cations (Na^{+}, Cu^{+}, Mg^{2+}), titration experiments monitored by fluorescence emission were conducted according to the general procedure[31] to better quantify the phenomena. A significant decrease of the fluorescence intensity was observed when one equivalent of $NaBAr_F$ was added, while another one equivalent of $NaBAr_F$ led to a small red shift of the emission (20 nm). No more variation on spectra was observed by adding 2.5 to 5 equivalents of $NaBAr_F$. This qualitative titration suggested the formation of a (1:2) host-guest (Figure 5-16). Similarly, one equivalent of $Cu(MeCN)_4BF_4$ greatly quenched the emission of **V3**, and two equivalents of cooper(I) led to the complete emission quenching which suggests a (1:2) coordination mode. A small variation in fluorescence emission was observed when cage **V3** was mixed with two equivalents of $Mg(OTf)_2$ which might account for the weak coordination of this cation, as already suggested by ^{1}H NMR analysis. Notably, five equivalents of magnesium afforded a slight decrease of emission which could indicate the degradation of the cage.

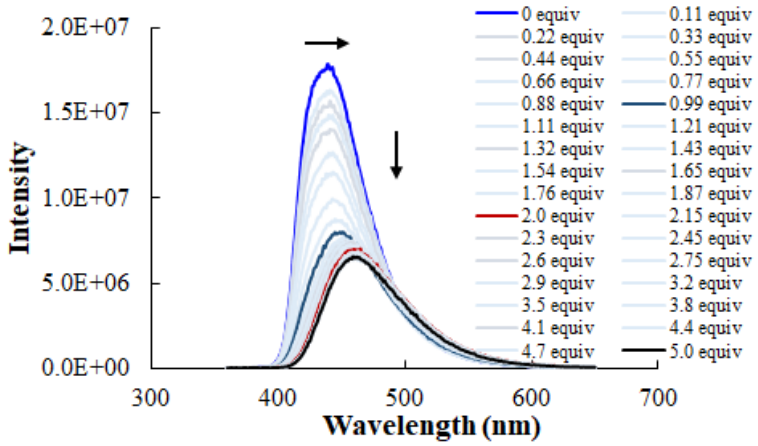

Figure 5-16. Coordination of $NaBAr_F$ by imine cage **V3** (20 μM in CH_2Cl_2) monitored by fluorescence emission under an excitation wavelength of 340 nm.

[31] To a dichloromethane solution of imine cage (20 μM) in volumetric flask was added certain amount of cation source, shake for one minute and the solution was measured by fluorescence spectroscopy. After each measurement, the sample was transferred back to the flask and ready to add another batch of cation source. Similarly, the next measurement was repeated as the first one.

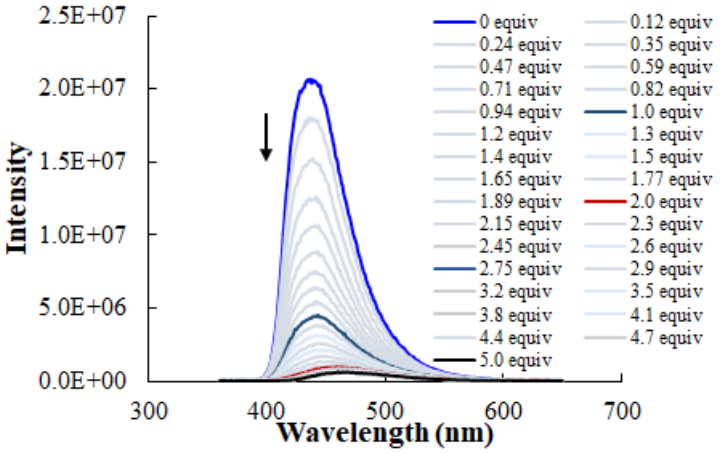

Figure 5-17. Coordination of $Cu(MeCN)_4BF_4$ by imine cage **V3** (20 µM in CH_2Cl_2) monitored by fluorescence emission under an excitation wavelength of 340 nm.

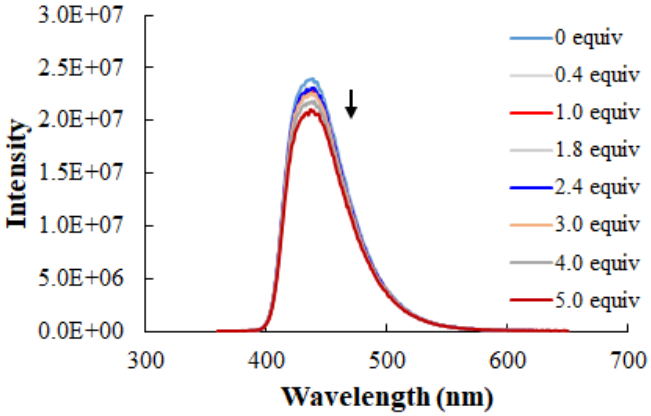

Figure 5-18. Coordination of $Mg(OTf)_2$ by imine cage **V3** (20 µM in CH_2Cl_2) monitored by fluorescence emission under an excitation wavelength of 340 nm.

5.5 Conclusion and perspectives

A self-assembled fluorescent imine cage **V3** was synthesized via dynamic chemistry in one single step using TREN as a cap and DPA-based bis-aldehyde as pillars. The use of other triamine caps and substituted DPA pillars failed to access to the corresponding self-assembled cages but led to polymerization which might be attributed to several factors (solubility, steric hindrance, pre-organisation). The switchability of the imine cage was examined in the presence of singlet oxygen and this (4+2) reaction was monitored by UV-vis and fluorescence emission spectroscopies and ^1H NMR and mass spectrometry. 3-Chlorotoluene was the optimized solvent for oxidation-cycloreversion cycles of cage **V3**. The kinetics studies in 3-chlorotoluene showed a different rate constant for both steps: 0.25 h^{-1} for oxidation vs 0.17 h^{-1} for cycloreversion. The DOSY NMR analysis of species along one cycle, i.e. endoperoxide cage **V4** and the parent imine cage **V3**,

indicated that both possess a similar globular structures. Finally, the coordination of various cations monitored by ^{1}H NMR and fluorescence emission showed high affinity towards sodium and cooper. Additionally, a fluorescent imine macrocycle with 9,10-diphenylanthracene (DPA) pillars can be readily obtained by using diethylenetriamine and DPA-based aldehyde (1:1) which can be further reduced to a macrocyclic amine.

In perspective, triamines with hindered substituents can be used to favor the preorganization of the reactive groups and thus allow the obtention of new cages. Meanwhile, efforts should also be put to transform the imine cage to a chemically robust amine or amide cage[356] and avoid decomposition due to the reversibility of the imine bond. Moreover, the reduced amine cage can be further transformed to water-soluble ammonium cage and explore the properties in aqueous medium. Finally, chiral amines as caps can be introduced to form cages or macrocycles that might lead to easy access to chiroptical properties.[357]

6 General conclusions

This thesis describes two research axes: one is the use of ligand design to prepare functional gold and silver complexes for catalysis, and the other concerns the development of 9,10-diphenylanthracene (DPA) based supramolecules which are chiral sulfoxides for tunable chiroptical properties and a reversible imine cage sensitive to singlet oxygen stimulus.

-Dialkylthioether ligands were conceived to form gold(III) chloride complexes with a well-defined stoichiometry. Stable for months, the latter complexes are readily obtained by a simple liquid-liquid extraction between ligands and inorganic salts. Independently of the ligand nature (anthracene, phenyl, alkyl), all gold(III) chloride complexes are rapidly photoreduced to the corresponding gold(I) chloride complexes using a 365-nm irradiation or visible light. The rate of this photoreduction was more rapid (30 min) than the thermal reduction at 80°C (12h). Moreover, we found no acceleration or reduction of the photoreduction kinetics ascribable to the presence of the diphenylanthracene chromophore since a possible antennae effect resulting from efficient intramolecular energy transfer between the DPA and the gold atoms. In the case of the dialkyl thioether gold complexes, the reductive elimination might be triggered by a direct excitation of the gold center and/or a ligand to metal charge transfer (LMCT) state. Based on the trapping experiments, several pathways for reductive elimination were proposed, notably the possible occurrence of a chloronium intermediate. All gold(III) chloride and *in situ* generated gold(I) chloride complexes showed excellent efficiency for single and sequential double cyclization reactions involving alkynes. This result demonstrates for the first time that photoreduced gold species are high efficient Lewis acid catalysts.

-Functionalized phosphine ligands were also elaborated and the corresponding gold(I) chloride complexes smoothly grafted onto silica nano-objects through a peptide coupling. A transfer of chirality from the chiral silica helices to the surface-bound gold complexes was confirmed using circular dichroism spectroscopy. In the presence of a silver salt, the inorganic silica nano-objects supported gold complexes exhibited a high efficiency in several alkyne-related cyclizations. The heterogeneous catalysts could be recycled up to an average 7 cycles without any loss of efficiency in the dearomative spirocyclization reaction of aryl alkynoate esters. Noteworthy, the recycled silica material appeared to gradually be transformed over time and cycles, from pure supported cationic gold(I) catalysts into a complex catalytic system possibly involving silver nanoparticles.

-Four DPA-based thioether ligands with stable *syn*- and *anti*- atropisomerism were designed and synthesized. They readily formed complexes with various silver salts whose geometry can be tuned by the nature of anion or by extending the length of the coordination chain. The silver complexes adopted various geometries such as macrocyclic M2**L**2, metallocage M6**L**4, discrete M2**L**, polymeric M2**L** and cyclic M**L**

which were identified by XRD analysis. Their activity in homogeneous catalysis was confirmed in two tandem addition/cycloisomerization of alkynes using 0.5-1 mol% of catalytic loading with efficiencies are similar to those of inorganic silver catalysts employed in higher loadings (2.5-5 mol%).

-DPA-based sulfoxides were synthesized by oxidation of the corresponding thioethers. The chiral sulfoxides were obtained by a chiral HPLC separation and their absolute configuration was determined by the comparison of calculated and experimental electronic circular dichroism (ECD) spectra. The oxidation of DPA-based sulfoxide by using singlet oxygen led to a major unusual diendoperoxide product **DPAO4** (1,4- and 9,10- position), possibly induced by the electronic or steric effects at the *ortho*-position, The thermal cycloreversion of this new stable diendoperoxide partially led to the parent DPA. A photochemical cycloreversion could be an alternative strategy. The evaluation of chiroptical properties of enantiopure DPA-sulfoxides is in progress.

- A self-assembled fluorescent [2+3] imine cage was synthesized via dynamic covalent chemistry using TREN as caps and DPA-based aldehyde as pillars. Notably, the structural variation for triamine caps and substituted DPA pillars failed to access to self-assembled cages but led to polymerization instead. The reversible reactivity of the imine cage towards singlet oxygen was followed by NMR spectrometry, UV-Vis and fluorescence spectroscopy. 3-Chlorotoluene was the best solvent allowing reversible cycles. The binding properties toward several cations were examined by ^{1}H NMR and fluorescence emission titration which showed a high affinity for cages towards sodium and coopper. Besides, using the same dynamic chemistry approach, a fluorescent imine macrocycle with 9,10-diphenylanthracene (DPA) pillars can be readily obtained by the [2+2] self-assembly of diethylenetriamine and DPA-based aldehyde. The imine macrocycle was further reduced to macrocyclic amine.

7 Experimental section

7.1 General information

All commercial reagents were used as received without further purification unless otherwise stated. All reactions were carried out using conventional Schlenk techniques under a static pressure of argon or nitrogen with dry solvents unless otherwise noted. Solvents (dichloromethane, THF) were dried over activated alumina columns on MBraun Solvent Purification System (SPS-800), dry toluene was freshly distilled over sodium. Flash column chromatography was performed using 40-63 μm (230-400 mesh) silica gel. Analytic thin layer chromatography was performed using silica gel 60 F_{254} pre-coated plates (Merk) with visualization by ultraviolet light (6 W). Organic solutions were concentrated under reduced pressure using a Buchi rotary evaporator.

All new compounds were characterized by NMR spectroscopy, high-resolution mass spectrometry, optical rotation (if applicable), and melting point analysis (if solids). ^{1}H, ^{13}C, and ^{19}F NMR spectra were recorded in (deuterated solvents) on a Bruker 300 MHz spectrometers using the residual solvent as internal reference at a constant temperature of 298 K. Chemical shifts for ^{1}H NMR are reported relative to TMS as follows: chemical shift in reference to residual $CHCl_3$ at 7.26 ppm (δ ppm), Chemical shifts for ^{13}C NMR are reported in terms of chemical shift in reference to the $CDCl_3$ solvent signal (77.16 ppm). Chemical shifts (δ) are given in ppm, and coupling constants (J) are given in Hz. The following abbreviations were used to explain the multiplicities: s = singlet, br s = broad singlet, d = doublet, t = triplet, q = quartet, sex = sextet, sep = septet, ddd= doublet of double of doublets, td = triplet of doublets, m = multiplet. Melting points were measured on a Stuart Scientific melting point apparatus SMP3. High resolution mass spectrometric data were obtained on an Agilent 6210 time-of-flight HPLC/MS spectrometer (ESI-TOF). UV-Vis spectra were recorded on a Varian 5000 UV-Vis-NIR spectrophotometer. Emission spectra were measured on a Horiba Scientific Fluoromax-4 spectrofluorometer.

7.2 Synthesis of ligands and substrates

7.2.1 Thioether ligands for gold complexes

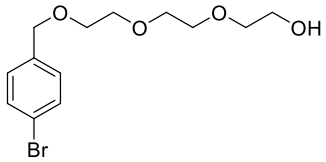

2-(2-(2-((4-Bromobenzyl)oxy)ethoxy)ethoxy)ethan-1-ol (II1-1): To an ice cold solution of sodium hydride (1.24 g, 52 mmol) in anhydrous THF (180 mL) was added ethylene glycol (6.4 mL, 48 mmol) under nitrogen atmosphere. The mixture was stirred at 0 °C for 1 h. Then, 4-bromobenzyl bromide was added to the mixture. The whole mixture was stirred at 0 °C for 1 h and allowed to warm up to ambient temperature stirred overnight. The mixture was cooled to 0 °C and saturated ammonium chloride (50 mL) was added, the

residue was extracted by ethyl acetate for 3 times (200 mL×3), the organic layer was dried over magnesium sulfate, then concentrated and purified by flash silica gel column chromatography (eluent: petrol ether/ethyl acetate = 10:3) to afford product (7.5 g, 60 % yield) as a clear oil.

^{1}H NMR (300 MHz, $CDCl_3$) δ 7.43-7.48 (m, 2H), 7.19-7.24 (m, 2H), 4.51 (s, 2H), 3.59-3.73 (m, 12H).

^{13}C NMR (75 MHz, $CDCl_3$) δ 137.3, 131.6, 129.5, 121.6, 72.6, 70.8, 70.7, 70.5, 69.6, 61.9.

HRMS (ESI+): m/z calculated for $C_{13}H_{19}O_4BrNa$ $[M+Na]^+$: 341.0364; found: 341.0350.

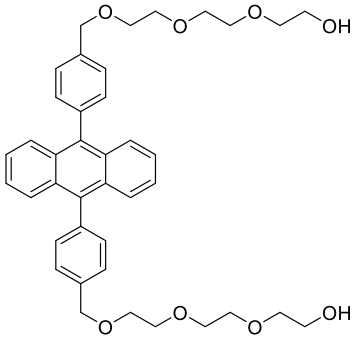

2,2'-(((((((Anthracene-9,10-diylbis(4,1-phenylene))bis(methylene))bis(oxy))bis(ethane-2,1-diyl))bis(oxy))bis(ethane-2,1-diyl))bis(oxy))bis(ethan-1-ol) (II1-2): An oven-dried Schlenk tube was charged with compound **II1-1** (159 mg, 0.5 mmol), 9,10-anthracene bis(pinacolato)diborane (86 mg, 0.2 mmol), palladium catalyst (10 mg, 4.3 mol%) and potassium carbonate(138 mg, 1.0 mmol). The mixture was degassed and flushed with nitrogen for 3 times, then a mixed solution of toluene/water = 8:1 (3.0 mL) was added via a syringe, The reaction was sealed and heated to 110 °C stirred for 48 h. After cooling to room temperature, dichloromethane (5 mL) was added and the mixture was filtered through a pad of celite, the organic layer was dried over magnesium sulfate and concentrated, then purified by silica gel column chromatography (eluent: CH_2Cl_2/methanol = 30:1) to afford product **II1-2** as a pale yellow solid (90 mg, 70 % yield).

^{1}H NMR (300 MHz, $CDCl_3$) δ 7.66-7.72 (m, 4H), 7.59 (d, *J* = 8.1 Hz, 4H), 7.45 (d, *J* = 8.1 Hz, 4H), 7.28-7.34 (m, 4H), 4.76 (s, 4H), 3.80 (br, 8H), 3.74 (br, 12 H), 3.63-3.66 (m, 4H), 2.49 (br, 2H).

^{13}C NMR (75 MHz, $CDCl_3$) δ 138.5, 137.5, 136.9, 131.4, 129.9, 127.9, 127.0, 125.0, 73.4, 72.6, 70.9, 70.8, 70.5, 69.9, 61.9.

HRMS (FD): *m/z* calculated for $C_{40}H_{46}O_8$ $[M]^{+\bullet}$: 654.3193; found: 654.3198.

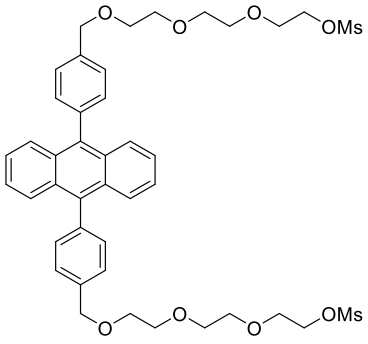

(((((((Anthracene-9,10-diylbis(4,1-phenylene))bis(methylene))bis(oxy))bis(ethane-2,1-diyl))bis(oxy))bis(ethane-2,1-diyl))bis(oxy))bis(ethane-2,1-diyl) dimethanesulfonate (II1-3): To a solution of **II1-2** (691 mg, 1.1 mmol) in anhydrous dichloromethane (6 mL) was added methanesulfonyl chloride (0.41 mL, 5.3 mmol) and triethylamine (0.74 mL, 5.3 mmol) at 0 °C under a nitrogen atmosphere. The mixture was allowed to warm to ambient temperature stirred overnight. Water (10 mL) was added and the mixture was extracted with dichloromethane 3 times (50 mL×3), the organic layer was dried over magnesium sulfate, then concentrated and purified by silica gel column chromatography (eluent: petrol ether/ ethyl acetate = 1:2) to afford product (670 mg, 78 % yield) as a pale yellow solid.

^{1}H NMR (300 MHz, $CDCl_3$) δ 7.69 (dd, *J* = 6.84, 3.27 Hz, 4H), 7.58 (d, *J* = 8.1 Hz, 4H), 7.46 (d, *J* = 8.1 Hz, 4H), 7.32 (dd, *J* = 6.84, 3.27 Hz, 4H), 4.75 (s, 4H), 4.38-4.41 (m, 4H), 3.73-3.81 (m, 20H), 3.07 (s, 6H).
^{13}C NMR (75 MHz, $CDCl_3$) δ 138.4, 137.5, 136.9, 131.4, 129.9, 127.8, 127.0, 125.1, 73.3, 70.8, 70.8, 70.7, 69.9, 69.3, 69.1, 37.8.

HRMS (FD): *m/z* calculated for $C_{42}H_{50}O_{12}S_2$ $[M]^{+\bullet}$: 810.2744; found: 810.2755.

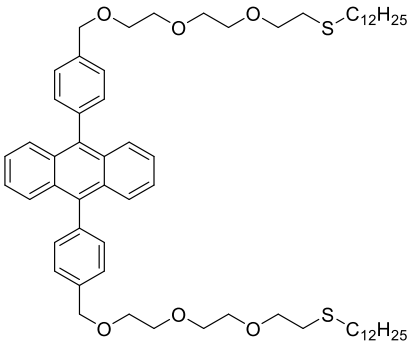

9,10-Bis(4-(2,5,8-trioxa-11-thiatricosyl)phenyl)anthracen (II1): To a cooled suspension of sodium hydride (dry, 95 %, 5 mg, 0.2 mmol) in anhydrous THF (1.5 mL) was added a solution of 1-dodecanethiol (36 μL, 0.15 mmol). The resulting solution was kept stirring at 0 °C for 30 min. Then a solution of compound **II1-3** (40 mg, 0.05 mmol) in anhydrous THF (1.0 mL) was added. The resulting mixture was allowed to warm to room temperature stirred for 5 h. The reaction was quenched with saturated ammonium chloride (2 mL), the mixture was extracted with dichloromethane (5 mL×3). The organic layer was dried over magnesium sulfate, concentrated and purified by silica gel column chromatography (eluent: petrol ether/ethyl acetate = 3:1) to get ligand **II1** (48 mg, 95 % yield) as a white solid.

^{1}H NMR (300 MHz, $CDCl_3$) δ 7.69 (dd, *J* = 6.83, 3.27 Hz, 4H), 7.59 (d, *J* = 8.16 Hz, 4H), 7.45 (d, *J* = 8.16 Hz, 4H), 7.31 (dd, *J* = 6.83, 3.27 Hz, 4H), 4.76 (s, 4H), 3.65-3.81 (m, 20H), 2.73 (t, *J* = 7.2 Hz, 4H), 2.53 (t, *J* = 7.26 Hz, 4H), 1.54-1.58 (m, 7H), 1.24 (br, 33H), 0.87 (t, *J* = 6.9 Hz, 6H).
^{13}C NMR (75 MHz, $CDCl_3$) δ 138.5, 137.6, 137.0, 131.4, 130.0, 127.9, 125.1, 73.4, 71.2, 70.9, 70.8, 70.5, 69.9, 32.7, 32.0, 31.5, 29.9, 29.7 (t, *J* = 1.86 Hz), 29.6, 29.4, 29.3, 29.0, 22.8, 14.2.

HRMS (FD): *m/z* calculated for $C_{64}H_{94}O_6S_2$ $[M]^{+\bullet}$: 1022.6492; found: 1022.6492.

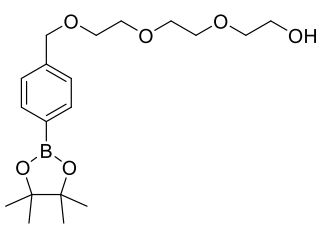

2-(2-(2-((4-(4,4,5,5-Tetramethyl-1,3,2-dioxaborolan-2-yl)benzyl)oxy) ethoxy)ethoxy)ethan-1-ol (II2-1): A flam-dried schlenk tube was charged with bromide compound **II1-1** (318 mg, 1.57 mmol), bis(pinacolato) diborane (500mg, 2.3 mmol), $Pd(dppf)_2Cl_2$ (51 mg, 6 mol%) and potassium acetate (294 mg, 4.7 mmol). The mixture was degassed and flushed with nitrogen for 3 times and 1,4-dioxane (5 mL) was subsequently added, the resulting mixture was stirred at 110 °C for 24 h. After cooling to room temperature, dichloromethane (15 mL) was added and the mixture was filtered through a pad of celite. The mixture was concentrated and purified by silica gel column chromatography. (eluent: petrol ether/ethyl acetate = 1:1) to afford product **II2-1** (325 mg, 89 % yield) as a yellow oil.

^{1}H NMR (300 MHz, $CDCl_3$) δ 7.78 (d, *J* = 8.1 Hz, 2H), 7.34 (d, *J* = 8.1 Hz, 2H), 4.58 (s, 2H), 3.59-3.73 (m, 12H), 1.33 (s, 12H).

^{13}C NMR (75 MHz, $CDCl_3$) δ 141.2, 134.6, 126.6, 83.5, 72.8, 72.4, 70.4, 70.3, 70.0, 69.2, 61.3, 24.6.

HRMS (ESI+): *m/z* calculated for $C_{19}H_{31}BO_6Na$ $[M+Na]^+$: 389.2111; found:389.2119.

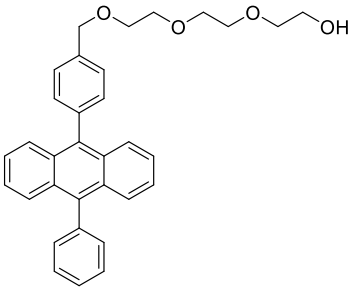

2-(2-(2-((4-(10-Phenylanthracen-9-yl)benzyl)oxy)ethoxy)ethoxy)ethan-1-ol (II2-2): A flame-dried schlenk tube was charged with bromide compound (187 mg, 0.56 mmol), boron compound **II2-1** (316 mg, 0.84 mmol), tetrakis(triphenylphosphine) palladium (33 mg, 5 mol%) and potassium acetate (386 mg, 2.8 mmol). The mixture was degassed and flushed with nitrogen for 3 times and then a mixed solvent of toluene/water (5 mL) was added, the resulting mixture was stirred at 110 °C for 24 h. After cooling to room temperature, the mixture was filtered through a pad of celite and washed with dichloromethane. The filtrate was concentrated and then purified by silica gel column chromatography (eluent: cyclohexane/ethyl acetate = 4:1) to afford product **II2-2** (190 mg, 69 % yield).

^{1}H NMR (300 MHz, $CDCl_3$) δ 7.66-7.72 (m, 4H), 7.55-7.64 (m, 5H), 7.46-7.50 (m, 4H), 7.30-7.35 (m, 4H), 4.76 (s, 2H), 3.75-3.81 (m, 10H), 3.64-3.67 (m, 2H).

^{13}C NMR (75 MHz, $CDCl_3$) δ 139.1, 138.5, 137.5, 137.2, 136.9, 131.5, 131.4, 130.0, 129.9, 128.5, 127.9, 127.5, 127.0, 125.1, 73.4, 72.6, 70.8, 70.8, 70.5, 69.9, 61.9.

HRMS (FD): *m/z* calculated for $C_{33}H_{32}O_4$ $[M]^{+\bullet}$: 492.2301; found: 492.2297.

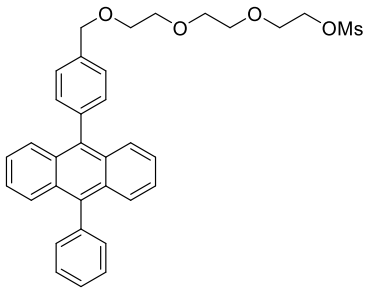

2-(2-(2-((4-(10-Phenylanthracen-9-yl)benzyl)oxy)ethoxy)ethoxy)ethyl methanesulfonate (II2-3): To a solution of compound **II2-2** (110 mg, 0.22 mmol) in anhydrous dichloromethane (3 mL) was added methanesulfonyl chloride (0.09 mL, 1.11 mmol) and triethyl amine (0.15 mL, 1.11 mmol) at 10 °C under nitrogen atmosphere. The mixture was stirred at room temperature overnight. Water (5 mL) was added and the mixture was extracted with ethyl acetate for 3 times (10 mL×3). The combined organic layer was dried over magnesium sulfate. Then concentrated and purified by silica gel column chromatography (eluent: petrol ether/ethyl acetate = 3:1) to afford product **II2-3** (100 mg, 79 % yield) as a yellow oil.

^{1}H NMR (300 MHz, $CDCl_3$) δ 7.69 (q, *J* = 6.8, 3.2 Hz, 4H), 7.55-7.63 (m, 5H), 7.45-7.49 (m, 4H),7.32 (d, *J* = 6.8, 3.2 Hz, 4H), 4.75 (s, 2H), 4.38-4.41 (m, 2H), 3.73-3.82 (m, 10H), 3.07 (s, 3H).

^{13}C NMR (75 MHz, $CDCl_3$) δ 139.1, 138.5, 137.2, 136.9, 131.5, 131.4, 130.0, 129.9, 129.9, 128.5, 127.9, 127.5, 127.1, 127.0, 125.1, 70.8, 70.8, 70.7, 69.9, 69.3, 69.2, 37.8.

HRMS (FD): *m/z* calculated for $C_{34}H_{34}O_6S$ $[M]^{+\bullet}$: 570.2076; found: 570.2089.

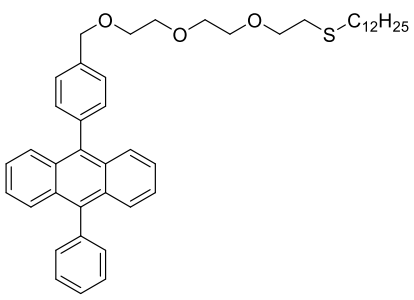

1-(4-(10-Phenylanthracen-9-yl)phenyl)-2,5,8-trioxa-11-thiatricosane (II2): To a suspension of sodium hydride (17 mg, 0.7 mmol) in THF (3 mL) was added 1-dodecanethiol (0.13 mL, 0.53 mmol) at 0 °C under nitrogen atmosphere. After 1 h, a solution of **II2-3** (100 mg, 0.17 mmol) was added. The mixture was stirred at ambient temperature overnight. Water (5.0 mL) was added, the mixture was extracted with ethyl acetate for 3 times (10 mL×3). The combined organic layers were dried over magnesium sulfate, then concentrated and purified by silica gel column chromatography (eluent: petrol ether/ ethyl acetate = 5:1) to afford ligand **II2** (88 mg, 74 % yield) as a white solid.

^{1}H NMR (300 MHz, $CDCl_3$) δ 7.70-7.74 (m, 4H), 7.58-7.62 (m, 5H), 7.47-7.50 (m, 4H), 7.31-7.36 (m, 4H), 4.77 (s, 4H), 3.67-3.82 (m,10H), 2.75 (t, *J* = 7.1 Hz, 2H), 2.56 (t, *J* = 7.38 Hz, 2H), 1.54-1.64 (m, 2H), 1.27-1.39 (m, 18H), 0.90 (t, *J* = 6.93 Hz, 3H);

^{13}C NMR (75 MHz, $CDCl_3$) δ 139.1, 138.4, 137.6, 137.2, 136.9, 131.4, 131.4, 129.9, 129.9, 128.4, 127.8, 127.5, 127.0, 125.0, 73.3, 71.1, 70.9, 70.8, 70.4, 69.9, 32.7, 32.0, 31.5, 29.9, 29.7, 29.7, 29.7, 29.6, 29.4, 29.3, 28.9, 22.7, 14.2;

HRMS (FD): *m/z* calculated for $C_{45}H_{56}O_3S$ $[M]^{+\bullet}$: 676.3950; found: 676.3924.

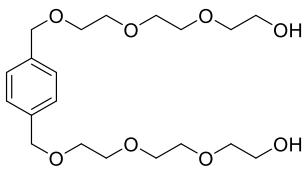

2,2'-((((((1,4-Phenylenebis(methylene))bis(oxy))bis(ethane-2,1-diyl))bis(oxy))bis(ethane-2,1-diyl))bis(oxy))bis(ethan-1-ol) (II3-1): A dry 250 mL two-neck flask was charged with ethylene glycol (9.0 mL, 67.6 mmol) and freshly prepared silver (I) oxide (18.8 g, 81.1 mmol) under nitrogen atmosphere, then anhydrous dichloromethane (40 mL) was injected into the flask. The resulting solution was kept stirring at room temperature for 30 min. Then *p*-xylene dibromide (8.1 g, 30.7 mmol) was added to the solution in one portion. The resulting mixture was stirred ambient temperature for 3 h, dichloromethane (100 mL) was added into flask, and the crude mixture was filtered by a Buchner funnel. The organic layer was evaporated on a rotary evaporator and purified by silica gel column chromatography (eluent: CH_2Cl_2/methanol = 30:1) to afford **II3-1** (6.8 g, 55 % yield) as clear oil.

^{1}H NMR (300 MHz, $CDCl_3$) δ 7.32 (d, *J* = 5.7 Hz, 4H), 4.55 (s, 4H), 3.58-3.71 (m, 24H).

^{13}C NMR (75 MHz, $CDCl_3$) δ 137.5, 127.9, 73.1, 72.6, 70.8, 70.7, 70.5, 69.5, 69.4, 61.8.

HRMS (ESI+): *m/z* calculated for $C_{20}H_{34}O_8Na$ $[M+Na]^+$: 425.2151; found: 425.2155.

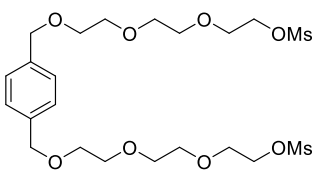

((((((1,4-Phenylenebis(methylene))bis(oxy))bis(ethane-2,1-diyl))bis(oxy))bis(ethane-2,1-diyl))bis(oxy))bis(ethane-2,1-diyl) dimethanesulfonate (II3-2): A flame-dried 25 mL flask was charged compound **II3-1** (5.6 g, 13.9 mmol) in anhydrous dichloromethane (4 mL), then the solution was cooled to

0 ˚C and methanesulfonyl chloride (3.23 mL, 41.7 mmol) and triethylamine (5.8 mL, 41.7 mmol) were added into this solution under nitrogen atmosphere. The mixture was stirred at 0 ˚C for 30 min then was allowed warm up to room temperature stirred for 5 h. Water (30 mL) was added and the resulting mixture was extracted with dichloromethane (100 mL×3). The combined organic layer was dried over magnesium sulfate, then concentrated and purified by silica gel column chromatography (eluent: ethyl acetate) to afford compound **II3-2** (6.0 g, 78 % yield).

^{1}H NMR (300 MHz, $CDCl_3$) δ 7.30 (s, 4H), 4.53 (s, 4H), 4.33-4.36 (m, 4H), 3.73-3.76 (m, 4H), 3.58-3.67 (m, 16H), 3.02 (s, 6H).

^{13}C NMR (75 MHz, $CDCl_3$) δ 137.7, 127.9, 73.1, 70.8, 70.7, 69.5, 69.4, 69.1, 37.8.

HRMS (ESI+): *m/z* calculated for $C_{22}H_{38}O_{12}S_2Na$ $[M+Na]^+$: 581.1702; found: 581.1701.

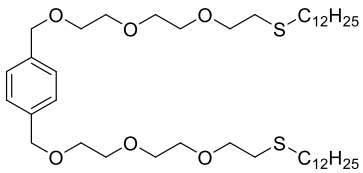

1,4-Di(2,5,8-trioxa-11-thiatricosyl)benzene (II3): To a cooled suspension of sodium hydride (dry, 95 %, 70 mg, 2.9 mmol) in anhydrous THF (10.0 mL) was added a solution of 1-dodecanethiol (0.52 mL, 2.1 mmol) in anhydrous THF (2.0 mL). The resulting solution was kept stirring at 0 ˚C for 30 min. Then a solution of compound **3-2** (400 mg, 0.72 mmol) in anhydrous THF (2 mL) was added. The whole mixture was allowed to warm up to room temperature stirred for 5 h. The reaction was quenched by saturated ammonium chloride (10 mL), the remaining system was extracted with dichloromethane (50 mL×3). The organic layer was dried over magnesium sulfate, then concentrated and purified by silica gel column chromatography (eluent: ethyl acetate) to get Ligand **II3** (435 mg, 79 %) as white solid.

^{1}H NMR (300 MHz, $CDCl_3$) δ 7.30 (s, 4H), 4.54 (s, 4H), 3.59-3.68 (m, 21H), 2.69 (t, *J* = 7.2 Hz, 4H), 2.52 (t, *J* = 7.2 Hz, 4H), 1.51-1.60 (m, 4H), 1.24 (br, 35H), 0.86 (t, *J* = 6.7 Hz, 6H).

^{13}C NMR (75 MHz, $CDCl_3$) δ 137.7, 127.8, 73.1, 71.1, 70.8, 70.7, 70.4, 69.5, 32.6, 32.0, 31.4, 29.9, 29.7, 29.6, 29.4, 29.3, 29.0, 22.7, 14.2.

HRMS (ESI+): *m/z* calculated for $C_{44}H_{82}O_6S_2Na$ $[M+Na]^+$: 793.5451; found: 793.5415.

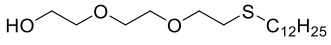

2-(2-(2-(Dodecylthio)ethoxy)ethoxy)ethan-1-ol (II4-1): A flame-dried Schlenk tube was charged with diethyl glycol monovinyl ether (500 mg, 3.8 mmol) and Irgacure 651 (98 mg, 0.38 mmol). The mixture was degassed and flushed with agron for 3 times. Then 1-dodecanthiol (0.94 mL, 3.8 mmol) was added. The whole mixture was stirred under 365 nm irradiation condition for 12 h. The mixture was purified by silica gel column chromatography. (eluent: petrol ether/ ethyl acetate = 5:1) to afford **II4-1** (1.16g, 92 % yield) as a clear oil.

^{1}H NMR (300 MHz, $CDCl_3$) δ 3.59-3.74 (m, 10H), 2.71 (t, *J* = 6.99 Hz, 2H), 2.53 (t, *J* = 7.29 Hz, 2H), 1.52-1.62 (m, 2H), 1.25-1.38 (m, 18H), 0.85-0.89 (m, 3H).

^{13}C NMR (75 MHz, $CDCl_3$) δ 72.6, 71.0, 70.3 (d, *J* = 5.0 Hz), 61.7, 32.6, 31.9, 31.4, 29.8, 29.7, 29.6, 29.5,

29.4, 29.3, 28.9.

HRMS (ESI+): *m/z* calculated for $C_{18}H_{38}NaO_3S$ $[M+Na]^+$: 357.2439; found: 357.2420.

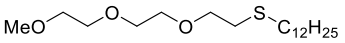

2,5,8-Trioxa-11-thiatricosane (II4): To a suspension of sodium hydride (14 mg, 0.6 mmol) in anhydrous THF (2 mL) was added a solution of compound **II4-1** (100 mg, 0.3 mmol) in THF (1 mL) at 0 °C under argon atmosphere. The reaction was kept at 0°C for 1 h and iodomethane (0.1 mL, 1.5 mmol) was added, the mixture was stirred at room temperature overnight. Water (5 mL) was added and the mixture was extracted with ethyl acetate for 3 times (10 mL×3). The combined organic layers were dried over magnesium sulfate hydrate, then concentrated and purified by silica gel column chromatography. (eluent: petrol ether/ ethyl acetate = 10:1) to afford ligand **II4** (85 mg, 82 % yield) as a clear oil.

^{1}H NMR (300 MHz, $CDCl_3$) δ 3.52-3.64 (m, 10H), 3.35 (s, 3H), 2.68 (t, *J* =7.08 Hz, 2H), 2.51 (t, *J* = 7.35 Hz, 2H), 1.50-1.59 (m, 2H), 1.25-1.36 (m, 18H), 0.85 (t, *J* = 6.99 Hz, 3H).

^{13}C NMR (75 MHz, $CDCl_3$) δ 72.0, 71.1, 70.7, 70.6, 70.3, 59.1, 32.6, 32.0, 31.4, 29.9, 29.7, 29.7, 29.6, 29.6, 29.4, 29.3, 28.9, 22.7, 14.2.

HRMS (ESI+): *m/z* calculated for $C_{19}H_{40}NaO_3S$ $[M+Na]^+$: 371.2596; found: 371.2580.

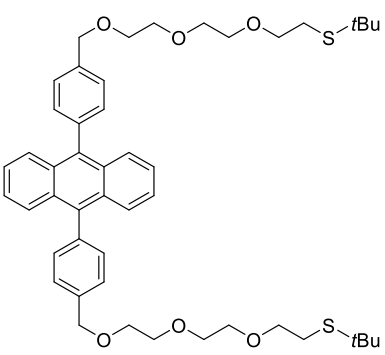

9,10-Bis(4-(12,12-dimethyl-2,5,8-trioxa-11-thiatridecyl)phenyl) anthracene (II23): To a solution of sodium hydride (12 mg, 0.5 mmol) in THF (1.5 mL) was added 2-methyl-2-propanethiol (45 μL, 0.4 mmol) at 0 °C under nitrogen atmosphere. After 1 h, a solution of **II1-3** (81 mg, 0.1 mmol) was added. The mixture was stirred at ambient temperature overnight. H_2O (3.0 mL) was added, the mixture was extracted with ethyl acetate for 3 times (10 mL×3). The combined organic layer was dried over magnesium, then concentrated and purified by silica gel column chromatography. (eluent: petrol ether/ ethyl acetate =5/1) to afford product **II23** (70 mg, 88 % yield) as a white solid.

^{1}H NMR (300 MHz, $CDCl_3$) δ 7.67-7.73 (m, 4H), 7.59 (d, J = 8.04 Hz, 4H), 7.46 (d, J = 8.04 Hz, 4H), 7.29-7.34 (m, 4H), 4.76 (s, 4H), 3.63-3.81 (m, 20H), 2.77 (t, J = 7.17 Hz, 4H), 1.31 (s, 18H).

^{13}C NMR (75 MHz, $CDCl_3$) δ 138.4, 137.6, 136.9, 131.4, 129.9, 127.8, 127.0, 125.0, 73.3, 71.3, 70.8, 70.7, 70.4, 69.9, 42.1, 31.1, 28.0.

HRMS (FD) calculated for [M, $C_{48}H_{62}O_6S_2]^{+\bullet}$: 798.3988; found: 798.3978.

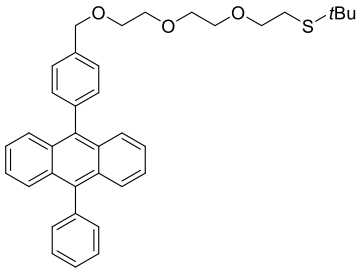

12,12-Dimethyl-1-(4-(10-phenylanthracen-9-yl)phenyl)-2,5,8-trioxa-11-thiatridecane (II24): To a solution of sodium hydride (13 mg, 0.56 mmol) in THF (2 mL) was added 2-methyl-2-propanethiol (0.05 mL, 0.42 mmol) at 0 °C under argon atmosphere. After 1 h, a solution of **II2-3** (80 mg, 0.14 mmol) was added. The mixture was stirred at ambient temperature overnight. H_2O (5.0 mL) was added, the mixture was extracted with ethyl acetate for 3 times (15 mL×3). The combined organic layer was dried over magnesium, then concentrated and purified by silica gel column chromatography. (eluent: petrol ether/ ethyl acetate = 5/1) to afford product 1-23-130-0 (71 mg, 90 % yield) as a yellow oil.

^{1}H NMR (300 MHz, $CDCl_3$) δ 7.69-7.73 (m, 4H), 7.55-7.64 (m, 5H), 7.46-7.50 (m, 4H), 7.30-7.36 (m, 4H), 4.77 (s, 2H), 3.65-3.82 (m, 10H), 2.78 (t, J = 7.29 Hz, 2H), 1.33 (s, 9H);

^{13}C NMR (75 MHz, $CDCl_3$) δ 139.1, 138.4, 137.6, 137.2, 136.9, 131.4 (d, J = 3.8 Hz), 129.9 (d, J = 2.3 Hz), 128.5, 127.9, 127.5, 127.0, 125.0, 73.4, 71.3, 70.9, 70.8, 70.4, 69.9, 42.2, 31.1, 28.0;

HRMS (TOF, positive) calculated for [M+Na, $C_{37}H_{40}O_3SNa]^+$: 587.2596; found: 587.2616.

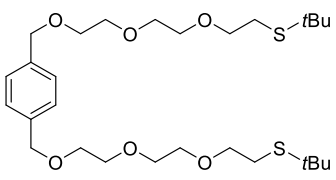

1,4-bis(12,12-dimethyl-2,5,8-trioxa-11-thiatridecyl)benzene (II25): To a suspension of sodium hydride (12 mg, 0.5 mmol) in THF (1.5 mL) was added 2-methyl-2-propanethiol (45 μL, 0.4 mmol) at 0 °C under nitrogen atmosphere. After 1 h, a solution of **II3-2** (56 mg, 0.1 mmol) was added. The mixture was stirred at ambient temperature overnight. H_2O (3.0 mL) was added, the mixture was extracted with ethyl acetate for 3 times (5 mL×3). The combined organic layers were dried over magnesium, then concentrated and purified by silica gel column chromatography. (eluent: petrol ether/ ethyl acetate = 3/1) to afford product 1-21-99-0 (36 mg, 67 % yield) as a clear oil.

^{1}H NMR (300 MHz, $CDCl_3$) δ 7.30 (s, 4H), 4.53 (s, 4H), 3.60-3.64 (m, 20H), 2.72 (t, *J* = 7.17 Hz, 4H), 1.30 (s, 18H);

^{13}C NMR (75 MHz, $CDCl_3$) δ 137.7, 127.8, 73.0, 71.2, 70.7, 70.7, 70.4, 69.4, 42.1, 31.1, 28.0

HRMS (ESI+) calculated for [M+Na, $C_{28}H_{50}NaO_6S_2]^+$: 569.2947; found: 569.2918.

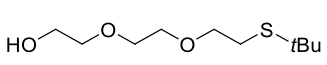

2-(2-(2-(*tert*-Butylthio)ethoxy)ethoxy)ethan-1-ol (II26-1): A flame-dried Schlenk tube was charged with diethyl glycol monovinyl ether (500 mg, 3.8 mmol) and Irgacure 651 (98 mg, 0.38 mmol). The mixture was degassed and flushed with agron for 3 times. Then, 2-methyl-2-propanethiol (0.45 mL, 3.8 mmol) was added. The whole mixture was stirred under 365 nm irradiation condition for 12 h. After the completion of the reaction, the mixture was purified by silica gel column chromatography. (eluent: petrol ether/ ethyl acetate = 5:1) to afford (1.16g, 92 % yield) as a clear oil.

^{1}H NMR (300 MHz, $CDCl_3$) δ 3.59-3.74 (m, 10H), 2.74 (t, *J* =7.38 Hz, 2H), 2.16 (br, 1H), 1.31 (m, 18H);

^{13}C NMR (75 MHz, $CDCl_3$) δ 72.6, 71.2, 70.4 (d, *J* = 4.4 Hz), 61.8, 42.2, 31.0, 27.9.

HRMS (TOF, positive ions) calculated for [M+Na, $C_{10}H_{22}NaO_3S]^+$: 245.1187; found:245.1119.

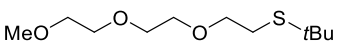

12,12-Dimethyl-2,5,8-trioxa-11-thiatridecane (II26): To a solution of sodium hydride (48 mg, 2.0 mmol) in anhydrous THF (2 mL) was added a solution of **II26-1** (222 mg, 1.0 mmol) in THF (1 mL) at 0 °C under argon atmosphere. After 1 h, iodomethane (0.31 mL, 5.0 mmol) was added, the mixture was stirred at room temperature overnight. After the completion of the reaction, H_2O (5 mL) was added and the mixture was extracted with ethyl acetate for 3 times (15 mL×3). The combined organic layer was dried over magnesium sulfate hydrate, then concentrated and purified by silica gel column chromatography. (eluent: petrol ether/ ethyl acetate = 7.5/1) to afford product **II26** (170 mg, 72 % yield) as a clear oil.

^{1}H NMR (300 MHz, $CDCl_3$) δ 3.54-3.65 (m, 10H), 3.37 (s, 3H), 2.73 (t, *J* =7.35 Hz, 2H), 1.31 (m, 9H);

^{13}C NMR (75 MHz, $CDCl_3$) δ 71.9, 71.2, 70.6, 70.5, 70.3, 59.0, 42.1, 31.0, 27.9;

HRMS (TOF, positive ions) calculated for [M+Na, $C_{11}H_{24}NaO_3S]^+$: 259.1344; found:259.1330.

7.2.2 Substrate for one pot reaction and final product

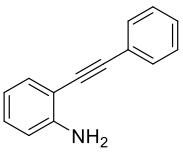

2-(Phenylethynyl)aniline (II18-1): To a mixture of 2-iodoaniline (2 g, 10.3 mmol), bis(triphenylphosphine) palladium acetate (180 mg, 0.23 mmol) and copper iodide (200 mg, 1.0 mmol) was added phenylacetylene (1.4 mL, 13.4 mmol) and triethylamine (10 mL) under argon atmosphere at room temperature. The mixture was stirred at ambient temperature overnight. Water (20 mL) was added and the mixture was extracted by dichloromethane for 3 times (20 mL×3). The combined organic phases were dried over magnesium sulfate, then concentrated and purified by silica gel column chromatography (eluent: petrol ether/ ethyl acetate = 50:1) to obtain product **II18-1** (1.23g, 70 % yield) as a brown solid.

^{1}H NMR (300 MHz, $CDCl_3$) δ 7.52-7.56 (m, 2H), 7.35-7.41 (m, 4H), 7.16 (td, *J* = 7.69, 1.45 Hz, 1H), 6.71-6.76 (m, 2H), 4.18 (br, 2H).

^{13}C NMR (75 MHz, $CDCl_3$) δ 147.8, 132.2, 131.5, 129.8, 128.4, 128.3, 123.4, 118.1, 114.4, 108.0, 94.8, 86.0;

HRMS (APCI, positive): *m/z* calculated for $C_{14}H_{11}N$ $[M]^+$: 193.0891; found: 193.0900.

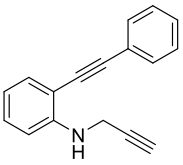

2-(Phenylethynyl)-N-(prop-2-yn-1-yl)aniline (II18-2): To a mixture of **II18-1** (860 mg, 4.45 mmol) and potassium carbonate (1.23 g, 8.9 mmol) in DMF (10 mL) was added propargyl bromide (0.77 mL, 8.9 mmol) under argon atmosphere at room temperature. The resulting mixture was stirred at ambient temperature overnight. Water (10 mL) was added and the mixture was extracted by dichloromethane for 3 times (20 mL×3). The collected organic phases were

dried over magnesium sulfate, then concentrated and purified by silica gel column chromatography (eluent: petrol ether/ ethyl acetate = 75:1) to afford product **II8-2** (683 mg, 72 % brsm yield) as a yellow oil.

^{1}H NMR (300 MHz, $CDCl_3$) δ 7.55-7.59 (m, 2H), 7.44 (d, *J* = 7.83, 1.56 Hz, 1H), 7.35-7.40 (m, 3H), 7.27-7.30 (m, 1H), 4.92 (br, 1H), 4.06 (d, *J* = 2.4 Hz, 2H), 2.28 (t, *J* = 2.43 Hz, 1H).

^{13}C NMR (75 MHz, $CDCl_3$) δ 147.6, 132.3, 131.6, 129.9, 128.5, 128.4, 123.2, 117.7, 110.3, 108.5, 95.3, 85.7, 80.7, 71.5, 33.3.

HRMS (APCI, positive): *m/z* calculated for $C_{17}H_{13}N$ $[M]^+$: 231.1048; found: 231.1048.

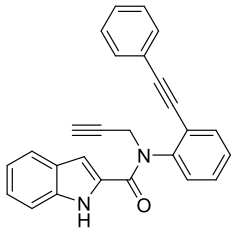

***N*-(2-(phenylethynyl)phenyl)-N-(prop-2-yn-1-yl)-1H-indole-2-carboxamide (II18-3)**: To an oven dried schlenk tube charged 1*H*-indole-2-carboxylic acid (32 mg, 0.198 mmol) in chloroform (2 mL) was added thionyl chloride (0.5 mL, 6.6 mmol) under argon atmosphere. The mixture was heated under reflux condition for 2 h. Then the solvent and excessive thionyl chloride was removed under reduced pressure and amine **II18-2** (41 mg, 0.188 mmol) and 4-dimethylaminopyridine (28 mg, 0.27 mmol) in chloroform (3 mL) were added. The system turned to dark and the mixture was heated under reflux condition overnight. After cooling to room temperature, the solvent was removed and purified by silica gel column chromatography (eluent: petrol ether/ ethyl acetate = 10:1) to afford product **II18-3** (51 mg, 77 % yield) as a yellow solid.

^{1}H NMR (300 MHz, $CDCl_3$) δ 9.93 (br, 1H), 7.69-7.72 (m, 1H), 7.38-7.54 (m, 7H), 7.19-7.28 (m, 4H), 7.70 (t, *J* = 7.4 Hz, 1H), 5.46 (s, 1H), 5.33 (d, *J* = 17.2 Hz, 1H), 4.39 (d, *J* = 17.2 Hz, 1H), 2.28 (t, *J* = 2.3 Hz, 1H).

^{13}C NMR (75 MHz, $CDCl_3$) δ 162.3, 143.0, 133.2, 131.7, 129.5, 128.8, 128.4, 127.7, 124.7, 123.6, 122.5, 122.3, 120.3, 111.9, 107.1, 95.3, 85.1, 78.8, 72.8, 39.1.

HRMS (ESI+): *m/z* calculated for $C_{26}H_{19}N_2O$ $[M+H]^+$: 375.1497; found: 375.1491.

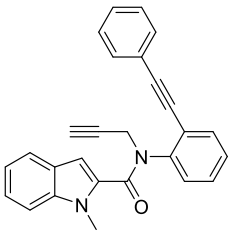

1-Methyl-N-(2-(phenylethynyl)phenyl)-N-(prop-2-yn-1-yl)-1H-indole-2-carboxamide (II18): To a suspension of sodium hydride (13 mg, 0.54 mmol) in anhydrous THF (4 mL) was added **II18-3** (100 mg, 0.27 mmol) under argon atmosphere at 0 °C. The mixture was kept stirring at 0 °C for 1 h, then iodomethane (0.2 mL, 2.7 mmol) was added and the mixture was allowed to warm up to ambient temperature overnight. Water (5 mL) was added and extracted with dichloromethane for 3 times (10 mL×3). The combined organic phases were dried over magnesium sulfate, then concentrated and purified by silica gel column chromatography (eluent: petrol ether/ ethyl acetate = 10:1) to afford product **II18** (90 mg, 87 % yield) as a white fluffy solid.

^{1}H NMR (300 MHz, $CDCl_3$) δ 7.55-7.58 (m, 2H), 7.47-7.51 (m, 2H), 7.35-7.43 (m, 5H), 7.19-7.31 (m, 3H), 6.20 (s, 1H), 5.11 (d, *J* = 16.47 Hz, 1H), 4.55 (d, *J* = 16.47 Hz, 1H), 3.87 (d, *J* = 0.57 Hz, 3H), 2.29 (t, *J* = 2.13 Hz, 1H). **^{13}C NMR (75 MHz, $CDCl_3$)** δ 163.8, 138.2, 133.2, 131.7, 131.3, 129.3 (d, *J* = 4.6 Hz), 129.1,

128.8, 128.5, 128.3, 128.1, 126.0, 125.3, 123.8, 122.9, 122.7, 122.0, 119.9, 109.9, 108.1, 94.5, 86.0, 79.0, 72.5, 38.8, 31.7.

HRMS (ESI+): *m/z* calculated for $C_{27}H_{20}N_2ONa$ $[M+Na]^+$: 411.1473; found: 411.1470.

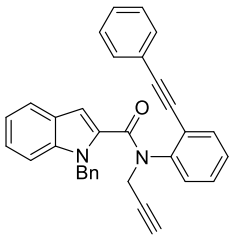

1-Benzyl-N-(2-(phenylethynyl)phenyl)-N-(prop-2-yn-1-yl)-1H-indole-2-carboxamide (II17): To a suspension of sodium hydride (6 mg, 0.27 mmol) in anhydrous THF (4 mL) was added **II18-3** (45 mg, 0.12 mmol) under argon atmosphere at 0 °C. The mixture was kept stirring at 0 °C for 1 h, then benzyl bromide (0.02 mL, 0.18 mmol) was added and the mixture was allowed to warm up to ambient temperature overnight. Water (5 mL) was added and extracted with dichloromethane for 3 times (10 mL×3). The combined organic phases were dried over magnesium sulfate, then concentrated and purified by silica gel column chromatography (eluent: petrol ether/ ethyl acetate = 10:1) to afford product **II17** (48 mg, 86 % yield) as a white solid.

^{1}H NMR (300 MHz, $CDCl_3$) δ 7.60–7.50 (m, 3H), 7.49–7.34 (m, 5H), 7.28 (t, *J* = 5.3 Hz, 2H), 7.25–7.16 (m, 3H), 7.07 (ddd, *J* = 14.8, 7.6, 2.1 Hz, 5H), 6.62–6.27 (m, 2H), 5.85 (d, *J* = 15.8 Hz, 1H), 5.43 (d, *J* = 15.5 Hz, 1H), 5.15 (d, *J* = 17.2 Hz, 1H), 4.39 (d, *J* = 17.0 Hz, 1H), 2.22 (t, *J* = 2.4 Hz, 1H).

^{13}C NMR (75 MHz, $CDCl_3$) δ 163.9, 143.9, 138.5, 138.0, 133.0, 131.8, 131.6, 131.3, 129.9, 129.2, 128.9, 128.6, 128.0, 127.3, 127.2, 126.4, 124.0, 122.6, 122.3, 122.2, 120.2, 110.5, 108.4, 95.3, 85.8, 78.8, 77.3, 72.3, 47.9, 38.4.;

HRMS (ESI+): *m/z* calculated for $C_{33}H_{25}N_2O$ $[M+H]^+$: 465.1967; found: 465.1954.

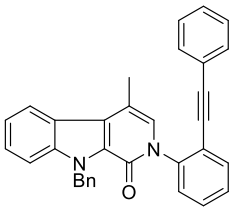

9-Benzyl-4-methyl-2-(2-(phenylethynyl)phenyl)-2,9-dihydro-1H-pyrido[3,4-b]indol-1-one (II21): To a solution of 2-amido-indole **II17** (11 mg, 21.5 µmol) in dichloromethane (2 mL) was added a solution of **II2**•$AuCl_3$ catalyst (2.2 µmol, 10 mol%) in dichloromethane (0.5 mL). The reaction was stirred at room temperature for 40 h. After concentration under vacuum, the residue was purified by column chromatography on silica gel (eluent: petrol ether/AcOEt, 10:1). Compound **II21** was isolated as a white solid (97 % yield)

^{1}H NMR (300 MHz, $CDCl_3$) δ 8.20 (d, *J* = 8.1 Hz, 1H), 7.75–7.67 (m, 1H), 7.54–7.40 (m, 5H), 7.32–7.27 (m, 1H), 7.23–7.00 (m, 11H), 6.96 (d, *J* = 1.2 Hz, 1H), 6.30 (d, *J* = 15.9 Hz, 1H), 6.02 (d, *J* = 15.8 Hz, 1H), 2.66 (d, *J* = 1.1 Hz, 3H).

MS (ESI+): *m/z* calculated for $C_{33}H_{25}N_2O$ $[M+H]^+$: 465.1967; found: 465.2

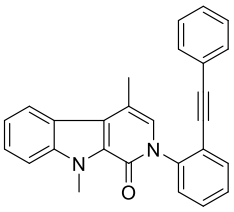

4,9-Dimethyl-2-(2-(phenylethynyl)phenyl)-2,9-dihydro-1H-pyrido[3,4-b]indol-1-one (II19): To a solution of 2-amido-indole **II18** (17 mg, 44 µmol) in dichloromethane (2 mL) was added a solution of **II1**•2$AuCl_3$ catalyst (2.2 µmol, 5 mol%) in dichloromethane (0.5 mL). The reaction was stirred at room temperature for 40 h. After concentration under vacuum, the residue was purified by column chromatography on silica gel (eluent: petrol ether/AcOEt, 1:1). Compound **II19** was isolated as a white solid (93 % yield). m.p. 163.7 °C; FTIR (NaCl): $\tilde{\nu}$ = 2923, 2854, 2219, 1663, 1590, 1331, 738 cm^{-1};

^{1}H NMR (300 MHz, $CDCl_3$) δ 8.18 (d, *J* = 8.1 Hz, 1H), 7.70-7.72 (m, 1H), 7.42-7.58 (m, 5H), 7.27-7.33 (m, 1H), 7.08-7.22 (m, 5H), 6.93 (d, *J* = 0.88 Hz, 1H), 4.35 (s, 3H), 2.63 (d, *J* = 0.88 Hz, 3H).

^{13}C NMR (75 MHz, $CDCl_3$) δ 156.0, 142.7, 141.2, 132.9, 131.5, 129.1, 128.6, 128.5, 128.4, 128.2, 126.8, 126.7, 126.5, 125.0, 122.9, 122.8, 122.3, 122.2, 120.2, 111.9, 110.3, 94.7, 85.5, 31.5, 17.0.

HRMS (ESI+): m/z calculated for $C_{27}H_{21}N_2O$ $[M+H]^+$: 389.1654; found: 389.1638.

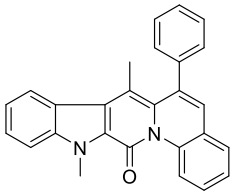

Indolino-4H-benzoquinolizin-4-one (II20): To a solution of 2-amido-indole **II19** (17 mg, 44 µmol) in dichloromethane (2 mL) was added a solution of gold catalyst (2.2 µmol, 5 mol%) in dichloromethane (0.5 mL). The reaction was stirred at room temperature for 8 h. Then, silver trifluoromethanesulfonate (1.0 mg, 7 mol%) was added and the reaction was stirred for 4 hours. The reaction medium was finally concentrated under vacuum. The residue was purified by column chromatography on silica gel (eluent: CH_2Cl_2/MeOH, 50:1). Compound **II20** was isolated as a sticky yellow oil (80 % yield): FTIR (NaCl): $\tilde{\nu}$ = 2925, 2854, 1630, 1525, 1334, 1266, 1030, 756, 637 cm^{-1};

^{1}H NMR (300 MHz, CD_3CN) δ 8.41 (s, 1H), 8.31 (d, *J* = 7.95 Hz, 1H), 8.06 (d, *J* = 8.28 Hz, 1H), 7.96 (d, *J* = 7.62 Hz, 1H), 7.62-7.82 (m, 5H), 7.40-7.53 (m, 4H), 6.96 (s, 1H), 3.91 (s, 3H), 2.90 (s, 3H).

^{13}C NMR (75 MHz, CD_3CN) δ 146.2, 144.6, 141.4, 134.8, 133.3, 132.9, 132.7, 2.1, 131.4, 130.3, 129.6, 129.4, 126.8, 126.1, 125.2, 124.2, 123.9, 123.5, 122.8, 122.2, 121.1, 119.9, 119.6, 112.3, 111.3, 34.0, 17.3.

HRMS (ESI+): m/z calculated for $C_{27}H_{21}N_2O$ $[M+H]^+$: 389.1654; found: 389.1648.

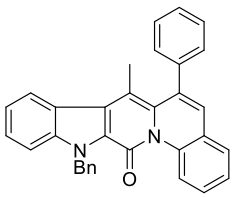

12-Benzyl-7-methyl-6-phenylindolo[3',2':4,5]pyrido[1,2-a]quinolin-13(12H)-one (II22): To a solution of **II17** (10.9 mg, 23.5 µmol) in $CDCl_3$ (2 mL) was added freshly prepared **II1**•2$AuCl_3$ (3~5 mg, 8 mol% ~13 mol%) under air at room temperature. The mixture was stirred at ambient temperature for 8 h. Then, silver trifluoromethanesulfonate (5 mg, 19.4 µmol) was added and the mixture was stirred under 365 nm UV lamp for 2 h. After the completion of the reaction as detected by TLC, the solvent was removed and purified by silica gel column chromatography (eluent: DCM/ MeOH = 75:1) to afford the cyclization product **II22** as a brown solid. Notes: it is very difficult to get the pure product even after 5th column chromatography even though it looks pure by TLC.

HRMS (ESI+) calculated for [M+H, $C_{33}H_{25}N_2O]^+$: 465.1967; found: 465.1963.

7.2.3 Pyridine ligands for gold(III) complexes

9,10-bis(3-(pyridin-2-yl)phenyl)anthracene: An oven-dried Schlenk tube was charged with 2-(3-bromophenyl)pyridine (163 mg, 0.69 mmol), 9,10-anthracene bis(pinacolato)diborane (100 mg, 0.23 mmol), palladium catalyst (21 mg, 8 mol%) and potassium carbonate(96 mg, 0.69 mmol). The mixture was degassed and flushed with nitrogen for 3 times, then a mixed solution of THF/water = 4:1 (5.0 mL) was added via syringe, The reaction was sealed and heated to 110 °C stirred for 24 h. After cooling to room temperature, dichloromethane (5 mL) was added and the mixture was filtered through a pad of celite, the organic layer was dried over magnesium sulfate and concentrated, then purified by silica gel column chromatography.

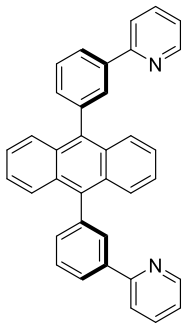

***Syn* 9,10-bis(3-(pyridin-2-yl)phenyl)anthracene (II27):**

(eluent: petrol ether/ethyl acetate = 20:1)

^{1}H NMR (300 MHz, $CDCl_3$) δ 8.68 (ddd, *J* = 4.8, 1.7, 1.0 Hz, 3H), 8.17 (t, *J* = 1.8 Hz, 3H), 7.90 (ddd, *J* = 7.8, 1.6, 1.1 Hz, 3H), 7.78–7.64 (m, 6H), 7.53 (ddd, *J* = 8.0, 2.0, 1.0 Hz, 3H), 7.32 (t, *J* = 7.9 Hz, 3H), 7.26–7.20 (m, 3H).

^{13}C NMR (75 MHz, $CDCl_3$) δ 155.8, 149.6, 141.1, 137.4, 132.2, 130.4, 130.2, 125.6, 123.2, 122.9, 120.9.

MS(ESI$^+$): calculated m/z $[M+H]^+$ for $[C_{36}H_{25}N_2]^+$: 485.2012, found: $[M+H]^+$: 485.2.

calculated m/z $[M+Na]^+$ for $[C_{36}H_{24}N_2Na]^+$: 507.1832, found: $[M+Na]^+$: 507.2.

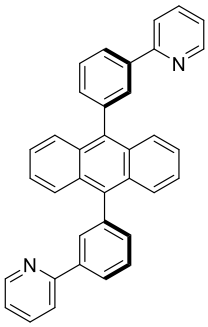

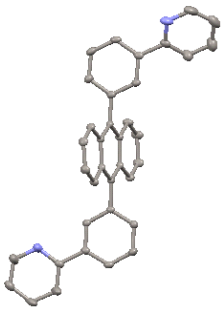

***Anti* 9,10-bis(3-(pyridin-2-yl)phenyl)anthracene (II28):**

(eluent: petrol ether/ethyl acetate = 5:1)

^{1}H NMR (300 MHz, $CDCl_3$) δ 8.72 (ddd, *J* = 4.7, 2.7, 1.5 Hz, 2H), 8.31–8.23 (m, 2H), 8.16–8.10 (m, 2H), 7.84–7.69 (m, 10H), 7.57 (ddd, *J* = 7.5, 2.9, 1.6 Hz, 2H), 7.39–7.31 (m, 4H), 7.27–7.21 (m, 2H).

^{13}C NMR (75 MHz, $CDCl_3$) δ 157.3, 149.8, 139.7, 137.1, 136.9, 132.1, 130.0, 129.9, 129.1, 127.1, 126.3, 125.3, 122.4, 120.8, 120.8.

HRMS(ESI$^+$): calculated m/z $[M+H]^+$ for $[C_{36}H_{25}N_2]^+$: 485.2012, found: $[M+H]^+$: 485.2020. calculated m/z $[M+Na]^+$ for $[C_{36}H_{24}N_2Na]^+$: 507.1832, found: $[M+Na]^+$: 507.1840.

7.2.4 Phosphine ligands for gold complexes

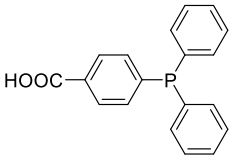

***p*-(Diphenylphosphino)benzoic acid (III1)**: A oven-dried schlenk tube was charged with 4-iodobenzoic acid (500 mg, 2.0 mmol) and palladium acetate (4.5 mg, 0.02 mmol). The mixture was degassed and refilled with argon three times, then dry acetonitrile (3 mL) was added. After the successive addition of triethylamine (0.56 mL, 4.0 mmol) and diphenylphosphine (0.52 mL, 3.0 mmol), the reaction mixture was stirred at reflux for 24 h. After full conversion (^{31}P NMR monitoring), the solvent was removed under reduced pressure and the crude residue was dissolved in an aqueous solution of KOH (3 mL, 1M). The solution was extracted with diethyl ether (3×20 mL). The aqueous phase was acidified with 6 N hydrochloric acid until the pH reaches 2-3. A brown solid appeared and was dissolved in the presence of dichloromethane (30 mL). The aqueous solution was extracted with dichloromethane (3×30 mL). The combined organic phases were dried over anhydrous magnesium sulfate, filtered and concentrated to afford compound **III1** (578 mg, 94% yield) as a brown solid. **^{1}H NMR (300 MHz, CDCl$_3$)** δ 8.03 (d, $^{3}J_{HP}$ = 7.7 Hz, 2H), 7.34 (br, 12H).

^{13}C NMR (75 MHz, CDCl$_3$) δ 171.7, 145.5 (d, J_{CP} = 15 Hz), 136.1 (d, J_{CP} = 10.4 Hz), 134.1 (d, J_{CP} = 19.9 Hz), 133.3 (d, J_{CP} = 18.4 Hz), 129.9 (d, J_{CP} = 6.3 Hz), 129.3, 129.2, 128.8 (d, J_{CP} = 7.3 Hz).

^{31}P NMR (121 MHz, CDCl$_3$) δ –4.7. The data is identical to literature.

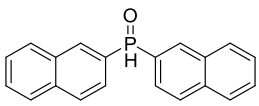

Bis(2-naphthalenyl)phosphine oxide (**III2-1**): An oven-dried Schlenk tube was charged with magnesium (360 mg, 15 mmol), then degassed and backfilled with argon for three times. A solution of 2-bromonaphtalene (1.5 g, 7.2 mmol) in dry THF (4.0 mL) was slowly added. The resulting mixture was heated at 50 °C for 1 h. After cooling the reaction mixture at 0 °C, diethyl phosphite (0.31 mL, 2.4 mmol) was added dropwise. The resulting mixture was allowed to stirred at room temperature overnight. After the addition of a saturated aqueous solution of ammonium chloride (3 mL) and water (20 mL), the mixture was extracted with diethyl ether (3×30 mL). The combined organic phases were dried over magnesium sulfate and concentrated. The crude residue was purified by column chromatography on silica gel (eluent: petrol ether/ ethyl acetate, 1:1) to afford **III2-1** (500 mg, 69 % yield) as a white solid.

^{1}H NMR (300 MHz, CDCl$_3$) δ 9.16 (s, CO_2H), 8.39 (d, $^{3}J_{HP}$ = 15.9 Hz, 2H), 7.85-7.95 (m, 6H), 7.55-7.67 (m, 6H). **^{13}C NMR (75 MHz, CDCl$_3$)** δ 135.2 (d, J_{CP} = 9.6 Hz), 133.0 (d, J_{CP} = 43.5 Hz), 132.6 (d, J_{CP} = 55.8 Hz), 129.3, 129.1, 128.9, 128.5, 128.1, 127.9, 127.3, 125.3 (d, J_{CP} = 49.3 Hz).

^{31}P NMR (121 MHz, CDCl$_3$) δ 21.7 (dt, $^{1}J_{HP}$ = 480 Hz, $^{3}J_{HP}$ = 12.4 Hz).

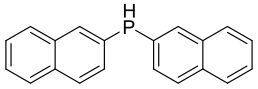

Bis(2-naphthalenyl)phosphine (**III2-2**): To a solution of DIBAL-H (3.7 mL, 4.5 mmol, 1.2 M in THF) at 65 °C under argon atmosphere was added a solution of

phosphine oxide **III2-1** (450 mg, 1.5 mmol) in THF (2.0 mL) over 10 min. The reaction was completed after 2 h (^{31}P NMR monitoring). After cooling to room temperature, sodium hydroxide (10 mL, 5 % aqueous solution) was slowly added. The mixture was extracted with hexane/diethyl ether (1:1; 4×10 mL). The combined organic phases were dried over magnesium sulfate under argon. The solution was transferred into a Schlenk tube and concentrated under vacuum to afford **III2-2** (400 mg, 93 % yield). Due to its ability to rapid oxidation, the compound was quickly used in the next step.

^{1}H NMR (300 MHz, $CDCl_3$) δ 8.03 (d, *J* = 9.0 Hz, 2H), 7.75-7.82 (m, 6H), 7.45-7.55 (m, 6H).

^{31}P NMR (121 MHz, $CDCl_3$) δ –39.8 (dt, $^{1}J_{HP}$ = 216 Hz, $^{3}J_{HP}$ = 6.2 Hz).

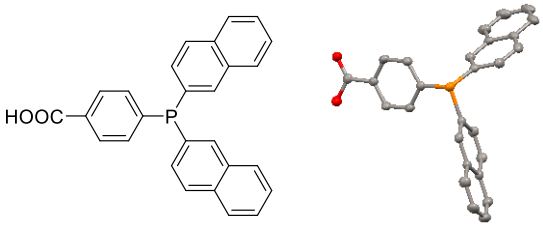

***p*-(Dinaphthylphosphino)benzoic acid (III2):** An oven-dried Schlenk tube was charged with 4-iodobenzoic acid (73 mg, 0.29 mmol), di-2-naphthalenylphosphine (100 mg, 0.35 mmol) and palladium acetate (5.1 mg, 1 mol%). After degassing (3 cycles of vacuum/argon), triethylamine (0.2 mL, 1.4 mmol) and dry acetonitrile (3 mL) were added. The reaction mixture was heated at 80 °C for 8 h. After concentration under reduced pressure, water (10 mL) was added and the mixture was extracted with diethyl ether (3×10 mL). The combined organic phases were dried over magnesium sulfate and concentrated. The crude product was purified by silica gel column chromatography (eluent: petrol ether/ ethyl acetate/ acetic acid, 100:10:0.3) to afford compound **III2** (89 mg, 76 % yield) as a white solid.

^{1}H NMR (300 MHz, $CDCl_3$) δ 8.05 (dd, *J* = 8.3 and 1.4 Hz, 2H), 7.92 (d, *J* = 9.4 Hz, 2H), 7.82-7.86 (m, 4H), 7.75-7.78 (m, 2H), 7.41-7.56 (m, 8H).

^{13}C NMR (75 MHz, $CDCl_3$) δ 171.9, 145.3 (d, *J* = 14.7 Hz), 134.9 (d, *J* = 24.3 Hz), 133.7, 133.5, 133.4 (d, *J* = 5.4 Hz), 133.3 (d, *J* = 4.4 Hz), 130.1 (d, *J* = 5.2 Hz), 130.0 (d, *J* = 5.1 Hz), 129.2, 128.4 (d, *J* = 6.7 Hz), 128.3, 127.8, 127.1, 126.6. ^{31}P NMR (121 MHz, $CDCl_3$) δ –3.7 (t, *J* = 6.3 Hz).

HRMS (ESI-): *m/z* calculated for $C_{27}H_{18}O_2P$ $[M-H]^-$: 405.1044, found: 405.1043.

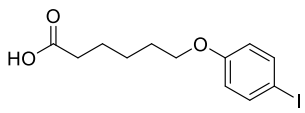

6-(4-Iodophenoxy)hexanoic acid (III3-1): To a solution of 4-bromophenol (1.0 g, 4.5 mmol) in a 10 % aqueous solution of KOH (15 mL) and ethanol (20 mL) under argon atmosphere at room temperature was added a solution of 6-bromohexanoic acid (1.1 g, 5.0 mmol) in an aqueous solution saturated with potassium carbonate (6 mL). The mixture was stirred under reflux overnight. After cooling to room temperature, an 18 % aqueous solution of HCl was added to acidify the solution (until pH = 2-3). A brown precipitate was formed and filtered. After washing with water (4×20 mL), the solid was dried to give 6-(4-iodophenoxy)hexanoic acid (660 mg, 44 % yield) as a solid.

^{1}H NMR (300 MHz, $CDCl_3$) δ 7.50-7.56 (m, 2H), 6.63-6.68 (m, 2H), 4.77 (s, 1H), 3.91 (t, *J* = 6.4 Hz, 2H),

2.38 (t, *J* = 7.3 Hz, 2H), 1.65-1.84 (m, 4H), 1.46-1.56 (m, 2H).

^{13}C NMR (75 MHz, $CDCl_3$) δ 179.6, 158.9, 138.2, 117.0, 82.6, 67.8, 34.0, 28.9, 25.6, 24.5.

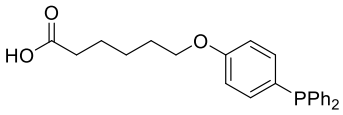

6-(4-(Diphenylphosphanyl)phenoxy)hexanoic acid (III3): An oven-dried Schlenk tube was charged with 6-(4-iodophenoxy)hexanoic acid (200 mg, 0.6 mmol) and palladium acetate (2 mg, 8 µmol). The mixture was degassed and refilled with argon for three times. Dry acetonitrile (3 mL), triethylamine (0.2 mL, 1.4 mmol) and diphenylphosphine (0.16 mL, 1.0 mmol) were successively added. The mixture was stirred at reflux overnight. After cooling at room temperature, the solvent was removed and water (10 mL) was added. The mixture was extracted with diethyl ether (3×10 mL). The combined organic phases were dried over magnesium sulfate and concentrated under reduced pressure. The crude solid was purified by silica gel column chromatography (eluent: petrol ether/ ethyl acetate/ acetic acid, 100:10:0.3) to afford **III3** (89 mg, 76 % yield) as a white solid.

^{1}H NMR (300 MHz, $CDCl_3$) δ 7.23-7.35 (m, 12H), 6.87 (d, *J* = 8.76 Hz, 2H), 3.96 (t, *J* = 6.33 Hz, 2H), 2.39 (t, *J* = 7.3 Hz, 2H), 1.67-1.85 (m, 4H), 1.47-1.58 (m, 2H).

^{13}C NMR (75 MHz, $CDCl_3$) δ 179.6, 159.9, 138.0 (d, *J* = 10.5 Hz), 135.7 (d, *J* = 21.2 Hz), 133.5 (d, *J* = 18.9 Hz), 128.5, 128.4, 127.5 (d, *J* = 7.9 Hz), 114.8 (d, *J* = 8.0 Hz), 67.6, 34.0, 29.0, 25.7, 24.5.

^{31}P NMR (121 MHz, $CDCl_3$) δ –7.0.

HRMS (ESI-): *m/z* calculated for $C_{24}H_{24}O_3P$ $[M-H]^-$: 391.1463, found: 391.1470.

7.2.5 Thioether ligands for silver complexes

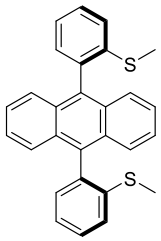

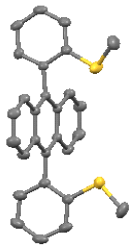

***Syn* 9,10-bis(2-(methylthio)phenyl)anthracene (IV2)**: An oven-dried schlenk tube was charged 9,10-dibromoanthracene (417 mg, 1.24 mmol), 2-(methylthio)phenylboronic acid (500 mg, 2.97 mmol), tetrakis(triphenylphosphine) palladium (72 mg, 0.062 mmol) and potassium carbonate (513 mg, 3.72 mmol). The mixture was evacuated and backfilled with argon for three times. Then, a mixture of toluene/EtOH/H_2O (4 mL/1 mL/ 1 mL) solvents was added. The whole mixture was stirred at 110°C for 24 h. After cooling to room temperature, dichloromethane (10 mL) was added and the mixture was dried over magnesium sulfate. The organic phase was concentrated and the residue was purified by silica gel column chromatography (eluent: petrol ether/ethyl acetate = 30:1) to afford *syn* **IV2** (166 mg, 32 % yield) as a yellow solid. m.p.: 252 °C

^{1}H NMR (300 MHz, $CDCl_3$) δ 7.52-7.59 (m, 6H, Anthr-H and Benz-H), 7.44 (d, *J* = 7.6 Hz, 2H, Benz-H), 7.31-7.40 (m, 8H, Anthr-H and Benz-H), 2.25 (m, 6H, SCH3).

^{13}C NMR (75 MHz, $CDCl_3$) δ 140.1, 137.0, 135.3, 131.6, 130.0, 128.6, 121.7, 125.5, 124.6, 15.3.

HRMS (FD): *m/z* calculated for $C_{13}H_{19}O_4BrNa$ $[M]^{+\bullet}$: 422.1163; found: 422.1180.

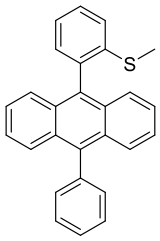

Methyl(2-(10-phenylanthracen-9-yl)phenyl)sulfane(IV1): 9-bromo-10-phenylanthracene (248 mg, 0.74 mmol), 2-(methylthio)phenylboronic acid (150 mg, 0.89 mmol), tetrakis(triphenylphosphine) palladium (43 mg, 0.037 mmol) and potassium carbonate (306 mg, 2.22 mmol) were successively charged in an oven-dried schlenk tube. The mixture was degassed under vacuum and backfilled with argon for three times. After the addition of solvents (6 mL, toluene/EtOH/H_2O: 4 /1/ 1), the mixture was stirred at 110°C for 24 h. After cooling to room temperature, dichloromethane (10 mL) was added and the mixture was dried over magnesium sulfate, the organic phase was concentrated and the residue purified by silica gel column chromatography (eluent: Petrol ether/ethyl acetate = 30:1) to afford product **IV1** (253 mg, 91 % yield) as a light yellow solid. m.p.: 235 °C

^{1}H NMR (300 MHz, $CDCl_3$) δ 7.68-7.75 (m, 2H), 7.52-7.64 (m, 7H), 7.44-7.49 (m, 2H), 7.30-7.41 (m, 6H), 2.31 (s, 3H).

^{13}C NMR (75 MHz, $CDCl_3$) δ 140.0, 139.1, 137.8, 137.1, 134.8, 131.8, 131.5, 131.4, 130.1, 129.8, 128.6, 128.4 (d, *J* = 1.6 Hz), 127.5, 127.3, 126.5, 125.4, 125.2, 124.7, 124.5, 15.4.

HRMS(ESI$^+$): calculated m/z $[M+H]^+$ for $[C_{27}H_{21}S]^+$: 377.1364, found: $[M+H]^+$: 377.1349; calculated for $[C_{27}H_{20}SNa]^+$: 399.1183, found: $[M+Na]^+$: 399.1169; calculated for $[C_{27}H_{20}SK]^+$: 415.0923 $[M+K]^+$: 415.0907.

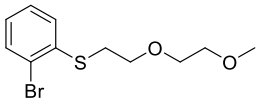

(2-Bromophenyl)(2-(2-methoxyethoxy)ethyl)sulfane (IV3-1): a flame-dried Schlenk tube was charged with 2'-bromothiophenol (500 mg, 2.64 mmol) and potassium carbonate (1.1 g, 7.9 mmol). The mixture was degassed and flushed with argon for three times. Then a solution of 2-(2-methoxyethoxy)ethyl 4-methylbenzenesulfonate (1.45 g, 5.38 mmol) in dry DMF (6 mL) was added under argon atmosphere. The resulting mixture was stirred at 100 °C for 24 h. After cooling to room temperature, water (20 mL) was added and the mixture was extracted with dichloromethane (3×30 mL). The combined organic phases were dried over magnesium sulfate, then concentrated and the residue was purified by silica gel column chromatography (eluent: petrol ether/ ethyl acetate = 10:1) to afford desired product **IV3-1** (691 mg, 90 %) as a colorless oil.

^{1}H NMR (300 MHz, $CDCl_3$) δ 7.52 (dd, *J* = 7.9, 1.2 Hz, 1H), 7.21-7.32 (m, 2H), 6.98-7.04 (m, 1H), 3.70 (t, *J* = 6.9 Hz, 2H), 3.59-3.63 (m, 2H), 3.51-3.54 (m, 2H), 3.37 (s, 3H), 3.15 (t, *J* = 7.1 Hz, 2H).

^{13}C NMR (75 MHz, $CDCl_3$) δ 137.5, 133.1, 128.2, 127.8, 126.8, 123.8, 71.9, 70.4, 69.5, 59.1, 32.3.

HRMS(ESI+): calculated m/z $[M+Na]^+$ for $[C_{11}H_{15}BrO_2SNa]^+$: 312.9874, found: $[M+Na]^+$: 312.9868.

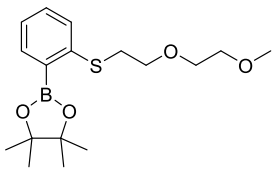

2-(2-((2-(2-Methoxyethoxy)ethyl)thio)phenyl)-4,4,5,5-tetramethyl-1,3,2-dioxaborolane (IV3-2): An oven-dried Schlenk tube was charged with compound **IV3-1** (500 mg, 1.72 mmol), bis(pinacolato)diboron (657 mg, 2.58 mmol), Pd(dppf)Cl_2 (70 mg, 0.086 mmol) and potassium acetate (505 mg, 5.16 mmol).

The mixture was degassed and refilled with argon for three times. After the addition of dry 1,4-dioxane (5 mL), the mixture was stirred at 110°C for 8 h. After cooling to room temperature, the dark solution was concentrated and dried. The crude boronic ester is used for the next step without any purification.

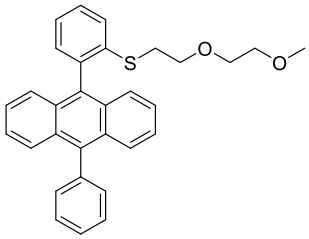

(2-(2-Methoxyethoxy)ethyl)(2-(10-phenylanthracen-9-yl)phenyl)sulfane (IV3): 9-bromo-10-phenylanthracene (477 mg, 1.43 mmol), tetrakis(triphenylphosphine) palladium (83 mg, 0.072 mmol) and potassium carbonate (592 mg, 4.29 mmol) were placed in a schlenk tube which was degassed and flushed with argon for three times. After the addition of solvents (4 mL, toluene/EtOH/H_2O: 4 /1/ 1), the mixture was stirred at 110°C for 24 h. After cooling to ambient temperature, dichloromethane (10 mL) was added and dried over magnesium sulfate, then concentrated and purified by silica gel column chromatography (eluent: petrol ether/ethyl acetate = 4:1) to afford product **IV3** (603 mg, 91 % yield) as a light yellow solid. m.p.: 136 °C

^{1}H NMR (300 MHz, $CDCl_3$) δ 7.67-7.74 (m, 2H), 7.45-7.63 (m, 9H), 7.29-7.42 (m, 6H), 3.41-3.51 (m, 6H), 3.32 (s, 3H), 2.97 (t, *J* = 7.7 Hz, 2H).

^{13}C NMR (75 MHz, $CDCl_3$) δ 139.1, 138.7, 137.7, 135.0, 132.2, 131.5, 131.4, 130.0, 129.9, 128.6, 128.4, 127.5, 127.3, 127.2, 126.5, 125.7, 125.4, 125.1, 71.9, 70.2, 69.9, 59.1, 31.6.

HRMS(ESI+): calculated m/z $[M+Na]^+$ for $[C_{31}H_{28}O_2SNa]^+$: 487.1708, found: $[M+Na]^+$: 487.1688.

9,10-Bis(2-((2-(2-methoxyethoxy)ethyl)thio)phenyl)anthracene *anti* (IV4) and *syn* (IV5): an oven-dried Schlenk tube was charged with compound **IV3-1** (77 mg, 0.267 mmol), 9,10-anthracene diboronic acid bis(pinacol) ester (50 mg, 0.116 mmol), tetrakis-(triphenylphosphine) palladium (13 mg, 0.0116 mmol) and potassium carbonate (80 mg, 0.58 mmol). The mixture was degassed under vacuum and refilled with argon for three times. After the addition of solvents (3.5 mL, toluene/EtOH/H_2O: 5 /1/ 1), the mixture was stirred at 110 °C for 48 h. After cooling to room temperature, the mixture was diluted with dichloromethane (30 mL) and dried over magnesium sulfate, then concentrated and purified by silica gel chromatography. A first eluent (petrol ether/ethyl acetate = 10:1) allowed the isolation of *anti* product **IV4** (116 mg, 42 % yield) as a white solid and the second eluent (petrol ether/ethyl acetate = 1:5) led to the obtention of *syn* product **IV5** (38 mg, 14 % yield) as a yellow oil. The *anti*/*syn* ratio is (3:1).

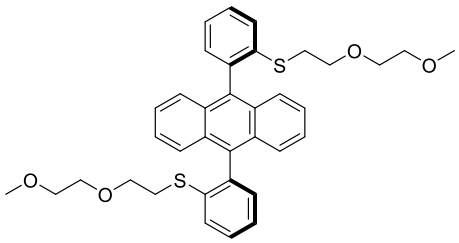
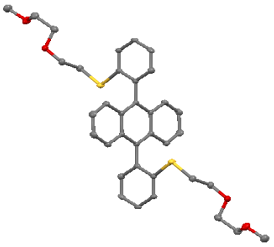

***Anti* 9,10-bis(2-((2- (2methoxy ethoxy)ethyl)thio)phenyl)anthracene (IV4):**

^{1}H NMR (300 MHz, $CDCl_3$) δ 7.61 (d, *J* = 7.8 Hz, 2H), 7.48-7.57 (m, 6H), 7.37-7.40 (m, 4H), 7.29-7.35 (m, 4H), 3.39-3.50 (m, 12H), 3.31 (s, 6H), 2.95 (t, *J* = 7.6 Hz, 4H)

^{13}C NMR (75 MHz, $CDCl_3$) δ 138.6, 137.6, 135.5, 132.3, 129.9, 128.6, 127.1, 126.7, 125.6, 125.4, 71.8, 70.2, 69.8, 59.1, 31.6.

HRMS(FD): calculated m/z $[M]^{+\bullet}$ for $[C_{36}H_{38}O_4S_2]^{+\bullet}$: 621.2109, found: $[M]^{+\bullet}$: 598.2211.

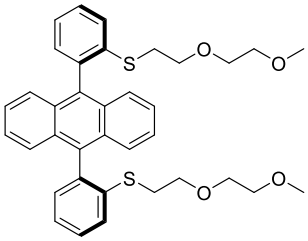

***Syn* 9,10-bis(2-((2-(2-methoxyethoxy)ethyl)thio)phenyl)anthracene (IV5):**

^{1}H NMR (300 MHz, $CDCl_3$) δ 7.62 (dd, *J* = 7.8, 1.0 Hz, 2H), 7.49-7.55 (m, 6H), 7.29-7.41 (m, 8H), 3.39-3.48 (m, 12H), 3.31 (s, 6H), 2.95 (t, *J* = 7.7 Hz, 4H)

^{13}C NMR (75 MHz, $CDCl_3$) δ 138.7, 137.8, 135.5, 132.1, 130.1, 130.0, 128.6, 127.4, 126.7, 125.6, 125.4, 71.9, 70.2, 69.9, 59.1, 31.6.

HRMS(FD): calculated m/z $[M]^{+\bullet}$ for $[C_{36}H_{38}O_4S_2]^{+\bullet}$: 598.2212, found: $[M]^{+\bullet}$: 598.2212.

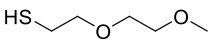

2-(2-Methoxyethoxy)ethane-1-thiol [32] **(IV6-1)**: To a solution of 2-(2-methoxyethoxy)ethyl 4-methylbenzenesulfonate (274 mg, 1.0 mmol) in EtOH/H_2O (3 mL/2 mL) was added thiourea (114 mg, 1.5 mmol) under argon atmosphere at room temperature. The resulting mixture was stirred at 100 °C for 24 h. After cooling to room temperature, water (20 mL) was added and the mixture was extracted with dichloromethane (3×30 mL). The combined organic phases were dried over magnesium sulfate, then concentrated and the residue was purified by silica gel column chromatography (eluent: petrol ether/ ethyl acetate = 5:1) to afford desired product **IV6-1** (40 mg, 29 %) as a colorless oil.

^{1}H NMR (300 MHz, $CDCl_3$) δ 3.61–3.54 (m, 4H), 3.53–3.48 (m, 2H), 3.34 (d, *J* = 1.7 Hz, 3H), 2.66 (dt, *J* = 8.2, 6.5 Hz, 2H), 1.54 (t, *J* = 8.2 Hz, 1H).

^{13}C NMR (75 MHz, $CDCl_3$) δ 73.0, 71.8, 70.1, 59.0, 24.2.

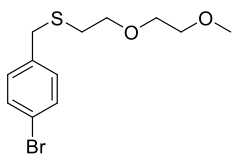

(4-Bromobenzyl)(2-(2-methoxyethoxy)ethyl)sulfane (IV6-2): To a suspension of potassium carbonate (61 mg, 0.44mmol) in acetonitrile (4 mL) was added 4-bromobenzyl bromide (92 mg, 0.37 mmol) and 2-(2-methoxyethoxy)ethane-1-thiol (50 mg, 0.37 mol) under argon atmosphere. The mixture was stirred at rt for 12 h. Solvent was removed and the residue was purified by silica gel column chromatography (eluent: petrol ether/

[32] S. S. Erdem, I. V. Nesterova, S. A. Soper and R. P. Hammer. *J. Org. Chem.*, **2009**, *74*, 9280-9286.

ethyl acetate = 10:1) to afford product (64 mg, 57% yield) as a colorless oil.

^{1}H NMR (300 MHz, $CDCl_3$) δ 7.44–7.37 (m, 2H), 7.22–7.15 (m, 2H), 3.69 (s, 2H), 3.57 (ddd, *J* = 5.9, 4.3, 3.8 Hz, 4H), 3.54–3.48 (m, 2H), 3.36 (s, 3H), 2.60 (t, *J* = 6.8 Hz, 2H).

^{13}C NMR (75 MHz, $CDCl_3$) δ 137.5, 131.6, 130.7, 120.8, 72.0, 71.0, 70.3, 59.1, 36.1, 30.6.

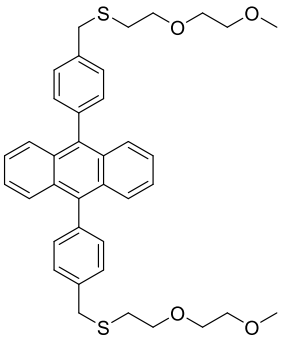

9,10-Bis(4-(((2-(2-methoxyethoxy)ethyl)thio)methyl)phenyl)anthracene (IV6): An oven-dried Schlenk tube was charged with (4-bromobenzyl)(2-(2-methoxyethoxy)ethyl)sulfane (60 mg, 0.2 mmol), 9,10-anthracene bis(pinacolato)diborane (39 mg, 0.09 mmol), palladium catalyst (10 mg, 10 mol%) and potassium carbonate(38 mg, 0.27 mmol). The mixture was degassed and flushed with nitrogen for 3 times, then a mixed solution of toluene/EtOH/water = 4:1:1 (3.0 mL) was added via a syringe, The reaction was sealed and heated to 110 °C stirred for 48 h. After cooling to room temperature, dichloromethane (5 mL) was added and the mixture was filtered through a pad of celite, the organic layer was dried over magnesium sulfate and concentrated, then purified by silica gel column chromatography (eluent: petrol ether/ ethyl acetate = 1:1) to afford product as a pale yellow solid **IV6** (20 mg, 36 % yield).

^{1}H NMR (300 MHz, $CDCl_3$) δ 7.73–7.66 (m, 4H), 7.57 (d, *J* = 8.1 Hz, 4H), 7.46–7.40 (m, 4H), 7.37–7.30 (m, 4H), 3.95 (s, 4H), 3.74 (t, *J* = 6.9 Hz, 4H), 3.67 (ddd, *J* = 3.8, 3.2, 1.2 Hz, 4H), 3.59 (ddd, *J* = 5.0, 3.3, 1.2 Hz, 4H), 3.41 (s, 6H), 2.82 (t, *J* = 6.9 Hz, 4H).

^{13}C NMR (75 MHz, $CDCl_3$) δ 137.9, 137.8, 136.9, 131.6, 130.0, 129.1, 127.0, 125.1, 72.1, 71.1, 70.4, 59.2, 36.8, 31.0.

HRMS (FD): *m/z* calculated for $C_{38}H_{42}O_4S_2$ $[M]^{+\bullet}$: 626.2525; found: 626.2531.

7.2.6 Oxidation of thioethers to sulfoxides

General procedure for the oxidation of IV1-5 to sulfoxides IV7-11: to a suspension of thioether in glacial acetic acid was added hydrogen peroxide (35 % aqueous solution, 1.5 equiv for **IV1** and **IV3**, 2.5 equiv for **IV2**, **IV4** and **IV5**). The resulting mixture was stirred at room temperature for 12 h under argon atmosphere. After the completion of the reaction (TLC monitoring), the solution was concentrated and the crude product was purified by column chromatography on silica gel to allow the isolation of sulfoxides **IV7-11**.

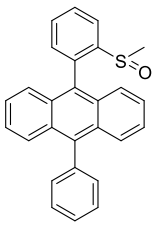

9-(2-(Methylsulfinyl)phenyl)-10-phenylanthracene (IV7): According to the general procedure, using thioether **R1** (205 mg, 0.55 mmol), hydrogen peroxide (79 mg, 0.82 mmol) and glacial acetic acid (3 mL), the crude product was purified by silica gel column chromatography (eluent: petrol ether/ethyl acetate = 1:1) to afford product **IV7** (187 mg, 88 % yield) as a light yellow solid. m.p.: 271 °C

^{1}H NMR (300 MHz, $CDCl_3$) δ 8.36 (dd, *J* = 7.9, 1.1 Hz, 1H), 7.85 (td, *J* = 7.5, 1.3 Hz, 1H), 7.70-7.76 (m, 3H), 7.55-7.63 (m, 5H), 7.31-7.47 (m, 7H), 2.24 (s, 3H).

^{13}C NMR (75 MHz, $CDCl_3$) δ 146.7, 139.0, 138.6, 136.1, 132.2, 131.3 (t, *J* = 1.5 Hz), 131.1, 130.2, 129.9 (d, *J* = 2.3 Hz), 129.8, 129.7, 128.5, 127.8, 127.3, 126.6, 126.1, 126.0, 125.7, 125.6, 125.1, 123.9, 43.5.
HRMS(ESI+): calculated m/z $[M+H]^+$ for $[C_{27}H_{21}OS]^+$: 393.1313, found: $[M+H]^+$: 393.1297; $[M+Na]^+$: 415.1117; $[2M+Na]^+$: 807.2341.

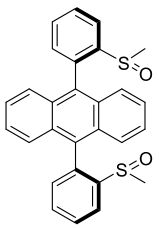

9,10-Bis(2-(methylsulfinyl)phenyl)anthracene (IV8): According to the general procedure, thioether *syn* **IV2** (236 mg, 0.56 mmol) and hydrogen peroxide (136 mg, 1.4 mmol, 35 % aqueous solution) were mixed in glacial acetic acid (3 mL) under argon atmosphere. The product was purified by silica gel column chromatography (eluent: dichlormethane/methanol = 50:1) to afford product *syn* **IV8** (170 mg, 72 % yield) as a yellow solid.

The mixture of diastereoisomers (ratio 1:1.3 based ^{1}H NMR) was separated by chiral HPLC.
(**Notes**: Two sets of NMR observed which were suspected as stereoisomers with a ratio of 1:1.3 based on the peak referred to CH_3 group). The data of this compound is not clear in the literature as no spectra was provided and the chemical shift of CH_3 is quite different (2.64 ppm) from our results (2.21 and 2.15 ppm).
m.p.: 345 °C
^{1}H NMR (300 MHz, $CDCl_3$) δ 8.32-8.36 (m, 2H), 7.84-7.90 (m, 2H), 7.73-7.80 (m, 2H), 7.57-7.61 (m, 2H), 7.36-7.51 (m, 8H), 2.21 (s, 3.4H), 2.15 (s, 2.6H).
^{13}C NMR (75 MHz, $CDCl_3$) δ 146.6, 146.5, 135.7, 135.5, 132.9, 132.8, 131.4, 131.3, 130.1, 130.1, 130.0, 129.7, 127.2, 126.7, 126.7, 126.4, 126.3, 125.8, 124.2, 124.1, 43.3, 42.8.
HRMS(ESI+): calculated m/z $[M+H]^+$ for $[C_{28}H_{23}O_2S_2]^+$: 455.1139, found: $[M+H]^+$: 455.1129; $[M+Na]^+$: 477.0948.
Enantiopure (*R*,*R*)-**IV8**: **^{1}H NMR (300 MHz, $CDCl_3$)** δ 8.33 (dd, *J* = 7.9, 1.0 Hz, 2H), 7.87 (td, *J* = 7.7, 1.4 Hz, 2H), 7.77 (td, *J* = 7.5, 1.4 Hz, 2H), 7.63–7.55 (m, 2H), 7.52–7.35 (m, 8H), 2.21 (s, 6H).
^{13}C NMR (75 MHz, $CDCl_3$) δ 146.6, 135.7, 132.8, 131.8, 131.4, 130.1, 129.7, 126.7, 126.7, 125.8, 124.1, 43.3.

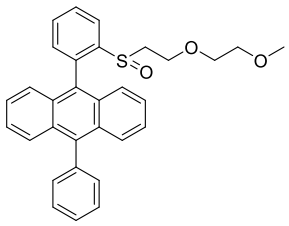

9-(2-((2-(2-Methoxyethoxy)ethyl)sulfinyl)phenyl)-10-phenylanthracene (IV9): According to the general procedure, thioether ligand **IV3** (280 mg, 0.58 mmol) and hydrogen peroxide (85 mg, 0.88 mmol, 35 % aqueous solution) were mixed in glacial acetic acid (3 mL) under argon atmosphere. The product was purified by silica gel column chromatography (eluent: ethyl acetate) to afford product **IV9** (271 mg, 97 % yield) as a yellow solid. m.p.: 149 °C
^{1}H NMR (300 MHz, $CDCl_3$) δ 8.29 (dd, *J* = 7.9, 1.1 Hz, 1H), 7.82 (td, *J* = 7.5, 1.3 Hz, 1H), 7.68-7.75 (m, 3H), 7.55-7.65 (m, 4H), 7.44-7.56 (m, 4H), 7.32-7.42 (m, 4H), 3.58-3.66 (m, 1H), 3.43-3.52 (m, 1H), 3.17 (s, 3H), 3.08-3.16 (m, 3H), 2.96-3.03 (m, 1H), 2.52-2.56 (m, 2H) .

^{13}C NMR (75 MHz, $CDCl_3$) δ 145.0, 138.9, 138.6, 136.3, 132.4, 131.3 (d, *J* = 2.1 Hz), 131.2, 131.1, 10.3, 129.8, 129.6, 129.4, 128.5, 127.8, 127.9, 127.3, 126.6, 126.2, 126.0, 125.8, 125.6, 125.2, 124.6, 71.5, 69.7, 63.2, 59.0, 55.6.

HRMS(ESI+): calculated m/z $[M+H]^+$ for $[C_{31}H_{29}O_3S]^+$: 481.1837, found: $[M+H]^+$: 481.1831; $[M+Na]^+$: 503.1649; $[2M+Na]^+$: 983.3410.

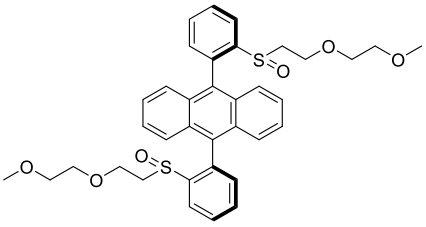

9,10-Bis(2-((2-(2-methoxyethoxy)ethyl)sulfinyl)phenyl)anthracene (IV10): According to the general procedure, thioether ligand **IV4** (204 mg, 0.34 mmol) and hydrogen peroxide (83 mg, 0.85 mmol, 35 % aqueous solution) were mixed in glacial acetic acid (3 mL) under argon atmosphere. The product was purified by silica gel column chromatography (eluent: dichlormethane/methanol = 75:1) to afford *anti* product **IV10** (172 mg, 80 % yield) as a yellow solid. m.p.: 136 °C

^{1}H NMR (300 MHz, $CDCl_3$) δ 8.29 (dd, *J* = 7.8, 1.1 Hz, 2H), 7.84 (t, *J* = 7.4 Hz, 2H), 7.70-7.77 (m, 2H), 7.56-7.64 (m, 2H), 7.36-7.53 (m, 8H), 3.57-3.65 (m, 2H), 3.42-3.54 (m, 2H), 2.92-3.23 (m, 14H), 2.57-2.94 (m, 4H).

^{13}C NMR (75 MHz, $CDCl_3$) δ 145.0, 144.9, 135.9, 132.9 (d, *J* = 1.1 Hz), 132.3 (d, *J* = 2.6 Hz), 131.2 (d, *J* = 2.1 Hz), 130.1, 129.7 (d, *J* = 2.1 Hz), 129.5 (d, *J* = 1.4 Hz), 127.0, 126.7, 126.5, 126.3, 126.1, 124.6, 71.5 (d, *J* = 2.6 Hz), 69.8 (d, *J* = 14.1 Hz), 63.1, 59.0 (d, *J* = 1.6 Hz), 55.6 (d, *J* = 14.4 Hz).

HRMS(ESI+): calculated m/z $[M+H]^+$ for $[C_{36}H_{39}O_6S_2]^+$: 631.2188, found: $[M+H]^+$: 631.2169; $[M+Na]^+$: 653.1987; $[2M+Na]^+$: 1283.4088.

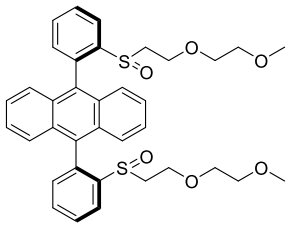

9,10-Bis(2-((2-(2-methoxyethoxy)ethyl)sulfinyl)phenyl)anthracene(IV11): According to the general procedure, thioether ligand **IV5** (75 mg, 0.125 mmol) and hydrogen peroxide (31 mg, 0.31 mmol, 35 % aqueous solution) were mixed in glacial acetic acid (3 mL) under argon atmosphere. The product was purified by silica gel column chromatography (eluent: ethyl acetate) to afford product **IV11** (63 mg, 80 % yield) as a sticky yellow oil.

^{1}H NMR (300 MHz, $CDCl_3$) δ 8.25 (dd, *J* = 7.9, 1.1 Hz, 2H), 7.77-7.84 (m, 2H), 7.68-7.75 (m, 2H), 7.48-7.59 (m, 4H), 7.34-7.46 (m, 6H), 3.44-3.60 (m, 4H), 3.18-3.36 (m, 12H), 3.11-3.16 (m, 2H), 2.30-2.57 (m, 4H).

^{13}C NMR (75 MHz, $CDCl_3$) δ 144.7, 144.4, 135.7 (d, *J* = 3.2 Hz), 132.8, 132.7, 132.0, 131.8, 131.1, 131.0, 130.1, 130.0 (d, *J* = 2.0 Hz), 129.6, 129.5, 129.4 (d, *J* = 2.3 Hz), 126.9, 126.6 (d, *J* = 1.7 Hz), 126.5, 126.3, 126.1, 126.0, 124.8, 124.7, 71.6 (d, *J* = 6.4 Hz), 69.8 (d, *J* = 27.9 Hz), 62.7 (d, *J* = 35.3 Hz), 58.9, 54.3 (d, *J* = 21.1 Hz).

HRMS(ESI+): calculated m/z $[M+H]^+$ for $[C_{36}H_{39}O_6S_2]^+$: 631.2188, found: $[M+H]^+$: 631.2175; $[M+Na]^+$: 653.1995; $[2M+Na]^+$: 1283.4103.

7.2.7 Amine and aldehyde motifs

7.2.7.1 Amine marcocycle and imine cage

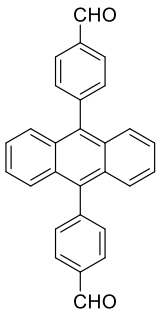

4,4'-(Anthracene-9,10-diyl)dibenzaldehyde [33] (V3-1): An oven-dried schlenk tube equipped with a stirring bar was charged with 9,10-dibromoanthracene (248 mg, 0.74 mmol), 2-(methylthio)phenylboronic acid (150 mg, 0.89 mmol), tetrakis(triphenylphosphine) palladium (43 mg, 0.037 mmol) and potassium carbonate (306 mg, 2.22 mmol). The mixture was evacuated and backfilled with argon for three times. Then, solvent Toluene/EtOH/H_2O (4 mL/1 mL/ 1 mL) was injected. The clear solution was stirred at 110°C for 24 h. At which point the system turned cloudy and a light yellow precipitation appeared. The solid was filtered and dried to afford the product (253 mg, 91 % yield) as a light yellow solid. The yellow crystals were obtained suitable for X-ray diffraction by solvent diffusion (hexane vapor into dichloromethane solution of **V3-1**).

^{1}H NMR (CD_2Cl_2, 300 MHz) δ 10.22 (s, 2H), 8.19–8.12 (m, 4H), 7.72–7.66 (m, 4H), 7.65–7.57 (m, 4H), 7.42–7.34 (m, 4H).

^{13}C NMR (CD_2Cl_2, 75 MHz) δ 192.13, 145.89, 136.29, 135.93, 132.26, 130.03, 129.53, 126.65, 125.83.

The data is identical to the literature.[34]

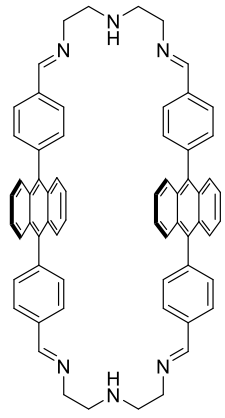

5,8,11,17,20,23-Hexaaza-2,14(9,10)-dianthracena-1,3,13,15(1,4)-tetrabenzenacyclotetracosaphane-4,11,16,23-tetraene (V1): To a solution of diethylenetriamine (0.11 mL, 1.0 mmol) in acetonitrile (5 mL) was added a solution of 4,4'-(anthracene-9,10-diyl)dibenzaldehyde (386 mg, 1.0 mmol) in dichloromethane (10 mL) over 1 h under argon atmosphere at room temperature. The resulting mixture was vigorously stirred at ambient temperature for 48 h, at which point a yellow precipitation appeared. The precipitate was filtered and washed with a mixed solvent (MeCN/CH_2Cl_2 5:1) (3 mL×3). The solid was dried to afford the product (360 mg, 89 % yield). *Notes: No carbon NMR was obtained due the poor solubility of the compound in common deuterated solvents.*

m.p.: > 350°C

[33] (a) C. Mongin, A. M. Ardoy, R. Méreau, D. M. Bassani and B. Bibal. *Chem. Sci.*, **2020**, *11*, 1478-1484; (b) W. Yang, A. Greenaway, X. Lin, R. Matsuda, A. J. Blake, C. Wilson, W. Lewis, P. Hubberstey, S. Kitagawa, N. R. Champness and M. Schröder. *J. Am. Chem. Soc.*, **2010**, *132*, 14457-14469.

[34] (a) C. Mongin, A. M. Ardoy, R. Méreau, D. M. Bassani and B. Bibal. *Chem. Sci.*, **2020**, *11*, 1478-1484; (b) W. Yang, A. Greenaway, X. Lin, R. Matsuda, A. J. Blake, C. Wilson, W. Lewis, P. Hubberstey, S. Kitagawa, N. R. Champness and M. Schröder. *J. Am. Chem. Soc.*, **2010**, *132*, 14457-14469.

^{1}H NMR ($CDCl_3$, 300 MHz) δ 8.59 (s, 4H), 7.95 (d, *J* = 7.9 Hz, 8H), 7.44 (dd, *J* = 6.8, 3.2 Hz, 8H), 7.35 (d, *J* = 7.9 Hz, 8H), 6.94 (dd, *J* = 6.9, 3.1 Hz, 8H), 3.98 (s, 8H), 3.49 (s, 2H), 3.16 (s, 8H).

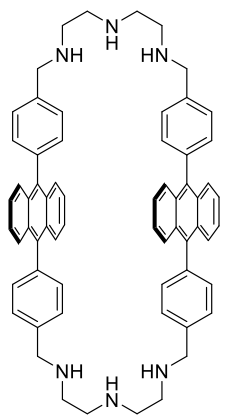

5,8,11,17,20,23-Hexaaza-2,14(9,10)-dianthracena-1,3,13,15(1,4)-tetrabenzenacyclotetracosaphane (V2): To a suspension of macrocyclic imine **V1** (222 mg, 0.24 mmol) in methanol (10 mL) and dichloromethane (15 mL) was added sodium borohydride (139 mg, 3.6 mmol) under argon atmosphere at ambient temperature. The mixture was stirred at room temperature for 16 h and the system turned to a clear solution. Then the solvent was removed and the residue was purified by column chromatography (Silica gel, eluent: CH_2Cl_2/MeOH/$NH_3 \cdot H_2O$ = 100: 5: 1) to deliver product (176 mg, 79 % yield) as a light yellow solid. m.p.: 320°C

^{1}H NMR ($CDCl_3$, 300 MHz) δ 7.56 (d, *J* = 7.8 Hz, 8H), 7.48 (dd, *J* = 6.8, 3.2 Hz, 8H), 7.27 (s, 4H), 7.24 (s, 4H), 6.93 (dd, *J* = 6.9, 3.2 Hz, 8H), 4.00 (s, 8H), 2.99 (dd, *J* = 26.2, 3.2 Hz, 16H).

^{13}C NMR ($CDCl_3$, 75 MHz) δ 139.73, 137.80, 136.61, 131.43, 129.74, 128.08, 126.72, 124.85, 54.20, 49.55, 49.24.

HRMS (ESI$^+$): calculated m/z $[M+H]^+$ for $[C_{64}H_{63}N_6]^+$: m/z 915.5114, found 915.5131

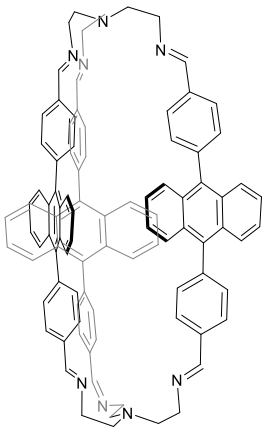

Imine cage (V3): To a solution of dialdehyde (122 mg, 0.32 mmol) in $CHCl_3$ (10 mL) was added a solution of tri(2-aminoethyl) amine (31 mg, 0.21 mmol) in $CHCl_3$ (10 mL) at room temperature under air. The resulting mixture was stirred at ambient temperature for 4 days. The yellow precipitate was filtered and washed with $CHCl_3$ (5 mL). Then the solid was dried under reduced pressure to afford the product (104 mg, 74 % yield) as a yellow solid. The yellow needle crystals were obtained by solvent diffusion (CH_3CN vapor into benzene or THF solution of **V3**, or cyclohexane vapor into THF solution of **V3**). *All the crystals showed no diffraction.* m.p.: > 350°C

^{1}H NMR (CD_2Cl_2, 300 MHz) δ 7.97 (s, 6H), 7.62 (dd, *J* = 6.8, 3.2 Hz, 12H), 7.51 (d, *J* = 7.6 Hz, 12H), 7.37–7.28 (m, 12H), 7.14 (dd, *J* = 6.8, 3.2 Hz, 12H), 3.67 (s, 12H), 2.95 (br, 12H).

^{13}C NMR (CD_2Cl_2, 75 MHz) δ 161.3, 141.8, 136.7, 136.5, 132.0, 129.8, 128.9, 126.9, 125.4, 77.9, 57.4.

HRMS (ESI$^+$): calculated m/z $[M+H]^+$ for $[C_{96}H_{79}N_8]^+$: m/z 1343.6428, found 1343.6471.

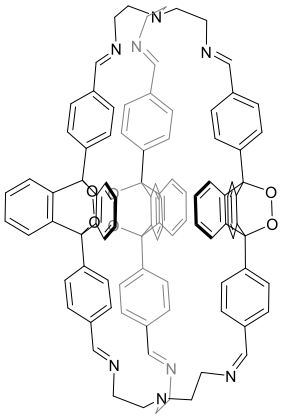

Endoperoxide (oxidized imine cage V4): An oven-dried Schlenk tube equipped with stirring bar was charged with imine cage **V3** (7 mg, 5.2 μmol), the system was evacuated and flushed with oxygen for five times. Then, a solution of methylene blue (0.03 mg, 0.1 μmol, 2 mol%) in dichloromethane (1 mL) was injected via a syringe. The mixture was stirred at room temperature under 656 nm-irradiation for 20 min in the oxygen atmosphere. Then the solution was passed through a pipette with cotton. The solution was concentrated to afford the oxidized imine cage in 90% yield (NMR yield). (Notes: methylene blue (2~3 mol%) is optimal loading for the oxidation process, if the loading is larger (for example: 10~30 mol%), decomposition product was observed. (Due to the solubility of oxidized cage, larger scale oxidized cage is not well-dissolved in CD_2Cl_2, thus ^{13}C NMR is not obtained.)

^{1}H NMR (300 MHz, CD_2Cl_2) δ 8.00 (m, 6H), 7.85–7.32 (m, 30H), 6.99 (m, 18H), 3.69 (s, 12H), 2.98 (s, 12H).

HRMS (ESI$^+$): calculated m/z $[M+2H]^{2+}$ for $[C_{96}H_{80}N_8O_6]^{2+}$: m/z 720.3095, found 720.3084.

7.2.7.2 Other triamines and OMe-substituted DPA-based aldehyde

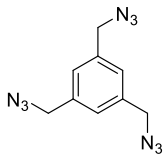

1,3,5-Tris(azidomethyl)benzene (V5-1): To a solution of 1,3,5-tris(bromomethyl)benzene (354 mg, 1.0 mmol) in DMF (10 mL) was added sodium azide (325 mg, 5.0 mmol) in three portions under argon atmosphere. Upon the completion of addition, the mixture was stirred at room temperature for 24 h. The mixture was diluted with dichloromethane (50 mL) and the organic system was washed with water for five times (30 mL×5). The organic layer was dried over magnesium sulfate, concentrated and dried to afford the pure product (200 mg, 82 % yield) as a white solid.

^{1}H NMR (300 MHz, $CDCl_3$) δ 7.25 (s, 3H), 4.40 (s, 6H).

^{13}C NMR (75 MHz, $CDCl_3$) δ 137.12, 127.61, 54.44.

Data in accordance with literature values.[35]

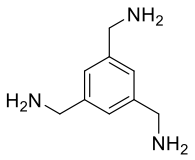

Benzene-1,3,5-triyltrimethanamine (V5-2): To a solution of 1,3,5-tris(azidomethyl)benzene (200 mg, 0.82 mmol) in absolute ethanol (5 mL) was added Pd/C (10 % Pd on carbon, 25 mg, 0.082 mmol) under an atmosphere of hydrogen (1 atm), the mixture was stirred at room temperature for 24 h. The mixture was filtered through a pad of celite, and the organic phase was comcentrated to afford the product (75 mg, 56 % yield) as a white solid.

^{1}H NMR (300 MHz, $CDCl_3$) δ 7.16 (s, 3H), 3.87 (s, 6H).

[35] L. Mancuso, T. Knobloch, J. Buchholz, J. Hartwig, L. Möller, K. Seidel, W. Collisi, F. Sasse and A. Kirschning. *Chem. Eur. J.*, **2014**, *20*, 17541-17551.

^{13}C NMR (75 MHz, $CDCl_3$) δ 144.03, 124.52, 46.55.

Data in accordance with literature values [36]

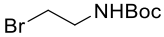

***tert*-Butyl (2-bromoethyl)carbamate (V6-1)**: An oven-dried 150 mL flask equipped with a stirring bar was charged with 2-bromoethylamine (2.0 g, 9.8 mmol), the system was degassed and flushed with argon for three times. Then, a solution of di-*tert*-butyl dicarbonate (1.88 mL, 8.8 mmol) in CH_2Cl_2 (25 mL) was added and followed by dropwise with triethylamine (2 mL, 14.6 mmol) at 0°C. The resulting mixture was stirred at 0°C for 30 min, the reaction mixture was allowed to warm to ambient temperature and stirred for 16 h. Water (50 mL) was added and the mixture was extracted with dicloromethane (40 mL×3). The combined organic phase was dried over magnesium sulfate and concentrated to afford the product (1.83 g, 93 % yield) without further purification. The data is identical to literature.[37]

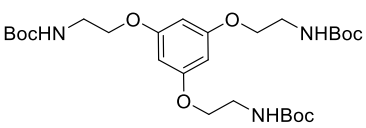

Tri-*tert*-butyl ((benzene-1,3,5-triyltris(oxy))tris(ethane-2,1-diyl))tri-carbamate (V6-2): A flame-dried 100 mL Schlenk tube was charged with phloroglucinol (259 mg, 2.1 mmol), compound 4-1 (1.83 g, 8.21 mmol) and potassium carbonate (1.45 g, 10.5 mmol). The system was evacuated and backfilled with argon for three times. DMF (20 mL) was added and the mixture was stirred at 50°C for 18 h. After cooling back to room temperature, water (50 mL) was added and the mixture was extracted by dicloromethane (40 mL×2). The combined organic phase was washed with water (50 mL×1). Then the organic phase was concentrated and purified by column chromatography (silica gel, eluent: petrol ether/ethyl acetate = 5:1) to furnish the product **V6-2** (767 mg, 72 % yield) as a white solid.

^{1}H NMR (300 MHz, $CDCl_3$) δ 6.07 (s, 3H), 4.96 (br s, 3H), 3.97 (t, *J* = 5.1 Hz, 6H), 3.59–3.40 (m, 6H), 1.45 (s, 27H).

^{13}C NMR (75 MHz, $CDCl_3$) δ 160.61, 155.99, 94.39, 79.73, 67.41, 40.16, 28.54.

HRMS (ESI^+): calculated m/z $[M+Na]^+$ for $[C_{27}H_{45}N_3NaO_9]^+$: m/z 578.3053, found 578.3055.

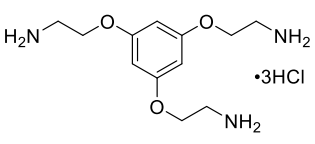

2,2',2''-(Benzene-1,3,5-triyltris(oxy))tris(ethan-1-amine) hydrochloric salt (V6-3): To a solution of compound **V6-2** (55.5 mg, 0.1 mmol) in CH_2Cl_2 (2 mL) was added a solution of hydrochloric acid (2 M in Et_2O, 1.0 mL, 2.0 mmol) under argon atmosphere at room temperature. The mixture was stirred at rt for 6 h, then solvent was removed and the residue was washed with dichloromethane (2 mL×3). The solid was dried to afford the pure hydrochloric salt product **V6-3** (35 mg, 97 % yield) as a white solid.

^{1}H NMR (300 MHz, D_2O) δ 6.37 (s, 3H), 4.36–4.24 (t, *J* = 4.9 Hz, 6H), 3.51–3.40 (t, *J* = 4.9 Hz, 6H).

^{13}C NMR (75 MHz, D_2O) δ 159.65, 95.02, 64.14, 38.88.

[36] a) J. L. Nallasivam and R. A. Fernandes. *Eur. J. Org. Chem.*, **2015**, *2015*, 2012-2022.
[37] M. U. Luescher, C.-V. T. Vo and J. W. Bode. *Org. Chem.*, **2014**, *16*, 1236-1239.

^{1}H NMR (300 MHz, CD_3OD) δ 6.36 (s, 3H), 4.59 (s, 6H), 4.29–4.17 (t, *J* = 4.9 Hz, 6H), 3.42–3.33 (t, *J* = 4.9 Hz, 6H).

^{13}C NMR (75 MHz, CD_3OD) δ 160.01, 94.88, 64.16, 38.87.

HRMS (ESI^+): calculated m/z $[M+H]^+$ for $[C_{12}H_{22}N_3O_3]^+$: m/z 256.1661, found 256.1658.

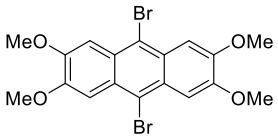

9,10-Dibromo-2,3,6,7-tetramethoxyanthracene [38] **(V7-1):** To a solution of 2,3,6,7-tetramethoxyanthracene (100 mg, 0.33 mmol) in $CHCl_3$ (10 mL) was added *N*-bromosuccinimide (239 mg, 1.34 mmol) in one portion. The mixture was stirred at room temperature for 12 h. Then the solvent was removed and the residue was purified by column chromatography (Silica gel, eluent: petrol ether/ ethyl acetate = 20:1) to deliver the desired product 9,10-dibromo-2,3,6,7-tetramethoxyanthracene (108 mg, 72 % yield) as a pale white solid.

^{1}H NMR (300 MHz, $CDCl_3$) δ 7.67–7.59 (m, 4H), 4.10 (s, 12H).

^{13}C NMR (75 MHz, $CDCl_3$) δ 150.75, 126.63, 118.53, 105.63, 56.20.

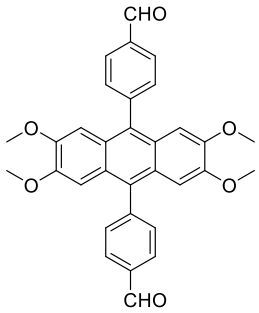

4,4'-(2,3,6,7-Tetramethoxyanthracene-9,10-diyl)dibenzaldehyde [39] **(V7-2)**: An oven-dried Schlenk tube equipped with stirring bar was charged with 9,10-dibromo-2,3,6,7-tetramethoxyanthracene (45 mg, 0.1 mmol), 4-formylboronic acid (38 mg, 0.25 mmol), tetrakis(triphenylphosphine) palladium (5.8 mg, 0.005 mmol) and potassium carbonate (69 mg, 0.5 mmol). The system was degassed and backfilled with argon for three times, then a mixed solvent toluene/EtOH/H_2O (2 mL/0.5 mL/1 mL) was injected via a syringe. The clear solution was stirred at 110°C for 48 h, at which point the system turned to cloudy and a light yellow precipitation appeared. The solid was filtered and dried to afford the product **V7-2** (48 mg, 95 % yield) as a light yellow solid.

^{1}H NMR (300 MHz, $CDCl_3$) δ 10.22 (s, 2H), 8.16 (d, *J* = 8.2 Hz, 4H), 7.69 (d, *J* = 8.0 Hz, 4H), 6.71 (s, 4H), 3.72 (s, 12H).

^{13}C NMR (75 MHz, $CDCl_3$) δ 192.2, 149.4, 146.8, 135.8, 132.0, 130.3, 125.5, 103.5, 55.7.

[38] F. Liu, L. Zhang, R. Wang, J. Sun, J. Yang, Z. Chen, X. Wang and D. Sun. *CrystEngComm.* **2014**, *16*, 2917-2928.
[39] T. S. Balaban, A. Eichhöfer, M. J. Krische and J.-M. Lehn. *Helv. Chim. Acta.*, **2006**, *89*, 333-351.

7.2.8 DPA-based phosphine oxides or phosphine sulfides for hemilabile ligands

7.2.8.1 Phosphine oxides

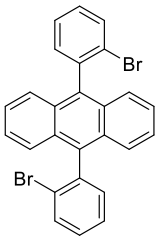

9,10-Bis(2-bromophenyl)anthracene (IV12-1): An oven-dried flask equipped with stirring bar was charged with 9,10-dibromoanthracene (500 mg, 1.5 mmol), 2-bromophenylboronic acid (747 mg, 3.7 mmol), tetrakis(triphenylphosphine) palladium (86 mg, 0.075 mmol) and potassium carbonate (925 mg, 7.5 mmol). The system was degassed and backfilled with argon for three times, then a mixed solvent dioxane/H_2O (2 mL/0.5 mL/1 mL) was injected via a syringe. The clear solution was stirred at 110°C for 24 h. After cooling room temperature, a white precipitation was appeared, the solid was filtered, washed with water and in vaccum to afford product (145 mg, 20 % yield).

^{1}H NMR (300 MHz, CD_2Cl_2) δ 7.93–7.86 (m, 2H), 7.63–7.45 (m, 10H), 7.43–7.35 (m, 4H).

^{13}C NMR (75 MHz, CD_2Cl_2) δ 141.2, 139.9, 136.7, 133.5, 133.3, 130.1, 129.8, 128.1, 126.8, 126.8, 126.0, 125.7.

HRMS(FD): calculated m/z $[M]^{\bullet+}$ for $[C_{26}H_{16}Br_2]^{\bullet+}$: 485.9619, found: $[M]^{\bullet+}$: 485.9627.

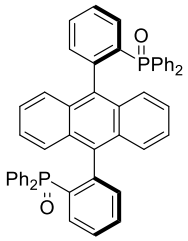

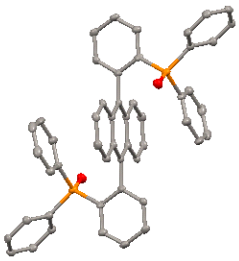

***Anti* (anthracene-9,10-diylbis(2,1-phenylene))bis(diphenyl-phosphineoxide) (IV12)**: To a solution of *ortho*-dibromodiphenylanthracene (64 mg, 0.13 mmol) in anhydrous THF (2.5 mL) was added *tert*-butyllithium (1.9 M, 0.063 mL, 0.12 mmol) at -78 °C under nitrogen atmosphere. The mixture was kept stirring at -78 °C for 1 h and it turned to a yellow solution. Then, chlorodiphenylphosphine (0.12 mL, 0.66 mmol) was added at the same temperature and the mixture was stirred for another 1 h. Then the mixture was allowed to warm up to room temperature stirred overnight. Saturated NH_4Cl (3 mL) was added and extracted with ethyl acetate 3 times (5 mL×3). The organic layer was dried over magnesium sulfate, then concentrated and purified by silica gel column chromatography. (eluent: dichloromethane/methanol = 50:1) to afford oxidized product (23 mg, 25 % yield) as a pale yellow solid. Cubic colorless crystal was obtained by slow evaporation: a solution of phosphine oxide in dichloromethane

^{1}H NMR (300 MHz, $CDCl_3$) δ 7.93 (ddd, *J* = 13.3, 7.8, 1.0 Hz, 2H), 7.76 (tt, *J* = 7.5, 1.4 Hz, 2H), 7.67–7.58 (m, 2H), 7.37–7.26 (m, 5H), 7.25 (d, *J* = 2.8 Hz, 1H), 7.22–7.06 (m, 16H), 6.90 (td, *J* = 7.8, 3.0 Hz, 8H).

^{13}C NMR (75 MHz, $CDCl_3$) δ 143.1, 143.0, 135.0, 135.0, 134.9, 134.4, 134.3, 133.7, 133.2, 132.9, 132.8, 131.9, 131.8, 131.2, 131.1, 130.7, 130.6, 129.9, 127.9, 127.2, 127.4, 127.3, 126.9, 124.8.

^{31}P NMR (121 MHz, $CDCl_3$) δ 25.9.

HRMS(FD): calculated m/z $[M]^{\bullet+}$ for $[C_{50}H_{36}O_2P_2]^{\bullet+}$: 730.2191, found: $[M]^{\bullet+}$: 730.2190.

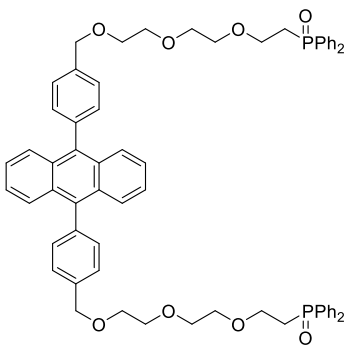

(((((((((Anthracene-9,10-diylbis(4,1-phenylene))bis(methylene))bis (oxy))bis(ethane-2,1-diyl))bis(oxy))bis(ethane-2,1-diyl))bis(oxy))bis (ethane-2,1-diyl))bis(diphenylphosphine oxide) (IV13): To a solution of diphenylphosphine (35 μL, 0.2 mmol) in anhydrous THF (1.0 mL) was added *n*-butyllithium (2.5 M, 0.08 mL, 0.2 mmol) at -78 °C under nitrogen atmosphere. The mixture was kept stirring at -78 °C for 1 h and it turned to deep red solution instantly. Then, a solution of **II1-3** (56 mg, 0.1 mmol) in THF (0.5 mL) was added at the same temperature and the mixture was stirred for another 1 h. Then, the mixture was allowed to warm up to room temperature stirred overnight. Saturated NH_4Cl (3 mL) was added and extracted with ethyl acetate for 3 times (5 mL×3). The organic layer was dried over magnesium sulfate, then concentrated and the residue was purified by silica gel column chromatography. (eluent: dichloromethane/methanol = 30:1) to afford oxidized product (31 mg, 30 % yield) as a yellow oil.

^{1}H NMR (300 MHz, $CDCl_3$) δ 7.78–7.66 (m, 13H), 7.57 (d, *J* = 7.9 Hz, 4H), 7.51–7.38 (m, 16H), 7.30 (dd, *J* = 6.8, 3.2 Hz, 4H), 4.72 (s, 4H), 3.89–3.53 (m, 20H), 2.69 (dt, *J* = 11.8, 7.6 Hz, 4H).

^{13}C NMR (75 MHz, $CDCl_3$) δ 138.4, 137.6, 136.9, 133.6, 132.3, 131.9, 131.8, 131.4, 130.8, 130.7, 129.9, 128.7, 128.6, 127.8, 127.0, 125.0, 73.3, 70.8, 70.5, 70.4, 69.8, 64.7, 31.4, 30.4.

^{31}P NMR (121 MHz, $CDCl_3$) δ 29.7.

HRMS(FD): calculated m/z $[M]^{\bullet+}$ for $[C_{64}H_{64}O_8P_2]^{\bullet+}$: 1022.4076, found: $[M]^{\bullet+}$: 1022.4082.

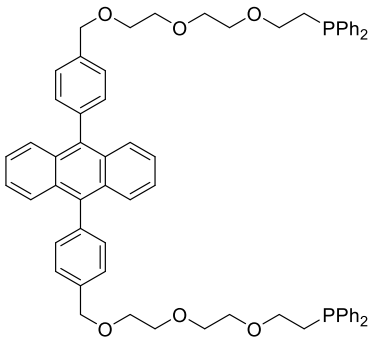

9,10-Bis(4-((2-(2-(2-(diphenylphosphanyl)ethoxy)ethoxy)ethoxy)methyl)phenyl)anthracene (IV14): To a solution of **IV13** (40 mg, 0.04 mmol) in anhydrous THF (3.0 mL) was added PMHS (0.1 mL, 0.4 mmol) and tetraisopropanolate titanium (0.13 mL, 0.4 mmol) at ambient temperature under argon atmosphere. The mixture was heated to 80 °C overnight. The reaction was detected by ^{31}P NMR. After the completion of the reaction for 4 h, the mixture was cooled to room temperature, 30 % aqueous NaOH (3 mL) was added. The mixture was further stirred at 60 °C for 1 h. After cooling to room temperature, the mixture was extracted with a solution of petrol ether/ ethyl acetate = 1/1 for 3 times (5 mL×3) and purified by passing through a neutral alumina plug to afford product. (Notes: the phosphine is easily to reoxidzed during purification)

^{31}P NMR (121 MHz, $CDCl_3$) δ -22.1.

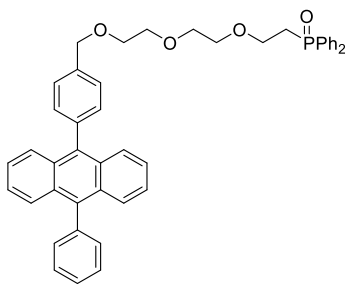

Diphenyl(2-(2-(2-((4-(10-phenylanthracen-9-yl)benzyl)oxy)ethoxy) ethoxy)ethyl)phosphine oxide (IV15): To a solution of diphenylphosphine (61 μL, 0.35 mmol) in anhydrous THF (1.5 mL) was added *n*-butyllithium (2.5 M, 0.14 mL, 0.35 mmol) at -78 °C under nitrogen atmosphere. The mixture was kept stirring at -78 °C for 1 h and it turned to deep red solution instantly. Then a solution of single-chain mesylate compound (100 mg, 0.175 mmol) in THF (1.0 mL) was added at the same temperature and the mixture was stirred for another 1 h. The mixture was allowed to warm to room temperature and stirred overnight. Saturated NH4Cl (3 mL) was added and extracted with ethyl acetate for 3 times (5 mL×3). The organic layer was dried over magnesium sulfate, then concentrated and the residue was purified by silica gel column chromatography. (eluent: dichloromethane/methanol = 30:1) to afford oxidized product (15 mg, 30 % yield) as a yellow oil

^{1}H NMR (300 MHz, $CDCl_3$) δ 7.82–7.68 (m, 8H), 7.58 (t, *J* = 9.2 Hz, 5H), 7.46 (dd, *J* = 11.9, 5.1 Hz, 11H), 7.32 (dd, *J* = 6.8, 3.2 Hz, 4H), 4.74 (s, 2H), 3.95–3.67 (m, 6H), 3.60 (s, 4H), 2.73 (dt, *J* = 11.9, 7.3 Hz, 2H).

^{13}C NMR (75 MHz, $CDCl_3$) δ 139.0, 138.3, 137.5, 137.1, 136.8, 133.3, 132.0, 131.9, 131.8, 131.3, 131.3, 130.8, 130.7, 129.9, 129.8, 128.7, 128.6, 128.4, 127.8, 127.5, 126.9, 125.0, 73.2, 70.7, 70.5, 70.3, 69.8, 64.6, 31.2, 30.3.

^{31}P NMR (121 MHz, $CDCl_3$) δ 30.8.

HRMS(FD): calculated m/z $[M]^{\bullet+}$ for $[C_{45}H_{41}O_4P]^{\bullet+}$: 676.2742, found: $[M]^{\bullet+}$: 676.2736.

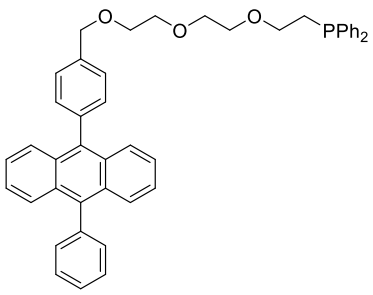

Diphenyl(2-(2-(2-((4-(10-phenylanthracen-9-yl)benzyl)oxy)ethoxy)et hoxy)ethyl)phosphane (IV16): To a solution of **IV15** (70 mg, 0.1 mmol) in anhydrous THF (3.0 mL) was added PMHS (0.1 mL, 0.4 mmol) and tetraisopropanolate titanium (0.13 mL, 0.4 mmol) at ambient temperature under argon atmosphere. The mixture was heated to 80 °C overnight. The reaction was followed by ^{31}P NMR. After the completion of the reaction, the mixture was cooled to room temperature, 30 % aqueous NaOH (3 mL) was added. The mixture was further stirred at 60 °C for 1 h. After cooling to room temperature, the mixture was extracted with a solution of petrol ether/ ethyl acetate = 1/1 for 3 times (5 mL×3) and purified by passing through a neutral alumina plug to afford product **IV16** (63 mg, 93 % yield) as a light yellow oil.

^{1}H NMR (300 MHz, $CDCl_3$) δ 7.76 – 7.69 (m, 4H), 7.66 – 7.55 (m, 5H), 7.53–7.41 (m, 9H), 7.38–7.28 (m, 10H), 4.76 (s, 2H), 3.85–3.60 (m, 10H), 2.45 (t, *J* = 7.4 Hz, 2H).

^{13}C NMR (75 MHz, $CDCl_3$) δ 139.2, 138.5, 138.3, 137.7, 137.2, 137.0, 132.9, 132.7, 131.5, 131.4, 130.0, 130.0, 128.7, 128.6, 128.5, 127.9, 127.6, 127.1, 125.1, 73.4, 70.9, 70.8, 70.3, 70.0, 68.9, 68.6, 29.0, 28.9.

^{31}P NMR (121 MHz, $CDCl_3$) δ -22.1.

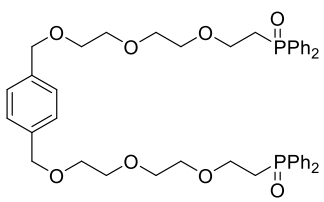

(((((((1,4-Phenylenebis(methylene))bis(oxy))bis(ethane-2,1diyl))bis(oxy)) bis(ethane-2,1-diyl))bis(oxy))bis(ethane-2,1-diyl))bis(diphenylphosphine oxide) (IV17): To a solution of diphenylphosphine (70 μL, 0.4 mmol) in anhydrous THF (1.5 mL) was added *n*-butyllithium (2.5 M, 0.16 mL, 0.4 mmol) at -78 °C under nitrogen atmosphere. The mixture was kept stirring at -78 °C for 1 h and it turned to deep red solution instantly. Then, a solution of **II3-2** (56 mg, 0.1 mmol) in THF (0.5 mL) was added at the same temperature and the mixture was stirred for another 1 h. Then the mixture was allowed to warm to room temperature stirred overnight. Saturated NH_4Cl (3 mL) was added and extracted with ethyl acetate for 3 times (5 mL×3). The organic layer was dried over magnesium sulfate, then concentrated and the residue was purified by silica gel column chromatography (eluent: dichloromethane/ methanol = 30:1) to afford oxidized product (32 mg, 43 % yield) as a clear oil.

^{1}H NMR (300 MHz, $CDCl_3$) δ 7.7–7.67 (m, 8H), 7.5 –7.40 (m, 12H), 7.28 (s, 4H), 4.51 (s, 4H), 3.79 (dt, *J* = 15.6, 7.7 Hz, 4H), 3.56 (dd, *J* = 12.4, 8.8 Hz, 16H), 2.73–2.60 (m, 4H).

^{13}C NMR (75 MHz, $CDCl_3$) δ 137.7, 133.7, 132.4, 131.9, 131.9, 130.9, 130.8, 128.8, 128.7, 127.9, 73.1, 70.7, 70.5, 70.4, 69.5, 64.7, 31.4, 30.5.

^{31}P NMR (121 MHz, $CDCl_3$) δ 29.6.

HRMS(ESI$^+$): calculated m/z $[M+Na]^+$ for $[C_{44}H_{52}NaO_8P_2]^+$: 793.3030, found: $[M+Na]^+$: 793.3004.

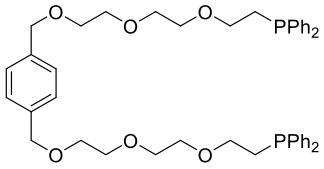

1,4-Bis((2-(2-(2-(diphenylphosphanyl)ethoxy)ethoxy)ethoxy)methyl) benzene (IV18): To a solution of **IV17** (77 mg, 0.1 mmol) in anhydrous THF (3.0 mL) was added PMHS (0.1 mL, 0.4 mmol) and tetraisopropanolate titanium (0.13 mL, 0.4 mmol) at ambient temperature under argon atmosphere. The mixture was heated to 80 °C overnight. The reaction was detected by ^{31}P NMR. After the completion of the reaction, the mixture was cooled to room temperature, 30 % aqueous NaOH (3 mL) was added. The mixture was further stirred at 60 °C for 1 h. After cooling to room temperature, the mixture was extracted with a solution of petrol ether/ ethyl acetate = 1:1 for 3 times (5 mL×3) and purified by passing through a neutral alumina plug to afford product (71 mg, 96 % yield) as a clear oil.

^{1}H NMR (300 MHz, $CDCl_3$) δ 7.48–7.38 (m, 8H), 7.37–7.27 (m, 16H), 4.54 (s, 4H), 3.67–3.53 (m, 20H), 2.47–2.35 (t, *J* = 7.9 Hz, 4H).

^{13}C NMR (75 MHz, $CDCl_3$) δ 138.5, 138.3, 137.8, 132.9, 132.7, 128.7, 128.6, 128.5, 127.9, 73.1, 70.8, 70.7, 70.3, 69.5, 68.8, 68.5, 29.0, 28.8.

^{31}P NMR (121 Hz, $CDCl_3$) δ -22.16.

7.2.8.2 Phosphine sulfides

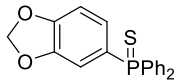

Benzo[d][1,3]dioxol-5-yldiphenylphosphine sulfide (IV19-1): To a solution of 4-bromo-1,2(methylenedioxy)benzene (0.3 mL, 2.5 mmol) in THF (4 mL) was added *n*-butyllithium (1.2 mL, 3.0 mmol) under argon atmosphere at -70°C. The mixture was stirred for 1 h then chlorodiphenylphosphine (0.67 mL, 3.75 mmol) was added. The mixture stirred at -70°C for another 1 h and allowed to stirred at rt overnight. Saturated NH_4Cl (2 mL) was added, after 5 min, sulfur powder (500 mg) was added and the mixture was stirred at rt for 8 h. The mixture was extracted with dichloromethane for 3 times (5 mL×3). The organic layer was dried over magnesium sulfate, then concentrated and the residue was purified by silica gel column chromatography (eluent: petrol ether/ethyl acetate = 30:1) to afford oxidized product (680 mg, 81 % yield) as a white solid.

^{1}H NMR (300 MHz, $CDCl_3$) δ 7.77–7.66 (m, 4H), 7.55–7.39 (m, 6H), 7.24–7.14 (m, 2H), 6.88–6.82 (m, 1H), 6.02 (s, 2H).

^{13}C NMR (75 MHz, $CDCl_3$) δ 150.79, 150.75, 148.3, 148.0, 133.8, 132.7, 132.4, 132.2, 131.7, 131.6, 128.7, 128.5, 128.0, 127.8, 126.6, 125.4, 112.1, 111.9, 108.6, 108.4, 101.9.

^{31}P NMR (121 MHz, $CDCl_3$) δ 43.7 (t, J_{CP} = 12.9 Hz).

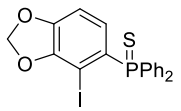

(4-Iodobenzo[d][1,3]dioxol-5-yl)diphenylphosphine sulfide (IV19-2): To a solution of benzo[d][1,3]dioxol-5-yldiphenylphosphine sulfide (50 mg, 0.15 mmol) in THF (2 mL) was added lithium diisopropylamide (0.3 mL, 0.6 mmol) at -78°C under argon atmosphere. The mixture was stirred for 30 min, then iodine (87 mg, 0.35 mmol) was added and the mixture was stirred at rt for 8 h. The product was used without purification.

^{1}H NMR (300 MHz, $CDCl_3$) δ 7.76–7.65 (m, 5H), 7.57–7.40 (m, 8H), 7.06 (dd, J = 12.2, 1.4 Hz, 1H), 6.08 (s, 2H).

^{31}P NMR (121 MHz, $CDCl_3$) δ 42.8 (t, J_{CP} = 12.7 Hz).

An oven-dried Schlenk tube was charged with (4-iodobenzo[d][1,3]dioxol-5-yl)diphenylphosphine sulfide (50 mg, 0.11 mmol), 9,10-anthracene bis(pinacolato)diborane (22 mg, 0.05 mmol), palladium catalyst (6 mg, 10 mol%) and potassium carbonate(35 mg, 0.26 mmol). The mixture was degassed and flushed with nitrogen for 3 times, then a mixed solution of toluene/EtOH/water = 4:1:1 (3.0 mL) was added via a syringe, The reaction was sealed and heated to 110 °C stirred for 48 h. After cooling to room temperature, dichloromethane (5 mL) was added and the mixture was filtered through a pad of celite, the organic layer was dried over magnesium sulfate and concentrated, then purified by silica gel column chromatography.

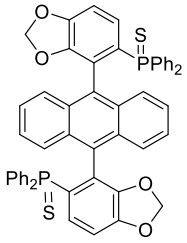

(Anthracene-9,10-diylbis(benzo[d][1,3]dioxole-4,5-diyl))bis(diphenylphosphine sulfide) (IV19):

^{1}H NMR (300 MHz, $CDCl_3$) δ 7.85–7.73 (m, 10H), 7.73–7.64 (m, 6H), 7.58 (dd, *J* = 12.9, 1.6 Hz, 2H), 7.54–7.36 (m, 22H), 7.22 (dt, *J* = 13.7, 1.7 Hz, 2H), 5.98 (d, *J* = 1.0 Hz, 4H).

^{31}P NMR (121 MHz, $CDCl_3$) δ 43.6 (t, J_{CP} = 13.2 Hz)

HRMS(ESI$^+$): calculated m/z $[M+H]^+$ for $[C_{52}H_{37}O_4P_2S_2]^+$: 851.1603, found: $[M+H]^+$: 851.1612.

(4-(Anthracen-9-yl)benzo[d][1,3]dioxol-5-yl)diphenylphosphine sulfide (IV20)

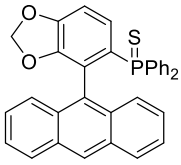

^{1}H NMR (300 MHz, $CDCl_3$) δ 8.46–8.41 (m, 2H), 7.85–7.75 (m, 4H), 7.66 (dd, *J* = 8.1, 0.7 Hz, 2H), 7.58 (dd, *J* = 13.0, 1.6 Hz, 1H), 7.53–7.36 (m, 11H), 7.10 (dd, *J* = 13.6, 1.6 Hz, 1H), 5.99 (s, 2H).

^{13}C NMR (75 MHz, $CDCl_3$) δ 149.51, 149.47, 148.63, 148.37, 135.37, 133.71, 132.57, 132.37, 132.23, 131.72, 131.68, 131.53, 130.87, 130.73, 129.52, 128.91, 128.74, 128.58, 127.01, 126.45, 125.85, 125.74, 125.66, 119.99, 119.78, 111.85, 111.66, 102.13, 84.71, 25.35.

^{31}P NMR (121 MHz, $CDCl_3$) δ 43.7 (t, J_{CP} = 13.2 Hz).

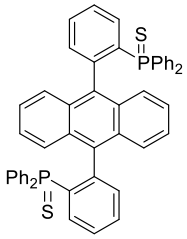

(Anthracene-9,10-diylbis(2,1-phenylene))bis(diphenylphosphine sulfide) (IV31):To a solution of *ortho*-dibromodiphenylanthracene (30 mg, 0.062 mmol) in anhydrous THF (2.5 mL) was added *tert*-butyllithium (1.9 M, 0.12 mL, 0.24 mmol) at -78 °C under nitrogen atmosphere. The mixture was kept stirring at -78 °C for 1 h and it turned to a yellow solution. Then, chlorodiphenylphosphine (54 μL, 0.3 mmol) was added at the same temperature and the mixture was stirred for another 1 h. Then the mixture was allowed to warm up to room temperature stirred overnight. Saturated NH_4Cl (3 mL) was added and excess sulfur (15 mg) was added afterwards. After stirring for 5 h at room temperature, water (10 mL) was added and the mixture was extracted with ethyl acetate for 3 times (5 mL×3). The organic layer was dried over magnesium sulfate, then concentrated and the residue was purified by silica gel column chromatography (eluent: dichloromethane/ methanol = 50:1) to afford product **IV31** (6 mg, 13 % yield) as a yellow solid.

^{1}H NMR (300 MHz, $CDCl_3$) δ 7.93 (ddd, *J* = 13.3, 7.8, 0.9 Hz, 2H), 7.79–7.72 (m, 2H), 7.65–7.56 (m, 2H), 7.33 (dd, *J* = 6.7, 4.4 Hz, 2H), 7.28 (s, 2H), 7.24 (d, *J* = 2.7 Hz, 2H), 7.19 – 7.07 (m, 16H), 6.88 (td, *J* = 8.1, 2.9 Hz, 8H).

^{13}C NMR (75 MHz, $CDCl_3$) δ 143.05 (d, *J* = 9.3 Hz), 135.00 (d, *J* = 11.1 Hz), 134.32 (d, *J* = 3.8 Hz), 133.5, 133.2, 132.6, 132.0, 131.6, 130.9 (dd, *J* = 34.6, 6.2 Hz), 130.6, 130.5, 129.9, 127.8 (d, *J* = 11.7 Hz), 127.4 (d, *J* = 12.2 Hz), 126.9, 124.9.

^{31}P NMR (121 MHz, $CDCl_3$) δ 26.2.

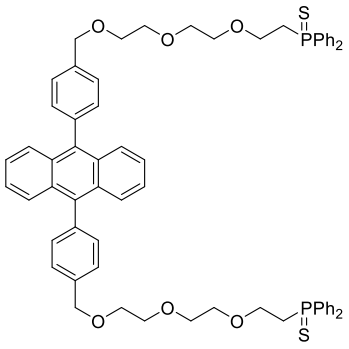

(((((((((Anthracene-9,10-diylbis(4,1-phenylene))bis(methylene))bis(oxy))bis(ethane-2,1-diyl))bis(oxy))bis(ethane-2,1-diyl))bis(oxy))bis(ethane-2,1-diyl))bis(diphenylphosphine sulfide) (IV32): To a solution of **IV13** (30mg, 0.029 mmol) in toluene (3 mL) was added Lawesson's reagent (47 mg, 0.117 mmol) under argon atmosphere, the mixture was heated at 110°C in a sealed Schlenck tube for 16 h. Then the solvent was removed and purified by silica gel column chromatography (eluent: dichloromethane/ methanol = 100:1) to afford product (5 mg, 17 % yield) as a yellow solid.

^{1}H NMR (300 MHz, $CDCl_3$) δ 7.85 (ddd, *J* = 13.1, 7.9, 1.6 Hz, 8H), 7.71 (dd, *J* = 6.8, 3.3 Hz, 4H), 7.60 (d, *J* = 8.1 Hz, 4H), 7.51 – 7.42 (m, 16H), 7.33 (dd, *J* = 6.9, 3.3 Hz, 4H), 4.76 (s, 4H), 3.97 – 3.85 (m, 4H), 3.83 – 3.68 (m, 8H), 3.66 – 3.55 (m, 8H), 2.87 (dt, *J* = 12.1, 7.4 Hz, 4H).

^{31}P NMR (121 MHz, $CDCl_3$) δ 38.4.

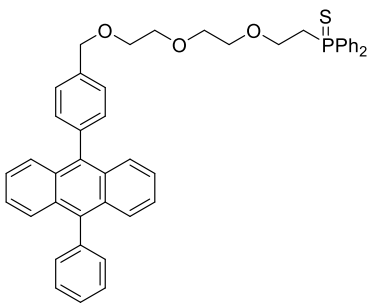

Diphenyl(2-(2-(2-((4-(10-phenylanthracen-9-yl)benzyl)oxy)ethoxy)ethoxy)ethyl)phosphine sulfide (IV33): To a solution of **II2-3** (350 mg, 0.61 mmol) in anhydrous THF (7 mL) was added *n*-butyllithium (2.5 M, 0.74 mL, 1.84 mmol) at -78 °C under nitrogen atmosphere. The mixture was kept stirring at -78 °C for 1 h and it turned to a yellow solution. Then chlorodiphenylphosphine (0.32 mL, 1.84 mmol) was added at the same temperature and the mixture was stirred for another 1 h. Then the mixture was allowed to warm up to room temperature stirred overnight. Saturated NH_4Cl (4 mL) was added and excess sulfur (96 mg) was then added. After stirring for 5 h at room temperature, water (30 mL) was added and the mixture was extracted with ethyl acetate for 3 times (20 mL×3). The organic layer was dried over magnesium sulfate, then concentrated and the residue was purified by silica gel column chromatography (eluent: dichloromethane/methanol = 50:1) to afford product **IV33** (315 mg, 75 % yield) as a yellow solid.

^{1}H NMR (300 MHz, $CDCl_3$) δ 7.80–7.66 (m, 8H), 7.64 – 7.52 (m, 5H), 7.52 – 7.40 (m, 10H), 7.37 – 7.28 (m, 4H), 4.74 (s, 2H), 3.90 – 3.68 (m, 6H), 3.65 – 3.54 (m, 4H), 2.70 (dt, *J* = 11.8, 7.6 Hz, 2H).

^{13}C NMR (75 MHz, $CDCl_3$) δ 137.6, 131.9 (d, *J* = 2.6 Hz), 131.4 (d, *J* = 3.4 Hz), 130.9 (d, *J* = 9.5 Hz), 130.2, 129.8, 129.0, 128.4, 127.9, 127.6, 127.1 (d, *J* = 1.2 Hz), 125.1, 73.4, 71.0, 70.3, 69.9, 64.8, 31.5, 30.6.

^{31}P NMR (121 MHz, $CDCl_3$) δ 29.6.

7.3 Reagent preparation

Synthesis of AgOTf(PPh$_3$)[40]

To a suspension of silver triflate (257 mg, 1.0 mmol) in diethyl ether (5 mL) was added a solution of triphenylphosphine (262 mg, 1.0 mmol) in diethyl ether (5 mL) under argon atmosphere. A white precipitate was formed instantly. The solid was filtered and rinsed with hexane (10 mL), then dried to afford the product in quantitative yield.

Synthesis of AgOTFA

To a suspension of silver oxide (1 g, 4.32 mmol) in water (15 mL) was added trifluoacetic acid (0.58 mL, 7.84 mmol) at room temperature under argon atmosphere. The mixture was stirred at room temperature overnight. The mixture was filtered to remove undissolved solid. Then, the aqueous phase was concentrated. The residue was re-dissolved in diethyl ether, the suspension was filtered and rinsed with diethyl ether (25 mL). The filtrate was concentrated and dried to afford the product (1.64 g, 95 % yield) as a white solid.

Synthesis of Ag(tht)OTf

To an dried flask was charged with silver triflate (291 mg, 1.13 mmol) in diethyl ether (10 mL) was added dropwise tetrahydrothiophene (0.1 mL) at room temperature. The mixture was stirred for 1 h and a white precipitate appeared. The suspension was filtered and dried to afford the product (360 mg, 92 % yield)

Synthesis of Au(tht)Cl[41]

To a solution of hydrogen tetrachloroaurate trihydrate (500 mg, 1.27 mmol) in ethanol (10 mL) was added dropwise with tetrahydrothiphene (5.6 mL, 6.35 mmol) under air. A yellow solid formed instantly, after 40 min, it turns to a white precipitate. The solid was filtered and washed by ethanol (20 mL) and dried to afford the product (406 mg, 100 % yield)

Synthesis of Ph$_3$P(S)AuCl[42]

To a solution of Au(tht)Cl (11 mg, 0.034 mmol) in dichloromethane (0.5 mL) was added dropwise a solution of triphenylphosphine sulfide (10 mg, 0.034 mmol) in CH_2Cl_2 (1.0 mL) under argon atmosphere at room temperature. The mixture was stirred at rt for 4 h, then the solution was concentrated to *ca*. 0.4 mL, diethyl ether (2 mL) was added to afford the product (16.4 mg, 92 % yield) as a white solid. Crystals suitable for X-ray diffraction was obtained by slow evaporation of the complex in CH_2Cl_2.

Synthesis of PhICl$_2$[43]

A two-neck flask equipped with a stirring bar was charged with an emulsion of iodobenzene (0.4 mL, 3.6 mmol) and diluted hydrochloric acid (8 mL, 5 M in aqueous). Sodium chlorite (2 g, 22 mmol) was added portionwise over 10 min. The resulting mixture was stirred for 4 h. A light yellow solid was precipitated. The solid was filtered and washed with water (20 mL) and hexane (10 mL), then dried in the dark to deliver the product as a fluffy yellow solid (907 mg, 92 % yield).

[40] T. G. Driver and K. A. Woerpel. *J. Am. Chem. Soc.*, **2004**, *126*, 9993-10002.
[41] M. J. Harper, E. J. Emmett, J. F. Bower and C. A. Russell. *J. Am. Chem. Soc.*, **2017**, *139*, 12386-12389.
[42] D. Upmann and P. G. Jones. *Dalton Trans.*, **2013**, *42*, 7526-7528.
[43] D. Canestrari, S. Lancianesi, E. Badiola, C. Strinna, H. Ibrahim and M. F. A. Adamo. *Org. Chem.*, **2017**, *19*, 918-921.

Synthesis of $Pd(PPh_3)_2O_2$[44]

A 100 mL Schlenk flask was charged with a suspension of $Pd(PPh_3)_4$ (300 mg, 0.26 mmol) in Et_2O (45 mL). Bubbling of dry O_2 into the solution for 10 min resulted in the precipitation of the product as a pale green solid, which was collected, washed with Et_2O (3 × 5 mL), and dried under vacuum (154.5 mg, 95% yield).

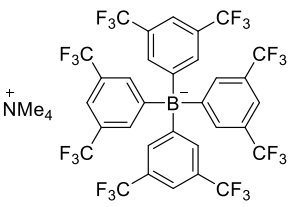

To a solution of tetramethylammounium chloride (16.8 mg, 0.154 mmol) in water/ethanol (1:1, 10 mL) was added a solution of $NaBAr_F$ (150 mg, 0.169 mmol) in water/ethanol (1:1, 15 mL) under air. The mixture was stirred for 5 h. The resulting solid was filtered and washed with water (5 mL). The solid was collected and dried under reduced pressure to afford product (120 mg, 83 % yield) as a white solid.

7.4 General procedure for the preparation of metal complexes

7.4.1 Preparation of thioether gold(III) complexes

An oven-dried centrifugation tube (50 mL) was charged with a solution of $NaAuCl_4 \cdot 2H_2O$ (5.0 equiv for **II1** and **II3** ligands; 3.0 equiv for **II2** and **II4** ligands) in MilliQ water (10 mL), and a solution of ligand (1.0 equiv) in toluene (12 mL). The samples were fixed on the orbital shaker and shaken at 3000 rpm in the dark for 1 to 2 hours. The two phases were separated by centrifugal force at 3000 rpm for 15 min, the organic phase was carefully collected with a pipette or a syringe, then the solvent was evaporated under reduced pressure and dried under vacuum to afford the pure thioether gold (III) complexes.

II1• $2AuCl_3$: **^{1}H NMR (300 MHz, $CDCl_3$)** δ 7.69 (dd, *J* = 6.9, 3.3 Hz, 4H), 7.59 (d, *J* = 8.0 Hz, 4H), 7.45 (d, *J* = 8.0 Hz, 4H), 7.32 (dd, *J* = 6.9, 3.3 Hz, 4H), 4.76 (s, 4H), 3.97-4.00 (m, 3H), 3.71-3.81 (m, 16H), 3.59-3.67 (m, 1H),3.42-3.51 (m, 1H), 3.27-3.35 (m, 1H), 2.98-3.07 (m, 3H), 2.72-2.89 (m, 1H), 1.72-1.91 (m, 1H), 1.37-1.50 (m, 4H), 1.24 (br, 34H), 0.87 (t, *J* = 6.6 Hz, 6H).

HRMS (FD): *m/z* calculated for $C_{64}H_{94}O_6S_2Au_2Cl_6$ $[M]^{+\bullet}$: 1626.3954; found: 1626.3929.

II2• $AuCl_3$: **^{1}H NMR (300 MHz, $CDCl_3$)** δ 7.66-7.71 (m, 4H), 7.52-7.58 (m, 5H), 7.45-7.49 (m, 4H), 7.29-7.35 (m, 4H), 4.76 (s, 2H), 3.97-4.00 (m, 1H), 3.60-3.81 (m, 9H), 3.27-3.48 (m, 1H), 2.97-3.06 (m, 1H), 1.73-1.88 (m, 2H), 1.24-1.49 (m, 20H), 0.87 (t, *J* = 6.6 Hz, 3H).

HRMS (FD): *m/z* calculated for $C_{45}H_{56}O_3SAuCl_3$ $[M]^{+\bullet}$: 978.2681; found: 978.2698.

II3• $2AuCl_3$: **^{1}H NMR (300 MHz, $CDCl_3$)** δ 7.32 (s, 4H), 4.55 (s, 4H), 3.82-3.95 (m, 4H), 3.62-3.75 (m, 16H), 3.54-3.60 (m, 1H), 3.39-3.48 (m, 1H), 3.25-3.33 (m, 1H), 3.17 (t, *J* = 5.5 Hz, 1H), 2.97-3.10 (m, 2H), 1.71-1.89 (m, 4H), 1.41-1.49 (m, 4H), 1.26 (br, 34H), 0.87 (t, *J* = 6.7 Hz, 6H).

II4• $AuCl_3$: **^{1}H NMR (300 MHz, $CDCl_3$)** δ 3.95 (t, *J* = 5.0 Hz, 1H), 3.84 (t, *J* = 5.5 Hz, 1H), 3.64-3.73 (m,

[44] Q. Liu, G. Li, J. He, J. Liu, P. Li and A. Lei. *Angew. Chem. Int. Ed.*, **2010**, *49*, 3371-3374.

5H), 3.45-3.65 (m, 4H), 3.31-3.41 (m, 4H), 3.14-3.25 (m, 1H), 3.01-3.13 (m, 1H), 1.73-1.90 (m, 2H), 1.40-1.49 (m, 2H), 1.26 (br, 16H), 0.87 (t, *J* = 6.7 Hz, 3H).

7.4.2 Preparation of silver complexes

To a solution of thioether ligands (1.0 equiv) in dichloromethane (1.0 mL) was added the silver salt (1.0 equiv) under an argon atmosphere. The mixture was stirred at room temperature for 4 h. Then, the solution was concentrated to *ca.* 0.3 mL and diethyl ether (2 mL) was added to afford a white precipitate. The solid was filtered, washed by diethyl ether and dried under reduced pressure to afford the desired complex.

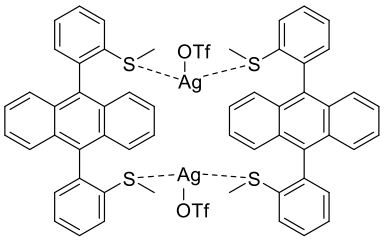

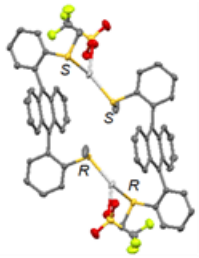

IV21a

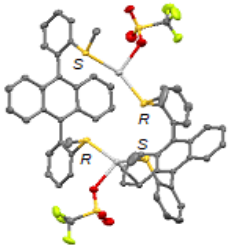

IV21b

According to the general procedure, *syn* **IV2** (15 mg, 0.0355 mol) and silver trifluoromethanesulfonate (9.1 mg, 0.0355 mmol) were employed to afford silver complex **IV21** [2(**IV2**)·2AgOTf] (22 mg, 92 % yield). Monocrystals (needles) were obtained by the slow diffusion of hexane into a solution of complex **IV21** (1.5 mg) in CH_2Cl_2 (0.2 mL). Two diastereoisomers (head to head coordination **IV21a** and head to tail coordination **IV21b**) were isolated and the structures were determined by XRD analysis.

M. p. 246 °C; FTIR (KBr): $\tilde{\nu}$ = 3440, 3057, 2927, 1620, 1474, 1437, 1383, 1279, 1243, 1221, 1162, 1026, 773, 753, 635 cm^{-1}.

^{1}H NMR (300 MHz, $CDCl_3$) δ 7.86 (d, *J* = 7.9 Hz, 4H, Benz-H), 7.73 (td, *J* = 7.4, 1.5 Hz, 4H, Benz-H), 7.65 (td, *J* = 7.4, 1.2 Hz, 4H, Benz-H), 7.52-7.58 (m, 12H, Anthr-H and Benz-H), 7.36-7.42 (m, 8H, Anthr-H) 2.38 (s, 12H, SCH_3).

^{13}C NMR (75 MHz, $CDCl_3$) δ 138.3, 134.4, 133.4, 131.7, 130.6, 130.1, 129.6, 128.6, 126.9, 125.4, 20.4.

^{19}F NMR (282 MHz, $CDCl_3$) δ -77.4.

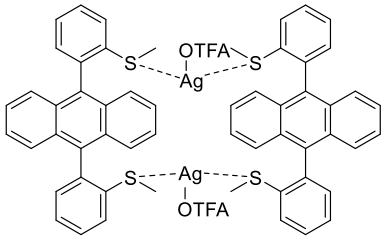

According to the general procedure, *syn* **IV2** (6 mg, 0.014 mol) and silver trifluoroacetate (3.1 mg, 0.014 mmol) were employed to deliver silver complex **IV22** [2(**IV2**)·2AgOTFA] (7 mg, 78 % yield).

M. p. 235 °C; FTIR (KBr): $\tilde{\nu}$ = 3426, 3052, 2919, 1620, 1473, 1434, 1384, 1299, 772, 754, 664 cm^{-1}

^{1}H NMR (300 MHz, $CDCl_3$) δ 7.61-7.67 (m, 4H, Benz-H), 7.55-7.59 (m, 8H, Anthr-H), 7.45-7.55 (m, 12H, Benz-H), 7.36-7.41 (m, 8H, Anthr-H), 2.40 (s, 12H, SCH_3).

^{13}C NMR (75 MHz, $CDCl_3$) δ 137.2, 136.5, 134.6, 131.7, 130.1, 129.8, 129.3, 126.6, 126.5, 125.8, 125.7,

17.1.

^{19}F NMR (282 MHz, $CDCl_3$) δ -73.7 ppm.

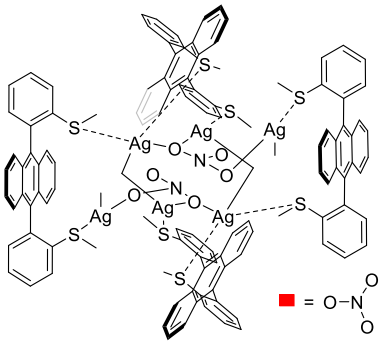

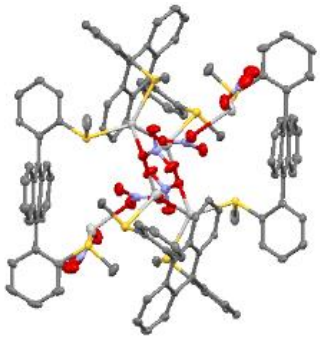

According to the general procedure, *syn* **IV2** (6 mg, 0.014 mol) and silver nitrate (2.4 mg, 0.014 mmol) were employed to deliver silver complex **IV23** [6(**IV2**)·4$AgNO_3$] (5.1 mg, 80 % yield). White needle monocrystals were grown by hexane diffusion into a solution of complex **IV22** (2 mg) in CH_2Cl_2 (0.3 mL).

M. p. 247.3 °C; FTIR (KBr): $\tilde{\nu}$ = 3428, 3052, 2919, 1620, 1473, 1434, 1384, 1300, 772, 754, 664 cm^{-1}

^{1}H NMR (300 MHz, $CDCl_3$) δ 7.63-7.69 (m, 8H, Benz-H), 7.47-7.63 (m, 40H, Anthr-H and Benz-H), 7.39-7.42 (m, 16H, Anthr-H), 2.37 (s, 24H, SCH_3).

^{13}C NMR (75 MHz, $CDCl_3$) δ 137.5, 135.3, 134.6, 131.7, 129.6 (d, *J* = 2.6 Hz), 127.4, 127.2, 126.7, 125.5, 18.4.

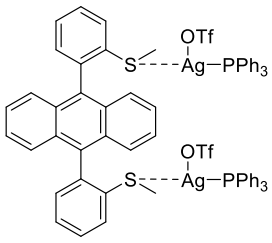

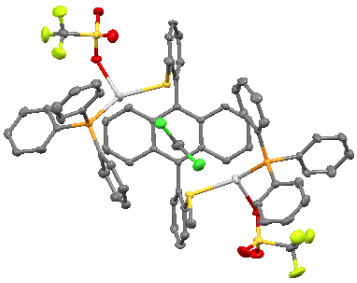

According to the general procedure, *syn* **IV2** (6 mg, 0.014 mol) and triphenylphosphine silver trifluoromethanesulfonate (7.4 mg, 0.014 mmol) were employed to deliver silver complex **IV24** [**IV2**·2AgOTf(PPh_3)] as a light yellow powder (8 mg, 77 % yield). Yellow monocystals were grown from hexane diffusion into a solution of complex **IV24** (1 mg) in CH_2Cl_2 (0.2 mL)

M. p. 125.8 °C; FTIR (KBr): $\tilde{\nu}$ = 3441, 3055, 2929, 1587, 1480, 1436, 1289, 1235, 1220, 1162, 1026, 779, 753, 694, 635, 516, 504 cm^{-1}.

^{1}H NMR (300 MHz, $CDCl_3$) δ 7.64-7.69 (m, 4H, Benz-H), 7.51-7.61 (m, 6H, Anthr-H and Benz-H), 7.42-7.48 (m, 8H, Anthr-H and Benz-H and PPh_3), 7.29-7.39 (m, 28H, PPh_3), 2.34 (s, 6H, SCH_3).

^{13}C NMR (75 MHz, $CDCl_3$) δ 137.4, 137.2, 135.4, 134.7, 133.9, 131.6, 131.1, 129.7, 129.3, 127.9, 127.1, 126.5, 125.6, 18.3.

^{19}F NMR (282 MHz, $CDCl_3$) δ -77.4.

^{31}P NMR (121 MHz, $CDCl_3$) δ 14.9 (br s).

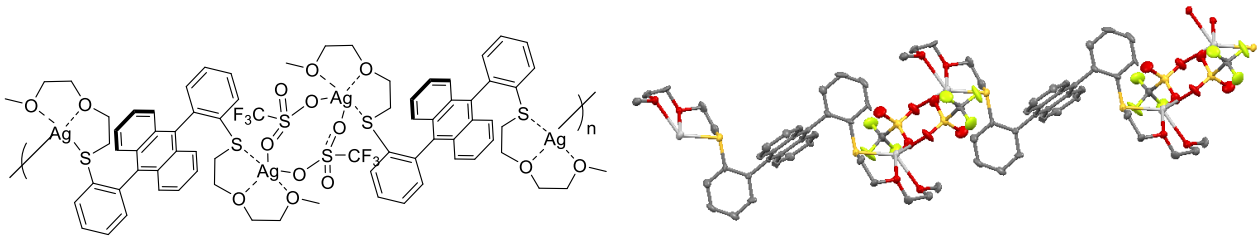

According to the general procedure, **IV4** (12 mg, 20 µmol) and silver trifluoromethanesulfonate (5.1 mg, 20 µmol) were employed to afford **IV25** (15.4 mg, 90 % yield) as a white solid. White needle crystals were grown from hexane diffusion into a solution of complex **IV25** in $CDCl_3$ (0.3 mL) with a drop of acetonitrile.

^{1}H NMR (300 MHz, $CDCl_3$) δ 7.60-7.63 (m, 2H), 7.51-7.57 (m, 6H), 7.39-7.45 (m, 4H), 7.32-7.37 (m, 4H), 3.40-3.50 (m, 12H), 3.30 (s, 6H), 2.97 (t, *J* = 7.1 Hz, 4H).

^{19}F NMR (282 MHz, $CDCl_3$) δ -77.5 ppm.

HRMS (MALDI): calculated m/z $[M+Ag]^+$ for $[C_{36}H_{38}O_4S_2Ag]^+$: 705.1262, found: [M+Ag]: 705.2510.

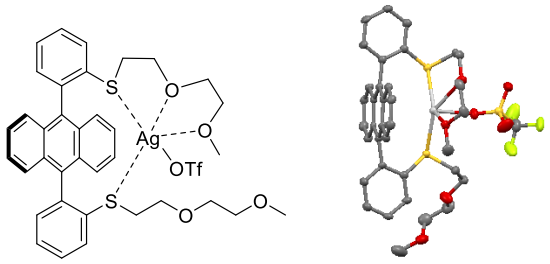

According to the general procedure, **IV5** (3 mg, 5 µmol) and silver trifluoromethanesulfonate (1.3 mg, 5 µmol) were employed to afford a small quantity of precipitate which was identified to be silver complex **IV26** [**IV5**·AgOTf].

Notes: The filtrate was also collected and put for NMR. The NMR of both solids are almost identical and the complex can be dissolved in Et_2O, and the ^{1}H NMR shows a large difference from ligand and the ^{19}F NMR shows a peak at -78.01 ppm.

The white crystals were grown by solvent diffusion: hexane vapor into a solution of silver complex in dichloromethane.

^{1}H NMR (300 MHz, $CDCl_3$) δ 7.82-7.88 (m, 2H), 7.64-7.72 (m, 6H), 7.52-7.57 (m, 4H), 7.43-7.48 (m, 4H), 3.38 (t, *J* = 5.5 Hz, 4H), 3.22-3.28 (m, 8H), 3.16 (s, 6H), 3.13 (t, *J* = 5.6 Hz, 4H).

^{13}C NMR (75 MHz, $CDCl_3$) δ 139.8, 134.1, 132.3, 132.0, 131.6, 130.1, 130.0, 129.6, 128.6, 127.0, 126.0, 71.4, 70.1, 67.3, 59.2.

^{19}F NMR (282 MHz, $CDCl_3$) δ -78.0 ppm.

MS (ESI^+): [**IV5**+Na]$^+$: 621.21 was observed.

7.4.3 Silver complexes with undetermined structures

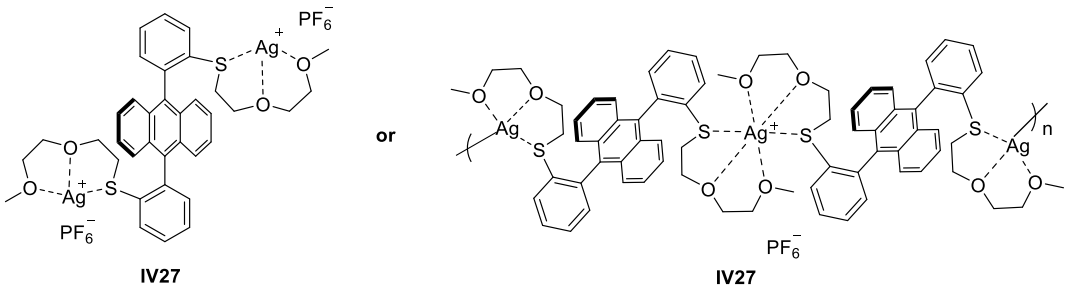

IV27 IV27

To a solution of **IV4** (12 mg, 20 μmol) in dichloromethane (1 mL) was added silver hexafluorophosphate (5.1 mg, 20 μmol) at ambient temperature under argon atmosphere. The mixture was stirred at room temperature for 4 h and the system become a turbid solution. Then, the mixture was concentrated to *ca*. 0.3 mL, and diethyl ether (1.0 mL) was added to afford a white precipitate. The precipitate was filtered and dried to afford silver complex **IV27** (15.4 mg, 90 % yield) as a white solid.

^{1}H NMR (300 MHz, CD_3CN) δ 7.57-7.68 (m, 4H), 7.42-7.51 (m, 6H), 7.32-7.41 (m, 6H), 3.44 (t, *J* = 6.6 Hz, 4H), 3.36-3.40 (m, 4H), 3.29-3.32 (m, 4H), 3.18 (s, 6H), 2.96 (t, *J* = 6.6 Hz, 4H).

^{19}F NMR (282 MHz, CD_3CN) δ -71.7, -74.2, -79.3.

^{31}P NMR (121 MHz, CD_3CN) δ -144.6 (q, J_{PF} = 703.1 Hz).

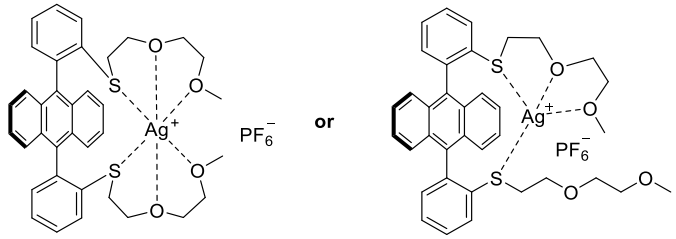

IV28 IV28

To a solution of **IV5** (6 mg, 10 μmol) in dichloromethane (1 mL) was added silver hexafluorophosphate (2.5 mg, 10 μmol) at ambient temperature under argon atmosphere. The mixture was stirred at room temperature for 5 h and the system become a turbid solution. Then the mixture was concentrated to *ca*. 0.2 mL, diethyl ether (1.0 mL) was added to afford a small amount precipitate. However, the complex also dissolved in diethyl ether. The silver complex was combined and dried to afford product **IV28** (6.2 mg, 74 % yield) as an oil-like solid.

^{1}H NMR (300 MHz, $CDCl_3$) δ 7.84-7.90 (m, 2H), 7.67-7.71 (m, 6H), 7.53-7.57 (m, 4H), 7.45-7.49 (m, 4H), 3.40 (t, *J* = 5.3 Hz, 4H), 3.26-3.32 (m, 8H), 3.18 (s, 6H), 3.12 (t, *J* = 5.4 Hz, 4H).

^{19}F NMR (282 MHz, $CDCl_3$) δ -77.9.

^{31}P NMR (121 MHz, $CDCl_3$) δ -77.7 (q, J_{PF} = 361.4 Hz).

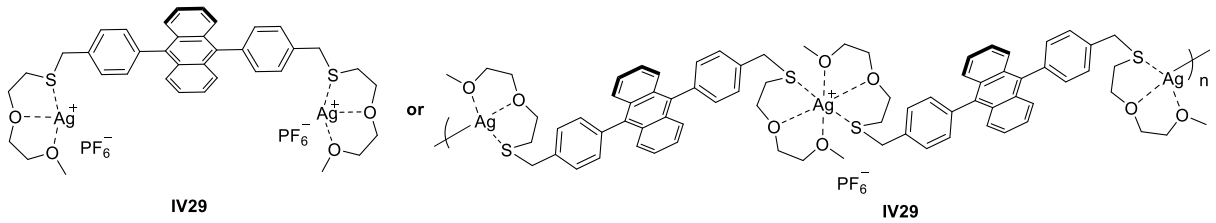

IV29 **IV29**

To a solution of **IV6** (5.5 mg, 8.7 µmol) in dichloromethane (1 mL) was added silver hexafluorophosphate (2.2 mg, 8.7 µmol) at ambient temperature under argon atmosphere. The mixture was stirred at room temperature for 3 h and the system becomes a turbid solution. Then the mixture was concentrated to *ca*. 0.2 mL, and diethyl ether (1.0 mL) was added to afford a white precipitate. The precipitate was filtered and dried to afford silver complex **IV29** (5.9 mg, 77 % yield) as an aicy solid.

^{1}H NMR (300 MHz, $CDCl_3$) δ 7.58 (dd, *J* = 6.8, 3.3 Hz, 4H), 7.48 (d, *J* = 8.0 Hz, 4H), 7.29 (d, *J* = 8.0 Hz, 4H), 7.24 (d, *J* = 6.8, 3.3 Hz, 4H), 4.19 (s, 4H), 3.85 (t, *J* = 5.6 Hz, 4H), 3.77 (dd, *J* = 5.6, 3.2 Hz, 4H), 3.65 (dd, *J* = 5.7, 3.1 Hz, 4H), 3.43 (s, 6H), 3.06 (t, *J* = 5.5 Hz, 4H).

^{19}F NMR (282 MHz, $CDCl_3$) δ -71.1, -73.6, -77.5, -81.5, -85.0.

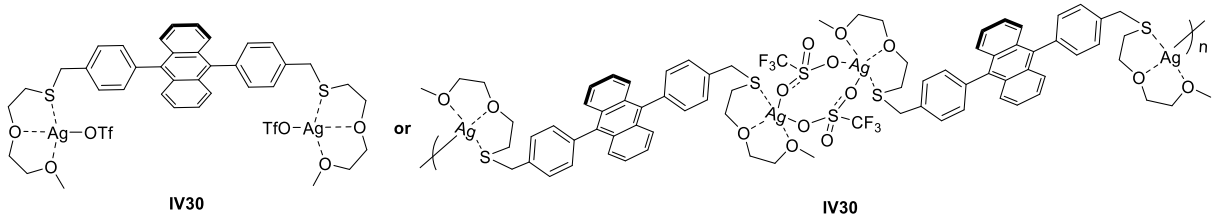

IV30 **IV30**

To a solution of **IV6** (5.5 mg, 8.7 µmol) in dichloromethane (1 mL) was added silver trifluoromethanesulfonate (2.3 mg, 8.7 µmol) at ambient temperature under argon atmosphere. The mixture was stirred at room temperature for 3 h and the system become a turbid solution. Then, the mixture was concentrated to *ca*. 0.2 mL, and diethyl ether (1.0 mL) was added to afford a white precipitation. The precipitate was filtered and dried to afford silver complex **IV30** (6.5 mg, 83 % yield) as an aicy solid.

^{1}H NMR (300 MHz, $CDCl_3$) δ 7.60 (dd, *J* = 6.8, 3.3 Hz, 4H), 7.50 (d, *J* = 8.1 Hz, 4H), 7.32 (d, *J* = 8.1 Hz, 4H), 7.26 (dd, *J* = 6.8, 3.3 Hz, 4H), 4.16 (s, 4H), 3.84 (t, *J* = 5.8 Hz, 4H), 3.75 (dd, *J* = 5.6, 3.1 Hz, 4H), 3.64 (dd, *J* = 5.6, 3.2 Hz, 4H), 3.42 (s, 6H), 3.02 (t, *J* = 5.8 Hz, 4H), 2.73 (s, 4H).

^{19}F NMR (282 MHz, $CDCl_3$) δ -77.7.

Details of crystals

Table **S1**. Crystal data and structure refinement for compound **II28**.

Empirical formula	$C_{54}H_{36}N_3$
Formula weight	726.86
Temperature	150(2) K
Wavelength	0.71073 Å
Crystal system, space group	Monoclinic, P 21/n
Unit cell dimensions	a = 17.0440(14) Å alpha = 90°
	b = 9.1290(7) Å beta = 98.317(2)°
	c = 24.4599(17) Å gamma = 90°
Volume	3765.8(5) $Å^3$
Z	4
Calculated density	1.282 Mg/m^3
Absorption coefficient	0.075 mm^{-1}
F(000)	1524
Crystal size	0.800× 0.330 × 0.150 mm^3
Theta range for data collection	1.368 to 28.826°.
Limiting indices	$-23 \le h \le 23$, $-12 \le k \le 12$, $-32 \le l \le 33$
Reflections collected / unique	43812 / 9808 [R(int) = 0.0395]
Completeness to theta = 25.242	99.9 %
Absorption correction	Semi-empirical from equivalents
Refinement method	Full-matrix least-squares on F^2
Data / restraints / parameters	9808 / 0 / 514
Goodness-of-fit on F^2	1.030
Final R indices [I>2sigma(I)]	R1 = 0.0485, wR2 = 0.1256
R indices (all data)	R1 = 0.0678, wR2 = 0.1378
Extinction coefficient	n/a
Largest diff. peak and hole	0.384 and -0.326 e. $Å^{-3}$

Table **S2**. Crystal data and structure refinement for compound **III2**.

Empirical formula	$C_{27}H_{19}O_2P$
Formula weight	406.39
Temperature	150(2) K
Wavelength	0.71073 Å
Crystal system, space group	Triclinic, P -1
Unit cell dimensions	a = 8.3472(11) Å alpha = 105.776(4)°
	b = 10.2653(15) Å beta = 96.071(4)°
	c = 14.109(2) Å gamma = 112.508(3)°
Volume	1044.5(3) $Å^3$
Z	2
Calculated density	1.292 Mg/m^3
Absorption coefficient	0.153 mm^{-1}
F(000)	424
Crystal size	0.070× 0.050 × 0.030 mm^3
Theta range for data collection	1.543 to 27.103°.
Limiting indices	$-10 \leq h \leq 10$, $-13 \leq k \leq 13$, $-18 \leq l \leq 17$
Reflections collected / unique	9518 / 4593 [R(int) = 0.0591]
Completeness to theta = 25.242	99.8 %
Absorption correction	Semi-empirical from equivalents
Refinement method	Full-matrix least-squares on F^2
Data / restraints / parameters	4593 / 0 / 272
Goodness-of-fit on F^2	1.002
Final R indices [I>2sigma(I)]	R1 = 0.0585, wR2 = 0.1039
R indices (all data)	R1 = 0.1233, wR2 = 0.1293
Extinction coefficient	n/a
Largest diff. peak and hole	0.280 and -0.328 e. $Å^{-3}$

Table **S3**. Crystal data and structure refinement for compound **IV2**.

CCDC number	1883674	
Empirical formula	$C_{56}H_{44}S_4$	
Formula weight	845.15	
Temperature	153(2) K	
Wavelength	1.54187 Å	
Crystal system	Monoclinic	
Space group	P21/c	
Unit cell dimensions	a = 20.742(3) Å	Alpha= 90°
	b = 8.9984(11) Å	Beta= 91.166(6) °
	c = 23.764(4) Å	Gamma = 90°
Volume	4434.5(11) $Å^3$	
Z	4	
Density (calculated)	1.266 Mg/m^3	
Absorption coefficient	2.250 mm^{-1}	
F(000)	1776	
Crystal size	0.12 × 0.06 × 0.02 mm^3	
Theta range for data collection	6.40 to 68.25∞.	
Index ranges	-24 ≤ h ≤ 24, -10 ≤ k ≤10, -28 ≤ l ≤ 27	
Reflections collected	31983	
Independent reflections	8075 [R(int) = 0.0161]	
Completeness to theta = 68.25°	99.5 %	
Absorption correction	Semi-empirical from equivalents	
Max. and min. transmission	0.9564 and 0.7740	
Refinement method	Full-matrix least-squares on F^2	
Data / restraints / parameters	8075 / 0 / 545	
Goodness-of-fit on F^2	1.039	
Final R indices [I>2sigma(I)]	R1 = 0.0385, wR2 = 0.1093	
R indices (all data)	R1 = 0.0445, wR2 = 0.1134	
Largest diff. peak and hole	0.788 and -0.815 $eÅ^{-3}$	

Table **S4**. Crystal data and structure refinement for silver complex **IV21a** (head-to-head coordination of ligands)

CCDC number	1883535
Empirical formula	$C_{58}H_{44}Ag_2F_6O_6S_6$
Formula weight	1359.03
Temperature	150(2) K
Wavelength	0.71073 Å
Crystal system	Triclinic
Space group	P -1
Unit cell dimensions	a = 13.4300(13) Å alpha = 117.822(2)°
	b = 14.8251(14) Å beta = 103.344(2)°
	c = 15.6390(13) Å gamma = 92.109(2)°
Volume	2641.4(4) $Å^3$
Z	2
Calculated density	1.709 Mg/m^{-3}
Absorption coefficient	1.053 mm^{-1}
F(000)	1368
Crystal size	0.120 × 0.100 × 0.030 mm^3
Theta range for data collection	1.534 to 26.381 °
Limiting indices	-16≤ h ≤16, -18≤ k ≤18, -18≤ l ≤19
Reflections collected / unique	29382 / 10564 [R(int) = 0.0524]
Completeness to theta = 25.242	98.1 %
Absorption correction	Semi-empirical from equivalents
Refinement method	Full-matrix least-squares on F^2
Data / restraints / parameters	10564 / 6 / 760
Goodness-of-fit on F^2	1.033
Final R indices [I>2sigma(I)]	R1 = 0.0393, wR2 = 0.0887
R indices (all data)	R1 = 0.0603, wR2 = 0.0993
Extinction coefficient	n/a
Largest diff. peak and hole	0.598 and -0.781 e.$Å^{-3}$

Table **S5**. Crystal data and structure refinement for silver complex **IV21b** (head-to-tail coordination of ligands)

CCDC number	1883532
Empirical formula	C_{58} H_{44} Ag_2 F_6 O_6 S_6
Formula weight	1359.03
Temperature	120(2) K
Wavelength	0.71073 Å
Crystal system	Monoclinic
Space group	P 21/c
Unit cell dimensions	a = 15.8914(11) Å alpha = 90 °
	b = 14.2792(10) Å beta = 94.932(2) °
	c = 26.5135(18) Å gamma = 90 °
Volume	5994.1 (7) $Å^3$
Z	4
Calculated density	1.506 Mg/m^{-3}
Absorption coefficient	0.928 mm^{-1}
F(000)	2736
Crystal size	0.600 × 0.150 × 0.060 mm^3
Theta range for data collection	1.542 to 26.760°
Limiting indices	-20≤ h ≤20, -18≤ k ≤18, -33≤ l ≤33
Reflections collected / unique	93239 / 12661 [R(int) = 0.0378]
Completeness to theta = 25.242	99.7 %
Absorption correction	Semi-empirical from equivalents
Max. and min. transmission	0.7454 and 0.6047
Refinement method	Full-matrix least-squares on F^2
Data / restraints / parameters	12661 / 1 / 707
Goodness-of-fit on F^2	1.040
Final R indices [I>2sigma(I)]	R1 = 0.0324, wR2 = 0.0744
R indices (all data)	R1 = 0.0380, wR2 = 0.0761
Extinction coefficient	n/a
Largest diff. peak and hole	0.721 and -0.513 e.$Å^{-3}$

Table **S6**. Crystal data and structure refinement for silver complex **IV23.**

CCDC number	1883538
Empirical formula	$C_{56}H_{44}Ag_3N_3O_9S_4$
Formula weight	1354.79
Temperature	150(2) K
Wavelength	0.71073 Å
Crystal system	Triclinic
Space group	P -1
Unit cell dimensions	a = 12.755(3) Å alpha = 111.882(5) °
	b = 13.140(3) Å beta = 102.770(4) °
	c = 16.721(4) Å gamma = 92.073(5) °
Volume	2514.4 (9) $Å^3$
Z	2
Calculated density	1.789 Mg/m^{-3}
Absorption coefficient	1.386 mm^{-1}
F(000)	1356
Crystal size	0.140 × 0.030 × 0.030 mm^3
Theta range for data collection	3.103 to 26.372 °
Limiting indices	-15≤ h ≤15, -16≤ k ≤16, -20≤ l ≤20
Reflections collected / unique	78956 / 10193 [R(int) = 0.0603]
Completeness to theta = 25.242	99.2 %
Absorption correction	Semi-empirical from equivalents
Max. and min. transmission	0.7454 and 0.6977
Refinement method	Full-matrix least-squares on F^2
Data / restraints / parameters	10193 / 0 / 680
Goodness-of-fit on F^2	1.023
Final R indices [I>2sigma(I)]	R1 = 0.0319, wR2 = 0.0661
R indices (all data)	R1 = 0.0494, wR2 = 0.0724
Extinction coefficient	n/a
Largest diff. peak and hole	0.971 and -0.739 e.$Å^{-3}$

Table **S7**. Crystal data and structure refinement for silver complex **IV24**

CCDC number	1883536
Empirical formula	$C_{67}H_{54}Ag_2Cl_2F_6O_6P_2S_4$
Formula weight	1545.92
Temperature	150(2) K
Wavelength	0.71073 Å
Crystal system	Orthorhombic
Space group	P n a 21
Unit cell dimensions	a = 26.230(2) Å alpha = 90 °
	b = 9.4521(8) Å beta = 90 °
	c = 25.912(2) Å gamma = 90 °
Volume	6424.2 (9) $Å^3$
Z	4
Calculated density	1.598 Mg/m^{-3}
Absorption coefficient	0.942 mm^{-1}
F(000)	3120
Crystal size	0.150 × 0.040 × 0.020 mm^3
Theta range for data collection	1.553 to 26.374 °
Limiting indices	-30≤ h ≤32, -11≤ k ≤11, -32≤ l ≤26
Reflections collected / unique	44069 / 11444 [R(int) = 0.0520]
Completeness to theta = 25.242	99.8 %
Absorption correction	Semi-empirical from equivalents
Max. and min. transmission	0.7454 and 0.6655
Refinement method	Full-matrix least-squares on F^2
Data / restraints / parameters	11444 / 1 / 805
Goodness-of-fit on F^2	1.021
Final R indices [I>2sigma(I)]	R1 = 0.0309, wR2 = 0.0547
R indices (all data)	R1 = 0.0404, wR2 = 0.0578
Extinction coefficient	n/a
Largest diff. peak and hole	0.353 and -0.346 e.$Å^{-3}$

Table **S8**. Crystal data and structure refinement for silver complex **IV4**.

Empirical formula	$C_{18}H_{19}O_2S$
Formula weight	299.39
Temperature	150(2) K
Wavelength	0.71073 Å
Crystal system, space group	Triclinic, P -1
Unit cell dimensions	a = 7.4778(10) Å alpha = 88.290(4)°
	b = 10.2771(15) Å beta = 80.076(3)°
	c = 10.5136(15) Å gamma = 73.107(3)°
Volume	761.36(19) $Å^3$
Z	2
Calculated density	1.306 Mg/m^3
Absorption coefficient	0.214 mm^{-1}
F(000)	318
Crystal size	0.200 × 0.120 × 0.020 mm^3
Theta range for data collection	1.967 to 25.973°.
Limiting indices	$-9 \leq h \leq 8, -12 \leq k \leq 12, -12 \leq l \leq 12$
Reflections collected / unique	8913 / 2963 [R(int) = 0.0285]
Completeness to theta = 25.242	99.6 %
Absorption correction	Semi-empirical from equivalents
Refinement method	Full-matrix least-squares on F^2
Data / restraints / parameters	2963 / 0 / 191
Goodness-of-fit on F^2	1.042
Final R indices [I>2sigma(I)]	R1 = 0.0364, wR2 = 0.0852
R indices (all data)	R1 = 0.0451, wR2 = 0.0897
Extinction coefficient	n/a
Largest diff. peak and hole	0.279 and -0.233 $e.Å^{-3}$

Table **S9**. Crystal data and structure refinement for silver complex **IV25**.

Empirical formula	$C_{19}H_{19}AgF_3O_5S_2$
Formula weight	556.33
Temperature	150(2) K
Wavelength	0.71073 Å
Crystal system, space group	Triclinic, P -1
Unit cell dimensions	a = 9.2390(15) Å alpha = 90.612(4)°
	b = 10.2526(16) Å beta = 104.659(3)°
	c = 12.2524(19) Å gamma = 112.816(4)°
Volume	1027.2(3) $Å^3$
Z	2
Calculated density	1.799 Mg/m^3
Absorption coefficient	1.240 mm^{-1}
F(000)	558
Crystal size	0.250 × 0.070 × 0.070 mm^3
Theta range for data collection	1.731 to 33.878°
Limiting indices	$-14 \leq h \leq 14$, $-16 \leq k \leq 16$, $-19 \leq l \leq 18$
Reflections collected / unique	39863 / 8144 [R(int) = 0.0316]
Completeness to theta = 25.242	99.5 %
Absorption correction	Semi-empirical from equivalents
Max. and min. transmission	0.7467 and 0.6838
Refinement method	Full-matrix least-squares on F^2
Data / restraints / parameters	8144 / 0 / 272
Goodness-of-fit on F^2	1.033
Final R indices [I>2sigma(I)]	R1 = 0.0295, wR2 = 0.0645
R indices (all data)	R1 = 0.0397, wR2 = 0.0690
Extinction coefficient	n/a
Largest diff. peak and hole	0.865 and -0.989 $e.Å^{-3}$

Table **S10**. Crystal data and structure refinement for silver complex **IV26**.

Empirical formula	$C_{37}H_{38}AgF_3O_7S_3$
Formula weight	855.72
Temperature	150(2) K
Wavelength	0.71073 Å
Crystal system, space group	Monoclinic, P -1
Unit cell dimensions	a = 33.262(4) Å alpha = 90°
	b = 9.3095(11) Å beta = 119.454(2)°
	c = 31.213(4) Å gamma = 90°
Volume	8415.9(18) $Å^3$
Z	8
Calculated density	1.351 Mg/m^3
Absorption coefficient	0.683 mm^{-1}
F(000)	3504
Crystal size	0.160 × 0.040 × 0.040 mm^3
Theta range for data collection	2.298 to 27.132°
Limiting indices	$-42 \leq h \leq 42, -11 \leq k \leq 11, -39 \leq l \leq 40$
Reflections collected / unique	66001 / 9255 [R(int) = 0.0878]
Completeness to theta = 25.242	99.5 %
Absorption correction	Semi-empirical from equivalents
Max. and min. transmission	0.7455 and 0.6546
Refinement method	Full-matrix least-squares on F^2
Data / restraints / parameters	9255 / 0 / 462
Goodness-of-fit on F^2	1.157
Final R indices [I>2sigma(I)]	R1 = 0.0623, wR2 = 0.1670
R indices (all data)	R1 = 0.0820, wR2 = 0.1764
Extinction coefficient	n/a
Largest diff. peak and hole	0.746 and -1.366 $e.Å^{-3}$

Appendix tables

Table S11. Optical rotation measurement for enantiomers of **IV7**

λ (nm)	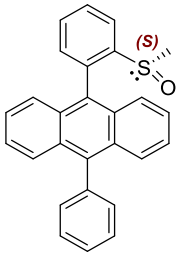 [α]$_\lambda^{25}$ (CH_2Cl_2, c =0.162)	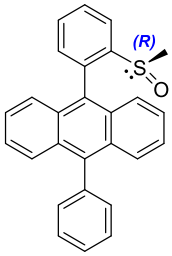 [α]$_\lambda^{25}$ (CH_2Cl_2, c =0.171)
589	- 128	+ 128
578	- 134	+ 134
546	- 155	+ 155
436	- 226	+ 227

Table S12. Optical rotation measurement for enantiomers of **IV8**

λ (nm)	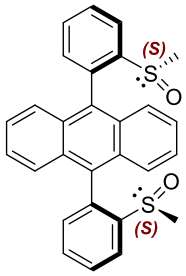 [α]$_\lambda^{25}$ (CH_2Cl_2, c =0.180)	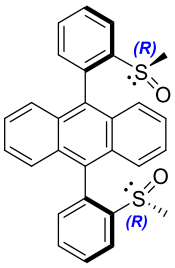 [α]$_\lambda^{25}$ (CH_2Cl_2, c =0.189)
589	- 180	+ 180
578	- 188	+ 188
546	- 215	+ 215
436	- 253	+ 254

Table S13. Optical rotation measurement for enantiomers of **IV9**

λ (nm)	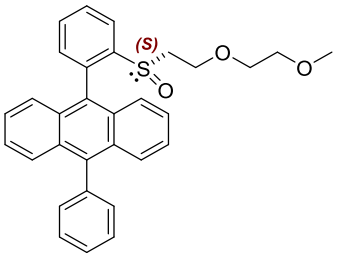 [α]$_\lambda^{25}$ (CH_2Cl_2, c =0.178)	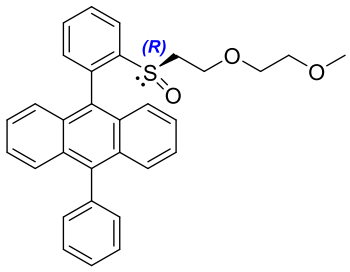 [α]$_\lambda^{25}$ (CH_2Cl_2, c =0.145)
589	- 185	+ 185
578	- 193	+ 192
546	- 224	+ 223
436	- 382	+ 378

Table S14. Optical rotation measurement for enantiomers of **IV10**

λ (nm)	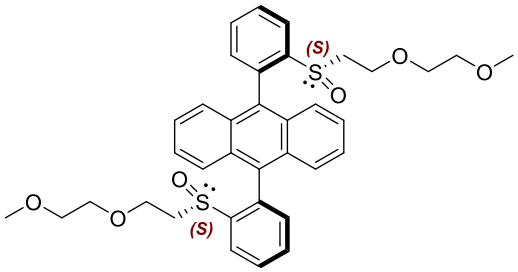 [α]$_\lambda^{25}$ (CH_2Cl_2, c =0.230)	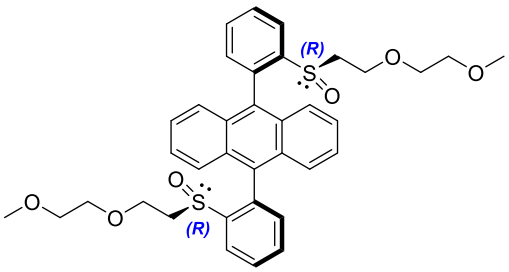 [α]$_\lambda^{25}$ (CH_2Cl_2, c =0.139)
589	- 286	+ 286
578	- 299	+ 300
546	- 349	+ 349
436	- 585	+ 585

Table S15. Optical rotation measurement for enantiomers of **IV11**

λ (nm)	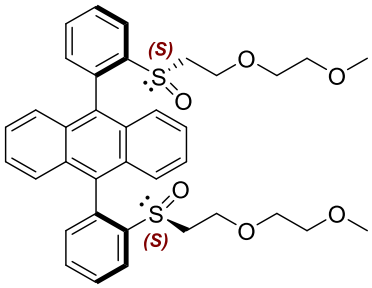 [α]$_\lambda^{25}$ (CH_2Cl_2, c =0.149)	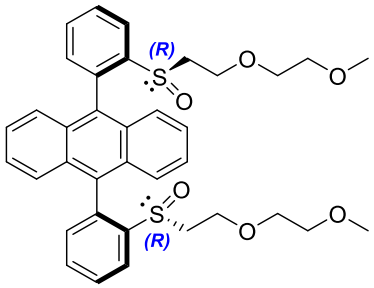 [α]$_\lambda^{25}$ (CH_2Cl_2, c =0.110)
589	- 302	+ 301
578	- 316	+ 315
546	- 369	+ 367
436	- 631	+ 629

Bibliography

[1] D. Seebach. "Organic Synthesis—Where now?" *Angew. Chem. Int. Ed.*, **1990**, *29*, 1320-1367.

[2] C. Thomas, A. Milet, F. Peruch and B. Bibal. "Activation of carbonyl bonds by quaternary ammoniums and a (Na^+:crown-ether) complex: investigation of the ring-opening polymerization of cyclic esters." *Polym. Chem.*, **2013**, *4*, 3491-3498.

[3] C. Thomas, F. Peruch, A. Deffieux, A. Milet, J.-P. Desvergne and B. Bibal. "Phenols and Tertiary Amines: An Amazingly Simple Hydrogen-Bonding Organocatalytic System Promoting Ring Opening Polymerization." *Adv. Synth. Catal.*, **2011**, *353*, 1049-1054.

[4] S. Koeller, J. Kadota, A. Deffieux, F. Peruch, S. Massip, J.-M. Léger, J.-P. Desvergne and B. Bibal. "Ring-Opening Polymerization of l-Lactide Efficiently Triggered by an Amido-Indole. X-ray Structure of a Complex between l-Lactide and the Hydrogen-Bonding Organocatalyst." *J. Am. Chem. Soc.*, **2009**, *131*, 15088-15089.

[5] C. Thomas, F. Peruch and B. Bibal. "Ring-opening polymerization of lactones using supramolecular organocatalysts under simple conditions." *RSC Adv.*, **2012**, *2*, 12851-12856.

[6] C. Thomas and B. Bibal. "Hydrogen-bonding organocatalysts for ring-opening polymerization." *Green Chem.*, **2014**, *16*, 1687-1699.

[7] C. Mongin, I. Pianet, G. Jonusauskas, D. M. Bassani and B. Bibal. "Supramolecular Photocatalyst for the Reduction of Au(III) to Au(I) and High-Turnover Generation of Gold Nanocrystals." *ACS Catal.*, **2015**, *5*, 380-387.

[8] Z. Cao, D. M. Bassani and B. Bibal. "Photoreduction of Thioether Gold(III) Complexes: Mechanistic Insight and Homogeneous Catalysis." *Chem. Eur. J.*, **2018**, *24*, 18779-18787.

[9] C. Mongin, A. M. Ardoy, R. Méreau, D. M. Bassani and B. Bibal. "Singlet oxygen stimulus for switchable functional organic cages." *Chem. Sci.*, **2020**, *11*, 1478-1484.

[10] M. S. Winston, W. J. Wolf and F. D. Toste. "Halide-Dependent Mechanisms of Reductive Elimination from Gold(III)." *J. Am. Chem. Soc.*, **2015**, *137*, 7921-7928.

[11] K. Kang, S. Liu, T. Xu, D. Wang, X. Leng, R. Bai, Y. Lan and Q. Shen. "C(sp^2)–C(sp^2) Reductive Elimination from Well-Defined Diarylgold(III) Complexes." *Organometallics.* **2017**, *36*, 4727-4740.

[12] W. J. Wolf, M. S. Winston and F. D. Toste. "Exceptionally fast carbon–carbon bond reductive elimination from gold(III)." *Nat. Chem.*, **2014**, *6*, 159-164.

[13] S. Komiya, T. A. Albright, R. Hoffmann and J. K. Kochi. "Reductive elimination and isomerization of organogold complexes. Theoretical studies of trialkylgold species as reactive intermediates." *J. Am. Chem. Soc.*, **1976**, *98*, 7255-7265.

[14] S. Komiya and J. K. Kochi. "Electrophilic cleavage of organogold complexes with acids. The mechanism of the reductive elimination of dialkyl(aniono)gold(III) species." *J. Am. Chem. Soc.*, **1976**, *98*, 7599-7607.

[15] A. Tamaki, S. A. Magennis and J. K. Kochi. "Catalysis by gold. Alkyl isomerization, *cis-trans* rearrangement, and reductive elimination of alkylgold(III) complexes." *J. Am. Chem. Soc.*, **1974**, *96*, 6140-6148.

[16] M. L. Marin, K. L. McGilvray and J. C. Scaiano. "Photochemical Strategies for the Synthesis of Gold Nanoparticles from Au(III) and Au(I) Using Photoinduced Free Radical Generation." *J. Am. Chem. Soc.*, **2008**, *130*, 16572-16584.

[17] K. L. McGilvray, J. Granger, M. Correia, J. T. Banks and J. C. Scaiano. "Opportunistic use of tetrachloroaurate photolysis in the generation of reductive species for the production of gold nanostructures." *Physical Chemistry Chemical Physics.* **2011**, *13*, 11914-11918.

[18] J. C. Scaiano, K. G. Stamplecoskie and G. L. Hallett-Tapley. "Photochemical Norrish type I reaction as a tool for metal nanoparticle synthesis: importance of proton coupled electron transfer." *Chem. Commun.*, **2012**, *48*, 4798-4808.

[19] P. Kwolek and M. Wojnicki. "The kinetic study of photoreduction of tetrachloroaurate acid by methanol in acidic media." *J. Photo. Photobio. A:* **2014**, *286*, 47-54.

[20] J. D. Keyes, R. J. Hilton, J. Farrer and R. K. Watt. "Ferritin as a photocatalyst and scaffold for gold nanoparticle synthesis." *J. Nanopart. Res.*, **2011**, *13*, 2563-2575.

[21] T. S. Teets and D. G. Nocera. "Halogen Photoreductive Elimination from Gold(III) Centers." *J. Am. Chem. Soc.*, **2009**, *131*, 7411-7420.

[22] C. Hirtenlehner, C. Krims, J. Hölbling, M. List, M. Zabel, M. Fleck, R. J. F. Berger, W. Schoefberger and U. Monkowius. "Syntheses, crystal structures, reactivity, and photochemistry of gold(III) bromides bearing N-heterocyclic carbenes." *Dalton Trans.*, **2011**, *40*, 9899-9910.

[23] M. J. Ghidiu, A. J. Pistner, G. P. A. Yap, D. A. Lutterman and J. Rosenthal. "Thermal versus Photochemical Reductive Elimination of Aryl Chlorides from NHC–Gold Complexes." *Organometallics.* **2013**, *32*, 5026-5029.

[24] A. S. K. Hashmi, J. P. Weyrauch, M. Rudolph and E. Kurpejović. "Gold Catalysis: The Benefits of N and N,O Ligands." *Angew. Chem. Int. Ed.*, **2004**, *43*, 6545-6547.

[25] C.-F. Xu, M. Xu, L.-Q. Yang and C.-Y. Li. "Synthesis of allenes via gold-catalyzed intermolecular reaction of propargylic alcohols and aromatic compounds." *J. Org. Chem.*, **2012**, *77*, 3010-3016.

[26] E. P. A. Talbot, M. Richardson, J. M. McKenna and F. D. Toste. "Gold-Catalyzed Redox Synthesis of Imidazo[1,2-a]pyridines using Pyridine *N*-Oxide and Alkynes." *Adv. Synth. Catal.*, **2014**, *356*, 687-691.

[27] F. Nzulu, A. Bontemps, J. Robert, M. Barbazanges, L. Fensterbank, J.-P. Goddard, M. Malacria, C. Ollivier, M. Petit, J. Rieger and F. Stoffelbach. "Gold-Catalyzed Polymerization Based on Carbene Polycyclopropanation." *Macromolecules.*, **2014**, *47*, 6652-6656.

[28] N. Morita, K. Oguro, S. Takahashi, M. Kawahara, S. Ban, Y. Hashimoto and O. Tamura. "Gold(III)-catalyzed synthesis of 2,3,4-trisubstituted dihydropyrans from propargylic alcohols with 1,3-dicarbonyl compounds." *Heterocycles.*, **2017**, *95*, 172-180.

[29] E. C. Minnihan, S. L. Colletti, F. D. Toste and H. C. Shen. "Gold(I)-Catalyzed Regioselective Cyclizations of Silyl Ketene Amides and Carbamates with Alkynes." *J. Org. Chem.*, **2007**, *72*, 6287-6289.

[30] N. Marien, B. Brigou, B. Pinter, F. De Proft and G. Verniest. "Synthesis of 2-Spiropseudoindoxyls via an Intramolecular Nitroalkyne Redox-Dipolar Cycloaddition Cascade." *Org. Lett.*, **2015**, *17*, 270-273.

[31] Y. Li, J. P. Brand and J. Waser. "Gold-Catalyzed Regioselective Synthesis of 2- and 3-Alkynyl Furans." *Angew. Chem., Int. Ed.*, **2013**, *52*, 6743-6747.

[32] S. Tosoni and G. Pacchioni. "Oxide-Supported Gold Clusters and Nanoparticles in Catalysis: A Computational Chemistry Perspective." *ChemCatChem.*, **2019**, *11*, 73-89.

[33] A. Corma and H. Garcia. "Supported gold nanoparticles as catalysts for organic reactions." *Chem. Soc. Rev.*, **2008**, *37*, 2096-2126.

[34] A. S. Alshammari. "Heterogeneous gold catalysis: from discovery to applications." *Catalysts.*, **2019**, *9*, 402.

[35] G. J. Hutchings. "Heterogeneous Gold Catalysis." *ACS Cent. Sci.*, **2018**, *4*, 1095-1101.

[36] M. Egi, K. Azechi and S. Akai. "Reusable and Durable Immobilized-Cationic Gold(I) Catalysts for Environmentally Benign Bond-Forming Reactions." *Adv. Synth. Catal.*, **2011**, *353*, 287-290.

[37] W. Cao and B. Yu. "A Recyclable Polystyrene-Supported Gold(I) Catalyst." *Adv. Synth. Catal.*, **2011**, *353*, 1903-1907.

[38] M. Raducan, C. Rodríguez-Escrich, X. C. Cambeiro, E. C. Escudero-Adán, M. A. Pericàs and A. M.

Echavarren. "A multipurpose gold(I) precatalyst." *Chem. Commun.*, **2011**, *47*, 4893-4895.

[39] Y. Zhu, S. Laval, Y. Tang, G. Lian and B. Yu. "A Polystyrene-Bound Triphenylphosphine Gold(I) Catalyst for the Glycosylation of Glycosyl ortho-Hexynylbenzoates." *Asian J. Org. Chem.*, **2015**, *4*, 1034-1039.

[40] R. Cai, X. Ye, Q. Sun, Q. He, Y. He, S. Ma and X. Shi. "Anchoring Triazole-Gold(I) Complex into Porous Organic Polymer To Boost the Stability and Reactivity of Gold(I) Catalyst." *ACS Catal.*, **2017**, *7*, 1087-1092.

[41] M. Chen, Z.-M. Zhang, Z. Yu, H. Qiu, B. Ma, H.-H. Wu and J. Zhang. "Polymer-Bound Chiral Gold-Based Complexes as Efficient Heterogeneous Catalysts for Enantioselectivity Tunable Cycloaddition." *ACS Catal.*, **2015**, *5*, 7488-7492.

[42] G. Villaverde, A. Corma, M. Iglesias and F. Sánchez. "Heterogenized Gold Complexes: Recoverable Catalysts for Multicomponent Reactions of Aldehydes, Terminal Alkynes, and Amines." *ACS Catal.*, **2012**, *2*, 399-406.

[43] W. Yang, R. Zhang, F. Yi and M. Cai. "A Heterogeneous Gold(I)-Catalyzed [2 + 2 + 1] Annulation of Terminal Alkynes, Nitriles, and Oxygen Atoms Leading to 2,5-Disubstituted Oxazoles." *J. Org. Chem.*, **2017**, *82*, 5204-5211.

[44] Q. Nie, F. Yi, B. Huang and M. Cai. "Efficient Heterogeneous Gold(I)-Catalyzed Direct C(sp^2)–C(sp) Bond Functionalization of Arylalkynes through a Nitrogenation Process to Amides." *Adv. Synth. Catal.*, **2017**, *359*, 3968-3976.

[45] X. Xia, J. Meng, H. Wu, T. Cheng and G. Liu. "Integration of multiple active sites on large-pore mesoporous silica for enantioselective tandem reactions." *Chem. Commun.*, **2017**, *53*, 1638-1641.

[46] X.-Z. Shu, S. C. Nguyen, Y. He, F. Oba, Q. Zhang, C. Canlas, G. A. Somorjai, A. P. Alivisatos and F. D. Toste. "Silica-Supported Cationic Gold(I) Complexes as Heterogeneous Catalysts for Regio- and Enantioselective Lactonization Reactions." *J. Am. Chem. Soc.*, **2015**, *137*, 7083-7086.

[47] W. Yang, L. Wei, T. Yan and M. Cai. "Highly efficient heterogeneous aerobic oxidative C–C coupling from Csp^3–H bonds by a magnetic nanoparticle-immobilized bipy–gold(III) catalyst." *Catal. Sci.*, **2017**, *7*, 1744-1755.

[48] W. Yang, L. Wei, F. Yi and M. Cai. "Magnetic nanoparticle-supported phosphine gold(i) complex: a highly efficient and recyclable catalyst for the direct reductive amination of aldehydes and ketones." *Catal. Sci.*, **2016**, *6*, 4554-4564.

[49] A. K. Clarke, M. J. James, P. O'Brien, R. J. K. Taylor and W. P. Unsworth. "Silica-Supported Silver Nitrate as a Highly Active Dearomatizing Spirocyclization Catalyst: Synergistic Alkyne Activation by Silver Nanoparticles and Silica." *Angew. Chem. Int. Ed.*, **2016**, *55*, 13798-13802.

[50] C. Du, S. Ye, Y. Liu, Y. Guo, T. Wu, H. Liu, J. Zheng, C. Cheng, M. Zhu and G. Yu. "Fused-seven-ring anthracene derivative with two sulfur bridges for high performance red organic light-emitting diodes." *Chem. Commun.*, **2010**, *46*, 8573-8575.

[51] S. K. Pedersen, J. Holmehave, F. H. Blaikie, A. Gollmer, T. Breitenbach, H. H. Jensen and P. R. Ogilby. "Aarhus Sensor Green: A Fluorescent Probe for Singlet Oxygen." *J. Org. Chem.*, **2014**, *79*, 3079-3087.

[52] A. Belyaev, Y.-T. Chen, S.-H. Su, Y.-J. Tseng, A. J. Karttunen, S. P. Tunik, P.-T. Chou and I. O. Koshevoy. "Copper-mediated phospha-annulation to attain water-soluble polycyclic luminophores." *Chem. Commun.*, **2017**, *53*, 10954-10957.

[53] A. Iida and S. Yamaguchi. "Intense solid-state blue emission with a small Stokes' shift: π-stacking protection of the diphenylanthracene skeleton." *Chem. Commun.*, **2009**, 3002-3004.

[54] J. C. C. Atherton and S. Jones. "Diels–Alder reactions of anthracene, 9-substituted anthracenes and 9,10-disubstituted anthracenes." *Tetrahedron.* **2003**, *59*, 9039-9057.

[55] T. Wilson, A. U. Khan and M. M. Mehrotra. "Spectral observation of singlet molecular oxygen fron aromatic

endoperoxides in solution." *Photochem. Photobio.*, **1986**, *43*, 661-662.

[56] R. Schmidt, H. D. Brauer and J. Rigaudy. "Reactions originating from different upper excited singlet states: The photocycloreversion of the endoperoxides of 1,4-dimethyl-9,10-diphenylanthracene." *J. Photochem.*, **1986**, *34*, 197-208.

[57] J.-M. Aubry, C. Pierlot, J. Rigaudy and R. Schmidt. "Reversible Binding of Oxygen to Aromatic Compounds." *Acc. Chem. Res.*, **2003**, *36*, 668-675.

[58] A. Caspar, S. Altenburger-Combrisson and F. Gobert. "Etude par RMN ^{13}C de Dérivés Aromatiques Phénylés: Observation de Substituants Phényles en Rotation Restreinte." *Org. Magn. Reson.*, **1978**, *11*, 603-606.

[59] P. J. Marriott and Y.-H. Lai. "Capillary column gas chromatographic method for the study of dynamic intramolecular interconversion behaviour." *J. Chromatogr.*, **1988**, *447*, 29-41.

[60] K. Nikitin, H. Müller-Bunz, Y. Ortin, J. Muldoon and M. J. McGlinchey. "Restricted Rotation in 9-Phenyl-anthracenes: A Prediction Fulfilled." *Org. Chem.*, **2011**, *13*, 256-259.

[61] D. Zehm, W. Fudickar and T. Linker. "Molecular Switches Flipped by Oxygen." *Angew. Chem. Int. Ed.*, **2007**, *46*, 7689-7692.

[62] R. Alberto, W. Nef, A. Smith, T. A. Kaden, M. Neuburger, M. Zehnder, A. Frey, U. Abram and P. A. Schubiger. "Silver(I) Complexes of the Derivatized Crown Thioether Ligands 3,6,9,12,15,18-Hexathianonadecanol and 3,6,9,13,16,19-Hexathiaicosanol. Determination of Stability Constants and the Crystal Structures of [Ag(19-aneS6-OH)OTf]and [Ag(20-aneS6-OH)BF_4]." *Inorg. Chem.*, **1996**, *35*, 3420-3427.

[63] G. A. Forsyth and J. C. Lockhart. "Macrocyclic thioether design by molecular modeling." *Supramol. Chem.*, **1994**, *4*, 17-29.

[64] A. J. Blake, R. O. Gould, W.-S. Li, V. Lippolis, S. Parsons, C. Radek and M. Schroeder. "Silver-Thioether Crown Complexes as Templates for the Synthesis of Extended Polyiodide Networks: Synthesis and X-ray Crystal Structures of [Ag_2([15]aneS5)$_2$]I_{12}, [Ag([18]aneS6)]I_7, [Ag([18]aneS6)]I_3, and [Ag([9]aneS3)$_2$]I_5." *Inorg. Chem.*, **1998**, *37*, 5070-5077.

[65] W. Liang, S. Liu, C. R. Lucas and D. O. Miller. "Silver, copper and nickel complexes of 1-oxa-4,7-dithiacyclononane and 1-oxa-4,8-dithiacyclodecane." *Polyhedron.* **1998**, *17*, 1323-1328.

[66] A. J. Blake, R. O. Gould, C. Radek, G. Reid, A. Taylor and M. Schroeder. "Structural mis-matches in silver and gold complexes of thioether macrocycles." *Spec. Publ. - R. Soc. Chem.*, **1993**, *131*, 95-101.

[67] X.-H. Bu, W. Chen, M. Du, K. Biradha, W.-Z. Wang and R.-H. Zhang. "Chiral Noninterpenetrated (10,3)-a Net in the Crystal Structure of Ag(I) and Bisthioether." *Inorg. Chem.*, **2002**, *41*, 437-439.

[68] X.-H. Bu, W.-F. Hou, M. Du, W. Chen and R.-H. Zhang. "Varying the Frameworks of Novel Silver(I) Coordination Polymers with Thioethers by Altering the Backbone or Terminal Groups of Ligands." *Cryst. Growth Des.*, **2002**, *2*, 303-307.

[69] Y. Zhang, D. Yang, Y. Li, B. Wang, X. Zhao and J. Qu. "Synthesis and characterization of a family of thioether-dithiolate-bridged heteronuclear iron complexes." *Dalton Trans.*, **2017**, *46*, 7030-7038.

[70] H.-J. Holdt, H. Mueller, M. Poetter, A. Kelling, U. Schilde, I. Starke, M. Heydenreich and E. Kleinpeter. "The first sandwich complex with an octa(thioether) coordination sphere: bis(maleonitrile-tetrathia-12-crown-4)silver(I)." *Eur. J. Inorg. Chem.*, **2006**, 2377-2384.

[71] A. J. Blake, N. R. Champness, S. M. Howdle, K. S. Morley, P. B. Webb and C. Wilson. "Silver(I)-thioether coordination polymers constructed using asymmetric diketonate anions." *CrystEngComm.* **2002**, *4*, 88-92.

[72] V. Rosa, C. Fliedel, A. Ghisolfi, R. Pattacini, T. Aviles and P. Braunstein. "Influence of a thioether function in short-bite diphosphine ligands on the nature of their silver complexes: structure of a trinuclear complex and of a coordination polymer." *Dalton Trans.*, **2013**, *42*, 12109-12119.

[73] A. J. Blake, N. R. Champness, S. M. Howdle and P. B. Webb. "Silver(I) Coordination Polymers Using Thioether Macrocycle Building Blocks." *Inorg. Chem.*, **2000**, *39*, 1035-1038.

[74] S. Park, L. F. Lindoy and S. S. Lee. "Assembly of Silver(I) Complexes of Isomeric NS_2-Macrocycles Displaying Cyclic Oligomer, Helix, and Zigzag Structures." *Cryst. Growth Des.*, **2012**, *12*, 1320-1329.

[75] A. Zeineddine, L. Estévez, S. Mallet-Ladeira, K. Miqueu, A. Amgoune and D. Bourissou. "Rational development of catalytic Au(I)/Au(III) arylation involving mild oxidative addition of aryl halides." *Nat. Commun.*, **2017**, *8*, 565-572.

[76] M. Joost, A. Zeineddine, L. Estévez, S. Mallet−Ladeira, K. Miqueu, A. Amgoune and D. Bourissou. "Facile Oxidative Addition of Aryl Iodides to Gold(I) by Ligand Design: Bending Turns on Reactivity." *J. Am. Chem. Soc.*, **2014**, *136*, 14654-14657.

[77] W. Shang, X. Zhu, T. Liang, C. Du, L. Hu, T. Li and M. Liu. "Chiral Reticular Self-Assembly of Achiral AIEgen into Optically Pure Metal-Organic Frameworks (MOFs) with Dual Mechano-Switchable Circularly Polarized Luminescence." *Angew. Chem., Int. Ed.*, **2020**, *59*, 12811-12816.

[78] K. Hirano, T. Ikeda, N. Fujii, T. Hirao, M. Nakamura, Y. Adachi, J. Ohshita and T. Haino. "Helical assembly of a dithienogermole exhibiting switchable circularly polarized luminescence." *Chem. Commun.*, **2019**, *55*, 10607-10610.

[79] Y. Kitagawa, M. Tsurui and Y. Hasegawa. "Steric and Electronic Control of Chiral Eu(III) Complexes for Effective Circularly Polarized Luminescence." *ACS Omega.* **2020**, *5*, 3786-3791.

[80] F. Gendron, B. Moore, II, O. Cador, F. Pointillart, J. Autschbach and B. Le Guennic. "*Ab Initio* Study of Circular Dichroism and Circularly Polarized Luminescence of Spin-Allowed and Spin-Forbidden Transitions: From Organic Ketones to Lanthanide Complexes." *J. Chem. Theory Comput.*, **2019**, *15*, 4140-4155.

[81] Y. Nagata, T. Nishikawa and M. Suginome. "Chirality-switchable circularly polarized luminescence in solution based on the solvent-dependent helix inversion of poly(quinoxaline-2,3-diyl)s." *Chem. Commun.*, **2014**, *50*, 9951-9953.

[82] B. Zhao, K. Pan and J. Deng. "Combining Chiral Helical Polymer with Achiral Luminophores for Generating Full-Color, On-Off, and Switchable Circularly Polarized Luminescence." *Macromolecules.*, **2019**, *52*, 376-384.

[83] T. Kimoto, T. Amako, N. Tajima, R. Kuroda, M. Fujiki and Y. Imai. "Control of Solid-state Circularly Polarized Luminescence of Binaphthyl Organic Fluorophores through Environmental Changes." *Asian J. Org. Chem.*, **2013**, *2*, 404-410.

[84] Z. Jiang, J. Wang, T. Gao, J. Ma, Z. Liu and R. Chen. "Rational Design of Axially Chiral Platinabinaphthalenes with Aggregation-Induced Emission for Red Circularly Polarized Phosphorescent Organic Light-Emitting Diodes." *ACS Appl. Mater. Inter.*, **2020**, *12*, 9520-9527.

[85] Z.-B. Sun, J.-K. Liu, D.-F. Yuan, Z.-H. Zhao, X.-Z. Zhu, D.-H. Liu, Q. Peng and C.-H. Zhao. "2,2'-Diamino-6,6'-diboryl-1,1'-binaphthyl: A Versatile Building Block for Temperature-Dependent Dual Fluorescence and Switchable Circularly Polarized Luminescence." *Angew. Chem., Int. Ed.*, **2019**, *58*, 4840-4846.

[86] K. Takase, K. Noguchi and K. Nakano. "Circularly Polarized Luminescence from Chiral Spiro Molecules: Synthesis and Optical Properties of 10,10'-Spirobi(indeno[1,2-b][1]benzothiophene) Derivatives." *Org. Lett.*, **2017**, *19*, 5082-5085.

[87] K. Ma, W. Chen, T. Jiao, X. Jin, Y. Sang, D. Yang, J. Zhou, M. Liu and P. Duan. "Boosting the circularly polarized luminescence of small organic molecules via multi-dimensional morphology control." *Chem. Sci.*, **2019**, *10*, 6821-6827.

[88] C. Schaack, L. Arrico, E. Sidler, M. Gorecki, L. Di Bari and F. Diederich. "Helicene Monomers and Dimers: Chiral Chromophores Featuring Strong Circularly Polarized Luminescence." *Chem. Eur. J.*, **2019**, *25*, 8003-

8007.

[89] W.-L. Zhao, M. Li, H.-Y. Lu and C.-F. Chen. "Advances in helicene derivatives with circularly polarized luminescence." *Chem. Commun.*, **2019**, *55*, 13793-13803.

[90] C. Shen, E. Anger, M. Srebro, N. Vanthuyne, K. K. Deol, T. D. Jefferson, G. Muller, J. A. G. Williams, L. Toupet, C. Roussel, J. Autschbach, R. Reau and J. Crassous. "Straightforward access to mono- and bis-cycloplatinated helicenes displaying circularly polarized phosphorescence by using crystallization resolution methods." *Chem. Sci.*, **2014**, *5*, 1915-1927.

[91] H. A. Wegner. "Molecular Switches. Second Edition. Edited by Ben L. Feringa and Wesley R. Browne." *Angew. Chem. Int. Ed.*, **2012**, *51*, 2281-2281.

[92] B. Mondal, A. K. Ghosh and P. S. Mukherjee. "Reversible Multistimuli Switching of a Spiropyran-Functionalized Organic Cage in Solid and Solution." *J. Org. Chem.*, **2017**, *82*, 7783-7790.

[93] Y. Ito, M. Sawamura and T. Hayashi. "Catalytic asymmetric aldol reaction: reaction of aldehydes with isocyanoacetate catalyzed by a chiral ferrocenylphosphine-gold(I) complex." *J. Am. Chem. Soc.*, **1986**, *108*, 6405-6406.

[94] Y. Fukuda and K. Utimoto. "Effective transformation of unactivated alkynes into ketones or acetals with a gold(III) catalyst." *J. Org. Chem.*, **1991**, *56*, 3729-3731.

[95] J. H. Teles, S. Brode and M. Chabanas. "Cationic Gold(I) Complexes: Highly Efficient Catalysts for the Addition of Alcohols to Alkynes." *Angew. Chem. Int. Ed.*, **1998**, *37*, 1415-1418.

[96] A. S. K. Hashmi, T. M. Frost and J. W. Bats. "Highly Selective Gold-Catalyzed Arene Synthesis." *J. Am. Chem. Soc.*, **2000**, *122*, 11553-11554.

[97] A. Leyva-Pérez and A. Corma. "Similarities and Differences between the "Relativistic" Triad Gold, Platinum, and Mercury in Catalysis." *Angew. Chem. Int. Ed.*, **2012**, *51*, 614-635.

[98] K. S. Pitzer. "Relativistic effects on chemical properties." *Acc. Chem. Res.*, **1979**, *12*, 271-276.

[99] P. Pyykko and J. P. Desclaux. "Relativity and the periodic system of elements." *Acc. Chem. Res.*, **1979**, *12*, 276-281.

[100] P. Pyykkö. "Relativity, Gold, Closed-Shell Interactions, and $CsAu{\cdot}NH_3$." *Angew. Chem. Int. Ed.*, **2002**, *41*, 3573-3578.

[101] P. Pyykkö. "Theoretical Chemistry of Gold." *Angew. Chem. Int. Ed.*, **2004**, *43*, 4412-4456.

[102] D. J. Gorin and F. D. Toste. "Relativistic effects in homogeneous gold catalysis." *Nature*, **2007**, *446*, 395-403.

[103] M. L. H. Green. "A new approach to the formal classification of covalent compounds of the elements." *J. Organomet. Chem.*, **1995**, *500*, 127-148.

[104] G. W. A. Fowles, D. A. Rice and M. J. Riedl. "The reaction of gold halides with some sulphur-containing ligands." *J. Less-Common Met.*, **1973**, *32*, 379-384.

[105] N. Marion and S. P. Nolan. "N-Heterocyclic carbenes in gold catalysis." *Chem. Soc. Rev.*, **2008**, *37*, 1776-1782.

[106] S. P. Nolan. "The Development and Catalytic Uses of N-Heterocyclic Carbene Gold Complexes." *Acc. Chem. Res.*, **2011**, *44*, 91-100.

[107] W. Zi and F. Dean Toste. "Recent advances in enantioselective gold catalysis." *Chem. Soc. Rev.*, **2016**, *45*, 4567-4589.

[108] G. Zuccarello, M. Zanini and A. M. Echavarren. "Buchwald-Type Ligands on Gold(I) Catalysis." *Isr. J. Chem.*, **2020**, *60*, 360-372.

[109] G. Zuccarello, J. G. Mayans, I. Escofet, D. Scharnagel, M. S. Kirillova, A. H. Pérez-Jimeno, P. Calleja, J. R. Boothe and A. M. Echavarren. "Enantioselective Folding of Enynes by Gold(I) Catalysts with a Remote C2-

Chiral Element." *J. Am. Chem. Soc.*, **2019**, *141*, 11858-11863.

[110] Z. Zhang, V. Smal, P. Retailleau, A. Voituriez, G. Frison, A. Marinetti and X. Guinchard. "Tethered Counterion-Directed Catalysis: Merging the Chiral Ion-Pairing and Bifunctional Ligand Strategies in Enantioselective Gold(I) Catalysis." *J. Am. Chem. Soc.*, **2020**, *142*, 3797-3805.

[111] K. Ji, Z. Zheng, Z. Wang and L. Zhang. "Enantioselective Oxidative Gold Catalysis Enabled by a Designed Chiral P,N-Bidentate Ligand." *Angew. Chem. Int. Ed.*, **2015**, *54*, 1245-1249.

[112] K. Yavari, P. Aillard, Y. Zhang, F. Nuter, P. Retailleau, A. Voituriez and A. Marinetti. "Helicenes with Embedded Phosphole Units in Enantioselective Gold Catalysis." *Angew. Chem. Int. Ed.*, **2014**, *53*, 861-865.

[113] Y. Li, W. Li and J. Zhang. "Gold-Catalyzed Enantioselective Annulations." *Chem. Eur. J.*, **2017**, *23*, 467-512.

[114] M. Barbazanges and L. Fensterbank. "Chiral Acyclic Diaminocarbene Complexes: a New Opportunity for Gold Asymmetric Catalysis." *ChemCatChem.* **2012**, *4*, 1065-1066.

[115] H. Teller, S. Flügge, R. Goddard and A. Fürstner. "Enantioselective Gold Catalysis: Opportunities Provided by Monodentate Phosphoramidite Ligands with an Acyclic TADDOL Backbone." *Angew. Chem. Int. Ed.*, **2010**, *49*, 1949-1953.

[116] Z. Wu, K. Isaac, P. Retailleau, J.-F. Betzer, A. Voituriez and A. Marinetti. "Planar Chiral Phosphoramidites with a Paracyclophane Scaffold: Synthesis, Gold(I) Complexes, and Enantioselective Cycloisomerization of Dienynes." *Chem. Eur. J.*, **2016**, *22*, 3278-3281.

[117] H. Duan, S. Sengupta, J. L. Petersen, N. G. Akhmedov and X. Shi. "Triazole−Au(I) Complexes: A New Class of Catalysts with Improved Thermal Stability and Reactivity for Intermolecular Alkyne Hydroamination." *J. Am. Chem. Soc.*, **2009**, *131*, 12100-12102.

[118] S. Bontemps, G. Bouhadir, K. Miqueu and D. Bourissou. "On the Versatile and Unusual Coordination Behavior of Ambiphilic Ligands *o*-$R_2P(Ph)BR'_2$." *J. Am. Chem. Soc.*, **2006**, *128*, 12056-12057.

[119] M. Sircoglou, S. Bontemps, M. Mercy, N. Saffon, M. Takahashi, G. Bouhadir, L. Maron and D. Bourissou. "Transition-Metal Complexes Featuring Z-Type Ligands: Agreement or Discrepancy between Geometry and dn Configuration?" *Angew. Chem. Int. Ed.*, **2007**, *46*, 8583-8586.

[120] F. Inagaki, C. Matsumoto, Y. Okada, N. Maruyama and C. Mukai. "Air-Stable Cationic Gold(I) Catalyst Featuring a Z-Type Ligand: Promoting Enyne Cyclizations." *Angew. Chem., Int. Ed.*, **2015**, *54*, 818-822.

[121] H. Yang and F. P. Gabbai. "Activation of a Hydroamination Gold Catalyst by Oxidation of a Redox-Noninnocent Chlorostibine Z-Ligand." *J. Am. Chem. Soc.*, **2015**, *137*, 13425-13432.

[122] F. Inagaki, K. Nakazawa, K. Maeda, T. Koseki and C. Mukai. "Substituent effects in the cyclization of yne-diols catalyzed by gold complexes featuring L2/Z-type diphosphinoborane ligands." *Organometallics.* **2017**, *36*, 3005-3008.

[123] R. Murakami and F. Inagaki. "Recent topics of gold catalyst featuring Z-type ligands." *Tetrahedron Lett.*, **2019**, *60*, 151231-15138.

[124] L. C. Wilkins, Y. Kim, E. D. Litle and F. P. Gabbai. "Stabilized Carbenium Ions as Latent, Z-type Ligands." *Angew. Chem. Int. Ed.*, **2019**, *58*, 18266-18270.

[125] L. Zhang. *Dichloro(pyridine-2-carboxylato)-gold(III)*. 2009. John Wiley & Sons, Ltd.

[126] X. Tian, L. Song, C. Han, C. Zhang, Y. Wu, M. Rudolph, F. Rominger and A. S. K. Hashmi. "Gold(III)-Catalyzed Formal [3 + 2] Annulations of *N*-Acyl Sulfilimines with Ynamides for the Synthesis of 4-Aminooxazoles." *Org. Lett.*, **2019**, *21*, 2937-2940.

[127] X. Tian, L. Song, M. Rudolph, Q. Wang, X. Song, F. Rominger and A. S. K. Hashmi. "*N*-Pyridinyl Sulfilimines as a Source for α-Imino Gold Carbenes: Access to 2-Amino-Substituted N-Fused Imidazoles." *Org. Lett.*, **2019**, *21*, 1598-1601.

[128] X. Tian, L. Song, K. Farshadfar, M. Rudolph, F. Rominger, T. Oeser, A. Ariafard and A. S. K. Hashmi. "Acyl

Migration versus Epoxidation in Gold Catalysis: Facile, Switchable, and Atom-Economic Synthesis of Acylindoles and Quinoline Derivatives." *Angew. Chem., Int. Ed.*, **2020**, *59*, 471-478.

[129]T. Roth, H. Wadepohl and L. H. Gade. "Cationic BPI-Gold(III) Complexes: Controlling Ligating and Nonligating Anions." *Eur. J. Inorg. Chem.*, **2016**, *2016*, 1184-1191.

[130]J. Serra, P. Font, E. D. Sosa Carrizo, S. Mallet-Ladeira, S. Massou, T. Parella, K. Miqueu, A. Amgoune, X. Ribas and D. Bourissou. "Cyclometalated gold(III) complexes: noticeable differences between (N,C) and (P,C) ligands in migratory insertion." *Chem. Sci.*, **2018**, *9*, 3932-3940.

[131]L. Huang, F. Rominger, M. Rudolph and A. S. K. Hashmi. "A general access to organogold(III) complexes by oxidative addition of diazonium salts." *Chem. Commun.*, **2016**, *52*, 6435-6438.

[132]J. Guenther, S. Mallet-Ladeira, L. Estevez, K. Miqueu, A. Amgoune and D. Bourissou. "Activation of Aryl Halides at Gold(I): Practical Synthesis of (P,C) Cyclometalated Gold(III) Complexes." *J. Am. Chem. Soc.*, **2014**, *136*, 1778-1781.

[133]C.-Y. Wu, T. Horibe, C. B. Jacobsen and F. D. Toste. "Stable gold(III) catalysts by oxidative addition of a carbon–carbon bond." *Nature*, **2015**, *517*, 449-454.

[134]V. K.-Y. Lo, K. K.-Y. Kung, M.-K. Wong and C.-M. Che. "Gold(III) (C,N) complex-catalyzed synthesis of propargylamines via a three-component coupling reaction of aldehydes, amines and alkynes." *J. Organomet. Chem.*, **2009**, *694*, 583-591.

[135]M. Joost, A. Amgoune and D. Bourissou. "Reactivity of Gold Complexes towards Elementary Organometallic Reactions." *Angew. Chem. Int. Ed.*, **2015**, *54*, 15022-15045.

[136]L. Zhang. "Tandem Au-Catalyzed 3,3-Rearrangement−[2 + 2] Cycloadditions of Propargylic Esters: Expeditious Access to Highly Functionalized 2,3-Indoline-Fused Cyclobutanes." *J. Am. Chem. Soc.*, **2005**, *127*, 16804-16805.

[137]C. Ferrer and A. M. Echavarren. "Gold-Catalyzed Intramolecular Reaction of Indoles with Alkynes: Facile Formation of Eight-Membered Rings and an Unexpected Allenylation." *Angew. Chem. Int. Ed.*, **2006**, *45*, 1105-1109.

[138]D. Lee, S. M. Kim, H. Hirao and S. H. Hong. "Gold(I)/Gold(III)-Catalyzed Selective Synthesis of *N*-Sulfonyl Enaminone Isomers from Sulfonamides and Ynones via Two Distinct Reaction Pathways." *Org. Chem.*, **2017**, *19*, 4734-4737.

[139]A. Fürstner and P. W. Davies. "Catalytic Carbophilic Activation: Catalysis by Platinum and Gold π-Acids." *Angew. Chem. Int. Ed.*, **2007**, *46*, 3410-3449.

[140]A. Arcadi. "Alternative Synthetic Methods through New Developments in Catalysis by Gold." *Chem. Rev.*, **2008**, *108*, 3266-3325.

[141]A. Corma, A. Leyva-Pérez and M. J. Sabater. "Gold-Catalyzed Carbon−Heteroatom Bond-Forming Reactions." *Chem. Rev.*, **2011**, *111*, 1657-1712.

[142]N. Krause and C. Winter. "Gold-Catalyzed Nucleophilic Cyclization of Functionalized Allenes: A Powerful Access to Carbo- and Heterocycles." *Chem. Rev.*, **2011**, *111*, 1994-2009.

[143]M. Rudolph and A. S. K. Hashmi. "Gold catalysis in total synthesis—an update." *Chem. Soc. Rev.*, **2012**, *41*, 2448-2462.

[144]L. Fensterbank and M. Malacria. "Molecular Complexity from Polyunsaturated Substrates: The Gold Catalysis Approach." *Acc. Chem. Res.*, **2014**, *47*, 953-965.

[145]D. Qian and J. Zhang. "Gold-catalyzed cyclopropanation reactions using a carbenoid precursor toolbox." *Chem. Soc. Rev.*, **2015**, *44*, 677-698.

[146]D. P. Day and P. W. H. Chan. "Gold-Catalyzed Cycloisomerizations of 1,*n*-Diyne Carbonates and Esters." *Adv. Synth. Catal.*, **2016**, *358*, 1368-1384.

[147]S. Kramer. "Recent Advances in Gold-Catalyzed Intermolecular Aryl C-H Functionalization." *Chem. Eur. J.*, **2016**, *22*, 15584-15598.

[148]D. Pflästerer and A. S. K. Hashmi. "Gold catalysis in total synthesis – recent achievements." *Chem. Soc. Rev.*, **2016**, *45*, 1331-1367.

[149]M. Jia and M. Bandini. "Counterion Effects in Homogeneous Gold Catalysis." *ACS Catal.*, **2015**, *5*, 1638-1652.

[150]Z. Lu, G. B. Hammond and B. Xu. "Improving Homogeneous Cationic Gold Catalysis through a Mechanism-Based Approach." *Acc. Chem. Res.*, **2019**, *52*, 1275-1288.

[151]A. S. K. Hashmi. "Isolable vinylgold intermediates - first access to phantoms of homogeneous gold catalysis." *Gold Bull.*, **2009**, *42*, 275-279.

[152]L.-P. Liu, B. Xu, M. S. Mashuta and G. B. Hammond. "Synthesis and Structural Characterization of Stable Organogold(I) Compounds. Evidence for the Mechanism of Gold-Catalyzed Cyclizations." *J. Am. Chem. Soc.*, **2008**, *130*, 17642-17643.

[153]Y. Wang, M. E. Muratore and A. M. Echavarren. "Gold Carbene or Carbenoid: Is There a Difference?" *Chem. Eur. J.*, **2015**, *21*, 7332-7339.

[154]R. J. Harris and R. A. Widenhoefer. "Gold carbenes, gold-stabilized carbocations, and cationic intermediates relevant to gold-catalysed enyne cycloaddition." *Chem. Soc. Rev.*, **2016**, *45*, 4533-4551.

[155]E. Jiménez-Núñez and A. M. Echavarren. "Molecular diversity through gold catalysis with alkynes." *Chem. Commun.*, **2007**, 333-346.

[156]C. Nieto-Oberhuber, S. López, M. P. Muñoz, D. J. Cárdenas, E. Buñuel, C. Nevado and A. M. Echavarren. "Divergent Mechanisms for the Skeletal Rearrangement and [2+2] Cycloaddition of Enynes Catalyzed by Gold." *Angew. Chem. Int. Ed.*, **2005**, *44*, 6146-6148.

[157]C. Nieto-Oberhuber, M. P. Muñoz, E. Buñuel, C. Nevado, D. J. Cárdenas and A. M. Echavarren. "Cationic Gold(I) Complexes: Highly Alkynophilic Catalysts for the exo- and endo-Cyclization of Enynes." *Angew. Chem. Int. Ed.*, **2004**, *43*, 2402-2406.

[158]D. Scharnagel, I. Escofet, H. Armengol-Relats, M. E. de Orbe, J. N. Korber and A. M. Echavarren. "Acetylene as a Dicarbene Equivalent for Gold(I) Catalysis: Total Synthesis of Waitziacuminone in One Step." *Angew. Chem. Int. Ed.*, **2020**, *59*, 4888-4891.

[159]G. Li and L. Zhang. "Gold-Catalyzed Intramolecular Redox Reaction of Sulfinyl Alkynes: Efficient Generation of α-Oxo Gold Carbenoids and Application in Insertion into R-CO Bonds." *Angew. Chem. Int. Ed.*, **2007**, *46*, 5156-5159.

[160]N. D. Shapiro and F. D. Toste. "Rearrangement of Alkynyl Sulfoxides Catalyzed by Gold(I) Complexes." *J. Am. Chem. Soc.*, **2007**, *129*, 4160-4161.

[161]Z. Zheng, Z. Wang, Y. Wang and L. Zhang. "Au-Catalysed oxidative cyclisation." *Chem. Soc. Rev.*, **2016**, *45*, 4448-4458.

[162]D. B. Huple, S. Ghorpade and R.-S. Liu. "Gold-Catalyzed Oxidative Cycloadditions to Activate a Quinoline Framework." *Chem. Eur. J.*, **2013**, *19*, 12965-12969.

[163]R. Dorel and A. M. Echavarren. "Gold(I)-Catalyzed Activation of Alkynes for the Construction of Molecular Complexity." *Chem. Rev.*, **2015**, *115*, 9028-9072.

[164]S. G. Modha, A. Kumar, D. D. Vachhani, J. Jacobs, S. K. Sharma, V. S. Parmar, L. Van Meervelt and E. V. Van der Eycken. "A Diversity-Oriented Approach to Spiroindolines: Post-Ugi Gold-Catalyzed Diastereoselective Domino Cyclization." *Angew. Chem. Int. Ed.*, **2012**, *51*, 9572-9575.

[165]P. M. Barbour, L. J. Marholz, L. Chang, W. Xu and X. Wang. "Gold Approaches to Polycyclic Indole Alkaloids." *Chemistry Letters.* **2014**, *43*, 572-578.

[166]A. S. K. Hashmi, M. Rudolph, J. Huck, W. Frey, J. W. Bats and M. Hamzić. "Gold Catalysis: Switching the Pathway of the Furan-Yne Cyclization." *Angew. Chem. Int. Ed.*, **2009**, *48*, 5848-5852.

[167]G. Fang and X. Bi. "Silver-catalysed reactions of alkynes: recent advances." *Chem. Soc. Rev.*, **2015**, *44*, 8124-8173.

[168]D. Weber and M. R. Gagné. "Dinuclear Gold−Silver Resting States May Explain Silver Effects in Gold(I)-Catalysis." *Org. Chem.*, **2009**, *11*, 4962-4965.

[169]D. Wang, R. Cai, S. Sharma, J. Jirak, S. K. Thummanapelli, N. G. Akhmedov, H. Zhang, X. Liu, J. L. Petersen and X. Shi. "“Silver Effect” in Gold(I) Catalysis: An Overlooked Important Factor." *J. Am. Chem. Soc.*, **2012**, *134*, 9012-9019.

[170]A. Zhdanko and M. E. Maier. "Explanation of "Silver Effects" in Gold(I)-Catalyzed Hydroalkoxylation of Alkynes." *ACS Catal.*, **2015**, *5*, 5994-6004.

[171]Z. Lu, J. Han, G. B. Hammond and B. Xu. "Revisiting the Influence of Silver in Cationic Gold Catalysis: A Practical Guide." *Org. Chem.*, **2015**, *17*, 4534-4537.

[172]A. Homs, I. Escofet and A. M. Echavarren. "On the Silver Effect and the Formation of Chloride-Bridged Digold Complexes." *Org. Lett.*, **2013**, *15*, 5782-5785.

[173]M. A. Tarselli, A. R. Chianese, S. J. Lee and M. R. Gagné. "Gold(I)-Catalyzed Asymmetric Cycloisomerization of Eneallenes into Vinylcyclohexenes." *Angew. Chem. Int. Ed.*, **2007**, *46*, 6670-6673.

[174]M. Veguillas, G. M. Rosair, M. W. P. Bebbington and A.-L. Lee. "Silver Effect in Regiodivergent Gold-Catalyzed Hydroaminations." *ACS Catal.*, **2019**, *9*, 2552-2557.

[175]H. A. Wegner. "Oxidative coupling reactions with gold." *Chimia.* **2009**, *63*, 44-48.

[176]A. Kar, N. Mangu, H. M. Kaiser, M. Beller and M. K. Tse. "A general gold-catalyzed direct oxidative coupling of non-activated arenes." *Chem. Commun.*, **2008**, 386-388.

[177]G. Zhang, Y. Peng, L. Cui and L. Zhang. "Gold-Catalyzed Homogeneous Oxidative Cross-Coupling Reactions." *Angew. Chem. Int. Ed.*, **2009**, *48*, 3112-3115.

[178]G. Zhang, L. Cui, Y. Wang and L. Zhang. "Homogeneous Gold-Catalyzed Oxidative Carboheterofunctionalization of Alkenes." *J. Am. Chem. Soc.*, **2010**, *132*, 1474-1475.

[179]T. de Haro and C. Nevado. "Gold-Catalyzed Ethynylation of Arenes." *J. Am. Chem. Soc.*, **2010**, *132*, 1512-1513.

[180]L. T. Ball, G. C. Lloyd-Jones and C. A. Russell. "Gold-Catalyzed Direct Arylation." *Science.* **2012**, *337*, 1644.

[181]L. T. Ball, G. C. Lloyd-Jones and C. A. Russell. "Gold-Catalyzed Oxidative Coupling of Arylsilanes and Arenes: Origin of Selectivity and Improved Precatalyst." *J. Am. Chem. Soc.*, **2014**, *136*, 254-264.

[182]M. Hofer, A. Genoux, R. Kumar and C. Nevado. "Gold-Catalyzed Direct Oxidative Arylation with Boron Coupling Partners." *Angew. Chem. Int. Ed.*, **2017**, *56*, 1021-1025.

[183]C. Fricke, A. Dahiya, W. B. Reid and F. Schoenebeck. "Gold-Catalyzed C–H Functionalization with Aryl Germanes." *ACS Catal.*, **2019**, *9*, 9231-9236.

[184]A. Dahiya, C. Fricke and F. Schoenebeck. "Gold-Catalyzed Chemoselective Couplings of Polyfluoroarenes with Aryl Germanes and Downstream Diversification." *J. Am. Chem. Soc.*, **2020**, *142*, 7754-7759.

[185]X. C. Cambeiro, T. C. Boorman, P. Lu and I. Larrosa. "Redox-Controlled Selectivity of C-H Activation in the Oxidative Cross-Coupling of Arenes." *Angew. Chem. Int. Ed.*, **2013**, *52*, 1781-1784.

[186]X. C. Cambeiro, N. Ahlsten and I. Larrosa. "Au-Catalyzed Cross-Coupling of Arenes via Double C–H Activation." *J. Am. Chem. Soc.*, **2015**, *137*, 15636-15639.

[187]R. A. Angnes, Z. Li, C. R. D. Correia and G. B. Hammond. "Recent synthetic additions to the visible light photoredox catalysis toolbox." *Org. Biomol. Chem.*, **2015**, *13*, 9152-9167.

[188]T. de Haro and C. Nevado. "Gold-Catalyzed Ethynylation of Arenes." *J. Am. Chem. Soc.*, **2010**, *132*, 1512-1513.

[189]T. de Haro and C. Nevado. "Flexible Gold-Catalyzed Regioselective Oxidative Difunctionalization of Unactivated Alkenes." *Angew. Chem. Int. Ed.*, **2011**, *50*, 906-910.

[190]M. Hofer and C. Nevado. "Cross-coupling of arene-gold(III) complexes." *Tetrahedron*. **2013**, *69*, 5751-5757.

[191]M. Hofer, A. Genoux, R. Kumar and C. Nevado. "Gold-Catalyzed Direct Oxidative Arylation with Boron Coupling Partners." *Angew. Chem., Int. Ed.*, **2017**, *56*, 1021-1025.

[192]X. C. Cambeiro, N. Ahlsten and I. Larrosa. "Au-Catalyzed Cross-Coupling of Arenes via Double C-H Activation." *J. Am. Chem. Soc.*, **2015**, *137*, 15636-15639.

[193]L. T. Ball, G. C. Lloyd-Jones and C. A. Russell. "Gold-Catalyzed Oxidative Coupling of Arylsilanes and Arenes: Origin of Selectivity and Improved Precatalyst." *J. Am. Chem. Soc.*, **2014**, *136*, 254-264.

[194]A. Johnson and R. J. Puddephatt. "Reactions of trifluoromethyl iodide with methylgold(I) complexes. Preparation of trifluoromethyl-gold(I) and -gold(III) complexes." *J. Chem. Soc. Dalton Trans.*, **1976**, 1360-1363.

[195]C. Aprile, M. Boronat, B. Ferrer, A. Corma and H. Garcia. "Radical Trapping by Gold Chlorides Forming Organogold Intermediates." *J. Am. Chem. Soc.*, **2006**, *128*, 8388-8389.

[196]B. Sahoo, M. N. Hopkinson and F. Glorius. "Combining Gold and Photoredox Catalysis: Visible Light-Mediated Oxy- and Aminoarylation of Alkenes." *J. Am. Chem. Soc.*, **2013**, *135*, 5505-5508.

[197]X.-z. Shu, M. Zhang, Y. He, H. Frei and F. D. Toste. "Dual Visible Light Photoredox and Gold-Catalyzed Arylative Ring Expansion." *J. Am. Chem. Soc.*, **2014**, *136*, 5844-5847.

[198]L. Huang, M. Rudolph, F. Rominger and A. S. K. Hashmi. "Photosensitizer-Free Visible-Light-Mediated Gold-Catalyzed 1,2-Difunctionalization of Alkynes." *Angew. Chem. Int. Ed.*, **2016**, *55*, 4808-4813.

[199]Q. Zhang, Z.-Q. Zhang, Y. Fu and H.-Z. Yu. "Mechanism of the Visible Light-Mediated Gold-Catalyzed Oxyarylation Reaction of Alkenes." *ACS Catal.*, **2016**, *6*, 798-808.

[200]S. Witzel, J. Xie, M. Rudolph and A. S. K. Hashmi. "Photosensitizer-Free, Gold-Catalyzed C-C Cross-Coupling of Boronic Acids and Diazonium Salts Enabled by Visible Light." *Adv. Synth. Catal.*, **2017**, *359*, 1522-1528.

[201]S. Witzel, K. Sekine, M. Rudolph and A. S. K. Hashmi. "New transmetalation reagents for the gold-catalyzed visible light-enabled C(sp or sp^2)-C(sp^2) cross-coupling with aryldiazonium salts in the absence of a photosensitizer." *Chem. Commun.*, **2018**, *54*, 13802-13804.

[202]J. Xie, K. Sekine, S. Witzel, P. Krämer, M. Rudolph, F. Rominger and A. S. K. Hashmi. "Light-Induced Gold-Catalyzed Hiyama Arylation: A Coupling Access to Biarylboronates." *Angew. Chem. Int. Ed.*, **2018**, *57*, 16648-16653.

[203]Y. Liu, Y. Yang, R. Zhu, C. Liu and D. Zhang. "The Dual Role of Gold(I) Complexes in Photosensitizer-Free Visible-Light-Mediated Gold-Catalyzed 1,2-Difunctionalization of Alkynes: A DFT Study." *Chem. Eur. J.*, **2018**, *24*, 14119-14126.

[204]I. Fernandez, L. P. Wolters and F. M. Bickelhaupt. "Controlling the oxidative addition of aryl halides to Au(I)." *J. Comput. Chem.*, **2014**, *35*, 2140-2145.

[205]C.-Y. Wu, T. Horibe, C. B. Jacobsen and F. D. Toste. "Stable gold(III) catalysts by oxidative addition of a carbon-carbon bond." *Nature*. **2015**, *517*, 449-454.

[206]A. Zeineddine, A. Amgoune, D. Bourissou, L. Estevez, K. Miqueu, L. Estevez and S. Mallet-Ladeira. "Rational development of catalytic Au(I)/Au(III) arylation involving mild oxidative addition of aryl halides." *Nat. Commun.*, **2017**, *8*, 565-572.

[207]A. Tlahuext-Aca, M. N. Hopkinson, C. G. Daniliuc and F. Glorius. "Oxidative Addition to Gold(I) by

Photoredox Catalysis: Straightforward Access to Diverse (C,N)-Cyclometalated Gold(III) Complexes." *Chem. Eur. J.*, **2016**, *22*, 11587-11592.

[208]S. Kim and F. D. Toste. "Mechanism of Photoredox-Initiated C–C and C–N Bond Formation by Arylation of IPrAu(I)–CF_3 and IPrAu(I)–Succinimide." *J. Am. Chem. Soc.*, **2019**, *141*, 4308-4315.

[209]M. N. Hopkinson, B. Sahoo and F. Glorius. "Dual Photoredox and Gold Catalysis: Intermolecular Multicomponent Oxyarylation of Alkenes." *Adv. Synth. Catal.*, **2014**, *356*, 2794-2800.

[210]Z. Xia, O. Khaled, V. Mouriès-Mansuy, C. Ollivier and L. Fensterbank. "Dual Photoredox/Gold Catalysis Arylative Cyclization of o-Alkynylphenols with Aryldiazonium Salts: A Flexible Synthesis of Benzofurans." *J. Org. Chem.*, **2016**, *81*, 7182-7190.

[211]C. Qu, S. Zhang, H. Du and C. Zhu. "Cascade photoredox/gold catalysis: access to multisubstituted indoles via aminoarylation of alkynes." *Chem. Commun.*, **2016**, *52*, 14400-14403.

[212]A. H. Bansode, S. R. Shaikh, R. G. Gonnade and N. T. Patil. "Intramolecular *ipso*-arylative cyclization of aryl-alkynoates and *N*-arylpropiolamides with aryldiazonium salts through merged gold/visible light photoredox catalysis." *Chem. Commun.*, **2017**, *53*, 9081-9084.

[213]Z.-S. Wang, T.-D. Tan, C.-M. Wang, D.-Q. Yuan, T. Zhang, P. Zhu, C. Zhu, J.-M. Zhou and L.-W. Ye. "Dual gold/photoredox-catalyzed bis-arylative cyclization of chiral homopropargyl sulfonamides with diazonium salts: rapid access to enantioenriched 2,3-dihydropyrroles." *Chem. Commun.*, **2017**, *53*, 6848-6851.

[214]B. Alcaide, P. Almendros, E. Busto, F. Herrera, C. Lázaro-Milla and A. Luna. "Photopromoted Entry to Benzothiophenes, Benzoselenophenes, 3H-Indoles, Isocoumarins, Benzosultams, and (Thio)flavones by Gold-Catalyzed Arylative Heterocyclization of Alkynes." *Adv. Synth. Catal.*, **2017**, *359*, 2640-2652.

[215]B. Alcaide, P. Almendros, E. Busto and C. Lazaro-Milla. "Photoinduced Gold-Catalyzed Domino C(sp) Arylation/Oxyarylation of TMS-Terminated Alkynols with Arenediazonium Salts." *J. Org. Chem.*, **2017**, *82*, 2177-2186.

[216]B. Alcaide, P. Almendros, B. Aparicio, C. Lazaro-Milla, A. Luna and O. N. Faza. "Gold-Photoredox-Cocatalyzed Tandem Oxycyclization/Coupling Sequence of Allenols and Diazonium Salts with Visible Light Mediation." *Adv. Synth. Catal.*, **2017**, *359*, 2789-2800.

[217]M. O. Akram, S. Banerjee, S. S. Saswade, V. Bedi and N. T. Patil. "Oxidant-free oxidative gold catalysis: the new paradigm in cross-coupling reactions." *Chem. Commun.*, **2018**, *54*, 11069-11083.

[218]Y. He, H. Wu and F. D. Toste. "A dual catalytic strategy for carbon–phosphorus cross-coupling via gold and photoredox catalysis." *Chem. Sci.*, **2015**, *6*, 1194-1198.

[219]A. Tlahuext-Aca, M. N. Hopkinson, B. Sahoo and F. Glorius. "Dual gold/photoredox-catalyzed C(sp)–H arylation of terminal alkynes with diazonium salts." *Chem. Sci.*, **2016**, *7*, 89-93.

[220]S. Kim, J. Rojas-Martin and F. D. Toste. "Visible light-mediated gold-catalysed carbon(sp^2)–carbon(sp) cross-coupling." *Chem. Sci.*, **2016**, *7*, 85-88.

[221]M. O. Akram, P. S. Mali and N. T. Patil. "Cross-Coupling Reactions of Aryldiazonium Salts with Allylsilanes under Merged Gold/Visible-Light Photoredox Catalysis." *Org. Lett.*, **2017**, *19*, 3075-3078.

[222]I. Chakrabarty, M. O. Akram, S. Biswas and N. T. Patil. "Visible light mediated desilylative C(sp^2)–C(sp^2) cross-coupling reactions of arylsilanes with aryldiazonium salts under Au(I)/Au(III) catalysis." *Chem. Commun.*, **2018**, *54*, 7223-7226.

[223]T. Cornilleau, P. Hermange and E. Fouquet. "Gold-catalysed cross-coupling between aryldiazonium salts and arylboronic acids: probing the usefulness of photoredox conditions." *Chem. Commun.*, **2016**, *52*, 10040-10043.

[224]V. Gauchot and A.-L. Lee. "Dual gold photoredox C(sp^2)–C(sp^2) cross couplings – development and mechanistic studies." *Chem. Commun.*, **2016**, *52*, 10163-10166.

[225]V. Gauchot, D. R. Sutherland and A. L. Lee. "Dual gold and photoredox catalyzed C-H activation of arenes for aryl-aryl cross couplings." *Chem. Sci.*, **2017**, *8*, 2885-2889.

[226]C. Sauer, Y. Liu, A. De Nisi, S. Protti, M. Fagnoni and M. Bandini. "Photocatalyst-free, Visible Light Driven, Gold Promoted Suzuki Synthesis of (Hetero)biaryls." *ChemCatChem.* **2017**, *9*, 4456-4459.

[227]J.-R. Deng, W.-C. Chan, N. Chun-Him Lai, B. Yang, C.-S. Tsang, C.-B. K. Ben, S. Lai-Fung Chan and M.-K. Wong. "Photosensitizer-free visible light-mediated gold-catalyzed *cis*-difunctionalization of silyl-substituted alkynes." *Chem. Sci.*, **2017**, *8*, 7537-7544.

[228]T. McCallum, S. Rohe and L. Barriault. "Thieme Chemistry Journals Awardees – Where Are They Now? What's Golden: Recent Advances in Organic Transformations Using Photoredox Gold Catalysis." *Synlett.* **2017**, *28*, 289-305.

[229]J. Xie, H. Jin and A. S. K. Hashmi. "The recent achievements of redox-neutral radical C–C cross-coupling enabled by visible-light." *Chem. Soc. Rev.*, **2017**, *46*, 5193-5203.

[230]M. Zidan, S. Rohe, T. McCallum and L. Barriault. "Recent advances in mono and binuclear gold photoredox catalysis." *Catal. Sci. Technol.*, **2018**, *8*, 6019-6028.

[231]C. M. Che, H. L. Kwong, V. W. W. Yam and K. C. Cho. "Spectroscopic properties and redox chemistry of the phosphorescent excited state of $[Au_2(dppm)_2]^{2+}$ [dppm = bis(diphenylphosphino)methane]." *J. Chem. Soc., Chem. Commun.*, **1989**, 885-886.

[232]G. Revol, T. McCallum, M. Morin, F. Gagosz and L. Barriault. "Photoredox Transformations with Dimeric Gold Complexes." *Angew. Chem. Int. Ed.*, **2013**, *52*, 13342-13345.

[233]C. Ma, C. T.-L. Chan, W.-P. To, W.-M. Kwok and C.-M. Che. "Deciphering Photoluminescence Dynamics and Reactivity of the Luminescent Metal-Metal-Bonded Excited State of a Binuclear Gold(I) Phosphine Complex Containing Open Coordination Sites." *Chem. Eur. J.*, **2015**, *21*, 13888-13893.

[234]C. D. McTiernan, M. Morin, T. McCallum, J. C. Scaiano and L. Barriault. "Polynuclear gold(I) complexes in photoredox catalysis: understanding their reactivity through characterization and kinetic analysis." *Catal. Sci. Technol.*, **2016**, *6*, 201-207.

[235]S. J. Kaldas, A. Cannillo, T. McCallum and L. Barriault. "Indole Functionalization via Photoredox Gold Catalysis." *Org. Chem.*, **2015**, *17*, 2864-2866.

[236]A. Cannillo, T. R. Schwantje, M. Bégin, F. Barabé and L. Barriault. "Gold-Catalyzed Photoredox C(sp^2) Cyclization: Formal Synthesis of (±)-Triptolide." *Org. Chem.*, **2016**, *18*, 2592-2595.

[237]F. M. Miloserdov, M. S. Kirillova, M. E. Muratore and A. M. Echavarren. "Unified Total Synthesis of Pyrroloazocine Indole Alkaloids Sheds Light on Their Biosynthetic Relationship." *J. Am. Chem. Soc.*, **2018**, *140*, 5393-5400.

[238]S. Rohe, T. McCallum, A. O. Morris and L. Barriault. "Transformations of Isonitriles with Bromoalkanes Using Photoredox Gold Catalysis." *J. Org. Chem.*, **2018**, *83*, 10015-10024.

[239]T. McCallum and L. Barriault. "Direct alkylation of heteroarenes with unactivated bromoalkanes using photoredox gold catalysis." *Chem. Sci.*, **2016**, *7*, 4754-4758.

[240]T. McCallum, E. Slavko, M. Morin and L. Barriault. "Light-Mediated Deoxygenation of Alcohols with a Dimeric Gold Catalyst." *Eur. J. Org. Chem.*, **2015**, *2015*, 81-85.

[241]H. Tran, T. McCallum, M. Morin and L. Barriault. "Homocoupling of Iodoarenes and Bromoalkanes Using Photoredox Gold Catalysis: A Light Enabled Au(III) Reductive Elimination." *Org. Chem.*, **2016**, *18*, 4308-4311.

[242]F. Nzulu, S. Telitel, F. Stoffelbach, B. Graff, F. Morlet-Savary, J. Lalevée, L. Fensterbank, J.-P. Goddard and C. Ollivier. "A dinuclear gold(I) complex as a novel photoredox catalyst for light-induced atom transfer radical polymerization." *Polym. Chem.*, **2015**, *6*, 4605-4611.

[243]J. Xie, T. Zhang, F. Chen, N. Mehrkens, F. Rominger, M. Rudolph and A. S. K. Hashmi. "Gold-Catalyzed Highly Selective Photoredox C(sp^2)–H Difluoroalkylation and Perfluoroalkylation of Hydrazones." *Angew. Chem. Int. Ed.*, **2016**, *55*, 2934-2938.

[244]J. Xie, J. Li, V. Weingand, M. Rudolph and A. S. K. Hashmi. "Intermolecular Photocatalyzed Heck-like Coupling of Unactivated Alkyl Bromides by a Dinuclear Gold Complex." *Chem. Eur. J.*, **2016**, *22*, 12646-12650.

[245]J. Xie, S. Shi, T. Zhang, N. Mehrkens, M. Rudolph and A. S. K. Hashmi. "A Highly Efficient Gold-Catalyzed Photoredox α-C(sp^3)-H Alkynylation of Tertiary Aliphatic Amines with Sunlight." *Angew. Chem. Int. Ed.*, **2015**, *54*, 6046-6050.

[246]Y. Zhao, J. Jin and P. W. H. Chan. "Gold Catalyzed Photoredox C1-Alkynylation of *N*-Alkyl-1,2,3,4-tetrahydroisoquinolines by 1-Bromoalkynes with UVA LED Light." *Adv. Synth. Catal.*, **2019**, *361*, 1313-1321.

[247]M. D. Levin and F. D. Toste. "Gold-Catalyzed Allylation of Aryl Boronic Acids: Accessing Cross-Coupling Reactivity with Gold." *Angew. Chem. Int. Ed.*, **2014**, *53*, 6211-6215.

[248]J. Serra, T. Parella and X. Ribas. "Au(III)-aryl intermediates in oxidant-free C–N and C–O cross-coupling catalysis." *Chem. Sci.*, **2017**, *8*, 946-952.

[249]R. Cai, M. Lu, E. Y. Aguilera, Y. Xi, N. G. Akhmedov, J. L. Petersen, H. Chen and X. Shi. "Ligand-Assisted Gold-Catalyzed Cross-Coupling with Aryldiazonium Salts: Redox Gold Catalysis without an External Oxidant." *Angew. Chem. Int. Ed.*, **2015**, *54*, 8772-8776.

[250]E. O. Asomoza-Solís, J. Rojas-Ocampo, R. A. Toscano and S. Porcel. "Arenediazonium salts as electrophiles for the oxidative addition of gold(I)." *Chem. Commun.*, **2016**, *52*, 7295-7298.

[251]M. Rigoulet, O. Thillaye du Boullay, A. Amgoune and D. Bourissou. "Gold(I)/Gold(III) Catalysis that Merges Oxidative Addition and π-Alkene Activation." *Angew. Chem. Int. Ed.*, **2020**, 10.1002/anie.202006074.

[252]A. G. Tathe, C. C. Chintawar, V. W. Bhoyare and N. T. Patil. "Ligand-enabled gold-catalyzed 1,2-heteroarylation of alkenes." *Chem. Commun.*, **2020**, *56*, 9304-9307.

[253]P. Lawrence Kuch and R. Stuart Tobias. "Synthesis of cationic dialkylgold(III) complexes: nature of the facile reductive elimination of alkane." *J. Organomet. Chem.*, **1976**, *122*, 429-446.

[254]S. Komiya, T. Sone, S. Ozaki, M. Ishikawa and N. Kasuga. "Synthesis, structure and properties of dimethyl(alkoxycarbonyl)gold(III) complexes having a triphenylphosphine ligand." *J. Organomet. Chem.*, **1992**, *428*, 303-313.

[255]S. Liu, K. Kang, S. Liu, D. Wang, P. Wei, Y. Lan and Q. Shen. "The Difluoromethylated Organogold(III) Complex *cis*-[Au(PCy_3)(4-F-C_6H_4)(CF_2H)(Cl)]: Preparation, Characterization, and Its C(sp^2)-CF_2H Reductive Elimination." *Organometallics.* **2018**, *37*, 3901-3908.

[256]D. M. Kaphan, M. D. Levin, R. G. Bergman, K. N. Raymond and F. D. Toste. "A supramolecular microenvironment strategy for transition metal catalysis." *Science.* **2015**, *350*, 1235-1238.

[257]J. Vicente, M. D. Bermúdez, J. Escribano, M. P. Carrillo and P. G. Jones. "Synthesis of intermediates in the C-H activation of acetone with 2-phenylazophenylgold(III) complexes and in the C-C coupling of aryl groups from diarylgold(III) complexes." *J. Chem. Soc. Dalton Trans.*, **1990**, 3083-3089.

[258]L. Rocchigiani, J. Fernandez-Cestau, P. H. M. Budzelaar and M. Bochmann. "Reductive Elimination Leading to C-C Bond Formation in Gold(III) Complexes: A Mechanistic and Computational Study." *Chem. Eur. J.*, **2018**, *24*, 8893-8903.

[259]A. Genoux, J. González, E. Merino, C. Nevado and E. Merino. "Mechanistic Insights into C(sp^2)-C(sp)N Reductive Elimination from Gold(III) Cyanide Complexes." *Angew. Chem. Int. Ed.*, **2020**,

10.1002/anie.202005731.

[260]K. K.-Y. Kung, H.-M. Ko, J.-F. Cui, H.-C. Chong, Y.-C. Leung and M.-K. Wong. "Cyclometalated gold(III) complexes for chemoselective cysteine modification via ligand controlled C-S bond-forming reductive elimination." *Chem. Commun.*, **2014**, *50*, 11899-11902.

[261]L. Currie, L. Rocchigiani, D. L. Hughes and M. Bochmann. "Carbon-sulfur bond formation by reductive elimination of gold(III) thiolates." *Dalton Trans.*, **2018**, *47*, 6333-6343.

[262]J. H. Kim, R. T. Mertens, A. Agarwal, S. Parkin, G. Berger and S. G. Awuah. "Direct intramolecular carbon(sp^2)-nitrogen(sp^2) reductive elimination from gold(III)." *Dalton Trans.*, **2019**, *48*, 6273-6282.

[263]Q. Wu, C. Du, Y. Huang, X. Liu, Z. Long, F. Song and J. You. "Stoichiometric to catalytic reactivity of the aryl cycloaurated species with arylboronic acids: insight into the mechanism of gold-catalyzed oxidative C(sp^2)-H arylation." *Chem. Sci.*, **2015**, *6*, 288-293.

[264]V. J. Scott, J. A. Labinger and J. E. Bercaw. "Mechanism of Reductive Elimination of Methyl Iodide from a Novel Gold(III)-Monomethyl Complex." *Organometallics.* **2010**, *29*, 4090-4096.

[265]M. Blaya, D. Bautista, J. Gil-Rubio and J. Vicente. "Synthesis of Au(I) Trifluoromethyl Complexes. Oxidation to Au(III) and Reductive Elimination of Halotrifluoromethanes." *Organometallics.* **2014**, *33*, 6358-6368.

[266]G. R. Dey, A. K. El Omar, J. A. Jacob, M. Mostafavi and J. Belloni. "Mechanism of Trivalent Gold Reduction and Reactivity of Transient Divalent and Monovalent Gold Ions Studied by Gamma and Pulse Radiolysis." *J. Phys. Chem. A.* **2011**, *115*, 383-391.

[267]M. J. Katz, K. Sakai and D. B. Leznoff. "The use of aurophilic and other metal-metal interactions as crystal engineering design elements to increase structural dimensionality." *Chem. Soc. Rev.*, **2008**, *37*, 1884-1895.

[268]H. Schmidbaur and A. Schier. "Aurophilic interactions as a subject of current research: an up-date." *Chem. Soc. Rev.*, **2012**, *41*, 370-412.

[269]J. P. Weyrauch, A. S. K. Hashmi, A. Schuster, T. Hengst, S. Schetter, A. Littmann, M. Rudolph, M. Hamzic, J. Visus, F. Rominger, W. Frey and J. W. Bats. "Cyclization of Propargylic Amides: Mild Access to Oxazole Derivatives." *Chem. Eur. J.*, **2010**, *16*, 956-963.

[270]D. B. England and A. Padwa. "Gold-Catalyzed Cycloisomerization of *N*-Propargylindole-2-carboxamides: Application toward the Synthesis of Lavendamycin Analogues." *Org. Chem.*, **2008**, *10*, 3631-3634.

[271]K. Nakamura, S. Furumi, M. Takeuchi, T. Shibuya and K. Tanaka. "Enantioselective Synthesis and Enhanced Circularly Polarized Luminescence of S-Shaped Double Azahelicenes." *J. Am. Chem. Soc.*, **2014**, *136*, 5555-5558.

[272]J. Li, Y. Yang, Z. Wang, B. Feng and J. You. "Rhodium(III)-Catalyzed Annulation of Pyridinones with Alkynes via Double C–H Activation: A Route to Functionalized Quinolizinones." *Org. Chem.*, **2017**, *19*, 3083-3086.

[273]H. Yu, G. Zhang and H. Huang. "Palladium-Catalyzed Dearomative Cyclocarbonylation by C-N Bond Activation." *Angew. Chem. Int. Ed.*, **2015**, *54*, 10912-10916.

[274]S. Wang and L. Zhang. "A Highly Efficient Preparative Method of α-Ylidene-β-Diketones via Au(III)-Catalyzed Acyl Migration of Propargylic Esters." *J. Am. Chem. Soc.*, **2006**, *128*, 8414-8415.

[275]S. Wang and L. Zhang. "A Gold-Catalyzed Unique Cycloisomerization of 1,5-Enynes: Efficient Formation of 1-Carboxycyclohexa-1,4-dienes and Carboxyarenes." *J. Am. Chem. Soc.*, **2006**, *128*, 14274-14275.

[276]A. Dar, K. Moss, S. M. Cottrill, R. V. Parish, C. A. McAuliffe, R. G. Pritchard, B. Beagley and J. Sandbank. "Complexes of gold(III) and mononegative bidentate N,O-ligands." *J. Chem. Soc., Dalton Trans.*, **1992**, 1907-1913.

[277]K. Sennewald, W. Vogt and H. Glaser, *Vinyl acetate*. 1967, DE1244766B, Knapsack.

[278]C. Wang and D. Astruc. "Nanogold plasmonic photocatalysis for organic synthesis and clean energy conversion." *Chem. Soc. Rev.*, **2014**, *43*, 7188-7216.

[279]D. Astruc, F. Lu and J. R. Aranzaes. "Nanoparticles as Recyclable Catalysts: The Frontier between Homogeneous and Heterogeneous Catalysis." *Angew. Chem. Int. Ed.*, **2005**, *44*, 7852-7872.

[280]M. Haruta, N. Yamada, T. Kobayashi and S. Iijima. "Gold catalysts prepared by coprecipitation for low-temperature oxidation of hydrogen and of carbon monoxide." *J. Catal.*, **1989**, *115*, 301-309.

[281]M. D. Hughes, Y.-J. Xu, P. Jenkins, P. McMorn, P. Landon, D. I. Enache, A. F. Carley, G. A. Attard, G. J. Hutchings, F. King, E. H. Stitt, P. Johnston, K. Griffin and C. J. Kiely. "Tunable gold catalysts for selective hydrocarbon oxidation under mild conditions." *Nature*, **2005**, *437*, 1132-1135.

[282]J. K. Edwards, B. Solsona, E. N. N, A. F. Carley, A. A. Herzing, C. J. Kiely and G. J. Hutchings. "Switching Off Hydrogen Peroxide Hydrogenation in the Direct Synthesis Process." *Science*, **2009**, *323*, 1037-1041.

[283]B. S. Takale, M. Bao and Y. Yamamoto. "Gold nanoparticle (AuNPs) and gold nanopore (AuNPore) catalysts in organic synthesis." *Org. Biomol. Chem.*, **2014**, *12*, 2005-2027.

[284]S. Liang, J. Jasinski, G. B. Hammond and B. Xu. "Supported Gold Nanoparticle-Catalyzed Hydration of Alkynes under Basic Conditions." *Org. Chem.*, **2015**, *17*, 162-165.

[285]S. Carrettin, M. C. Blanco, A. Corma and A. S. K. Hashmi. "Heterogeneous Gold-Catalysed Synthesis of Phenols." *Adv. Synth. Catal.*, **2006**, *348*, 1283-1288.

[286]S. Carrettin, J. Guzman and A. Corma. "Supported Gold Catalyzes the Homocoupling of Phenylboronic Acid with High Conversion and Selectivity." *Angew. Chem. Int. Ed.*, **2005**, *44*, 2242-2245.

[287]B. Nkosi, N. J. Coville and G. J. Hutchings. "Reactivation of a supported gold catalyst for acetylene hydrochlorination." *J. Chem. Soc. Chem. Commun.*, **1988**, 71-72.

[288]H. Gu, X. Sun, Y. Wang, H. Wu and P. Wu. "Highly efficient mesoporous polymer supported phosphine-gold(I) complex catalysts for amination of allylic alcohols and intramolecular cyclization reactions." *RSC Adv.*, **2018**, *8*, 1737-1743.

[289]C. Lothschütz, J. Szlachetko and J. A. van Bokhoven. "Heterogenized Gold(I)–Carbene as a Single-Site Catalyst in Continuous Flow." *ChemCatChem.*, **2014**, *6*, 443-448.

[290]S. Tšupova, A. Cadu, S. A. C. Carabineiro, M. Rudolph and A. S. K. Hashmi. "Solid-supported nitrogen acyclic carbene (SNAC) complexes of gold: Preparation and catalytic activity." *J. Catal.*, **2017**, *350*, 97-102.

[291]J. T. Sarmiento, S. Suárez-Pantiga, A. Olmos, T. Varea and G. Asensio. "Silica-Immobilized NHC-Gold(I) Complexes: Versatile Catalysts for the Functionalization of Alkynes under Batch and Continuous Flow Conditions." *ACS Catal.*, **2017**, *7*, 7146-7155.

[292]M. Jiang, Q. Nie and M. Cai. "Heterogeneous gold(I)-catalyzed cyclization between ynals and amidines: An efficient and practical synthesis of 2,4-disubstituted pyrimidines." *Synth. Commun.*, **2019**, *49*, 2488-2500.

[293]F. Yi, B. Huang, Q. Nie and M. Cai. "A heterogeneous gold(I)-catalyzed ring expansion of unactivated alkynylcyclopropanes with sulfonamides leading to (*E*)-2-alkylidenecyclobutanamines." *Tetrahedron Lett.*, **2016**, *57*, 4405-4410.

[294]C. Vriamont, M. Devillers, O. Riant and S. Hermans. "A covalently anchored homogeneous gold complex on carbon nanotubes: a reusable catalyst." *Chem. Commun.*, **2013**, *49*, 10504-10506.

[295]C. Vriamont, M. Devillers, O. Riant and S. Hermans. "Catalysis with Gold Complexes Immobilised on Carbon Nanotubes by π–π Stacking Interactions: Heterogeneous Catalysis versus the Boomerang Effect." *Chem. Eur. J.*, **2013**, *19*, 12009-12017.

[296]D. Ventura-Espinosa, S. Sabater and J. A. Mata. "Enhancement of gold catalytic activity and stability by immobilization on the surface of graphene." *J. Catal.*, **2017**, *352*, 498-504.

[297]R. Oda, I. Huc and S. J. Candau. "Gemini Surfactants as New, Low Molecular Weight Gelators of Organic

Solvents and Water." *Angew. Chem. Int. Ed.*, **1998**, *37*, 2689-2691.

[298]R. Oda, I. Huc, M. Schmutz, S. J. Candau and F. C. MacKintosh. "Tuning bilayer twist using chiral counterions." *Nature*. **1999**, *399*, 566-569.

[299]M. Attoui, E. Pouget, R. Oda, D. Talaga, G. Le Bourdon, T. Buffeteau and S. Nlate. "Optically Active Polyoxometalate-Based Silica Nanohelices: Induced Chirality from Inorganic Nanohelices to Achiral POM Clusters." *Chem. Eur. J.*, **2018**, *24*, 11344-11353.

[300]J. Cheng, G. Le Saux, J. Gao, T. Buffeteau, Y. Battie, P. Barois, V. Ponsinet, M.-H. Delville, O. Ersen, E. Pouget and R. Oda. "GoldHelix: Gold Nanoparticles Forming 3D Helical Superstructures with Controlled Morphology and Strong Chiroptical Property." *ACS Nano.* **2017**, *11*, 3806-3818.

[301]R. E. Ebule, D. Malhotra, G. B. Hammond and B. Xu. "Ligand Effects in the Gold Catalyzed Hydration of Alkynes." *Adv. Synth. Catal.*, **2016**, *358*, 1478-1481.

[302]M. D. Aparece and P. A. Vadola. "Gold-Catalyzed Dearomative Spirocyclization of Aryl Alkynoate Esters." *Org. Chem.*, **2014**, *16*, 6008-6011.

[303]C. M. Cobley, S. E. Skrabalak, D. J. Campbell and Y. Xia. "Shape-Controlled Synthesis of Silver Nanoparticles for Plasmonic and Sensing Applications." *Plasmonics.*, **2009**, *4*, 171-179.

[304]P. K. Jain, I. H. El-Sayed and M. A. El-Sayed. "Au nanoparticles target cancer." *Nano Today.* **2007**, *2*, 18-29.

[305]S. Hübner, J. G. de Vries and V. Farina. "Why Does Industry Not Use Immobilized Transition Metal Complexes as Catalysts?" *Adv. Synth. Catal.*, **2016**, *358*, 3-25.

[306]D. Zehm, W. Fudickar, M. Hans, U. Schilde, A. Kelling and T. Linker. "9,10-Diarylanthracenes as Molecular Switches: Syntheses, Properties, Isomerisations and Their Reactions with Singlet Oxygen." *Chem. Eur. J.*, **2008**, *14*, 11429-11441.

[307]S. Liao, C.-Y. Su, H.-X. Zhang, J.-L. Shi, Z.-Y. Zhou, H.-Q. Liu, A. S. C. Chan and B.-S. Kang. "Helical complexes from the self-assembly of silver salts and the polydentate thioether α,α'-bis(8-thioquinoline)-*m*-xylene." *Inorg. Chim. Acta.* **2002**, *336*, 151-156.

[308]M. Dell'Acqua, B. Castano, C. Cecchini, T. Pedrazzini, V. Pirovano, E. Rossi, A. Caselli and G. Abbiati. "Mild Regiospecific Synthesis of 1-Alkoxy-isochromenes Catalyzed by Well-Defined [Silver(I)(Pyridine-Containing Ligand)] Complexes." *J. Org. Chem.*, **2014**, *79*, 3494-3505.

[309]E. Parker, N. Leconte, T. Godet and P. Belmont. "Silver-catalyzed furoquinolines synthesis: from nitrogen effects to the use of silver imidazolate polymer as a new and robust silver catalyst." *Chem. Commun.*, **2011**, *47*, 343-345.

[310]T. J. Harrison, J. A. Kozak, M. Corbella-Pané and G. R. Dake. "Pyrrole Synthesis Catalyzed by AgOTf or Cationic Au(I) Complexes." *J. Org. Chem.*, **2006**, *71*, 4525-4529.

[311]A. J. Chalk. "1,5-Cyclooctadiene Complexes of Gold(I) and Gold(III)." *J. Am. Chem. Soc.*, **1964**, *86*, 4733-4734.

[312]F.-B. Xu, Q.-S. Li, L.-Z. Wu, X.-B. Leng, Z.-C. Li, X.-S. Zeng, Y. L. Chow and Z.-Z. Zhang. "Formation of Group 11 Metal(I)-Arene Complexes: Bonding Mode and Molecule-Responsive Spectral Variations." *Organometallics.* **2003**, *22*, 633-640.

[313]Q.-S. Li, C.-Q. Wan, R.-Y. Zou, F.-B. Xu, H.-B. Song, X.-J. Wan and Z.-Z. Zhang. "Gold(I) η^2-Arene Complexes." *Inorg. Chem.*, **2006**, *45*, 1888-1890.

[314]E. Herrero-Gómez, C. Nieto-Oberhuber, S. López, J. Benet-Buchholz and A. M. Echavarren. "Cationic η^1/η^2-Gold(I) Complexes of Simple Arenes." *Angew. Chem. Int. Ed.*, **2006**, *45*, 5455-5459.

[315]H. Schmidbaur and A. Schier. "Gold η^2-Coordination to Unsaturated and Aromatic Hydrocarbons: The Key Step in Gold-Catalyzed Organic Transformations." *Organometallics.*, **2010**, *29*, 2-23.

[316]H. Tanaka, Y. Inoue and T. Mori. "Circularly Polarized Luminescence and Circular Dichroisms in Small

Organic Molecules: Correlation between Excitation and Emission Dissymmetry Factors." *ChemPhotoChem.*, **2018**, *2*, 386-402.

[317]H. Maeda, Y. Bando, K. Shimomura, I. Yamada, M. Naito, K. Nobusawa, H. Tsumatori and T. Kawai. "Chemical-Stimuli-Controllable Circularly Polarized Luminescence from Anion-Responsive π-Conjugated Molecules." *J. Am. Chem. Soc.*, **2011**, *133*, 9266-9269.

[318]P. Reiné, A. M. Ortuño, S. Resa, L. Álvarez de Cienfuegos, V. Blanco, M. J. Ruedas-Rama, G. Mazzeo, S. Abbate, A. Lucotti, M. Tommasini, S. Guisán-Ceinos, M. Ribagorda, A. G. Campaña, A. Mota, G. Longhi, D. Miguel and J. M. Cuerva. "OFF/ON switching of circularly polarized luminescence by oxophilic interaction of homochiral sulfoxide-containing o-OPEs with metal cations." *Chem. Commun.*, **2018**, *54*, 13985-13988.

[319]N. Saleh, B. Moore Ii, M. Srebro, N. Vanthuyne, L. Toupet, J. A. G. Williams, C. Roussel, K. K. Deol, G. Muller, J. Autschbach and J. Crassous. "Acid/Base-Triggered Switching of Circularly Polarized Luminescence and Electronic Circular Dichroism in Organic and Organometallic Helicenes." *Chem. Eur. J.*, **2015**, *21*, 1673-1681.

[320]K. Takaishi, K. Iwachido and T. Ema. "Solvent-Induced Sign Inversion of Circularly Polarized Luminescence: Control of Excimer Chirality by Hydrogen Bonding." *J. Am. Chem. Soc.*, **2020**, *142*, 1774-1779.

[321]Z.-B. Sun, J.-K. Liu, D.-F. Yuan, Z.-H. Zhao, X.-Z. Zhu, D.-H. Liu, Q. Peng and C.-H. Zhao. "2,2'-Diamino-6,6'-diboryl-1,1'-binaphthyl: A Versatile Building Block for Temperature-Dependent Dual Fluorescence and Switchable Circularly Polarized Luminescence." *Angew. Chem. Int. Ed.*, **2019**, *58*, 4840-4846.

[322]J.-L. Ma, Q. Peng and C.-H. Zhao. "Circularly Polarized Luminescence Switching in Small Organic Molecules." *Chem. Eur. J.*, **2019**, *25*, 15441-15454.

[323]Y. Gao, C. Ren, X. Lin and T. He. "The Progress and Perspective of Organic Molecules With Switchable Circularly Polarized Luminescence." *Front. Chem.*, **2020**, 10.3389/fchem.2020.00458.

[324]R. Schmidt, W. Drews and H. D. Brauer. "Photolysis of the endoperoxide of heterocoerdianthrone. A concerted, adiabatic cycloreversion originating from an upper excited singlet state." *J. Am. Chem. Soc.*, **1980**, *102*, 2791-2797.

[325]K. B. Eisenthal, N. J. Turro, C. G. Dupuy, D. A. Hrovat, J. Langan, T. A. Jenny and E. V. Sitzmann. "State-selective photochemistry of singlet oxygen precursors: kinetics and wavelength dependence of the photodissociation of anthracene endoperoxides." *J. Phys. Chem.*, **1986**, *90*, 5168-5173.

[326]D. MacDowell and J. Nelson. "Facile synthesis of a new family of cage molecules." *Tetrahedron Lett.*, **1988**, *29*, 385-386.

[327]M. L. C. Quan and D. J. Cram. "Constrictive binding of large guests by a hemicarcerand containing four portals." *J. Am. Chem. Soc.*, **1991**, *113*, 2754-2755.

[328]S. Mendoza, P. D. Davidov and A. E. Kaifer. "Electrochemistry of Encapsulated Guests: Ferrocene inside Cram's Hemicarcerands." *Chem. Eur. J.*, **1998**, *4*, 864-870.

[329]S. Ro, S. J. Rowan, A. R. Pease, D. J. Cram and J. F. Stoddart. "Dynamic Hemicarcerands and Hemicarceplexes." *Org. Chem.*, **2000**, *2*, 2411-2414.

[330]J.-M. Lehn. "Dynamic Combinatorial Chemistry and Virtual Combinatorial Libraries." *Chem. Eur. J.*, **1999**, *5*, 2455-2463.

[331]J. J. Gassensmith, J. M. Baumes, J. Eberhard and B. D. Smith. "Cycloaddition to an anthracene-derived macrocyclic receptor with supramolecular control of regioselectivity." *Chem. Commun.*, **2009**, 2517-2519.

[332]W. Liu, A. G. Oliver and B. D. Smith. "Macrocyclic Receptor for Precious Gold, Platinum, or Palladium Coordination Complexes." *J. Am. Chem. Soc.*, **2018**, *140*, 6810-6813.

[333]H. Bouas-Laurent, A. Castellan, J.-P. Desvergne and R. Lapouyade. "Photodimerization of anthracenes in

fluid solution: structural aspects." *Chem. Soc. Rev.*, **2000**, *29*, 43-55.

[334]M. Yoshizawa and J. K. Klosterman. "Molecular architectures of multi-anthracene assemblies." *Chem. Soc. Rev.*, **2014**, *43*, 1885-1898.

[335]Y. Liu, X. Liu and R. Warmuth. "Multicomponent Dynamic Covalent Assembly of a Rhombicuboctahedral Nanocapsule." *Chem. Eur. J.*, **2007**, *13*, 8953-8959.

[336]M. Mastalerz. "One-pot synthesis of a shape-persistent endo-functionalised nano-sized adamantoid compound." *Chem. Commun.*, **2008**, 4756-4758.

[337]O. Francesconi, A. Ienco, G. Moneti, C. Nativi and S. Roelens. "A Self-Assembled Pyrrolic Cage Receptor Specifically Recognizes β-Glucopyranosides." *Angew. Chem. Int. Ed.*, **2006**, *45*, 6693-6696.

[338]K. Acharyya and P. S. Mukherjee. "A fluorescent organic cage for picric acid detection." *Chem. Commun.*, **2014**, *50*, 15788-91.

[339]T. Kunde, E. Nieland, H. V. Schröder, C. A. Schalley and B. M. Schmidt. "A porous fluorinated organic [4+4] imine cage showing CO_2 and H_2 adsorption." *Chem. Commun.*, **2020**, *56*, 4761-4764.

[340]J. C. Lauer, W.-S. Zhang, F. Rominger, R. R. Schröder and M. Mastalerz. "Shape-Persistent [4+4] Imine Cages with a Truncated Tetrahedral Geometry." *Chem. Eur. J.*, **2018**, *24*, 1816-1820.

[341]M. Arunachalam, I. Ravikumar and P. Ghosh. "A New Hexaaza Bicyclic Cyclophane with Dual Binding Sites." *J. Org. Chem.*, **2008**, *73*, 9144-9147.

[342]P. Mateus, R. Delgado, P. Brandão and V. Félix. "Polyaza Cryptand Receptor Selective for Dihydrogen Phosphate." *J. Org. Chem.*, **2009**, *74*, 8638-8646.

[343]R. L. Greenaway, V. Santolini, M. J. Bennison, B. M. Alston, C. J. Pugh, M. A. Little, M. Miklitz, E. G. B. Eden-Rump, R. Clowes, A. Shakil, H. J. Cuthbertson, H. Armstrong, M. E. Briggs, K. E. Jelfs and A. I. Cooper. "High-throughput discovery of organic cages and catenanes using computational screening fused with robotic synthesis." *Nat. Commun.*, **2018**, *9*, 2849.

[344]K. E. Jelfs, X. Wu, M. Schmidtmann, J. T. A. Jones, J. E. Warren, D. J. Adams and A. I. Cooper. "Large Self-Assembled Chiral Organic Cages: Synthesis, Structure, and Shape Persistence." *Angew. Chem. Int. Ed.*, **2011**, *50*, 10653-10656.

[345]T. Hasell, M. Schmidtmann, C. A. Stone, M. W. Smith and A. I. Cooper. "Reversible water uptake by a stable imine-based porous organic cage." *Chem. Commun.*, **2012**, *48*, 4689-4691.

[346]S. Jiang, H. J. Cox, E. I. Papaioannou, C. Tang, H. Liu, B. J. Murdoch, E. K. Gibson, I. S. Metcalfe, J. S. O. Evans and S. K. Beaumont. "Shape-persistent porous organic cage supported palladium nanoparticles as heterogeneous catalytic materials." *Nanoscale.*, **2019**, *11*, 14929-14936.

[347]H. Ding, Y. Yang, B. Li, F. Pan, G. Zhu, M. Zeller, D. Yuan and C. Wang. "Targeted synthesis of a large triazine-based [4+6] organic molecular cage: structure, porosity and gas separation." *Chem. Commun.*, **2015**, *51*, 1976-1979.

[348]B. Teng, M. A. Little, T. Hasell, S. Y. Chong, K. E. Jelfs, R. Clowes, M. E. Briggs and A. I. Cooper. "Synthesis of a Large, Shape-Flexible, Solvatomorphic Porous Organic Cage." *Cryst. Growth Des.*, **2019**, *19*, 3647-3651.

[349]M. M. Safont-Sempere, G. Fernández and F. Würthner. "Self-Sorting Phenomena in Complex Supramolecular Systems." *Chem. Rev.*, **2011**, *111*, 5784-5814.

[350]R. Kramer, J. M. Lehn and A. Marquis-Rigault. "Self-recognition in helicate self-assembly: spontaneous formation of helical metal complexes from mixtures of ligands and metal ions." *Proc. Natl. Acad. Sci.*, **1993**, *90*, 5394.

[351]K. Acharyya and P. S. Mukherjee. "Hydrogen-Bond-Driven Controlled Molecular Marriage in Covalent Cages." *Chem. Eur. J.*, **2014**, *20*, 1646-1657.

[352]M. Kołodziejski, A. R. Stefankiewicz and J.-M. Lehn. "Dynamic polyimine macrobicyclic cryptands – self-sorting with component selection." *Chem. Sci.*, **2019**, *10*, 1836-1843.

[353]S. Bera, K. Dey, T. K. Pal, A. Halder, S. Tothadi, S. Karak, M. Addicoat and R. Banerjee. "Porosity Switching in Polymorphic Porous Organic Cages with Exceptional Chemical Stability." *Angew. Chem. Int. Ed.*, **2019**, *58*, 4243-4247.

[354]D. Samanta, D. Galaktionova, J. Gemen, L. J. W. Shimon, Y. Diskin-Posner, L. Avram, P. Král and R. Klajn. "Reversible chromism of spiropyran in the cavity of a flexible coordination cage." *Nat. Commun.*, **2018**, *9*, 641.

[355]D. Zhang, J. R. Cochrane, S. Di Pietro, L. Guy, H. Gornitzka, J.-P. Dutasta and A. Martinez. "“Breathing” Motion of a Modulable Molecular Cavity." *Chem. Eur. J.*, **2017**, *23*, 6495-6498.

[356]A. S. Bhat, S. M. Elbert, W.-S. Zhang, F. Rominger, M. Dieckmann, R. R. Schröder and M. Mastalerz. "Transformation of a [4+6] Salicylbisimine Cage to Chemically Robust Amide Cages." *Angew. Chem. Int. Ed.*, **2019**, *58*, 8819-8823.

[357]M. Zgorzelak, J. Grajewski, J. Gawroński and M. Kwit. "Solvent-assisted synthesis of a shape-persistent chiral polyaza gigantocycle characterized by a very large internal cavity and extraordinarily high amplitude of the ECD exciton couplet." *Chem. Commun.*, **2019**, *55*, 2301-2304.

Titre: Complexes fonctionnels d'or et d'argent et supramolécules à base de 9,10 diphenylanthracènes: photoactivité, catalyse et propriétés chiroptiques

Résumé: Cette thèse décrit principalement la conception de ligands et la synthèse de leurs complexes d'or fonctionnels pour la catalyse. Des ligands thioéther ont été développés pour accéder aux complexes d'or (III) chlorure qui peuvent être photoréduits en l'or (I), en utilisant la lumière UV ou visible. Ces deux espèces d'or ont été exploitées en catalyse homogène en tant qu'acides de Lewis, lors d'une réaction 'one pot' de cyclisation en cascade conduisant à une composé polyhétéroaromatique fusionné. Des ligands de phosphine ont aussi été élaborés puis les complexes d'or(I) chlorure correspondants ont été greffés sur des nano-objets de silices pour la catalyse hétérogène. L'induction chirale des hélices de silices chirales sur les complexes d'or a été observée par dichroïsme circulaire. En présence de sels d'argent, les catalyseurs d'or immobilisés de manière covalente ont montré une réactivités élevée et une bonne recyclabilité lors de réactions de sipirocyclisation d'esters d'aryl alkynoates. D'autres ligands thioéther encombrés à base de 9,10-diphénylanthracène (DPA) ont été utilisés pour former des complexes d'argent, dont l'auto-assemblage peut être ajustée en fonction de la nature de l'anion associé à l'argent et en prolongeant la longueur de la chaîne de coordination. Leur forte activité en catalyse a été démontrée au cours de deux reactions tandem d'addition/ cycloisomérisation d'alcynes en utilisant une charge catalytique de 0.5 à 1 % mol. Finalement, la réactivité régiosélective et réversible du 9,10-DPA vis-à-vis de l'oxygène singulet a été exploitée sur deux systèmes moléculaires à propriétés commutables: d'une part, une cage hexa-imine commutable auto-assemblée comportant trois piliers DPA qui montre une affinité pour les ions métalliques et d'autre part, différents sulfoxydes chiraux positionnés sur la plateforme DPA dont les propriétés chiroptique sont conçues pour être commutables.

Mots clés: Ligand thioéther, complexes d'or, complexes d'argent, catalyse homo/hétérogène, cage moleculaire, sulfoxyde, propriétés chiroptiques

---

Title: Functional gold and silver complexes and supramolecules based on 9,10 diphenylanthracenes: Photoactivity, catalysis and chiroptical properties

Abstract: This thesis mainly describes the use of ligand design to achieve functional gold complexes for catalysis. Thioethers ligands were designed to form gold(III) chloride complexes which can be photoreduced to gold(I) using UV or visible light. Both gold species are lewis acids that are catalytically active and can be used in a 'one pot' cascade cyclization reaction leading to a fused polyheteroaromatic compound. Functionalized phosphine ligands were also elaborated and the corresponding gold(I) chloride complexes smoothly grafted onto silica nano-objects for heterogeneous catalysis. Chiral induction to the surface-bound gold complexes from the chiral silica helices was confirmed using circular dichroism. In the presence of a silver salt, the covalently bound gold catalysts exhibited high reactivity and good recyclability in the dearomative spirocyclization reaction of aryl alkynoate esters. 9,10-Diphenylanthracene (DPA) based thioether ligands were also used to form silver complexes whose self-assembly can be tuned by the nature of the counteranion or by extending the length of the coordination chain. Their activity in homogeneous catalysis was effective in two tandem addition/cycloisomerization of alkynes using 0.5-1 mol% of catalytic loading. Based on the reversible covalent transformation of DPA upon cycloaddition of singlet oxygen, two systems demonstrating switchable properties were developed: a switchable [2+3] imine cage with three DPA pillars exhibiting an affinity for metal ions, and DPA-based chiral sulfoxides designed to exhibit tunable chiroptical properties.

Keywords: Thioether ligand, gold complexes, silver complexes, homo-/heterogeneous catalysis, molecular cage, sulfoxide, chiroptical properties

---

Unité de recherche

Institut des Sciences Moléculaires, CNRS UMR 5255, Groupe NEO, Bâtiment A12, 351 cours de lalibération, 33405 Talence cedex

A list of DPA-based compounds

DPA-based ligands

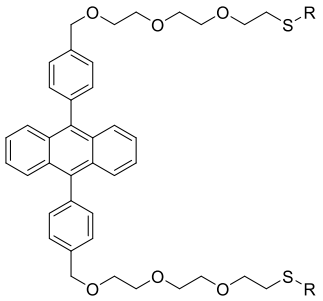

R = $C_{12}H_{25}$, **II1**
R = *t*Bu, **II23**

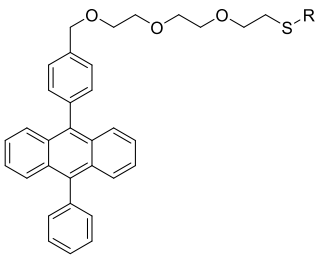

R = $C_{12}H_{25}$, **II2**
R = *t*Bu, **II24**

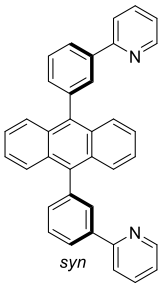

II27

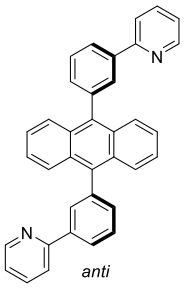

II28

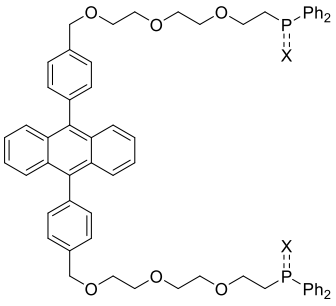

X = O, **IV13**
X = S, **IV32**
X = none, **IV14**

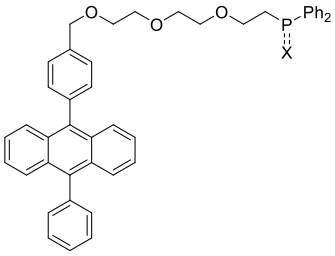

X = O, **IV15**
X = S, **IV33**
X = none, **IV16**

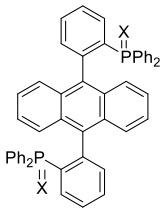

X = O, **IV12**
X = S, **IV31**

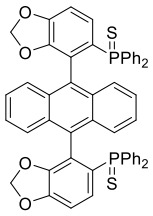

Unidentified configuration
IV19

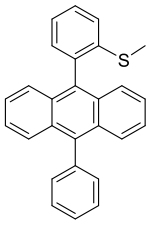

IV1

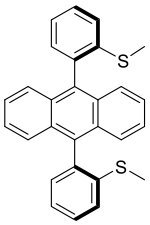

IV2

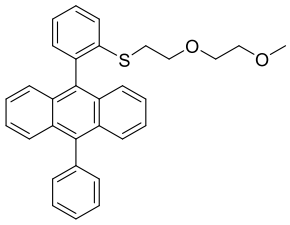

IV3

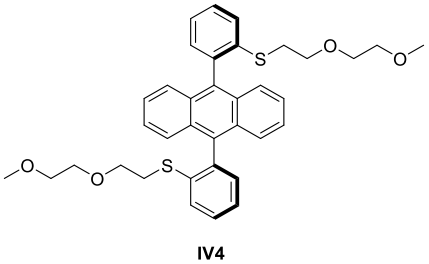

IV4

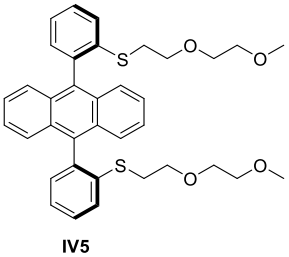

IV5

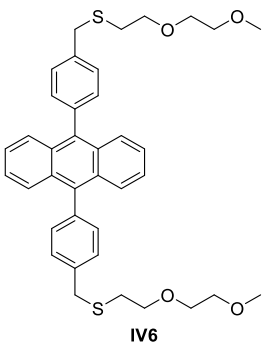

IV6

DPA-based sulfoxides

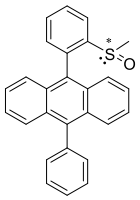

IV7

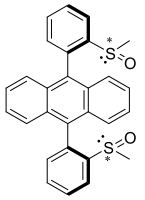

IV8

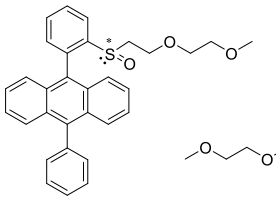

IV9

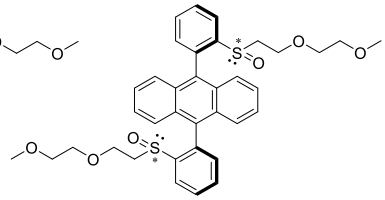

IV10

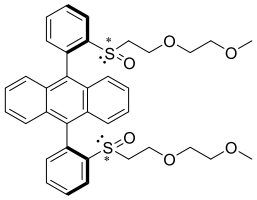

IV11

DPA-supported macrocycle and cage

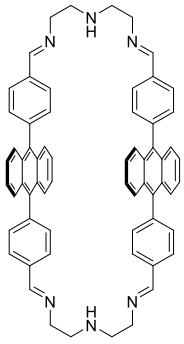

V1

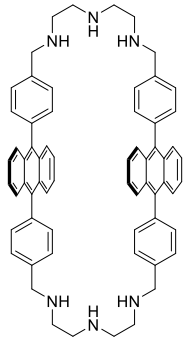

V2

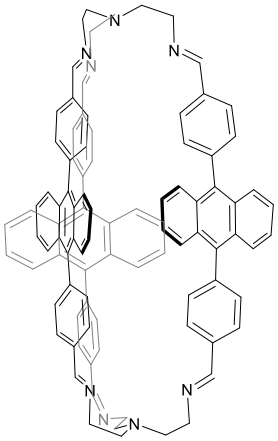

V3

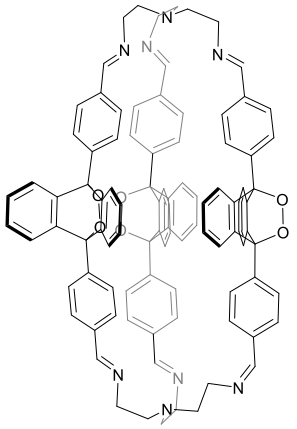

V4